NEW DEVELOPMENTS IN UNDERSTANDING BRAIN AND CEREBROMICROVASCULAR AGING: TOWARD PREVENTION OF VASCULAR COGNITIVE IMPAIRMENT AND ALZHEIMER'S DISEASE

EDITED BY: Stefano Tarantini, Prasad V. Katakam, William Sonntag, Mariagiovanna Cantone and Nicola Vanacore

PUBLISHED IN: Frontiers in Aging Neuroscience and Frontiers in Public Health

frontiers Research Topics

frontiers

ISSN 1664-8714
ISBN 978-2-88976-507-2
DOI 10.3389/978-2-88976-507-2

About Frontiers

Frontiers is more than just an open-access publisher of scholarly articles: it is a pioneering approach to the world of academia, radically improving the way scholarly research is managed. The grand vision of Frontiers is a world where all people have an equal opportunity to seek, share and generate knowledge. Frontiers provides immediate and permanent online open access to all its publications, but this alone is not enough to realize our grand goals.

Frontiers Journal Series

The Frontiers Journal Series is a multi-tier and interdisciplinary set of open-access, online journals, promising a paradigm shift from the current review, selection and dissemination processes in academic publishing. All Frontiers journals are driven by researchers for researchers; therefore, they constitute a service to the scholarly community. At the same time, the Frontiers Journal Series operates on a revolutionary invention, the tiered publishing system, initially addressing specific communities of scholars, and gradually climbing up to broader public understanding, thus serving the interests of the lay society, too.

Dedication to Quality

Each Frontiers article is a landmark of the highest quality, thanks to genuinely collaborative interactions between authors and review editors, who include some of the world's best academicians. Research must be certified by peers before entering a stream of knowledge that may eventually reach the public - and shape society; therefore, Frontiers only applies the most rigorous and unbiased reviews.
Frontiers revolutionizes research publishing by freely delivering the most outstanding research, evaluated with no bias from both the academic and social point of view. By applying the most advanced information technologies, Frontiers is catapulting scholarly publishing into a new generation.

What are Frontiers Research Topics?

Frontiers Research Topics are very popular trademarks of the Frontiers Journals Series: they are collections of at least ten articles, all centered on a particular subject. With their unique mix of varied contributions from Original Research to Review Articles, Frontiers Research Topics unify the most influential researchers, the latest key findings and historical advances in a hot research area! Find out more on how to host your own Frontiers Research Topic or contribute to one as an author by contacting the Frontiers Editorial Office: frontiersin.org/about/contact

NEW DEVELOPMENTS IN UNDERSTANDING BRAIN AND CEREBROMICROVASCULAR AGING: TOWARD PREVENTION OF VASCULAR COGNITIVE IMPAIRMENT AND ALZHEIMER'S DISEASE

Topic Editors:
Stefano Tarantini, University of Oklahoma Health Sciences Center, United States
Prasad V. Katakam, Tulane University, United States
William Sonntag, University of Oklahoma Health Sciences Center, United States
Mariagiovanna Cantone, ASP Caltanissetta, Italy
Nicola Vanacore, National Institute of Health (ISS), Italy

Citation: Tarantini, S., Katakam, P. V., Sonntag, W., Cantone, M., Vanacore, N., eds. (2022). New Developments in Understanding Brain and Cerebromicrovascular Aging: Toward Prevention of Vascular Cognitive Impairment and Alzheimer's Disease. Lausanne: Frontiers Media SA. doi: 10.3389/978-2-88976-507-2

Table of Contents

frontiers | Frontiers in Aging Neuroscience

TYPE Editorial
PUBLISHED 16 September 2022
DOI 10.3389/fnagi.2022.1020271

OPEN ACCESS

EDITED AND REVIEWED BY
Allison B. Reiss,
New York University, United States

*CORRESPONDENCE
Stefano Tarantini
Stefano-tarantini@ouhsc.edu

SPECIALTY SECTION
This article was submitted to Alzheimer's Disease and Related Dementias, a section of the journal Frontiers in Aging Neuroscience

RECEIVED 16 August 2022
ACCEPTED 24 August 2022
PUBLISHED 16 September 2022

CITATION
Sanford M, Negri S and Tarantini S (2022) Editorial: New developments in understanding brain and cerebromicrovascular aging: Toward prevention of vascular cognitive impairment and Alzheimer's disease. *Front. Aging Neurosci.* 14:1020271. doi: 10.3389/fnagi.2022.1020271

Editorial: New developments in understanding brain and cerebromicrovascular aging: Toward prevention of vascular cognitive impairment and Alzheimer's disease

Madison Sanford[1,2], Sharon Negri[1,2,3] and Stefano Tarantini[1,2,4]*

[1]Department of Biochemistry and Molecular Biology, Center for Geroscience and Healthy Brain Aging, University of Oklahoma Health Sciences Center, Oklahoma City, OK, United States, [2]Peggy and Charles Stephenson Cancer Center, University of Oklahoma Health Sciences Center, Oklahoma City, OK, United States, [3]Department of Biology and Biotechnology "Lazzaro Spallanzani", Laboratory of General Physiology, University of Pavia, Pavia, Italy, [4]Hudson College of Public Health, University of Oklahoma Health Sciences Center, Oklahoma City, OK, United States

KEYWORDS

neurovascular, brain aging, VCID, ADRD, Alzheimer's disease

Editorial on the Research Topic
New developments in understanding brain and cerebromicrovascular aging: Toward prevention of vascular cognitive impairment and Alzheimer's disease

Cardiovascular and cerebrovascular diseases are the most common cause of death among older people in the United States, accounting for ~1/3 of all deaths in the US at the age of 65, and nearly 2/3 at the age of 85. With a projected increase in the number of adults over 65 years old from 12 to 22% in the next 30 years, addressing age-related vascular diseases is of critical importance, as the annual cost to care for the older population is expected to more than double in that same time frame. Aging in the brain is characterized by a vast array of functional and structural alterations of the microcirculation, contributing to the pathogenesis of a range of age-related diseases including vascular cognitive impairment (VCI), Alzheimer's disease (AD), and mild cognitive impairment (MCI). The collection of articles published in the Research Topic titled: "*New Developments in Understanding Brain and Cerebromicrovascular Aging: Toward Prevention of Vascular Cognitive Impairment and Alzheimer's Disease*" highlights the recent growing interest and understanding of the role of the aging vasculature in the context of the age-related loss of cognitive function. The goal of this collection is to stimulate interest and gather evidence that relates to the mechanisms underlying the neurodegenerative diseases that associate with aging, with particular emphasis on treatment and interventions that aim to prevent or delay the onset of vascular cognitive impairment and Alzheimer's disease.

VCI and AD are the most common forms of cognitive disorder associated with cerebrovascular diseases and are related to increased morbidity and mortality among the older population (Wiesmann et al., 2013). Growing evidence highlighted in this Research Topic emphasizes the multifactorial nature of age-related cerebrovascular disease. Despite the evidence that reversal of vascular dementias has shown mixed results, we now understand that many of the risk factors are largely preventable. Such risk factors examined in this special issue include the effects of obesity, sedentary lifestyle, eating behaviors, hypertension, diabetes, circulating endocrine factors, and others. The current challenges and efforts in the field will also be briefly explored, while novel biomarkers of cerebrovascular disease and AD will be discussed.

Bliss et al. investigate the effects of aerobic exercise training on cerebrovascular and cognitive function in sedentary, obese, older adults. In their study, the authors showed that cerebrovascular function and cognition improved following 16 weeks of exercise and determined the presence of a dose-response relationship between the amount of exercise sessions performed and cerebrovascular reactivity to cognitive stimuli. Lifestyle interventions aimed at delaying or preventing age-related pathophysiology include exercise (Lucas et al., 2015; Bliss et al., 2021) and alterations in diet (Dobreva et al., 2022; Maroto-Rodriguez et al., 2022) [i.e. caloric restriction, intermittent fasting (Balasubramanian et al., 2020; Bray et al., 2022), or methionine restriction]. These highly translatable interventions have been shown to be effective in mediating increased health and lifespan in mice and other model organisms. Thelen and Brown-Borg reviewed the existing evidence to better understand the therapeutic potential of diets to act as a future treatment option for AD patients.

Circulating insulin-like growth factor-1 (IGF-1) deficiency is a well-known predictor of cognitive decline. For instance, previous studies established a causal link among age-related decline in circulating levels of IGF-1, neurovascular dysfunction, and cognitive impairment (Tarantini et al., 2021). Miller et al. further describe how IGF-1 deficiency is associated with increased susceptibility to cerebral microhemorrhages and signs of microvascular degeneration in the retina in response to hypertension. The formation of microhemorrhages, which associate with cognitive impairments, psychiatric disorders, and gait dysfunctions in patients is also caused by mild traumatic brain injury (mTBI). In this context, Toth et al. have investigated the effect of mTBI on cerebral microhemorrhages in aging and have reported that aging enhances the formation of parietal and occipital microhemorrhages after mTBIs.

The properties of the brain cerebral microvasculature can be also studied in the retina (Newman, 2013), as those micro vessels are closely related to those in the brain (Ptito et al., 2021). In addition to the work from Miller et al., illustrated above, Cheng et al. utilized the retina as model to study the association between diabetic retinopathy and cognitive impairment in this extensive systematic review. This timely work better examines the correlation of diabetic retinopathy with cognitive impairment, which has not been well-studied yet.

Normal brain function is dependent on moment-to-moment adjustment of cerebral blood flow to match the increased demands of active brain regions (Masamoto and Vazquez, 2018; Yabluchanskiy et al., 2021). The underlying biological mechanism termed neurovascular coupling (NVC) is dependent on the production of the endothelium-derived vasodilator molecule nitric oxide in response to multiple mediators released from activated astrocytes. Csipo et al. studied how geriatric sepsis affects endothelial dysfunction and impaired NVC responses precede cognitive impairment in a mouse model of geriatric sepsis, suggesting that sepsis-associated endothelial dysfunction and impairment of NVC responses may contribute to long-term cognitive deficits in older sepsis survivors. In addition, Liu et al. aimed to explore the characteristics and contributions of cerebral hemodynamics and carotid atherosclerosis to cognitive dysfunction. The authors discovered that pathological changes in macrovascular structure and function are correlated with cognitive impairment in dementia. This is intriguing as recent studies have shown that macrovascular aberrations closely associated with decreased microvascular health in aging (Xu et al., 2017). Shabaan et al. were also interested in examining the link between cognition and cerebrovascular reactivity in midlife women with both preeclampsia and maternal vascular malperfusion (MVM). Their data suggested that MVM in women with preeclampsia is a promising sex-specific indicator of cerebrovascular integrity in midlife (Shabaan et al.).

Another challenge in the field of cerebromicrovascular aging has been identifying a reliable indicator or biomarker to detect patients with different forms of dementia at an early stage (Zampino et al., 2022). Liu et al. showed that basal ganglia perivascular spaces were associated with increased cardiovascular risk burden and regional differences in cerebral blood flow and gray matter volume, thereby advancing the idea that perivascular spaces are an important associated phenotypic indicator of VCI with a larger population of cognitively intact individuals. Similarly, Yao et al. suggested that in a population of frail patients with cardiovascular disease the urinary 8-oxoGsn (a typical marker of oxidative modification of RNA) adjusted by urinary creatine levels, may be a useful indicator for the early screening of MCI. In their study, Sun et al. searched for an endothelial-specific biological marker to better understand the pathogenesis of cerebral small vessel disease (CSVD). Intriguingly, they found a relationship between ADAMTS13 activity and white matter hyperintensity (WMH), subcortical infarction, but not with cerebral microhemorrhage. In addition, ADAMTS13 (which regulates the activity of endothelium-derived von Willebrand factor by cutting it into smaller, less active molecules) may play an essential role in the progression of CSVD. Another typical marker that associates with CSVD

are WMHs. In their study Bauer et al. perform an extensive assessment of WMH volume and location. Notably, their results suggest that white matter microstructure may be a better predictor of WMHs volume than either brain iron levels or cerebral blood flow (CBF) but also draws attention to the possibility that some early WMH markers may be location specific. Furthermore, Vettore et al. add that the association between WMH burden and connectivity strength, during resting-state functional networks, is different between amnestic and non-amnestic MCI patients. Despite the exploratory nature of this study, these results suggest that clinical profiles reveal mechanistic interactions that may play a critical role in the classification of diagnostic vs. prognostic conditions. In another study, Liu et al. developed an innovative transfer learning model based on speech and natural language processing (NLP) technology to effectively improve the early diagnosis of AD.

Genetic variability is another interesting factor that can play a major effect in the development of cerebral vasculature (Bogorad et al., 2019), and as a determinant for age-related cerebrovascular disease and AD, as demonstrated in both clinical and experimental studies (Korstanje et al., 2021; Kulminski et al., 2022). Recent genetic mutation studies done in rodents have elucidated how different genetic backgrounds can significantly affect flow-mediated outward remodeling in the bilateral posterior communicating arteries after unilateral occlusion of a middle cerebral artery. Therefore, Eto et al. aimed to investigate the relationship between anatomical variations in the circle of Willis in cerebrovascular disease. This study sets up an important framework in which future investigations can further expand to understand what genetic variants are critical in determining anatomical variations in the circle of Willis, thus increasing vulnerability to age-related vascular disease. Additionally, Ehret et al. draw attention to an important point mutation in *Notch3* (N3), which is known to cause Cerebral Autosomal Dominant Arteriopathy with Subcortical Infarcts and Leukoencephalopathy (CADASIL). N3 is expressed in neural stem and progenitor cells in the hippocampus, where the authors previously demonstrated that it is a critical regulator of precursor cell proliferation and differentiation in the neurogenic niche of the murine hippocampus. Based on the previous results, they now suggest that N3 might exert regulatory influences on neuronal plasticity that could impact hippocampus-dependent learning and memory. The hippocampus together with the pre-frontal cortex constitute a very important brain area involved in the regulation of emotion and cognition. Qi et al. described how a bilateral hippocampal microinjection of streptozotocin can induce AD-like behavioral performance in mice, and adaptive changes in synaptic plasticity against neuroinflammatory and endocrinal injuries. The authors interpret these findings and hypothesize the underlying mechanisms to be associated with the inadequate balance in the hippocampal expression of the key proteins involved in Wnt signaling pathway.

Lastly, Takeuchi et al. discovered that the RNA transcription analysis of metabolism related genes in circulating white blood cells (WBCs) has the potential to provide significant information relating to impaired cell-cell interaction between WBCs and endothelial cells of aged mice. Additionally, this can serve as a tool to evaluate the change of the cell-cell interaction caused by various treatments or diseases.

Author contributions

ST: Conceptualization, funding acquisition, writing-original draft, and writing-review and editing. MS and SN: Writing-review and editing. All authors contributed to the article and approved the submitted version.

Funding

This work was supported by grants from the National Institute on Aging (NIA R03AG070479 and NIA K01AG073614), the American Heart Association AHA CDA941290, the NIA-supported Geroscience Training Program in Oklahoma (T32AG052363), the NIA-supported Oklahoma Nathan Shock Center, and the NIGMS supported Center of Biomedical Research Excellence (CoBRE) (1P20GM125528-01A1).

Conflict of interest

The authors declare that the research was conducted in the absence of any commercial or financial relationships that could be construed as a potential conflict of interest.

Publisher's note

References

Balasubramanian, P., DelFavero, J., Ungvari, A., Papp, M., Tarantini, A., Price, N., et al. (2020). Time-restricted feeding (TRF) for prevention of age-related vascular cognitive impairment and dementia. *Ageing Res. Rev.* 64:101189. doi: 10.1016/j.arr.2020.101189

Bliss, E. S., Wong, R. H., Howe, P. R., and Mills, D. E. (2021). Benefits of exercise training on cerebrovascular and cognitive function in ageing. *J. Cereb. Blood Flow Metab.* 41, 447–470. doi: 10.1177/0271678X20957807

Bogorad, M. I., DeStefano, J. G., Linville, R. M., Wong, A. D., and Searson, P. C. (2019). Cerebrovascular plasticity: Processes that lead to changes in the architecture of brain microvessels. *J. Cereb. Blood Flow Metab.* 39, 1413–1432. doi: 10.1177/0271678X19855875

Bray, E. E., Zheng, Z., Tolbert, M. K., and McCoy, B. M. (2022). Once-daily feeding is associated with better health in companion dogs: results from the Dog Aging Project. *Geroscience* 44, 1779–1790. doi: 10.1007/s11357-022-00575-7

Dobreva, I., Marston, L., and Mukadam, N. (2022). Which components of the Mediterranean diet are associated with dementia? A UK Biobank cohort study. *Geroscience*. doi: 10.1007/s11357-022-00615-2

Korstanje, R., Peters, L. L., Robinson, L. L., Krasinski, S. D., and Churchill, G. A. (2021). The Jackson Laboratory Nathan Shock Center: impact of genetic diversity on aging. *Geroscience* 43, 2129–2137. doi: 10.1007/s11357-021-00421-2

Kulminski, A. M., Loiko, E., Loika, Y., and Culminskaya, I. (2022). Pleiotropic predisposition to Alzheimer's disease and educational attainment: insights from the summary statistics analysis. *Geroscience* 44, 265–280. doi: 10.1007/s11357-021-00484-1

Lucas, S. J., Cotter, J. D., Brassard, P., and Bailey, D. M. (2015). High-intensity interval exercise and cerebrovascular health: curiosity, cause, and consequence. *J. Cereb. Blood Flow Metab.* 35, 902–911. doi: 10.1038/jcbfm.2015.49

Maroto-Rodriguez, J., Delgado-Velandia, M., Ortolá R., Carballo-Casla, A., García-Esquinas, E., Rodríguez-Artalejo, F., et al. (2022). Plant-based diets and risk of frailty in community-dwelling older adults: the Seniors-ENRICA-1 cohort. *Geroscience*. doi: 10.1007/s11357-022-00614-3

Masamoto, K., and Vazquez, A. (2018). Optical imaging and modulation of neurovascular responses. *J. Cereb. Blood Flow Metab.* 38, 2057–2072. doi: 10.1177/0271678X18803372

Newman, E. A. (2013). Functional hyperemia and mechanisms of neurovascular coupling in the retinal vasculature. *J. Cereb. Blood Flow Metab.* 33, 1685–1695. doi: 10.1038/jcbfm.2013.145

Ptito, M., Bleau, M., and Bouskila, J. (2021). The retina: a window into the brain. *Cells* 10:e23269. doi: 10.3390/cells10123269

Tarantini, S., Nyúl-Tóth, Á., Yabluchanskiy, A., Csipo, T., Mukli, P., Balasubramanian, P., et al. (2021). Endothelial deficiency of insulin-like growth factor-1 receptor (IGF1R) impairs neurovascular coupling responses in mice, mimicking aspects of the brain aging phenotype. *Geroscience* 43, 2387–2394. doi: 10.1007/s11357-021-00405-2

Wiesmann, M., Kiliaan, A. J., and Claassen, J. A. (2013). Vascular aspects of cognitive impairment and dementia. *J. Cereb. Blood Flow Metab.* 33, 1696–1706. doi: 10.1038/jcbfm.2013.159

Xu, X., Wang, B., Ren, C., Hu, J., Greenberg, D. A., Chen, T., et al. (2017). Recent progress in vascular aging: mechanisms and its role in age-related diseases. *Aging Dis.* 8, 486–505. doi: 10.14336/AD.2017.0507

Yabluchanskiy, A., Nyul-Toth, A., Csiszar, A., Gulej, R., Saunders, D., Towner, R., et al. (2021). Age-related alterations in the cerebrovasculature affect neurovascular coupling and BOLD fMRI responses: Insights from animal models of aging. *Psychophysiology* 58:e13718. doi: 10.1111/psyp.13718

Zampino, M., Polidori, M. C., Ferrucci, L., O'Neill, D., Pilotto, A., Gogol, M., et al. (2022). Biomarkers of aging in real life: three questions on aging and the comprehensive geriatric assessment. *Geroscience* 7, 1–12. doi: 10.1007/s11357-022-00613-4

frontiers in Aging Neuroscience

REVIEW
published: 23 December 2020
doi: 10.3389/fnagi.2020.617071

Does Diet Have a Role in the Treatment of Alzheimer's Disease?

Mitchell Thelen† *and Holly M. Brown-Borg**

Department of Biomedical Sciences, University of North Dakota School of Medicine and Health Sciences, Grand Forks, ND, United States

The aging process causes many changes to the brain and is a major risk factor for the development of neurodegenerative diseases such as Alzheimer's Disease (AD). Despite an already vast amount of research on AD, a greater understanding of the disease's pathology and therapeutic options are desperately needed. One important distinction that is also in need of further study is the ability to distinguish changes to the brain observed in early stages of AD vs. changes that occur with normal aging. Current FDA-approved therapeutic options for AD patients have proven to be ineffective and indicate the need for alternative therapies. Aging interventions including alterations in diet (such as caloric restriction, fasting, or methionine restriction) have been shown to be effective in mediating increased health and lifespan in mice and other model organisms. Because aging is the greatest risk factor for the development of neurodegenerative diseases, certain dietary interventions should be explored as they have the potential to act as a future treatment option for AD patients.

Keywords: aging, diet, interventions, Alzheimer's disease, lifespan

OPEN ACCESS

Edited by:
Stefano Tarantini, University of Oklahoma Health Sciences Center, United States

Reviewed by:
Andriy Yabluchanskiy, University of Oklahoma Health Sciences Center, United States
Priya Balasubramanian, University of Oklahoma Health Sciences Center, United States

***Correspondence:**
Holly M. Brown-Borg
Holly.brown.borg@und.edu

†*Mitchell Thelen is a second-year medical student that wrote this review to fulfill requirements for the Research Experience for Medical Students program at the University of North Dakota School of Medicine, Health Sciences*

Received: *13 October 2020*
Accepted: *30 November 2020*
Published: *23 December 2020*

Citation:
Thelen M and Brown-Borg HM (2020) Does Diet Have a Role in the Treatment of Alzheimer's Disease? Front. Aging Neurosci. 12:617071. doi: 10.3389/fnagi.2020.617071

INTRODUCTION

Aging is the major risk factor for many diseases but the factors that drive age-related changes and promote dysfunction are poorly understood. Slowing or even delaying these processes may lead to extended periods of health in humans. With each passing year, aging has a greater impact on the U.S. healthcare system. As of the year 2020, the older adult population (65 years and older) is comprised of 56 million people and is expected to increase to nearly 90 million by the year 2050 (Alzheimer's Association, 2020a). In fact, projections point toward the year 2030 as being the first time in U.S. history where the population of those over the age of 65 will outnumber those 18 years and younger (Mendiola-Precoma et al., 2016). Aging is associated with an increased risk of disease and death; therefore, an aging population will place increased burden on our healthcare system and will have a greater financial impact on individuals throughout the country (Rose, 2009; Mendiola-Precoma et al., 2016).

Aging occurs in nearly all organisms and is represented by a physiological decline in function. Decades of work by many scientists led to the identification of several hallmarks of aging, many of which impact the brain as will be later presented. Various versions of the list exist but many agree about the general contributors. However, despite the identified hallmarks, the exact mechanisms underlying or driving biological aging remain inadequate to develop therapies to truly combat aging as a whole. This has led to alternative hypotheses suggesting that random cellular dysfunctions may be the greatest contributor to aging, potentially explaining why organisms of the same genotype (monozygotic twins) who are raised in a common environment have significantly different life spans (Kirkwood et al., 2005).

An aging population warrants increased attention toward understanding the mechanisms that drive the aging process. This includes considering therapies to slow, delay or prevent aging. Past and current treatment options have focused on interventions specific for one disease process at a time (such as FDA drug approval for specific diseases). This has been one approach contributing to the increase in population health over a span of decades, as evidenced by an increase in U.S. life expectancy from 69.9 to 78.9 years from the years 1959 to 2016. However, recent data suggests that U.S. life expectancy is reaching a plateau or even slightly decreasing (Woolf and Schoomaker, 2019). A greater understanding of aging offers vast potential toward the field of medicine. It provides hope for slower disease progression and increased life expectancy in humans. However, the ultimate goal is to lengthen the overall time individuals remain disease-free (increased health-span), which would have a major positive impact on individuals and the healthcare system.

BRAIN AGING AND AD

Aging impacts many organ systems, but the brain garners a large share of the interest and funding. The brain undergoes prominent structural and functional changes throughout a lifetime. Structurally, normal brain aging involves atrophy seen through reductions in both gray and white matter and an associated enlargement of the cerebral ventricles (Drayer, 1988). These age-related reductions in gray matter are most notable in the frontal and temporal lobes (Jack et al., 1997). Much of this normal brain atrophy appears to be due to neuronal loss, neuronal morphology changes, and dendritic and synaptic reductions (Terry and Katzman, 2001; Dumitriu et al., 2010). Other structural brain changes observed in normal aging include increased visualization of amyloid-β plaques, neurofibrillary tangles, white matter injuries, small-vessel ischemia, and microhemorrhages (Terry and Katzman, 2001; Park et al., 2013; Prins and Scheltens, 2015; Shim et al., 2015; Ramirez et al., 2016). Functional changes to the brain with increased age include a gradual decline in attention, memory, decision-making speed, learning, motor coordination, and sensory perceptions (Alexander et al., 2012; Dykiert et al., 2012; Levin et al., 2014). Cognitive function is most affected in the areas of executive function, working memory, and episodic memory (Alexander et al., 2012).

Aging is the greatest risk factor for developing many neurodegenerative diseases (Hou et al., 2019). Broad classification of neurodegenerative diseases includes amyloidoses, tauopathies, synucleinopathies, and TDP-43 proteinopathies (Dugger and Dickson, 2017). Alzheimer's Disease (AD), a mixed amyloidose and tauopathy pathology, is the most common neurodegenerative disease in the U.S. Currently, AD is five times more prevalent than Parkinson's Disease, the second most common neurodegenerative disease, and this margin is expected to continue increasing. To date, AD affects nearly five million Americans (1 in 10 people over the age of 65) and is the sixth leading cause of death in the U.S. These numbers are expected to grow as 13.8 million people are projected to be living with AD by the year 2050. Furthermore, AD and related dementias will cost the U.S. over $300 billion in 2020 with an expectation to increase to more than $1 trillion by the year 2050 (Alzheimer's Association, 2020a).

Despite great effort from the scientific community, the primary cause of AD remains unknown. Risk factors for developing familial AD (leading to early onset symptoms) include mutations in the amyloid precursor protein (APP), presenilin 1 and presenilin 2 genes (Bekris et al., 2010). However, risk factors for the much more common sporadic development of AD include increased age and mutations to the ApoE4 allele (Liu et al., 2013). Features of an AD brain involve noticeable amyloid-beta (Aβ) plaques and p-tau neurofibrillary tangles (Bloom, 2014). Aβ peptides are produced after the proteolysis of the type I integral membrane protein amyloid precursor protein (APP) (Esch et al., 1990; Shoji et al., 1992; Haass and Selkoe, 1993; Haass et al., 1993; Jarrett et al., 1993). Aβ plaque and p-tau neurofibrillary tangle formation starts with altered APP cleavage by β-secretases (BACE1) and γ-secretases to produce insoluble Aβ fibrils. These Aβ fibrils then polymerize into insoluble amyloid fibrils which aggregate into plaques (Fontana et al., 2004; Simunkova et al., 2019). Polymerization of Aβ fibrils cause activation of kinases which hyperphosphorylate microtubule associated p-tau and lead to their polymerization into insoluble neurofibrillary tangles. Accumulation of Aβ plaques and p-tau neurofibrillary tangles lead to microglial activation and are associated with neurotoxicity (Long and Holtzman, 2019).

Disruption of cerebral vasculature is associated with neuroinflammation in mice studies and has also been shown to contribute to aging and AD (Tarantini et al., 2017; Fulop et al., 2019). Regions of the brain with increased activity rely on a mechanism known as neurovascular coupling (NVC) to receive a compensatory uptick in regional oxygen and glucose. NVC works through the release of the vasodilating molecule nitric oxide (NO) from microvascular endothelial cells surrounding areas of metabolically active neurons and astrocytes (Toth et al., 2014, 2015; Tarantini et al., 2017, 2018, 2019a). Interruption of the NVC mechanism tends to be found in older adults and it also leads to cognitive impairment in mice (Fabiani et al., 2014; Tarantini et al., 2017, 2018, 2019a; Lipecz et al., 2019). In fact, in mouse models of aging, interventions which improve NVC and cerebral microvasculature also improve cognitive function (Csiszar et al., 2019; Tarantini et al., 2019b; Wiedenhoeft et al., 2019). Currently functional MRI (fMRI) is one method of measuring NVC in humans, yet many new technologies are being studied for their usefulness in monitoring the cerebral microvascular changes that accompany aging (Csipo et al., 2019; Lipecz et al., 2019).

AD is a slow progressing disease characterized by a decline in cognitive function. Recent estimates report the preclinical (asymptomatic) stage of AD occurs for up to 15 to 20 years prior to clinical symptom emergence (Morris et al., 2001; Sperling et al., 2011, 2013). This is based upon examinations of brains of older individuals, who die with no cognitive impairment or mild cognitive impairment, often revealing similar pathology to those with apparent AD (Mufson et al., 1999; Price and Morris, 1999; Bennett et al., 2005; Markesbery et al., 2006). AD is classified

into early stage (mild), middle stage (moderate), and late stages (severe forms). Mild and moderate stages may last for years at a time as the individual's memory, cognitive ability, and ability to live independently slowly decline. By the late stage of AD, the individual loses their ability to respond to their environment, carry on a conversation, and eventually control movement. Memory and cognition also continue to decline during this time. Most people only live for 4 to 8 years following first diagnosis (Alzheimer's Association, 2020b).

A closer look at the specific hallmarks of aging as they relate to the central nervous system is warranted. The nine hallmarks of aging include genomic instability, telomere attrition, epigenetic alterations, loss of proteostasis, mitochondrial dysfunction, cellular senescence, dysregulated nutrient sensing, stem cell exhaustion, and altered intercellular communication and immune function (López-Otín et al., 2013). Many of these hallmarks are associated with neurodegenerative diseases such as AD. Studies have found increased DNA damage and altered DNA repair mechanisms in the brains of AD patients (Lovell et al., 1999). Certain epigenetic markers, such as methylation patterns in APP promoters of primates, are related to neurodegenerative features (Bradley-Whitman and Lovell, 2013). The mitophagy process seems to be defective in AD, such that stimulation of mitophagy in nematode and mouse models improved memory (Fang et al., 2019). Brain cells from AD models demonstrate reduced glucose and oxygen metabolic rates (Camandola and Mattson, 2017). Additionally, Aβ oligomers trigger senescence of neurons *in vitro* and senescent astrocytes, microglia, and neurons are found in greater numbers in human AD brains (He et al., 2013). *In vivo* and *in vitro* studies have found that APP expression on microglial cells is required for their proinflammatory activation to Aβ oligomers (Manocha et al., 2016). Thus, several aspects of the underlying pathology and clinical features found with AD, mirror those observed in the established hallmarks of aging.

Distinguishing normal changes to the brain with age vs. pathological changes remains a challenge to date. Difficulty arises from evidence indicating that many of the structural changes to the brain found in neurodegenerative diseases such as AD, resemble the structural changes observed in a normal aging brain. High levels of amyloid-β plaques, neurofibrillary tangles, synaptic loss, and neuroinflammation are hallmarks of AD. As previously discussed, these changes also comprise part of normal aging of the brain and it is not uncommon for these same features to be seen in a non-demented, older individual (Denver and McClean, 2018). However, many of the structural changes displayed in neurodegenerative diseases are more frequent and more severe than in the normal aging process (Park et al., 2013; Prins and Scheltens, 2015; Shim et al., 2015; Ramirez et al., 2016). Unfortunately, in the case of AD, by the time these structural changes have accumulated enough to begin manifesting in symptoms, the neuropathology is irreversible. A greater ability to distinguish AD pathology, especially in its early stages, vs. normal aging would lead to improved diagnostic capabilities and potential new drug discoveries (Denver and McClean, 2018).

THERAPIES FOR AD

Therapies to treat AD progression range from FDA-approved compounds to exercise, nutraceuticals and dietary interventions (**Figure 1**). Importantly, current treatment options for Alzheimer's Disease lack effectiveness. Only two therapeutic options are approved by the FDA, that being cholinesterase inhibitors (Donepezil, Rivastigmine, and Galantamine) and Memantine (an NMDA receptor antagonist/dopamine agonist) (Howard et al., 2012; Grossberg et al., 2013). Both options offer mild symptom management with no effect on long term progression of the disease. Additionally, over 20 compounds have reached large phase 3, double-blind, randomized control trials in cohorts of AD patients at various stages of disease progression, yet none have shown the ability to improve global functioning or slow cognitive decline (Long and Holtzman, 2019).

Due to the ineffectiveness of AD therapeutics, alternative treatment options are being explored. Huperzine A, a nutraceutical, has been shown to increase memory and activities of daily living in AD patients (Xing et al., 2014). This compound, along with other herbal drugs such as huperzine B, ginseng, corilagen, and curcumin offer therapeutic potential for AD due to their ability to cross the blood brain barrier (BBB) and act through the inhibition of acetylcholinesterase (AChE), chelation of redox-active metals, inhibition of the aggregation of Aβ and reduction of neuroinflammation (Simunkova et al., 2019). However, these drugs are not approved by the FDA and may suffer from lack of purity and potency (Xing et al., 2014). Recently, several small clinical studies have shown a relationship between a ketogenic diet and improved cognition in AD and other neurodegenerative disease patients (Rusek et al., 2019). Administration of medium-chain triglyceride-based ketogenic formula for 12 weeks to 20 patients with mild-to-moderate AD led to a significant increase in working memory, short-term memory, and processing speed. Specifically, these patients showed improvements in the digit-symbol coding test as well as the immediate and delayed logical memory tests (Ota et al., 2019). Many treatments for AD are designed to target the production and/or accumulation of Aβ and tau proteins, but this approach has not been promising so far. Monoclonal antibodies designed to target and remove abnormal amyloid beta have shown no improvement in cognitive function in early and late stage AD patients (Doody et al., 2014; Salloway et al., 2014; Honig et al., 2018). Potential vaccines against tau protein are currently under investigation as well as deep brain stimulation and gamma-frequency oscillation therapies (Weller and Budson, 2018; Koseoglu, 2019). Thus, although numerous therapies have been explored, very few clinical options are currently available to stop or slow progression of neurodegenerative disorders. There are numerous reports showing an association between diet, exercise, and reduced risk of developing neurodegenerative diseases, but these are not considered in this discussion of treatments for ongoing disease.

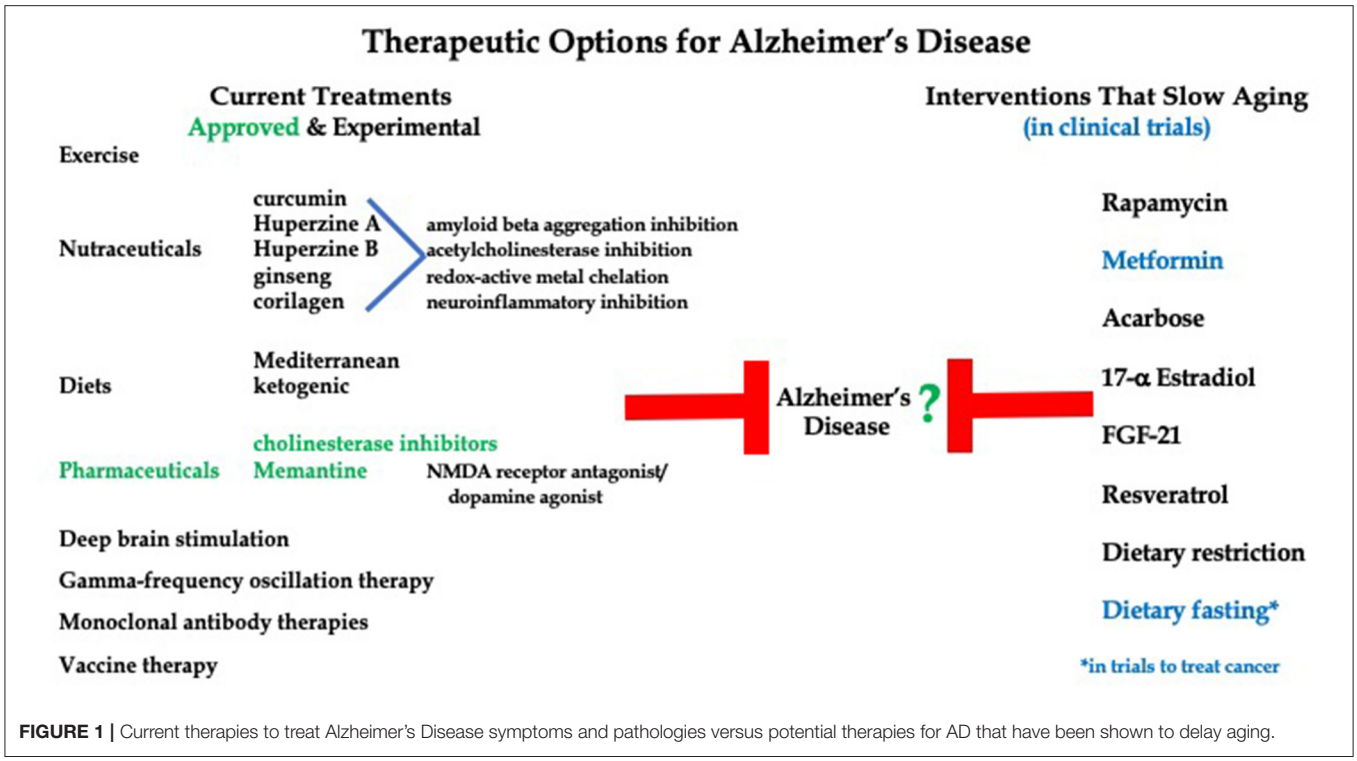

FIGURE 1 | Current therapies to treat Alzheimer's Disease symptoms and pathologies versus potential therapies for AD that have been shown to delay aging.

MODELS OF AD

AD is modeled in the laboratory to address the biology of specific cell types as well as in mice primarily, to study disease onset, progression, and treatment. Mouse models, including transgenic and non-transgenic options, are most common for the investigation of AD and offer a variety of pros and cons (Puzzo et al., 2015). Several transgenic mouse lines have been created to mimic human AD pathology. These animals are genetically engineered to overexpress one or more of the proteins found in human AD patients and often include APP, tau, and/or presenilin. One commonly used mouse line is the double transgenic APP/PS1 which develop a robust deposition of amyloid-beta plaques due to mutations in APP on chromosome 21 and presenilin 1 (PS1) on chromosome 14. These mice show increased levels of soluble Aβ40 and Aβ42 at an early age which allows for study of an AD-related phenotype (Puzzo et al., 2015).

Behavior studies of transgenic mice aim to assess the cognitive domains of these AD models in ways that are similar to what is observed in human AD. Alterations to working memory, executive function, and attention are common aspects of cognition which are disrupted in human AD and can also be studied in transgenic mice. In humans, working memory is assessed through verbal tasks, yet working memory is typically studied in mice through maze-type tasks in which spatial working memory is evaluated. AD transgenic mice show deficits in working memory by taking longer to learn where the food reward is located and which aspects of the maze they have previously visited (Webster et al., 2014). Executive function requires higher order cognition such as planning, reasoning, and cognitive flexibility and is observed in humans through tests such as the Wisconsin Card Sorting Task (Drewe, 1974; Robinson et al., 1980; Arnett et al., 1994). AD transgenic mice show deficits in executive function abilities through tasks involving set-shifting, reversal learning, and response inhibition (Zhuo et al., 2007; Papadopoulos et al., 2013; Romberg et al., 2013). The most widely used method of examining disruptions in attention for transgenic mice is through tasks, such as the five-choice serial-reaction time task (5-CSRTT), that utilize sustained attention divided among multiple spatial locations, where a large number of trials and errors of commission, omission, and reaction time are scored (Webster et al., 2014). These rodent tests most closely resemble Leonard's 5-CSRTT and Continuous Performance Tests (CPT) of sustained attention used in humans, however, there remains difficulty translating attention results from mice AD models to those seen in humans (Rosvold et al., 1956; Wilkinson, 1963; Young et al., 2009).

The study of AD through transgenic mice (including APP/PS1 mice) is limited in some ways. First, transgenic mice express a genetic form of AD while most cases in humans are not genetically based, but rather develop sporadically at older ages. Additionally, transgenic mutations introduced into mice are not able to match the complexity seen in AD such that no mouse models can reproduce the full spectrum of human AD symptoms and pathology (Tai et al., 2017). Non-transgenic models of AD typically involve molecular (such as Aβ or tau) intracerebroventricular or intrahippocampal injections into mice. This method of investigation offers the benefit of studying acute effects on brain tissue of Aβ or tau exposure, which is more like the sporadic development of AD pathology typically

occurring in humans when compared to transgenic mice. Yet, non-transgenic mice do not reproduce the gradual rise of Aβ that occurs over many years in humans and it does not replicate the spreading of pathology through regions of the brain, which is a major component of AD pathology (Puzzo et al., 2015). Ultimately, while there remains uncertainty as to how similar pathogenic pathways found in mice are to those in humans, mouse models are a valuable tool for the study of the AD process (Shineman et al., 2011).

THERAPIES FOR AGING

Currently, there are no FDA approved interventions to slow and/or delay aging. However, the search is on for drugs that may alter the aging process in humans. To date, several drugs presently approved and prescribed to treat symptoms or slow specific disease processes have shown the ability to also slow aging in model systems. Examples include Rapamycin, Metformin and Acarbose. The advantage of studying these medications is that their safety for use in humans is already known. Notable non-FDA approved options also under current study, include 17α -Estradiol (17α-E2), Fibroblast-growth factor-21 (FGF21), and Resveratrol. Further, interventions targeting the sirtuins, NAD biosynthesis, amino acids, autophagy, and senescence pathways have shown promise as well and are actively being investigated in models of aging and health (Gonzalez-Freire et al., 2020).

Rapamycin use is FDA approved for its immunosuppressive and anti-graft rejection properties (Camardo, 2003). However, Rapamycin and other rapalogs have shown an ability to increase lifespan in animal studies through inhibition of the mammalian target of rapamycin (mTOR) pathway. The mTOR pathway is a metabolic regulator whose activation is triggered by the insulin/IGF-1 axis, amino acid levels, and glucose levels which all signal cellular energy status. Signals act through two multiprotein complexes (mTORC1 and mTORC2) and lead to different outcomes. In short, mTORC1 activation leads to protein translation and cell growth, whereas its inhibition blocks growth and induces stress response pathways, such as autophagy, leading to pro-longevity effects (Laplante and Sabatini, 2012; Saxton and Sabatini, 2017). Pharmacological mTORC1 inhibition extends lifespan in mice and involves multiple processes including autophagy, lipid synthesis, mitochondrial metabolism, ribosomal biogenesis, and modulation of the senescence-associated secretory phenotypes (Pan and Finkel, 2017). Contrarily, mTORC2 inactivation is believed to be responsible for the unwanted insulin resistance associated with rapamycin treatment (Saxton and Sabatini, 2017). Inhibition of mTORC1 occurs following both acute and chronic administration of rapamycin while the unwanted inhibition of mTORC2 requires long-term rapamycin treatment (Li J. et al., 2014). Thus, rapamycin and other rapalogs remain potential candidates for use to interfere with aging processes and extend health span.

Metformin is another drug currently approved for use in humans that has shown promising age-altering effects in animal studies. Metformin is a safe biguanide-class drug used as the first line defense for type II diabetes in humans. Its effectiveness in type II diabetes management comes from its ability to lower hepatic glucose production and insulin resistance. However, there are reports that metformin use seems to offer other health benefits, one of which is its anti-aging properties. Administration of metformin leads to caloric restriction-like benefits such as improved insulin sensitivity, AMP-activated protein kinase (AMPK) activity, and better antioxidant protection (Martin-Montalvo et al., 2013). Neonatal mice injected with a single dose of metformin on the 3rd, 5th, and 7th days after birth showed a significant increase in lifespan for males and a slight (non-significant) increase in females (Anisimov et al., 2015). In both male and female neonatally-treated mice, hormonal and metabolic serum testing was unaltered compared to control. However, metformin-treated males had decreased body weight plus food and water consumption compared to control mice. Female treated mice showed no such difference compared to controls (Anisimov et al., 2015). Contrarily, administration of metformin to 2-year-old male mice leads to improved health without increased lifespan (Alfaras et al., 2017). Based on its promising results from cellular and animal studies on aging and its known safety in humans, a ground-breaking clinical trial termed TAME (Targeting Aging with Metformin) is underway. TAME is the first drug trial approved by the FDA that directly targets aging. The study plans to examine metformin's ability to delay age-related diseases beyond its effects on glucose metabolism through the study of 3,000 subjects across the U.S. between the ages of 65 to 79. Results of TAME could have a profound impact on the health care and research community. If metformin shows the ability to modulate aging and related diseases, outside of its impact on diabetes, it would be the first step in the development of drugs specifically targeting the biology of aging (Barzilai et al., 2016).

Acarbose is an alpha-glucoside inhibitor used to treat hyperglycemia and type II diabetes. When consumed with a carbohydrate-rich meal, acarbose competitively inhibits complex carbohydrate breakdown along the brush border of the small intestine resulting in delayed dietary carbohydrate breakdown and absorption (Caspary and Graf, 1979). Administration of acarbose seems to have a positive impact on both short-term and long-term blood glucose and insulin levels while also receiving reports of decreased body weight in both animal and human studies (Brewer et al., 2016). In animal studies, acarbose administration leads to extended lifespan and improved health-span particularly in male mice through an increase in fibroblast growth factor-21 (FGF21) and a decrease in IGF-1 levels (Harrison et al., 2014).

17α -Estradiol (17α-E2), Fibroblast-growth factor-21 (FGF21), and Resveratrol lack FDA approved use in humans but studies of each have shown promise for an ability to curb detrimental effects of aging in mice. 17α-E2 is a non-feminizing hormone found in humans whose administration in mice leads to reduced body weight, extended lifespan, and mitigated metabolic and age-related chronic inflammation. However, these effects were limited to only male mice (Stout et al., 2017). Fibroblast-growth factor-21 (FGF21) is a protein hormone which attenuates GH/IGF1 signaling in mice (Mendelsohn and Larrick,

2012). Transgenic overexpression of FGF21 leads to increased lifespan (Zhang et al., 2012). Finally, Resveratrol is a polyphenol found in mulberries, peanuts, and red grapes. Supplementation of this polyphenol in monkeys has shown increased health while supplementation in C. Elegans leads to increased lifespan. There have been mixed results in human studies (Gonzalez-Freire et al., 2020). Currently, there are new compounds being tested and older drugs being repurposed for potential utilization to slow aging processes and extend health in older persons, but more studies are needed.

DIET, ALZHEIMER'S DISEASE AND AGING

Since aging is the major risk factor for neurodegenerative disease, one therapeutic tactic could be to investigate agents that slow or delay aging processes and evaluate the impact on progression of AD and related dementias (**Figure 1**). Little research has looked at the potential role of diet on AD progression. There is evidence for certain dietary practices, such as Mediterranean diet (MD) and vitamin supplementation, offering protection against neurodegenerative disease development, but the effects of dietary intervention on the management of AD is relatively unknown (Mendiola-Precoma et al., 2016; McGrattan et al., 2019). A few small clinical studies have showed a relationship between ketogenic diet and improved cognition in AD patients (Rusek et al., 2019). These findings seem to be supported by studies showing AD patients consistently exhibit reductions in cerebral glucose utilization without alteration in brain ketone metabolism (Castellano et al., 2015; Taylor et al., 2019).

More specifically, diet has been proposed to directly affect many of the underlying features of AD progression–including amyloidogenesis, oxidative stress, and inflammation (Wu et al., 2004; Gómez-Pinilla, 2008; Murphy et al., 2014). Specific components of diet have been heavily studied for their potential role in the development and/or management of AD. For example, elevated levels of cholesterol cause increased amyloid beta production through the increased activity of APP cleaving enzymes γ-secretase and BACE1 as well as facilitating a conformational change from a helical-rich Aβ structure to an aggregation prone β-pleated sheet (Kakio et al., 2001; Thirumangalakudi et al., 2008; Xiong et al., 2008). Therapeutic lowering of cholesterol via statin therapies has also shown an association with decreased amyloid beta accumulation and AD development (Shepardson et al., 2011; Lin et al., 2015). However, a gradual decline in serum cholesterol is typically seen with dementias which shows the complexity of AD pathogenesis (Mielke et al., 2010; Presečki et al., 2011). Studies on fatty acids have yielded contradicting results, but generally saturated fats, trans-fats, and ω-6 fatty acids offer no benefit or may be detrimental in the context of AD while ω-3 fatty acids have demonstrated some potential benefits (Liyanage et al., 2019).

The association between a diet rich in carbohydrates and AD progression is strong and there is speculation as to whether altered glucose metabolism may be causative in AD. Consistently high levels of dietary sugars is linked with insulin resistance, which has been proposed as a contributive factor for AD development (Liyanage et al., 2019). Interestingly, brains of AD patients have shown decreased levels of the glucose transporters GLUT1 and GLUT3, which allow glucose to cross the blood brain barrier and provide energy to the CNS (Szablewski, 2017). Decreased glucose delivery to the brain leads to glucose starvation and stimulates AD neuropathologies, vascular degeneration, and impaired cognition (Iadecola, 2015; Winkler et al., 2015). Additionally, proper insulin signaling, which is disturbed in the AD brain, has also been suggested for appropriate regulation of amyloid beta and tau proteins (Hong and Lee, 1997; Qiu et al., 1998; Vekrellis et al., 2000; Planel et al., 2007; El Khoury et al., 2014). Insulin resistance also triggers inflammation, which may worsen AD pathology (Creegan et al., 2015).

In general, alterations to dietary protein intake modifies lifespan. Mice fed one-of-many diets varying in the ratio of macronutrients and total energy content (as seen in the Geometric Framework) found that those on low protein/high carbohydrate (LPHC) diets had the greatest improvements in longevity and metabolic health compared to all other diets (Solon-Biet et al., 2014; Le Couteur et al., 2016). In humans, a national representative study of nutrition involving a United States population (6,381 individuals aged 50 years and over) found that individuals who got more of their dietary calories from protein had significantly increased risk of all-cause cancer and cancer-related mortality. Interestingly, this relationship only applied to those under 66 years of age, as those older showed reduction in all-cause mortality when getting more of their calories from protein. The protective effect of increased dietary protein found in the older group may be explained by preventing sarcopenia and frailty development, which are more commonly observed with increased age (Levine et al., 2014). The source of protein may also be important, as a large cohort study reported an association between higher animal protein consumption and increased risk of all-cause mortality, when compared to plant-based protein intake (Song et al., 2016). Whether protein intake impacts AD directly is an area that is underexplored.

Adherence to a Mediterranean diet (MD) has been linked with improved health outcomes. Recent research is finding that MD may also offer cognitive and/or neurological benefits (Baumgart et al., 2015). MD consists of a high intake in fruits, vegetables, fish, nuts, monounsaturated fats, whole grains, and legumes while limiting intake of red meat, saturated fats, dairy, and refined grains. Results of many clinical trials have been suggestive, but not definite, for MD having a protective effect on dementias and improved cognitive performance with aging (Gardener and Caunca, 2018). The mechanism through which MD may be neuroprotective is not fully understood. MD has been shown to decrease rates of stroke and other vascular diseases (such as obesity, hypertension, and diabetes). Vascular events are associated with the development of dementia and may mediate a connection between MD and neuroprotection. Further, the antioxidants and anti-inflammatory agents found in MD have been hypothesized to play a protective role. Mouse models given extra virgin olive oil (which is high in monounsaturated fats) had improved cognitive performance and reduced beta-amyloid

and tau proteins (Qosa et al., 2015). Additionally, neuronal cells treated with oleocanthal (a polyphenol found in extra virgin olive oil) led to reduced amyloid-beta oligomer-mediated astrocyte inflammation and synaptic proteins (Batarseh et al., 2017).

DIETARY RESTRICTION AND NUTRIENT SIGNALING

A common pathway involved in many interventions aimed at slowing aging processes is the somatotropic axis. Genetic alterations to this axis have dramatic effects on an organism's health and life span that is well-conserved evolutionarily. For example, low levels of growth hormone (GH) signaling, found in both Ames dwarf and growth hormone receptor (GHR) knockout mice, can extend the life of mice by over 50% (Brown-Borg, 2016). In humans with GHR deficiency and subsequent decreased GH signaling as observed in Laron syndrome (LS), protection from diabetes and fatal neoplasms occurs (Guevara-Aguirre et al., 2011). Additionally, studies of centenarians have found that low plasma levels of insulin-like growth factor-1 (IGF-1) predict survival in these long-lived people (Milman et al., 2014). Currently there are several classes of compounds approved for use in patients with acromegaly which inhibit the GH/IGF-1 axis (Trainer et al., 2000; Giustina et al., 2014). While these therapeutics have not been studied for their effects on aging and health span in humans, their safety and the known effects of decreased GH/IGF-1 levels on the health span of mice shows a promising area of future research (Longo et al., 2015).

Many dietary interventions have been found to lower signaling through the GH/IGF axis and thus positively impact health and lifespan. Reduced mTOR signaling is also frequently observed in models of extended lifespan from dietary manipulation (Papadopoli et al., 2019). It has long been known that diet impacts health in humans, but more recent work has now found new connections between diet and aging. The three most common dietary interventions include caloric restriction (CR), fasting, and methionine restriction. Each have been shown to increase lifespan in mice and will be discussed in further depth.

Protocols for caloric restriction (CR; aka dietary restriction) in rodents generally call for reduced total caloric intake by 20–50% compared to ad libitum food administration (Vaughan et al., 2018). The following of these guidelines generally produces a significant increase in lifespan in mice. However, further studies have observed that mice of differing genetic backgrounds are affected by CR differently. 42 different recombinant inbred strains of mice subjected to CR led to extended lifespan in nine strains, significantly reduced lifespan in four strains, and no significant change to 29 strains (Liao et al., 2010; Rikke et al., 2010). These results show a need for continued study of the pathways relating diet to health and aging. Current understanding seems to indicate that CR's beneficial effects on aging work through the key nutrient and stress-responsive metabolic signaling pathways including IIS/FOXO, mTOR, AMPK, sirtuins, NRF2, and autophagy (Hwangbo et al., 2020). Application of CR to human studies has begun. To an extent, chronic CR has shown to be beneficial to human health such that moderate CR without malnutrition causes a protective effect against obesity, type II diabetes, inflammation, hypertension and cardiovascular disease, all of which are major causes of morbidity, disability and mortality (Fontana et al., 2004). However, there remains valid concerns against CR since the duration and severity required for optimal health and anti-aging benefits is not feasible for most people over long periods of time and could lead to undesirable side effects (Longo et al., 2015).

Dietary fasting has also been studied for its impact on health and aging. There are many forms of fasting but common types include intermittent fasting (IF), which involves cycling between ad libitum feeding and periods of fasting, and time restricted fasting (TRF), in which food intake is limited to 6–12 h each day without a change in the total calorie intake of the normal diet (Hwangbo et al., 2020). Model studies has shown IF to lead to improved health with some reports of improved lifespan as well (Goodrick et al., 1990; Honjoh et al., 2009; Catterson et al., 2018; de Cabo and Mattson, 2019). TRF has also shown the potential to improve health and extend lifespan (Hwangbo et al., 2020). Compared to CR, the mechanisms relating fasting to aging are not as well-understood and results from rodent studies signify that IF and TRF effects on aging act through differing pathways. There have been proposed models, however, linking CR and IF through common key metabolic pathways (such as mTOR, IIS, and sirtuin) (Pan and Finkel, 2017). One relatively well-understood mechanism is that in the yeast Saccharomyces cerevisiae, in which fasting causes the activation of the stress resistance transcription factors Msn2/4 and Gis1 that regulate many protective and metabolic genes (Wei et al., 2008). In general, though, fasting is believed to be a time in which the organism activates alternative metabolic pathways which are important for repair and health maintenance (fasting physiology) (Longo and Panda, 2016). IF and TRF allow the organism to spend more time in this metabolic state which could contribute to greater health and lifespan. Human studies have found IF and TRF to be safe and to have the ability to improve metabolic health and physiological function, especially in obese individuals (Hwangbo et al., 2020; Martens et al., 2020). Yet, there are still dangers accompanying fasting implementation in certain populations of patients, especially those low in BMI, frail and old, and patients with diabetes receiving insulin or insulin-like drugs.

Although restrictions in total protein is associated with increased health and lifespan, studies have found that restrictions in specific amino acids (such as methionine or branched chain amino acids) cause similar effects. The benefits observed with methionine restriction in mice are also like those seen with CR (Brown-Borg, 2016). The longevity benefit of methionine restriction relies on GH signaling, as in the absence of GH signaling no lifespan extension is observed (Brown-Borg et al., 2014). Dietary amino acid levels are sensed by at least two evolutionarily conserved mechanisms—mTOR and GCN2 (general control non-derepressible two). The GCN2 pathway becomes activated by the absence of many amino acids while mTOR is activated by specific dietary amino acids (Li W. et al., 2014). mTORC1, a serine/threonine kinase subunit of mTOR, has been heavily studied and is an important regulator of cell growth

and metabolism based on nutrient and growth factor levels (Kim and Guan, 2019). Pharmacologic inhibition of mTORC1 extends lifespan in mice and reduced levels of methionine leads to similar decreased activity in mTORC1 (Harrison et al., 2009). The conversion of methionine to S-adenosylmethionine (SAM), and the downstream SAM pathway, has been identified as the link between methionine and mTORC1 signaling. In short, less dietary intake in methionine leads to decreased mTORC1 signaling and increased health and lifespan (Kitada et al., 2019). Importantly, mice on LPHC diets in the Geometric Framework study showed low circulating branched chain amino acids which correlated with decreased activation of hepatic mTOR (Solon-Biet et al., 2014). This highlights mTOR as an important pathway in regulating health and lifespan.

Neurovascular coupling (NVC) disruptions and cerebral microvasculature changes are also being studied as potential targets for pharmacological therapies of the cognitive decline typically seen with aging, but dietary intervention offers another avenue of research into this topic. Increases in ROS production (especially mitochondrial-derived) as well as decreased production of oxidative stress protecting molecules, such as antioxidants and anti-inflammatories, are associated with vascular aging and disease (Ungvari et al., 2011, 2018, 2019; Springo et al., 2015). Contrarily, elevated levels of certain antioxidant enzymes, such as mitochondrial catalase, are associated with protection of cerebral microvasculature and the NVC mechanism in aging mice (Csiszar et al., 2019). As previously discussed, integration of dietary changes like caloric restriction and fasting increase an organism's stress response pathways which are known for their anti-inflammatory and health maintenance qualities. This raises an interesting question as to what role diet could have on maintenance and/or improvement of NVC and cerebral microvasculature in older adults and AD patients.

CONCLUSION

Aging is a major risk factor for the development of neurodegenerative diseases such as Alzheimer's Disease (AD). Current therapeutic approaches toward the treatment of AD have proved to be ineffective and emphasize the need for alternative options. Certain medications (such as Rapamycin and Metformin) are intriguing because of their known safety in humans as well as their ability to improve health and lifespan in model organisms, but dietary interventions may be the most feasible and yet understudied option. Diet has long been known to impact human health and following certain diets (such as Mediterranean) is associated with decreased incidence of neurodegenerative diseases as well as increased health and lifespan. Early findings from a few small studies show that dietary changes (such as ketogenic diet) may be useful in the management of AD. However, much more work is needed to examine the plausibility of dietary interventions for the management of certain neurodegenerative diseases.

AUTHOR CONTRIBUTIONS

MT and HB-B wrote and edited the manuscript. Both authors contributed to the article and approved the submitted version.

FUNDING

Support provided by the University of North Dakota REMS program.

REFERENCES

Alexander, G. E., Ryan, L., Bowers, D., Foster, T. C., Bizon, J. L., Geldmacher, D. S., et al. (2012). Characterizing cognitive aging in humans with links to animal models. *Front. Aging Neurosci*. 4:21. doi: 10.3389/fnagi.2012.00021

Alfaras, I., Mitchell, S. J., Mora, H., Lugo, D. R., Warren, A., Navas-Enamorado, I., et al. (2017). Health benefits of late-onset metformin treatment every other week in mice. *NPJ Aging Mech. Dis*. 3:16. doi: 10.1038/s41514-017-0018-7

Alzheimer's Association (2020b). *Stages of Alzheimer's*. Chicago, IL: Alzheimer's Dementia.

Alzheimer's Association (2020a). *Alzheimer's Disease Facts and Figures*. Chicago, IL: Alzheimers Dementia.

Anisimov, V. N., Popovich, I. G., Zabezhinski, M. A., Egormin, P. A., Yurova, M. N., Semenchenko, A. V., et al. (2015). Sex differences in aging, life span and spontaneous tumorigenesis in 129/Sv mice neonatally exposed to metformin. *Cell Cycle* 14, 46–55. doi: 10.4161/15384101.2014.973308

Arnett, P. A., Rao, S. M., Bernardin, L., Grafman, J., Yetkin, F. Z., and Lobeck, L. (1994). Relationship between frontal lobe lesions and Wisconsin Card sorting test performance in patients with multiple sclerosis. *Neurology* 44(3 Part 1), 420–425. doi: 10.1212/WNL.44.3_Part_1.420

Barzilai, N., Crandall, J. P., Kritchevsky, S. B., and Espeland, M. A. (2016). Metformin as a tool to target aging. *Cell Metab*. 23, 1060–1065. doi: 10.1016/j.cmet.2016.05.011

Batarseh, Y. S., Mohamed, L. A., Al Rihani, S. B., Mousa, Y. M., Siddique, A. B., El Sayed, K. A., et al. (2017). Oleocanthal ameliorates amyloid-β oligomers' toxicity on astrocytes and neuronal cells: *in vitro* studies. *Neuroscience* 352, 204–215. doi: 10.1016/j.neuroscience.2017.03.059

Baumgart, M., Snyder, H. M., Carrillo, M. C., Fazio, S., Kim, H., and Johns, H. (2015). Summary of the evidence on modifiable risk factors for cognitive decline and dementia: a population-based perspective. *Alzheimer's Dement*. 11, 718–726. doi: 10.1016/j.jalz.2015.05.016

Bekris, L. M., Yu, C. E., Bird, T. D., and Tsuang, D. W. (2010). Genetics of Alzheimer disease. *J. Geriatr. Psychiatry Neurol*. 23, 213–227. doi: 10.1177/0891988710383571

Bennett, D. A., Schneider, J. A., Bienias, J. L., Evans, D. A., and Wilson, R. S. (2005). Mild cognitive impairment is related to Alzheimer disease pathology and cerebral infarctions. *Neurology* 64, 834–841. doi: 10.1212/01.WNL.0000152982.47274.9E

Bloom, G. S. (2014). Amyloid-β and tau: the trigger and bullet in Alzheimer disease pathogenesis. *JAMA Neurol*. 71, 505–508. doi: 10.1001/jamaneurol.2013.5847

Bradley-Whitman, M. A., and Lovell, M. A. (2013). Epigenetic changes in the progression of Alzheimer's disease. *Mech. Ageing Dev*. 134, 486–495. doi: 10.1016/j.mad.2013.08.005

Brewer, R. A., Gibbs, V. K., and Smith, D. L. Jr. (2016). Targeting glucose metabolism for healthy aging. *Nutr. Health. Aging* 4, 31–46. doi: 10.3233/NHA-160007

Brown-Borg, H. M. (2016). Reduced growth hormone signaling and methionine restriction: interventions that improve metabolic health and extend life span. *Ann. N. Y. Acad. Sci*. 1363, 40–49. doi: 10.1111/nyas.12971

Brown-Borg, H. M., Rakoczy, S. G., Wonderlich, J. A., Rojanathammanee, L., Kopchick, J. J., Armstrong, V., et al. (2014). Growth hormone signaling

is necessary for lifespan extension by dietary methionine. *Aging Cell* 13, 1019–1027. doi: 10.1111/acel.12269

Camandola, S., and Mattson, M. P. (2017). Brain metabolism in health, aging, and neurodegeneration. *EMBO J*. 36, 1474–1492. doi: 10.15252/embj.201695810

Camardo, J. (2003). "The Rapamune era of immunosuppression 2003: the journey from the laboratory to clinical transplantation," in *Transplantation Proceedings* (London, UK: Elsevier), 35. S18–S24.

Caspary, W. F., and Graf, S. (1979). Inhibition of human intestinalα-glucosidehydrolases by a new complex oligosaccharide. *Res. Exp. Med*. 175, 1–6. doi: 10.1007/BF01851228

Castellano, C. A., Nugent, S., Paquet, N., Tremblay, S., Bocti, C., Lacombe, G., et al. (2015). Lower brain 18F-fluorodeoxyglucose uptake but normal 11C-acetoacetate metabolism in mild Alzheimer's disease dementia. *J. Alzheimer's Dis*. 43, 1343–1353. doi: 10.3233/JAD-141074

Catterson, J. H., Khericha, M., Dyson, M. C., Vincent, A. J., Callard, R., Haveron, S. M., et al. (2018). Short-term, intermittent fasting induces long-lasting gut health and TOR-independent lifespan extension. *Curr. Biol*. 28, 1714–1724. doi: 10.1016/j.cub.2018.04.015

Creegan, R., Hunt, W., McManus, A., and Rainey-Smith, S. R. (2015). Diet, nutrients and metabolism: cogs in the wheel driving Alzheimer's disease pathology?. *Br. J. Nutr*. 113, 1499–1517. doi: 10.1017/S0007114515000926

Csipo, T., Mukli, P., Lipecz, A., Tarantini, S., Bahadli, D., Abdulhussein, O., et al. (2019). Assessment of age-related decline of neurovascular coupling responses by functional near-infrared spectroscopy (fNIRS) in humans. *Geroscience* 41, 495–509. doi: 10.1007/s11357-019-00122-x

Csiszar, A., Yabluchanskiy, A., Ungvari, A., Ungvari, Z., and Tarantini, S. (2019). Overexpression of catalase targeted to mitochondria improves neurovascular coupling responses in aged mice. *Geroscience* 41, 609–617. doi: 10.1007/s11357-019-00111-0

de Cabo, R., and Mattson, M. P. (2019). Effects of intermittent fasting on health, aging, and disease. *N. Engl. J. Med.* 381, 2541–2551. doi: 10.1056/NEJMra1905136

Denver, P., and McClean, P. L. (2018). Distinguishing normal brain aging from the development of Alzheimer's disease: inflammation, insulin signaling and cognition. *Neural Regen. Res*. 13, 1719–1730. doi: 10.4103/1673-5374.238608

Doody, R. S., Thomas, R. G., Farlow, M., Iwatsubo, T., Vellas, B., Joffe, S., et al. (2014). Phase 3 trials of solanezumab for mild-to-moderate Alzheimer's disease. *N. Engl. J. Med*. 370, 311–321. doi: 10.1056/NEJMoa1312889

Drayer, B. P. (1988). Imaging of the aging brain. part I. normal findings. *Radiology* 166, 785–796. doi: 10.1148/radiology.166.3.3277247

Drewe, E. A. (1974). The effect of type and area of brain lesion on Wisconsin Card sorting test performance. *Cortex* 10, 159–170. doi: 10.1016/S0010-9452(74)80006-7

Dugger, B. N., and Dickson, D. W. (2017). Pathology of neurodegenerative diseases. *Cold Spring Harb. Perspect. Biol*. 9:a028035. doi: 10.1101/cshperspect.a028035

Dumitriu, D., Hao, J., Hara, Y., Kaufmann, J., Janssen, W. G., Lou, W., et al. (2010). Selective changes in thin spine density and morphology in monkey prefrontal cortex correlate with aging-related cognitive impairment. *J. Neurosci*. 30, 7507–7515. doi: 10.1523/JNEUROSCI.6410-09.2010

Dykiert, D., Der G, Starr, J. M., and Deary, I. J. (2012). Age differences in intra-individual variability in simple and choice reaction time: systematic review and meta-analysis. *PLoS ONE* 7:e45759. doi: 10.1371/journal.pone.0045759

El Khoury, N., Gratuze, M., Papon, M. A., Bretteville, A., and Planel, E. (2014). Insulin dysfunction and Tau pathology. *Front. Cell. Neurosci*. 8:22. doi: 10.3389/fncel.2014.00022

Esch, F. S., Keim, P. S., Beattie, E. C., Blacher, R. W., Culwell, A. R., Oltersdorf, T., et al. (1990). Cleavage of amyloid beta peptide during constitutive processing of its precursor. *Science* 248, 1122–1124. doi: 10.1126/science.2111583

Fabiani, M., Gordon, B. A., Maclin, E. L., Pearson, M. A., Brumback-Peltz, C. R., Low, K. A., et al. (2014). Neurovascular coupling in normal aging: a combined optical, ERP and fMRI study. *Neuroimage* 85, 592–607. doi: 10.1016/j.neuroimage.2013.04.113

Fang, E. F., Hou, Y., Palikaras, K., Adriaanse, B. A., Kerr, J. S., Yang, B., et al. (2019). Mitophagy inhibits amyloid-β and tau pathology and reverses cognitive deficits in models of Alzheimer's disease. *Nat. Neurosci*. 22, 401–412. doi: 10.1038/s41593-018-0332-9

Fontana, L., Meyer, T. E., Klein, S., and Holloszy, J. O. (2004). Long-term calorie restriction is highly effective in reducing the risk for atherosclerosis in humans. *Proc. Natl. Acad. Sci. U.S.A.* 101, 6659–6663. doi: 10.1073/pnas.0308291101

Fulop, G. A., Ahire, C., Csipo, T., Tarantini, S., Kiss, T., Balasubramanian, P., et al. (2019). Cerebral venous congestion promotes blood-brain barrier disruption and neuroinflammation, impairing cognitive function in mice. *Geroscience* 41, 575–589. doi: 10.1007/s11357-019-00110-1

Gardener, H., and Caunca, M. R. (2018). Mediterranean diet in preventing neurodegenerative diseases. *Curr. Nutr. Rep*. 7, 10–20. doi: 10.1007/s13668-018-0222-5

Giustina, A., Chanson, P., Kleinberg, D., Bronstein, M. D., Clemmons, D. R., Klibanski, A., et al. (2014). Expert consensus document: a consensus on the medical treatment of acromegaly. *Nat. Rev. Endocrinol*. 10, 243–248. doi: 10.1038/nrendo.2014.21

Gómez-Pinilla, F. (2008). Brain foods: the effects of nutrients on brain function. *Nat. Rev. Neurosci*. 9, 568–578. doi: 10.1038/nrn2421

Gonzalez-Freire, M., Diaz-Ruiz, A., Hauser, D., Martinez-Romero, J., Ferrucci, L., Bernier, M., et al. (2020). The road ahead for health and lifespan interventions. *Ageing Res. Rev*. 25:101037. doi: 10.1016/j.arr.2020.101037

Goodrick, C. L., Ingram, D. K., Reynolds, M. A., Freeman, J. R., and Cider, N. (1990). Effects of intermittent feeding upon body weight and lifespan in inbred mice: interaction of genotype and age. *Mech. Ageing Dev*. 55, 69–87. doi: 10.1016/0047-6374(90)90107-Q

Grossberg, G. T., Manes, F., Allegri, R. F., Gutiérrez-Robledo, L. M., Gloger, S., Xie, L., et al. (2013). The safety, tolerability, and efficacy of once-daily memantine (28 mg): a multinational, randomized, double-blind, placebo-controlled trial in patients with moderate-to-severe Alzheimer's disease taking cholinesterase inhibitors. *CNS Drugs* 27, 469–478. doi: 10.1007/s40263-013-0077-7

Guevara-Aguirre, J., Balasubramanian, P., Guevara-Aguirre, M., Wei, M., Madia, F., Cheng, C. W., et al. (2011). Growth hormone receptor deficiency is associated with a major reduction in pro-aging signaling, cancer, and diabetes in humans. *Sci. Transl. Med*. 3:70ra13. doi: 10.1126/scitranslmed.3001845

Haass, C., Hung, A. Y., Schlossmacher, M. G., Oltersdorf, T., Teplow, D. B., and Selkoe, D. J. (1993). Normal cellular processing of the β-amyloid precursor protein results in the secretion of the amyloid β peptide and related molecules a. *Ann. N. Y. Acad. Sci*. 695, 109–116. doi: 10.1111/j.1749-6632.1993.tb23037.x

Haass, C., and Selkoe, D. J. (1993). Cellular processing of β-amyloid precursor protein and the genesis of amyloid β-peptide. *Cell* 75, 1039–1042. doi: 10.1016/0092-8674(93)90312-E

Harrison, D. E., Strong, R., Allison, D. B., Ames, B. N., Astle, C. M., Atamna, H., et al. (2014). Acarbose, 17-α-estradiol, and nordihydroguaiaretic acid extend mouse lifespan preferentially in males. *Aging Cell* 13, 273–282. doi: 10.1111/acel.12170

Harrison, D. E., Strong, R., Sharp, Z. D., Nelson, J. F., Astle, C. M., Flurkey, K., et al. (2009). Rapamycin fed late in life extends lifespan in genetically heterogeneous mice. *Nature* 460, 392–395. doi: 10.1038/nature08221

He, N., Jin, W. L., Lok, K. H., Wang, Y., Yin, M., and Wang, Z. J. (2013). Amyloid-β 1–42 oligomer accelerates senescence in adult hippocampal neural stem/progenitor cells via formylpeptide receptor 2. *Cell Death Dis*. 4:e924. doi: 10.1038/cddis.2013.437

Hong, M., and Lee, V. M. (1997). Insulin and insulin-like growth factor-1 regulate tau phosphorylation in cultured human neurons. *J. Biol. Chem*. 272, 19547–19553. doi: 10.1074/jbc.272.31.19547

Honig, L. S., Vellas, B., Woodward, M., Boada, M., Bullock, R., Borrie, M., et al. (2018). Trial of solanezumab for mild dementia due to Alzheimer's disease. *N. Engl. J. Med*. 378, 321–330. doi: 10.1056/NEJMoa1705971

Honjoh, S., Yamamoto, T., Uno, M., and Nishida, E. (2009). Signalling through RHEB-1 mediates intermittent fasting-induced longevity in *C. elegans*. *Nature* 457, 726–730. doi: 10.1038/nature07583

Hou, Y., Dan, X., Babbar, M., Wei, Y., Hasselbalch, S. G., Croteau, D. L., et al. (2019). Ageing as a risk factor for neurodegenerative disease. *Nat. Rev. Neurol*. 15, 565–581. doi: 10.1038/s41582-019-0244-7

Howard, R., McShane, R., Lindesay, J., Ritchie, C., Baldwin, A., Barber, R., et al. (2012). Donepezil and memantine for moderate-to-severe Alzheimer's disease. *N. Engl. J. Med*. 366, 893–903. doi: 10.1056/NEJMoa1106668

Hwangbo, D. S., Lee, H. Y., Abozaid, L. S., and Min, K. J. (2020). Mechanisms of lifespan regulation by calorie restriction and intermittent fasting in model organisms. *Nutrients* 12:1194. doi: 10.3390/nu12041194

Iadecola, C. (2015). Sugar and Alzheimer's disease: a bittersweet truth. *Nat. Neurosci*. 18, 477–478. doi: 10.1038/nn.3986

Jack, C. R., Petersen, R. C., Xu, Y. C., Waring, S. C., O'Brien, P. C., Tangalos, E. G., et al. (1997). Medial temporal atrophy on MRI in normal aging and very mild Alzheimer's disease. *Neurology* 49, 786–794. doi: 10.1212/WNL.49.3.786

Jarrett, J. T., Berger, E. P., and Lansbury, P. T. Jr. (1993). The carboxy terminus of the. beta. amyloid protein is critical for the seeding of amyloid formation: implications for the pathogenesis of Alzheimer's disease. *Biochemistry* 32, 4693–4697. doi: 10.1021/bi00069a001

Kakio, A., Nishimoto, S. I., Yanagisawa, K., Kozutsumi, Y., and Matsuzaki, K. (2001). Cholesterol-dependent formation of GM1 ganglioside-bound amyloid β-protein, an endogenous seed for Alzheimer amyloid. *J. Biol. Chem*. 276, 24985–24990. doi: 10.1074/jbc.M100252200

Kim, J., and Guan, K. L. (2019). mTOR as a central hub of nutrient signalling and cell growth. *Nat. Cell Biol*. 21, 63–71. doi: 10.1038/s41556-018-0205-1

Kirkwood, T. B., Feder, M., Finch, C. E., Franceschi, C., Globerson, A., Klingenberg, C. P., et al. (2005). What accounts for the wide variation in life span of genetically identical organisms reared in a constant environment? *Mech. Ageing Dev*. 126, 439–443. doi: 10.1016/j.mad.2004.09.008

Kitada, M., Ogura, Y., Monno, I., and Koya, D. (2019). The impact of dietary protein intake on longevity and metabolic health. *EBioMedicine* 43, 632–640. doi: 10.1016/j.ebiom.2019.04.005

Koseoglu, E. (2019). New treatment modalities in Alzheimer's disease. *World J. Clin. Cases* 7, 1764–1774. doi: 10.12998/wjcc.v7.i14.1764

Laplante, M., and Sabatini, D. M. (2012). mTOR signaling in growth control and disease. *Cell* 149, 274–293. doi: 10.1016/j.cell.2012.03.017

Le Couteur, D. G., Solon-Biet, S., Cogger, V. C., Mitchell, S. J., Senior, A., de Cabo, R., et al. (2016). The impact of low-protein high-carbohydrate diets on aging and lifespan. *Cell. Mol. Life Sci*. 73, 1237–1252. doi: 10.1007/s00018-015-2120-y

Levin, O., Fujiyama, H., Boisgontier, M. P., Swinnen, S. P., and Summers, J. J. (2014). Aging and motor inhibition: a converging perspective provided by brain stimulation and imaging approaches. *Neurosci. Biobehav. Rev*. 43, 100–117. doi: 10.1016/j.neubiorev.2014.04.001

Levine, M. E., Suarez, J. A., Brandhorst, S., Balasubramanian, P., Cheng, C. W., Madia, F., et al. (2014). Low protein intake is associated with a major reduction in IGF-1, cancer, and overall mortality in the 65 and younger but not older population. *Cell Metab*. 19, 407–417. doi: 10.1016/j.cmet.2014.02.006

Li, J., Kim, S. G., and Blenis, J. (2014). Rapamycin: one drug, many effects. *Cell Metab*. 19, 373–379. doi: 10.1016/j.cmet.2014.01.001

Li, W., Li, X., and Miller, R. A. (2014). ATF 4 activity: a common feature shared by many kinds of slow-aging mice. *Aging Cell* 13, 1012–1018. doi: 10.1111/acel.12264

Liao, C. Y., Rikke, B. A., Johnson, T. E., Diaz, V., and Nelson, J. F. (2010). Genetic variation in the murine lifespan response to dietary restriction: from life extension to life shortening. *Aging Cell* 9, 92–95. doi: 10.1111/j.1474-9726.2009.00533.x

Lin, F. C., Chuang, Y. S., Hsieh, H. M., Lee, T. C., Chiu, K. F., Liu, C. K., et al. (2015). Early statin use and the progression of Alzheimer disease: a total population-based case-control study. *Medicine* 94:e2143. doi: 10.1097/MD.0000000000002143

Lipecz, A., Csipo, T., Tarantini, S., Hand, R. A., Ngo, B. N., Conley, S., et al. (2019). Age-related impairment of neurovascular coupling responses: a dynamic vessel analysis (DVA)-based approach to measure decreased flicker light stimulus-induced retinal arteriolar dilation in healthy older adults. *Geroscience* 41, 341–349. doi: 10.1007/s11357-019-00078-y

Liu, C. C., Kanekiyo, T., Xu, H., and Bu, G. (2013). Apolipoprotein E and Alzheimer disease: risk, mechanisms and therapy. *Nat. Rev. Neurol*. 9, 106–118. doi: 10.1038/nrneurol.2012.263

Liyanage, S. I., Vilekar, P., and Weaver, D. F. (2019). Nutrients in Alzheimer's disease: the interaction of diet, drugs and disease. *Canad. J. Neurol. Sci*. 46, 23–34. doi: 10.1017/cjn.2018.353

Long, J. M., and Holtzman, D. M. (2019). Alzheimer disease: an update on pathobiology and treatment strategies. *Cell* 179, 312–339. doi: 10.1016/j.cell.2019.09.001

Longo, V. D., Antebi, A., Bartke, A., Barzilai, N., Brown-Borg, H. M., Caruso, C., et al. (2015). Interventions to slow aging in humans: are we ready? *Aging Cell* 14, 497–510. doi: 10.1111/acel.12338

Longo, V. D., and Panda, S. (2016). Fasting, circadian rhythms, and time-restricted feeding in healthy lifespan. *Cell Metab*. 23, 1048–1059. doi: 10.1016/j.cmet.2016.06.001

López-Otín, C., Blasco, M. A., Partridge, L., Serrano, M., and Kroemer, G. (2013). The hallmarks of aging. *Cell* 153, 1194–1217. doi: 10.1016/j.cell.2013.05.039

Lovell, M. A., Gabbita, S. P., and Markesbery, W. R. (1999). Increased DNA oxidation and decreased levels of repair products in Alzheimer's disease ventricular CSF. *J. Neurochem*. 72, 771–776. doi: 10.1046/j.1471-4159.1999.0720771.x

Manocha, G. D., Floden, A. M., Rausch, K., Kulas, J. A., McGregor, B. A., Rojanathammanee, L., et al. (2016). APP regulates microglial phenotype in a mouse model of Alzheimer's disease. *J. Neurosci*. 36, 8471–8486. doi: 10.1523/JNEUROSCI.4654-15.2016

Markesbery, W. R., Schmitt, F. A., Kryscio, R. J., Davis, D. G., Smith, C. D., and Wekstein, D. R. (2006). Neuropathologic substrate of mild cognitive impairment. *Arch. Neurol*. 63, 38–46. doi: 10.1001/archneur.63.1.38

Martens, C. R., Rossman, M. J., Mazzo, M. R., Jankowski, L. R., Nagy, E. E., Denman, B. A., et al. (2020). Short-term time-restricted feeding is safe and feasible in non-obese healthy midlife and older adults. *GeroScience* 23, 667–686. doi: 10.1007/s11357-020-00156-6

Martin-Montalvo, A., Mercken, E. M., Mitchell, S. J., Palacios, H. H., Mote, P. L., Scheibye-Knudsen, M., et al. (2013). Metformin improves healthspan and lifespan in mice. *Nat. Commun*. 4:2192. doi: 10.1038/ncomms3192

McGrattan, A. M., McGuinness, B., McKinley, M. C., Kee, F., Passmore, P., Woodside, J. V., et al. (2019). Diet and inflammation in cognitive ageing and Alzheimer's disease. *Curr. Nutr. Rep*. 8, 53–65. doi: 10.1007/s13668-019-0271-4

Mendelsohn, A. R., and Larrick, J. W. (2012). Fibroblast growth factor-21 is a promising dietary restriction mimetic. *Rejuvenation Res*. 15, 624–628. doi: 10.1089/rej.2012.1392

Mendiola-Precoma, J., Berumen, L. C., Padilla, K., and Garcia-Alcocer, G. (2016). Therapies for prevention and treatment of Alzheimer's disease. *Biomed Res. Int*. 2016:2589276. doi: 10.1155/2016/2589276

Mielke, M. M., Zandi, P. P., Shao, H., Waern, M. M., Östling, S., Guo XM, Björkelund, C., et al. (2010). The 32-year relationship between cholesterol and dementia from midlife to late life. *Neurology* 75, 1888–1895. doi: 10.1212/WNL.0b013e3181feb2bf

Milman, S., Atzmon, G., Huffman, D. M., Wan, J., Crandall, J. P., Cohen, P., et al. (2014). Low insulin-like growth factor-1 level predicts survival in humans with exceptional longevity. *Aging Cell* 13, 769–771. doi: 10.1111/acel.12213

Morris, J. C., Storandt, M., Miller, J. P., McKeel, D. W., Price, J. L., Rubin, E. H., et al. (2001). Mild cognitive impairment represents early-stage Alzheimer disease. *Arch. Neurol*. 58, 397–405. doi: 10.1001/archneur.58.3.397

Mufson, E. J., Chen, E. Y., Cochran, E. J., Beckett, L. A., Bennett, D. A., and Kordower, J. H. (1999). Entorhinal cortex β-amyloid load in individuals with mild cognitive impairment. *Exp. Neurol*. 158, 469–490. doi: 10.1006/exnr.1999.7086

Murphy, T., Dias, G. P., and Thuret, S. (2014). Effects of diet on brain plasticity in animal and human studies: mind the gap. *Neural Plast*. 2014:563160. doi: 10.1155/2014/563160

Ota, M., Matsuo, J., Ishida, I., Takano, H., Yokoi, Y., Hori, H., et al. (2019). Effects of a medium-chain triglyceride-based ketogenic formula on cognitive function in patients with mild-to-moderate Alzheimer's disease. *Neurosci. Lett*. 690, 232–236. doi: 10.1016/j.neulet.2018.10.048

Pan, H., and Finkel, T. (2017). Key proteins and pathways that regulate lifespan. *J. Biol. Chem*. 292, 6452–6460. doi: 10.1074/jbc.R116.771915

Papadopoli, D., Boulay, K., Kazak, L., Pollak, M., Mallette, F., Topisirovic, I., et al. (2019). mTOR as a central regulator of lifespan and aging. *F1000Res* 8:998. doi: 10.12688/f1000research.17196.1

Papadopoulos, P., Rosa-Neto, P., Rochford, J., and Hamel, E. (2013). Pioglitazone improves reversal learning and exerts mixed cerebrovascular effects in a mouse model of Alzheimer's disease with combined amyloid-β and cerebrovascular pathology. *PLoS ONE* 8:e68612. doi: 10.1371/journal.pone.0068612

Park, J. H., Seo, S. W., Kim, C., Kim, G. H., Noh, H. J., Kim, S. T., et al. (2013). Pathogenesis of cerebral microbleeds: in vivo imaging of amyloid and subcortical ischemic small vessel disease in 226 individuals with cognitive impairment. *Ann. Neurol*. 73, 584–593. doi: 10.1002/ana.23845

Planel, E., Tatebayashi, Y., Miyasaka, T., Liu, L., Wang, L., Herman, M., et al. (2007). Insulin dysfunction induces in vivo tau hyperphosphorylation

through distinct mechanisms. *J. Neurosci.* 27, 13635–13648. doi: 10.1523/JNEUROSCI.3949-07.2007

Presečki, P., Mück-Šeler, D., Mimica, N., Pivac, N., Mustapić M., Stipčević T., et al. (2011). Serum lipid levels in patients with Alzheimer's disease. *Coll. Antropol.* 35, 115–120.

Price, J. L., and Morris, J. C. (1999). Tangles and plaques in nondemented aging and "preclinical" Alzheimer's disease. *Ann. Neurol.* 45, 358–368. doi: 10.1002/1531-8249(199903)45:3<358::AID-ANA12>3.0.CO;2-X

Prins, N. D., and Scheltens, P. (2015). White matter hyperintensities, cognitive impairment and dementia: an update. *Nat. Rev. Neurol.* 11, 157–165. doi: 10.1038/nrneurol.2015.10

Puzzo, D., Gulisano, W., Palmeri, A., and Arancio, O. (2015). Rodent models for Alzheimer's disease drug discovery. *Expert Opin. Drug Discov.* 10, 703–711. doi: 10.1517/17460441.2015.1041913

Qiu, W. Q., Walsh, D. M., Ye, Z., Vekrellis, K., Zhang, J., Podlisny, M. B., et al. (1998). Insulin-degrading enzyme regulates extracellular levels of amyloid β-protein by degradation. *J. Biol. Chem.* 273, 32730–32738. doi: 10.1074/jbc.273.49.32730

Qosa, H., Mohamed, L. A., Batarseh, Y. S., Alqahtani, S., Ibrahim, B., LeVine, I. I. I. H., et al. (2015). Extra-virgin olive oil attenuates amyloid-β and tau pathologies in the brains of TgSwDI mice. *J. Nutr. Biochem.* 26, 1479–1490. doi: 10.1016/j.jnutbio.2015.07.022

Ramirez, J., Berezuk, C., McNeely, A. A., Gao, F., McLaurin, J., and Black, S. E. (2016). Imaging the perivascular space as a potential biomarker of neurovascular and neurodegenerative diseases. *Cell. Mol. Neurobiol.* 36, 289–299. doi: 10.1007/s10571-016-0343-6

Rikke, B. A., Liao, C. Y., McQueen, M. B., Nelson, J. F., and Johnson, T. E. (2010). Genetic dissection of dietary restriction in mice supports the metabolic efficiency model of life extension. *Exp. Gerontol.* 45, 691–701. doi: 10.1016/j.exger.2010.04.008

Robinson, A. L., Heaton, R. K., Lehman, R. A., and Stilson, D. W. (1980). The utility of the Wisconsin card sorting test in detecting and localizing frontal lobe lesions. *J. Consult. Clin. Psychol.* 48, 605–614. doi: 10.1037/0022-006X.48.5.605

Romberg, C., Horner, A. E., Bussey, T. J., and Saksida, L. M. (2013). A touch screen-automated cognitive test battery reveals impaired attention, memory abnormalities, and increased response inhibition in the TgCRND8 mouse model of Alzheimer's disease. *Neurobiol. Aging* 34, 731–744. doi: 10.1016/j.neurobiolaging.2012.08.006

Rose, M. R. (2009). Adaptation, aging, and genomic information. *Aging* 1, 444–450. doi: 10.18632/aging.100053

Rosvold, H. E., Mirsky, A. F., Sarason, I., Bransome Jr, E. D., and Beck, L. H. (1956). A continuous performance test of brain damage. *J. Consult. Psychol.* 20, 343–350. doi: 10.1037/h0043220

Rusek, M., Pluta, R., Ułamek-Kozioł, M., and Czuczwar, S. J. (2019). Ketogenic diet in Alzheimer's disease. *Int. J. Mol. Sci.* 20:3892. doi: 10.3390/ijms20163892

Salloway, S., Sperling, R., Fox, N. C., Blennow, K., Klunk, W., Raskind, M., et al. (2014). Two phase 3 trials of bapineuzumab in mild-to-moderate Alzheimer's disease. *N. Engl. J. Med.* 370, 322–333. doi: 10.1056/NEJMoa1304839

Saxton, R. A., and Sabatini, D. M. (2017). mTOR signaling in growth, metabolism, and disease. *Cell* 168, 960–976. doi: 10.1016/j.cell.2017.02.004

Shepardson, N. E., Shankar, G. M., and Selkoe, D. J. (2011). Cholesterol level and statin use in Alzheimer disease: II. review of human trials and recommendations. *Arch. Neurol.* 68, 1385–1392. doi: 10.1001/archneurol.2011.242

Shim, Y. S., Yang, D. W., Roe, C. M., Coats, M. A., Benzinger, T. L., Xiong, C., et al. (2015). Pathological correlates of white matter hyperintensities on magnetic resonance imaging. *Dement. Geriatr. Cogn. Disord.* 39, 92–104. doi: 10.1159/000366411

Shineman, D. W., Basi, G. S., Bizon, J. L., Colton, C. A., Greenberg, B. D., Hollister, B. A., et al. (2011). Accelerating drug discovery for Alzheimer's disease: best practices for preclinical animal studies. *Alzheimer's Res. Ther.* 3:28. doi: 10.1186/alzrt90

Shoji, M., Golde, T. E., Ghiso, J., Cheung, T. T., Estus, S., Shaffer, L. M., et al. (1992). Production of the Alzheimer amyloid beta protein by normal proteolytic processing. *Science* 258, 126–129. doi: 10.1126/science.1439760

Simunkova, M., Alwasel, S. H., Alhazza, I. M., Jomova, K., Kollar, V., Rusko, M., et al. (2019). Management of oxidative stress and other pathologies in Alzheimer's disease. *Arch. Toxicol.* 93, 2491–2513. doi: 10.1007/s00204-019-02538-y

Solon-Biet, S. M., McMahon, A. C., Ballard, J. W., Ruohonen, K., Wu, L. E., Cogger, V. C., et al. (2014). The ratio of macronutrients, not caloric intake, dictates cardiometabolic health, aging, and longevity in ad libitum-fed mice. *Cell Metab.* 19, 418–430. doi: 10.1016/j.cmet.2014.02.009

Song, M., Fung, T. T., Hu, F. B., Willett, W. C., Longo, V. D., Chan, A. T., et al. (2016). Association of animal and plant protein intake with all-cause and cause-specific mortality. *JAMA Intern. Med.* 176, 1453–1463. doi: 10.1001/jamainternmed.2016.4182

Sperling, R. A., Aisen, P. S., Beckett, L. A., Bennett, D. A., Craft, S., Fagan, A. M., et al. (2011). Toward defining the preclinical stages of Alzheimer's disease: recommendations from the National Institute on Aging-Alzheimer's association workgroups on diagnostic guidelines for Alzheimer's disease. *Alzheimer's Dement.* 7, 280–292. doi: 10.1016/j.jalz.2011.03.003

Sperling, R. A., Karlawish, J., and Johnson, K. A. (2013). Preclinical Alzheimer disease—the challenges ahead. *Nat. Rev. Neurol.* 9, 5458. doi: 10.1038/nrneurol.2012.241

Springo, Z., Tarantini, S., Toth, P., Tucsek, Z., Koller, A., Sonntag, W. E., et al. (2015). Aging exacerbates pressure-induced mitochondrial oxidative stress in mouse cerebral arteries. *J. Gerontol. A Biomed. Sci. Med. Sci.* 70, 1355–1359. doi: 10.1093/gerona/glu244

Stout, M. B., Steyn, F. J., Jurczak, M. J., Camporez, J. P., Zhu, Y., Hawse, J. R., et al. (2017). 17α-Estradiol alleviates age-related metabolic and inflammatory dysfunction in male mice without inducing feminization. *J. Gerontol. A Biomed. Sci. Med. Sci.* 72, 3–15. doi: 10.1093/gerona/glv309

Szablewski, L. (2017). Glucose transporters in brain: in health and in Alzheimer's disease. *J. Alzheimer's Dis.* 55, 1307–1320. doi: 10.3233/JAD-160841

Tai, L. M., Balu, D., Avila-Munoz, E., Abdullah, L., Thomas, R., Collins, N., et al. (2017). EFAD transgenic mice as a human APOE relevant preclinical model of Alzheimer's disease. *J. Lipid Res.* 58, 1733–1755. doi: 10.1194/jlr.R076315

Tarantini, S., Tran, C. H., Gordon, G. R., Ungvari, Z., and Csiszar, A. (2017). Impaired neurovascular coupling in aging and Alzheimer's disease: contribution of astrocyte dysfunction and endothelial impairment to cognitive decline. *Exp. Gerontol.* 94, 52–58. doi: 10.1016/j.exger.2016.11.004

Tarantini, S., Valcarcel-Ares, M. N., Toth, P., Yabluchanskiy, A., Tucsek, Z., Kiss, T., et al. (2019a). Nicotinamide mononucleotide (NMN) supplementation rescues cerebromicrovascular endothelial function and neurovascular coupling responses and improves cognitive function in aged mice. *Redox Biol.* 24:101192. doi: 10.1016/j.redox.2019.101192

Tarantini, S., Valcarcel-Ares, N. M., Yabluchanskiy, A., Fulop, G. A., Hertelendy, P., Gautam, T., et al. (2018). Treatment with the mitochondrial-targeted antioxidant peptide SS-31 rescues neurovascular coupling responses and cerebrovascular endothelial function and improves cognition in aged mice. *Aging Cell* 17:e12731. doi: 10.1111/acel.12731

Tarantini, S., Yabluchanskiy, A., Csipo, T., Fulop, G., Kiss, T., Balasubramanian P,DelFavero, J., et al. (2019b). Treatment with the poly(ADP-ribose) polymerase inhibitor PJ-34 improves cerebromicrovascular endothelial function, neurovascular coupling responses and cognitive performance in aged mice, supporting the NAD+ depletion hypothesis of neurovascular aging. *Geroscience* 41, 533–542. doi: 10.1007/s11357-019-00101-2

Taylor, M. K., Swerdlow, R. H., and Sullivan, D. K. (2019). Dietary neuroketotherapeutics for Alzheimer's disease: An evidence update and the potential role for diet quality. *Nutrients* 11:1910. doi: 10.3390/nu11081910

Terry, R. D., and Katzman, R. (2001). Life span and synapses: will there be a primary senile dementia? *Neurobiol. Aging* 22, 347–348. doi: 10.1016/S0197-4580(00)00250-5

Thirumangalakudi, L., Prakasam, A., Zhang, R., Bimonte-Nelson, H., Sambamurti, K., Kindy, M. S., et al. (2008). High cholesterol-induced neuroinflammation and amyloid precursor protein processing correlate with loss of working memory in mice. *J. Neurochem.* 106, 475–485. doi: 10.1111/j.1471-4159.2008.05415.x

Toth, P., Tarantini, S., Davila, A., Valcarcel-Ares, M. N., Tucsek, Z., Varamini, B., et al. (2015). Purinergic glio-endothelial coupling during neuronal activity: role of P2Y1 receptors and eNOS in functional hyperemia in the mouse

somatosensory cortex. *Am. J. Physiol. Heart Circ. Physiol.* 309, H1837–H1845. doi: 10.1152/ajpheart.00463.2015

Toth, P., Tarantini, S., Tucsek, Z., Ashpole, N. M., Sosnowska, D., Gautam, T., et al. (2014). Resveratrol treatment rescues neurovascular coupling in aged mice: role of improved cerebromicrovascular endothelial function and downregulation of NADPH oxidase. *Am. J. Physiol. Heart Circ. Physiol.* 306, H299–H308. doi: 10.1152/ajpheart.00744.2013

Trainer, P. J., Drake, W. M., Katznelson, L., Freda, P. U., Herman-Bonert, V., van der Lely, A. J., et al. (2000). Treatment of acromegaly with the growth hormone–receptor antagonist pegvisomant. *N. Engl. J. Med.* 342, 1171–1177. doi: 10.1056/NEJM200004203421604

Ungvari, Z., Bailey-Downs, L., Gautam, T., Sosnowska, D., Wang, M., Monticone, R. E., et al. (2011). Age-associated vascular oxidative stress, Nrf2 dysfunction, and NF-κB activation in the nonhuman primate *Macaca mulatta*. *J. Gerontol. A Biomed. Sci. Med. Sci.* 66, 866–875. doi: 10.1093/gerona/glr092

Ungvari, Z., Tarantini, S., Donato, A. J., Galvan, V., and Csiszar, A. (2018). Mechanisms of vascular aging. *Circ. Res.* 123, 849–867. doi: 10.1161/CIRCRESAHA.118.311378

Ungvari, Z., Tarantini, S., Nyúl-Tóth, Á., Kiss, T., Yabluchanskiy, A., Csipo, T., et al. (2019). Nrf2 dysfunction and impaired cellular resilience to oxidative stressors in the aged vasculature: from increased cellular senescence to the pathogenesis of age-related vascular diseases. *Geroscience* 41, 727–738. doi: 10.1007/s11357-019-00107-w

Vaughan, K. L., Kaiser, T., Peaden, R., Anson, R. M., de Cabo, R., and Mattison, J. A. (2018). Caloric restriction study design limitations in rodent and nonhuman primate studies. *J. Gerontol. A* 73, 48–53. doi: 10.1093/gerona/glx088

Vekrellis, K., Ye, Z., Qiu, W. Q., Walsh, D., Hartley, D., Chesneau, V., et al. (2000). Neurons regulate extracellular levels of amyloid β-protein via proteolysis by insulin-degrading enzyme. *J. Neurosci.* 20, 1657–1665. doi: 10.1523/JNEUROSCI.20-05-01657.2000

Webster, S. J., Bachstetter, A. D., Nelson, P. T., Schmitt, F. A., and Van Eldik, L. J. (2014). Using mice to model Alzheimer's dementia: an overview of the clinical disease and the preclinical behavioral changes in 10 mouse models. *Front. Genet.* 5:88. doi: 10.3389/fgene.2014.00088

Wei, M., Fabrizio, P., Hu, J., Ge, H., Cheng, C., Li, L., et al. (2008). Life span extension by calorie restriction depends on Rim15 and transcription factors downstream of Ras/PKA, Tor, and Sch9. *PLoS Genet.* 4:e13. doi: 10.1371/journal.pgen.0040013

Weller, J., and Budson, A. (2018). Current understanding of Alzheimer's disease diagnosis and treatment. *F1000Res.* 7:1161. doi: 10.12688/f1000research.14506.1

Wiedenhoeft, T., Tarantini, S., Nyúl-Tóth, Á., Yabluchanskiy, A., Csipo, T., Balasubramanian, P., et al. (2019). Fusogenic liposomes effectively deliver resveratrol to the cerebral microcirculation and improve endothelium-dependent neurovascular coupling responses in aged mice. *Geroscience* 41, 711–725. doi: 10.1007/s11357-019-00102-1

Wilkinson, R. T. (1963). Interaction of noise with knowledge of results and sleep deprivation. *J. Exp. Psychol.* 66, 332–337. doi: 10.1037/h0044161

Winkler, E. A., Nishida, Y., Sagare, A. P., Rege, S. V., Bell, R. D., Perlmutter, D., et al. (2015). GLUT1 reductions exacerbate Alzheimer's disease vasculo-neuronal dysfunction and degeneration. *Nat. Neurosci.* 18, 521–530. doi: 10.1038/nn.3966

Woolf, S. H., and Schoomaker, H. (2019). Life expectancy and mortality rates in the United States, 1959-2017. *JAMA* 322, 1996–2016. doi: 10.1001/jama.2019.16932

Wu, A., Ying, Z., and Gomez-Pinilla, F. (2004). The interplay between oxidative stress and brain-derived neurotrophic factor modulates the outcome of a saturated fat diet on synaptic plasticity and cognition. *Eur. J. Neurosci.* 19, 1699–1707. doi: 10.1111/j.1460-9568.2004.03246.x

Xing, S. H., Zhu, C. X., Zhang, R., and An, L. (2014). Huperzine a in the treatment of Alzheimer's disease and vascular dementia: a meta-analysis. *Evid. Based Complement Alternat. Med.* 2014:363985. doi: 10.1155/2014/363985

Xiong, H., Callaghan, D., Jones, A., Walker, D. G., Lue, L. F., Beach, T. G., et al. (2008). Cholesterol retention in Alzheimer's brain is responsible for high β- and γ-secretase activities and Aβ production. *Neurobiol. Dis.* 29, 422–437. doi: 10.1016/j.nbd.2007.10.005

Young, J. W., Light, G. A., Marston, H. M., Sharp, R., and Geyer, M. A. (2009). The 5-choice continuous performance test: evidence for a translational test of vigilance for mice. *PLoS ONE* 4:e4227. doi: 10.1371/journal.pone.0004227

Zhang, Y., Xie, Y., Berglund, E. D., Coate, K. C., He, T. T., Katafuchi, T., et al. (2012). The starvation hormone, fibroblast growth factor-21, extends lifespan in mice. *Elife* 1:e00065. doi: 10.7554/eLife.00065

Zhuo, J. M., Prescott, S. L., Murray, M. E., Zhang, H. Y., Baxter, M. G., and Nicolle, M. M. (2007). Early discrimination reversal learning impairment and preserved spatial learning in a longitudinal study of Tg2576 APPsw mice. *Neurobiol. Aging* 28, 1248–1257. doi: 10.1016/j.neurobiolaging.2006.05.034

Conflict of Interest: The authors declare that the research was conducted in the absence of any commercial or financial relationships that could be construed as a potential conflict of interest.

frontiers in Aging Neuroscience

ORIGINAL RESEARCH
published: 01 March 2021
doi: 10.3389/fnagi.2021.633495

Impaired Learning and Memory Ability Induced by a Bilaterally Hippocampal Injection of Streptozotocin in Mice: Involved With the Adaptive Changes of Synaptic Plasticity

Cong-Cong Qi[1†], *Xing-Xing Chen*[2,3,4†], *Xin-Ran Gao*[2,3,4], *Jing-Xian Xu*[2,3,4], *Sen Liu*[2,3,4] *and Jin-Fang Ge*[2,3,4*]

[1] *Department of Laboratory Animal Science, Fudan University, Shanghai, China,* [2] *School of Pharmacy, Anhui Medical University, Hefei, China,* [3] *Anhui Provincial Laboratory of Inflammatory and Immunity Disease, Anhui Institute of Innovative Drugs, Hefei, China,* [4] *The Key Laboratory of Anti-inflammatory and Immune Medicine, Ministry of Education, Anhui Medical University, Hefei, China*

OPEN ACCESS

Edited by:
Stefano Tarantini, University of Oklahoma Health Sciences Center, United States

Reviewed by:
Albert Orock, University of Oklahoma Health Sciences Center, United States
Xavier Xifró, University of Girona, Spain

***Correspondence:**
Jin-Fang Ge
gejinfang@ahmu.edu.cn

†These authors have contributed equally to this work

Received: *25 November 2020*
Accepted: *09 February 2021*
Published: *01 March 2021*

Citation:
Qi C-C, Chen X-X, Gao X-R, Xu J-X, Liu S and Ge J-F (2021) Impaired Learning and Memory Ability Induced by a Bilaterally Hippocampal Injection of Streptozotocin in Mice: Involved With the Adaptive Changes of Synaptic Plasticity. Front. Aging Neurosci. 13:633495. doi: 10.3389/fnagi.2021.633495

Background: Alzheimer's disease (AD) is a neurodegenerative disease characterized by progressive cognitive decline, psychiatric symptoms and behavioral disorders, resulting in disability, and loss of self-sufficiency.

Objective: To establish an AD-like mice model, investigate the behavioral performance, and explore the potential mechanism.

Methods: Streptozotocin (STZ, 3 mg/kg) was microinjected bilaterally into the dorsal hippocampus of C57BL/6 mice, and the behavioral performance was observed. The serum concentrations of insulin and nesfatin-1 were measured by ELISA, and the activation of hippocampal microglia and astrocytes was assessed by immunohistochemistry. The protein expression of several molecular associated with the regulation of synaptic plasticity in the hippocampus and the pre-frontal cortex (PFC) was detected via western blotting.

Results: The STZ-microinjected model mice showed a slower bodyweight gain and higher serum concentration of insulin and nesfatin-1. Although there was no significant difference between groups with regard to the ability of balance and motor coordination, the model mice presented a decline of spontaneous movement and exploratory behavior, together with an impairment of learning and memory ability. Increased activated microglia was aggregated in the hippocampal dentate gyrus of model mice, together with an increase abundance of $A\beta_{1-42}$ and Tau in the hippocampus and PFC. Moreover, the protein expression of NMDAR2A, NMDAR2B, SynGAP, PSD95, BDNF, and p-β-catenin/β-catenin were remarkably decreased in the hippocampus and the PFC of model mice, and the expression of p-GSK-3β (ser9)/GSK-3β were reduced in the hippocampus.

Conclusion: A bilateral hippocampal microinjection of STZ could induce not only AD-like behavioral performance in mice, but also adaptive changes of synaptic plasticity against neuroinflammatory and endocrinal injuries. The underlying mechanisms might be associated with the imbalanced expression of the key proteins of Wnt signaling pathway in the hippocampus and the PFC.

Keywords: Alzheimer disease, streptozotocin, BDNF, nesfatin-1 (NUCB2), NMDAR

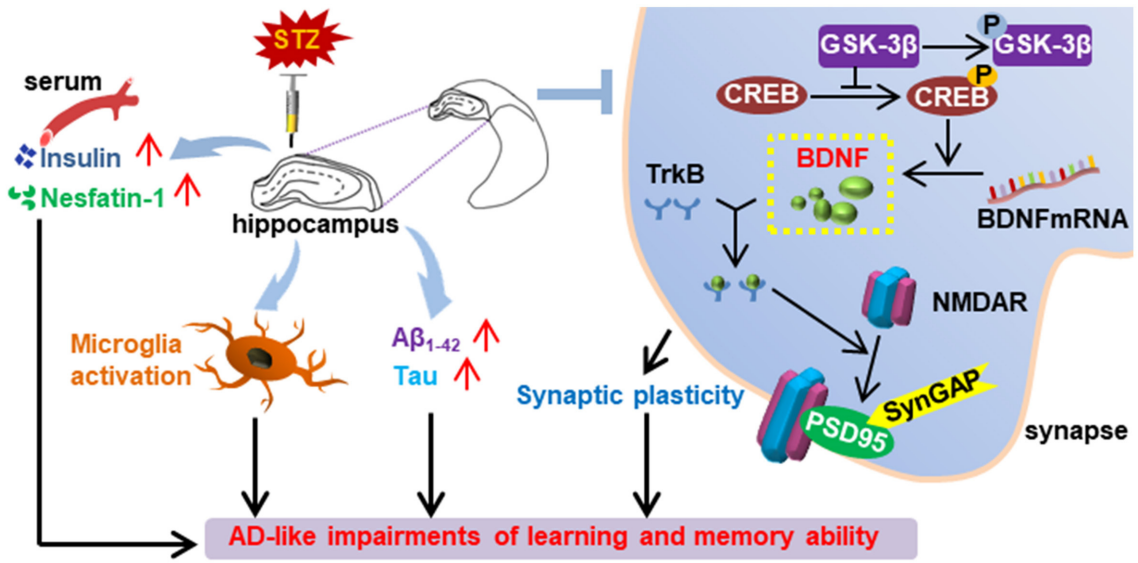

Graphical Abstract | Summary of the effect of bilaterally hippocampal injection of streptozotocin on the mice.

INTRODUCTION

Alzheimer's disease (AD) is a devastating neurodegenerative disorder characterized by a progressive deterioration of cognitive functions (Zameer et al., 2019). Targeted at increasing the activity of cholinergic neurons, cholinesterase inhibitors such as tacrine are clinically used in the treatment for AD with limited effect, but they could not slow or reverse the progress of AD. According to the classical amyloid cascade hypothesis, the deposition of amyloid beta (Aβ) is taken as the trigger of AD leading to the formation of senile plaques (SPs) and nerve fiber tangles (NFTs), resulting in the death of nerve cells and dementia eventually. However, the results of considerable clinical trials of anti-AD agents targeting at Aβ are mostly ended in failure (Hung and Fu, 2017). Although sodium oligomannate has received its first approval in 2019 in China for the treatment of mild to moderate AD (Wang et al., 2019; Syed, 2020), it is still one of the most imperative scientific issues to explore the pathogenesis of AD clearly, find potential therapeutic targets, and develop effective therapeutic agents in the field of neuropsychiatric diseases and public health.

Increasing evidence shows the important role of glutamate-mediated excitotoxity in the pathogenesis of AD, basing on which N-methyl-D-aspartate receptor (NMDARs/GluN) antagonist memantine has been approved by American Food and Drug Administration (FDA) in treatment for AD. Classical NMDAR is a heterotetramer composed of two GluN1 subunits and two GluN2 (A/B) combinations (Henneberger et al., 2013). It has been reported that GluN2A and GluN2B promote the induction and prolongation of synaptic plasticity in different ways (Brigman et al., 2010; Wang et al., 2011; Ballesteros et al., 2016). Declined NMDAR subunits are found in the hippocampus of AD patients, with a significant association with the abnormal presynaptic changes and cognitive deficits (Sze et al., 2001).

NMDARs are reported to be involved in the pathogenesis of AD via regulating the synaptic function (Muller et al.,

Abbreviations: Aβ, amyloid beta; AD, Alzheimer's disease; ADDLs, Aβ-derived diffusible ligands; CFC, contextual fear conditioning test; CREB, cAMP response element-binding protein; DCX, doublecortin; ELISA, enzyme-linked immunosorbent assay; FDA, American Food and Drug Administration; GFAP, glial fibrillary acidic protein; GLUT2, glucose transporters protein 2; Iba-1, ionized calcium-binding adapter molecule 1; IGF, insulin-like growth factor; MWM, Morris water maze; NFTs, nerve fiber tangles; NMDARs, N-methyl-D-aspartate receptor; NOR, novel object recognition test; OFT, open field test; PFC, pre-frontal cortex; PSD95, postsynaptic density protein 95; RT, rotarod test; SPs, senile plaques; SPI, sucrose preference index; SPT, sucrose preference test; STZ, streptozotocin; SynGAP, Synaptic Ras GTPase activation protein; TST, tail suspension test.

2018). Synaptic Ras GTPase activation protein (SynGAP) located at excitatory synapses is reported to integrate with postsynaptic density protein 95 (PSD95), Shank and Ca^{2+}/CaM kinase II (CaMKII) into key signaling protein complexes. The complex is responsible for the membrane binding between synaptic terminals and the neurotransmitter receptors including NMDARs and AMPAR in the postsynaptic density (Chen et al., 2015). These results suggest that NMDARs perhaps take part in the etiopathology of neuropsychiatric injury in AD, with different physiological and molecular characteristics for different subunits of NMDARs.

The canonical Wnt/β-catenin signaling pathway is required for the maintenance of normal brain structure and function (Gaesser and Fyffe-Maricich, 2016), and the deficit of Wnt/β-catenin pathway has been demonstrated in the brain of AD patients (Folke et al., 2019). Results of animal studies showed that blocking of the Wnt pathway could exacerbate the Tau hyper-phosphorylation, the formation and deposition of $A\beta_{1-42}$, and the memory impairment (Tapia-Rojas and Inestrosa, 2018). Note that, abnormal function of Wnt signaling pathway can promote the production of Aβ, while Aβ, in turn, can inhibit the Wnt/β-catenin signaling pathway to aggravate the course of AD (Magdesian et al., 2008; Rodriguez et al., 2011; Liu et al., 2014).

The hippocampus and the pre-frontal cortex (PFC) are very important brain areas involving with the regulation of emotion and cognition (Hiser and Koenigs, 2018), and increasing data have demonstrated their structural and functional changes in AD patients or animal models (Teixeira et al., 2018; Zhong et al., 2018) (Jahanshahi et al., 2019). Given the important role of insulin resistance in the mechanism of both AD and type 2 diabetes mellitus, streptozotocin (STZ), a glucosamine-nitrosourea and DNA alkylating reagent that could result in insulin resistance, are used widely to establish animal models of AD or diabetes mellitus with multiple administration methods (Zameer et al., 2019). Results of animal studies showed that peripheral or central administration of STZ could result in not only insulin resistance, but also structural or functional dysfunction in hippocampus and PFC (Li et al., 2018; Mishra et al., 2018). Moreover, it has been reported that hippocampal injection of AAV-CD82 could induce AD-like cognitive deficits and impairments in neuronal spine density in young adult mice (Zhao et al., 2020). Targeted hippocampal overexpression of tumor necrosis factor-α-induced protein 8-like 2 (TIPE2) in APP/PS1 mice could result in an improvement of learning and memory, together with a reduced expression of inflammatory cytokines and increased expression of anti-inflammatory cytokines (Miao et al., 2019). These findings suggest that hippocampal targeted injection of stimulants or therapeutic drugs can be used effectively in research focusing on the pathogenesis of AD and evaluation of therapeutic effects.

It is a crucial experimental means and premise to establish effective animal models mimicking the pathophysiological process of human diseases. The main purpose of this study was to characterize the AD mice model via bilaterally hippocampal microinjection of STZ. The behavioral performance was observed via the sucrose preference test (SPT), rotarod test (RT), open field test (OFT), tail suspension test (TST), novel object recognition (NOR) test, Morris water maze (MWM), and contextual fear conditioning (CFC) test. The serum concentrations of insulin and nesfatin-1 were tested via enzyme-linked immunosorbent assay (ELISA). The activation of microglia and astrocytes and neurogenesis in the hippocampus was detected by immunofluorescent staining with ionized calcium-binding adapter molecule 1 (Iba-1), CD68, glial fibrillary acidic protein (GFAP), and doublecortin (DCX) respectively. The expression of $A\beta_{1-42}$, Tau, synaptic plasticity related molecules, and key proteins of the Wnt pathway in the hippocampus and the pre-frontal cortex (PFC) were detected via western blot.

MATERIALS AND METHODS

Animals

Twenty-six adult C57BL /6 male mice (bodyweight 25∼30 g, aging 3 months) were purchased from and kept in the experimental animal center of Tongji University School of Medicine under the condition equipped with a commutative 12 h light/dark schedule. The mice were randomly divided into a control group (CON) and a STZ-injection model group (MOD) with 4–5 mice per cage and access to food and water *ad libitum*. The ambient temperature was maintained at 20 ± 2°C with 50 ± 5% relative humidity. All the animal care practices and experiment procedures were reviewed and approved by the Animal Experimentation Ethics Committee of Tongji University School of Medicine, in compliance with the National Institutes of Health Guide for the Care and Use of Laboratory Animals (NIH publication No.85-23, revised 1985).

Stereotactic Intra-Hippocampal Microinjection of STZ and Experiment Design

Each mouse was anesthetized by intraperitoneal injection of 5% chloral hydrate (0.1 ml/10 g), secured to a platform placed in a stereotaxic apparatus (David Kopf; Tujunga, CA, USA) and the scalp incised. After the bregma was located, a rotary tool was used to drill into the skull and get two burr holes, according to the following sites of 2.1 mm posterior, 1.3 mm lateral, and 1.8 mm below. Mice in the MOD group received bilateral infusions of STZ (Sigma-Aldrich, s0130; 3 mg/kg) dissolved in 0.9% sterile saline into the hippocampus on both coordinates with a constant rate (500 nL/min) pulled by a micropipette puller. Correspondingly, mice in the CON group received bilateral infusions of 0.9% sterile saline. After the wound was closed, the animals were placed on the 37°C warming pad to recover until their respiration and locomotor activity returned to normal (Zhang et al., 2016).

Bodyweight of mouse was monitored once a week. After 2 weeks of recovery from surgery, all mice were submitted to a chain of behavioral paradigms. The schedule of the experimental design is shown in **Figure 1**.

Behavioral Test

All behavioral experiments were performed during the light phase of the light/dark cycle and in a sound-proof room with a neutral environment. All the mice in this study were given a

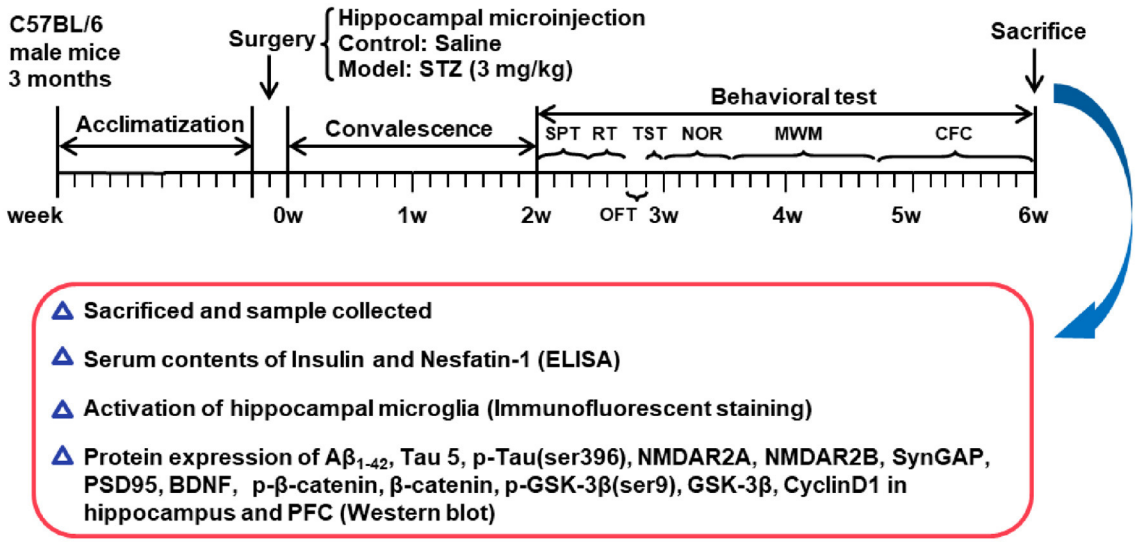

FIGURE 1 | Schedule of the experimental design. STZ, streptozotocin; SPT, sucrose preference test; RT, rotarod test; OFT, open field test; TST, tail suspension test; NOR, novel object recognition test; MWM, Morris water maze; CFC, contextual fear conditioning test; BDNF, brain derived neurotrophic factor; PFC, pre-frontal cortex.

30-min habituation time after transported to the experimental rooms and subjected to the following behavioral tests. The experimenter was blind to the group identity of the tested mice. The behavioral tests were recorded with a camera and a trained researcher analyzed these videos.

The behavioral tests began with the SPT, followed in sequence by the RT, OFT, TST, NOR, MWM, and CFC test, which was shown in **Figure 1**.

Sucrose Preference Test (SPT)

The SPT was used to detect the anhedonia behavior in rodents (Ke et al., 2020). After a deprivation of food and water for 12 h, the mice were housed solely and had free access to two identical water bottles filled with either sterile water or 1% (w/v) sucrose solution, respectively. To eliminate the interference of the location factor, the positions of the bottles were swapped after 12 h. The mass of water and sucrose solution consumed were weighed after 12 and 24 h, respectively. The sucrose preference index (SPI) is defined as the ratio of the sucrose water ingested to the total amount of liquid intake.

Rotarod Test (RT)

Motor coordination and balance of mice was assessed by RT in a reliable way. The test was divided into two stages, namely the training period and the test period. The training period consisted of a uniform 10 rpm for 1 min, and an acceleration period of 4–40 rpm for 5 min with relaxing 30 min at least. The mice were placed on the rotating apparatus with their backs to the operator. Note that, once the mouse fell during the training, it will be put back immediately to make sure completion. The test period was conducted on the second day after the training by three trails on the rotating rod, and inter-trial interval was 1 h for each mouse. During the process of accelerating the rod device from 4 to 40 rpm over the course 5 min, the latency to fall off and the maximal rotation rate before the mouse fell down were recorded and evaluated (Kandimalla et al., 2018).

Open Field Test (OFT)

The OFT was conducted to synchronously explore the locomotion and exploration. The apparatus was made up of a square arena, with a white floor divided into 9 squares (10 cm × 10 cm) and enclosed by continuous 20.3 cm-high walls made of transparent plexiglass. Each mouse was put into it at one corner and headed toward the wall. The total distance traveled, latency to the central square, distance and duration in the central square, as well as the frequency through the central square over a 30 min period were recorded and analyzed by Activity Monitor software (Med Associates, St. Albans, VT, United States) (Zhang et al., 2019).

Tail Suspension Test (TST)

The TST was conducted as previously described (Zhou et al., 2016) with some modifications. Briefly, mice were individually suspended by tail (20 cm from floor) using a paper tape (1.5 cm from the tip of the end). Each mouse was suspended for a total of 6 min, and the duration of immobility was recorded during the final 4 min interval of the test. Mice were considered immobile only when they hung passively and completely motionless. In addition, the mouse that once climbed up their tails was not involved in this assay.

Novel Object Recognition (NOR) Test

The NOR test was performed to assess non-spatial memory in a 25 cm × 25 cm × 25 cm and black soundproof box (Zhu et al., 2014). The test consisted of three phase: habituation, training, and retention sessions. In the first stage, the single mouse was placed into the box facing the wall, having a preceding 10 min habituation once a day, for 3 consecutive days.

During the training session, two indistinguishable objects were symmetrically fixed to the floor of the box, and each mouse was allowed to travel in the apparatus freely for 10 min. After the training, the mice were immediately returned to their home cages for 60 min at least. Ultimately, during the retention test, each mouse was placed back into the same box, with one of the familiar objects substituted by a novel object. Test mouse was then allowed to freely explore for 5 min and videotaped. New object recognition index, a ratio of the amount of time spent exploring the novel object over the total time spent exploring the both, was used to evaluate cognitive function. A mouse was scored as exploring the object when touching or sniffing the object with its nose or front legs, and facing the object at a distance within 1 cm (Wang D. et al., 2018).

Morris Water Maze (MWM) Test

MWM serves as a method of evaluating different aspects of spatial memory in rodents. The maze was equipped with a circular blue pool (diameter 120 cm, height 60 cm, filled with water to 40 cm high at 21°C), which was divided into four hypothetical, equal quadrants. A circular platform (11 cm diameter) was submerged approximately 1 cm below the surface of water in the center of the target quadrant. Several complex visual cues surrounded the pool diagonally and were used for facilitating orientation.

The test consisted of a 7-day acquisition phase and a 1-day probe test on the 8th day. During the acquisition phase, each mouse received 4 trials per day, and was trained to find the hidden platform. The mouse was placed into the pool facing the wall individually to find the submerged platform within 60 s, and stayed on it for 20 s. If the hidden-platform was not found within 60 s, the mouse was gently guided to the platform and held for 20 s. On the 8th day, the probe test was performed to determine memory retention, and the platform was removed. Each mouse was put into the pool from the diagonally opposite side of the previous platform, and permitted to swim for 60 s freely. The escape latency in the acquisition phase, total distance to the platform, the duration spent in and frequency to the target quadrant in the probe test were monitored and measured automatically by Noldus software (EthoVision XT 8.0, Noldus Technology) (Kandimalla et al., 2018).

Contextual Fear Conditioning (CFC) Test

The CFC paradigm was considered to assess the ability of associating a distinct context with aversive footshocks through hippocampus-dependent cognitive mechanisms in rodents as described previously (Dai et al., 2008). The mouse was subjected to a CFC test in a sound attenuating chamber (30 × 25 × 20 cm), the floor of which was consisted of parallel 2 mm diameter stainless steel rods spaced 8 mm apart. A preceding 10 min habituation was subjected to reduce the contribution of anxiety and stress on the outcome. 24 h later, mice were placed in the same chamber and allowed to explore freely for 120 s before receiving 8 unsignaled foot shocks (1.0 mA, 2 s) with inter-shock intervals of 60 s. Mice were immediately returned to their home cages 2 min after the final foot shock. The behavioral freezing to the context of mice was measured to evaluate contextual fear memory at three points: 1, 24, and 1 week after fear conditioning. The mice were placed back to the same context and scored freezing behavior for 660 s by the automated FreezeFrame system (Coulbourn Instruments), which digitizes the video signal at 4 Hz and compares movement frame by frame to score the amount of freezing. Freezing was defined as the absence of all movement except for that needed for breathing (Devi and Ohno, 2013).

Measurement of the Serum Concentrations of Insulin and Nesfatin-1

Twenty-four hours after the last behavioral test, all mice were sacrificed and the blood was collected. The serum levels of insulin and nesfatin-1 were detected using commercially available enzyme-linked immunosorbent assay (ELISA) kits (insulin: Yuanye Biotech. Co., LTD, Shanghai, China; nesfatin-1: Cusabio Biotech. Co., LTD, Wuhan, China) according to the manufacturers' instructions.

Immunofluorescent Staining

Three mice in each group were selected randomly and transcardially perfused with 0.01 M phosphate-buffered saline (PBS, pH 7.4) followed by 4% paraformaldehyde (PFA) in PBS. The whole brains were dissected out and post-fixed in 4% PFA overnight, followed by cryoprotection in 30% sucrose in PBS overnight. After embedded with optimum cutting temperature compound (OCT), the brains were cut into sagittal sections (25 m thick), and then stored at −80°C for immunostaining (Pruski et al., 2019).

Immunohistochemistry was performed as described previously (Zhu et al., 2014) with some modifications. Sections were re-hydrated washed in PBS for 3 × 10 min in a microwave followed by incubation with a blocking solution containing 5 % bovine serum albumin (BSA) and 0.1% Tween-20 in PBS (pH 7.4) for 6 min at 95°C to retrieve the antigen. Then, brain sections were incubated with rabbit anti-Iba-1 (1:1,000; LAK4357, Wako, Japan), rat anti-CD68 (1:200; MCA1957GA, Bio-Rad Company, United States), guinea pig anti-DCX (1:300; AB2253, Millipore, USA), or rabbit anti-GFAP (1:1,000; z0334, Dako, USA), at 4°C overnight. After several washes in PBS, sections were incubated with donkey anti-rabbit Alexa Fluor 488-conjugated IgG (1:500; R37118, Invitrogen, Carlsbad, CA, USA), and biotinylated horse anti-rat or horse anti-guinea pig IgG (1:500, Jackson ImmunoResearch, USA) at room temperature for 2 h. Ultimately, brain sections were incubated with streptavidin-Cy3 (1:1,000, 016160084, Jackson ImmunoResearch, West Grove, PA, USA) and counterstained with Hoechst 33258 (1:2,000, 94403, Sigma, St.Louis, MO, USA) at room temperature for 1 h. Fluorescent images were taken on a laser-scanning confocal fluorescent microscope (Leica TCS SP8, Leica Microsystems, Wetzlar, Germany).

Western Blot Assays

Another 3 mice were selected randomly in each group, and sacrificed by cervical dislocation 24 h after the last behavioral test. The hippocampus and the PFC were dissected promptly, frozen in liquid nitrogen and stored at −80°C. The western blot protocol was carried out as described in our previous study. Briefly, the

tissues were lysed in ice-cold radio immunoprecipitation assay (RIPA) buffer containing protease inhibitor cocktail (Roche, IN, USA) and the phosphatase inhibitor PhosSTOP (Roche, IN, USA). Determine equal amounts of proteins (20 μg) using the BCA Protein Assay Reagent Kit before loading onto the 12.5% SDS-PAGE. After separated from each other, the proteins were subsequently transferred onto the polyvinylidene difluoride membrane (PVDF). The membrane was blocked 2 h with 5% BSA in TBST at RT followed by incubation with primary antibodies respectively at 4°C overnight. The primary antibodies were as follows: anti-Aβ_{1-42} (1:1,000; 25524-1-AP; Proteintech), anti-Tau 5 (1:200; sc-58860; Santa Cruz), anti-p-Tau (ser396) (1:1,000; sc-32275; Santa Cruz), anti-NMDAR2A (1:2,000; 19953-1-AP; Proteintech), anti-NMDAR2B (1:2,000; 21920-1-AP; Proteintech), anti-SynGAP (1:2,000; 19739-1-AP; Proteintech), anti-PSD95 (1:2,000; MA1-045; Thermo), anti-BDNF (1:1,000; sc-546; Santa Cruz), anti-p-β-catenin (1:1,000; 9561; Cell Signaling Technology), anti-β-catenin (1:1,000; 9562; Cell Signaling Technology), anti-p-GSK-3β(ser9) (1:1,000; 9323; Cell Signaling Technology), anti-GSK-3β (1:1,000; 9315; Cell Signaling Technology), anti-CyclinD1 (1:1,000; ab190564; Abcam), and β-actin (1:2,000; TA-09; Zhongshan Biotechnology). Then the membranes were further incubated with a horseradish peroxidase-conjugated secondary antibody, goat anti-rabbit or goat anti-mouse secondary antibodies (Abcam), at RT for 1 h. All procedures were performed by rinsing in TBST for 10 min and repeated three times. After developed with the Easy Enhanced Chemiluminescence Western Blot Kit (Pierce Biotechnology, Rockford, IL, USA), the protein blots were visualized by a gel imaging system (Tanon Science and Technology Co., Ltd., Shanghai, China) and then images were processed and analyzed using Image J software (NIH) (Chen et al., 2019).

Statistical Analysis

All statistical analyses were performed using SPSS (version 12.0.1, SPSS Inc., Chicago, IL, United States). The difference between groups was examined using Student's *t*-test. Data are expressed as means ± SEM and $P < 0.05$ was considered statistically significant. Correlation analysis was performed using a Pearson's correlation test.

RESULTS

Bilaterally Hippocampal Injection of STZ Induced a Decreased Tendency of Body Weight-Gain

Figure 2 shows the bodyweight and bodyweight gain of mice in the two groups. As compared with that in the control group, the tendency of the bodyweight gain in the bilaterally hippocampal STZ-injected group was decreased, with a significant difference between groups during the 2nd week post-operation (t (24) =2.160, $P = 0.041$; **Figure 2B**).

Bilaterally Hippocampal Injection of STZ Induced a Decrease of Locomotor Activity and Exploration Behavior in Mice in the OFT Without Significant Changes in the RT, TST, and SPT

General behavior performances of mice are shown in **Figure 3**, including the balance and motor coordination, automatic activity, exploratory and despair behavior, and anhedonia. As shown in **Figures 3A,B**, there was no significant difference between the two groups as regard to the falling time (t (24) = 0.561, $P = 0.041$; **Figure 3A**) and falling speed (t (24) = 0.496, $P = 0.624$; **Figure 3B**) in the RT. In the OFT, although there was no significant difference between groups with regards to the latency (t (24) = −1.439, $P = 0.173$; **Figure 3C**) and frequency (t (24) = −1.950, $P = 0.063$; **Figure 3D**) to the center, and duration in the center (t (24) = 0.856, $P = 0.401$; **Figure 3E**), the bilaterally hippocampal STZ-injected mice showed significantly decreased total ambulatory distance traveling in the area (t (24) = 2.474, $P = 0.024$; **Figure 3F**), as well as the ambulatory distance (t (24) =2.611, $P = 0.017$; **Figure 3G**) and ambulatory time (t (24) = 2.598, $P = 0.017$; **Figure 3H**) in the center zone as compared with the control ones. The immobility time in the TST (t (24) = 1.445, $P = 0.161$; **Figure 3I**) and the sucrose preference index in the SPT

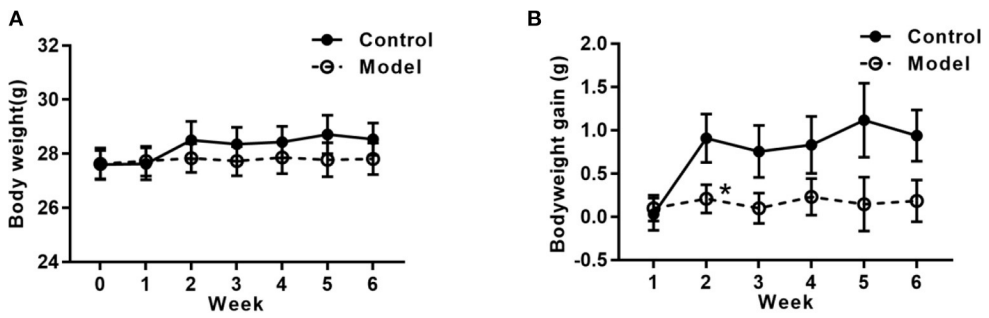

FIGURE 2 | Effects of bilaterally hippocampal injection of STZ on the bodyweight gain in mice. The data are presented as the mean ± SEM, with 13 mice in each group. Although there was no significant difference between groups with regard to the bodyweight **(A)**, the net bodyweight gain **(B)** of mice injected by STZ in the model group was lower than that in the control group in the 2nd week. *$P < 0.05$, compared with the control group.

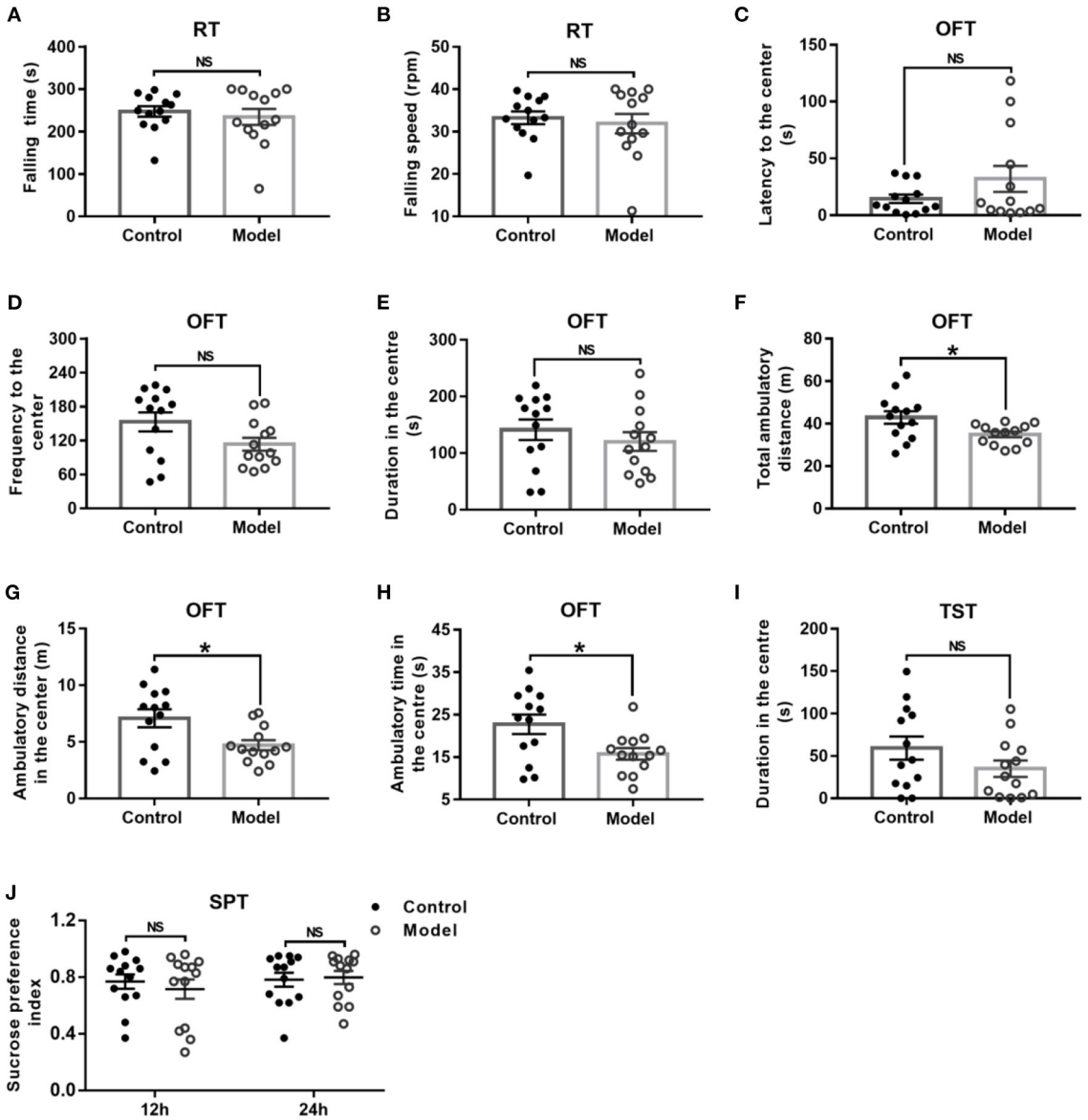

FIGURE 3 | Effect of bilaterally hippocampal injection of STZ on the behavior performance of mice in the RT, OFT, TST, and SPT. The data are presented as the mean ± SEM, with 13 mice in each group. There was no significant difference between the two groups as regard to the falling time **(A)** and falling speed **(B)** in the RT. In the OFT, although there was no significant difference in the latency **(C)** and frequency **(D)** to the center, duration **(E)** in the center between the two groups, bilaterally hippocampal STZ-injected mice showed significant decreased total ambulatory distance traveled **(F)** in the area, as well as the ambulatory distance **(G)** and time **(H)** in the center zone than control mice. The immobility time **(I)** in the TST and the SPI **(J)** in the SPT are not remarkably different between groups. *$P < 0.05$; compared with the control group, NS is no significance.

(12 h, t (24) = −0.257, P = 0.799; 24 h, t (24) = −0.239, P = 0.813, **Figure 3J**) were not remarkably different between groups.

Bilaterally Hippocampal Injection of STZ Induced an Impairment of Learning and Memory Ability in Mice in the NOR and MWM, but Not CFC

Behavioral performance of mice in the NOR task is shown in **Figure 4A**. As compared with the control mice, the bilaterally hippocampal STZ-injected mice spent less time exploring the novel object, with a significant decrease of the novel object recognition index (t (24) = 2.091, P = 0.047; **Figure 4A**).

Figure 4B shows the performance of mice in the stage of fear memory formation in the CFC test, and there was no significant difference between the two groups. Moreover, the amount of freezing to context (**Figure 4C**) of the bilaterally hippocampal STZ-injected mice was not observably different from that of control ones, when the fear memories were extracted in the same

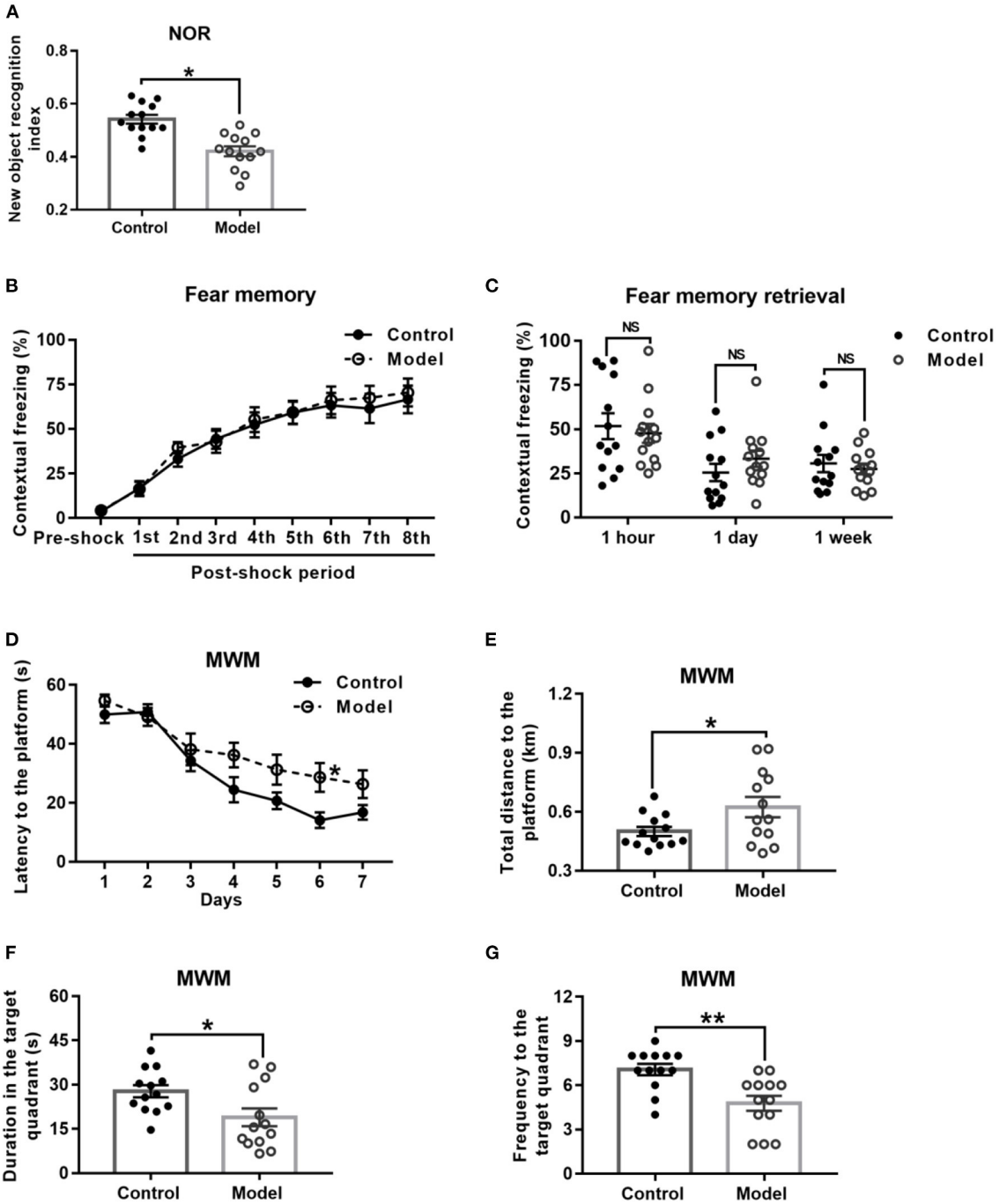

FIGURE 4 | Effect of bilaterally hippocampal injection of STZ on the behavior performance of mice in the NOR, CFC and MWM. The data are presented as the mean ± SEM, with 13 mice in each group. In the NOR, compared with control mice, the novel object recognition index of model mice **(A)** was remarkably reduced. There was no significant difference between the two groups in the stage of fear memory formation **(B)** and freezing time of mice when the fear memory was extracted after 1 h, 1 day, and 1 week **(C)** in the CFC. In the MWM, during the acquisition phase, bilaterally hippocampal STZ-injected mice took longer time to find the submerged platform than the control mice did on 6th day **(D)**. During the probe trial, the model mice showed increased total swimming distance to the platform **(E)**, decreased duration **(F)** and less frequency **(G)** in the target quadrant. $^{*}P < 0.05$, $^{**}P < 0.01$; compared with the control group, NS is no significance.

environment 1 h, 1 and 7 days after formation of fear memory (1 h, $t\ (24) = 0.448$, $P = 0.658$; 1 day, $t\ (24) = -1.158$, $P = 0.258$; 7 days, $t\ (24) = 0.542$, $P = 0.592$, **Figure 4C**).

The performance of mice during the acquisition phase in the MWM is shown in **Figure 4D**. All the mice in this study learned how to locate the platform, as revealed by the sharp decline in

the escape latency to the submerged platform. Moreover, the bilaterally hippocampal STZ-injected mice spent a longer time to find the escape platform than the control ones did on the sixth day (t (24) = −2.611, P = 0.017; **Figure 4D**). In the probe test, as compared with that of the control group, the total swimming distance to the platform (t (24) = −2.179, P = 0.044; **Figure 4E**) of the model mice was significantly extended, together with a shorter duration (t (24) = 2.411, P = 0.024; **Figure 4F**) in and less the frequency (t (24) = 3.625, P = 0.001; **Figure 4G**) to the target quadrant.

Bilaterally Hippocampal Injection of STZ Increased the Serum Concentrations of Insulin and Nesfatin-1 in Mice

As **Figure 5** shown, compared with those in the control mice, the serum concentrations of insulin (t (24) = −3.665, P = 0.001; **Figure 5A**) and nesfatin-1 (t (24) = −4.850, P < 0.001; **Figure 5B**) were observably increased in the bilaterally hippocampal STZ-injected mice.

Bilaterally Hippocampal Injection of STZ Promoted Microglia to Aggregate and Activate in the Hippocampus of Mice

Figures 6A–F shows the typical immunofluorescent images of Iba-1 (green) and CD68 (red) in the mice hippocampal sections. As shown in **Figures 6A,D**, the Iba-1 (green) positive microglia clustered at the dentate gyrus (DG) of the bilaterally hippocampal STZ-injected mice, while such a phenomenon was not detected in the control group. Interestingly, as shown in **Figure 6K**, a dramatic ascending number of positive Iba-1 (green) marked microglia (t (4) = −2.796, P = 0.049; **Figure 6K**) and CD68 (red) marked activated microglia (t (4) = −3.806, P = 0.019; **Figure 6K**) were presented in the DG of the hippocampal tissues of model mice, and the activated microglial marker CD68 was mostly clustered around the hippocampal injection site.

Figures 6G–J shows the typical immunofluorescent images of DCX (red) and GFAP (green) in the mice brain sections. There was no significant difference between groups as regard to the number of DCX (red) positive cells (t (4) = 0.417, P = 0.698; **Figures 6G,H,L**). As shown in the **Figures 6I,J,L**, the GFAP (green) positive cells in the mice brain of the two groups were uniformly distributed in the hippocampus (t (4) =1.814, P = 0.210; **Figure 6L**).

Bilaterally Hippocampal Injection of STZ Induced an Increased Expression of $A\beta_{1-42}$ and Both the Total and Phosphorylated Tau in the Hippocampus and the PFC in Mice

Figure 7 shows the expression of $A\beta_{1-42}$, p-Tau (ser396) and Tau 5 in the hippocampus and PFC of the mice. As compared with that in the control group, the relative expression of $A\beta_{1-42}$ was remarkably increased in the hippocampus (t (4) = 2.947, P = 0.046; **Figure 7B**) and PFC (t (4) = 2.175, P = 0.032; **Figure 7C**), and both the expression level of p-Tau (ser396) and Tau 5 were significant increase in the hippocampus (t (4) = 2.195, P = 0.008; **Figure 7B**; t (4) = 4.092, P = 0.007; **Figure 7B**) and the PFC (t (4) = 1.389, P = 0.001; **Figure 7C**; t (4) = 8.196, P = 0.035; **Figure 7C**).

Bilaterally Hippocampal Injection of STZ Induced an Imbalanced Expression of Synaptic Plasticity Related Proteins in the Hippocampus and the PFC in Mice

Figure 8 shows the protein expressions of NMDAR2A, NMDAR2B, SynGAP, PSD95, and BDNF in the hippocampus and PFC of mice. Compared with those in the control mice, the expression levels of NMDAR2A (Hippocampus: t (4) = 7.037, P = 0.002, **Figure 8B**; PFC: t (4) = 6.490, P = 0.003, **Figure 8C**), NMDAR2B (Hippocampus: t (4) = 3.962, P = 0.017, **Figure 8B**; PFC: t (4) = 9.076, P = 0.001, **Figure 8C**), SynGAP (Hippocampus: t (4) = 3.391, P = 0.028, **Figure 8B**; PFC: t (4) = 6.613, P = 0.003, **Figure 8C**), PSD95 (Hippocampus: t (4) = 4.461, P = 0.011, **Figure 8B**; PFC: t (4) = 3.280, P = 0.030, **Figure 8C**) and BDNF (Hippocampus: t (4) = 6.092, P = 0.004, **Figure 8B**; PFC: t (4) = 3.423, P =

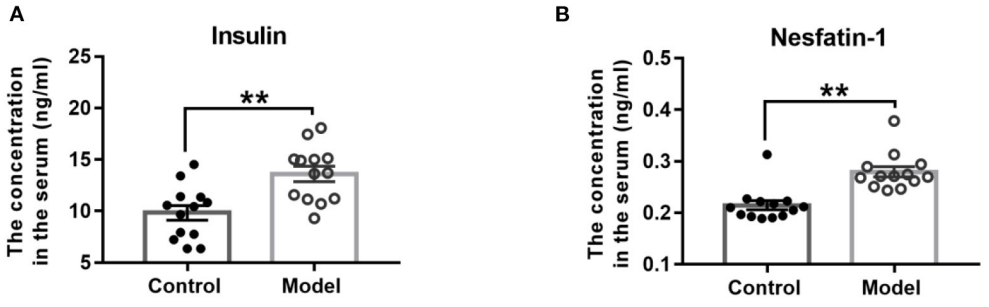

FIGURE 5 | Effect of bilaterally hippocampal injection of STZ on the serum concentrations of insulin and nesfatin-1. The data are presented as the mean ± SEM, with 13 mice in each group. Compared with those in the control mice, the serum concentrations of insulin **(A)** and nesfatin-1 **(B)** were observably increased in the bilaterally hippocampal STZ-injected mice. $^{**}P < 0.01$, compared with the control group.

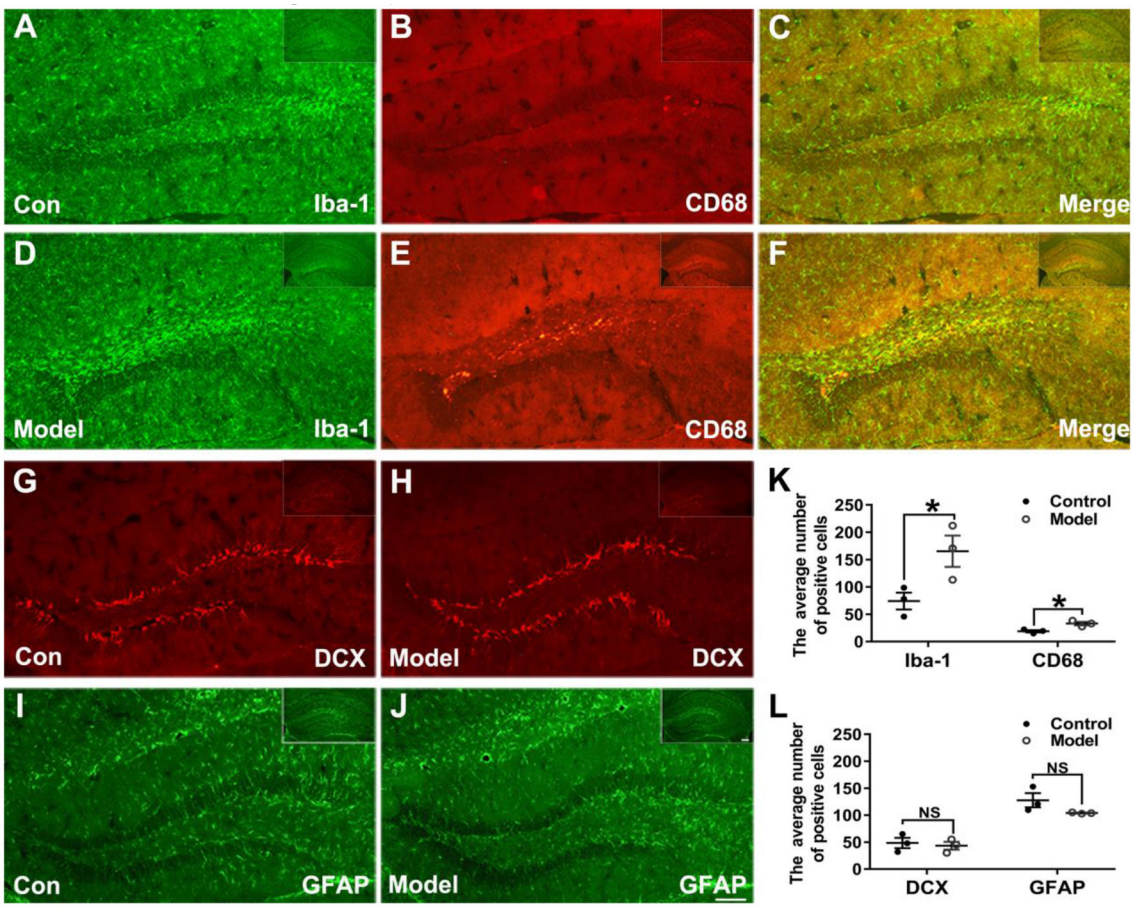

FIGURE 6 | Effects of bilaterally hippocampal injection of STZ on the activation of microglias in the dentate gyrus of hippocampus of mice. **(A–F)** shows immunofluorescent microscopy of Iba-1 (green) and CD68 (red) in hippocampus tissues and the dentate gyrus. **(G–J)** shows immunofluorescent microscopy of DCX (red) and GFAP (green) in hippocampus tissues and the dentate gyrus (DG). Compared with those in the control mice, the number of Iba-1 **(A,D)** and CD68 **(B,E)** positive microglia ascends significantly in the DG tissues of the model group **(K)**. There was no significant difference in the number of positive cells of DCX **(G,H)** and GFAP **(I,J)** between the two groups. The data in **(K)** and **(L)** are presented as the mean ± SEM, with 3 mice in each group. Scale bars = 100 μm in J (applies to **A–J**), 200 μm in insets. *$P < 0.05$; compared with the control group, NS is no significance.

0.027, **Figure 8C**) were remarkably decreased in both the hippocampus and the PFC of bilaterally hippocampal STZ-injected mice. Despite the small sample size, significant positive correlations were observed between the protein expression of BDNF and NMDAR2A (Hippocampus: $r = 0.996$, $P < 0.001$, **Supplementary Figure 1A**; PFC: $r = 0.960$, $P = 0.002$, **Supplementary Figure 1B**), SynGAP (Hippocampus: $r = 0.850$, $P = 0.032$, **Supplementary Figure 1C**; PFC: $r = 0.880$, $P = 0.021$, **Supplementary Figure 1D**), or PSD95 (Hippocampus: $r = 0.857$, $P = 0.029$, **Supplementary Figure 1E**; PFC: $r = 0.894$, $P = 0.016$, **Supplementary Figure 1F**). Moreover, significant positively correlations were also observed between the protein expression of NMDAR2A and NMDAR2B (Hippocampus: $r = 0.820$, $P = 0.045$, **Supplementary Figure 2A**; PFC: $r = 0.985$, $P < 0.001$, **Supplementary Figure 2B**), SynGAP (Hippocampus: $r = 0.848$, $P = 0.033$, **Supplementary Figure 2C**; PFC: $r = 0.952$, $P = 0.003$, **Supplementary Figure 2D**), or PSD95 (Hippocampus: $r = 0.851$, $P = 0.032$, **Supplementary Figure 2E**; PFC: $r = 0.871$, $P = 0.024$, **Supplementary Figure 2F**).

Bilaterally Hippocampal Injection of STZ Induced a Dysregulation of Wnt/β-catenin Signaling Pathway in the Hippocampus and the PFC in Mice

Figure 9 shows the expression of key proteins in the Wnt/β-catenin pathway in the hippocampus and PFC of the mice. As compared with that in the control group, the relative expression of p-β-catenin/β-catenin in both the hippocampus (t (4) =3.111, $P = 0.036$; **Figure 9B**) and the PFC (t (4) = 9.748, $P = 0.001$; **Figure 9C**) were remarkably declined in bilaterally hippocampal STZ-injected mice, and the expression of p-GSK-3β (ser9)/GSK-3β was decreased in the hippocampus (t (4) = 4.306, $P = 0.013$; **Figure 9B**), but not the PFC (t (4) = 1.821, $P = 0.143$; **Figure 9C**).

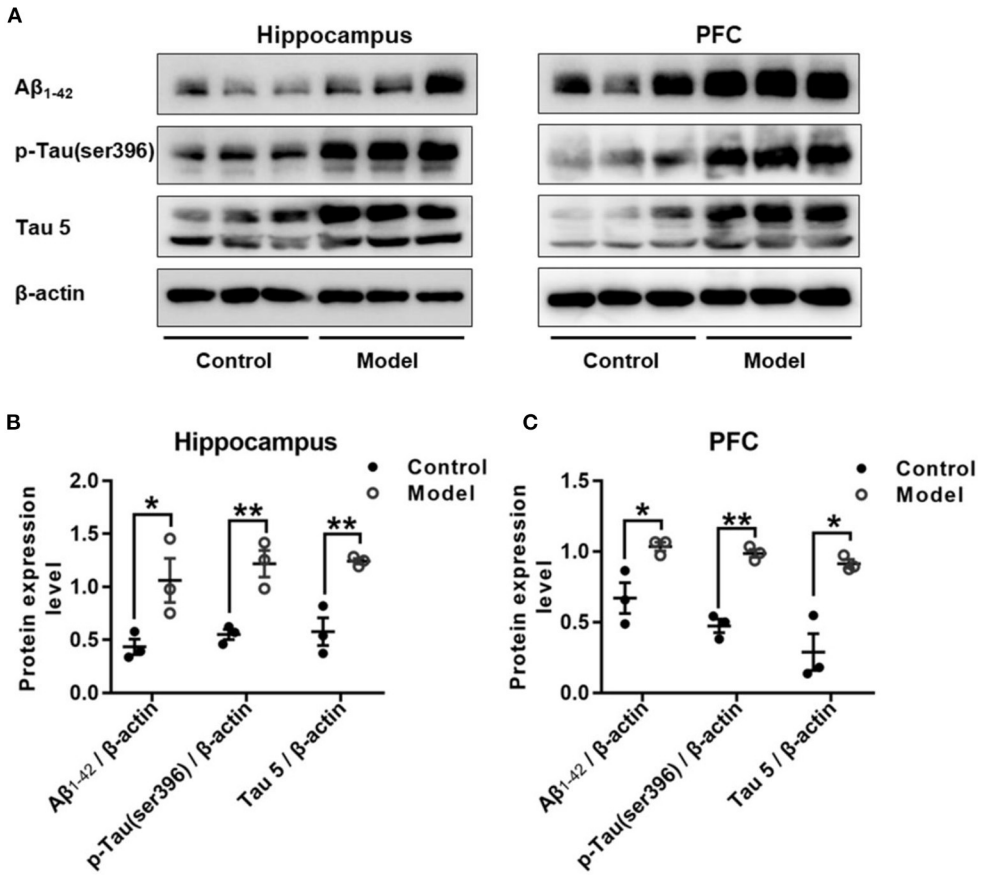

FIGURE 7 | Effect of bilaterally hippocampal injection of STZ on amyloid beta and Tau protein in the hippocampus and PFC of model mice. Typical graph **(A)** and statistical analyses **(B,C)** of the western blot results. Data in **(B,C)** are presented as the mean ± SEM ($n = 3$ for each group). Compared with that in the control mice, the relative expression of $A\beta_{1-42}$, p-Tau (ser396) and Tau 5 was increased in the hippocampus **(A,B)** and the PFC **(A,C)** of the model mice. $^{*}P < 0.05$, $^{**}P < 0.01$; compared with the control group.

No significant changes were found between groups as regard to the protein expression of CyclinD1 in both the hippocampus (t (4) = 1.284, $P = 0.269$; **Figure 9B**) and the PFC (t (4) = 1.988, $P = 0.118$; **Figure 9C**). The results of Pearson's correlation analysis showed that the protein expression of p-GSK-3β/GSK-3β was positively correlated with BDNF ($r = 0.939$, $P = 0.005$; **Supplementary Figure 3A**), NMDAR2A (r =0.937, $P = 0.006$; **Supplementary Figure 3B**), or synGAP ($r = 0.960$, $P = 0.002$; **Supplementary Figure 3C**) in the hippocampus.

DISCUSSION

In the present study, an AD mouse model was established via bilaterally hippocampal injection of STZ. The results showed that a bilaterally hippocampal injection of STZ could induce a decreased tendency of bodyweight gain in mice, together with remarkably increased serum concentrations of insulin and nesfatin-1. Results of behavioral tests demonstrated that the spontaneous movement and exploratory behavior were decreased in the bilaterally hippocampal STZ-injected mice as compared with the control ones. More importantly, the model mice showed a task-specific impairment of learning and memory, as indicated by the declined novel object recognition index in the NOR, and the longer escape latency and swimming distance in the acquisition of MWM, decreased duration and less frequency in the target quadrant during the navigation phase of MWW. Moreover, our results showed that the microglia was aggregated around the injection site, and the number of activated microglia increased remarkably in the DG of the model mice. Furthermore, apart from the increased abundance of $A\beta_{1-42}$ and Tau in the hippocampus and PFC of the model mice, the expression of NMDAR2A, NMDAR2B, SynGAP, PSD95, BDNF, and phosphorylated β-catenin were remarkably reduced in the hippocampus and the PFC, and the phosphorylation of GSK-3β was declined in the hippocampus. The alterations in the neuroinflammatory and neuroendocrine responses, together with the adaptive changes of synapse plasticity and Wnt signaling pathway, supported again the network hypothesis of AD that compromised functionality of relevant neural networks may underlie the development of AD symptomatology.

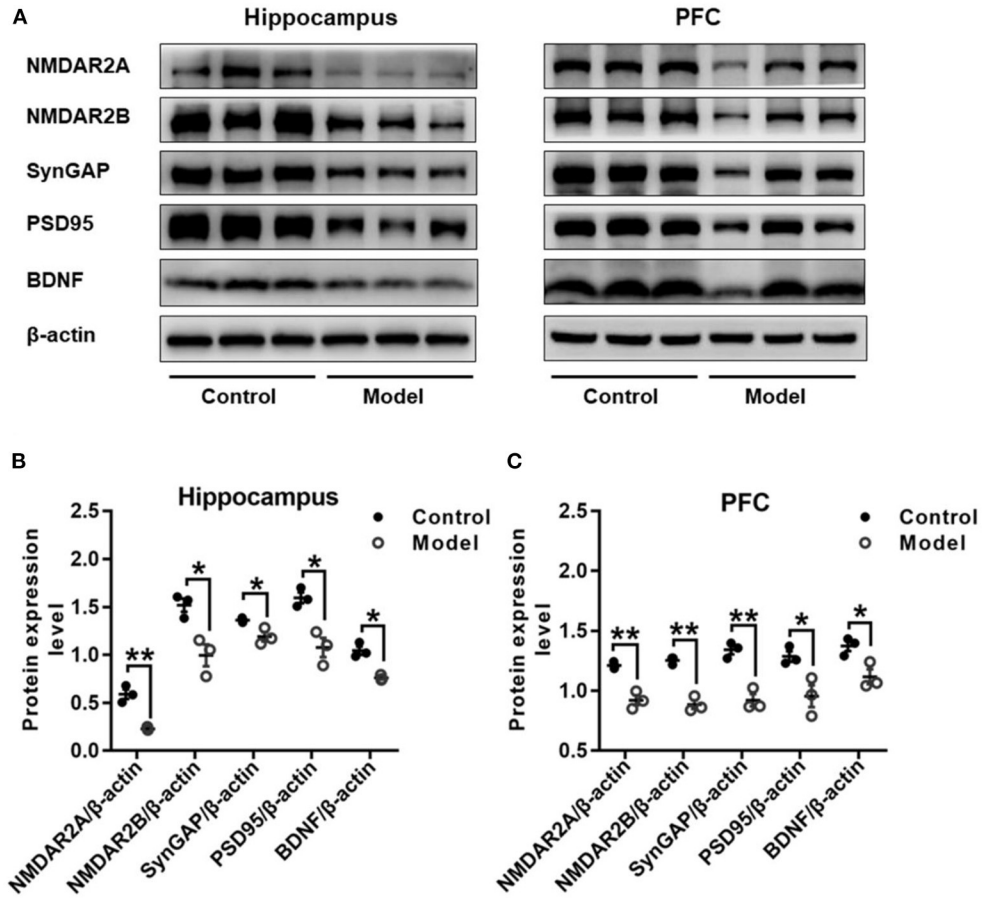

FIGURE 8 | Effects of bilaterally hippocampal injection of STZ on the expression of synaptic plasticity related proteins in the hippocampus and PFC of model mice. Typical graph **(A)** and statistical analyses **(B,C)** of the western blot results. Data in **(B,C)** are presented as the mean ± SEM ($n = 3$ for each group). In the hippocampus **(A,B)**, the expression of NMDAR2A, NMDAR2B, SynGAP, PSD95, and BDNF was all decreased in the model group. The proteins expression situation in PFC is similar to that in hippocampus **(A,C)**. $^{*}P < 0.05$, $^{**}P < 0.01$; compared with the control group.

STZ belongs to the family of glucosamine-nitrosourea compound and DNA alkylating reagent, and could be transferred to the cells alone by means of glucose transporters protein 2 (GLUT2). Peripheral injection of STZ is used widely to induce animal models of diabetes mellitus, as it could kill the pancreatic β cells high selectively at a dose-dependently manner and induce glucose metabolism disorder. Given the important role of insulin in the regulation of synaptic plasticity and the close relationship between diabetes mellitus and AD, STZ is also reported to be used in establishing AD animal models (Agrawal et al., 2011; Rai et al., 2014). It has been reported that intracerebroventricular (icv) injection of STZ could cause not only the dysfunction of insulin/ insulin-like growth factor (IGF) pathway, but also the impaired learning and memory ability in mice (Agrawal et al., 2011). Consistently, in the present study, our results showed that bilateral injection of STZ into the dorsal hippocampus could induce a significant increase of serum insulin level in mice. These results suggest that there might other mechanism underling the effect of STZ on insulin secretion and glucose regulation, besides directly killing the pancreatic β cells.

To investigate the behavioral changes induced by central administration of STZ and its subsequent increase of serum insulin concentration, a series of behavioral tests were performed in the present study. The results showed that hippocampal injected with STZ could induce an impairment of learning and memory in mice, together with decreased spontaneous movement and exploratory behaviors, which was consistent with the findings in previous studies of STZ icv injected mice (Zhang et al., 2016; Sorial and El Sayed, 2017; Moreira-Silva et al., 2018). There was no significant difference between groups as regard to the behavioral performance in the TST, SPT, and RT, indicating that a bilaterally hippocampal injection of STZ might not enough to induce despair, anhedonia, and impairments of balance and coordination activity in mice. On the whole, these results showed that bilateral hippocampal STZ injection could successfully induce a turbulence of insulin abundance and trigger task-specific AD-like behavior changes in mice. Together with the increased expression $A\beta_{1-42}$ and Tau in the hippocampus and PFC, our results indicated that bilaterally hippocampal injection of STZ should be an effective method to establish an AD-like mice

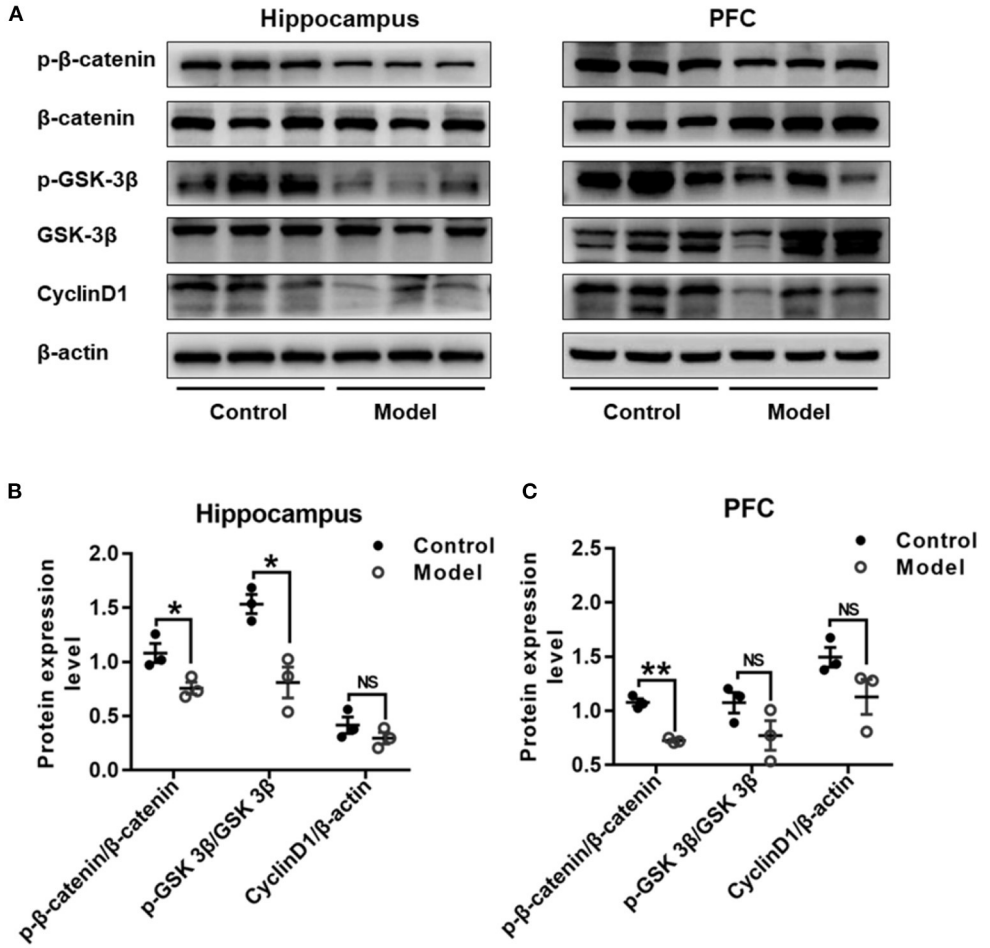

FIGURE 9 | Effect of bilaterally hippocampal injection of STZ on the key protein expression of Wnt/β-catenin pathway in the hippocampus and prefrontal cortex of model mice. Typical graph **(A)** and statistical analyses **(B,C)** of the western blot results. Data in **(B,C)** are presented as the mean ± SEM ($n = 3$ for each group). In the hippocampus **(A,B)**, the expression of p-β-catenin/β-catenin and p-GSK-3β(ser9)/GSK-3β was decreased in the model group, without CyclinD1. In PFC **(A,C)**, although the expression of p-β-catenin/β-catenin of model mice was lesser than that of control mice, but not p-GSK-3β (ser9)/GSK-3β and CyclinD1. $^{*}P < 0.05$, $^{**}P < 0.01$; compared with the control group, NS is no significance.

model, with the advantages of clear location, accurate dose and direct effect.

Nesfatin-1 is a satiety factor widely expressed in both central and peripheral tissues. Apart from the function of regulating feeding behavior and energy metabolism, nesfatin-1 has been reported to participate in the pathogenesis of anxiety, depression and other neuropsychiatric behaviors. Results of our previous study demonstrated that peripheral abundance of nesfatin-1 could be changed by high-fat diet and chronic stress, and ip injection of nesfatin-1 could induce anxiety and depression-like behavioral disorder in rats, together with the change of hippocampal synaptic plasticity (Ge et al., 2015; Chen et al., 2019). Higher plasma level of nesfatin-1 was also reported in AD or diabetes mellitus patients and animal models (Dong et al., 2013; Alpua and Kisa, 2019), with significant correlation to the cognitive dysfunction. In the present study, our results showed that the serum nesfatin-1 concentration was increased in the bilaterally hippocampal STZ-injected mice. Although the mechanism remains unclear, these results provide new evidence that nesfatin-1 might be involved with the insulin metabolism disorder-associated cognitive impairment in AD.

Neuro-inflammation has long been taken as a critical factor in the pathological of AD. It has been demonstrated that microglia can be activated by Aβ deposition, thereby secreting various inflammatory cytokines and inducing the activation of the complement system (Marttinen et al., 2018). In turn, the reactive inflammatory response will induce a further activation of microglia, as a vicious circle, ultimately leading to the neuronal dysfunction. Iba-1 is a specific marker of microglia, and CD68 is also used to label activated microglia. Increased expressions of Iba-1 and GFAP have been identified in the hippocampus of adult rats or mice received icv administration of STZ (Dos Santos et al., 2020). In line with these findings, in the present study, the activation of microglia was observed in the STZ model

group as indicated by aggregation and increased expression of Iba-1 and CD68 in the dentate gyrus of hippocampal tissues, The data is consistent with the phenomenon of a marked increase in CD68-labeled activated microglia in AD brain slices of APP/PS1 transgenic mouse (Gallagher et al., 2012). However, there was no significant difference between groups as regard to the expression of GFAP, which is taken as a marker of astrocytes activation. Although there was no exact interpret for this discrepancy, it has been reported that microglial cells act as first line of defense against immune responses in the brain, while astrocytes are neurosupportive in nature (Kraft et al., 2009; Kirkley et al., 2017). Microglial responses are often rapid, as compared with the more delayed activation of astrocytes against stimulation (Zhang et al., 2010; Kaur et al., 2019). Moreover, in many neurodegenerative diseases including AD, activation of microglia is reported to precede astrogliosis and overt neuronal loss (Kirkley et al., 2017). Although the dynamic changes of both microglia and astrocytes activation were not observed in this study, our results, together with the findings in other reports, suggested again that temporally distinct signaling events are required for a reactive phenotype in different type of glial cell.

The doublecortin (DCX) is considered as a molecular marker of neurogenesis in hippocampal dentate gyrus and only expressed in the newborn neurons, and significantly reduced number of newborn neurons labeled with DCX was demonstrated in the hippocampus of an AD rat model induced by icv injection of STZ (Mishra et al., 2018). In this present study, there was just a downward trend of DCX immune-positive cells in the dentate gyrus of the model mice, without a significant difference between groups. These results indicated that the reactive inflammatory response was activated after bilaterally hippocampal injection of STZ, together with subtle decline of neurogenesis. These changes might interpret partly the impairment of learning and memory of AD-like model mice induced by STZ hippocampal injection. However, more detailed investigation should be carried out focusing on the delicate shifts and the potential mechanism in the future.

Brain-derived neurotrophic factor (BDNF) can provide neurotrophic support for different neuronal populations including 5-HT and is a seminal regulator of synaptic plasticity. Decreased BDNF concentration has been reported in serum and CSF of AD patients, with a significantly positive relationship between the degree of decline and the severity of cognitive dysfunction (Li et al., 2009; Ng et al., 2019). Moreover, it has been demonstrated that lateral ventricle injection of nerve growth factor can significantly improve the cognitive abilities of AD transgenic mice by up-regulating the hippocampal expression of BDNF. Furthermore, BDNF can reverse neuron loss, improve cognitive impairment, and provide substantial protection for important neural circuits associated with AD (Nigam et al., 2017). Consistent with these findings, our results showed a decreased protein expression of BDNF in the hippocampus and the PFC of bilaterally hippocampal STZ-injected mice, suggesting the central role of BDNF in the pathogenesis of AD again. It has been reported that astrocytes could secrete BDNF to promote the development and survival of the central nervous system (de Pins et al., 2019). However, in the present study, the results of immunofluorescent staining showed no significant difference between groups about the number of astrocytes in the DG, indicating that the decreased expression of BDNF in the hippocampus and PFC of STZ-injected mice may not be regulated totally by the astrocytes.

NMDARs serve as modulators of synaptic transmission in the mammalian central nervous system with both short-term and long-lasting effects, and take responsible for maintaining the neuronal excitability, Ca^{2+} influx, and memory formation (Kamat et al., 2016). BDNF is reported to bind with TrkB and promote the activation of NMDAR and the aggregation of PSD95 through the PI3K-Akt pathway to regulate synaptic plasticity (Yoshii and Constantine-Paton, 2007). Over-activation of NMDAR could lead to neuronal cell death, excessive influx of Ca^{2+}, and abnormal generation of free radicals, which drives synaptic dysfunction and hyper-phosphorylation of Tau protein (Rai et al., 2013). Memantine, the NMDA receptor antagonist, has been reported to improve the cognitive function of AD patients by improving the activity of glutamatergic neurons (Hong et al., 2018; Jason and Andrew, 2018). Besides, the content of phosphorylated and non-phosphorylated NMDAR subunits in the hippocampus of AD patients are reduced (Sze et al., 2001). Consistently, in SAMP8 mice or AD models injected with $A\beta_{25-35}$ or $A\beta_{1-42}$, the expression of NMDAR1, NMDAR2A, and NMDAR2B were decreased markedly in the hippocampus or cortex (Xu et al., 2016; Wang K. et al., 2018; Chang et al., 2020). Moreover, it has been demonstrated that ketamine, a non-competitive NMDAR antagonist, could ameliorate the impaired learning and memory of developing mice induced by repetitive mechanical stress, and the mechanism may be associated with the increased hippocampal BDNF expression (Peng et al., 2011; Chang et al., 2018). In this present study, the expression of NMDAR2A and NMDAR2B in the hippocampus and PFC of mice were significantly down-regulated after bilaterally hippocampal injection of STZ, and a significant positive correlation was found between the protein expression of BDNF and NMDAR2A. These results further confirmed the central role of BDNF in the pathogenesis of AD and the close relationship between BDNF and NMDARs.

Synaptic plasticity is the material basis for regulating learning and memory functions and emotional states. The PDZ domain of PSD95 can be combined with the intracellular domain of the NMDAR2 subunit, thereby anchoring NMDAR to the post-synaptic densities, based on which NMDAR can exert a biological function on synapses (Chen et al., 2015). Unsurprising, PSD95 is reported decreased in the hippocampus of APP/PS1 AD transgenic mice (Zhang et al., 2020). SynGAP, a protein enriched in excitatory synapses, can integrate with PSD95, Shank and Ca^{2+}/CaMKII to form a complex that plays a key role in synaptic plasticity (Kim et al., 1998). Aβ oligomers have been reported to be capable of instigating synapse dysfunction and deterioration via binding with SynGAP, subsequently aggravating the course of AD (Ding et al., 2019). Results of postmortem study showed that the SynGAP levels in the PSD were remarkably declined in the PFC of AD patients (Gong et al., 2009). Compared with that of control group, the expressions of SynGAP and PSD95 in the hippocampus and the PFC of AD model mice

was significantly down-regulated in the present study. Apart from the significant positive correlation between BDNF and NMDAR2A, the protein expression of SynGAP and PSD95 were also remarkably correlated with the expression of BDNF. Together with the shifted expression of BDNF and NMDARs in this study, our result suggests again that the synaptic plasticity, involved with the balance of multiple proteins and multiple receptors, play a critical role in the pathogenesis of AD.

Dysfunction of the Wnt/β-catenin signaling pathway is also involved in the progress of AD, which is manifested by the decreased level in β-catenin and increased activity of GSK-3β. The inhibition of Wnt/β-catenin pathway is reported to promote massive accumulation of Aβ and Tau hyper-phosphorylation, and Aβ in turn inhibits the Wnt/β-catenin pathway, eventually resulting in neurofibrillary tangles in AD patients and worsening the course of AD (Jia et al., 2019). Moreover, it has been demonstrated that blocking Wnt/β-catenin pathway could down-regulate the expression of BDNF induced by NMDAR activation in the primary cortical neurons of mice, whereas activation of Wnt/β-catenin pathway could stimulate and increase BDNF expression (Zhang et al., 2018). In this present study, the phosphorylation of β-catenin and GSK-3β (ser9) were decreased in the hippocampus or PFC of mice after bilaterally hippocampal injection of STZ, although the expression of CyclinD1 was not significantly different between groups. The phosphorylation of GSK-3β at ser9 inhibited the activity of GSK-3β, and the reduced phosphorylation of GSK-3β (ser9) in the hippocampus indicated the abnormal increased activity of GSK-3β. It has been demonstrated that GSK-3β could directly inhibit the expression of BDNF by phosphorylation of CREB (Grimes and Jope, 2001). In the present study, the protein expression of p-GSK-3β/GSK-3β was positively correlated with BDNF. These results indicated again the expression pattern of Wnt/β-catenin signaling pathway might be associated with the pathogenesis of STZ-induced AD, and BDNF might be taken as an important factor linking the imbalanced protein expression to the changed synaptic plasticity.

There were several limitations in the current study. First, although the central role of BDNF in the AD-like neurobiological changes induced by bilateral hippocampal STZ injection was suggested, it was not further identified by intervening the abundance or function of BDNF. Moreover, the correlation between BDNF and insulin or nesfatin-1, need to be observed in our further studies. Additionally, although increased expression of $A\beta_{1-42}$ and Tau was demonstrated in this study, it is better to investigate the abundance of Aβ and more phosphorylation-site of Tau in detail.

In summary, our results showed that a bilaterally hippocampal injection of STZ could successfully induce AD-like behaviors in mice. Moreover, dysfunctional neuroendocrine response was also found in the bilaterally hippocampal STZ-injected mice, as indicated by the increased serum concentration of insulin and nesfatin-1. Apart from the hippocampal inflammatory response, the mechanism might be associated with the imbalanced expression of synaptic plasticity-related proteins in hippocampus and PFC, including NMDAR2A, NMDAR2B, SynGAP, PSD95, and BDNF. Moreover, the dysfunction of Wnt/β-catenin pathway, especially the decrease in the phosphorylation of β-catenin and GSK-3β, may also be involved in AD-like pathological process. Given the relationship between BDNF and the imbalanced expression of proteins associated with regulation of synaptic plasticity in the hippocampus and the PFC, the central role of BDNF was self-evident. These findings might provide new evidence for understanding the pathogenesis of STZ-associated AD.

DATA AVAILABILITY STATEMENT

The original contributions presented in the study are included in the article/**Supplementary Material**, further inquiries can be directed to the corresponding author.

ETHICS STATEMENT

The animal study was reviewed and approved by the Animal Experimentation Ethics Committee of Tongji University School of Medicine.

AUTHOR CONTRIBUTIONS

C-CQ and X-XC performed most of the experiments, analyzed the data, and wrote the manuscript. X-RG performed Western blotting analysis. J-XX and SL modified the pictures. C-CQ and J-FG designed of the study. J-FG conceived the study and revised the manuscript. All authors read and approved the final manuscript.

FUNDING

Funding for this study was provided by the Natural Science Foundation of China (81870403, 81401122) and Anhui Medical University Basic and Clinical Cooperative Research Promotion Plan (2020xkjT036). These institutions had no role in the study design; the collection, analysis, or interpretation of the data; the writing of the manuscript, or the decision to submit the paper for publication.

ACKNOWLEDGMENTS

The authors would like to thank Dr. Qiong Zhang and Ling Hu who assisted in the experiments of molecular biology and statistical analysis of data. The preprint of this manuscript has been displayed in bioRxiv without copyright.

SUPPLEMENTARY MATERIAL

The Supplementary Material for this article can be found online at: https://www.frontiersin.org/articles/10.3389/fnagi.2021.633495/full#supplementary-material

REFERENCES

Agrawal, R., Tyagi, E., Shukla, R., and Nath, C. (2011). Insulin receptor signaling in rat hippocampus: a study in STZ (ICV) induced memory deficit model. *Eur. Neuropsychopharmacol.* 21, 261–273. doi: 10.1016/j.euroneuro.2010.11.009

Alpua, M., and Kisa, U. (2019). Nesfatin-1 and caspase-cleaved cytokeratin-18: promising biomarkers for Alzheimer's disease? *Bratisl. Lek. Listy* 120, 295–298. doi: 10.4149/BLL_2019_046

Ballesteros, J. J., Buschler, A., Köhr, G., and Manahan-Vaughan, D. (2016). Afferent input selects NMDA receptor subtype to determine the persistency of hippocampal LTP in freely behaving mice. *Front. Synaptic Neurosci.* 8:33. doi: 10.3389/fnsyn.2016.00033

Brigman, J. L., Wright, T., Talani, G., Prasad-Mulcare, S., Jinde, S., Seabold, G. K., et al. (2010). Loss of GluN2B-containing NMDA receptors in CA1 hippocampus and cortex impairs long-term depression, reduces dendritic spine density, and disrupts learning. *J. Neurosci.* 30, 4590–4600. doi: 10.1523/JNEUROSCI.0640-10.2010

Chang, C. H., Su, C. L., and Gean, P. W. (2018). Mechanism underlying NMDA blockade-induced inhibition of aggression in post-weaning socially isolated mice. *Neuropharmacology* 143, 95–105. doi: 10.1016/j.neuropharm.2018.09.019

Chang, K. W., Zong, H. F., Rizvi, M. Y., Ma, K. G., Zhai, W., Wang, M., et al. (2020). Modulation of the MAPKs pathways affects Abeta-induced cognitive deficits in Alzheimer's disease via activation of alpha7nAChR. *Neurobiol. Learn. Mem.* 168:107154. doi: 10.1016/j.nlm.2019.107154

Chen, X., Levy, J. M., Hou, A., Winters, C., Azzam, R., Sousa, A. A., et al. (2015). PSD-95 family MAGUKs are essential for anchoring AMPA and NMDA receptor complexes at the postsynaptic density. *Proc. Natl. Acad. Sci. U. S. A.* 112, E6983–6992. doi: 10.1073/pnas.1517045112

Chen, X.-X., Xu, Y.-Y., Wu, R., Chen, Z., Fang, K., Han, Y.-X., et al. (2019). Resveratrol reduces glucolipid metabolic dysfunction and learning and memory impairment in a NAFLD rat model: involvement in regulating the imbalance of Nesfatin-1 abundance and Copine 6 expression. *Front. Endocrinol. (Lausanne)* 10:434. doi: 10.3389/fendo.2019.00434

Dai, J. X., Han, H. L., Tian, M., Cao, J., Xiu, J. B., Song, N. N., et al. (2008). Enhanced contextual fear memory in central serotonin-deficient mice. *Proc. Natl. Acad. Sci. U. S. A.* 105, 11981–11986. doi: 10.1073/pnas.0801329105

de Pins, B., Cifuentes-Diaz, C., Farah, A. T., Lopez-Molina, L., Montalban, E., Sancho-Balsells, A., et al. (2019). Conditional BDNF delivery from astrocytes rescues memory deficits, spine density, and synaptic properties in the 5xFAD mouse model of Alzheimer disease. *J. Neurosci.* 39, 2441–2458. doi: 10.1523/JNEUROSCI.2121-18.2019

Devi, L., and Ohno, M. (2013). Effects of levetiracetam, an antiepileptic drug, on memory impairments associated with aging and Alzheimer's disease in mice. *Neurobiol. Learn. Mem.* 102, 7–11. doi: 10.1016/j.nlm.2013.02.001

Ding, Y., Zhao, J., Zhang, X., Wang, S., Viola, K. L., Chow, F. E., et al. (2019). Amyloid beta oligomers target to extracellular and intracellular neuronal synaptic proteins in Alzheimer's disease. *Front. Neurol.* 10:1140. doi: 10.3389/fneur.2019.01140

Dong, J., Xu, H., Xu, H., Wang, P. F., Cai, G. J., Song, H. F., et al. (2013). Nesfatin-1 stimulates fatty-acid oxidation by activating AMP-activated protein kinase in STZ-induced type 2 diabetic mice. *PLoS ONE* 8:e83397. doi: 10.1371/journal.pone.0083397

Dos Santos, J. P. A., Vizuete, A. F., and Goncalves, C. A. (2020). Calcineurin-mediated hippocampal inflammatory alterations in streptozotocin-induced model of dementia. *Mol. Neurobiol.* 57, 502–512. doi: 10.1007/s12035-019-01718-2

Folke, J., Pakkenberg, B., and Brudek, T. (2019). Impaired Wnt signaling in the prefrontal cortex of Alzheimer's disease. *Mol. Neurobiol.* 56, 873–891. doi: 10.1007/s12035-018-1103-z

Gaesser, J. M., and Fyffe-Maricich, S. L. (2016). Intracellular signaling pathway regulation of myelination and remyelination in the CNS. *Exp. Neurol.* 283, 501–511. doi: 10.1016/j.expneurol.2016.03.008

Gallagher, J. J., Finnegan, M. E., Grehan, B., Dobson, J., Collingwood, J. F., and Lynch, M. A. (2012). Modest amyloid deposition is associated with iron dysregulation, microglial activation, and oxidative stress. *J. Alzheimers. Dis.* 28, 147–161. doi: 10.3233/JAD-2011-110614

Ge, J.-F., Xu, Y.-Y., Qin, G., Peng, Y.-N., Zhang, C.-F., Liu, X.-R., et al. (2015). Depression-like behavior induced by Nesfatin-1 in rats: involvement of increased immune activation and imbalance of synaptic vesicle proteins. *Front. Neurosci.* 9:429. doi: 10.3389/fnins.2015.00429

Gong, Y., Lippa, C. F., Zhu, J., Lin, Q., and Rosso, A. L. (2009). Disruption of glutamate receptors at Shank-postsynaptic platform in Alzheimer's disease. *Brain Res.* 1292, 191–198. doi: 10.1016/j.brainres.2009.07.056

Grimes, C. A., and Jope, R. S. (2001). CREB DNA binding activity is inhibited by glycogen synthase kinase-3 beta and facilitated by lithium. *J. Neurochem.* 78, 1219–1232. doi: 10.1046/j.1471-4159.2001.00495.x

Henneberger, C., Bard, L., King, C., Jennings, A., and Rusakov, D. A. (2013). NMDA receptor activation: two targets for two co-agonists. *Neurochem. Res.* 38, 1156–1162. doi: 10.1007/s11064-013-0987-2

Hiser, J., and Koenigs, M. (2018). The multifaceted role of the ventromedial prefrontal cortex in emotion, decision making, social cognition, and psychopathology. *Biol. Psychiatry* 83, 638–647. doi: 10.1016/j.biopsych.2017.10.030

Hong, Y. J., Choi, S. H., Jeong, J. H., Park, K. W., and Na, H. R. (2018). Effectiveness of anti-dementia drugs in extremely severe Alzheimer's disease: a 12-week, multicenter, randomized, single-blind study. *J. Alzheimers. Dis.* 63, 1035–1044. doi: 10.3233/JAD-180159

Hung, S. Y., and Fu, W. M. (2017). Drug candidates in clinical trials for Alzheimer's disease. *J. Biomed. Sci.* 24:47. doi: 10.1186/s12929-017-0355-7

Jahanshahi, M., Saeidi, M., Nikmahzar, E., Babakordi, F., and Bahlakeh, G. (2019). Effects of hCG on reduced numbers of hCG receptors in the prefrontal cortex and cerebellum of rat models of Alzheimer's disease. *Biotech. Histochem.* 94, 360–365. doi: 10.1080/10520295.2019.1571228

Jason, W., and Andrew, B. (2018). Current understanding of Alzheimer's disease diagnosis and treatment. F1*000Research* 7:1. doi: 10.12688/f1000research.14506.1

Jia, L., Pina-Crespo, J., and Li, Y. (2019). Restoring Wnt/beta-catenin signaling is a promising therapeutic strategy for Alzheimer's disease. *Mol. Brain* 12:104. doi: 10.1186/s13041-019-0525-5

Kamat, P. K., Kalani, A., Rai, S., Swarnkar, S., Tota, S., Nath, C., et al. (2016). Mechanism of oxidative stress and synapse dysfunction in the pathogenesis of Alzheimer's disease: understanding the therapeutics strategies. *Mol. Neurobiol.* 53, 648–661. doi: 10.1007/s12035-014-9053-6

Kandimalla, R., Manczak, M., Yin, X., Wang, R., and Reddy, P. H. (2018). Hippocampal phosphorylated tau induced cognitive decline, dendritic spine loss and mitochondrial abnormalities in a mouse model of Alzheimer's disease. *Hum. Mol. Genet.* 27, 30–40. doi: 10.1093/hmg/ddx381

Kaur, D., Sharma, V., and Deshmukh, R. (2019). Activation of microglia and astrocytes: a roadway to neuroinflammation and Alzheimer's disease. *Inflammopharmacology* 27, 663–677. doi: 10.1007/s10787-019-00580-x

Ke, F., Li, H.-R., Chen, X.-X., Gao, X.-R., Huang, L.-L., Du, A.-Q., et al. (2020). Quercetin alleviates LPS-induced depression-like behavior in rats via regulating BDNF-related imbalance of copine 6 and TREM1/2 in the hippocampus and PFC. *Front. Pharmacol.* 10:1544. doi: 10.3389/fphar.2019.01544

Kim, J. H., Liao, D., Lau, L. F., and Huganir, R. L. (1998). SynGAP: a synaptic RasGAP that associates with the PSD-95/SAP90 protein family. *Neuron* 20, 683–691. doi: 10.1016/S0896-6273(00)81008-9

Kirkley, K. S., Popichak, K. A., Afzali, M. F., Legare, M. E., and Tjalkens, R. B. (2017). Microglia amplify inflammatory activation of astrocytes in manganese neurotoxicity. *J. Neuroinflammation.* 14:99. doi: 10.1186/s12974-017-0871-0

Kraft, A. D., McPherson, C. A., and Harry, G. J. (2009). Heterogeneity of microglia and TNF signaling as determinants for neuronal death or survival. *Neurotoxicology* 30, 785–793. doi: 10.1016/j.neuro.2009.07.001

Li, G., Peskind, E. R., Millard, S. P., Chi, P., Sokal, I., Yu, C. E., et al. (2009). Cerebrospinal fluid concentration of brain-derived neurotrophic factor and cognitive function in non-demented subjects. *PLoS ONE* 4:e5424. doi: 10.1371/journal.pone.0005424

Li, H., Wu, J., Zhu, L., Sha, L., Yang, S., Wei, J., et al. (2018). Insulin degrading enzyme contributes to the pathology in a mixed model of Type 2 diabetes and Alzheimer's disease: possible mechanisms of IDE in T2D and AD. *Biosci. Rep.* 38:BSR20170862. doi: 10.1042/BSR20170862

Liu, C. C., Tsai, C. W., Deak, F., Rogers, J., Penuliar, M., Sung, Y. M., et al. (2014). Deficiency in LRP6-mediated Wnt signaling contributes to synaptic abnormalities and amyloid pathology in Alzheimer's disease. *Neuron* 84, 63–77. doi: 10.1016/j.neuron.2014.08.048

Magdesian, M. H., Carvalho, M. M., Mendes, F. A., Saraiva, L. M., Juliano, M. A., Juliano, L., et al. (2008). Amyloid-beta binds to the extracellular cysteine-rich domain of Frizzled and inhibits Wnt/beta-catenin signaling. *J. Biol. Chem.* 283, 9359–9368. doi: 10.1074/jbc.M707108200

Marttinen, M., Takalo, M., Natunen, T., Wittrahm, R., Gabbouj, S., Kemppainen, S., et al. (2018). Molecular mechanisms of synaptotoxicity and neuroinflammation in Alzheimer's disease. *Front. Neurosci.* 12:963. doi: 10.3389/fnins.2018.00963

Miao, Y., Wang, N., Shao, W., Xu, Z., Yang, Z., Wang, L., et al. (2019). Overexpression of TIPE2, a negative regulator of innate and adaptive immunity, attenuates cognitive deficits in APP/PS1 mice. *J. Neuroimmune Pharmacol.* 14, 519–529. doi: 10.1007/s11481-019-09861-2

Mishra, S. K., Singh, S., Shukla, S., and Shukla, R. (2018). Intracerebroventricular streptozotocin impairs adult neurogenesis and cognitive functions via regulating neuroinflammation and insulin signaling in adult rats. *Neurochem. Int.* 113, 56–68. doi: 10.1016/j.neuint.2017.11.012

Moreira-Silva, D., Carrettiero, D. C., Oliveira, A. S. A., Rodrigues, S., Dos Santos-Lopes, J., Canas, P. M., et al. (2018). Anandamide effects in a streptozotocin-induced Alzheimer's disease-like sporadic dementia in rats. *Front. Neurosci.* 12:653. doi: 10.3389/fnins.2018.00653

Muller, M. K., Jacobi, E., Sakimura, K., Malinow, R., and von Engelhardt, J. (2018). NMDA receptors mediate synaptic depression, but not spine loss in the dentate gyrus of adult amyloid Beta (Abeta) overexpressing mice. *Acta Neuropathol Commun.* 6:110. doi: 10.1186/s40478-018-0611-4

Ng, T. K. S., Ho, C. S. H., Tam, W. W. S., Kua, E. H., and Ho, R. C. (2019). Decreased serum brain-derived neurotrophic factor (BDNF) levels in patients with Alzheimer's Disease (AD): a systematic review and meta-analysis. *Int. J. Mol. Sci.* 20:57. doi: 10.3390/ijms20020257

Nigam, S. M., Xu, S., Kritikou, J. S., Marosi, K., Brodin, L., and Mattson, M. P. (2017). Exercise and BDNF reduce Abeta production by enhancing alpha-secretase processing of APP. *J. Neurochem.* 142, 286–296. doi: 10.1111/jnc.14034

Peng, S., Zhang, Y., Wang, H., Ren, B., and Zhang, J. (2011). Anesthetic ketamine counteracts repetitive mechanical stress-induced learning and memory impairment in developing mice. *Mol. Biol. Rep.* 38, 4347–4351. doi: 10.1007/s11033-010-0561-9

Pruski, M., Hu, L., Yang, C., Wang, Y., Zhang, J. B., Zhang, L., et al. (2019). Roles for IFT172 and primary cilia in cell migration, cell division, and neocortex development. *Front Cell Dev Biol.* 7:287. doi: 10.3389/fcell.2019.00287

Rai, S., Kamat, P. K., Nath, C., and Shukla, R. (2013). A study on neuroinflammation and NMDA receptor function in STZ (ICV) induced memory impaired rats. *J. Neuroimmunol.* 254, 1–9. doi: 10.1016/j.jneuroim.2012.08.008

Rai, S., Kamat, P. K., Nath, C., and Shukla, R. (2014). Glial activation and post-synaptic neurotoxicity: the key events in Streptozotocin (ICV) induced memory impairment in rats. *Pharmacol. Biochem. Behav.* 117, 104–117. doi: 10.1016/j.pbb.2013.11.035

Rodriguez, J. J., Noristani, H. N., Olabarria, M., Fletcher, J., Somerville, T. D., Yeh, C. Y., et al. (2011). Voluntary running and environmental enrichment restores impaired hippocampal neurogenesis in a triple transgenic mouse model of Alzheimer's disease. *Curr. Alzheimer Res.* 8, 707–717. doi: 10.2174/156720511797633214

Sorial, M. E., and El Sayed, N. (2017). Protective effect of valproic acid in streptozotocin-induced sporadic Alzheimer's disease mouse model: possible involvement of the cholinergic system. *Naunyn Schmiedebergs. Arch. Pharmacol.* 390, 581–593. doi: 10.1007/s00210-017-1357-4

Syed, Y. Y. (2020). Correction to: Sodium oligomannate: first approval. *Drugs* 80, 445–446. doi: 10.1007/s40265-020-01274-3

Sze, C.-I., Bi, H., Kleinschmidt-DeMasters, B. K., Filley, C. M., and Martin, L. J. (2001). N -Methyl- d -aspartate receptor subunit proteins and their phosphorylation status are altered selectively in Alzheimer's disease. *J. Neurol. Sci.* 182, 151–159. doi: 10.1016/S0022-510X(00)00467-6

Tapia-Rojas, C., and Inestrosa, N. C. (2018). Loss of canonical Wnt signaling is involved in the pathogenesis of Alzheimer's disease. *Neural Regen. Res.* 13, 1705–1710. doi: 10.4103/1673-5374.238606

Teixeira, C. M., Pallas-Bazarra, N., Bolos, M., Terreros-Roncal, J., Avila, J., and Llorens-Martin, M. (2018). Untold New beginnings: adult hippocampal neurogenesis and Alzheimer's disease. *J. Alzheimers Dis.* 64, 497–505. doi: 10.3233/JAD-179918

Wang, C.-C., Held, R. G., Chang, S.-C., Yang, L., Delpire, E., Ghosh, A., et al. (2011). A critical role for GluN2B-containing NMDA receptors in cortical development and function. *Neuron* 72, 789–805. doi: 10.1016/j.neuron.2011.09.023

Wang, D., Wang, C., Liu, L., and Li, S. (2018). Protective effects of evodiamine in experimental paradigm of Alzheimer's disease. *Cogn. Neurodyn.* 12, 303–313. doi: 10.1007/s11571-017-9471-z

Wang, K., Sun, W., Zhang, L., Guo, W., Xu, J., Liu, S., et al. (2018). Oleanolic acid ameliorates abeta25-35 injection-induced memory deficit in Alzheimer's disease model rats by maintaining synaptic plasticity. *CNS Neurol. Disord. Drug Targets* 17, 389–399. doi: 10.2174/1871527317666180525113109

Wang, X., Sun, G., Feng, T., Zhang, J., Huang, X., Wang, T., et al. (2019). Sodium oligomannate therapeutically remodels gut microbiota and suppresses gut bacterial amino acids-shaped neuroinflammation to inhibit Alzheimer's disease progression. *Cell Res.* 29, 787–803. doi: 10.1038/s41422-019-0216-x

Xu, P., Xu, S. P., Wang, K. Z., Lu, C., Zhang, H. X., Pan, R. L., et al. (2016). Cognitive-enhancing effects of hydrolysate of polygalasaponin in SAMP8 mice. *J. Zhejiang Univ. Sci. B* 17, 503–514. doi: 10.1631/jzus.B1500321

Yoshii, A., and Constantine-Paton, M. (2007). BDNF induces transport of PSD-95 to dendrites through PI3K-AKT signaling after NMDA receptor activation. *Nat. Neurosci.* 10, 702–711. doi: 10.1038/nn1903

Zameer, S., Kaundal, M., Vohora, D., Ali, J., Kalam Najmi, A., and Akhtar, M. (2019). Ameliorative effect of alendronate against intracerebroventricular streptozotocin induced alteration in neurobehavioral, neuroinflammation and biochemical parameters with emphasis on Abeta and BACE-1. *Neurotoxicology* 70, 122–134. doi: 10.1016/j.neuro.2018.11.012

Zhang, C. T., Lin, J. R., Wu, F., Ghosh, A., Tang, S. S., Hu, M., et al. (2016). Montelukast ameliorates streptozotocin-induced cognitive impairment and neurotoxicity in mice. *Neurotoxicology* 57, 214–222. doi: 10.1016/j.neuro.2016.09.022

Zhang, D., Hu, X., Qian, L., O'Callaghan, J. P., and Hong, J. S. (2010). Astrogliosis in CNS pathologies: is there a role for microglia? *Mol. Neurobiol.* 41, 232–241. doi: 10.1007/s12035-010-8098-4

Zhang, Q., Huang, Y., Zhang, L., Ding, Y. Q., and Song, N. N. (2019). Loss of Satb2 in the cortex and hippocampus leads to abnormal behaviors in mice. *Front. Mol. Neurosci.* 12:33. doi: 10.3389/fnmol.2019.00033

Zhang, W., Shi, Y., Peng, Y., Zhong, L., Zhu, S., Zhang, W., et al. (2018). Neuron activity-induced Wnt signaling up-regulates expression of brain-derived neurotrophic factor in the pain neural circuit. *J. Biol. Chem.* 293, 15641–15651. doi: 10.1074/jbc.RA118.002840

Zhang, X., Zhao, F., Wang, C., Zhang, J., Bai, Y., Zhou, F., et al. (2020). AVP(4-8) improves cognitive behaviors and hippocampal synaptic plasticity in the APP/PS1 Mouse model of Alzheimer's disease. *Neurosci. Bull.* 36, 254–262. doi: 10.1007/s12264-019-00434-0

Zhao, Y., Kiss, T., DelFavero, J., Li, L., Li, X., Zheng, L., et al. (2020). CD82-TRPM7-Numb signaling mediates age-related cognitive impairment. *Geroscience* 42, 595–611. doi: 10.1007/s11357-020-00166-4

Zhong, S., Zhang, S., Fan, X., Wu, Q., Yan, L., Dong, J., et al. (2018). A single-cell RNA-seq survey of the developmental landscape of the human prefrontal cortex. *Nature* 555, 524–528. doi: 10.1038/nature25980

Zhou, Y., Wang, X., Zhao, Y., Liu, A., Zhao, T., Zhang, Y., et al. (2016). Elevated thyroid peroxidase antibody increases risk of post-partum depression by decreasing prefrontal cortex BDNF and 5-HT levels in mice. *Front. Cell. Neurosci.* 10:307. doi: 10.3389/fncel.2016.00307

Zhu, F., Zheng, Y., Ding, Y. Q., Liu, Y., Zhang, X., Wu, R., et al. (2014). Minocycline and risperidone prevent microglia activation and rescue behavioral deficits induced by neonatal intrahippocampal injection of lipopolysaccharide in rats. *PLoS ONE* 9:e93966. doi: 10.1371/journal.pone.0093966

Conflict of Interest: The authors declare that the research was conducted in the absence of any commercial or financial relationships that could be construed as a potential conflict of interest.

frontiers in Aging Neuroscience

BRIEF RESEARCH REPORT
published: 04 May 2021
doi: 10.3389/fnagi.2021.637574

Cognition and Cerebrovascular Reactivity in Midlife Women With History of Preeclampsia and Placental Evidence of Maternal Vascular Malperfusion

C. Elizabeth Shaaban[1,2], Caterina Rosano[1], Ann D. Cohen[3], Theodore Huppert[4,5], Meryl A. Butters[3], James Hengenius[1], W. Tony Parks[6,7] and Janet M. Catov[1,8]*

[1] Department of Epidemiology, University of Pittsburgh, Pittsburgh, PA, United States, [2] Center for the Neural Basis of Cognition, University of Pittsburgh, Pittsburgh, PA, United States, [3] Department of Psychiatry, University of Pittsburgh, Pittsburgh, PA, United States, [4] Department of Radiology, University of Pittsburgh, Pittsburgh, PA, United States, [5] Department of Bioengineering, University of Pittsburgh, Pittsburgh, PA, United States, [6] Department of Pathology and Laboratory Medicine, Mount Sinai Hospital, Toronto, ON, Canada, [7] Department of Laboratory Medicine and Pathobiology, University of Toronto, Toronto, ON, Canada, [8] Department of Obstetrics, Gynecology and Reproductive Sciences, University of Pittsburgh, Pittsburgh, PA, United States

OPEN ACCESS

Edited by:
Stefano Tarantini, University of Oklahoma Health Sciences Center, United States

Reviewed by:
Johannes Duvekot, Erasmus MC, Netherlands
Joseph Arnold Fisher, University Health Network (UHN), Canada

***Correspondence:**
C. Elizabeth Shaaban
Beth.Shaaban@pitt.edu

Received: *03 December 2020*
Accepted: *09 April 2021*
Published: *04 May 2021*

Citation:
Shaaban CE, Rosano C, Cohen AD, Huppert T, Butters MA, Hengenius J, Parks WT and Catov JM (2021) Cognition and Cerebrovascular Reactivity in Midlife Women With History of Preeclampsia and Placental Evidence of Maternal Vascular Malperfusion. Front. Aging Neurosci. 13:637574. doi: 10.3389/fnagi.2021.637574

Background: Preeclampsia is emerging as a sex-specific risk factor for cerebral small vessel disease (SVD) and dementia, but the reason is unknown. We assessed the relationship of maternal vascular malperfusion (MVM), a marker of placental SVD, with cognition and cerebral SVD in women with and without preeclampsia. We hypothesized women with both preeclampsia and MVM would perform worst on information processing speed and executive function.

Methods: Women (n = 45; mean 10.5 years post-delivery; mean age: 41 years; 42.2% Black) were classified as preeclampsia-/MVM-, preeclampsia+/MVM-, or preeclampsia+/MVM+. Information processing speed, executive function, and memory were assessed. In a pilot sub-study of cerebrovascular reactivity (CVR; n = 22), cerebral blood flow during room-air breathing and breath-hold induced hypercapnia were obtained via arterial spin labeling MRI. Non-parametric tests and regression models were used to test associations.

Results: Between-group cognitive differences were significant for information processing speed (p = 0.02); preeclampsia+/MVM+ had the lowest scores. Cerebral blood flow increased from room-air to breath-hold, globally and in all regions in the three groups, except the preeclampsia+/MVM+ parietal region (p = 0.12). Lower parietal CVR (less change from room-air breathing to breath-holding) was correlated with poorer information processing speed (partial ρ = 0.63, p = 0.005) and executive function (ρ = 0.50, p = 0.03) independent of preeclampsia/MVM status.

Conclusion: Compared to women without preeclampsia and MVM, midlife women with both preeclampsia and MVM have worse information processing speed and may have blunted parietal CVR, an area important for information processing speed and executive function. MVM in women with preeclampsia is a promising sex-specific indicator of cerebrovascular integrity in midlife.

Keywords: arterial spin labeling, cerebral blood flow, cognitive function, hypercapnia, hypertensive disorders of pregnancy, vascular contributions to cognitive impairment and dementia

INTRODUCTION

Preeclampsia, characterized by *de novo* hypertension and end-organ dysfunction (American College of Obstetricians and Gynecologists, 2020), occurs in as many as 8% of pregnancies and affects up to 15% of women (Auger et al., 2016; Garovic et al., 2020). A common finding in preeclampsia is insufficient vascular remodeling to develop the maternal side of the placenta, the maternal decidua, with lower perfusion and small vessel disease (SVD) in the placenta (Parks, 2015).

Preeclampsia is emerging as a sex-specific risk factor for vascular contributions to cognitive impairment and dementia (VCID) in later life (Theilen et al., 2016; Basit et al., 2018; Elharram et al., 2018; Gannon et al., 2019; Andolf et al., 2020). Studies indicate preeclampsia-related differences in information processing speed, executive function, and, to some extent, also memory (Brussé et al., 2008; Fields et al., 2017; Miller et al., 2019). Neuroimaging studies indicate preeclampsia-related gray matter atrophy (Mielke et al., 2016; Siepmann et al., 2017; Miller et al., 2019) and white matter hyperintensities (Wiegman et al., 2014; Siepmann et al., 2017). Recent evidence also suggests preeclampsia-related lower cerebrovascular reactivity (CVR), an early sign of cerebral SVD, using carotid or total brain transcranial Doppler 35–40 years after pregnancy (mean age, 60 years) (Barnes et al., 2018).

The reason for the occurrence of neurovascular and cognitive deficits in preeclampsia is unknown. Associations are overall independent of cardiometabolic risk factors and cardiovascular diseases. A possible explanation is that women with preeclampsia have more severe SVD not only in the placenta, but also affecting the cerebral vasculature, which can manifest as cerebral SVD later in life. Histopathological measures of placental SVD may hold the key to capturing SVD severity during pregnancy. Decidual vasculopathy and concomitant hypoxia/reperfusion lesions in the placenta are collectively termed maternal vascular malperfusion (MVM) (Parks, 2015). MVM is emerging as a risk factor for maternal vascular risk later in life for both large (Staff et al., 2010, 2013; Stevens et al., 2014, 2015; Catov et al., 2018; Holzman et al., 2020) and small vessels (Pepine et al., 2015; Bairey Merz, 2019). We have recently found that 8–10 years after pregnancy, women with MVM have excess masked hypertension (Catov et al., 2019), sublingual microvascular dysfunction (Hauspurg et al., 2020), and reduced coronary flow reserve (Countouris et al., 2020). However, prior studies of cerebrovascular integrity did not have direct measures of SVD severity during pregnancy, and hence could not assess the relationship between preeclampsia, MVM, and cerebral dysfunction. Our primary objectives were to test the associations of MVM and preeclampsia with cognition and to carry out a pilot study to assess the feasibility of measuring CVR in whole brain and regions of interest (ROIs) in these women. We hypothesized that women with both preeclampsia and MVM would perform worst on information processing speed and executive function. Our secondary aim was to explore associations of CVR with MVM, preeclampsia, and cognition.

METHODS

Participants

Participants were drawn from an observational study of women's post-partum cardiovascular health, the WINDOWS BP Study (N = 71). Twenty-six women were enrolled before cognitive assessments began, and therefore N = 45 women were included in this study of cognitive assessments (see study participation flow in **Figure 1A**). We report neuroimaging pilot study results in N = 22. A detailed description of the neuroimaging study participation flow is provided in the Results section "Pilot Study Feasibility" and **Figure 1B**. WINDOWS BP participants were drawn from the parent WINDOWS Study (N = 498), an ancillary study to our pregnancy registry with data for all births from 2008 to 2010 at Magee-Womens Hospital, Pittsburgh, PA, United States (N = 6632); they were women who delivered a liveborn, singleton infant at Magee-Womens Hospital and who had a clinical placenta pathology report (for the index delivery). Extensive characterization of preeclampsia and placental MVM data were collected at the time of birth (2008–2010) and validated via chart review and blinded review of pathology specimens. Data on vascular and cardiometabolic factors were collected 8–10 years after delivery at the WINDOWS study visit, unless otherwise indicated. WINDOWS study participants were not currently pregnant or pregnant within the last 6 months. At the cognitive assessment study visit [mean (SD): 10.5 (0.6) years after delivery], cognitive testing and MRI were collected. Eligibility criteria for our MRI pilot study included that participants had no MRI contraindications such as claustrophobia or non-MRI cleared metal in the body. All WINDOWS study participants were stroke-free.

By design, we enrolled women with preeclampsia regardless of MVM status and women without preeclampsia had no MVM. We focused on placental severity as opposed to clinical preeclampsia severity, and we hypothesized that women with both preeclampsia and MVM would have the most adverse profile.

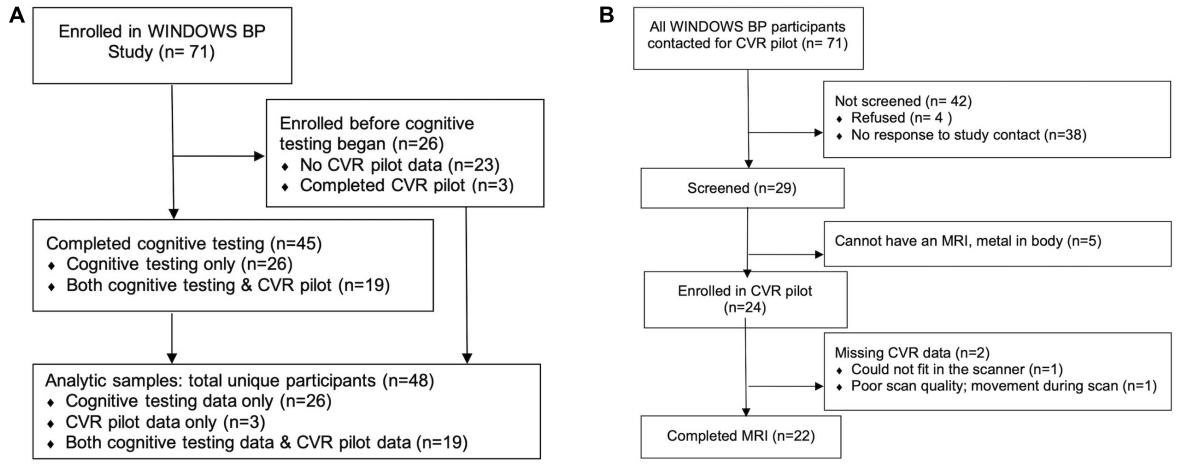

FIGURE 1 | Study participation flow diagrams. CVR, cerebrovascular reactivity. **(A)** Overall study flow diagram and **(B)** detailed study flow diagram for the cerebrovascular reactivity (CVR) pilot study.

This study was approved by the University of Pittsburgh Institutional Review Board, and all participants provided written informed consent before any study procedures were carried out.

MRI Pilot Study

In preparation for a larger planned study, we invited all participants of the WINDOWS BP study to complete an MRI with measures of CVR. We aimed to assess the feasibility of recruitment and carrying out our CVR imaging protocol and to obtain estimates of: CVR by study group, variance, and association effect sizes for cognition and CVR.

We follow the reporting guidance of Strengthening the Reporting of Observational Studies in Epidemiology (STROBE) (von Elm et al., 2007) and the Consolidated Standards of Reporting Trials (CONSORT) extension to randomized pilot and feasibility trials (Eldridge et al., 2016) based on recommendations for reporting non-randomized pilot studies that serve as preparation for larger studies and which test preliminary associations (Lancaster and Thabane, 2019).

Predictors

Preeclampsia

Preeclampsia is based on the registry medical record data for the index delivery and validated via chart abstraction. Cases were identified based on American College of Obstetricians and Gynecologists (ACOG) criteria: new-onset hypertension ($\geq$140/90 mmHg) after 20-weeks' gestation accompanied by proteinuria or other organ involvement (American College of Obstetricians and Gynecologists, 2020).

To characterize the clinical severity of preeclampsia, we report the proportion of women with the following based on the index delivery: preeclampsia with severe features based on ICD-9 code, pulmonary edema, seizures, any headache, a pre-term delivery (<37 weeks' gestation), and an infant that was small for gestational age. We also report gestational age and birth weight.

Maternal Vascular Malperfusion

Placental histopathology was used to detect MVM (Staff et al., 2010) using uniform consensus criteria (Khong et al., 2016). We classified MVM as present in the placenta if any of the following consensus rated features were identified: decidual vasculopathy, villous infarction, accelerated villous maturation, perivillous fibrin deposition, or intervillous fibrin deposition (defined in **Supplementary Table 1**). Specimens were retrieved and reviewed by an expert perinatal pathologist (WTP), blinded to all clinical information except gestational age. There was substantial agreement between the blinded review and the clinical report of MVM (kappa = 0.78). Cases with disagreement underwent an additional round of review for adjudication.

Outcomes

Cognition

Cognitive assessments were administered by trained raters overseen by a neuropsychologist. Our domains of interest were information processing speed, executive function, and memory. The information processing speed domain included Digit Symbol Coding (Wechsler, 1997a) and Stroop Word Reading and Color Naming (Golden, 1978). Tests in the executive function domain included the Similarities and Matrix Reasoning subtests of the Wechsler Adult Intelligence Scale-III (Wechsler, 1997a) and Stroop Color Word Interference (Golden, 1978). Tests in the memory domain included Logical Memory Immediate and Delayed Recall (Wechsler, 1997b). Cognitive test z-scores were created, and domain composite z-scores were then calculated as the average of the test *z*-scores for that domain. A higher score is better for all domains.

Cerebrovascular Reactivity

Cerebrovascular reactivity, a measure of vessel response to a vasoactive stimulus (e.g., increased CO_2), is an excellent marker of cerebral SVD (Bakker et al., 1999; Rane et al., 2018).

We evaluated global and regional CVR non-invasively as change in blood flow from room-air breathing to blood flow during a 24-s breath-hold using a validated arterial spin labeling MRI imaging protocol (Urback et al., 2017; Cohen and Wang, 2019). We used this less invasive approach to induce hypercapnia for our pilot study in order to assess feasibility of, lay groundwork for, and justify using the more invasive and logistically complicated approach of CO_2 challenge in a larger study (e.g., administration of CO_2 requires an Investigational New Drug approval). We did not measure end-tidal CO_2, but breath-holding calibrates well against direct administration of CO_2 to induce hypercapnia (Kastrup et al., 2001; Bulte et al., 2009), and this breath-holding approach has been used to successfully induce hypercapnia in other population-based studies (Haight et al., 2015). Details of our standardized CVR protocol and methods can be found in the **Supplementary Methods section** and details of ROIs in **Supplementary Table 2**.

Covariates and Other Study Characteristics

Systolic blood pressure (SBP) and diastolic blood pressure (DBP) were measured in a standardized way by trained study staff based on our established protocol using a Microlife A6 PC / BP 3GUI-8X (Guangdong, China). Following a 5-min rest, BP was measured three times on the non-dominant arm with 1-min intervals with an appropriate cuff size based on arm measurement. The average of these three measures was used for data analyses. Body mass index (BMI) at the parent study visit was calculated as $\frac{weight\ (kg)}{[height\ (m)]^2}$ based on measured height (using a stadiometer) and weight (Tanita scale TBF-300A) after women removed their shoes, socks, and excessive clothing. Waist circumference was measured with a tape measure at end-expiration at the level of the iliac crest. Total cholesterol, high-density lipoprotein cholesterol (HDL-C), low-density lipoprotein cholesterol (LDL-C), triglycerides, glycated hemoglobin (HbA1c), and high sensitivity C-reactive protein (hs-CRP) were measured in fasting blood samples at the University of Pittsburgh Medical Center (UPMC) Presbyterian Hospital Automated Testing Laboratory. Any values that were less than the assay's level of detection were set to the test value/2. Smoking status (yes/no) was recorded from the registry medical record during pregnancy. Gestational diabetes (yes/no) was any pregnancy prior to the parent study visit with gestational diabetes based on the registry medical record. Menopausal status (yes/no) was assessed via reproductive history questionnaire, aligned with the landmark SWAN study to record date of last menstruation, hysterectomy, oophorectomy history, and use of hormonal contraception (Tseng et al., 2012; Cortes et al., 2017).

Statistical Analysis

We calculated sample characteristics overall and by preeclampsia/MVM status in the 45 cognitive assessment study participants. They are presented as means and standard deviations for continuous variables or numbers and percentages for categorical variables. Group comparisons were carried out using ANOVA for normally distributed continuous variables, Kruskal–Wallis tests for non-normally distributed continuous variables, and Fisher's exact tests for categorical variables. We did not conduct inferential statistical tests on the preeclampsia severity variables due to small sample and cell sizes.

For primary aim hypothesis testing involving cognition, we set alpha to 0.05 and corrected for multiple comparisons using the Bonferroni correction. Because the neuroimaging aim of this study was a pilot study, we wanted to increase the likelihood of exploring promising results in our larger planned study, making us more concerned with erroneously ruling out a potential finding (false negative) than with false positives (Rothman, 1990). Thus, we set alpha at 0.10, and we did not correct for multiple comparisons in analyses involving CVR. Statistical analyses were carried out in SPSS version 25.0, SAS version 9.4, and *R* version 4.0.2.

Cognition

Forty-five women had cognitive assessments (**Figure 1**). Differences in information processing speed, executive function, and memory by preeclampsia/MVM status were tested using ANOVA. Significant tests were repeated adjusting for education alone and in combination with SBP, BMI, or both SBP and BMI using generalized linear models (GLMs). For any cognitive domain significantly associated with preeclampsia/MVM status in education adjusted models, we followed up with Bonferroni adjusted pairwise comparisons, and we also tested whether cognitive performance differences were driven by preeclampsia or MVM using ANOVA and education adjusted GLMs. For all of these models, education was treated as a continuous variable.

Pilot Study Feasibility

We report descriptive statistics as *N* (%) for participants' response to invitation to participate, screening, enrollment, and usable CVR data.

CVR

Twenty-two participants had usable CVR data (**Figure 1**). We analyzed CVR (change from room-air breathing to breath-hold) and also computed percent signal change as (mean of breath-hold − mean of room-air breathing) / mean of room-air breathing × 100; higher CVR values indicate increased flow in response to breath-holding. Due to small sample size, we tested within preeclampsia/MVM group change from room-air breathing to breath-hold using Wilcoxon Signed Rank tests (non-parametric paired tests). We also tested between group differences in room-air breathing, breath-hold, and percent change using Kruskal–Wallis tests.

Associations of CVR With Cognition

Nineteen participants had data on both CVR and cognition (**Figure 1**). We evaluated associations of global and regional CVR with cognition independent of preeclampsia/MVM status using Spearman partial correlations. We further adjusted these partial correlations one at a time for years of education, gestational diabetes, menopause, preeclamspia

severity, pre-term birth, and any variables which differed significantly by preeclampsia/MVM status.

RESULTS

Participant characteristics are presented in **Table 1**. Overall, the participants were about 31 years of age at delivery and 41 years of age at the time of cognitive assessments. About 42% of the participants were of Black race/ethnicity, and most had greater than high school education. Among the participants, $n = 24$ had neither preeclampsia nor MVM, $n = 8$ had preeclampsia only, and $n = 13$ had preeclampsia with MVM. There were no significant differences in participant characteristics by preeclampsia/MVM status with the exception of DBP. Women with both preeclampsia and MVM had the highest DBP ($p = 0.04$, **Table 1**).

Clinical features of preeclampsia severity by MVM status are reported in **Table 1**. Compared to women without MVM, women with MVM were likelier to have severe preeclampsia, report headaches, and to have an infant that was small for gestational age, although numbers were small, so we did not perform statistical tests of these differences. No women had pulmonary edema or seizures.

Cognition

Boxplots of unadjusted cognitive scores by preeclampsia/MVM status are shown in **Figure 2**. We found women with both preeclampsia and MVM had the worst information processing speed, mean (SD): preeclampsia-/MVM-, +0.19 (0.63); preeclampsia+/MVM-, +0.32 (0.72); preeclampsia+/MVM+, −0.55 (1.06) (overall $p = 0.02$). In pairwise comparisons, preeclampsia-/MVM- vs. preeclampsia+/MVM+ were significantly different at a Bonferroni adjusted alpha of 0.017 for three comparisons (pairwise $p = 0.01$), but not preeclampsia+/MVM- vs. preeclampsia+/MVM+ ($p = 0.06$) or preeclampsia-/MVM- vs. preeclampsia+/MVM- ($p = 0.64$). Preeclampsia+/MVM+ women also had the lowest executive function scores, although the overall difference was not significant (overall $p = 0.26$). There was no significant difference in memory scores (overall $p = 0.76$). Differences in information processing speed appeared driven more by MVM rather than preeclampsia (MVM+ vs. MVM-, $p = 0.004$; preeclampsia+ vs. preeclampsia-, $p = 0.11$). Overall

TABLE 1 | Characteristics of study participants overall and by preeclampsia and maternal vascular malperfusion status.

Characteristic	Overall ($n = 45$)		PreE-/MVM- ($n = 24$)		PreE+/MVM-($n = 8$)		PreE+/MVM+($n = 13$)		p
Age at delivery, years	30.6	5.6	31.3	5.3	27.9	6.2	30.8	5.6	0.31
Age at Cognitive test, years	41.0	5.5	41.6	5.3	38.5	5.9	41.5	5.5	0.35
Education, years*	15.2	2.6	15.4	2.6	15.3	2.8	14.8	2.5	0.77
Education, <HS	10	22.2%	5	20.8%	1	12.5%	4	30.8%	0.70
Smoking during pregnancy[#]	7	16.3%	5	20.8%	0	0%	2	18.2%	0.46
Gestational diabetes	6	13.3%	3	12.5%	2	25%	1	7.7%	0.60
Black	19	42.2%	11	45.8%	3	37.5%	5	38.4%	0.49
BMI, kg/m^2 at parent study visit	31.6	7.7	29.9	7.6	31.6	7.9	34.5	7.4	0.22
Waist circumference, inches	39.7	7.1	38.3	7.2	40.2	9.0	42.0	5.4	0.33
SBP, mmHg*	119.7	14.4	117.2	15.6	118.3	11.4	125.0	13.4	0.15
DBP, mmHg*	78.4	10.1	75.6	9.8	78.0	10.1	83.8	9.0	0.04
Total cholesterol, mg/dl^	181.0	41.8	182.8	36.3	162.7	43.6	187.5	50.4	0.44
LDL-C, mg/dl^	100.9	33.2	99.5	29.4	87.0	35.0	111.0	38.1	0.30
HDL-C, mg/dl^	58.9	16.4	62.6	17.2	58.0	19.5	52.5	11.7	0.20
Triglycerides, mg/dl^*	106.7	67.3	104.6	65.7	88.3	35.7	120.5	83.1	0.80
hsCRP, mg/dl^*	0.4	0.9	0.3	0.4	1.1	2.0	0.3	0.3	0.60
HbA1c, percent^*	5.8	1.8	5.4	0.5	6.4	3.1	6.2	2.4	0.28
Post-menopausal	3	6.7%	2	8.3%	0	0%	1	7.7%	>0.99
Severe preeclampsia	–	–	–	–	1	12.5%	6	46.2%	–
Pulmonary edema	–	–	–	–	0^^	0%	0[$]	0%	–
Seizures	–	–	–	–	0^^	0%	0[$]	0%	–
Headache[&]	–	–	–	–	1	12.5%	3[@]	23.1%	–
Pre-term birth	–	–	–	–	2	25.0%	4	30.8%	–
Gestational age, weeks	–	–	–	–	37.0	2.0	36.3	3.8	–
Small for gestational age	–	–	–	–	1	12.5%	5	38.5%	–
Birth weight	–	–	–	–	3,137.4	629.8	2,637.4	1,080.9	–

*[#]N = 43; ^N = 44; ^^N = 7; [&]N = 6; [$]N = 10; and [@]N = 11. Mean and standard deviations or numbers (%) are presented for continuous and categorical variables, respectively. P-values for continuous variables are from ANOVA for normally distributed variables and from Kruskal–Wallis tests for non-normally distributed variables (indicated by *), and p-values for categorical variables are from Fisher's exact tests. BMI, body mass index; DBP, diastolic blood pressure; HbA1c, glycated hemoglobin; HDL-C, high-density lipoprotein cholesterol; HS, high school; hsCRP, high sensitivity c-reactive protein; LDL-C, low-density lipoprotein cholesterol; MVM, maternal vascular malperfusion; PreE, preeclampsia; SBP, systolic blood pressure.*

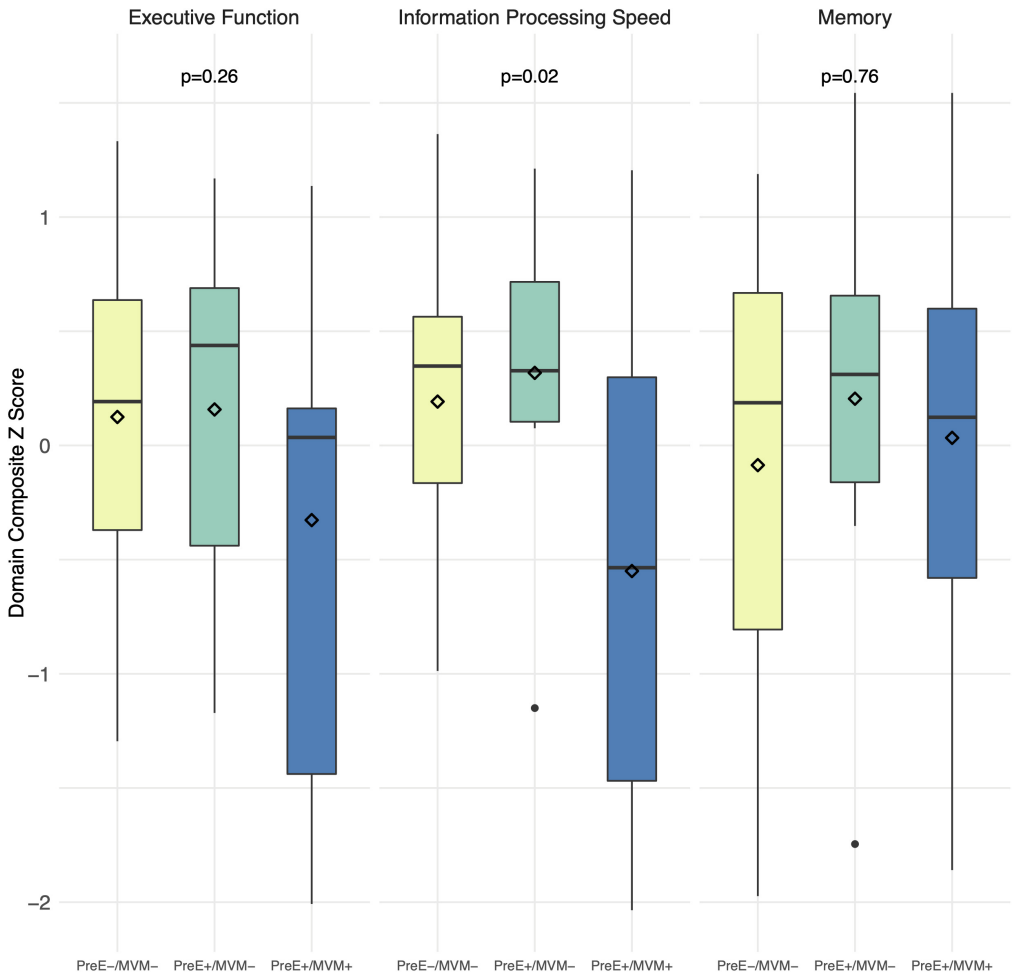

FIGURE 2 | Cognitive performance by preeclampsia and maternal vascular malperfusion status. Boxplots of unadjusted composite *z*-scores for each cognitive domain. Domain composite *z*-scores are average *z*-scores of the tests comprising the domain. Diamonds = mean score. *P* values are from ANOVAs. MVM, maternal vascular malperfusion; PreE, preeclampsia.

associations of preeclampsia/MVM status with information processing speed remained similar after adjustment for years of education, SBP, and BMI.

Pilot Study Feasibility

Detailed pilot study participation flow is shown in **Figure 1B**. Out of the 71 WINDOWS BP participants who were invited to participate in the CVR pilot study, 38 (53.5%) were non-responsive. The frank refusal rate was 5.6% ($n = 4$). We screened 29 (40.8%) for participation, and of those, 5 (17.2%) were MRI screen failures. We enrolled 24 (33.8%) participants. Two participants were missing CVR data: one participant was unable to fit in the scanner, and one had poor scan quality due to motion while in the scanner. This resulted in 22 (31.0%) participants with usable CVR data.

Cerebrovascular Reactivity

Across the full study sample, cerebral blood flow increased during breath-hold compared to room-air breathing (average global CVR increase: 12%). This was true of global blood flow within the three preeclampsia/MVM groups as well. But using regional spatial distribution, preeclampsia+/MVM+ women demonstrated a less robust CVR response in the parietal lobe; they showed no statistically significant difference between room-air breathing and breath-hold, while preeclampsia-/MVM- and preeclampsia+/MVM- women did (**Table 2**). All groups significantly increased blood flow from room air breathing to breath-hold in the other ROIs. Although there was a consistent pattern across ROIs for preeclampsia+/MVM+ women to have the lowest cerebral blood flow under room-air breathing conditions, all between-group differences for cerebral blood flow during room-air breathing or breath-hold, or for percent signal change—CVR— were not statistically significant (all $p > 0.1$).

Associations of CVR With Cognition

Scatterplots, partial correlations, and *p*-values of cognitive scores by CVR for significant correlations are shown in **Supplementary Figure 1**. We found significant correlations of lower CVR

TABLE 2 | Cerebral blood flow during room-air breathing and breath-hold stratified by preeclampsia and maternal vascular malperfusion status.

	PreE-/MVM- (*n* = 9)			PreE+/MVM- (*n* = 5)			PreE+/MVM+ (*n* = 8)		
	Room-air	Breath- hold	Within arm p	Room-air	Breath- hold	Within arm p	Room-air	Breath- hold	Within arm p
Global	11.7 (1.6)	12.9 (2.2)	0.038	12.0 (1.4)	13.6 (0.8)	0.080	11.1 (2.0)	12.4 (1.8)	0.012
Parietal	10.8 (2.1)	11.6 (2.5)	0.051	11.0 (1.2)	12.5 (1.1)	0.080	10.1 (1.9)	10.9 (1.7)	0.123
Precuneus	14.2 (1.9)	15.3 (2.3)	0.038	14.2 (1.4)	15.9 (0.6)	0.080	12.8 (1.9)	14.6 (3.4)	0.012
Anterior Cingulate	14.3 (2.5)	16.1 (3.1)	0.028	15.1 (1.8)	17.4 (2.2)	0.043	13.2 (2.6)	15.6 (3.5)	0.012
Posterior Cingulate	15.7 (2.0)	17.0 (3.1)	0.066	16.1 (2.5)	17.7 (1.5)	0.080	14.2 (1.9)	16.9 (3.5)	0.012

N = 22. Values are mean (standard deviation). P-values are based on Wilcoxon Signed Rank tests, non-parametric paired tests. MVM, maternal vascular malperfusion; PreE, preeclampsia.

in the parietal lobe with worse information processing speed and executive function (**Supplementary Figure 1**), but not memory ($p = 0.16$), independent of preeclampsia/MVM status. Anterior and posterior cingulate CVR were significantly inversely associated with memory (**Supplementary Figure 1**), but not information processing speed or executive function (all $p > 0.1$). Lower global CVR was significantly correlated with worse information processing speed (**Supplementary Figure 1**), but not executive function or memory ($p > 0.1$), independent of preeclampsia/MVM status. These relationships survived additional one at a time adjustments for education, DBP, gestational diabetes, menopause, preeclampsia severity, and preterm birth, except: parietal CVR with executive function adjusted for education ($\rho = 0.38$, $p = 0.13$) and both anterior cingulate CVR with memory ($\rho = -0.39$, $p = 0.11$) and global CVR with information processing speed ($\rho = 0.41$, $p = 0.11$) adjusted for preeclampsia severity. Correlations of CVR in other ROIs with cognition were not significant (all $p > 0.1$).

DISCUSSION

Consistent with our hypothesis, midlife women with a history of both preeclampsia and MVM had poorer information processing speed compared to women with neither preeclampsia nor MVM, and nearly so compared to women with preeclampsia only; these differences appeared driven by MVM rather than preeclampsia. While preeclampsia-related poorer information processing speed has been previously reported (Brussé et al., 2008; Fields et al., 2017; Miller et al., 2019), our results that women with both MVM and preeclampsia had worse cognitive function are novel. Our pilot study demonstrated the feasibility of enrolling such women originally drawn from a birth registry for our future larger study incorporating advanced neuroimaging, with 41% of women in our parent study screened, 34% enrolled, and 31% with usable neuroimaging data. Further characterizing the cerebrovascular integrity of women with histories of preeclampsia and MVM in a larger study is important, as our pilot results demonstrate that the women with both preeclampsia and MVM also appeared to have blunted CVR localized in the parietal lobe, a region important for information processing speed and executive function. Our results raise the intriguing possibility that small vessel impairments in the placenta may additionally mark the subset of women with preeclampsia who are susceptible to poorer cognition and cerebral SVD. Future studies to identify mechanisms are needed.

The possible blunted CVR response in women with both preeclampsia and MVM may be localized in the parietal lobe for several reasons. Both in older and younger adults with high vascular risk, cerebral SVD is more common in fronto-parietal and subcortical areas, due to poor collateral vascularity (watershed areas) (Pantoni, 2010). Of note, in this group, the parietal lobe may have been more susceptible to lower CVR because it had lower baseline flow. Cerebral SVD in fronto-parietal areas affect executive function regulation (Wardlaw et al., 2013), planning, problem-solving, and decision-making (Salthouse, 1996; Erel and Levy, 2016; Igelström and Graziano, 2017; Ardila et al., 2018; Bubb et al., 2018; Froudist-Walsh et al., 2018; Gratton et al., 2018; Nguyen et al., 2019; Worringer et al., 2019). In older age, cerebral SVD is an established risk factor for dementia (Saxton et al., 2004; Backman et al., 2005; Rapp and Reischies, 2005; Rosano and Newman, 2006; Debette et al., 2019), and associations of lower CVR with dementia risk have been documented (Di Marco et al., 2015; De Silva and Faraci, 2016; Nelson et al., 2016; Peng et al., 2018). While direct evidence for these associations is sparser in midlife (Jorgensen et al., 2018), lower neurocognitive integrity in midlife may reduce brain reserve, increasing vulnerability to age-related risk factors, and lowering the threshold for clinical manifestations of brain changes (Wang et al., 2017; Windham et al., 2019; Xu et al., 2019). Our work extends this to indicate that neurocognitive differences in the reproductive years may be detectable, a critical step to identification of high-risk individuals who may be susceptible to later life impairments. In sum, focal changes in CVR in early midlife women with preeclampsia may be an early risk factor for development of VCID.

Strengths and Limitations

The strengths of our study include our evaluation of women in early midlife at a time in which risk factors for VCID are more amenable to intervention. Our study sample included a large proportion of Black women. Prior work has primarily been in white women, yet hypertensive disorders of pregnancy and pregnancy-related morbidity and mortality are disproportionately experienced by Black women (Breathett et al., 2014; Shahul et al., 2015; Miller et al., 2020). We also applied rigorous measurement of study variables. Our characterization of

preeclampsia was drawn from our birth registry, with the medical record reviewed and diagnosis adjudicated and applied according to current American College of Obstetricians and Gynecologists criteria. We evaluated MVM, a novel measure of SVD in the placenta, a vascular bed not typically considered in cerebral SVD studies. Our evaluation of MVM was based on expert review of placental histopathology, with chance of rater bias reduced by blinding to nearly all participant clinical information, including preeclampsia diagnosis. We used a functional measure of cerebral microvascular dysfunction—CVR—which is capable of capturing early changes in cerebrovascular integrity; these changes can appear without yet corresponding to the structural degradation of tissue-based markers of cerebral SVD (Shaaban et al., 2019). We used a standardized breath-hold-based CVR protocol to enhance consistency across participants. In addition, our imaging methods captured two novel aspects of CVR compared to prior methods relying on transcranial Doppler: the spatial distribution of cerebral blood flow at the regional level, and the contribution of signal from smaller sized vessels. Transcranial doppler is limited to capturing changes in large arteries and precludes parsing vascular changes regionally as we have done (Blair et al., 2016). Our regional approach allowed us to connect cognitive performance in specific domains with cerebral SVD in brain regions that subserve these functions.

There are several limitations which should be kept in mind when considering our study results. We did not have additional details on severity and neurological symptoms of preeclampsia beyond what we reported in **Table 1**. Our neuroimaging sample was small, and the associated analyses were, by design for a pilot study, exploratory. We noted large standard deviations in our CVR measures; thus absence of significant relationships may be true or may be due simply to small sample size and large variability. We also used breath-holding to induce hypercapnia and did not measure end-tidal CO_2. These pilot study results lay groundwork for our larger planned study where we will be able to further evaluate and confirm these results using CO_2 challenge to induce hypercapnia; this is expected to elicit a stronger response with a larger effect size compared to breath-holding, making it easier to detect. This study provides only one timepoint of CVR and cognitive measures; change over time was not evaluated, and we also cannot know what these participants' cognitive performance and CVR were prior to our assessments nor prior to preeclampsia or MVM onset. Understanding how these factors in midlife evolve and relate to late-life cognitive function will require longitudinal studies.

Future Directions

Our results suggest that regional CVR may more precisely reveal preeclampsia-related injury than global CVR, especially in relatively young women. Therefore, regional CVR measures should be incorporated in future longitudinal studies linking preeclampsia to long-term brain health. Future studies can incorporate other methods that induce a greater hypercapnic response, such as CO_2 challenge. Larger, longitudinal studies using a broader-based cognitive battery are warranted to further evaluate the relationships of preeclampsia, MVM, cognition, and CVR. Specifically, a better understanding of how preeclampsia and MVM impact information processing speed and whether cognitive functions worsen from early midlife into late-life will identify if pregnancy is a key window of opportunity for risk identification and targeted intervention.

DATA AVAILABILITY STATEMENT

Data are available from the University of Pittsburgh Institutional Data Access/Ethics Committee for researchers who meet the criteria for access to confidential data. Requests to access the datasets should be directed to JC, jmcst43@pitt.edu.

ETHICS STATEMENT

The studies involving human participants were reviewed and approved by University of Pittsburgh Institutional Review Board. The patients/participants provided their written informed consent to participate in this study.

AUTHOR CONTRIBUTIONS

JC, CR, WP, AC, TH, and CS contributed to conception and design of the study. CR and CS performed the statistical analysis. JC, CR, WP, MB, AC, TH, and CS interpreted the data for the work. CS wrote the first draft of the manuscript. JC and CR drafted sections of the manuscript. All authors contributed to manuscript revision and read and approved the submitted version.

FUNDING

This research was funded by American Heart Association Grants 16SFRN27810001 and 18SCG34350001 (https://www.heart.org/) and the Jewish Healthcare Foundation (https://www.jhf.org/) (all to JC). CS was funded by NIH grant T32 AG055381 from the National Institute on Aging (https://www.nia.nih.gov/). The funders had no role in study design, data collection and analysis, decision to publish, or preparation of the manuscript.

ACKNOWLEDGMENTS

The authors would like to thank our study participants, Cassandra Berkey and Samantha Bryan who were instrumental in data acquisition, and the University of Pittsburgh Magnetic Resonance Research Center.

SUPPLEMENTARY MATERIAL

The Supplementary Material for this article can be found online at: https://www.frontiersin.org/articles/10.3389/fnagi.2021.637574/full#supplementary-material

REFERENCES

American College of Obstetricians and Gynecologists (2020). Gestational hypertension and preeclampsia: acog practice bulletin, Number 222. *Obstet. Gynecol.* 135, e237–e260. doi: 10.1097/aog.0000000000003891

Andolf, E., Bladh, M., Möller, L., and Sydsjö, G. (2020). Prior placental bed disorders and later dementia: a retrospective Swedish register-based cohort study. *BJOG* 127, 1090–1099. doi: 10.1111/1471-0528.16201

Ardila, A., Bernal, B., and Rosselli, M. (2018). Executive functions brain system: an activation likelihood estimation meta-analytic study. *Arch. Clin. Neuropsychol.* 33, 379–405. doi: 10.1093/arclin/acx066

Auger, N., Luo, Z. C., Nuyt, A. M., Kaufman, J. S., Naimi, A. I., Platt, R. W., et al. (2016). Secular trends in Preeclampsia incidence and outcomes in a large canada database: a longitudinal study over 24 years. *Can. J. Cardiol.* 32:987.e15-23. doi: 10.1016/j.cjca.2015.12.011

Backman, L., Jones, S., Berger, A. K., Laukka, E. J., and Small, B. J. (2005). Cognitive impairment in preclinical Alzheimer's disease: a meta-analysis. *Neuropsychology* 19, 520–531. doi: 10.1037/0894-4105.19.4.520

Bairey Merz, C. N. (2019). Testing for coronary microvascular dysfunction. *JAMA* 322, 2358–2358. doi: 10.1001/jama.2019.16625

Bakker, S. L., de Leeuw, F. E., de Groot, J. C., Hofman, A., Koudstaal, P. J., and Breteler, M. M. (1999). Cerebral vasomotor reactivity and cerebral white matter lesions in the elderly. *Neurology* 52, 578–583. doi: 10.1212/wnl.52.3.578

Barnes, J. N., Harvey, R. E., Miller, K. B., Jayachandran, M., Malterer, K. R., Lahr, B. D., et al. (2018). Cerebrovascular reactivity and vascular activation in postmenopausal women with histories of preeclampsia. *Hypertension* 71, 110–117. doi: 10.1161/hypertensionaha.117.10248

Basit, S., Wohlfahrt, J., and Boyd, H. A. (2018). Pre-eclampsia and risk of dementia later in life: nationwide cohort study. *BMJ* 363:k4109. doi: 10.1136/bmj.k4109

Blair, G. W., Doubal, F. N., Thrippleton, M. J., Marshall, I., and Wardlaw, J. M. (2016). Magnetic resonance imaging for assessment of cerebrovascular reactivity in cerebral small vessel disease: a systematic review. *J. Cereb. Blood Flow Metab.* 36, 833–841. doi: 10.1177/0271678x16631756

Breathett, K., Muhlestein, D., Foraker, R., and Gulati, M. (2014). Differences in Preeclampsia rates between African American and Caucasian women: trends from the National Hospital Discharge Survey. *J. Womens Health* 23, 886–893. doi: 10.1089/jwh.2014.4749

Brussé, I., Duvekot, J., Jongerling, J., Steegers, E., and De Koning, I. (2008). Impaired maternal cognitive functioning after pregnancies complicated by severe pre-eclampsia: a pilot case-control study. *Acta Obstet. Gynecol. Scand.* 87, 408–412. doi: 10.1080/00016340801915127

Bubb, E. J., Metzler-Baddeley, C., and Aggleton, J. P. (2018). The cingulum bundle: anatomy, function, and dysfunction. *Neurosci. Biobehav. Rev.* 92, 104–127. doi: 10.1016/j.neubiorev.2018.05.008

Bulte, D. P., Drescher, K., and Jezzard, P. (2009). Comparison of hypercapnia-based calibration techniques for measurement of cerebral oxygen metabolism with MRI. *Magn. Reson. Med.* 61, 391–398. doi: 10.1002/mrm.21862

Catov, J., Assibey-Mensah, V., Muldoon, M. F., Sun, B., and Parks, W. T. (2019). *Maternal Vascular Lesions in the Placenta May Identify Women Susceptible to Masked Hypertension a Decade after Delivery*. Houston, TX: American Heart Association EPI/Lifestyle 2019 Scientific Sessions.

Catov, J. M., Muldoon, M. F., Reis, S. E., Ness, R. B., Nguyen, L. N., Yamal, J. M., et al. (2018). Preterm birth with placental evidence of malperfusion is associated with cardiovascular risk factors after pregnancy: a prospective cohort study. *BJOG* 125, 1009–1017. doi: 10.1111/1471-0528.15040

Cohen, A. D., and Wang, Y. (2019). Improving the assessment of breath-holding induced cerebral vascular reactivity using a multiband multi-echo ASL/BOLD sequence. *Sci. Rep.* 9:5079. doi: 10.1038/s41598-019-41199-w

Cortes, Y. I., Catov, J. M., Brooks, M., Harlow, S. D., Isasi, C. R., Jackson, E. A., et al. (2017). History of adverse pregnancy outcomes, blood pressure, and subclinical vascular measures in late midlife: SWAN (Study of Women's Health Across the Nation). *J. Am. Heart Assoc.* 7:e007138. doi: 10.1161/jaha.117.007138

Countouris, M. E., Catov Janet, M., de Jong, N., Brands, J., Chen, X., Berlacher, K., et al. (2020). *Hypertensive Disorders of Preganancy and Placental Maternal Vascular Malperfusion Lesions are Associated With Abnormal Coronary Microvascular Function 8 to 10 Years After Delivery*. Chicago, IL: JACC.

De Silva, T. M., and Faraci, F. M. (2016). Microvascular dysfunction and cognitive impairment. *Cell. Mol. Neurobiol.* 36, 241–258. doi: 10.1007/s10571-015-0308-1

Debette, S., Schilling, S., Duperron, M. G., Larsson, S. C., and Markus, H. S. (2019). Clinical significance of magnetic resonance imaging markers of vascular brain injury: a systematic review and meta-analysis. *JAMA Neurol.* 76, 81–94. doi: 10.1001/jamaneurol.2018.3122

Di Marco, L. Y., Venneri, A., Farkas, E., Evans, P. C., Marzo, A., and Frangi, A. F. (2015). Vascular dysfunction in the pathogenesis of Alzheimer's disease–a review of endothelium-mediated mechanisms and ensuing vicious circles. *Neurobiol. Dis.* 82, 593–606. doi: 10.1016/j.nbd.2015.08.014

Eldridge, S. M., Chan, C. L., Campbell, M. J., Bond, C. M., Hopewell, S., Thabane, L., et al. (2016). CONSORT 2010 statement: extension to randomised pilot and feasibility trials. *BMJ* 355, i5239. doi: 10.1136/bmj.i5239

Elharram, M., Dayan, N., Kaur, A., Landry, T., and Pilote, L. (2018). Long-term cognitive impairment after Preeclampsia: a systematic review and meta-analysis. *Obstet. Gynecol.* 132, 355–364. doi: 10.1097/aog.0000000000002686

Erel, H., and Levy, D. A. (2016). Orienting of visual attention in aging. *Neurosci. Biobehav. Rev.* 69, 357–380. doi: 10.1016/j.neubiorev.2016.08.010

Fields, J. A., Garovic, V. D., Mielke, M. M., Kantarci, K., Jayachandran, M., White, W. M., et al. (2017). Preeclampsia and cognitive impairment later in life. *Am. J. Obstet. Gynecol.* 217, 74.e1–74.e11. doi: 10.1016/j.ajog.2017.03.008

Froudist-Walsh, S., López-Barroso, D., José Torres-Prioris, M., Croxson, P. L., and Berthier, M. L. (2018). Plasticity in the working memory system: life span changes and response to injury. *Neuroscientist* 24, 261–276. doi: 10.1177/1073858417717210

Gannon, O. J., Robison, L. S., Custozzo, A. J., and Zuloaga, K. L. (2019). Sex differences in risk factors for vascular contributions to cognitive impairment & dementia. *Neurochem. Int.* 127, 38–55. doi: 10.1016/j.neuint.2018.11.014

Garovic, V. D., White, W. M., Vaughan, L., Saiki, M., Parashuram, S., Garcia-Valencia, O., et al. (2020). Incidence and long-term outcomes of hypertensive disorders of pregnancy. *J. Am. Coll. Cardiol.* 75, 2323–2334. doi: 10.1016/j.jacc.2020.03.028

Golden, C. J. (1978). *A Manual for the Clinical and Experimental Use of the Stroop Color and Word Test*. Chicago, IL: Stoelting.

Gratton, C., Sun, H., and Petersen, S. E. (2018). Control networks and hubs. *Psychophysiology* 55:e13032. doi: 10.1111/psyp.13032

Haight, T. J., Bryan, R. N., Erus, G., Davatzikos, C., Jacobs, D. R., D'Esposito, M., et al. (2015). Vascular risk factors, cerebrovascular reactivity, and the default-mode brain network. *Neuroimage* 115, 7–16. doi: 10.1016/j.neuroimage.2015.04.039

Hauspurg, A., Brands, J., Gandley, R. E., Parks, W., Hubel, C., and Catov Janet, M. (2020). *Evidence of Impaired Microvascular Function a Decade After Delivery in Women With Placental Malperfusion Lesions*. Phoenix, AZ: American Heart Association EPI/Lifestyle 2020 Scientific Sessions.

Holzman, C., Senegore, P., Xu, J., Dunietz, G., Strutz, K., Tian, Y., et al. (2020). Maternal risk of hypertension 7-15 Years after pregnancy: clues from the placenta. *BJOG.* 128, 827–836.

Igelström, K. M., and Graziano, M. S. A. (2017). The inferior parietal lobule and temporoparietal junction: a network perspective. *Neuropsychologia* 105, 70–83. doi: 10.1016/j.neuropsychologia.2017.01.001

Jorgensen, D. R., Shaaban, C. E., Wiley, C. A., Gianaros, P. J., Mettenburg, J., and Rosano, C. (2018). A population neuroscience approach to the study of cerebral small vessel disease in midlife and late life: an invited review. *Am. J. Physiol. Heart. Circ. Physiol.* 314, H1117–H1136. doi: 10.1152/ajpheart.00535.2017

Kastrup, A., Krüger, G., Neumann-Haefelin, T., and Moseley, M. E. (2001). Assessment of cerebrovascular reactivity with functional magnetic resonance imaging: comparison of CO(2) and breath holding. *Magn. Reson. Imaging* 19, 13–20. doi: 10.1016/s0730-725x(01)00227-2

Khong, T. Y., Mooney, E. E., Ariel, I., Balmus, N. C., Boyd, T. K., Brundler, M. A., et al. (2016). Sampling and definitions of placental lesions: Amsterdam placental workshop group consensus statement. *Arch. Pathol. Lab. Med.* 140, 698–713. doi: 10.5858/arpa.2015-0225-CC

Lancaster, G. A., and Thabane, L. (2019). Guidelines for reporting non-randomised pilot and feasibility studies. *Pilot Feasibility Stud.* 5:114. doi: 10.1186/s40814-019-0499-1

Mielke, M. M., Milic, N. M., Weissgerber, T. L., White, W. M., Kantarci, K., Mosley, T. H., et al. (2016). Impaired cognition and brain atrophy decades after hypertensive pregnancy disorders. *Circ. Cardiovasc. Qual. Outcomes.* 9(2 Suppl. 1), S70–S76. doi: 10.1161/circoutcomes.115.002461

Miller, E. C., Zambrano Espinoza, M. D., Huang, Y., Friedman, A. M., Boehme, A. K., Bello, N. A., et al. (2020). Maternal race/ethnicity, hypertension, and risk for stroke during delivery admission. *J. Am. Heart Assoc.* 9:e014775. doi: 10.1161/jaha.119.014775

Miller, K. B., Miller, V. M., and Barnes, J. N. (2019). Pregnancy history, hypertension, and cognitive impairment in postmenopausal women. *Curr. Hypertens. Rep.* 21:93. doi: 10.1007/s11906-019-0997-9

Nelson, A. R., Sweeney, M. D., Sagare, A. P., and Zlokovic, B. V. (2016). Neurovascular dysfunction and neurodegeneration in dementia and Alzheimer's disease. *Biochim. Biophys. Acta* 1862, 887–900. doi: 10.1016/j.bbadis.2015.12.016

Nguyen, L., Murphy, K., and Andrews, G. (2019). Cognitive and neural plasticity in old age: a systematic review of evidence from executive functions cognitive training. *Ageing Res. Rev.* 53:100912. doi: 10.1016/j.arr.2019.100912

Pantoni, L. (2010). Cerebral small vessel disease: from pathogenesis and clinical characteristics to therapeutic challenges. *Lancet Neurol.* 9, 689–701. doi: 10.1016/s1474-4422(10)70104-6

Parks, W. T. (2015). Placental hypoxia: the lesions of maternal malperfusion. *Semin. Perinatol.* 39, 9–19. doi: 10.1053/j.semperi.2014.10.003

Peng, S. L., Chen, X., Li, Y., Rodrigue, K. M., Park, D. C., and Lu, H. (2018). Age-related changes in cerebrovascular reactivity and their relationship to cognition: a four-year longitudinal study. *Neuroimage* 174, 257–262. doi: 10.1016/j.neuroimage.2018.03.033

Pepine, C. J., Ferdinand, K. C., Shaw, L. J., Light-McGroary, K. A., Shah, R. U., Gulati, M., et al. (2015). Emergence of nonobstructive coronary artery disease: a woman's problem and need for change in definition on angiography. *J Am Coll Cardiol* 66, 1918–1933. doi: 10.1016/j.jacc.2015.08.876

Rane, S., Koh, N., Boord, P., Madhyastha, T., Askren, M. K., Jayadev, S., et al. (2018). Quantitative cerebrovascular pathology in a community-based cohort of older adults. *Neurobiol. Aging.* 65, 77–85. doi: 10.1016/j.neurobiolaging.2018.01.006

Rapp, M. A., and Reischies, F. M. (2005). Attention and executive control predict alzheimer disease in late life: results from the berlin aging study (BASE). *Am. J. Geriatr. Psychiatry* 13, 134–141. doi: 10.1176/appi.ajgp.13.2.134

Rosano, C., and Newman, A. B. (2006). Cardiovascular disease and risk of Alzheimer's disease. *Neurol. Res.* 28, 612–620. doi: 10.1179/016164106x130407

Rothman, K. J. (1990). No adjustments are needed for multiple comparisons. *Epidemiology* 1, 43–46.

Salthouse, T. A. (1996). The processing-speed theory of adult age differences in cognition. *Psychol. Rev.* 103, 403–428.

Saxton, J., Lopez, O. L., Ratcliff, G., Dulberg, C., Fried, L. P., Carlson, M. C., et al. (2004). Preclinical Alzheimer disease: neuropsychological test performance 1.5 to 8 years prior to onset. *Neurology* 63, 2341–2347.

Shaaban, C. E., Jorgensen, D. R., Gianaros, P. J., Mettenburg, J., and Rosano, C. (2019). Cerebrovascular disease: neuroimaging of cerebral small vessel disease. *Prog. Mol. Biol. Transl. Sci.* 165, 225–255. doi: 10.1016/bs.pmbts.2019.07.008

Shahul, S., Tung, A., Minhaj, M., Nizamuddin, J., Wenger, J., Mahmood, E., et al. (2015). Racial disparities in comorbidities. complications, and maternal and fetal outcomes in women with preeclampsia/eclampsia. *Hypertens. Pregnancy* 34, 506–515. doi: 10.3109/10641955.2015.1090581

Siepmann, T., Boardman, H., Bilderbeck, A., Griffanti, L., Kenworthy, Y., Zwager, C., et al. (2017). Long-term cerebral white and gray matter changes after preeclampsia. *Neurology* 88, 1256–1264. doi: 10.1212/wnl.0000000000003765

Staff, A. C., Dechend, R., and Pijnenborg, R. (2010). Learning from the placenta: acute atherosis and vascular remodeling in preeclampsia-novel aspects for atherosclerosis and future cardiovascular health. *Hypertension* 56, 1026–1034. doi: 10.1161/HYPERTENSIONAHA.110.157743

Staff, A. C., Dechend, R., and Redman, C. W. G. (2013). Review: preeclampsia, acute atherosis of the spiral arteries and future cardiovascular disease: two new hypotheses. *Placenta* 34, S73–S78. doi: 10.1016/j.placenta.2012.11.022

Stevens, D. U., Al-Nasiry, S., Fajta, M. M., Bulten, J., van Dijk, A. P., van der Vlugt, M. J., et al. (2014). Cardiovascular and thrombogenic risk of decidual vasculopathy in preeclampsia. *Am. J. Obstet. Gynecol.* 210:545.e1-6. doi: 10.1016/j.ajog.2013.12.029

Stevens, D. U., Smits, M. P., Bulten, J., Spaanderman, M. E., van Vugt, J. M., and Al-Nasiry, S. (2015). Prevalence of hypertensive disorders in women after preeclamptic pregnancy associated with decidual vasculopathy. *Hypertens. Pregnancy* 34, 332–341. doi: 10.3109/10641955.2015.1034803

Theilen, L. H., Fraser, A., Hollingshaus, M. S., Schliep, K. C., Varner, M. W., Smith, K. R., et al. (2016). All-cause and cause-specific mortality after hypertensive disease of pregnancy. *Obstet. Gynecol.* 128, 238–244. doi: 10.1097/aog.0000000000001534

Tseng, L. A., El Khoudary, S. R., Young, E. A., Farhat, G. N., Sowers, M., Sutton-Tyrrell, K., et al. (2012). The association of menopause status with physical function: the Study of Women's Health Across the Nation. *Menopause (New York N.Y.)* 19, 1186–1192. doi: 10.1097/gme.0b013e3182565740

Urback, A. L., MacIntosh, B. J., and Goldstein, B. I. (2017). Cerebrovascular reactivity measured by functional magnetic resonance imaging during breath-hold challenge: a systematic review. *Neurosci. Biobehav. Rev.* 79, 27–47. doi: 10.1016/j.neubiorev.2017.05.003

von Elm, E., Altman, D. G., Egger, M., Pocock, S. J., Gøtzsche, P. C., and Vandenbroucke, J. P. (2007). The Strengthening the Reporting of Observational Studies in Epidemiology (STROBE) statement: guidelines for reporting observational studies. *Lancet* 370, 1453–1457. doi: 10.1016/s0140-6736(07)61602-x

Wang, H. X., MacDonald, S. W., Dekhtyar, S., and Fratiglioni, L. (2017). Association of lifelong exposure to cognitive reserve-enhancing factors with dementia risk: a community-based cohort study. *PLoS Med* 14:e1002251. doi: 10.1371/journal.pmed.1002251

Wardlaw, J. M., Smith, C., and Dichgans, M. (2013). Mechanisms of sporadic cerebral small vessel disease: insights from neuroimaging. *Lancet Neurol.* 12, 483–497. doi: 10.1016/s1474-4422(13)70060-7

Wechsler, D. (1997a). *WAIS-III Manual*. New York, NY: Psychological Corp.

Wechsler, D. (1997b). *Wechsler Memory Scale (WMS-III)*. San Antonio, TX: Psychological corporation.

Wiegman, M. J., Zeeman, G. G., Aukes, A. M., Bolte, A. C., Faas, M. M., Aarnoudse, J. G., et al. (2014). Regional distribution of cerebral white matter lesions years after preeclampsia and eclampsia. *Obstet. Gynecol.* 123, 790–795. doi: 10.1097/aog.0000000000000162

Windham, B. G., Griswold, M. E., Wilkening, S. R., Su, D., Tingle, J., Coker, L. H., et al. (2019). Midlife smaller and larger infarctions. white matter hyperintensities, and 20-year cognitive decline: a cohort study. *Ann. Intern. Med.* 171, 389–396. doi: 10.7326/m18-0295

Worringer, B., Langner, R., Koch, I., Eickhoff, S. B., Eickhoff, C. R., and Binkofski, F. C. (2019). Common and distinct neural correlates of dual-tasking and task-switching: a meta-analytic review and a neuro-cognitive processing model of human multitasking. *Brain Struct. Funct.* 224, 1845–1869. doi: 10.1007/s00429-019-01870-4

Xu, H., Yang, R., Qi, X., Dintica, C., Song, R., Bennett, D. A., et al. (2019). Association of lifespan cognitive reserve indicator with dementia risk in the presence of brain pathologies. *JAMA Neurol.* 76, 1184–1191. doi: 10.1001/jamaneurol.2019.2455

Conflict of Interest: The authors declare that the research was conducted in the absence of any commercial or financial relationships that could be construed as a potential conflict of interest.

frontiers in Aging Neuroscience

ORIGINAL RESEARCH
published: 14 May 2021
doi: 10.3389/fnagi.2021.644733

Endothelial Dysfunction and Impaired Neurovascular Coupling Responses Precede Cognitive Impairment in a Mouse Model of Geriatric Sepsis

*Tamas Csipo[1,2], Benjamin R. Cassidy[3], Priya Balasubramanian[1], Douglas A. Drevets[3,4], Zoltan I. Ungvari[1,3,5] and Andriy Yabluchanskiy[1]**

[1] Center for Geroscience and Healthy Brain Aging, Department of Biochemistry and Molecular Biology, University of Oklahoma Health Sciences Center, Oklahoma City, OK, United States, [2] International Training Program in Geroscience, Department of Public Health, Doctoral School of Basic and Translational Medicine, Semmelweis University, Budapest, Hungary, [3] Department of Medicine, University of Oklahoma Health Sciences Center, Oklahoma City, OK, United States, [4] Department of Veterans Affairs Medical Center, Oklahoma City, OK, United States, [5] International Training Program in Geroscience, Departments of Medical Physics and Informatics, Theoretical Medicine Doctoral School University of Szeged, Szeged, Hungary

Sepsis is a life-threatening condition, the incidence of which is significantly increased in elderly patients. One of the long-lasting effects of sepsis is cognitive impairment defined as a new deficit or exacerbation of preexisting deficits in global cognition or executive function. Normal brain function is dependent on moment-to-moment adjustment of cerebral blood flow to match the increased demands of active brain regions. This homeostatic mechanism, termed neurovascular coupling (NVC, also known as functional hyperemia), is critically dependent on the production of vasodilator NO by microvascular endothelial cells in response to mediators released from activated astrocytes. The goal of this study was to test the hypothesis that sepsis in aging leads to impairment of NVC responses early after treatment and that this neurovascular dysfunction associates with impairments in cognitive performance and vascular endothelial dysfunction. To test this hypothesis, we used a commonly studied bacterial pathogen, *Listeria monocytogenes*, to induce sepsis in experimental animals (males, 24 months of age) and subjected experimental animals to a standard clinical protocol of 3 doses of ampicillin i.p. and 14 days of amoxicillin added to the drinking water. NVC responses, endothelial function and cognitive performance were measured in septic and age-matched control groups within 14 days after the final antibiotic treatment. Our data demonstrate that sepsis in aging significantly impairs NVC responses measured in somatosensory cortex during whisker stimulation, significantly impairs endothelial function in isolated and pressure cannulated aorta rings in response to acetylcholine stimulation. No significant impairment of cognitive function in post-sepsis aged animals has been observed when measured using the PhenoTyper homecage based system. Our findings suggest that sepsis-associated endothelial dysfunction and impairment of NVC responses may contribute to long-term cognitive deficits in older sepsis survivors.

Keywords: aging, sepsis, neurovascular coupling, endothelial dysfunction, cognition

OPEN ACCESS

Edited by:
Prasad V. Katakam,
Tulane University, United States

Reviewed by:
Fan Fan,
University of Mississippi Medical Center, United States
Efrat Levy,
New York University, United States

****Correspondence:***
Andriy Yabluchanskiy
andriy-yabluchanskiy@ouhsc.edu

Received: *21 December 2020*
Accepted: *19 April 2021*
Published: *14 May 2021*

Citation:
Csipo T, Cassidy BR, Balasubramanian P, Drevets DA, Ungvari ZI and Yabluchanskiy A (2021) Endothelial Dysfunction and Impaired Neurovascular Coupling Responses Precede Cognitive Impairment in a Mouse Model of Geriatric Sepsis. Front. Aging Neurosci. 13:644733. doi: 10.3389/fnagi.2021.644733

INTRODUCTION

Sepsis is a life-threatening condition, the incidence of which is significantly increased and the outcomes are dramatically worsened in elderly patients (Angus et al., 2001; Martin et al., 2003; Lagu et al., 2012; Corrales-Medina et al., 2015). Older adults (>65 years of age) are 10–15 times more likely to be hospitalized with sepsis than younger individuals and over 60% of older adults admitted to the intensive care unit present with sepsis upon admission (Marik, 2006). Severe sepsis accounts for up to half of bed-days in older adults (Wood and Angus, 2004; Hall et al., 2011). The incidence of sepsis in older adults is likely even higher than reported because many elderly dying patients with infection are not documented as having "sepsis" as they often receive palliative care rather than being sent to the ICU for aggressive treatment (Starr and Saito, 2014). Thus, sepsis in elderly patients is one of the most expensive conditions treated in the US hospitals, the costs for which are exceeding $60 billion per year (Andrews and Elixhauser, 2006; Wier and Andrews, 2006).

The hallmark of sepsis is exaggerated systemic inflammatory response to infection, the consequences of which include generalized microvascular dysfunction, impaired tissue perfusion, endothelial activation and coagulation abnormalities (Hotchkiss et al., 2016). It is now established that a number of sepsis survivors experience residual physical and psychological effects long after treatment and discharge from the hospital (Iwashyna et al., 2010; Calsavara et al., 2018a). One of the long-lasting effects of sepsis is cognitive impairment defined as a new deficit or exacerbation of preexisting deficits in global cognition or executive function (Calsavara et al., 2018a). Clinical data demonstrate that nearly 35% of elderly develop post-sepsis cognitive deficits in the magnitude comparable to individuals with moderate traumatic brain injury or mild Alzheimer's disease (Pandharipande et al., 2013).

Normal brain function is critically dependent on moment-to-moment adjustment of cerebral blood flow to match the increased demands of active brain regions (Toth et al., 2014, 2015a,b; Tucsek et al., 2014; Tarantini et al., 2015). This homeostatic mechanism, termed neurovascular coupling (NVC, also known as functional hyperemia), depends on the production of vasodilator NO by microvascular endothelial cells in response to mediators released from activated astrocytes. Extensive clinical and pre-clinical data demonstrate that NVC is impaired in aging (Csiszar et al., 2019; Farias Quipildor et al., 2019; Tarantini et al., 2019b) due, at least in part, to cerebromicrovascular endothelial dysfunction and is causally linked to cognitive impairment (Toth et al., 2014; Tarantini et al., 2015; Ungvari et al., 2017). Further, there is emerging evidence from experimental studies that restoration of NVC responses in aged animals leads to improved cognitive performance (Tarantini et al., 2018, 2019a; Csipo et al., 2019b; Lipecz et al., 2019). There is strong evidence that sepsis is associated with significant endothelial dysfunction, which contributes to the pathogenesis of multiple organ failure in severe cases (Aird, 2003; Peters et al., 2003; Szabo and Goldstein, 2011; Vachharajani et al., 2012; Coletta et al., 2014; De Backer et al., 2014). Aging is associated with impaired endothelial stress resilience (Ungvari et al., 2011a,b; Fulop et al., 2018) and there are strong experimental data suggesting that sepsis in aged mice is associated with exacerbated endothelial dysfunction (Coletta et al., 2014). However, the impact of sepsis on NVC responses in aging is currently unknown.

This study was designed to test the hypothesis that sepsis in aging leads to impairment of NVC responses early after treatment and that this neurovascular dysfunction associates with impairments in cognitive performance and vascular endothelial dysfunction. To test this hypothesis, we used a commonly studied bacterial pathogen, *Listeria monocytogenes*, to induce sepsis in experimental animals. In humans, *L. monocytogenes* is a food-borne pathogen known to primarily affect the elderly population in whom it causes sepsis and central nervous system infections (Yildiz et al., 2007). For example, adults >65 years of age are over 4 times more likely than the general population to experience invasive *L. monocytogenes* infections, and patients with *L. monocytogenes* CNS infections typically have worse outcomes than those infected with other common neuroinvasive bacteria (Tubiana et al., 2020). To mimic the clinical scenario, antibiotic treatment was administered. Cognitive performance, NVC responses and vascular endothelial function were measured 30 days after sepsis induction and within 2 weeks after antibiotic treatment completion.

MATERIALS AND METHODS

Sepsis Model and Experimental Animals

L. monocytogenes was used to induce sepsis in experimental animals. *L. monocytogenes* strain EGD was originally obtained from P.A. Campbell (Dramsi et al., 1996). Bacteria were stored in brain-heart infusion (BHI) broth (Difco, Detroit, MI) at 109 CFU/mL at −80°C. For experiments, the stock culture was diluted 1:10,000 into BHI and cultured overnight at 37°C with shaking.

This study was carried out with the approval from Institutional Animal Care and use Committee (IACUC) of the University of Oklahoma HSC (OUHSC). All animals were obtained from the NIA Aged Rodent Colony (Charles River Laboratories, Wilmington, MA).

Male C57BL/6N mice 24 months of age were used in experiments as indicated. The biological age of 24 months old mice corresponds to that of 65 year old humans. Mice were injected i.p. with 500–1,000 μL PBS containing 2.0–7.5 × 104 CFU *L. monocytogenes* (sepsis group, n = 27) or vehicle (sham group, n = 11), and then treated with antibiotics as previously described (Zhang et al., 2018). Although *L. monocytogenes* is a foodborne bacterial pathogen in humans, the choice for i.p. administration in our experimental design was based on amino acid difference between human and murine E cadherin. This difference significantly limits the invasion of *L. monocytogenes* through the GI in mice (Bonazzi et al., 2009), therefore the i.v. or i.p. injections are commonly used to bypass the GI tract in mice and to establish systemic infection in a reproducible fashion (Zhang et al., 2018; Cassidy et al., 2020).

Septic and sham mice were injected i.p. with 2 mg ampicillin (Butler Schein Animal Health, Dublin, OH) three times at

10–12 h intervals beginning 48 h post-infection. Bubblegum-flavored amoxicillin (2 mg/mL final concentration) was added to the drinking water 3 days post-infection and continued until sacrifice or 14 days post-infection. All solutions were warmed to body temperature prior to injection. Mice were weighed daily for 14 days. Mice were euthanized by CO_2 asphyxiation and transcardially perfused with ice cold PBS.

Measurement of Neurovascular Coupling Responses

Mice in each group were anesthetized with isoflurane (4% induction for 1–2 min, 1% maintenance during surgical preparation, and 0.5% during NVC measurements), endotracheally intubated and ventilated (MousVent G500; Kent Scientific Co., Torrington, CT) as described previously (Tarantini et al., 2017). A thermostatic heating pad (Kent Scientific Co., Torrington, CT) was used to maintain rectal temperature at 37°C. End-tidal CO_2 was controlled between 3.2 and 3.7% to keep blood gas values within the physiological range. Cannulation of the right femoral artery was performed for arterial blood pressure measurement (Living Systems Instrumentations, Burlington, VT). The blood pressure was within the physiological range throughout the experiments (90–110 mmHg). Mice were immobilized and placed on a stereotaxic frame (Leica Microsystems, Buffalo Grove, IL), the scalp and periosteum were pulled aside, and the skull was gently thinned using a dental drill while cooled with dripping buffer.

Prior to assessment of NVC responses, experimental animals were maintained on 0.5% isoflurane for 20 min. To assess NVC, a laser speckle contrast imager (Perimed, Järfälla, Sweden) was placed 10 cm above the thinned skull and differential perfusion maps of the brain surface were captured (Tarantini et al., 2017). Changes in cerebral blood flow were monitored above the left and right whisker barrel cortex in six consecutive and alternating trials of left and right whisker stimulation, separated by 5–10 min intervals.

For data evaluation, the relative change in the CBF signal was compared between the baseline of the region of interest (ROI) and during stimulation. To rule out an unspecific increase of cerebral blood flow, the difference between the relative change for both lateral ROI's was used for further evaluation to determine specific changes for the contralateral somatosensory cortex. In each study, the experimenter was blinded to the treatment of the animals.

Assessment of Endothelial Nitric Oxide (NO)-Mediated Vasodilation in Aorta

Assessment of endothelium-dependent vasorelaxation was performed in isolated aorta ring preparations as previously described (Horvath et al., 2005; Csiszar et al., 2008; Pearson et al., 2008; Csiszar et al., 2009; Bailey-Downs et al., 2012). In brief, vessels were cut into ring segments approximately 1.5 mm in length and were mounted in wire myograph chambers (Danish Myo Technology A/S, Inc., Denmark) for measurement of isometric tension. The chambers were filled with Krebs buffer solution (118 mM NaCl, 4.7 mM KCl, 1.5 mM $CaCl_2$, 25 mM $NaHCO_3$, 1.1 mM $MgSO_4$, 1.2 mM KH_2PO_4, and 5.6 mM glucose; at 37°C; gassed with 95% O_2 and 5% CO_2). Optimal passive tension was applied to the rings (as determined from the vascular length-tension relationship). After 1 h equilibration, rings were pre-constricted with 10 μM phenylephrine. Acetylcholine-mediated vasodilation was quantified as a normalized relaxation compared to phenylephrine preconstriction. Endothelial NO-dependent relaxation was measured in the presence and absence of the NO synthase inhibitor N(ω)-nitro-L-arginine methyl ester in response to acetylcholine (from 1 nM up to 10 μM). Endothelium independent relaxation was determined in response to sodium nitroprusside (SNP, 0.1 nM to 10 μ M).

Assessment of Cognitive Function Using the PhenoTyper Home Cage System

Cognitive performance was tested using the automated home-cage testing apparatus, PhenoTyper (Model 3000, Noldus Information Technology, Netherlands), as described previously (Logan et al., 2019). Mice were continuously monitored during the light and dark cycles. During cognitive testing, mice were rewarded with a food pellet after five successful entries into the correct hole (FR5; fixed ratio 5) as previously described (Logan et al., 2018). In brief, the percentage of correct entries made in a moving window of the trailing 30 entries was calculated and trials to reach an 80% success rate were determined. Data was tracked for the dark and light phases over the course of 4 days. For initial learning phase, mice were required to pass through the left entrance of the CognitionWall to obtain a food reward (Dustless Precision Rodent Pellets, F05684, Bio-Serv, Flemington, NJ), which was dispensed using an FR5 schedule. In 48 hours, the task was modified, and the correct response was changed to the right entry requiring the animal to extinguish the previous learning and acquire a new response, and the cognitive flexibility was calculated. The data were processed using Python programming language. The Leaning Index for initial learning and cognitive flexibility phases was calculated as correct entries minus the incorrect entries divided by the total number of entries.

Statistical Analysis

Mortality rates were analyzed using Chi-square test and data were presented in the form of Kaplan-Meier curves. NVC responses were evaluated using the appropriate unpaired *t*-test after testing the dataset for normality. Relaxation of aorta rings were expressed as the change of ring tension relative to the tension evoked by the preconstriction. Raw tension data of rings not exhibiting a constriction greater than 1 mN and/or endothelium-dependent vasorelaxation were excluded from further analysis. Multiple aorta ring measurements were then averaged for each animal, and two-way repeated measures ANOVA with Sidak's *post hoc* test was used to compare relaxation between groups. Cognitive data from the PhenoTyper cages was calculated and presented as changes in initial learning during the first 2 days of cognitive assessment, and as cognitive flexibility during the reversal phase of cognitive assessment. Initial learning and cognitive flexibility were calculated as a number of ([correct

entries-incorrect entries]/total entries) during the hours 3–12 and 51–62, respectively. Cognitive data were analyzed using the parametric unpaired *t*-test after passing the normality test. All statistical analysis was performed in GraphPad Prism 8.4.2 (GraphPad Software, LLC, United States). Data are shown as mean ± SEM. A $p < 0.05$ was considered statistically significant.

RESULTS

The Effect of *L. monocytogenes* Induced Sepsis on Mortality Rates and Body Weights in Aged Mice

Survival curves of aged mice after infection with *L. monocytogenes* are shown in **Figure 1A**. The weight loss is considered a key biological feature of sepsis in mouse models (Stortz et al., 2019) and the time course of changes in body weight associated with *L. monocytogenes* induced sepsis is shown in **Figure 1B**. The weight loss in current project was similar to reported data that previously utilized similar sepsis model (Cassidy et al., 2020). The timescale of observed mortality and weight loss in our sepsis model was also similar to sepsis timescale in humans, when the vast majority of deaths in first 72 h after admission to the ICU are due to primary infection-related multiple organ failure (Daviaud et al., 2015).

One mouse from the experimental group was euthanized per recommendations of attending veterinarian for conditions not associated with experimental sepsis protocol and were removed from analysis.

Sepsis Impairs NVC Responses in Aged Animals

To determine the effect of sepsis on NVC responses in aging, we assessed functional hyperemia in the whisker barrel cortex in mice 5 days after completion of antibiotic treatment in infected and sham-treated aged animals ($n = 13$ and $n = 7$, respectively). One mouse in sham group died due to complications with the surgical preparation and their aortas were immediately removed for vascular functional assessment.

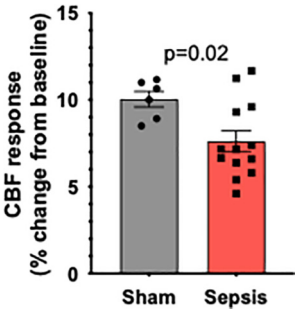

FIGURE 2 | Sepsis impairs NVC responses in aged animals. Sepsis ($n = 13$) significantly impaired CBF responses during whisker stimulation when compared to sham controls ($n = 7$). Data are presented as a%-change from baseline values prior to sham or *l.* monocytogenes treatment. $p = 0.002$.

We found that in aged mice sepsis significantly impaired NVC responses evoked by contralateral whisker stimulation (**Figure 2**). Our data demonstrate that sepsis-induced chronic neurovascular dysfunction persists even after a complete course of translationally relevant antibiotic treatment.

Sepsis Impairs Vascular Endothelial Function in Aged Animals

To assess the effect of *L. monocytogenes* induced sepsis on endothelial function, acetylcholine-mediated relaxation was measured in aorta rings under isometric conditions ($n = 13$ for the septic group, $n = 7$ for sham). Acetylcholine-induced relaxation was compared with two-way repeated measures ANOVA (**Figure 3A**), which showed that sepsis accounted for 5.122% of variance [$F_{(1,14)} = 9.64$, $p = 0.008$]. *Post hoc* multiple Sidak's test showed a significant difference between groups at acetylcholine concentration of 4 μM (mean difference: 22.12%, 95% CI: 1.51–42.72, $p = 0.03$). Inhibition of endothelial NO synthase abolished acetylcholine-evoked relaxation in both groups (data not shown). Endothelium independent vasorelaxation in response to sodium nitroprusside was not different between the groups (**Figure 3B**). These data suggest that

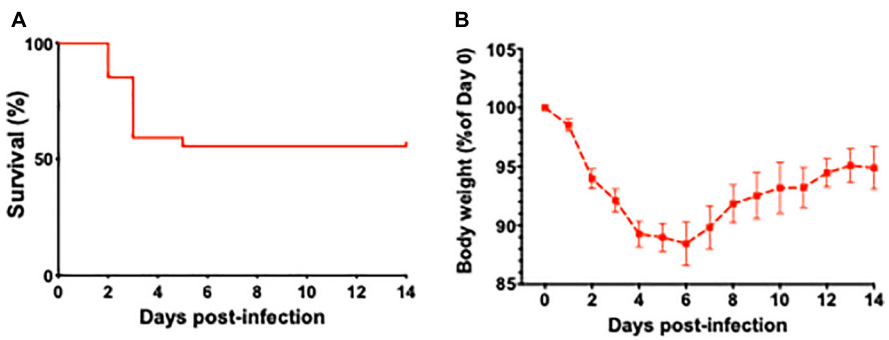

FIGURE 1 | The effect of *L. monocytogenes* induced sepsis on mortality rates and body weights in aged mice. **(A)** Survival curve of 24-month-old mice after *L. monocytogenes* infection and antibiotic treatment. Over the course of the experiment, 13 out of 27 *L. monocytogenes* infected mice died due to sepsis. Antibiotic treatment was initiated 48 h post-infection. **(B)** Time course of changes in body weight associated with *L. monocytogenes* induced sepsis in aged mice.

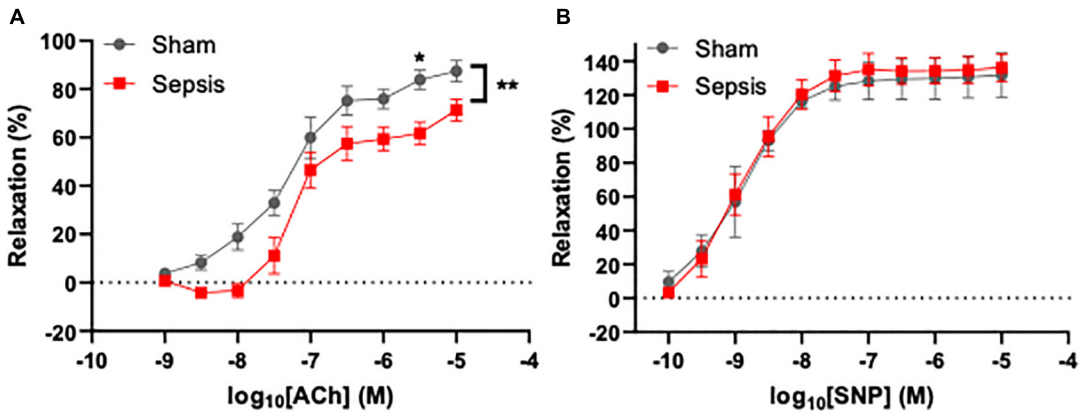

FIGURE 3 | Sepsis caused by *L. monocytogenes* was associated with endothelial dysfunction. Endothelium-dependent vasodilation was measured using wire myography in aorta rings under isometric conditions. **(A)** Sepsis significantly reduced endothelial function in aged animals. A significant difference in dilation between groups was observed when 4 μM acetylcholine (ACh) was applied to aorta rings. **(B)** Endothelium-independent relaxation evoked by sodium nitroprusside (SNP) was not different between groups (right panel). $^{*}p < 0.05$; $^{**}p < 0.01$.

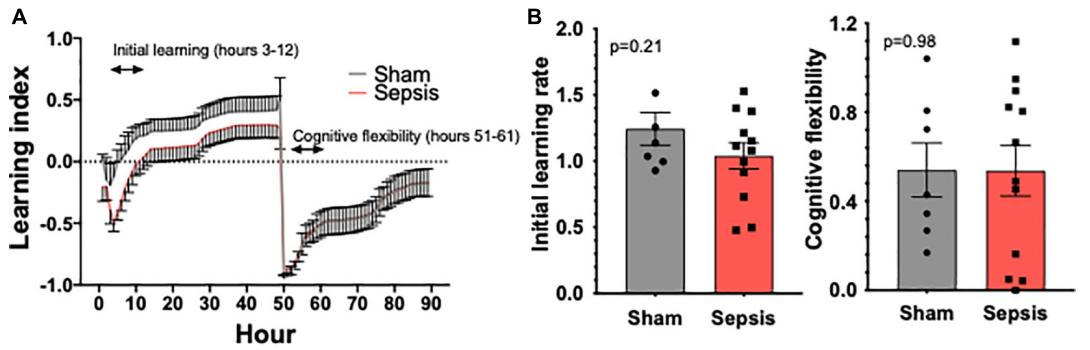

FIGURE 4 | Sepsis effects on cognitive performance in aged animals. PhenoTyper homecage system was used to evaluate the impact of sepsis on cognitive performance (n = 13 in sepsis group and n = 7 in sham group). **(A)** All experimental animals were tested for the duration of 4 days, during which Initial Learning and Cognitive Flexibility were evaluated. Our data demonstrate a trend toward an impairment of cognitive performance measured during the initial learning phase **(B)**. Cognitive flexibility was unaltered by sepsis.

sepsis induces endothelial dysfunction, which persists even after completion of a full antibiotic treatment.

Sepsis Effects on Cognitive Performance in Aged Animals

To evaluate whether *L. monocytogenes* induced sepsis has an impact on cognition, experimental animals were evaluated for cognitive performance using the PhenoTyper homecage system (n = 13 in sepsis group and n = 7 in sham group, **Figure 4A**). One mouse in sepsis group was excluded from the analysis due failure in food reward/pellet dispensing system. No significant effect on cognitive performance measured using the PhenoTyper homecage system in *L. monocytogenes* induced sepsis in this model was observed (**Figure 4B**).

DISCUSSION

In this study, we utilized a clinically relevant *in vivo* model of sepsis via infection of aged mice with *L. monocytogenes*, an important cause of bacterial sepsis in older adults (Yildiz et al., 2007). The key finding of this study is that in aged mice, *L. monocytogenes* induced sepsis impairs NVC responses and promotes endothelial dysfunction, a finding which persists even after treatment with a clinically relevant regimen of antibiotics.

This is the first study to demonstrate compromised NVC responses in a relevant preclinical animal model of geriatric sepsis. Previous clinical studies reported multifaceted effects of sepsis on cerebral blood flow regulation (Terborg et al., 2001; Bowie et al., 2003; Pfister et al., 2008; Toksvang et al., 2014; Vasko et al., 2014; de Azevedo et al., 2017; Crippa et al., 2018; Masse et al., 2018). The emerging concept is that both reduced cerebral blood flow and altered autoregulation contribute to sepsis-associated encephalopathy. Our data are in line with this concept, suggesting that impaired moment-to-moment regulation of cerebral blood flow is casually linked to the pathogenesis of cognitive impairment associated with geriatric sepsis. There is a temporal evolution of cerebral hemodynamic impairments in sepsis. Our data suggest that

persisting neurovascular dysfunction is manifested even after adequate antibiotic treatment in aged mice.

An abundant body of evidence demonstrates that sepsis due to a wide range of bacterial infections results in generalized endothelial dysfunction (Szabo and Goldstein, 2011; Becker et al., 2012; Wexler et al., 2012). Here we provide evidence that *L. monocytogenes* infection also causes marked endothelial dysfunction, which persists after antibiotic treatment. Various bacterial species can exert either a direct effect on the vascular endothelium or promote endothelial dysfunction through the induction of pro-inflammatory mediators and oxidative stress (Al-Obaidi and Desa, 2018). *L. monocytogenes* is known to release the pore-forming toxin listeriolysin O, which confers deleterious effects on endothelial cells (Drevets, 1998; Wilson and Drevets, 1998; Kayal et al., 1999; Kayal et al., 2002). Additionally, *L. monocytogenes* can also invade brain microvascular endothelial cells (Drevets et al., 1995; Greiffenberg et al., 1998). Our findings that *L. monocytogenes* infection promotes significant endothelial dysfunction in aged mice is translationally relevant, as healthy endothelial function is a prerequisite for normal NVC responses. The limitation to our findings is that endothelial function measured in aorta rings cannot be directly translated to the function of endothelial cells in the cerebral microcirculation due to known significant morphological and functional differences between endothelial cells from different anatomic sites (Sengoelge et al., 2005). However, recent studies suggest that the extent of generalized endothelial dysfunction predicts cognitive performance in older adults (Csipo et al., 2019a), providing additional evidence on the role of endothelial dysfunction in impairment of NVC responses in sepsis. Further, while not the part of this study, future experiments are warranted to evaluate the contribution of endothelial function in hemodynamic responses of NVC measured *in vivo* (such as in L-NAME and acetylcholine infused animals).

A growing body of clinical evidence demonstrates that persisting cognitive impairment is one of the major complications observed in sepsis survivors (Iwashyna et al., 2010). Recent meta-analysis studies report that cognitive impairment is observed in up to 21% of sepsis survivors and that sepsis may affect different domains of cognition including attention, cognitive flexibility, processing speed and working memory (Calsavara et al., 2018b). The study reports that cognitive decline can be observed as early as 24 h after discharge from the intensive care unit in young and middle-aged sepsis survivors of 34–64 years of age. When tested 1 year after sepsis incident, all subjects presented with a general improvement in cognitive performance for Verbal Fluency, Mini Mental State Examination, Word Listing Learning, Word List Recall, Word List Recognition and Praxis Recall. Interestingly, cognitive performance based on Modified Boston Naming Test and Constructional Praxis remained unchanged from the time of discharge from intensive care unit, suggesting sepsis has profound and long-lasting effects on cognitive performance in young and middle-aged adults (Calsavara et al., 2018b). Further, clinical studies report that cognitive impairment among sepsis survivors of > 65 years of age is significantly associated with substantial and persistent new cognitive impairments and functional disability 1-year post-sepsis, with the magnitude of these deficits likely leading to loss of independence and severely reduced quality of life. In our study, we did not observe significant difference in cognitive performance early post-sepsis when compared to control animals. Possible explanation for non-significant difference in cognitive performance, but just a trend, could be due to the sample size and due to the choice of behavioral test. PhenoTyper homecage system that was used in our experiments is the food reward-based spatial memory task (Logan et al., 2018), and while it evaluates hippocampal function, it does not allow evaluation of other domains of cognitive function that are known to be most affected in sepsis in humans (Calsavara et al., 2018b). Therefore, whether cognitive deficits observed in the model used in the current study are present in other domains of cognition and whether the relationship between impairment of NVC responses and cognitive dysfunction exist is yet to be studied.

CONCLUSION

In conclusion, findings from our study suggest that sepsis-associated endothelial dysfunction and impairment of NVC responses in aged animals may contribute to long-term cognitive deficits in older sepsis survivors. Future studies are warranted to determine whether pharmacological interventions aimed at restoration of endothelial function and NVC responses are effective in improving cognitive function in sepsis survivors.

DATA AVAILABILITY STATEMENT

The raw data supporting the conclusions of this article will be made available by the authors, without undue reservation.

ETHICS STATEMENT

The animal study was reviewed and approved by The Institutional Animal Care and Use Committee at the University of Oklahoma Health Sciences Center, Protocol #17-072-SSL.

AUTHOR CONTRIBUTIONS

TC, BC, DD, ZU, and AY designed and performed the study. All authors contributed to the article and approved the submitted version.

FUNDING

This work was supported by the Oklahoma Center for the Advancement of Science and Technology, Presbyterian Heath Foundation, American Federation for Aging Research, National Institute on Aging (R01-AG055395 and R01-AG068295), National Institute of Neurological Disorders and Stroke (R01-NS100782), NIA-supported Geroscience Training Program in Oklahoma (T32AG052363), and the Cellular and Molecular GeroScience CoBRE (P20GM125528, sub#5337).

REFERENCES

Aird, W. C. (2003). The role of the endothelium in severe sepsis and multiple organ dysfunction syndrome. *Blood* 101, 3765–3777. doi: 10.1182/blood-2002-06-1887

Al-Obaidi, M. M. J., and Desa, M. N. M. (2018). Mechanisms of blood brain barrier disruption by different types of bacteria, and bacterial-host interactions facilitate the bacterial pathogen invading the brain. *Cell Mol. Neurobiol.* 38, 1349–1368. doi: 10.1007/s10571-018-0609-2

Andrews, R. M., and Elixhauser, A. (2006). *The National Hospital Bill: Growth Trends and 2005 Update on the Most Expensive Conditions by Payer: Statistical Brief #42*. Rockville, MD: Healthcare Cost and Utilization Project (HCUP) Statistical Briefs.

Angus, D. C., Linde-Zwirble, W. T., Lidicker, J., Clermont, G., Carcillo, J., and Pinsky, M. R. (2001). Epidemiology of severe sepsis in the United States: analysis of incidence, outcome, and associated costs of care. *Crit. Care Med.* 29, 1303–1310. doi: 10.1097/00003246-200107000-00002

Bailey-Downs, L. C., Sosnowska, D., Toth, P., Mitschelen, M., Gautam, T., Henthorn, J. C., et al. (2012). Growth hormone and IGF-1 deficiency exacerbate high-fat diet-induced endothelial impairment in obese lewis dwarf rats: implications for vascular aging. *J. Gerontol. A Biol. Sci. Med. Sci.* 67, 553–564. doi: 10.1093/gerona/glr197

Becker, L., Prado, K., Foppa, M., Martinelli, N., Aguiar, C., Furian, T., et al. (2012). Endothelial dysfunction assessed by brachial artery ultrasound in severe sepsis and septic shock. *J. Crit. Care* 27, 316 e9-e14. doi: 10.1016/j.jcrc.2011.08.002

Bonazzi, M., Lecuit, M., and Cossart, P. (2009). Listeria monocytogenes internalin and E-cadherin: from structure to pathogenesis. *Cell Microbiol.* 11, 693–702. doi: 10.1111/j.1462-5822.2009.01293.x

Bowie, R. A., O'Connor, P. J., and Mahajan, R. P. (2003). Cerebrovascular reactivity to carbon dioxide in sepsis syndrome. *Anaesthesia* 58, 261–265. doi: 10.1046/j.1365-2044.2003.29671.x

Calsavara, A. J. C., Costa, P. A., Nobre, V., and Teixeira, A. L. (2018a). Factors associated with short and long term cognitive changes in patients with sepsis. *Sci. Rep.* 8:4509. doi: 10.1038/s41598-018-22754-3

Calsavara, A. J. C., Nobre, V., Barichello, T., and Teixeira, A. L. (2018b). Post-sepsis cognitive impairment and associated risk factors: a systematic review. *Aust. Crit. Care* 31, 242–253. doi: 10.1016/j.aucc.2017.06.001

Cassidy, B. R., Zhang, M., Sonntag, W. E., and Drevets, D. A. (2020). Neuroinvasive Listeria monocytogenes infection triggers accumulation of brain CD8(+) tissue-resident memory T cells in a miR-155-dependent fashion. *J. Neuroinflammation* 17:259. doi: 10.1186/s12974-020-01929-8

Coletta, C., Modis, K., Olah, G., Brunyanszki, A., Herzig, D. S., Sherwood, E. R., et al. (2014). Endothelial dysfunction is a potential contributor to multiple organ failure and mortality in aged mice subjected to septic shock: preclinical studies in a murine model of cecal ligation and Puncture. *Crit. Care* 18:511. doi: 10.1186/s13054-014-0511-3

Corrales-Medina, V. F., Alvarez, K. N., Weissfeld, L. A., Angus, D. C., Chirinos, J. A., Chang, C. C., et al. (2015). Association between hospitalization for Pneumonia and subsequent risk of Cardiovascular disease. *JAMA* 313, 264–274. doi: 10.1001/jama.2014.18229

Crippa, I. A., Subira, C., Vincent, J. L., Fernandez, R. F., Hernandez, S. C., Cavicchi, F. Z., et al. (2018). Impaired cerebral autoregulation is associated with brain dysfunction in patients with sepsis. *Crit. Care* 22:327. doi: 10.1186/s13054-018-2258-8

Csipo, T., Lipecz, A., Fulop, G. A., Hand, R. A., Ngo, B. N., Dzialendzik, M., et al. (2019a). Age-related decline in peripheral vascular health predicts cognitive impairment. *Geroscience* 41, 125–136. doi: 10.1007/s11357-019-00063-5

Csipo, T., Mukli, P., Lipecz, A., Tarantini, S., Bahadli, D., Abdulhussein, O., et al. (2019b). Assessment of age-related decline of neurovascular coupling responses by functional near-infrared spectroscopy (fNIRS) in humans. *Geroscience* 41, 495–509. doi: 10.1007/s11357-019-00122-x

Csiszar, A., Labinskyy, N., Jimenez, R., Pinto, J. T., Ballabh, P., Losonczy, G., et al. (2009). Anti-oxidative and anti-inflammatory vasoprotective effects of caloric restriction in aging: role of circulating factors and SIRT1. *Mech. Ageing Dev.* 130, 518–527. doi: 10.1016/j.mad.2009.06.004

Csiszar, A., Labinskyy, N., Perez, V., Recchia, F. A., Podlutsky, A., Mukhopadhyay, P., et al. (2008). Endothelial function and vascular oxidative stress in long-lived GH/IGF-deficient Ames dwarf mice. *Am. J. Physiol. Heart Circ. Physiol.* 295, H1882–H1894. doi: 10.1152/ajpheart.412.2008

Csiszar, A., Yabluchanskiy, A., Ungvari, A., Ungvari, Z., and Tarantini, S. (2019). Overexpression of catalase targeted to mitochondria improves neurovascular coupling responses in aged mice. *Geroscience* 41, 609–617. doi: 10.1007/s11357-019-00111-0

Daviaud, F., Grimaldi, D., Dechartres, A., Charpentier, J., Geri, G., Marin, N., et al. (2015). Timing and causes of death in septic shock. *Ann. Intensive Care* 5:16. doi: 10.1186/s13613-015-0058-8

de Azevedo, D. S., Salinet, A. S. M., de Lima Oliveira, M., Teixeira, M. J., Bor-Seng-Shu, E., and de Carvalho Nogueira, R. (2017). Cerebral hemodynamics in sepsis assessed by transcranial Doppler: a systematic review and meta-analysis. *J. Clin. Monit. Comput.* 31, 1123–1132. doi: 10.1007/s10877-016-9945-2

De Backer, D., Orbegozo Cortes, D., Donadello, K., and Vincent, J. L. (2014). Pathophysiology of microcirculatory dysfunction and the pathogenesis of septic shock. *Virulence* 5, 73–79. doi: 10.4161/viru.26482

Dramsi, S., Lebrun, M., and Cossart, P. (1996). Molecular and genetic determinants involved in invasion of mammalian cells by Listeria monocytogenes. *Curr. Top. Microbiol. Immunol.* 209, 61–77. doi: 10.1007/978-3-642-85216-9_4

Drevets, D. A. (1998). Listeria monocytogenes virulence factors that stimulate endothelial cells. *Infect. Immun.* 66, 232–238. doi: 10.1128/IAI.66.1.232-238.1998

Drevets, D. A., Sawyer, R. T., Potter, T. A., and Campbell, P. A. (1995). Listeria monocytogenes infects human endothelial cells by two distinct mechanisms. *Infect. Immun.* 63, 4268–4276. doi: 10.1128/IAI.63.11.4268-4276.1995

Farias Quipildor, G. E., Mao, K., Hu, Z., Novaj, A., Cui, M. H., Gulinello, M., et al. (2019). Central IGF-1 protects against features of cognitive and sensorimotor decline with aging in male mice. *Geroscience* 41, 185–208. doi: 10.1007/s11357-019-00065-3

Fulop, G. A., Kiss, T., Tarantini, S., Balasubramanian, P., Yabluchanskiy, A., Farkas, E., et al. (2018). Nrf2 deficiency in aged mice exacerbates cellular senescence promoting cerebrovascular inflammation. *Geroscience* 40, 513–521. doi: 10.1007/s11357-018-0047-6

Greiffenberg, L., Goebel, W., Kim, K. S., Weiglein, I., Bubert, A., Engelbrecht, F., et al. (1998). Interaction of Listeria monocytogenes with human brain microvascular endothelial cells: InlB-dependent invasion, long-term intracellular growth, and spread from macrophages to endothelial cells. *Infect. Immun.* 66, 5260–5267. doi: 10.1128/IAI.66.11.5260-5267.1998

Hall, M. J., Williams, S. N., DeFrances, C. J., and Golosinskiy, A. (2011). Inpatient care for septicemia or sepsis: a challenge for patients and hospitals. *NCHS Data Brief.* 1–8.

Horvath, B., Orsy, P., and Benyo, Z. (2005). Endothelial NOS-mediated relaxations of isolated thoracic aorta of the C57BL/6J mouse: a methodological study. *J. Cardiovasc. Pharmacol.* 45, 225–231. doi: 10.1097/01.fjc.0000154377.90069.b9

Hotchkiss, R. S., Moldawer, L. L., Opal, S. M., Reinhart, K., Turnbull, I. R., and Vincent, J. L. (2016). Sepsis and septic shock. *Nat. Rev. Dis. Primers* 2:16045. doi: 10.1038/nrdp.2016.45

Iwashyna, T. J., Ely, E. W., Smith, D. M., and Langa, K. M. (2010). Long-term cognitive impairment and functional disability among survivors of severe sepsis. *JAMA* 304, 1787–1794. doi: 10.1001/jama.2010.1553

Kayal, S., Lilienbaum, A., Join-Lambert, O., Li, X., Israel, A., and Berche, P. (2002). Listeriolysin O secreted by Listeria monocytogenes induces NF-kappaB signalling by activating the IkappaB kinase complex. *Mol. Microbiol.* 44, 1407–1419. doi: 10.1046/j.1365-2958.2002.02973.x

Kayal, S., Lilienbaum, A., Poyart, C., Memet, S., Israel, A., and Berche, P. (1999). Listeriolysin O-dependent activation of endothelial cells during infection with Listeria monocytogenes: activation of NF-kappa B and upregulation of adhesion molecules and chemokines. *Mol. Microbiol.* 31, 1709–1722. doi: 10.1046/j.1365-2958.1999.01305.x

Lagu, T., Rothberg, M. B., Shieh, M. S., Pekow, P. S., Steingrub, J. S., and Lindenauer, P. K. (2012). Hospitalizations, costs, and outcomes of severe sepsis in the United States 2003 to 2007. *Crit. Care Med.* 40, 754–761. doi: 10.1097/CCM.0b013e318232db65

Lipecz, A., Csipo, T., Tarantini, S., Hand, R. A., Ngo, B. N., Conley, S., et al. (2019). Age-related impairment of neurovascular coupling responses: a dynamic vessel analysis (DVA)-based approach to measure decreased flicker light stimulus-induced retinal arteriolar dilation in healthy older adults. *Geroscience* 41, 341–349. doi: 10.1007/s11357-019-00078-y

Logan, S., Owen, D., Chen, S., Chen, W. J., Ungvari, Z., Farley, J., et al. (2018). Simultaneous assessment of cognitive function, circadian rhythm, and spontaneous activity in aging mice. *Geroscience* 40, 123–137. doi: 10.1007/s11357-018-0019-x

Logan, S., Royce, G. H., Owen, D., Farley, J., Ranjo-Bishop, M., Sonntag, W. E., et al. (2019). Accelerated decline in cognition in a mouse model of increased oxidative stress. *Geroscience* 41, 591–607. doi: 10.1007/s11357-019-00105-y

Marik, P. E. (2006). Management of the critically ill geriatric patient. *Crit. Care Med.* 34(9 Suppl.), S176–S182. doi: 10.1097/01.CCM.0000232624.14883.9A

Martin, G. S., Mannino, D. M., Eaton, S., and Moss, M. (2003). The epidemiology of sepsis in the United States from 1979 through 2000. *N. Engl. J. Med.* 348, 1546–1554. doi: 10.1056/NEJMoa022139

Masse, M. H., Richard, M. A., D'Aragon, F., St-Arnaud, C., Mayette, M., Adhikari, N. K. J., et al. (2018). Early evidence of sepsis-associated hyperperfusion-a study of cerebral blood flow measured with MRI arterial spin labeling in critically Ill septic patients and control subjects. *Crit. Care Med.* 46, e663–e669. doi: 10.1097/CCM.0000000000003147

Pandharipande, P. P., Girard, T. D., Jackson, J. C., Morandi, A., Thompson, J. L., Pun, B. T., et al. (2013). Long-term cognitive impairment after critical illness. *N. Engl. J. Med.* 369, 1306–1316. doi: 10.1056/NEJMoa1301372

Pearson, K. J., Baur, J. A., Lewis, K. N., Peshkin, L., Price, N. L., Labinskyy, N., et al. (2008). Resveratrol delays age-related deterioration and mimics transcriptional aspects of dietary restriction without extending life Span. *Cell Metabolism* 8, 157–168. doi: 10.1016/j.cmet.2008.06.011

Peters, K., Unger, R. E., Brunner, J., and Kirkpatrick, C. J. (2003). Molecular basis of endothelial dysfunction in sepsis. *Cardiovasc. Res.* 60, 49–57. doi: 10.1016/S0008-6363(03)00397-3

Pfister, D., Siegemund, M., Dell-Kuster, S., Smielewski, P., Ruegg, S., Strebel, S. P., et al. (2008). Cerebral perfusion in sepsis-associated delirium. *Crit. Care* 12:R63. doi: 10.1186/cc6891

Sengoelge, G., Luo, W., Fine, D., Perschl, A. M., Fierlbeck, W., Haririan, A., et al. (2005). A SAGE-based comparison between glomerular and aortic endothelial cells. *Am. J. Physiol. Renal. Physiol.* 288, F1290–F1300. doi: 10.1152/ajprenal.00076.2004

Starr, M. E., and Saito, H. (2014). Sepsis in old age: review of human and animal studies. *Aging Dis.* 5, 126–136. doi: 10.14336/AD.2014.0500126

Stortz, J. A., Hollen, M. K., Nacionales, D. C., Horiguchi, H., Ungaro, R., Dirain, M. L., et al. (2019). Old mice demonstrate organ Dysfunction as well as prolonged inflammation, immunosuppression, and weight loss in a modified surgical sepsis model. *Crit. Care Med.* 47, e919–e929. doi: 10.1097/CCM.0000000000003926

Szabo, C., and Goldstein, B. (2011). Endothelial dysfunction as predictor of mortality in sepsis. *Crit. Care Med.* 39, 878–879. doi: 10.1097/CCM.0b013e31820a52ba

Tarantini, S., Fulop, G. A., Kiss, T., Farkas, E., Zolei-Szenasi, D., Galvan, V., et al. (2017). Demonstration of impaired neurovascular coupling responses in TG2576 mouse model of Alzheimer's disease using functional laser speckle contrast imaging. *Geroscience* 39, 465–473. doi: 10.1007/s11357-017-9980-z

Tarantini, S., Hertelendy, P., Tucsek, Z., Valcarcel-Ares, M. N., Smith, N., Menyhart, A., et al. (2015). Pharmacologically-induced neurovascular uncoupling is associated with cognitive impairment in mice. *J. Cereb. Blood Flow Metab.* 35, 1871–1881. doi: 10.1038/jcbfm.2015.162

Tarantini, S., Valcarcel-Ares, M. N., Toth, P., Yabluchanskiy, A., Tucsek, Z., Kiss, T., et al. (2019a). Nicotinamide mononucleotide (NMN) supplementation rescues cerebromicrovascular endothelial function and neurovascular coupling responses and improves cognitive function in aged mice. *Redox Biol.* 24:101192. doi: 10.1016/j.redox.2019.101192

Tarantini, S., Valcarcel-Ares, N. M., Yabluchanskiy, A., Fulop, G. A., Hertelendy, P., Gautam, T., et al. (2018). Treatment with the mitochondrial-targeted antioxidant peptide SS-31 rescues neurovascular coupling responses and cerebrovascular endothelial function and improves cognition in aged mice. *Aging Cell* 17:e12731. doi: 10.1111/acel.12731

Tarantini, S., Yabluchanskiy, A., Csipo, T., Fulop, G., Kiss, T., Balasubramanian, P., et al. (2019b). Treatment with the poly(ADP-ribose) polymerase inhibitor PJ-34 improves cerebromicrovascular endothelial function, neurovascular coupling responses and cognitive performance in aged mice, supporting the NAD+ depletion hypothesis of neurovascular aging. *Geroscience* 41, 533–542. doi: 10.1007/s11357-019-00101-2

Terborg, C., Schummer, W., Albrecht, M., Reinhart, K., Weiller, C., and Rother, J. (2001). Dysfunction of vasomotor reactivity in severe sepsis and septic shock. *Intensive Care Med.* 27, 1231–1234. doi: 10.1007/s001340101005

Toksvang, L. N., Plovsing, R. R., Petersen, M. W., Moller, K., and Berg, R. M. (2014). Poor agreement between transcranial Doppler and near-infrared spectroscopy-based estimates of cerebral blood flow changes in sepsis. *Clin. Physiol. Funct. Imaging* 34, 405–409. doi: 10.1111/cpf.12120

Toth, P., Tarantini, S., Ashpole, N. M., Tucsek, Z., Milne, G. L., Valcarcel-Ares, N. M., et al. (2015a). IGF-1 deficiency impairs neurovascular coupling in mice: implications for cerebromicrovascular aging. *Aging Cell* 14, 1034–1044. doi: 10.1111/acel.12372

Toth, P., Tarantini, S., Davila, A., Valcarcel-Ares, M. N., Tucsek, Z., Varamini, B., et al. (2015b). Purinergic glio-endothelial coupling during neuronal activity: role of P2Y1 receptors and eNOS in functional hyperemia in the mouse somatosensory cortex. *Am. J. Physiol. Heart Circ. Physiol.* 309, H1837–H1845. doi: 10.1152/ajpheart.00463.2015

Toth, P., Tarantini, S., Tucsek, Z., Ashpole, N. M., Sosnowska, D., Gautam, T., et al. (2014). Resveratrol treatment rescues neurovascular coupling in aged mice:role of improved cerebromicrovascular endothelial function and down-regulation of NADPH oxidas. *Am. J. Physiol. Heart Circ. Physiol.* 306, H299–H308. doi: 10.1152/ajpheart.00744.2013

Tubiana, S., Varon, E., Biron, C., Ploy, M. C., Mourvillier, B., Taha, M. K., et al. (2020). Community-acquired bacterial meningitis in adults: in-hospital prognosis, long-term disability and determinants of outcome in a multicentre prospective cohort. *Clin. Microbiol. Infect* 26, 1192–1200. doi: 10.1016/j.cmi.2019.12.020

Tucsek, Z., Toth, P., Tarantini, S., Sosnowska, D., Gautam, T., Warrington, J. P., et al. (2014). Aging exacerbates obesity-induced cerebromicrovascular rarefaction, neurovascular uncoupling, and cognitive decline in mice. *J. Gerontol. A Biol. Sci. Med. Sci.* 69, 1339–1352. doi: 10.1093/gerona/glu080

Ungvari, Z., Bailey-Downs, L., Gautam, T., Sosnowska, D., Wang, M., Monticone, R. E., et al. (2011a). Age-associated vascular oxidative stress, Nrf2 dysfunction and NF-kB activation in the non-human primate *Macaca mulatta*. *J. Gerontol. A Biol. Sci. Med. Sci.* 66, 866–875. doi: 10.1093/gerona/glr092

Ungvari, Z., Bailey-Downs, L., Sosnowska, D., Gautam, T., Koncz, P., Losonczy, G., et al. (2011b). Vascular oxidative stress in aging: a homeostatic failure due to dysregulation of Nrf2-mediated antioxidant response. *Am. J. Physiol. Heart Circ. Physiol.* 301, H363–H372. doi: 10.1152/ajpheart.01134.2010

Ungvari, Z., Tarantini, S., Hertelendy, P., Valcarcel-Ares, M. N., Fülöp, G. Á, Logan, S., et al. (2017). Cerebromicrovascular dysfunction predicts cognitive decline and gait abnormalities in a mouse model of whole brain irradiation-induced accelerated brain senescence. *GeroScience* 39, 33–42. doi: 10.1007/s11357-017-9964-z

Vachharajani, V., Cunningham, C., Yoza, B., Carson, J., Vachharajani, T. J., and McCall, C. (2012). Adiponectin-deficiency exaggerates sepsis-induced microvascular dysfunction in the mouse brain. *Obesity* 20, 498–504. doi: 10.1038/oby.2011.316

Vasko, A., Siro, P., Laszlo, I., Szatmari, S., Molnar, L., Fulesdi, B., et al. (2014). Assessment of cerebral tissue oxygen saturation in septic patients during acetazolamide provocation – a near infrared spectroscopy study. *Acta Physiol. Hung.* 101, 32–39. doi: 10.1556/APhysiol.101.2014.1.4

Wexler, O., Morgan, M. A., Gough, M. S., Steinmetz, S. D., Mack, C. M., Darling, D. C., et al. (2012). Brachial artery reactivity in patients with severe sepsis: an observational study. *Crit. Care* 16:R38. doi: 10.1186/cc1 1223

Wier, L. M., and Andrews, R. M. (2006). *The National Hospital Bill: The Most Expensive Conditions by Payer, 2008: Statistical Brief # 107*. Rockville, MD: Healthcare Cost and Utilization Project (HCUP) Statistical Briefs.

Wilson, S. L., and Drevets, D. A. (1998). Listeria monocytogenes infection and activation of human brain microvascular endothelial cells. *J. Infect. Dis.* 178, 1658–1666. doi: 10.1086/314490

Wood, K. A., and Angus, D. C. (2004). Pharmacoeconomic implications of new therapies in sepsis. *Pharmacoeconomics* 22, 895–906. doi: 10.2165/00019053-200422140-00001

Yildiz, O., Aygen, B., Esel, D., Kayabas, U., Alp, E., Sumerkan, B., et al. (2007). Sepsis and meningitis due to Listeria monocytogenes. *Yonsei Med. J.* 48, 433–439. doi: 10.3349/ymj.2007.48.3.433

Zhang, M., Gillaspy, A. F., Gipson, J. R., Cassidy, B. R., Nave, J. L., Brewer, M. F., et al. (2018). Neuroinvasive Listeria monocytogenes infection triggers IFN-activation of Microglia and Upregulates Microglial miR-155. *Front. Immunol.* 9:2751.

Conflict of Interest: The authors declare that the research was conducted in the absence of any commercial or financial relationships that could be construed as a potential conflict of interest.

frontiers in Aging Neuroscience

ORIGINAL RESEARCH
published: 21 May 2021
doi: 10.3389/fnagi.2021.617733

Notch3-Dependent Effects on Adult Neurogenesis and Hippocampus-Dependent Learning in a Modified Transgenic Model of CADASIL

*Fanny Ehret[1], Ricardo Moreno Traspas[2], Marie-Theres Neumuth[1], Bianca Hamann[1], Daniela Lasse[1] and Gerd Kempermann[1,2]**

[1] German Center for Neurodegenerative Diseases (DZNE), Dresden, Germany, [2] Center for Regenerative Therapies Dresden, TU Dresden, Dresden, Germany

We and others have reported that Notch3 is a regulator of adult hippocampal neurogenesis. *Cerebral Autosomal Dominant Arteriopathy with Subcortical Infarcts and Leukoencephalopathy* (CADASIL), the most common genetic form of vascular dementia, is caused by mutations in *Notch3*. The present study intended to investigate whether there is a correlation between altered adult hippocampal neurogenesis and spatial memory performance in CADASIL transgenic mice. To overcome visual disabilities that hampered behavioral testing of the original mice (on an FVB background) we back-crossed the existing TgN3^{R169C} CADASIL mouse model onto the C57BL/6J background. These animals showed an age-dependent increase in the pathognomonic granular osmiophilic material (GOM) deposition in the hippocampus. Analysis in the Morris water maze task at an age of 6 and 12 months revealed deficits in re-learning and perseverance in the CADASIL transgenic mice. Overexpression of Notch3 alone resulted in deficits in the use of spatial strategies and diminished adult neurogenesis in both age groups. The additional CADASIL mutation compensated the effect on strategy usage but not on adult neurogenesis. In brain bank tissue samples from deceased CADASIL patients we found signs of new neurons, as assessed by calretinin immunohistochemistry, but no conclusive quantification was possible. In summary, while our study confirmed the role of Notch3 in adult neurogenesis, we found a specific effect of the CADASIL mutation only on the reversion of the Notch3 effect on behavior, particularly visible at 6 months of age, consistent with a loss of function. The mutation did not revert the Notch3-dependent changes in adult neurogenesis or otherwise affected adult neurogenesis in this model.

Keywords: adult neurogenesis, CADASIL, dentate gyrus, hippocampus, Notch3, spatial learning, human brain, mouse model

OPEN ACCESS

Edited by:
Prasad V. Katakam, Tulane University, United States

Reviewed by:
Shanting Zhao, Northwest A&F University, China
Diego Sepulveda-Falla, University Medical Center Hamburg-Eppendorf, Germany

***Correspondence:**
Gerd Kempermann
gerd.kempermann@dzne.de; gerd.kempermann@tu-dresden.de

Received: *15 October 2020*
Accepted: *08 April 2021*
Published: *21 May 2021*

Citation:
Ehret F, Moreno Traspas R, Neumuth M-T, Hamann B, Lasse D and Kempermann G (2021) Notch3-Dependent Effects on Adult Neurogenesis and Hippocampus-Dependent Learning in a Modified Transgenic Model of CADASIL. Front. Aging Neurosci. 13:617733. doi: 10.3389/fnagi.2021.617733

Abbreviations: BrdU, Bromodeoxyuridine; CADASIL, Cerebral autosomal dominant arteriopathy with subcortical infarcts and leukoencephalopathy; DG, dentate gyrus; GFAP, glial fibrillary acidic protein; GOM, granular osmiophilic material; PFA, paraformaldehyde; N3, Notch3; RT, room temperature; TBS, tris-buffered saline; TgN3^{WT}, transgenic mice overexpressing rat wild type Notch3; TgN3^{R169C}, transgenic mice overexpressing rat CADASIL mutant Notch3; SGZ, subgranular zone.

INTRODUCTION

Cerebral Autosomal Dominant Arteriopathy with Subcortical Infarcts and Leukoencephalopathy (CADASIL), the most common genetic cause of stroke and vascular dementia, results in accumulation of granular osmiophilic material (GOM) in small and medium sized arteries (Chabriat et al., 2009). We previously identified GOMs in the vasculature of the adult hippocampus in an established transgenic mouse model overexpressing *Notch3* (N3*)* with a CADASIL-causing point mutation (Ehret et al., 2015). In that model we saw effects on adult hippocampal neurogenesis but could not assess any potential role in hippocampus-dependent behavior, because the existing mice, which are on a FVB background, cannot be feasibly tested for spatial memory because of a genetic visual deficit (Voikar et al., 2001; Farley et al., 2011). The current project aimed at overcoming that limitation in order to support our original hypothesis that neurogenesis-related impairments due to the N3 mutation in neural stem cells might contribute to the overall phenotype in CADASIL.

The hippocampus is one of the first structures affected in dementias, playing an essential role in memory processing. Particularly the consolidation of declarative memory, which includes semantic and episodic memory, is processed by the hippocampus (O'Keefe and Dostrovsky, 1971; reviewed by Morris, 2007). Even though only a few studies have specified the memory deficits seen in CADASIL patients and despite the limitations of the neuropsychological assessment strategies used, some interesting commonalties have arisen. CADASIL patients often present deficits in episodic memory, executive function and working memory prior to stroke and age-dependent cognitive decline (Buffon et al., 2006; Epelbaum et al., 2011). This pattern of memory impairment suggests, besides the involvement of subcortical-frontal regions, connections to the hippocampal subfields. Furthermore, a correlation has been identified between hippocampal volume and cognitive performance in CADASIL patients, independent of vascular lesions (O'Sullivan et al., 2009). Hence, these findings point to potential role of the hippocampus in the manifestation of CADASIL.

Besides its pivotal role in memory processing, the hippocampus is also unique in that it maintains lifelong adult neurogenesis. The current view suggests that neurogenesis in this region provides increased plasticity, which is critical for lifelong cognitive flexibility (Burghardt et al., 2012; Kempermann, 2012; Spalding et al., 2013; Garthe et al., 2014). This process is tightly controlled by internal and external factors acting on residing stem and progenitor cells. The Notch super-family is one of such transcriptional regulators that play a central role in stem cell quiescence and maintenance, progenitor cell proliferation and differentiation in the developing and adult brain (Ehm et al., 2010; Imayoshi et al., 2010; Lugert et al., 2010). Since CADASIL is due to a diversity of point mutations in N3, the Notch signaling pathway is of particular relevance. Although most of the work focuses on *Notch1* (N1), some aspects regarding the critical function of N3 in stem cell quiescence and neurogenesis have been identified (Kawai et al., 2017; Than-Trong et al., 2018). In adult mice, N3 is expressed in neural stem and progenitor cells in the subependymal zone of the lateral ventricles (Kawai et al., 2017) and the subgranular zone of the hippocampus (Ehret et al., 2015). Importantly, our previous research identified N3 as a critical regulator of precursor cell proliferation and differentiation in the neurogenic niche of the murine hippocampus (Ehret et al., 2015). Although a detailed analysis in human cells and tissues is still lacking, these findings already suggest that N3 might exert regulatory influences on neuronal plasticity that could impact hippocampus-dependent learning and memory.

The N3 signaling pathway is of outstanding relevance in CADASIL, since mutations in the N3 gene are disease-causative. We already proved the presence of altered hippocampal neurogenesis independent to overt vascular abnormalities in a transgenic mouse model of CADASIL (Ehret et al., 2015). In the current study we aimed at confirming whether N3 dysfunction might be an additional underlying mechanism accounting for the learning and memory deficits seen in CADASIL patients, possibly independent of vascular dysfunction but related to a dysfunction in neural stem cells in the hippocampus. For that purpose, we backcrossed the established mouse model TgN3^{R169C} (Joutel et al., 2010) onto a C57BL/6J background in order to allow unconstrained behavioral testing in the classical Morris water maze task. We used a concrete testing paradigm, which we had previously identified as highly sensitive to the contribution of adult-generated neurons to spatial learning (Garthe et al., 2009, 2014). Additionally, we intended to investigate whether we could find signs of altered adult hippocampal neurogenesis in samples from CADASIL patients.

MATERIALS AND METHODS

Animals and Tissue Preparation

TgN3^{WT} and TgN3^{R169C} generated by Joutel et al. (2010) and crossed back for 10 generations to C57BL/6J (Charles River), were maintained at the CRTD – Center for Regenerative Therapies Dresden, Dresden, Germany. WT littermates from both strains were used as controls. All experiments were conducted in accordance with the applicable European and National regulations (Tierschutzgesetz) and approved by the responsible authority (Landesdirektion Dresden, approval number 24-9168.11-1/2012-26). Animals were maintained on a 12 h light/dark cycle with food and water provided *ad libitum*. TgN3^{WT} and TgN3^{R169C} mice were genotyped by PCR (*Notch3* forward: 5′ TTC AGTGGTGGCGGGCGTC 3′ *Notch3* reverse: 5′GCCTACAGGTGCCACCATTA CGGC 3′; Vector forward: 5′ AACAGGAAGAATCGCAACGTTAAT 3′ Vector reverse: 5′ AATGCA GCGATCAACGCCTTCTC 3′). *Notch3* PCR products from TgN3^{WT} and TgN3^{R169C} mice were sequenced and the genetic mutation site was identified to confirm the correct genotype of the strains used. The effect on protein expression has been analyzed in the original TgN3^{WT} and TgN3^{R169C} mice and is shown in **Supplementary Figure 4**.

Female and male C57BL/6J, TgN3^{WT}, and TgN3^{R169C} mice received intraperitoneal injections of 5-bromo-2-deoxyuridine (BrdU, Sigma-Aldrich) at 50 mg/kg, dissolved in sterile 0.9%

NaCl (10 mg/ml). BrdU was delivered three times every 6 h for 6 months old animals and seven times every 24 h for 12 months old animals. Mice were killed 28 days after BrdU administration by using a mixture of ketamine and xylazine and transcardial perfusion with 0.9% NaCl and 4% paraformaldehyde (PFA). The brains were left in 4% PFA for 24 h at 4°C, transferred to 30% sucrose and cut into 40 μm thick serial coronal sections on a freezing microtome (HM430, Thermo Scientific). Sections were stored at −20°C in cryoprotectant solution (25% ethylene glycol, 25% glycerol in 0.1 M phosphate buffer, pH 7.4).

Human Samples

Post-mortem human hippocampus samples (N = 7 CADASIL and N = 6 Control samples) were obtained from the CADASIL brain bank, Leiden University, Netherlands (age range 48–70 years, including both sexes). Out of the seven CADASIL patients, six had a mutation on exon 4 and one in exon 8. The modeled R169C mutation was not present in the human samples. All participants gave informed consent that their samples could be used for research and publication, nevertheless to prevent traceability the data are only presented in charts. For details on the influence of age, sex or post mortem delay on the obtained (but ultimately inconclusive) data see **Supplementary Figure 1**.

Immunohistochemistry

Animal Tissue

As described previously (Kempermann et al., 2003), for BrdU detection every sixth brain section from C57BL/6J, TgN3^{WT}, TgN3^{R169C} animals at 6 months and 12 months of age were used (group size at 6 months WT = 15, TgN3 both 12 and at 12 months WT = 19, TgN3 both 13). Briefly for BrdU detection, sections were quenched with 0.6% H_2O_2 for 30 min, incubated in 2 N HCl for 30 min at 37°C followed by 1 h blocking with TBS^{++} (10% donkey serum, 0.2% Triton-X 100 in TBS) and incubation in monoclonal rat anti-BrdU antibody (1:500; OBT0030, Serotec) overnight at 4°C in TBS^{+} (3% donkey serum in TBS). For calretinin detection an analog protocol was used, but without the HCl denaturing step. Sections were incubated with primary antibody rabbit anti-calretinin (1:2000, CR7697, Swant). To determine the total number of labeled cells, the peroxidase method was used with biotinylated donkey anti-rat or anti-rabbit antibody (similarly as described for the human tissue). However, no counter stain was performed and sections were mounted on gelatine-coated slides and cover-slipped with Neo-Mount (Merck). For phenotyping of BrdU^{+} cells, immunofluorescence was performed. Free-floating sections were washed, incubated with 2 N HCL for 30 min at 37°C, blocked for 1 h in TBS^{++} and incubated over night at 4°C with the following primary antibodies: rat anti-BrdU (as above), mouse anti-NeuN (1:500; MAB377, Millipore), rabbit anti-S100β (1:1000; ab52642, Abcam). The next day, sections were washed and incubated with secondary antibody for 2 h at RT. All secondary antibodies were purchased from Dianova: anti-mouse Dye-Light 549, anti-rat Alexa 488, anti-rabbit Alexa 647. After a final washing step, sections were incubated for 10 min in Hoechst (1:4000 in TBS; 33342, Sigma-Aldrich) and then mounted on glass slides using 2.5% PVA-DABCO.

Human Tissue

Paraffin-fixed sections of 5 μm thickness were taken from three different blocks per human hippocampus. Per patient six sections two per each block were analyzed. Tissue sections were dewaxed with xylene and rehydrated with decreasing concentrations of ethanol. Unmasking was performed using 1 mM EDTA (pH 8) at 110°C in a pressure cooker for 5 min. Sections were afterward incubated with 3% H_2O_2 for 30 min, blocked for 1 h in TBS^{+} (containing 10% donkey serum) and subsequently Avidin-Biotin blocked (SP2001, Vector labs) followed by incubation with calretinin antibody (1:2000, CR7697, Swant) overnight at 4°C in TBS^{+} (containing 5% donkey serum).

To determine the number of labeled cells, the peroxidase method (Vectastain Elite ABC kit, Vector laboratories) was used with biotinylated donkey anti-rabbit antibody (1:500, Dianova) and diaminobenzidine (DAB, Sigma) as a chromogen. Sections were finally haematoxylin counter stained (Richard-Allan Scientific Hematoxylin, Thermo Scientific), sequentially dehydrated and cover-slipped with Entellan (Sigma-Aldrich).

Image Quantification

Bromodeoxyuridine and calretinin cell quantification were performed on coded slides using widefield light microscopy with a Leica microscope (DM 750, Leica). The number of immunopositive (+) cells present in the SGZ of the DG was quantified by manually counting all DAB-positive cells present within 40 μm of the granular cell layer of the DG formation (i.e., from Bregma −1.06 to Bregma −3.88). Fluorescence images for BrdU phenotyping were obtained on a fluorescence microscope with 2D structured illumination (ApoTome.2, Zeiss). Images were processed with Zen software (Zeiss), Fiji and Illustrator CS5 (Adobe). Only general contrast and color level adjustments were made; otherwise images were not digitally manipulated. Net neurogenesis and gliogenesis were calculated for each animal separately by multiplying the proportion of BrdU differentiation obtained through fluorescent double labeling (NeuN^{+}BrdU^{+} or S100β^{+}BrdU^{+}) with the number of BrdU^{+} cells obtained through DAB.

Morris Water Maze Task

Mice were trained in the reference memory version of the Morris water maze task to locate a hidden escape platform in a circular pool (2 m diameter). In opaque water (by adding non-toxic titan white) at 19–20°C, mice had to swim six trials a day for five consecutive days for 6 months-old mice, or seven consecutive days for 12 months-old mice. The experimental design (see **Figures 2A**, **4A**) contained 3 or 4 days acquisition (for 6 and 12 months old mice, respectively) followed by 2 or 3 days of reversal, where the platform position was switched to the opposite quadrant. Mice were released every day from a new starting position and allowed to search for the hidden platform for a maximum of 120 s. During each day the starting position remained constant. At the end of each trial and irrespective of trial performance, mice were guided to the platform and allowed to remain there for at least 15 s. At the last day a final trial with a visual platform in a new position was performed to evaluate the visual abilities of the mice. Swim paths were recorded using

EthoVision (Noldus) and further analyzed using Matlab (The Mathworks). To visualize spatial preference for the goal position in the probe trials, a heat map like occupancy plot was divided into 10 cm × 10 cm wide sectors and the probability of an animal to be found in each sector was calculated. Search strategies were classified according to parameters and an algorithm described in our previous study (Garthe et al., 2014), originally based on (Balschun et al., 2003). Strategies were defined by no more than two parameters that are not dependent on pool dimensions. In detail, the swim path data from EthoVision (Noldus) were used to derive the time-tagged x, y-coordinates for the dominant search strategies by an algorithm implemented in Matlab (Mathworks). For analysis of these search strategies a logistic regression model was applied and evaluated using the working environment R (for details see statistics).

Electron Microscopy

Female and male mice were perfused with 0.9% NaCl followed by Karnovsky's fixative (2% glutaraldehyde, 2% paraformaldehyde, 20 mM HEPES). The brains were left in Karnovsky solution overnight followed by vibratome sectioning (Model 1200 Leica) at a thickness of 200 μm. Tissue was contrasted for 2 h in 1% OsO_4 at 4°C, washed, *en bloc* contrasted with 1% uranyl acetate for 2 h at 4°C, washed and gradually dehydrated in ethanol. This was followed by infiltration of Epon 812 resin, embedding in molds and polymerization at 60°C for 24 h. Semithin sections were stained with 1% toluidine blue and 0.5% Borax (TB/Borax) and inspected with widefield microscope BZ 8000 (Keyence). Ultrathin 70 nm sections were analyzed on a transmission electron microscope (Morgagni 268D, FEI).

Statistics

For analysis of human post-mortem samples we used unpaired *t*-test since data was normally distributed.

For analysis of adult neurogenesis rates in transgenic animals we used one-way ANOVA, since the data passed the D'Agostino & Pearson normality test, with Bonferroni *post-hoc* test.

For statistical analysis of the effect of WT, $TgN3^{WT}$, and $TgN3^{R169C}$ on water maze performance (swim speed, latency, and path length), we performed the non-parametric testing of Friedman with Dunn's *post-hoc* test since the data was not normally distributed. For probe trial performance we used Kruskal–Wallis test at 6 months of age since data was not normally distributed, and one-way ANOVA at 12 months of age since data was normally distributed (tested with D'Agostino & Pearson normality test).

For statistical analysis of the effect of WT, $TgN3^{WT}$, and $TgN3^{R169C}$ on the search strategies, we applied a logistic regression (LR) (as discribed previously Garthe et al., 2016). Using the LR model with nested effect, we estimated the odds ratios for the three different genotypes (WT, $TgN3^{WT}$, and $TGN3^{R169C}$), thus comparing the chance of using more versus less hippocampus-dependent search strategies. Corresponding *p*-values are based on ANOVA. Calculations for search strategy analysis were done in working environment R, all other statistical calculations were done in Prism 7 (GraphPad).

RESULTS

Based on the previous observation of reduced adult hippocampal neurogenesis (Ehret et al., 2015) in the CADASIL transgenic mouse model established by Joutel et al. (2010), we aimed at identifying behavioral deficits in hippocampus-dependent spatial learning by the Morris water maze task. Therefore, this CADASIL transgenic mouse model was back-crossed onto the C57BL/6J background (B6) to overcome the limitations of the FVB/N background (Pugh et al., 2004) like impaired vision (Voikar et al., 2001).

Accumulation of Granular Osmiophilic Material Starts at 6 Months in CADASIL Transgenic Mice on the B6 Background

We first confirmed that in the new backcrossed model, neuropathological characteristics of CADASIL would be maintained. Accumulations of electron dense GOMs in small and medium sized arteries, a key feature of the disease process, appears in some transgenic animal models but not in all. Especially in the used animal model of $TgN3^{R169C}$ on FVB/N background, GOM deposits started to occur at 5 months in the pial arteries and became widely distributed throughout the brain by 10–12 months of age (Joutel et al., 2010). On the B6 background, we now carried out a detailed electron microscopic analysis to observe the disease progression. Surprisingly, we found GOM accumulations already at 6 months of age in $TgN3^{R169C}$ on C57BL/6 background in the hippocampus (**Figure 1**). GOMs can be found close to the 3rd ventricle and around medium-sized vessels of the hippocampal fissure.

Deficits in Hippocampus-Dependent Learning in Aged $TgN3^{WT}$ and $TgN3^{R169C}$ Mice on the B6 Background

An extended protocol was used for this task, consisting of 4 days of acquisition and 3 days of reversal, to cope with age-dependent deficits (experimental protocol **Figure 2A**). At 12 months of age, the transgenic mice showed specific deficits in relearning of a new platform position in the old context (reversal) while the initial acquisition was not impaired. In detail, the analysis of latency to find the hidden platform was unimpaired (Chi-Square = 0.857, $p = 0.768$; **Figure 2C**), but since swim speed differed significantly (Chi-Square = 12.29, $p = 0.003$ with $TgN3^{WT} < TgN3^{R169C}$, $p = 0.0015$; **Figure 2D**), the analysis of path lengths is a more reliable measure (Chi-Square = 6, $p = 0.05$ with $TgN3^{WT}$ vs. $TgN3^{R169C}$ $p = 0.048$; **Figure 2B**). Relearning of a new platform position was impaired in CADASIL mice, as the analysis of path-length during reversal showed (Chi-Square = 6, $p = 0.027$ with WT vs. $TgN3^{R169C}$ $p = 0.04$). Nevertheless, the initial memory of the previous platform position was not impaired, as analyzed during a probe trial by measuring the time the mouse spent in the relevant target zone [$F_{(2,40)} = 1.667$, $p = 0.20$] and the number of former goal crossings [$F_{(2,40)} = 0.86$ $p = 0.43$; **Figures 2G,J**]. In addition, we asked how many trials it took each mouse after goal reversal to regain a mean path length that was equal or shorter than on the last day of acquisition. Although there were variations

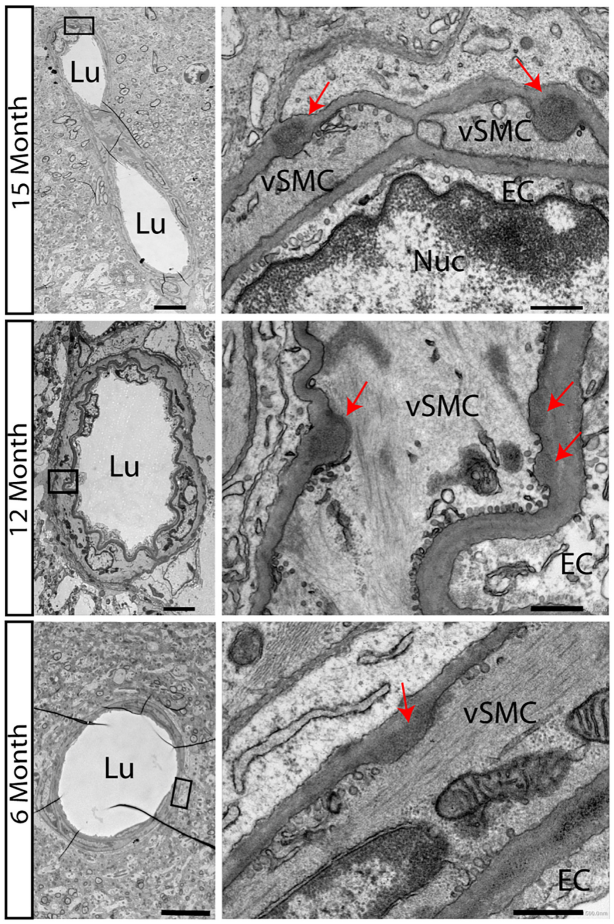

FIGURE 1 | Accumulations of GOMs in hippocampus of TgN3^{R169C} mice. Electron microscopic analysis of the hippocampus in TgN3^{R169C} mice showed accumulation of electron dense granular osmiophilic material at 15 and 12 months of age and less dense accumulation already at 6 months of age, as highlighted by the red arrow. Scale bar for left column 5 μm, right column 0.5 μm. EC, endothelial cells; Lu, Lumen; Nuc, Nucleus; vSMC, vascular smooth muscle cells.

between the different lines, no statistically significant difference could be detected [ANOVA $F_{(2,40)} = 2.45$, $p = 0.09$; **Figure 2K**]. The low p-value of 0.09 nevertheless indicates that further studies with increased power might reveal an effect of the mutation on the N3-dependent impairment.

In conclusion, the old platform position could be easily remembered, but CADASIL TgN3^{R169C} mice showed deficits in up-dating the old context. A detailed analysis of the search strategies revealed that the mice used different strategies to locate the hidden platform. These strategies are indicative of the underlying cognitive processes and brain structures involved (Balschun et al., 2003; Garthe et al., 2009). Thus, we analyzed the search patterns (**Figure 2E**) of the mice while they were navigating to the hidden goal during task acquisition (days 1–4) and the reversal (days 5–7). Specifically, we compared the ratio of spatially directed effective search patterns to less directed patterns and thus less effective strategies shown by the TgN3^{WT} and TgN3^{R169C} mice compared to WT mice (**Figures 2F,H**). Using a logistic regression, we statistically assessed changes in the chance (odds) for using either a more or less hippocampus-dependent strategy. The estimated odds-ratio (OR) for transgenic mice overexpressing N3 compared to WT was OR = 0.777 ($p = 0.004$), whereas the CADASIL mutation resulted in estimated OR = 0.936 ($p = 0.063$). Consequently, overexpression of N3 significantly impaired the use of spatial, more hippocampus-dependent strategies, while the CADASIL mutation *per se* (in comparison to N3 overexpression) resulted in less severe deficits in the use of spatial strategies. In the reversal phase, perseverance could be seen predominantly in the N3 and CADASIL transgenic mice. We therefore applied the logistic regression model to the perseverance and found a significantly increased perseverance in CADASIL mutant mice (OR = 2.61, $p = 0.003$) in addition to the perseverance seen in N3 overexpressing mice (OR = 2.36, $p < 0.001$; **Figure 2I**). These findings highlight that the R169C mutation resulted in deficits in up-dating of the allocentric map at this age, thereby resulting in an increased perseverance. These deficits are potentially due to a combined effect of vascular changes in the hippocampal niche (Ehret et al., 2015) and reduced adult neurogenesis. To confirm these neurogenic deficits in the modified mouse model, we carried out histological analysis of adult hippocampal neurogenesis.

Deficits in Adult Neurogenesis in Aged N3 and CADASIL Transgenic Mice on the B6 Background

We had previously found alterations in adult neurogenesis in these N3 and CADASIL transgenic mouse models on the FVB/N background (Ehret et al., 2015). In the new modified transgenic mouse model deficits due to N3 overexpression could be found at 12 months of age, which is in agreement with our previous observation. Also in line with the previous report, the CADASIL mutation did not additionally impact precursor proliferation and neuronal survival, as only differences to WT animals could be detected but not to the N3 overexpressing controls in this age group.

In detail, analysis of adult neurogenesis by BrdU revealed a reduction in cell survival in TgN3^{R169C} [ANOVA $F_{(2,44)} = 5.54$, $p = 0.007$, with TgN3^{R169C} < WT $p = 0.006$; **Figure 3B**]. Further phenotyping of BrdU$^+$ cells showed a decreased proportion of neuronal differentiation [NeuN$^+$; ANOVA $F_{(2,43)} = 20.62$, $p < 0.001$ with TgN3^{WT} < WT $p < 0.001$ and TgN3^{R169C} < WT $p < 0.001$] and an increase in astrocytic differentiation [$F_{(2,43)} = 12.01$, $p < 0.0001$ with TgN3^{WT} > WT $p = 0.013$ and TgN3^{R169C} > WT $p < 0.0001$; **Figure 3C,E,F**]. While net gliogenesis was not altered [ANOVA $F_{(2,44)} = 0.39$ $p = 0.67$], net neurogenesis was reduced in both N3 and CADASIL transgenic animals [ANOVA $F_{(2,44)} = 12.19$, $p < 0.0001$ with TgN3^{WT} < WT $p = 0.002$ and TgN3^{R169C} > WT $p = 0.0002$; **Figure 3D**]. The morphology of BrdU$^+$ new neurons and new astrocytes in both N3 and CADASIL transgenic mice appeared normal as shown in **Figures 3E,F**. For further confirmation of these results, we counted the number of calretinin$^+$ cells in the SGZ of the DG as an independent marker for immature neurons in

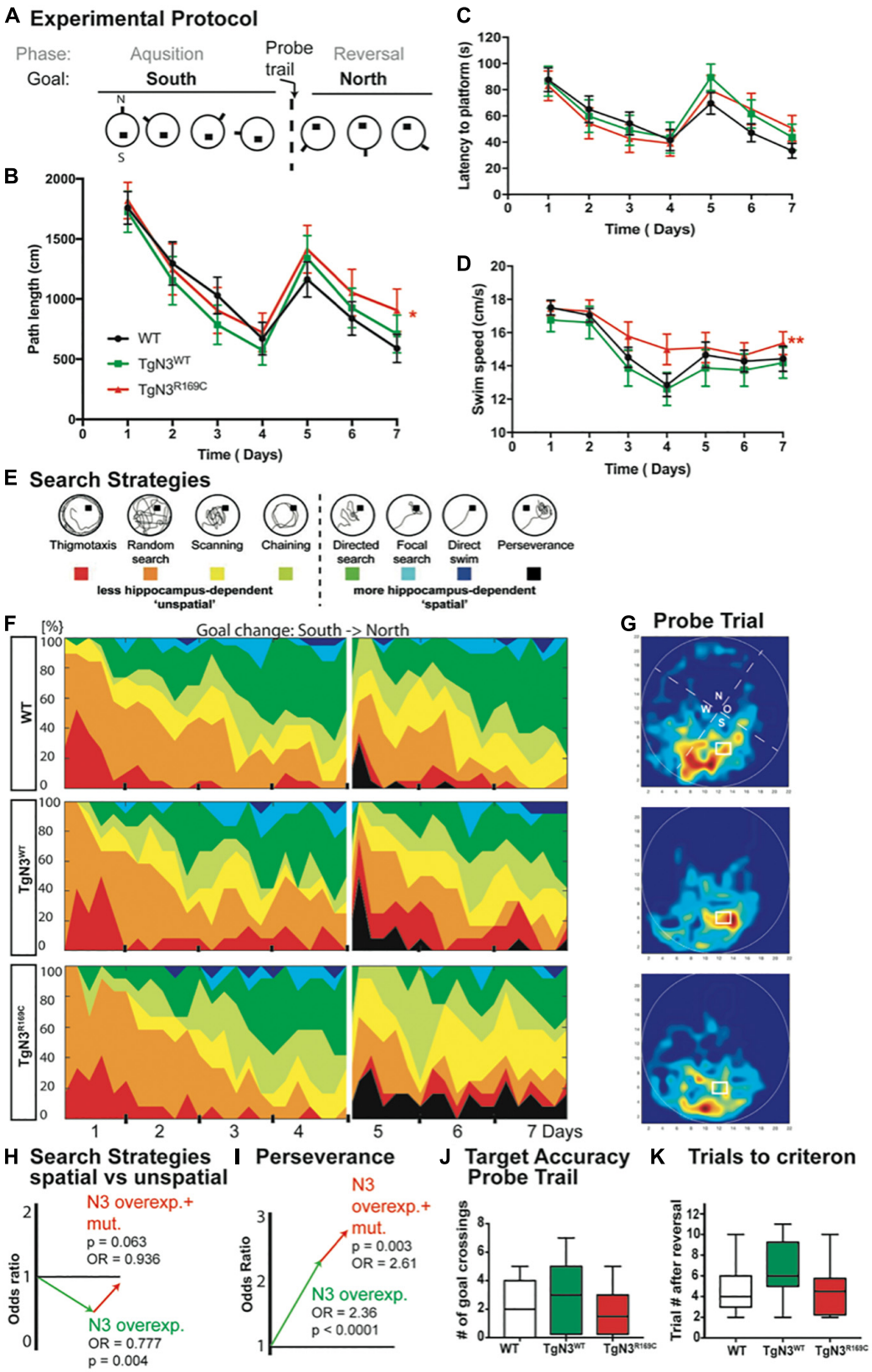

FIGURE 2 | Continued

FIGURE 2 | Impaired spatial learning in the Morris water maze task in *Notch*3 and CADASIL transgenic mice at 12 months of age. **(A)** The experimental protocol of the Morris water maze task adjusted for aged animals and thus containing 4 days of acquisition and 3 days of reversal. **(B)** Analysis of path length showed an impaired performance after platform relocation in CADASIL mice (* represents $p < 0.05$). **(C)** Analysis of latency shows similar trends but no significant effect since the swim speed is significant higher in TgN3^{R169C}. **(D)** Swim speed of CADASIL mice differed significantly compared to N3 transgenic controls (**$p < 0.01$). **(E)** Examples for classification of search strategies used to define "unspatial" vs. "spatial" more hippocampus-dependent patterns. **(F)** Contribution of the respective search strategies to group performance, color code as indicated in **(E)**. **(G)** Heat maps from the respective animal groups of the probe trial performance (only the first 30 s). **(H)** Graphic illustration of the induced change in the odds to choose a more hippocampus-dependent strategy as uncovered by logistic regression analysis based on previous classification shown in **(E)**. **(I)** Graphic illustration of the induced change in the odds for perseverance based strategy in the reversal phase of the Morris water maze task. **(J)** Analysis of former goal crossings as an indicator of target accuracy in the probe trials. No impairment in previous goal location can be seen in transgenic mice. **(K)** Number of trials an individual animal needed to regain the average path length of day 4.

the adult dentate gyrus (Kempermann et al., 2004; Mattiesen et al., 2009; Knoth et al., 2010). A reduction in the number of calretinin$^+$ cells was found [ANOVA $F_{(2,46)} = 8.61$ $p = 0.0007$ with TgN3^{WT} < WT $p = 0.018$ and TgN3^{R169C} < WT $p = 0.001$; **Figure 3A**], and thus these results were in line with the BrdU data (representative images shown in **Supplementary Figure 1**).

In conclusion, N3 overexpression reduced survival and differentiation potential of precursor cells in adulthood with no significant additional effect of the CADASIL mutation. A correlation analysis was carried out (**Supplementary Figure 2**) to gain further information about a link between the mutation, the neurogenesis effect and the behavioral findings. In the TgN3^{WT} mice, a strong cluster of neurogenesis and gliogenesis parameters was found, which was weaker in WT and TgN3^{R169C} animals. Further, a positive correlation between water maze performance and adult neurogenesis was detected as described previously (Kempermann and Gage, 2002). Adult neurogenesis correlated well to the performance on the last day of acquisition (day 4) when the mice were most efficient in finding the hidden platform. CADASIL transgenic animals on the other hand did not show such strong positive correlations between adult neurogenesis and hippocampus-dependent learning, although they overexpressed N3 to the same extent. Thus, TgN3^{R169C} showed clusters of positive correlations for water maze performance throughout all trials, which indicated that these mice behaved more predictable and therefore, presumably, less flexible. This is corroborated by the finding that a correlation to neurogenesis could be detected only on the first day of reversal, when relearning is just starting and mice randomly search for the new platform.

In conclusion, the correlation analysis indicated that N3 is a regulator of adult neurogenesis and gliogenesis and might influence hippocampus-dependent learning in our animal model. The CADASIL mutation partly reverted the behavioral effects of N3 but not on adult neurogenesis.

Deficits in Spatial Learning and Reduced Neurogenesis in N3 Transgenic Mice at 6 Months of Age

As first GOM accumulations were already present at 6 months of age (**Figure 1**), we also asked whether the described phenotypes were already present at this much younger age, possibly offering insight into the developmental process that leads to the described changes.

At 6 months of age, CADASIL and N3 transgenic mice on the B6 background learned the Morris water maze task quickly and did not show any deficits during acquisition. The analysis of latencies throughout the experiment, with 3 days acquisition and 2 days reversal (**Figure 4A**), showed no significant differences of N3 transgenic mice to find the hidden platform (Chi-Square = 5.2, $p = 0.09$; **Figure 4C**). Swim speed, however, differed significantly (Chi-Square = 8.4, $p = 0.008$; **Figure 4D**), as TgN3^{WT} mice were significantly slower compared to WT ($p = 0.006$). Consequently, the analysis of path length as a less confounded measure was used, but did not reveal a significant difference (Chi-Square = 0.77 $p = 0.76$; **Figure 4B**). Although CADASIL mice showed slight deficits in remembering the previous platform location as the heat maps of the probe trial illustrate (**Figure 4G**). Nevertheless, analysis of probe trial performance revealed no significant differences in target accuracy, which was assessed by the number of former goal crossings (Chi-Square = 0.625, $p = 0.73$; **Figure 4J**) and the time spent in the target zone [ANOVA $F_{(2,53)} = 2.073$, $p = 0.135$; **Figure 4I**]. A closer look into the learning strategies (**Figure 4E**) revealed that N3 overexpression led to a reduction of spatial, hippocampus-dependent strategies (**Figure 4F**). Analysis of the spatial versus non-spatial strategies by logistic regression revealed an OR = 0.62 ($p = 0.007$) for N3 overexpressing mice (**Figure 4H**). The CADASIL mutation on the other side resulted in an OR = 1.436 ($p = 0.009$), indicating that at this age CADASIL mice used more spatial cues as N3 transgenic controls.

As hippocampus-dependent learning seemed to be partially impaired in N3 transgenic mice at 6 months of age, we carried out a detailed analysis of precursor proliferation and differentiation in the adult hippocampus. As expected from our study on the FVB/N background (Ehret et al., 2015), histological analysis revealed that adult neurogenesis, in particular precursor proliferation and differentiation, was impaired at 6 months in N3 and CADASIL transgenic mice to the same extent. Hence, also the number of young neurons, as analyzed by calretinin immune labeling (**Supplementary Figure 1**), was significantly reduced in N3 and CADASIL transgenic mice [ANOVA $F_{(2,35)} = 85$, $p < 0.0001$ with TgN3^{WT} < WT, $p < 0.0001$ and TgN3^{R169C} < WT $p < 0.0001$; **Figure 5A**]. Similar results were obtained by the analysis of BrdU$^+$ cells 28 days post injection [ANOVA $F_{(2,35)} = 19.56$, $p < 0.0001$ with TgN3^{WT} < WT, $p < 0.0001$ and TgN3^{R169C} < WT, $p < 0.0001$; **Figure 5B**; representative images **Supplementary Figure 1**].

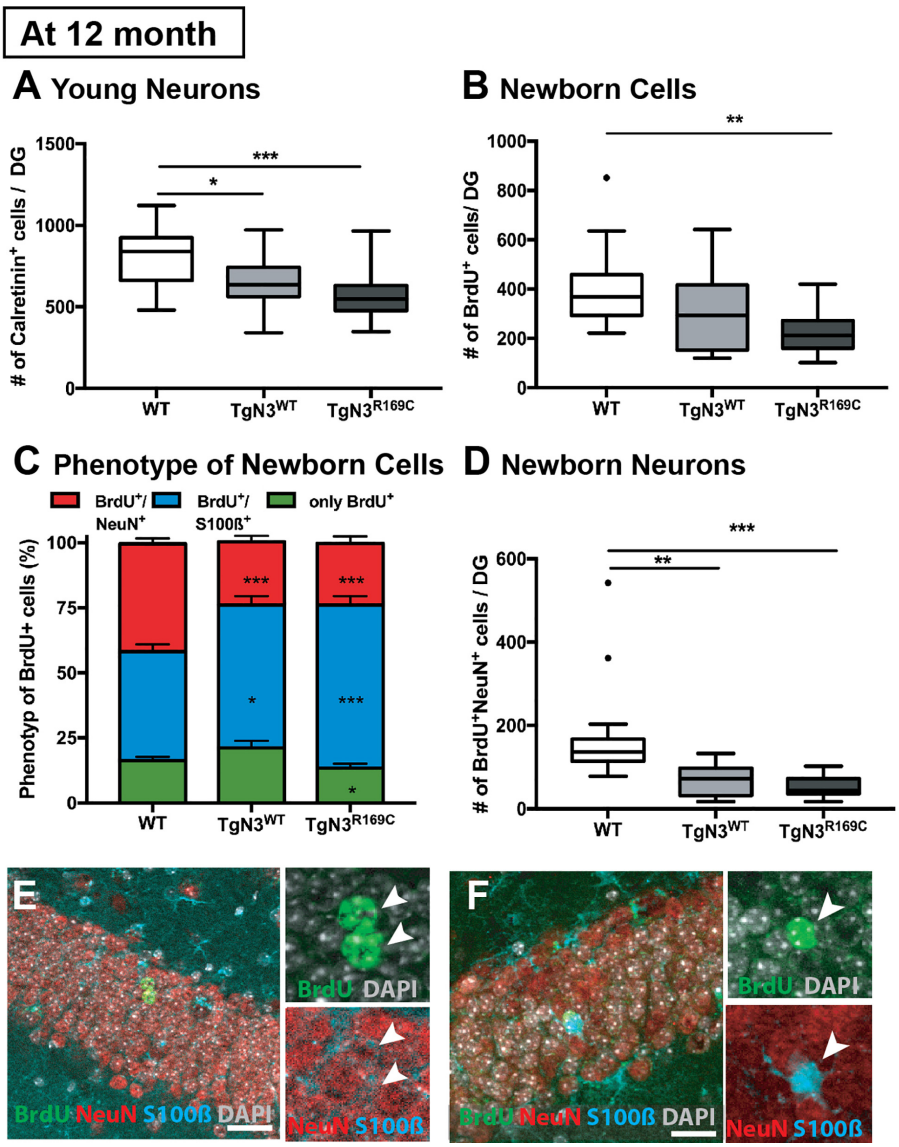

FIGURE 3 | Reduced adult neurogenesis in *Notch3* and CADASIL transgenic mice at 12 months of age. **(A)** The number of calretinin$^+$ cells, as a marker for young neurons, is reduced in the SGZ of the DG of Notch3 and CADASIL transgenic mice. **(B)** Analysis of adult neurogenesis by the number of BrdU$^+$ cells 28 days post injection showed a reduction in CADASIL transgenic animals. **(C)** Phenotyping of BrdU$^+$ cells located in the SGZ of the DG with neuronal marker (NeuN) and astrocyte marker (S100β) showed decreased neuronal differentiation and an increased astrocytic differentiation of Notch3 and CADASIL transgenic mice compared to WT, Data = Mean ± SEM. **(D)** Net neurogenesis, as calculated by number of BrdU$^+$/NeuN$^+$ cells, is reduced in Notch3 and CADASIL transgenic mice. **(E,F)** Representative image from TgN3^{R169C} mice of two BrdU$^+$/NeuN$^+$ neurons **(E)** and a BrdU$^+$/S100β$^+$ astrocyte **(F)**, scale bar 30 μm. *N* = 19 for WT and 13 for TgN3^{WT} and TGN3^{C169C} for all graphs. Asterisks indicate statistical significance (*$p < 0.05$, **$p < 0.01$, ***$p < 0.005$); DG, dentate gyrus; SGZ, subgranular zone.

Phenotyping of BrdU$^+$ cells revealed a reduction in neuronal differentiation (as measured by % of BrdU$^+$/NeuN$^+$ co-labeling) in CADASIL transgenic mice in comparison to WT mice [ANOVA $F_{(2,25)} = 3.41$, $p = 0.0049$ with TgN3^{R169C} < WT, $p = 0.047$; **Figure 5C**]. Further, an increase in astrocytic differentiation (measured by % of BrdU$^+$/S100β$^+$ co-labeling) in CADASIL transgenic mice in comparison to WT mice [ANOVA $F_{(2,25)} = 4.62$, $p = 0.019$; TgN3^{R169C} > WT $p = 0.025$] was observed. As a result, net neurogenesis was reduced in N3 and CADASIL transgenic mice [ANOVA $F_{(2,13)} = 10$, $p = 0.002$ with TgN3^{WT} < WT, $p = 0.004$ and TgN3^{R169C} < WT, $p = 0.007$; **Figure 5D**]. Nevertheless, net gliogenesis was not altered [ANOVA $F_{(2,13)} = 1.2$, $p = 0.32$]. These results indicate that in N3 overexpressing mice, adult neurogenesis is already impaired at an early age, which is in line with the observed albeit mild deficits in hippocampus-dependent spatial search strategies in the Morris water maze task. The CADASIL mutation in contrast, did not lead to an additional impairment in precursor proliferation or differentiation in this transgenic mouse model on C57BL/6J background.

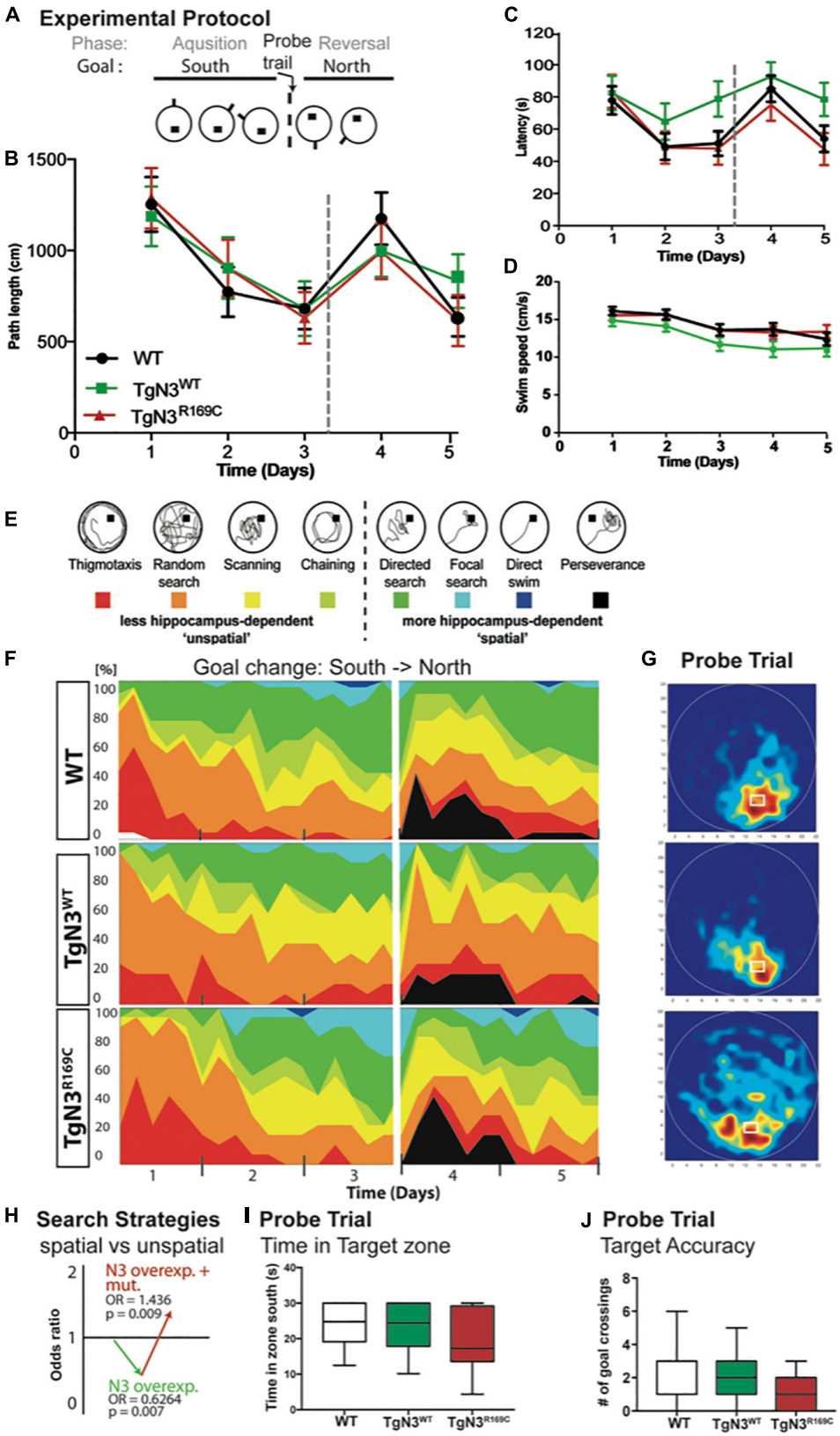

FIGURE 4 | Continued

FIGURE 4 | Morris water maze task in *Notch3* and CADASIL transgenic mice at 6 months of age. **(A)** The experimental protocol of the Morris water maze task containing 3 days of acquisition and 2 days of reversal. **(B)** Analysis of path length showed no deficits in performance. **(C)** Analysis of latency showed deficits, but since swim speed is reduced in TgN3^{WT} path length is a more reliable measure. **(D)** Swim speed of TgN3^{WT} mice is reduced compared to WT and TgN3^{R169C}. **(E)** Classification of search strategies. **(F)** Contribution of the respective search strategies to group performance, color code as indicated in **(E)**. **(G)** Probe trial performance of the respective animal groups indicated by heat maps (only the first 30 s were plotted). Dark-red zones represent a 6-fold presence probability. **(H)** Graphic illustration of the induced change in the odds to choose a more hippocampus-dependent strategy, which is determined by logistic regression analysis based on classification shown in **(E)**. The values indicated that Notch3 overexpression leads to the use of less spatial cues and that the CADASIL mutation *per se* results in the use of more spatial cues, which brought TGN3^{R169C} mice back to WT levels. **(I)** Analysis of time spent in target zone during the first 30 s of probe trial as indicator of target accuracy. **(J)** Analysis of former goal crossings as a precise indicator of target accuracy in the probe trials. Although CADASIL transgenic mice showed less target accuracy of the previous goal location, no significant changes can be detected with the applied measures.

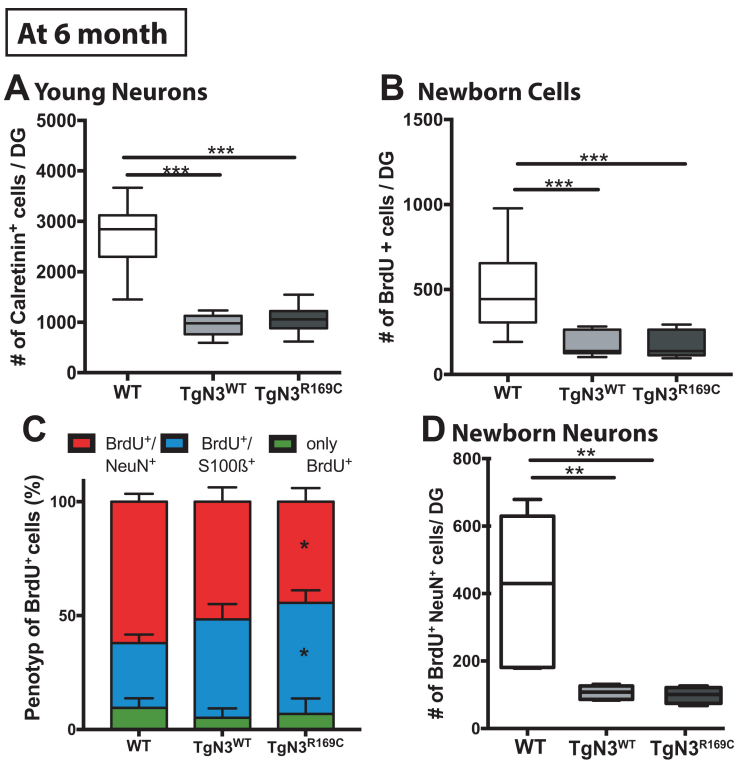

FIGURE 5 | Reduced adult neurogenesis in *Notch3* and CADASIL transgenic mice at 6 months of age. **(A)** The number of calretinin$^+$ cells, as a marker for young neurons, is reduced in the SGZ of the DG of Notch3 and CADASIL transgenic mice. **(B)** Analysis of adult neurogenesis by the number of BrdU$^+$ cells 28 days post injection showed a reduction in Notch 3 and CADASIL transgenic animals. **(C)** Phenotyping of BrdU$^+$ cells with neuronal marker (NeuN) and astrocyte marker (S100β) showed decreased neuronal differentiation and an increased astrocytic differentiation in CADASIL transgenic mice compared to WT, Data = Mean ± SEM. **(D)** Net neurogenesis, as calculated by number of BrdU$^+$/NeuN$^+$ cells, is reduced in Notch3 and CADASIL transgenic mice. *N* = 15 WT and 12 for TgN3WT and TgN3^{R169C} in all graphs. Asterisks indicate statistical significance (*$p < 0.05$, **$p < 0.01$, ***$p < 0.005$), DG, dentate gyrus; SGZ, subgranular zone.

Attempt to Study Adult Neurogenesis in CADASIL Patient Samples

Based on our current and previous observation (Ehret et al., 2015) of a potential direct regulatory influence of N3 on adult hippocampal neurogenesis and the loss-of-function deficits seen in CADASIL transgenic mice, we intended to analyze adult neurogenesis also in patient samples. We were aware of the fact that there are substantial challenges to assessing adult neurogenesis in human specimens (Kempermann et al., 2018; Moreno-Jimenez et al., 2019). Histological analysis on hippocampal samples collected from the CADASIL brain bank (Leiden, Netherlands) showed calretinin-positive cells in the dentate gyrus (**Figure 6B**) of both patient and control specimens, indicative of adult hippocampal neurogenesis (Brandt et al., 2003; Mattiesen et al., 2009; Knoth et al., 2010; Boldrini et al., 2018). Interneurons were distinguished from immature granular cells based on size and location (shown in **Figures 6C,D**). Additional neurogenic markers were tested but did not produce convincing results in these specimens (see **Supplementary Table B**). All samples were checked for confounding effects of age, sex and post-mortem interval, when the areal density of calretinin-positive cells was assessed (**Supplementary Figure 3**). Altough post-mortem delay did not negatively influence density, no statistical differences in density of calretinin-positive cells were found (**Figure 6A**). Given the rareness of this disease

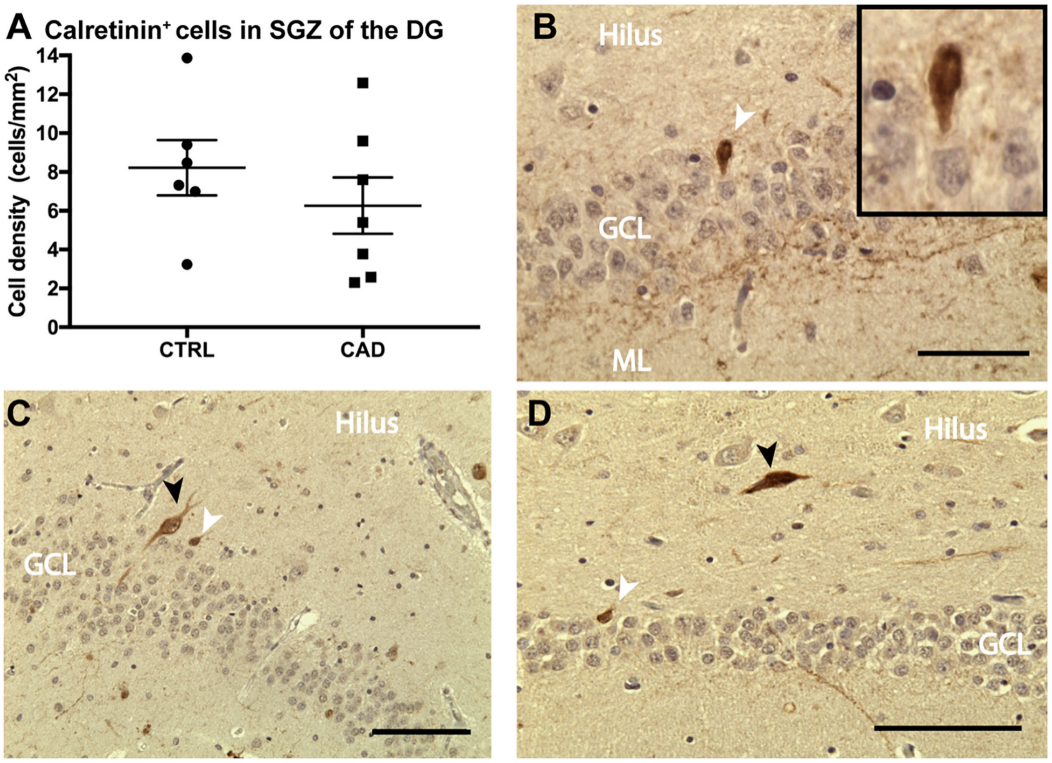

FIGURE 6 | Calretinin expression in the dentate gyrus of CADASIL post-mortem samples. **(A)** Number of calretinin$^+$ new born neurons per area of the granular cell layer (GCL) of control (CTRL) and CADASIL (CAD) patient samples. Cell density was averaged over 4–6 sections per patient. **(B–D)** Representative micrograph of calretinin$^+$ new born neurons (white arrow) and larger Interneurons (black arrow), which are mainly found the hilus of human DG from CADASIL **(B,D)** and Control patients **(C)**. Tissue was counter stained by haematoxylin. ML, molecular layer. Data = Mean ± SEM, *N* = 6–7, Scale bar 50 μm.

(and related tissue samples), it was unfortunate that no stereological quantification was possible and the results remain unconclusive with respect to a potential effect of CADASIL on adult neurogenesis.

DISCUSSION

The present study aimed at further elucidating the potential involvement of the hippocampus and failing adult neurogenesis in the manifestation of CADASIL. We had previously shown that N3 plays an essential role in adult neurogenesis, controlling aspects of precursor proliferation, activation and differentiation (Ehret et al., 2015). This is of particular relevance for CADASIL, since the functional consequences of the several established CADASIL mutations, including the R169C mutation investigated here, have still no yet been comprehensively described. The current study identified deficits in hippocampus-dependent spatial memory in CADASIL transgenic mice. The observed behavioral phenotype was mild and could not be explained by N3-dependent effects on adult neurogenesis, because the mutation did not affect the neurogenesis phenotype beyond the N3 effect.

At the same time we confirmed that a regulatory influence of N3 appears to be critical for a variety of neural stem and precursor cells (Kawai et al., 2017; Than-Trong et al., 2018). The differential activation and differentiation of stem and precursor cells might lead to a deficient use of spatial search strategies. Previous studies had shown that, if adult neurogenesis was abolished, as for example in Cyclin D2 knockout mice (Garthe et al., 2014), after irradiation (Snyder et al., 2005), or after treatment with a cytostatic agent (Garthe et al., 2009; Goodman et al., 2010), flexible re-learning was impaired. In the present study we could show that with increasing age especially this reversal learning is impaired in R169C CADASIL transgenic mice. So far, only one other CADASIL study had looked into spatial learning, but re-learning had not been assessed (Liu et al., 2015). The limitation of the model lies on the fact that it relies on N3 overexpression. Some of the effects of the mutation (on the ratio of spatial vs. unspatial strategies but not on perseverance) unveiled a loss of function that reverted or counteracted the pure N3 effects.

The used animal model is based on a strong (4-fold overexpression) of N3 with an endogenous-like expression pattern due to a PAC-based transgenesis approach (Joutel et al., 2010). Both transgenic lines express rat N3 at similar levels in addition to the endogenous mouse N3 protein (**Supplementary**

Figure 4). Since the overexpression *per se* has such a strong effect on stem and progenitor cells, the additional functional deficits observed through the mutation are rather small and thus hard to distinguish from the overexpression phenotype. Nevertheless only models with at least 2–4 fold overexpression have been able to represent the spectrum of disorders observed in CADASIL patients like the occurrence of GOMs, white matter brain lesions and vascular deficits (Joutel et al., 2010). In comparison to the previous evaluation of this model on the FVB/N background, fewer deficits could be detected in neurogenesis at the early stage of 6 months. Our studies thus add to the body of literature that describes how strongly the effect of a mutation depends on the genetic background.

Generally, in dementias, such as in Alzheimer's disease, re-learning and recall are prominently affected (Karantzoulis and Galvin, 2011; Tort-Merino et al., 2017). In CADASIL patients this has not yet been specifically analyzed and only deficits in working memory, short-term memory, recall of verbal memory as well as executive and organizational functions have been studied (Taillia et al., 1998; Amberla et al., 2004; Epelbaum et al., 2011). Impaired adult neurogenesis does not affect spatial learning *per se*; it is relevant for specific aspects like up-dating of a previously formed cognitive map (Zhang et al., 2008; Garthe et al., 2014) and behavioral pattern separation (Clelland et al., 2009). There is theoretical and experimental evidence to support that adult neurogenesis levels do not correlate with probe trial performance but with water maze acquisition (Kempermann and Gage, 2002). Our data further support this view since adult neurogenesis ($BrdU^+/NeuN^+$) correlated to water maze performance (Day 2 and 4) for WT and $TgN3^{WT}$ mice (**Supplementary Figure 2**). However, no correlation between adult neurogenesis and the acquisition phase of Morris water maze was found in CADASIL transgenic mice; only a correlation to the reversal phase and perseverance was observed. This indicates that aged CADASIL transgenic mice partially lack the flexibility of relearning a new spatial position. The use of spatial search strategies was impaired in N3 transgenic mice and almost back to WT levels in CADASIL transgenic mice, which partially supports a partial loss of function phenotype as found previously for this CADASIL mutation (Ehret et al., 2015). N3 overexpression on the side leads to predominantly less hippocampus-dependent strategies (**Figure 2H**) and perseverance after platform reversal.

Thus, these results confirm the critical involvement of N3 in precursor cell proliferation, activation and differentiation (Ehret et al., 2015; Kawai et al., 2017; Than-Trong et al., 2018), which might have direct functional consequences for the flexible integration of new information into previously established contexts (Garthe et al., 2009; Garthe and Kempermann, 2013). On the other hand, these results show that the impairment seen in CADASIL transgenic mice due to the mutation itself seems to be an additional component diminishing only certain aspects of plasticity and thus influencing the up-dating of the existing allocentric map, but do not *per se* lead to a loss of function phenotype. GOM accumulations and other subtle aspects of the pathology might additionally impair hippocampal function. Taken together, a complex relationship of vascular and neurogenic origin might influence hippocampus-dependent function in CADASIL, specifically with respect to the R169C mutation.

Since we know the limitation of the available murine CADASIL models, we also intended to analyze adult neurogenesis in human tissue sections. We had the opportunity to undertake the present study with rare CADASIL tissue samples from Leiden University and tested several histological markers (DCX, PCNA, Prox1, Sox2) and protocols (for details see **Supplementary Table B**) based on previously described markers (Knoth et al., 2010). Of these, only Calretinin immune reactivity could be consistently established. Further the structural diversity in the human hippocampal samples made stereological investigations impossible so that no strong quantitative data could be obtained. This limitation was further aggravated by the fact that cell counts needed to be normalized to area of the granular cell layer (Moreno-Jimenez et al., 2019), a common approach to compensate for the comprehensive stereotaxic analysis that would otherwise be desirable but relies on homogenous tissue samples or very high N. Nevertheless, to grossly evaluate potential region-specific differences, we subdivided the hippocampus into head, body and tail structures (Duvernoy and Vannson, 1988). Of these, the head region seemed to show some prominent changes in cell density (**Supplementary Figure 5**). Regional specific differences have not been evaluated by MRI in CADASIL patients so far, but the hippocampal head is sensitively affected in Alzheimer's disease and mild cognitive impairment (Wang et al., 2003; Feng et al., 2018), schizophrenia (O'Driscoll et al., 2001), epilepsy (Bernasconi et al., 2003), and traumatic brain injury (Ariza et al., 2006). Regional differences, if confirmed, would therefore be in line with other studies. Other than that, our study unfortunately remained inconclusive with respect to adult neurogenesis in patient samples.

We present the data nevertheless, because omitting the description of the unsuccessful attempt would create a publication bias in that positive findings are generally more likely to be published than negative or ambiguous results. Data on adult hippocampal neurogenesis in humans are scarce and problematic to obtain, partly because of the limited availability of specimen to be studied. This applies particularly to disease cases, such as CADASIL. With calretinin we could only assess one, obviously robust, marker, which by itself could not settle the case. But it is important that attempts are published and the difficulties and challenges are made public, because of the high expectations on studies on adult neurogenesis in disease contexts to include human data.

Independent of this question, our study provides evidence for an involvement of N3 in structural and functional plasticity of the hippocampus by controlling aspects of cell proliferation, activation and differentiation, which has functional consequences for spatial memory. In addition, the CADASIL mutation seems to

partially impair N3 function affecting spatial memory function in the Morris water maze task.

DATA AVAILABILITY STATEMENT

The raw data supporting the conclusions of this article will be made available by the authors, without undue reservation.

ETHICS STATEMENT

The animal study was reviewed and approved by the Landesdirektion Sachsen, Dresden, Germany. For the provided human data, all participants gave informed consent that their samples could be used for research and publication.

AUTHOR CONTRIBUTIONS

FE and GK planned the study and wrote the manuscript. FE, RMT, M-TN, BH, and DL performed the experiments. FE analyzed the data. GK supervised the entire project and provided financial support. All authors contributed to the article and approved the submitted version.

FUNDING

This work was financed by basic institutional funds (DZNE). FE was supported by Peter and Traudl Engelhorn-Stiftung.

ACKNOWLEDGMENTS

The authors like to thank Saskia A. J. Lesnik Oberstein (Leiden University) for collaboration on the human tissue samples from the Leiden brain bank, Ingrid Hegeman for human sample preparation, Sandra Günter and Anne Karasinsky for mouse handling, Peggy Oloth for technical assistance, Christina Steinhauer for molecular work, Benedikt Asay for help with EM preparations, and Thomas Kurth for EM preparations and imaging.

SUPPLEMENTARY MATERIAL

The Supplementary Material for this article can be found online at: https://www.frontiersin.org/articles/10.3389/fnagi.2021.617733/full#supplementary-material

REFERENCES

Amberla, K., Waljas, M., Tuominen, S., Almkvist, O., Poyhonen, M., Tuisku, S., et al. (2004). Insidious cognitive decline in CADASIL. *Stroke J. Cerebral Circ.* 35, 1598–1602. doi: 10.1161/01.STR.0000129787.92085.0a

Ariza, M., Serra-Grabulosa, J. M., Junque, C., Ramirez, B., Mataro, M., Poca, A., et al. (2006). Hippocampal head atrophy after traumatic brain injury. *Neuropsychologia* 44, 1956–1961. doi: 10.1016/j.neuropsychologia.2005.11.007

Balschun, D., Wolfer, D. P., Gass, P., Mantamadiotis, T., Welzl, H., Schutz, G., et al. (2003). Does cAMP response element-binding protein have a pivotal role in hippocampal synaptic plasticity and hippocampus-dependent memory? *J. Neurosci.* 23, 6304–6314.

Bernasconi, N., Bernasconi, A., Caramanos, Z., Antel, S. B., Andermann, F., and Arnold, D. L. (2003). Mesial temporal damage in temporal lobe epilepsy: a volumetric MRI study of the hippocampus, amygdala and parahippocampal region. *Brain* 126(Pt 2), 462–469.

Boldrini, M., Fulmore, C. A., Tartt, A. N., Simeon, L. R., Pavlova, I., Poposka, V., et al. (2018). Human hippocampal neurogenesis persists throughout aging. *Cell Stem Cell* 58:e585. doi: 10.1016/j.stem.2018.03.015

Brandt, M. D., Jessberger, S., Steiner, B., Kronenberg, G., Reuter, K., Bick-Sander, A., et al. (2003). Transient calretinin expression defines early postmitotic step of neuronal differentiation in adult hippocampal neurogenesis of mice. *Mol. Cell Neurosci.* 24, 603–613.

Buffon, F., Porcher, R., Hernandez, K., Kurtz, A., Pointeau, S., Vahedi, K., et al. (2006). Cognitive profile in CADASIL. *J. Neurol. Neurosurg. Psychiatry* 77, 175–180. doi: 10.1136/jnnp.2005.068726

Burghardt, N. S., Park, E. H., Hen, R., and Fenton, A. A. (2012). Adult-born hippocampal neurons promote cognitive flexibility in mice. *Hippocampus* 22, 1795–1808. doi: 10.1002/hipo.22013

Chabriat, H., Joutel, A., Dichgans, M., Tournier-Lasserve, E., and Bousser, M. G. (2009). Cadasil. *Lancet Neurol.* 8, 643–653. doi: 10.1016/S1474-4422(09)70127-9

Clelland, C. D., Choi, M., Romberg, C., Clemenson, G. D. Jr., Fragniere, A., Tyers, P., et al. (2009). A functional role for adult hippocampal neurogenesis in spatial pattern separation. *Science* 325, 210–213. doi: 10.1126/science.1173215

Duvernoy, H. M., and Vannson, J. L. (1988). *The Human Hippocampus : An Atlas of Applied Anatomy*. München: J.F. Bergmann-Verlag München.

Ehm, O., Goritz, C., Covic, M., Schaffner, I., Schwarz, T. J., Karaca, E., et al. (2010). RBPJkappa-dependent signaling is essential for long-term maintenance of neural stem cells in the adult hippocampus. *J. Neurosci.* 30, 13794–13807. doi: 10.1523/JNEUROSCI.1567-10.2010

Ehret, F., Vogler, S., Pojar, S., Elliott, D. A., Bradke, F., Steiner, B., et al. (2015). Mouse model of CADASIL reveals novel insights into Notch3 function in adult hippocampal neurogenesis. *Neurobiol. Dis.* 75, 131–141. doi: 10.1016/j.nbd.2014.12.018

Epelbaum, S., Benisty, S., Reyes, S., O'Sullivan, M., Jouvent, E., During, M., et al. (2011). Verbal memory impairment in subcortical ischemic vascular disease: a descriptive analysis in CADASIL. *Neurobiol. Aging* 32, 2172–2182. doi: 10.1016/j.neurobiolaging.2009.12.018

Farley, S. J., McKay, B. M., Disterhoft, J. F., and Weiss, C. (2011). Reevaluating hippocampus-dependent learning in FVB/N mice. *Behav. Neurosci.* 125, 871–878. doi: 10.1037/a0026033

Feng, F., Wang, P., Zhao, K., Zhou, B., Yao, H., Meng, Q., et al. (2018). Radiomic features of hippocampal subregions in Alzheimer's disease and amnestic mild cognitive impairment. *Front. Aging Neurosci.* 10:290. doi: 10.3389/fnagi.2018.00290

Garthe, A., Behr, J., and Kempermann, G. (2009). Adult-generated hippocampal neurons allow the flexible use of spatially precise learning strategies. *PLoS One* 4:e5464. doi: 10.1371/journal.pone.0005464

Garthe, A., Huang, Z., Kaczmarek, L., Filipkowski, R. K., and Kempermann, G. (2014). Not all water mazes are created equal: Cyclin D2 knockout mice with constitutively suppressed adult hippocampal neurogenesis do show specific spatial learning deficits. *Genes Brain Behav.* 13, 357–364. doi: 10.1111/gbb.12130

Garthe, A., and Kempermann, G. (2013). An old test for new neurons: refining the Morris water maze to study the functional relevance of adult hippocampal neurogenesis. *Front. Neurosci.* 7:63. doi: 10.3389/fnins.2013.00063

Garthe, A., Roeder, I., and Kempermann, G. (2016). Mice in an enriched environment learn more flexibly because of adult hippocampal neurogenesis. *Hippocampus* 26, 261–271. doi: 10.1002/hipo.22520

Goodman, T., Trouche, S., Massou, I., Verret, L., Zerwas, M., Roullet, P., et al. (2010). Young hippocampal neurons are critical for recent and remote spatial memory in adult mice. *Neuroscience* 171, 769–778. doi: 10.1016/j.neuroscience.2010.09.047

Imayoshi, I., Sakamoto, M., Yamaguchi, M., Mori, K., and Kageyama, R. (2010). Essential roles of Notch signaling in maintenance of neural stem cells in developing and adult brains. *J. Neurosci.* 30, 3489–3498. doi: 10.1523/JNEUROSCI.4987-09.2010

Joutel, A., Monet-Lepretre, M., Gosele, C., Baron-Menguy, C., Hammes, A., Schmidt, S., et al. (2010). Cerebrovascular dysfunction and microcirculation rarefaction precede white matter lesions in a mouse genetic model of cerebral ischemic small vessel disease. *J. Clin Investig.* 120, 433–445. doi: 10.1172/JCI39733

Karantzoulis, S., and Galvin, J. E. (2011). Distinguishing Alzheimer's disease from other major forms of dementia. *Expert Rev. Neurother.* 11, 1579–1591. doi: 10.1586/ern.11.155

Kawai, H., Kawaguchi, D., Kuebrich, B. D., Kitamoto, T., Yamaguchi, M., Gotoh, Y., et al. (2017). Area-specific regulation of quiescent neural stem cells by notch3 in the adult mouse subependymal zone. *J. Neurosci.* 37, 11867–11880. doi: 10.1523/JNEUROSCI.0001-17.2017

Kempermann, G. (2012). New neurons for 'survival of the fittest'. *Nat. Rev. Neurosci.* 13, 727–736. doi: 10.1038/nrn3319

Kempermann, G., Gage, F. H., Aigner, L., Song, H., Curtis, M. A., Thuret, S., et al. (2018). Human adult neurogenesis: evidence and remaining questions. *Cell Stem Cell* 23, 25–30. doi: 10.1016/j.stem.2018.04.004

Kempermann, G., and Gage, F. H. (2002). Genetic determinants of adult hippocampal neurogenesis correlate with acquisition, but not probe trial performance, in the water maze task. *Eur. J. Neurosci.* 16, 129–136.

Kempermann, G., Gast, D., Kronenberg, G., Yamaguchi, M., and Gage, F. H. (2003). Early determination and long-term persistence of adult-generated new neurons in the hippocampus of mice. *Development* 130, 391–399.

Kempermann, G., Jessberger, S., Steiner, B., and Kronenberg, G. (2004). Milestones of neuronal development in the adult hippocampus. *Trends Neurosci.* 27, 447–452. doi: 10.1016/j.tins.2004.05.013

Knoth, R., Singec, I., Ditter, M., Pantazis, G., Capetian, P., Meyer, R. P., et al. (2010). Murine features of neurogenesis in the human hippocampus across the lifespan from 0 to 100 years. *PLoS One* 5:e8809. doi: 10.1371/journal.pone.0008809

Liu, X. Y., Gonzalez-Toledo, M. E., Fagan, A., Duan, W. M., Liu, Y., Zhang, S., et al. (2015). Stem cell factor and granulocyte colony-stimulating factor exhibit therapeutic effects in a mouse model of CADASIL. *Neurobiol. Dis.* 73, 189–203. doi: 10.1016/j.nbd.2014.09.006

Lugert, S., Basak, O., Knuckles, P., Haussler, U., Fabel, K., Gotz, M., et al. (2010). Quiescent and active hippocampal neural stem cells with distinct morphologies respond selectively to physiological and pathological stimuli and aging. *Cell Stem Cell* 6, 445–456. doi: 10.1016/j.stem.2010.03.017

Mattiesen, W. R., Tauber, S. C., Gerber, J., Bunkowski, S., Bruck, W., and Nau, R. (2009). Increased neurogenesis after hypoxic-ischemic encephalopathy in humans is age related. *Acta Neuropathol.* 117, 525–534. doi: 10.1007/s00401-009-0509-0

Moreno-Jimenez, E. P., Flor-Garcia, M., Terreros-Roncal, J., Rabano, A., Cafini, F., Pallas-Bazarra, N., et al. (2019). Adult hippocampal neurogenesis is abundant in neurologically healthy subjects and drops sharply in patients with Alzheimer's disease. *Nat. Med.* 25, 554–560. doi: 10.1038/s41591-019-0375-9

Morris, R. (2007). *The Hippocampus Book*. Oxford: Oxford University Press.

O'Driscoll, G. A., Florencio, P. S., Gagnon, D., Wolff, A. V., Benkelfat, C., Mikula, L., et al. (2001). Amygdala-hippocampal volume and verbal memory in first-degree relatives of schizophrenic patients. *Psychiatry Res.* 107, 75–85.

O'Keefe, J., and Dostrovsky, J. (1971). The hippocampus as a spatial map. Preliminary evidence from unit activity in the freely-moving rat. *Brain Res.* 34, 171–175.

O'Sullivan, M., Ngo, E., Viswanathan, A., Jouvent, E., Gschwendtner, A., Saemann, P. G., et al. (2009). Hippocampal volume is an independent predictor of cognitive performance in CADASIL. *Neurobiol. Aging* 30, 890–897. doi: 10.1016/j.neurobiolaging.2007.09.002

Pugh, P. L., Ahmed, S. F., Smith, M. I., Upton, N., and Hunter, A. J. (2004). A behavioural characterisation of the FVB/N mouse strain. *Behav. Brain Res.* 155, 283–289. doi: 10.1016/j.bbr.2004.04.021

Snyder, J. S., Hong, N. S., McDonald, R. J., and Wojtowicz, J. M. (2005). A role for adult neurogenesis in spatial long-term memory. *Neuroscience* 130, 843–852. doi: 10.1016/j.neuroscience.2004.10.009

Spalding, K. L., Bergmann, O., Alkass, K., Bernard, S., Salehpour, M., Huttner, H. B., et al. (2013). Dynamics of hippocampal neurogenesis in adult humans. *Cell* 153, 1219–1227. doi: 10.1016/j.cell.2013.05.002

Taillia, H., Chabriat, H., Kurtz, A., Verin, M., Levy, C., Vahedi, K., et al. (1998). Cognitive alterations in non-demented CADASIL patients. *Cerebrovasc. Dis.* 8, 97–101.

Than-Trong, E., Ortica-Gatti, S., Mella, S., Nepal, C., Alunni, A., and Bally-Cuif, L. (2018). Neural stem cell quiescence and stemness are molecularly distinct outputs of the Notch3 signalling cascade in the vertebrate adult brain. *Development* 145, dev161034. doi: 10.1242/dev.161034

Tort-Merino, A., Valech, N., Penaloza, C., Gronholm-Nyman, P., Leon, M., Olives, J., et al. (2017). Early detection of learning difficulties when confronted with novel information in preclinical Alzheimer's disease stage 1. *J. Alzheimers Dis.* 58, 855–870. doi: 10.3233/JAD-161173

Voikar, V., Koks, S., Vasar, E., and Rauvala, H. (2001). Strain and gender differences in the behavior of mouse lines commonly used in transgenic studies. *Physiol. Behav.* 72, 271–281.

Wang, L., Swank, J. S., Glick, I. E., Gado, M. H., Miller, M. I., Morris, J. C., et al. (2003). Changes in hippocampal volume and shape across time distinguish dementia of the Alzheimer type from healthy aging. *Neuroimage* 20, 667–682. doi: 10.1016/S1053-8119(03)00361-6

Zhang, C. L., Zou, Y., He, W., Gage, F. H., and Evans, R. M. (2008). A role for adult TLX-positive neural stem cells in learning and behaviour. *Nature* 451, 1004–1007. doi: 10.1038/nature06562

Conflict of Interest: The authors declare that the research was conducted in the absence of any commercial or financial relationships that could be construed as a potential conflict of interest.

frontiers in Aging Neuroscience

SYSTEMATIC REVIEW
published: 30 June 2021
doi: 10.3389/fnagi.2021.692911

Association Between Diabetic Retinopathy and Cognitive Impairment: A Systematic Review and Meta-Analysis

Dihe Cheng[1], *Xue Zhao*[1], *Shuo Yang*[1], *Guixia Wang*[1]* *and Guang Ning*[2]*

[1] *Department of Endocrinology and Metabolism, The First Hospital of Jilin University, Changchun, China,* [2] *Key Laboratory for Endocrine and Metabolic Diseases of Ministry of Health of China, Shanghai National Clinical Research Center for Endocrine and Metabolic Diseases, Shanghai Institute for Endocrine and Metabolic Diseases, Ruijin Hospital, Shanghai Jiaotong University School of Medicine, Shanghai, China*

Diabetic retinopathy (DR) is one of the most common microvascular complications associated with diabetes mellitus. However, its correlation with another diabetes-related disorder, cognitive impairment, has not been well studied. This systematic review and meta-analysis aimed to explore the association between DR and cognitive impairment. MEDLINE (PubMed), the Cochrane Library, and EMBASE databases were searched for observational studies that reported an association between DR and cognitive impairment. Data from selected studies were extracted, and a meta-analysis was conducted using fixed-effects modeling. Fifteen observational studies were included in the systematic review, and 10 studies were included in the meta-analysis. The odds ratio of the association between DR and cognitive impairment was 2.24 (95% confidence interval [CI], 1.89–2.66; $I^2 = 0.8\%$). The hazard ratio of the association between DR and cognitive impairment was significant in four studies, ranging from 1.09–1.32. Minimal or mild DR was not significantly associated with cognitive impairment (odds ratio [OR], 2.04; 95% CI, 0.87–4.77). However, the association between proliferative DR and cognitive impairment (OR, 3.57; 95% CI, 1.79–7.12; $I^2 = 16.6\%$) was not stronger than the association between moderate or worse DR and cognitive impairment (OR, 4.26; 95% CI, 2.01–9.07; $I^2 = 0.0\%$). DR is associated with cognitive impairment, and screening for DR will be helpful for the early identification of individuals with cognitive impairment. Further studies are needed to confirm the association between proliferative DR and cognitive impairment.

Keywords: diabetes mellitus, diabetic retinopathy, cognitive impairment, mild cognitive impairment, dementia

OPEN ACCESS

Edited by:
Prasad V. Katakam,
Tulane University, United States

Reviewed by:
Maria E. Jimenez-Capdeville,
Autonomous University of San Luis Potosí, Mexico
Jia-Da Li,
Central South University, China

***Correspondence:**
Guang Ning
gning@sibs.ac.cn
Guixia Wang
gwang168@jlu.edu.cn

Received: *09 April 2021*
Accepted: *07 June 2021*
Published: *30 June 2021*

Citation:
Cheng D, Zhao X, Yang S, Wang G and Ning G (2021) Association Between Diabetic Retinopathy and Cognitive Impairment: A Systematic Review and Meta-Analysis. Front. Aging Neurosci. 13:692911. doi: 10.3389/fnagi.2021.692911

INTRODUCTION

Diabetes mellitus is a group of metabolic diseases characterized by hyperglycemia caused by defective secretion of insulin, the impaired biological action of insulin, or both. In 2015, 415 million people were estimated to have diabetes, with a projected increase to 642 million by 2040 (Chatterjee et al., 2017). The overall prevalence of diabetic retinopathy (DR) is 35% among patients with diabetes worldwide (Hammes, 2018). As one of the most common microvascular complications of diabetes mellitus, screening for DR has been widely performed in clinical practice.

Cognition is a process in which the human brain receives information from the outside world, processes it, and transforms it into internal psychological activities to acquire or apply knowledge. It includes memory, language, visual space, execution, computation, understanding, and judgment. Cognitive impairment mainly includes mild cognitive impairment and dementia. Mild cognitive impairment (MCI) is defined as acquired cognitive complaints with objective abnormal test results in one or more domains on formal cognitive testing, and dementia is defined as the most severe stage of cognitive dysfunction, with objective impairment of multiple cognitive domains, by definition affecting activities of daily life (Biessels and Whitmer, 2020). Although the lack of standardized diagnostic criteria and differences in the characteristics of different study samples lead to significant uncertainties in these estimates, the prevalence of MCI is approximately 10–20% (Langa and Levine, 2014), and the incidence of dementia is ∼7% in people over 65 years of age (Prince et al., 2013).

Both cognitive impairment and diabetes mellitus are closely associated with aging. Although cognitive impairment is not unique to diabetes, diabetes-related cognitive impairment is now recognized as a complication of diabetes. The risk of incident MCI (up to 60%) and dementia (50–100%) is higher in patients with type 2 diabetes than in those without (Srikanth et al., 2020). In one retrospective study, the risk of incident dementia in hospital-admitted patients with type 1 diabetes was 1.65 times higher than that in people without diabetes (Smolina et al., 2015). Although the risk of developing cognitive impairment in diabetes has received much attention, clinical guidelines have recently begun to emphasize its importance.

The prediction and identification of cognitive impairment in individuals with diabetes will be helpful in early intervention. Furthermore, since the eyes are the "window" to the brain, damage to the retina may be a sign of neurodegenerative diseases of the brain (Simó et al., 2018). Therefore, if DR is associated with cognitive impairment, it will be beneficial for predicting and preventing diabetes-related cognitive impairment and further emphasizes the importance of DR screening.

However, the relationship between DR and cognitive impairment has not been fully studied, and the findings are ambiguous. To date, one systematic review of DR and cognitive impairment in patients with type 2 diabetes has been published (Crosby-Nwaobi et al., 2012), but only three studies were included in the review, and there was a lack of population-based cohort studies. Therefore, the present systematic review and meta-analysis aimed to explore the association between DR and cognitive impairment as well as the association between the grades of DR and cognitive impairment.

METHODS

Literature Search Strategy

Relevant studies were identified by systematically searching MEDLINE (PubMed), the Cochrane Library, and EMBASE databases from inception to November 6, 2020 (date last searched), using a combination of Medical Subject Heading terms with related free-text terms ("diabetic retinopathy," "cognitive dysfunction," "dementia," "Alzheimer disease"). Additional articles were identified via manual search of the reference lists of relevant articles and previous review articles.

During this process, two independent investigators (Cheng and Zhao) completed this work to reduce selection bias. If there were disputes, a third investigator (Wang) resolved the disagreements.

Inclusion and Exclusion Criteria

Articles were included if they fulfilled the following criteria: 1) were cohort study, cross-sectional study, or case-control study design; 2) had DR as the exposure of interest; 3) included people without diabetic retinopathy as the control group; 4) had cognitive impairment including dementia as an outcome of interest; and 5) odds ratios (ORs) or hazard ratios (HRs) and 95% confidence intervals (CIs) were reported or could be calculated. The studies were limited to those conducted in the human population and English. Studies were excluded if categorized as editorials, literature reviews, case reports, and conference abstracts. Included and excluded studies were collected following the Preferred Reporting Items for Systematic Reviews and Meta-Analyses (PRISMA) flow diagram (Moher et al., 2009). The current systematic review and meta-analysis followed the Meta-analysis of Observational Studies in Epidemiology guidelines for meta-analysis of observational studies (Stroup et al., 2000).

Study Selection and Data Extraction

Eligible studies were assessed for overlap based on authors, study region, study population, sample size, and variable measurements. If there was an overlap of the study groups, articles of better quality were selected for the analysis. In addition, the following information was extracted from each study: authors, year of publication, country, study design, definition of cognitive impairment and DR, participant characteristics, sample size, outcome of interest, adjusted confounders (if possible), and duration of follow-up (if possible). During this process, two independent investigators independently screened the titles and abstracts of the identified searches, followed by a full-text review of potentially eligible articles to reduce selection bias.

Quality Assessment

The Newcastle-Ottawa Scale was used in the current systematic review and meta-analysis to evaluate the quality of cohort studies and case-control studies in terms of study group selection, group comparability, and exposure or outcome of interest (Stang, 2010). The scale uses a star system (with a maximum of nine stars). Studies with stars 0–3 were considered as "low quality," with stars 4–6 were considered as "moderate quality," and with stars 7–9 were considered as "high quality." We also evaluated the quality of cross-sectional studies according to the standards recommended by the Agency for Healthcare Research and Quality (https://www.ncbi.nlm.nih.gov/books/NBK35156/). The methodological quality of the included studies was assessed using an 11-item checklist. An item would be scored "0" if it was

answered "NO" or "UNCLEAR;" if it were answered "YES," then the item would be scored "1." Thus, studies with scores 0–3 were considered of "low quality," with scores 4–7 were considered of "moderate quality," and with scores 8–11 were considered of "high quality." Two authors (Cheng and Yang) independently assessed the risk of bias.

Data Synthesis and Analysis

Summary estimates and corresponding 95% CIs for the outcome of the relationship between DR and the risk of cognitive impairment were pooled, if possible. In the case of studies reporting ORs or HRs with various degrees of adjustment, we always used fully adjusted estimates and their 95% CIs.

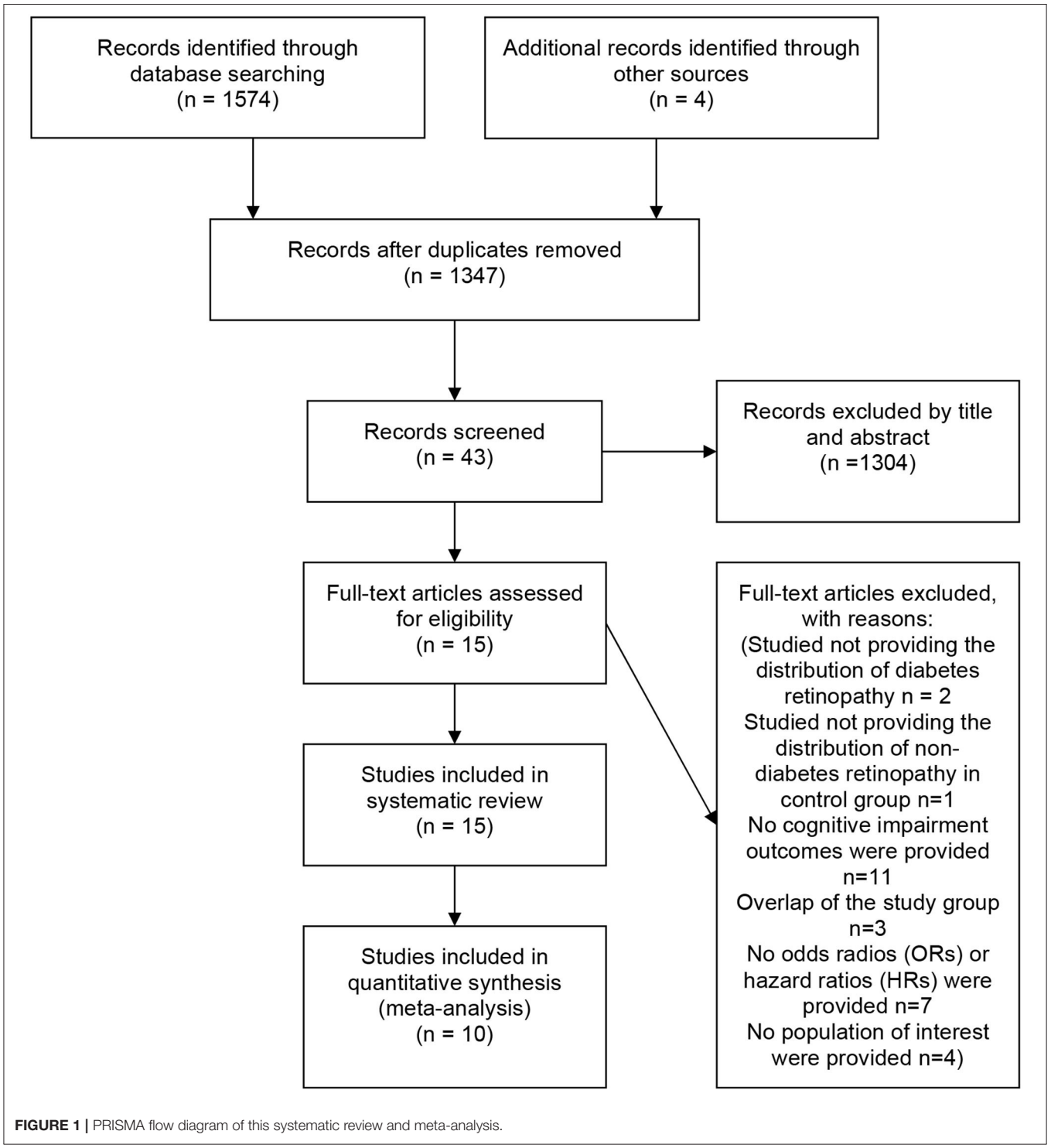

FIGURE 1 | PRISMA flow diagram of this systematic review and meta-analysis.

For studies that did not estimate ORs of the relationship between DR and the risk of cognitive impairment, we calculated the unadjusted ORs and 95% CIs using a two-by-two table. A fixed-effects model was used to pool the ORs across the selected studies. Cochran's *Q*-test and I^2 statistics were used to quantify heterogeneity, with values of $I^2 > 50\%$ representing medium heterogeneity (Lijmer et al., 2002; Li et al., 2015). We also performed a subgroup analysis to identify potential effect modifiers. If a study included multiple grades of DR, each result was analyzed separately in the subgroup analysis. Subgroup analyses by study type, duration of follow-up, and whether confounding factors had been adjusted (studies that provided unadjusted ORs and 95% CIs were grouped with those in which we calculated ORs using a two-by-two table) were also performed. Given the expected heterogeneity of the eligible studies, a sensitivity analysis was performed. We used the funnel plot and the Egger test to evaluate publication bias. A *P*-value of less than 0.05 was considered statistically significant. All analyses were conducted with STATA 15.1. Due to the high heterogeneity, a quantitative meta-analysis could not be performed to pool HRs across the selected studies.

RESULTS

Literature Search

The initial literature search yielded 1574 articles. Four additional articles were identified via manual search. Among all articles, 231 were duplicates. After screening the abstracts and titles, 43 articles remained. After a full-text review, 27 studies were excluded for the reasons specified in the PRISMA diagram. Fifteen observational studies were included in the systematic review, and 10 studies were included in the meta-analysis (**Figure 1**).

Study Characteristics

As summarized in **Table 1**, among the eligible studies reporting ORs and 95% CIs, four studies had a cross-sectional study design (Baker et al., 2007; Umegaki et al., 2008; Ogurel et al., 2015; Xia et al., 2020), two studies had a case-control study design (Roberts et al., 2008; Gorska-Ciebiada et al., 2015), and four studies had a cohort design (Kadoi et al., 2005; Bruce et al., 2014; Nunley et al., 2015; Gupta et al., 2019). Overall, there were 4769 adult participants among the 10 studies included in the meta-analysis. A total of five studies were carried out in Asia (China, Singapore, Turkey, and Japan) (Kadoi et al., 2005; Umegaki et al., 2008; Ogurel et al., 2015; Gupta et al., 2019; Xia et al., 2020), one study was carried out in Europe (Gorska-Ciebiada et al., 2015), two studies were carried out in North America (Roberts et al., 2008; Nunley et al., 2015), and two studies were carried out in Oceania (Baker et al., 2007; Bruce et al., 2014). Most of these studies were conducted on older subjects. Among the included studies, three studies used the Early Treatment of Diabetic Retinopathy Study (ETDRS) or modified ETDRS criteria to define DR (Kadoi et al., 2005; Ogurel et al., 2015; Gupta et al., 2019), four studies used other methods to define DR (Baker et al., 2007; Umegaki et al., 2008; Bruce et al., 2014; Nunley et al., 2015), and three studies did not mention how to define DR (Roberts et al., 2008; Gorska-Ciebiada et al., 2015; Xia et al., 2020). The control groups of the nine studies included the diabetic population (Kadoi et al., 2005; Baker et al., 2007; Umegaki et al., 2008; Bruce et al., 2014; Gorska-Ciebiada et al., 2015; Nunley et al., 2015; Ogurel et al., 2015; Gupta et al., 2019; Xia et al., 2020), while the control group of one study consisted of a non-diabetic population (Roberts et al., 2008).

As summarized in **Table 2**, among the eligible studies reporting HRs and 95% CIs, all five studies had a cohort design (Exalto et al., 2014; Rodill et al., 2018; Deal et al., 2019; Lee et al., 2019; Yu et al., 2020), and four of them were carried out in the USA (Exalto et al., 2014; Rodill et al., 2018; Deal et al., 2019; Lee et al., 2019). Two studies used the same database but different populations (Exalto et al., 2014; Rodill et al., 2018). In these five studies, there were 1,957,187 participants (10.2% with DR, $n =$ 200,323) aged 40 years or older. The mean duration of follow-up ranged from 5.1 to 16 years. All studies conducted multivariable-adjusted analyses with important confounders, including age and sex. The outcomes were dementia, including Alzheimer's disease and vascular dementia. Due to the high heterogeneity, a quantitative meta-analysis could not be performed to pool HRs across the selected studies.

Of the 15 included studies, six were of fair quality (Roberts et al., 2008; Exalto et al., 2014; Rodill et al., 2018; Deal et al., 2019; Gupta et al., 2019; Lee et al., 2019), while others were of moderate quality (Kadoi et al., 2005; Baker et al., 2007; Umegaki et al., 2008; Bruce et al., 2014; Gorska-Ciebiada et al., 2015; Nunley et al., 2015; Ogurel et al., 2015; Xia et al., 2020; Yu et al., 2020) (**Supplementary Tables 1, 2**).

DR and Cognitive Impairment

The OR of the association between DR and cognitive impairment was 2.24 (95% CI, 1.89–2.66; $I^2 = 0.8\%$), pooled from all included studies in **Table 1** (**Figure 2**). The OR was 2.12 (95% CI, 1.55–2.88; $I^2 = 0.0\%$), pooled from studies in which confounding factors had been adjusted, and the OR was 2.30 (95% CI, 1.87–2.83; $I^2 = 49.2\%$), pooled from studies in which confounding factors had not been adjusted (**Figure 3**). When the comparison was stratified by study type, the association between DR and cognitive impairment was significant in all study types (**Figure 3**). When the comparison was stratified by the duration of follow-up, the association between DR and cognitive impairment was more significant with a follow-up of over 10 years (OR, 2.92; 95% CI, 1.55–5.48) than with a follow-up of less than 10 years (OR, 2.39; 95% CI, 1.72–3.32) (**Figure 3**). Finally, eliminating each of the included studies from the analysis did not affect the overall association between DR and cognitive impairment (**Supplementary Figure 1**). The Egger test did not show statistically significant asymmetry in the funnel plot ($P =$ 0.538, **Figure 4**), indicating no significant publication bias.

The HRs of the association between DR and cognitive impairment were significant in four out of five studies, ranging from 1.09 to 1.32. Only one study showed that there was no connection between DR and cognitive impairment (HR, 1.12; 95% CI, 0.82–1.54).

TABLE 1 | Characteristics of the study providing odds ratios.

References	Country	Definition of diabetic retinopathy	Definition of cognitive impairment	Participant characteristics	Enrolled sample number	Study design	Follow-up	OR (95%)	Adjusted confounders
Xia et al. (2020)	China	Not mentioned	CDR score was bounded by 1.0/0.5 for dementia, 0.5/0 for MCI. MMSE score was bounded by 23/24 for dementia, and MOCA score by 25/26 for MCI. For the participants who had 12 years of education or fewer, a point was added to his/ her total MOCA score.	Hospital patients: T2DM subjects aged 45–74 years old	DR: 146 Control: 151	Cross-sectional	/	**Dementia:** DR: 2.197 (1.035–4.664)	Age, sex and education level.
Gupta et al. (2019)	Singapore	Modified airlie house classification system: none (early treatment of diabetic retinopathy study level 10), minimal/mild (level 20–35) and moderate or worse DR (level 43–90) using data from the better eye.	Validated AMT: scores of ≤6 and ≤8 for those with 0–6 and >6 years of formal education.	SEED-1 study: participants with diabetes who were ≥60 years	DR :199 Control: 483	Cohort	6 years	**Cognitive impairment:** DR: 2.32 (1.07–5.03) Minimal or mild DR: 2.04 (0.87–4.76) Moderate or worse DR: 3.41 (1.06 −11.00)	Age, gender, race, education, income, spherical equivalent, HbA1c, diabetes duration, hypertension, CVD and presence of eye conditions (cataract, age-related macular degeneration, glaucoma and undercorrected refractive error in the better eye), better eye presenting visual acuity.
Ogurel et al. (2015)	Turkey	The criteria of the early treatment diabetic retinopathy study.	The cut off score <21 on the MoCA.	Patients with diabetes	DR: 90 Control: 30	Cross-sectional	/	**Cognitive impairment:** DR: 3.5 (1.464-8.365) Moderate or worse DR: 5.0 (1.864-13.409) PDR: 6.5 (1.820-23.213)	No
Nunley et al. (2015)	USA	Proliferative retinopathy was defined as receiving laser therapy for proliferative diabetic retinopathy.	Individual raw test scores ≥1.5 SD worse than published norms (Ardila, 2007; Dominic, 2007; Dore et al., 2007).	EDC study: middle-aged adults with T1DM diagnosed before age 18 years	DR: 46 Control: 51	Cohort	About 27 years	**Cognitive impairment:** PDR: 2.79 (1.23–6.33)	Years of education
Gorska-Ciebiada et al. (2015)	Poland	Not mentioned	MCI was diagnosed based on criteria established by the 2006 European Alzheimer's Disease Consortium.	Hospital patients: Patients aged 65 and over with T2DM	DR: 121 Control: 155	Case-control	/	**MCI:** DR: 2.24 (1.7–2.96)	No
Bruce et al. (2014)	Australia	Ophthalmoscopy and/or detailed specialist assessment or retinal photography.	Normal cognition (CDR 0), cognitive impairment but not demented (CDR 0.5), and mild/moderate/severe dementia (CDR 1–3)	FDS study: T2DM patients aged 50 years or more	DR: 30 Control: 290	Cohort	14.7 years	**Cognitive impairment:** DR: 3.11 (1.15–8.38)	No

(Continued)

TABLE 1 | Continued

References	Country	Definition of diabetic retinopathy	Definition of cognitive impairment	Participant characteristics	Enrolled sample number	Study design	Follow-up	OR (95%)	Adjusted confounders
Umegaki et al. (2008)	Japan	Diabetic retinopathy was classified into two categories: mild (no retinopathy or intraretinal hemorrhages and hard exudates), or serious (soft exudates, intraretinal microvascular abnormalities, venous caliber abnormalities, venous beading, neovascularization of the disc or other areas in the retina, preretinal fibrous tissue proliferation, preretinal or vitreous hemorrhage, and/or retinal detachment).	Having an MMSE score of 23 or less.	J-EDIT study: Japanese people with diabetes aged 65 years or more	DR: 448 Control: 459	Cross-sectional	/	**Cognitive impairment:** DR: 1.730 (0.998–2.997)	Age
Roberts et al. (2008)	USA	Not mentioned	MCI was defined according to the following published criteria: cognitive concern by physician, patient, or nurse; impairment in 1 or more of the 4 cognitive domains; essentially normal functional activities; and not demented. A diagnosis of dementia was based on the Diagnostic and Statistical Manual of Mental Disorders, 4th edition criteria.	Olmsted county residents: subjects were found to be free of dementia aged 70 through 89 years	DR: 43 Control: 1558	Case-control	/	**MCI:** DR: 2.15 (1.09-4.22)	Age, sex, education, hypertension, stroke or transient ischemic attack, cigarette smoking, coronary artery disease, and body mass index.
Baker et al. (2007)	Australia	The photographs were evaluated according to a standardized protocol into 4 broad categories for: (1) retinopathy signs (microaneurysms, retinal hemorrhages, cotton wool spots, hard exudates, macular edema, intraretinal microvascular abnormalities, venous beading, new vessels at the disc or elsewhere, and vitreous hemorrhage); (2) arteriovenous nicking; (3) focal arteriolar narrowing; and (4) retinal arteriolar and venular caliber.	Definition of dementia correlates very closely to criteria used in the Diagnostic and Statistical Manual of Mental Disorders, 4th edition.	CHS study: diabetes adults 65 years of age and older	Total: 289	Cross-sectional	/	**Dementia:** DR: 0.32 (0.07- 1.44)	Not mentioned

(Continued)

TABLE 1 | Continued

References	Country	Definition of diabetic retinopathy	Definition of cognitive impairment	Participant characteristics	Enrolled sample number	Study design	Follow-up	OR (95%)	Adjusted confounders
Kadoi et al. (2005)	Japan	A modification of the diabetic retinopathy study and the early treatment diabetic retinopathy study grading scale.	Cognitive functioning was assessed with the following tests: (1) Mini-Mental State Examination, (2) Rey Auditory Verbal Learning Test, (3) Trail-Making Test (part A), (4) Trail-Making Test (part B), (5) Digit Span Forward, and (6) Grooved Pegboard. Significant impairment was defined as a decline from preoperative testing of more than 1 SD on more than 20% of test measures (at least 2 of 6).	Hospital patients: patients with T2DM who were scheduled for elective coronary artery bypass grafting	DR: 51 Control: 129	Cohort	7 days and 6 months	**All cognitive impairment:** DR: 2.4 (1.4-2.9) **Short-term cognitive impairment:** DR: 2.0 (1.3-3.0) **Long-term cognitive impairment:** DR: 2.1 (1.2-2.7)	No

CDR, clinical dementia rating; MCI, mild cognitive impairment; MMSE, Mini-Mental State Examination; MOCA, montreal cognitive assessment; T2DM, type 2 diabetes mellitus; DR, diabetic retinopathy; AMT, abbreviated mental test; HbA1c, glycosylated hemoglobin; CVD, cardiovascular disease; T1DM, type 1 diabetes mellitus; PDR, proliferative diabetic retinopathy.

Grades of DR and Cognitive Impairment

The distribution of studies by the estimate of the association between the grades of DR and cognitive impairment is plotted in **Figure 5**. Compared to other groups, minimal or mild DR was not significantly associated with cognitive impairment (OR, 2.04; 95% CI, 0.87–4.77). However, although proliferative diabetic retinopathy (PDR) was further distinguished, the association between PDR and cognitive impairment (OR, 3.57; 95% CI, 1.79–7.12; $I^2 = 16.6\%$) was not stronger than the association between moderate or worse DR and cognitive impairment (OR, 4.26; 95% CI, 2.01–9.07; $I^2 = 0.0\%$). Only one study reported HR data on patients with grades of DR, and a similar result was reported: compared to moderate or severe DR groups, mild DR was not significantly associated with cognitive impairment (HR, 1.5; 95% CI, 0.9–2.5).

DISCUSSION

In this systematic review and meta-analysis of observational studies, DR was found to be associated with cognitive impairment. Our meta-analysis provided evidence that patients with DR were more than twice as likely to develop cognitive impairment than were those without DR. The positive association was consistent across different study types, duration of follow-up, and regardless of whether confounding factors had been adjusted. In most of the included studies that reported HRs, there was also a positive association between DR and cognitive impairment. However, among the studies that provided HRs, the only study that found no link between DR and cognitive impairment was performed in a large group of patients with diabetes who survived to older ages (Rodill et al., 2018). As this study population included a healthy survivor group that outlived many peers, the relationship between DR and cognitive impairment might be underestimated.

Although DR is a common microvascular complication of diabetes, only one systematic review has previously investigated its association with cognitive impairment (Crosby-Nwaobi et al., 2012). However, only three studies were included in the systematic review, and the only cohort study was not population-based. In addition, the cohort study in that systematic review utilized a group of people who were about to undergo coronary artery bypass grafting, which might cause a certain degree of bias and reduce the applicability of the results. Moreover, the previous systematic review did not show whether patients with moderate to worse DR had more severe cognitive impairment than those without or with mild DR. Therefore, the current study attempted to quantitatively analyze the relationship between diabetic retinopathy and cognitive impairment based on more studies, especially cohort studies, and further explore the relationship between the degree of DR and cognitive impairment.

We found that minimal or mild DR was not significantly associated with cognitive impairment, but moderate to worse DR or PDR was strongly associated with cognitive impairment. Crosby-Nwaobi et al. found that patients with no or minimal DR demonstrated more cognitive impairment than did those with PDR (Crosby-Nwaobi et al., 2013), and this conclusion

TABLE 2 | Characteristics of the study providing hazard radios.

References	Country	Definition of diabetic retinopathy	Definition of cognitive impairment	Participant characteristics	Enrolled sample number	Study design	Mean follow-up	HR (95%)	Adjusted confounders
Yu et al. (2020)	Korea	ICD-10 code H36.0.	Prescribed anti-dementia medications (rivastigmine, galantamine, memantine, or donepezil) along with ICD-10 codes (F00, F01, F02, F03, G30, or G31).	NHIS: 40 years of age or older with diabetes	DR: 195449 Control: 1722253	Cohort	5.1 years	**Any type of dementia:** DR: 1.09 (1.07–1.11) **Alzheimer's disease:** DR: 1.10 (1.07–1.12) **Vascular dementia:** DR: 1.08 (1.03–1.14)	Age, sex, smoking, alcohol intake, exercise, income, plasma glucose concentration, duration of diabetes, BMI, dyslipidemia, hypertension, diabetic retinopathy, CKD, stroke, IHD, depression, number of OHAs, and treatment with insulin.
Deal et al. (2019)	USA	Modified Airlie House classification, as used in the Early Treatment Diabetic Retinopathy Study.	Modified CDR interviews with informants confirming a hospital ICD-9 discharge or death certificate dementia code, or on hospital or death certificate dementia codes alone.	ARIC study: Diabetes aged 50-73 years	DR: 324 Control: 1581	Cohort	16 years	**Dementia:** Moderate/severe retinopathy: 2.14 (1.50–3.04) Mild retinopathy: 1.5(0.9-2.5)	Age (linear and quadratic terms), education, sex, race center interaction, BMI, drinking status, smoking status, diabetes, hypertensive status, CHD, and history of stroke.
Lee et al. (2019)	USA	ICD-9 codes: DR (362.01, 363.02, 362.03, 362.04, 362.05, 362.06).	late-onset clinical Alzheimer's disease as defined by NINCDS-ADRDA criteria. Dementia diagnoses were determined at consensus conferences using the Diagnostic and Statistical Manual of Mental Disorders, 4th Version, criteria.	ACT participants (Kaiser Permanente Washington membership): Adults aged ≥65 who were dementia-free	DR: 248 Control: 3629	Cohort	>8 years	**Alzheimer's disease**: 0–5 years: 1.67 (1.01, 2.74) More than 5 years: 1.50 (1.05, 2.15)	Age, sex, education, self-reported white race, any APOE ε4 alleles, and time-dependent smoking status.
Rodill et al. (2018)	USA	ICD-9 diagnostic and CPT-4 procedural codes were used. PDR (ICD-9: 362.02; CPT-4: 67228), macular edema (ICD-9: 362.07, 362.53, 362.83; CPT-4: 67208, 67210) or nonspecific DR (ICD-9: 250.5x, 362.0x).	Dementia were identified using the following ICD-9 diagnostic codes: Alzheimer disease (331.0), vascular dementia (290.4x), and nonspecific dementia (290.0, 290.1x, 290.2x, 290.3, 294.1x, 294.2x, and 294.8).	KPNC database: Members with T1DM, with no prevalent dementia diagnoses, and at least 50 years old	DR: 2294 Control: 1448	Cohort	6.2 years	**Dementia:** DR: 1.12 (0.82, 1.54)	Age, sex and race, baseline glycosylated hemoglobin and comorbidities.
Exalto et al. (2014)	USA	PDR: panretinal photocoagulation to treat proliferative retinopathy (CTP4 code 67228), for diabetic macular edema: focal and grid photocoagulation to treat macular edema (CTP4 codes 67208 67210); or outpatient diagnoses made in ophthalmology: (ICD 9 codes 250.5 + 362.02 for PDR; ICD 9 codes 250.5 + 362.53 or 250.5 + 362.83 for diabetic macular edema).	Dementia was identified using ICD-9-CM diagnosis codes; senile dementia uncomplicated (290.0), Alzheimer disease (331.0), vascular dementia (290.4x), and dementia not otherwise specified (290.1). Using diagnoses made in primary care (ICD 9 codes 290.0, 290.1x) and neurology or memory clinic visits (ICD 9 codes 331.0, 290.1x, 290.2x, 290.3, 290.4x).	KPNC database: Patients aged ≥60 years with T2DM	DR: 2008 Control: 27953	Cohort	6.6 years	**Dementia:** DR: 1.32 (1.17, 1.49)	Age (as time scale), gender, race and education, medical utilization, diabetes mellitus composite, vascular composite, BMI and smoking status.

ICD, international classification of diseases; DR, diabetic retinopathy; BMI, body mass index; CKD, chronic kidney disease; IHD, schemic heart diseases; OHAs, oral hypoglycemic agents; CDR, Clinical Dementia Rating; CHD, coronary heart disease; NINCDS-ADRDA, national institute of neurological and communicative disorders and stroke–alzheimer's disease and related disorders association; APOE, apolipoprotein E; CPT-4, current procedural terminology, 4th edition; PDR, proliferative diabetic retinopathy; T1DM, type 1 diabetes mellitus; T2DM, type 1 diabetes mellitus.

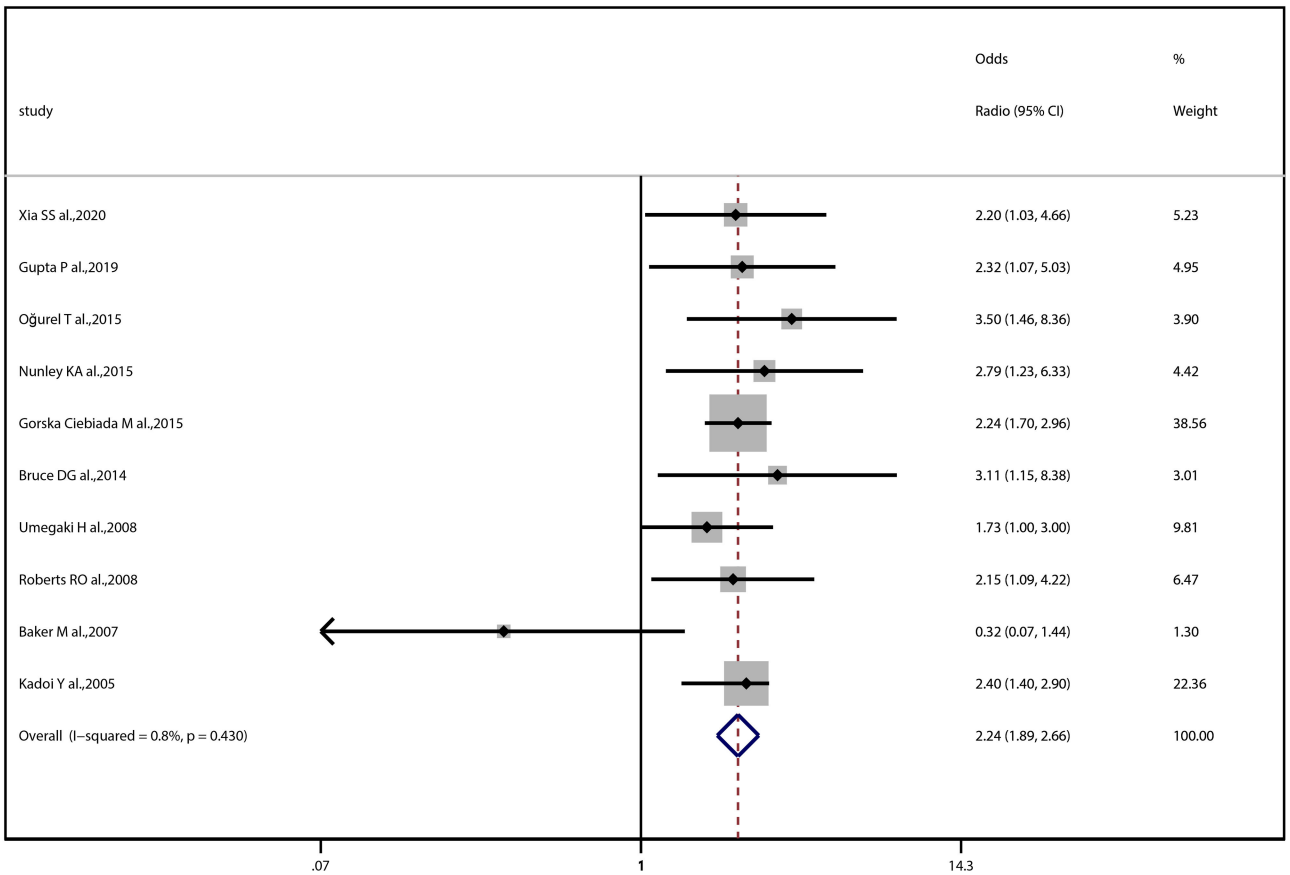

FIGURE 2 | Forest plot and pooled estimates of the association between diabetic retinopathy and cognitive impairment. Each study corresponds to a horizontal line and a square. The size of the square represents the weight of the study in the pooled analysis, and the length of the horizontal line represents the 95% confidence interval (CI). The pooled fixed-effect estimate and its 95% CI are represented by a dashed vertical and a diamond. The vertical at 1 indicates that diabetic retinopathy is not associated with cognitive impairment.

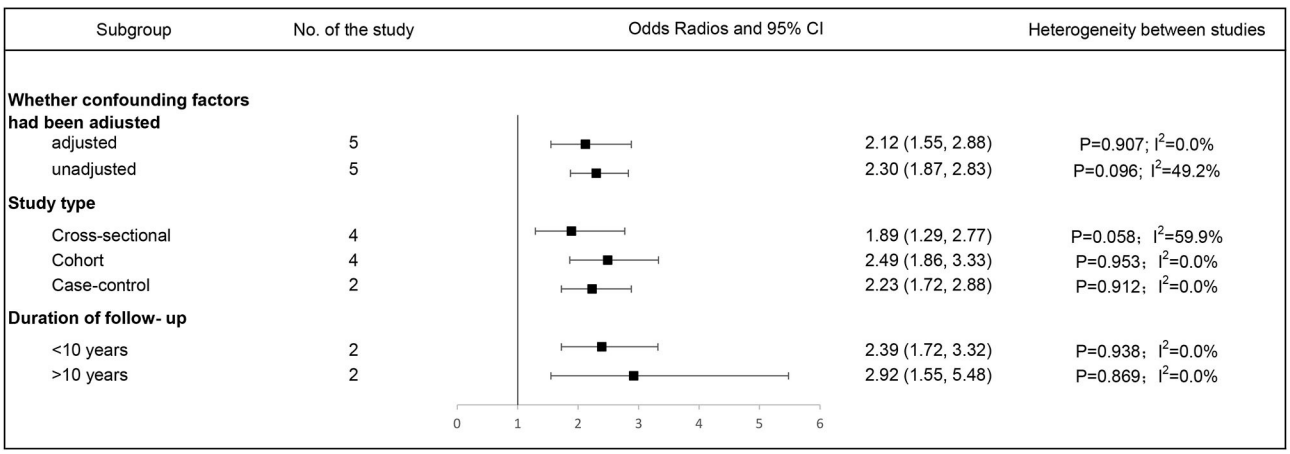

FIGURE 3 | Subgroup analysis of the association between diabetic retinopathy and cognitive impairment. Forest plot and pooled estimates of the association between diabetic retinopathy and cognitive impairment, stratified by whether confounding factors had been adjusted, study type, and duration of follow-up. Each subgroup corresponds to a horizontal line and a square. The square represents the pooled estimate, and the length of the horizontal line represents the 95% confidence interval. The vertical at 1 indicates that diabetic retinopathy is not associated with cognitive impairment.

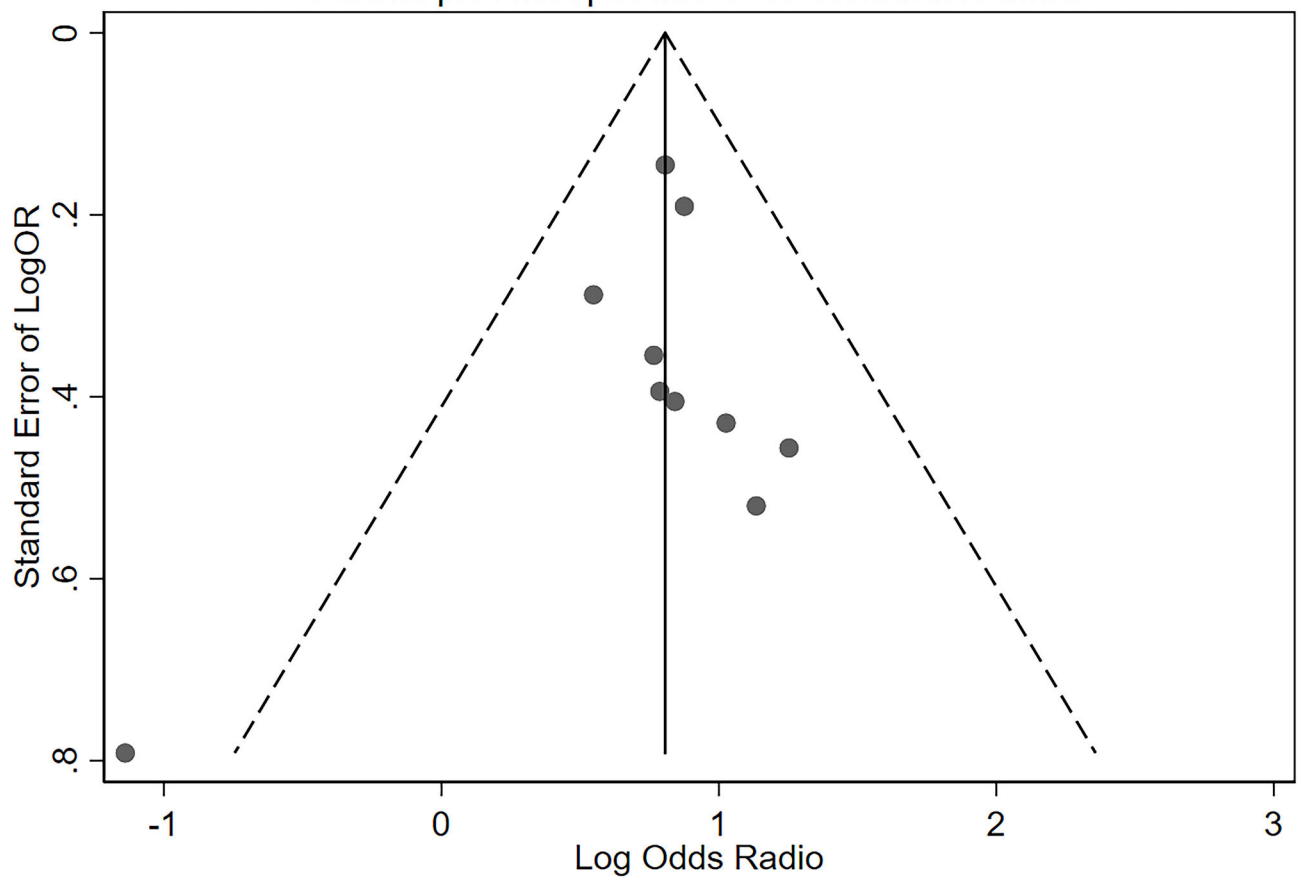

FIGURE 4 | Funnel plot of standard error of log odds ratio (OR) for the association of diabetic retinopathy and cognitive impairment. The vertical line represents the summary estimate of log OR. Diagonal dashed lines estimate the expected distribution of studies; The Egger test did not show statistically significant asymmetry of the funnel plot ($P = 0.538$).

was inconsistent with ours. However, there were two important limitations in the previous study that may account for the discrepancy between their conclusions and ours. First, the authors combined people without DR with mild DR as a control group, which may have weakened the association between PDR and cognitive impairment. Second, the level of education was different between the no/mild DR and PDR groups. Education level is associated with cognitive impairment, which may have influenced the final results.

Unfortunately, the mechanisms underlying the association between DR and cognitive impairment have not been well-explained. DR highlights hyperglycemia-induced microvascular damage as a specific complication of diabetes. The relationship between hyperglycemia and microvascular dysfunction is bidirectional and constitutes a vicious cycle (Stehouwer, 2018). Due to retinal vascular shared origin and drainage with the cerebrovascular circulation (Moss, 2015), one possible hypothesis is that DR may indicate diabetes-induced microvascular changes in the brain, which may ultimately cause cognitive impairment. Neurovascular coupling dysfunction and destruction of the blood–brain barrier are common in diabetic cerebrovascular dysfunction (van Sloten et al., 2020). Similarly, neurovascular coupling dysfunction (Garhöfer et al., 2020) and destruction of the blood–retinal barrier (Starr et al., 2003) are common in DR. This suggests that DR and cerebral microangiopathy have similar pathophysiological changes. This idea is further supported by the presence of microbleeds (Woerdeman et al., 2014), white matter lesions, and lacunes (Sanahuja et al., 2016) in the brains of patients with DR. Diabetes cerebral microvascular dysfunction and damage may lead to ischemia, hemorrhage, abnormal neuronal function, neuronal cell death, and altered neuronal connectivity, which contribute to cognitive dysfunction (van Sloten et al., 2020). The proximity of the onset of retinopathy to the onset of some cognitive domain damage also seems to support this idea. Within 5 years of diagnosis, 14% of patients with type 1 diabetes and 33% of patients with type 2 diabetes may develop DR (Cheung et al., 2010), and verbal memory and fluency are also likely to decline (Callisaya et al., 2019).

However, this hypothesis about the mechanism of the association between DR and cognitive impairment cannot fully

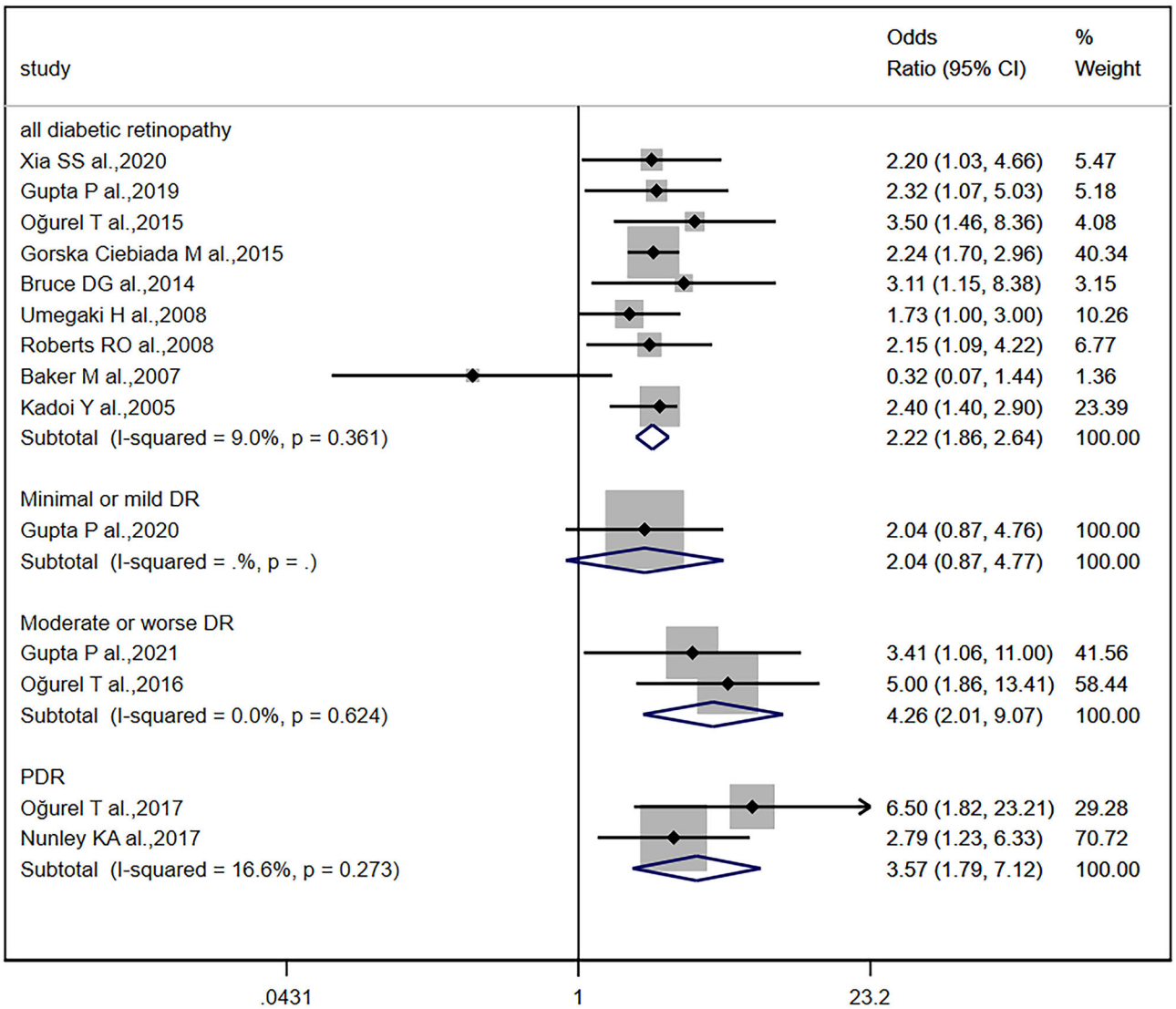

FIGURE 5 | Grades of diabetic retinopathy and cognitive impairment. Forest plot and pooled estimates of the association between diabetic retinopathy and cognitive impairment, stratified by the grade of diabetic retinopathy. Each study corresponds to a horizontal line and a square. The size of the square represents the weight of the study in the pooled analysis, and the length of the horizontal line represents the 95% confidence interval (CI). The pooled fixed-effect estimate and its 95% CI are represented by a dashed vertical and diamond. The vertical at 1 indicates that diabetic retinopathy is not associated with cognitive impairment.

explain the results of the current meta-analysis and systematic review. First, if this hypothesis is correct, then since the severity of DR is associated with the risk of cerebral microangiopathy (Modjtahedi et al., 2020), the severity of DR should also be associated with the risk of cognitive impairment. However, what was puzzling was that although some included studies focused on the relationship between PDR and cognitive impairment (OR, 3.57; 95% CI, 1.79–7.12; $I^2 = 16.6\%$), the relationship was not stronger than that between moderate to worse DR and cognitive impairment (OR, 4.26; 95% CI, 2.01–9.07; $I^2 = 0.0\%$). A possible explanation could be that moderate to worse DR included PDR in most of the included studies, and, therefore, its association with cognitive impairment has been overestimated. Second, in most of the cohort studies we included, why was there still a time gap between the onset of diabetic retinopathy and cognitive impairment, and the longer the time gap, the stronger the relationship? We speculated that it may be because even though cerebrovascular and some cognitive domains are damaged early, it still needs a certain degree of time to accumulate before it can be reflected in global cognitive tools, but this speculation still lacks necessary evidence. Third, the tools used to evaluate cognitive impairment, such as the Mini-Mental State Examination and Montreal Cognitive Assessment, can only evaluate the cognitive level of patients but cannot confirm the occurrence of cerebral microvascular disease. Therefore, the results of this meta-analysis and systematic review do not provide strong support for this

hypothesis. More evidence is needed to confirm whether there is a clear mechanistic link between DR and cognitive impairment.

The included cohort studies that reported HRs mostly showed that DR could predict dementia (**Table 2**). Dementia typically occurs after the age of 65–70 years, and no evidence exists that diabetes increases the risk of early-onset dementia (Biessels et al., 2014). This may indicate that different stages of cognitive impairment in patients with diabetes should not be regarded as a continuum (Biessels and Despa, 2018). Our results suggest that strategies that focus on DR screening may be useful in identifying individuals at risk of dementia, which could expand the role of diabetic retinopathy screening.

LIMITATION

There are some limitations to this systematic review and meta-analysis. First, whether PDR, the most severe form of DR, is most strongly associated with cognitive impairment remains unresolved. If the risk of cognitive impairment is related to the grade of retinopathy, the mechanistic link between DR and cognitive impairment is more plausible. However, although researchers were aware of the problem, PDR was not separated from moderate or worse DR. Second, some studies have reported that mild DR was not associated with cognitive impairment, but we were not able to obtain the data. Third, because some studies did not report adjustments or reported incomplete adjustments for potential confounders, we were not able to combine models with studies that adjusted for the same set of confounding factors. Fourth, because the definitions of DR and cognitive impairment varied in the included studies, we did not compare the results for different retinopathy diagnostic criteria, cognitive impairment diagnostic criteria, or cognitive testing tools. Fifth, since the included studies evaluated global cognitive function, we were unable to assess the relationship between DR and different cognitive domains. Sixth, many of the included studies did not specify the type of diabetes, even though the mechanisms of cognitive impairment caused by different types of diabetes may differ (McCrimmon et al., 2012). Finally, there is clear evidence of sex differences in cognitive impairment, and the rate of cognitive decline with aging is also different between the sexes (Li and Singh, 2014). However, because most of the included studies adjusted for sex as a confounding factor and the lack of information on retinopathy in sex, we were unable to use these studies to analyze males and females separately. A previous study suggested that negative associations between DR and several cognitive measures were statistically significant only in males (Ding et al., 2010), but the significantly greater number of men with DR than females in this study may have exaggerated the results. Therefore, further research is needed to confirm whether the relationship between DR and cognitive impairment differs between the sexes.

CONCLUSION

In conclusion, the present systematic review and meta-analysis demonstrated that DR is associated with an increased risk of cognitive impairment. Screening for DR may help identify individuals with cognitive impairment at an earlier stage. More studies are needed to confirm the association between PDR and cognitive impairment.

DATA AVAILABILITY STATEMENT

The original contributions presented in the study are included in the article/**Supplementary Material**, further inquiries can be directed to the corresponding authors.

AUTHOR CONTRIBUTIONS

GW and GN contributed to conception and design of the study. DC, XZ, and SY organized the database. DC performed the statistical analysis and wrote the first draft of the manuscript. All authors contributed to manuscript revision, read, and approved the submitted version.

FUNDING

This work was supported by the National Natural Science Foundation of China [grant numbers 81670732]; the National Key R&D Program of China [grant numbers 2016YFC0901204].

ACKNOWLEDGMENTS

We thank Yongqiang Yang for improving image quality.

SUPPLEMENTARY MATERIAL

The Supplementary Material for this article can be found online at: https://www.frontiersin.org/articles/10.3389/fnagi.2021.692911/full#supplementary-material

REFERENCES

Ardila, A. (2007). Normal aging increases cognitive heterogeneity: analysis of dispersion in WAIS-III scores across age. *Arch. Clin. Neuropsychol.* 22, 1003–1011. doi: 10.1016/j.acn.2007.08.004

Baker, M. L., Marino Larsen, E. K., Kuller, L. H., Klein, R., Klein, B. E., Siscovick, D. S., et al. (2007). Retinal microvascular signs, cognitive function, and dementia in older persons: the cardiovascular health study. *Stroke* 38, 2041–2047. doi: 10.1161/STROKEAHA.107.483586

Biessels, G. J., and Despa, F. (2018). Cognitive decline and dementia in diabetes mellitus: mechanisms and clinical implications. *Nat. Rev. Endocrinol.* 14, 591–604. doi: 10.1038/s41574-018-0048-7

Biessels, G. J., Strachan, M. W., Visseren, F. L., Kappelle, L. J., and Whitmer, R. A. (2014). Dementia and cognitive decline in type 2 diabetes and prediabetic stages: towards targeted interventions. *Lancet Diabetes Endocrinol.* 2, 246–255. doi: 10.1016/S2213-8587(13)70088-3

Biessels, G. J., and Whitmer, R. A. (2020). Cognitive dysfunction in diabetes: how to implement emerging guidelines. *Diabetologia* 63, 3–9. doi: 10.1007/s00125-019-04977-9

Bruce, D. G., Davis, W. A., Starkstein, S. E., and Davis, T. M. (2014). Mid-life predictors of cognitive impairment and dementia in type 2 diabetes mellitus: the fremantle diabetes study. *J. Alzheimers Dis.* 42, S63–S70. doi: 10.3233/JAD-132654

Callisaya, M. L., Beare, R., Moran, C., Phan, T., Wang, W., and Srikanth, V. K. (2019). Type 2 diabetes mellitus, brain atrophy and cognitive decline in older people: a longitudinal study. *Diabetologia* 62, 448–458. doi: 10.1007/s00125-018-4778-9

Chatterjee, S., Khunti, K., and Davies, M. J. (2017). Type 2 diabetes. *Lancet* 389, 2239–2251. doi: 10.1016/S0140-6736(17)30058-2

Cheung, N., Mitchell, P., and Wong, T. Y. (2010). Diabetic retinopathy. *Lancet* 376, 124–136. doi: 10.1016/S0140-6736(09)62124-3

Crosby-Nwaobi, R., Sivaprasad, S., and Forbes, A. (2012). A systematic review of the association of diabetic retinopathy and cognitive impairment in people with type 2 diabetes. *Diabetes Res. Clin. Pract.* 96, 101–110. doi: 10.1016/j.diabres.2011.11.010

Crosby-Nwaobi, R. R., Sivaprasad, S., Amiel, S., and Forbes, A. (2013). The relationship between diabetic retinopathy and cognitive impairment. *Diabetes Care* 36, 3177–3186. doi: 10.2337/dc12-2141

Deal, J. A., Sharrett, A. R., Albert, M., Bandeen-Roche, K., Burgard, S., Thomas, S. D., et al. (2019). Retinal signs and risk of incident dementia in the Atherosclerosis risk in communities study. *Alzheimers Dement.* 15, 477–486. doi: 10.1016/j.jalz.2018.10.002

Ding, J., Strachan, M. W. J., Reynolds, R. M., Frier, B. M., Deary, I. J., Fowkes, F. G. R., et al. (2010). Diabetic retinopathy and cognitive decline in older people with type 2 diabetes: the edinburgh type 2 diabetes study. *Diabetes* 59, 2883–2889. doi: 10.2337/db10-0752

Dominic, C. (2007). E. Strauss, E. M. S. Sherman, & O. Spreen, a compendium of neuropsychological tests: administration, norms, and commentary. *J. Appl. Neuropsychol.* 14, 62–63. doi: 10.1080/09084280701280502

Dore, G. A., Elias, M. F., Robbins, M. A., Elias, P. K., and Brennan, S. L. (2007). Cognitive performance and age: norms from the maine-syracuse study. *Exp. Aging Res.* 33, 205–271. doi: 10.1080/03610730701319087

Exalto, L. G., Biessels, G. J., Karter, A. J., Huang, E. S., Quesenberry, C. P. Jr, and Whitmer, R. A. (2014). Severe diabetic retinal disease and dementia risk in type 2 diabetes. *J. Alzheimer's Dis.* 42, S109–S117. doi: 10.3233/JAD-132570

Garhöfer, G., Chua, J., Tan, B., Wong, D., Schmidl, D., and Schmetterer, L. (2020). Retinal neurovascular coupling in diabetes. *J. Clin. Med.* 9:2829. doi: 10.3390/jcm9092829

Gorska-Ciebiada, M., Saryusz-Wolska, M., Borkowska, A., Ciebiada, M., and Loba, J. (2015). C-Reactive protein, advanced glycation end products, and their receptor in type 2 diabetic, elderly patients with mild cognitive impairment. *Front. Aging Neurosci.* 7:209. doi: 10.3389/fnagi.2015.00209

Gupta, P., Gan, A. T. L., Man, R. E. K., Fenwick, E. K., Sabanayagam, C., Mitchell, P., et al. (2019). Association between diabetic retinopathy and incident cognitive impairment. *Br. J. Ophthalmol.* 103, 1605–1609. doi: 10.1136/bjophthalmol-2018-312807

Hammes, H. P. (2018). Diabetic retinopathy: hyperglycaemia, oxidative stress and beyond. *Diabetologia* 61, 29–38. doi: 10.1007/s00125-017-4435-8

Kadoi, Y., Saito, S., Fujita, N., and Goto, F. (2005). Risk factors for cognitive dysfunction after coronary artery bypass graft surgery in patients with type 2 diabetes. *J. Thorac. Cardiovasc. Surg.* 129, 576–583. doi: 10.1016/j.jtcvs.2004.07.012

Langa, K. M., and Levine, D. A. (2014). The diagnosis and management of mild cognitive impairment: a clinical review. *Jama* 312, 2551–2561. doi: 10.1001/jama.2014.13806

Lee, C. S., Larson, E. B., Gibbons, L. E., Lee, A. Y., McCurry, S. M., Bowen, J. D., et al. (2019). Associations between recent and established ophthalmic conditions and risk of Alzheimer's disease. *Alzheimers Dement.* 15, 34–41. doi: 10.1016/j.jalz.2018.06.2856

Li, R., and Singh, M. (2014). Sex differences in cognitive impairment and Alzheimer's disease. *Front. Neuroendocrinol.* 35, 385–403. doi: 10.1016/j.yfrne.2014.01.002

Li, S. J., Jiang, H., Yang, H., Chen, W., Peng, J., Sun, M. W., et al. (2015). The dilemma of heterogeneity tests in meta-analysis: a challenge from a simulation study. *PLoS ONE* 10:e0127538. doi: 10.1371/journal.pone.0127538

Lijmer, J. G., Bossuyt, P. M., and Heisterkamp, S. H. (2002). Exploring sources of heterogeneity in systematic reviews of diagnostic tests. *Stat. Med.* 21, 1525–1537. doi: 10.1002/sim.1185

McCrimmon, R. J., Ryan, C. M., and Frier, B. M. (2012). Diabetes and cognitive dysfunction. *Lancet* 379, 2291–2299. doi: 10.1016/S0140-6736(12)60360-2

Modjtahedi, B. S., Wu, J., Luong, T. Q., Gandhi, N. K., Fong, D. S., and Chen, W. (2020). Severity of diabetic retinopathy and the risk of future cerebrovascular disease, cardiovascular disease, and all-cause mortality. *Ophthalmology* doi: 10.1016/j.ophtha.2020.12.019

Moher, D., Liberati, A., Tetzlaff, J., and Altman, D. G. (2009). Preferred reporting items for systematic reviews and meta-analyses: the PRISMA statement. *PLoS Med.* 6:e1000097. doi: 10.1371/journal.pmed.1000097

Moss, H. E. (2015). Retinal vascular changes are a marker for cerebral vascular diseases. *Curr. Neurol. Neurosci. Rep.* 15:40. doi: 10.1007/s11910-015-0561-1

Nunley, K. A., Rosano, C., Ryan, C. M., Jennings, J. R., Aizenstein, H. J., Zgibor, J. C., et al. (2015). Clinically relevant cognitive impairment in middle-aged adults with childhood-onset type 1 diabetes. *Diabetes Care* 38, 1768–1776. doi: 10.2337/dc15-0041

Ogurel, T., Ogurel, R., Özer, M. A., Türkel, Y., Dag, E., and Örnek, K. (2015). Mini-mental state exam versus montreal cognitive assessment in patients with diabetic retinopathy. *Niger. J. Clin. Pract.* 18, 786–789. doi: 10.4103/1119-3077.163274

Prince, M., Bryce, R., Albanese, E., Wimo, A., Ribeiro, W., and Ferri, C. P. (2013). The global prevalence of dementia: a systematic review and metaanalysis. *Alzheimers Dement.* 9, 63-75.e62. doi: 10.1016/j.jalz.2012.11.007

Roberts, R. O., Geda, Y. E., Knopman, D. S., Christianson, T. J., Pankratz, V. S., Boeve, B. F., et al. (2008). Association of duration and severity of diabetes mellitus with mild cognitive impairment. *Arch. Neurol.* 65, 1066–1073. doi: 10.1001/archneur.65.8.1066

Rodill, L. G., Exalto, L. G., Gilsanz, P., Biessels, G. J., Quesenberry, C. P. Jr., and Whitmer, R. A. (2018). Diabetic retinopathy and dementia in type 1 diabetes. *Alzheimer Dis. Assoc. Disord.* 32, 125–130. doi: 10.1097/WAD.0000000000000230

Sanahuja, J., Alonso, N., Diez, J., Ortega, E., Rubinat, E., Traveset, A., et al. (2016). Increased burden of cerebral small vessel disease in patients with type 2 diabetes and retinopathy. *Diabetes Care* 39, 1614–1620. doi: 10.2337/dc15-2671

Simó, R., Stitt, A. W., and Gardner, T. W. (2018). Neurodegeneration in diabetic retinopathy: does it really matter? *Diabetologia* 61, 1902–1912. doi: 10.1007/s00125-018-4692-1

Smolina, K., Wotton, C. J., and Goldacre, M. J. (2015). Risk of dementia in patients hospitalised with type 1 and type 2 diabetes in England, 1998-2011: a retrospective national record linkage cohort study. *Diabetologia* 58, 942–950. doi: 10.1007/s00125-015-3515-x

Srikanth, V., Sinclair, A. J., Hill-Briggs, F., Moran, C., and Biessels, G. J. (2020). Type 2 diabetes and cognitive dysfunction-towards effective management of both comorbidities. *Lancet Diabetes Endocrinol.* 8, 535–545. doi: 10.1016/S2213-8587(20)30118-2

Stang, A. (2010). Critical evaluation of the newcastle-ottawa scale for the assessment of the quality of nonrandomized studies in meta-analyses. *Eur. J. Epidemiol.* 25, 603–605. doi: 10.1007/s10654-010-9491-z

Starr, J. M., Wardlaw, J., Ferguson, K., MacLullich, A., Deary, I. J., and Marshall, I. (2003). Increased blood-brain barrier permeability in type II diabetes demonstrated by gadolinium magnetic resonance imaging. *J. Neurol. Neurosurg. Psychiatry* 74, 70–76. doi: 10.1136/jnnp.74.1.70

Stehouwer, C. D. A. (2018). Microvascular dysfunction and hyperglycemia: a vicious cycle with widespread consequences. *Diabetes* 67, 1729–1741. doi: 10.2337/dbi17-0044

Stroup, D. F., Berlin, J. A., Morton, S. C., Olkin, I., Williamson, G. D., Rennie, D., et al. (2000). Meta-analysis of observational studies in epidemiology: a proposal for reporting. meta-analysis of observational studies in epidemiology (MOOSE) group. *Jama* 283, 2008–2012. doi: 10.1001/jama.283.15.2008

Umegaki, H., Iimuro, S., Kaneko, T., Araki, A., Sakurai, T., Ohashi, Y., et al. (2008). Factors associated with lower mini mental state examination scores in elderly Japanese diabetes mellitus patients. *Neurobiol. Aging* 29, 1022–1026. doi: 10.1016/j.neurobiolaging.2007.02.004

van Sloten, T. T., Sedaghat, S., Carnethon, M. R., Launer, L. J., and Stehouwer, C. D. A. (2020). Cerebral microvascular complications of type 2 diabetes: stroke, cognitive dysfunction, and depression. *Lancet Diabetes Endocrinol.* 8, 325–336. doi: 10.1016/S2213-8587(19)30405-X

Woerdeman, J., van Duinkerken, E., Wattjes, M. P., Barkhof, F., Snoek, F. J., Moll, A. C., et al. (2014). Proliferative retinopathy in type 1 diabetes is associated with cerebral microbleeds, which is part of generalized microangiopathy. *Diabetes Care* 37, 1165–1168. doi: 10.2337/dc13-1586

Xia, S. S., Xia, W. L., Huang, J. J., Zou, H. J., Tao, J., and Yang, Y. (2020). The factors contributing to cognitive dysfunction in type 2 diabetic patients. *Ann. Transl. Med.* 8:104. doi: 10.21037/atm.2019.12.113

Yu, J. H., Han, K., Park, S., Cho, H., Lee, D. Y., Kim, J. W., et al. (2020). Incidence and risk factors for dementia in type 2 diabetes mellitus: a nationwide population-based study in Korea. *Diabetes Metabol. J.* 44, 113–124. doi: 10.4093/dmj.2018.0216

Conflict of Interest: The authors declare that the research was conducted in the absence of any commercial or financial relationships that could be construed as a potential conflict of interest.

frontiers in Aging Neuroscience

ORIGINAL RESEARCH
published: 05 July 2021
doi: 10.3389/fnagi.2021.617947

White Matter Hyperintensity Volume and Location: Associations With WM Microstructure, Brain Iron, and Cerebral Perfusion

Christopher E. Bauer[1], *Valentinos Zachariou*[1], *Elayna Seago*[1] *and Brian T. Gold*[1,2]*

[1] Department of Neuroscience, University of Kentucky, Lexington, KY, United States, [2] Sanders-Brown Center on Aging, University of Kentucky, Lexington, KY, United States

Cerebral white matter hyperintensities (WMHs) represent macrostructural brain damage associated with various etiologies. However, the relative contributions of various etiologies to WMH volume, as assessed via different neuroimaging measures, is not well-understood. Here, we explored associations between three potential early markers of white matter hyperintensity volume. Specifically, the unique variance in total and regional WMH volumes accounted for by white matter microstructure, brain iron concentration and cerebral blood flow (CBF) was assessed. Regional volumes explored were periventricular and deep regions. Eighty healthy older adults (ages 60–86) were scanned at 3 Tesla MRI using fluid-attenuated inversion recovery, diffusion tensor imaging (DTI), multi-echo gradient-recalled echo and pseudo-continuous arterial spin labeling sequences. In a stepwise regression model, DTI-based radial diffusivity accounted for significant variance in total WMH volume (adjusted R^2 change = 0.136). In contrast, iron concentration (adjusted R^2 change = 0.043) and CBF (adjusted R^2 change = 0.027) made more modest improvements to the variance accounted for in total WMH volume. However, there was an interaction between iron concentration and location on WMH volume such that iron concentration predicted deep ($p = 0.034$) but not periventricular ($p = 0.414$) WMH volume. Our results suggest that WM microstructure may be a better predictor of WMH volume than either brain iron or CBF but also draws attention to the possibility that some early WMH markers may be location-specific.

Keywords: cerebral small vessel disease, DTI, white matter hyperintensities, cerebral perfusion, brain iron, QSM

OPEN ACCESS

Edited by:
Nicola Vanacore,
National Institute of Health (ISS), Italy

Reviewed by:
Henk J. M. M. Mutsaerts,
VU University
Amsterdam, Netherlands
Owen T. Carmichael,
Pennington Biomedical Research Center, United States

***Correspondence:**
Brian T. Gold
brian.gold@uky.edu

Received: *15 October 2020*
Accepted: *31 May 2021*
Published: *05 July 2021*

Citation:
Bauer CE, Zachariou V, Seago E and Gold BT (2021) White Matter Hyperintensity Volume and Location: Associations With WM Microstructure, Brain Iron, and Cerebral Perfusion. Front. Aging Neurosci. 13:617947. doi: 10.3389/fnagi.2021.617947

INTRODUCTION

Cerebral white matter hyperintensities (WMHs) are diffuse regions of high signal intensity on T2-weighted magnetic resonance imaging scans (MRI; Hachinski et al., 1987; Wardlaw et al., 2015). The high signal intensity associated with WMHs reflect alterations in local tissue properties, including increased water content and myelin rarefaction (Fazekas et al., 1993; Pantoni and Garcia, 1997). WMHs are very common in older adults, with prevalence rates of ∼60–80% in those above 65 years of age (de Leeuw et al., 2001; Wen and Sachdev, 2004). While non-specific in etiology, WMHs are generally associated with cerebral small vessel disease (cSVD; Pantoni and Garcia, 1995; Wardlaw et al., 2013a).

WMHs are thought to reflect "macrostructural" damage associated with moderate-to-advanced stages of cSVD (Debette and Markus, 2010; Gouw et al., 2011; Wardlaw et al., 2015). Consistent with this possibility, pathology studies suggest that WMHs are associated with structural brain changes such as gliosis, axonal degeneration, myelin loss and vacuolation (Gouw et al., 2011; Valdés Hernández et al., 2015). Further, a meta-analysis of 22 studies showed that WMHs were associated with progressive cognitive impairment, a 2-fold increase in the risk of dementia and a 3-fold increase in stroke risk (Debette and Markus, 2010). In addition, WMHs are associated with decreased physical ability (Sachdev et al., 2005), depression (Taylor et al., 2003) and increased risk of mortality (Debette and Markus, 2010).

A number of other MRI metrics have been suggested as potentially earlier markers of WMH volume (Wardlaw et al., 2013b; Smith and Beaudin, 2018). Identification of earlier neuroimaging markers of WMH volume is an important goal toward early identification of participants for enrollment in cSVD clinical trials (Charidimou et al., 2016; Boulouis et al., 2017). Ultimately, earlier markers of WMH will be defined as those which predict subsequent changes in vascular-related cognitive processes or WMH growth with high accuracy. Several studies have shown that baseline DTI-based measures in normal-appearing white matter (NAWM) predict WMH growth 1 to 2 years later (Maillard et al., 2014; Promjunyakul et al., 2018). However, while longitudinal studies are the gold-standard, they are also expensive and time-consuming. Results from cross-sectional studies may prove useful in guiding the selection of promising predictors of WMHs for use in future longitudinal studies. A number of previous cross-sectional studies have suggested significant relationships between either DTI metrics in NAWM (Maillard et al., 2011; Pelletier et al., 2016; Promjunyakul et al., 2016) or ASL (ten Dam et al., 2007; Brickman et al., 2009; Bahrani et al., 2017) and WMH volume. More recently, several studies have reported significant associations between brain iron and WMH volume (Yan et al., 2013; Valdés Hernández et al., 2016; Sun et al., 2017). However, no studies have considered these predictors simultaneously. Doing so is critical to identify which predictors account for the most unique variance in WMH volume after controlling for shared variance between predictors.

In addition to considering associations with total WMH volume, WMHs are often studied based on their specific location (Wardlaw et al., 2013a). In particular, specific regions of periventricular (PV) and deep WMH volume are often compared (Gouw et al., 2011; Griffanti et al., 2018). However, it remains unclear whether PV and deep WMHs reflect different pathologies (Gouw et al., 2011) or similar pathologies at different stages of cSVD severity (Ryu et al., 2014). Exploring potential interactions between predictors and WM location may help address this question.

Abbreviations: cSVD, Cerebral Small Vessel Disease; MRI, Magnetic Resonance Imaging; WMH, White Matter Hyperintensity; PV, Periventricular; DTI, Diffusion Tensor Imaging; FA, Fractional Anisotropy; RD, Radial Diffusivity; CBF, Cerebral Blood Flow; QSM, Quantitative Susceptibility Mapping; GM, Gray Matter.

TABLE 1 | Group demographics and Montreal Cognitive Assessment (MoCA[a]) scores.

	Mean (S.D.)	*N*
Age (Years)	70.4 (5.6)	80
Sex Ratio (F:M)	48:32	80
Education (Years)	16.4 (2.4)	80
MoCA[a]	27.1 (2.5)	69

The table lists the mean (±sd) for age, the female/male ratio, and the mean (±sd) years of education and MoCA scores.
[a]*Nasreddine et al., 2005.*

Here, we explored the associations between several potential early stage markers of WMH volume. White matter (WM) microstructure, cerebral blood flow, and brain iron were used as predictors of WMH volume. Of key relevance, comprehensive models were used to assess the variance in WMH volume associated with each individual predictor, after controlling for variance associated with the other predictors to assess potential additive and synergistic effects on WMH volume and location. In addition, we explored whether each predictor contributed preferentially to PV or deep WMH volume.

MATERIALS AND METHODS

Participants

Eighty healthy older adults (48 women, age range 60–86 years) were recruited for the experiment. All participants provided informed consent under a protocol approved by the Institutional Review Board of the University of Kentucky. Participants were recruited from an existing longitudinal cohort at the Sanders-Brown Center on Aging (SBCoA) and the Lexington community. Participants from the SBCoA were cognitively intact based on clinical consensus diagnosis and scores from the Uniform Data Set (UDS3) used by US ADRCs (Besser et al., 2018). Participants recruited from the community did not complete the UDS3 battery but were required to score 26 or more on the Montreal Cognitive Assessment (MoCA; Nasreddine et al., 2005) as a study inclusion criteria. Exclusion criteria were significant head injury (defined as loss of consciousness for more than 5 min), heart disease, stroke, neurological or psychiatric disorders, claustrophobia, pacemakers, the presence of metal fragments or any metal implants that are incompatible with MRI, diseases affecting the blood (anemia, kidney/heart disease etc.) or significant brain abnormalities detected during imaging. One participant was excluded from the sample due to the presence of an old stroke within the right motor cortex that was not clinically evident at study enrollment. Detailed characteristics of the final group of participants are shown in **Table 1**.

Magnetic Resonance Imaging Protocol

Participants were screened to ensure magnetic safety for scanning within the Siemens Magnetom Prisma 3T (software version E11C) with a 64-channel head coil at the University of Kentucky's Magnetic Resonance Imaging and Spectroscopy Center (MRISC).

The following scans were acquired: (1) a 3D multi-echo, T1-weighted Magnetization Prepared Rapid Gradient Echo (T1) scan, (2) a 3D fluid-attenuated inversion recovery (FLAIR) scan, (3) a diffusion tensor imaging (DTI) scan, (4) a 3D, multi-echo gradient-recalled echo scan used for quantitative susceptibility mapping (QSM), and (5) a pseudo-continuous arterial spin labeling (PCASL) perfusion scan. Several other sequences were collected during the scanning session related to other scientific questions and are not discussed further here.

The T1 sequence covered the entire brain [1 mm isotropic voxels, 256 × 256 × 176 mm acquisition matrix, repetition time (TR) = 2,530 millisecond (ms), inversion time = 1,100 ms, flip angel (FA) = 7°, scan duration = 5.88 min] and had four echoes [First echo time (TE1) =1.69 ms, echo spacing (ΔTE = 1.86 ms)]. The 3D FLAIR sequence covered the entire brain (1 mm isotropic voxels, 256 × 256 × 176 acquisition matrix, TR = 5,000 ms, TE = 388 ms, inversion time = 1,800 ms, scan duration = 6.45 min). The DTI sequence was acquired with 126 separate diffusion directions (2 mm isotropic voxels, 81 slices, TR = 3,400 ms, TE = 71 ms, scan duration = 7.45 min, posterior-to-anterior phase encoding direction) and 4 b-values (0 s/mm^2, 500 s/mm^2, 1,000 s/mm^2 and 2,000 s/mm^2). A short (28 s) reverse phase-encoding direction scan was also obtained with the same parameters as the main DTI scan and used to correct for susceptibility-induced distortions in the main DTI scan. The 3D spoiled gradient-recalled echo sequence was used for QSM (1.2 mm isotropic voxels, 144 slices, FA = 15°, 24 millisecond TR, scan duration = 6.3 min) with eight separate TEs (TE1 = 2.98 ms, ΔTE = 2.53 ms). A 3DGRASE PCASL sequence was used with 9 control-label pairs [3 segments (echo planar imaging factor = 63, turbo factor = 14), 9 tagged and 9 untagged volumes and 1 M0 for calibration, 3.4 × 3.4 × 4.0 mm voxels, 220 × 220 × 144 mm acquisition matrix (36 slices), TR = 5,070 ms, TE = 31.4 ms, FA = 120°, labeling duration = 2,025 ms, post-labeling delay = 2,500 ms, scan duration = 5.15 min].

WMH Analyses

WMH volumes were computed using a validated 4-tissue segmentation method (DeCarli et al., 2013). Participants' FLAIR images were first registered to their own T1 [the four echoes averaged into a root mean square (RMS) image] image using FLIRT from FMRIB Software Library version 6.0.1 (FSL; Jenkinson et al., 2012), corrected for inhomogeneities using a previously published local histogram normalization (DeCarli et al., 1996), and then non-linearly aligned to a standard atlas (DeCarli et al., 2013). WMHs were estimated in standard space using Bayesian probability based on histogram fitting and prior probability maps. Voxels labeled as WMHs based on these maps also must have exceeded 3.5 SDs above the mean WM signal intensity. WMH volumes were calculated in participants' native FLAIR space after back-transformation and reported in cubic millimeters. WMHs were visually validated to ensure quality.

Periventricular and Deep WMH ROIs

WMH volume was further subdivided into periventricular (PV) and deep regions of interest (ROIs; **Figure 1**). PV WMHs were defined as being located within ∼10 mm of the ventricles and deep WMHs were defined as those located outside this radius (Griffanti et al., 2018). These ROIs were delineated using a validated group mask of the lateral ventricles, the Automatic Lateral Ventricle delIneatioN (ALVIN) mask, which was created using data from 275 healthy adults (age range 18–94; Kempton et al., 2011).

In order to accomplish this, each participant's RMS T1 image was first skull-stripped and segmented using FreeSurfer 6.0 (Fischl et al., 2004). The resulting images were then aligned to the participants' FLAIR images using the analysis of functional neuroimages (AFNI) and a local Pearson correlation cost function. A binary mask was then created from these FLAIR aligned T1 images for later use in masking deep WMHs (described below). Subsequently, the aligned non-binarized T1 images were warped to MNI space using the MNI ICBM152 atlas (1 mm, 6th generation; Grabner et al., 2006) and a non-linear transformation. The inverse transformation matrix was then applied to the ALVIN mask (which is in MNI space) to bring it back to each participant's native space, using AFNI and a nearest neighbor interpolation method.

The ALVIN mask extends beyond the lateral ventricles into brain parenchyma (∼7–11 mm in most participants) to ensure inclusion of the lateral ventricles across participants with varying brain size. Typically, subsequent multiplication with a segmented CSF image is then performed to exclude parenchyma from the ventricular mask (Kempton et al., 2011). Here, rather than performing this step, each participant's WMH mask was multiplied by their native-space ALVIN mask (**Figure 1**, top panel, PV ROI) to produce PV WMH masks (**Figure 2**). Lastly, deep ROIs were created by subtracting the participant's native-space ALVIN masks from their binarized FLAIR aligned T1 masks (**Figure 1**, bottom panel). Each participant's deep ROI was then multiplied by their WMH mask to produce deep WMH masks (**Figure 2**).

QSM Analyses

QSM images were processed in MATLAB using the Morphology Enabled Dipole Inversion toolbox (MEDI toolbox, release of 11/06/2017; Liu et al., 2012, 2013). This approach generates QSM images by inverting an estimate of the magnetic field to generate a distribution of local magnetic susceptibility used to calculate values for the underlying anatomy. The anatomical information required for MEDI was a (skull-stripped) magnitude image obtained during the same scan. The following steps were performed during MEDI: (1) non-linear fitting to the multi-echo data was used to estimate the magnetic field inhomogeneity. (2) Phase unwrapping using the magnitude image as a guide (Liu et al., 2013). (3) Removal of the background field by applying a projection onto the dipole field (Liu et al., 2011). (4) The remaining field was inverted to calculate the quantitative susceptibility map in parts per billion (PPB). (5) Local magnetic susceptibility in CSF was used to scale the QSM maps for susceptibility normalization such that positive values correspond to local magnetic susceptibility greater than CSF while negative values correspond to susceptibility less than CSF.

For the final step, ventricular reference masks were created for each participant by first registering the RMS T1 scans to the

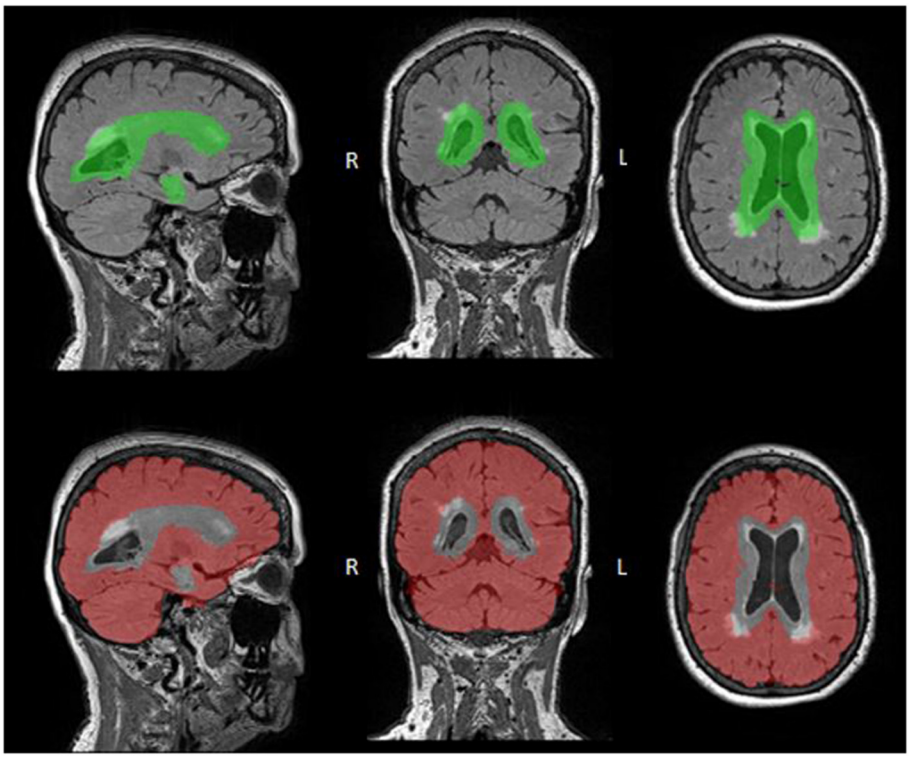

FIGURE 1 | WMH Regional ROI Masks. PV (top: green) and deep (bottom: red) ROI masks are overlaid onto FLAIR images. These ROIs were defined by registering the ALVIN mask to each participant's native FLAIR space, with the area within the ALVIN mask defined as the PV ROI and the area outside defined as the deep ROI. Although both ROIs include all tissues, not just WMHs, these ROIs were multiplied by the participants WMH mask resulting in only WMH volume in each region.

QSM magnitude image. The aligned RMS T1 scan was then used with ALVIN (Kempton et al., 2011) and SPM12 to create lateral ventricle masks for each participant, which were eroded by one voxel to prevent partial volume effects with surrounding gray and white matter. These masks were resampled to the QSM voxel resolution (1.2 mm isotropic) and used in the MEDI toolbox as the CSF reference mask (step 5).

Gray Matter QSM Measurement

Average GM QSM measures were calculated using FreeSurfer-derived ROIs from the cortex and dorsal striatum (caudate and putamen) as described in detail in our previous work (Zachariou et al., 2020). Briefly, these regions were selected based on previous literature indicating that iron in these areas increase with age (Aquino et al., 2009; Acosta-Cabronero et al., 2016). First, each participant's RMS T1 image was skull-stripped and segmented using FreeSurfer 6.0. Next, per participant cortical ROIs were created by combining the relevant GM segmented neocortical and allocortical (i.e., hippocampus) structures. Similarly, per participant subcortical ROIs were created from the FreeSurfer segmentations of the caudate and putamen.

The cortical and subcortical ROIs for each participant were then registered to their QSM images in native space using the following steps. First, each participant's RMS T1 was registered to the QSM magnitude image using the AFNI align_epi_anat.py function and a local Pearson correlation cost function. The resulting transformation matrices were then applied to each participants' cortical and subcortical ROIs using the AFNI function 3dAllineate with a nearest neighbor interpolation method. Finally, these ROIs were eroded by one voxel to prevent partial volume effects and were resampled to the QSM voxel resolution (1 to 1.2 mm isotropic voxels).

Due to significantly higher iron concentrations (over 10 times higher) in subcortical compared to cortical GM regions, per participant mean QSM values were extracted separately from the cortical and subcortical ROIs using fslstats. These values were then converted into z-scores and the mean of these z-scores across the 3 ROIs was used to create a single GM QSM measure for each participant.

CBF Analyses

PCASL images were processed in FSL. First, all tagged/untagged pairs were motion corrected to the M_0 image using FSL MCFLIRT. A perfusion image was subsequently calculated by taking the mean difference between the tagged and untagged pairs using asl_file in the BASIL toolbox (https://fsl.fmrib.ox.ac.uk/fsl/fslwiki/BASIL), which also helps correct for partial volume effects. Oxford_asl, which is also part of the BASIL toolbox, was then used for per-voxel calibration (using the M_0 image) resulting in a calibrated map of tissue perfusion (ml/100 g/min).

Gray Matter CBF Measurement

Participants' FreeSurfer GM ROIs were registered to their PCASL images in native space using the following steps. Each

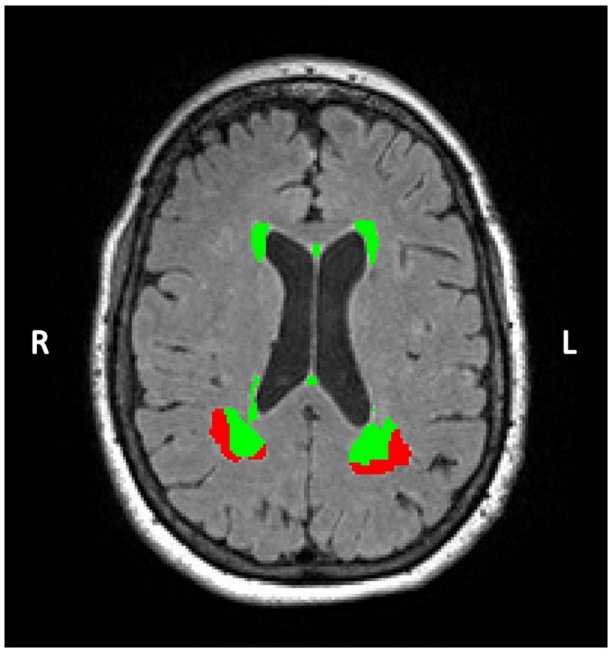

FIGURE 2 | A Sample Segmented WMH Mask. In this axial FLAIR slice, WMHs in a representative participant are color-coded according to being in either PV (green) or deep (red) regions. WMH volume was extracted from each region separately for every participant.

participant's RMS T1 was aligned to their PCASL M_0 image using AFNI and a local Pearson correlation cost function. The resulting transformation matrices were then applied to each participants' FreeSurfer GM ROIs using AFNI and a nearest neighbor interpolation method. Lastly, these ROIs were eroded by one voxel to prevent partial volume effects and were resampled to the PCASL voxel resolution (1 to 3.4 mm isotropic voxels).

Unlike with QSM, mean GM CBF signal was similar across the caudate, putamen, and cortical ROIs. Therefore, these ROIs were combined into a single ROI for our CBF measurement. Mean GM CBF signal was then extracted from the combined ROI using FSL.

DTI Analyses

DTI was analyzed with FSL's tract-based spatial statistics (TBSS) pipeline (Smith et al., 2006), as described in detail in our previous work (Brown et al., 2016, 2019). Briefly, each participant's diffusion data was corrected for susceptibility induced field distortions using FSL's topup (Andersson et al., 2003), skull-stripped using BET (Smith, 2002), and non-linearly corrected for eddy currents and participant motion simultaneously with eddy (Andersson and Sotiropoulos, 2016). Greater than 2 mm subject motion per slice was used as a guideline for examination of excessive motion, although no slices from any participants were ultimately removed (minimal motion artifacts). The diffusion tensor model and eigenvalues (λ_1, λ_2, λ_3) were computed within each voxel using DTIFIT, which were used to calculate fractional anisotropy (FA) images. After the initial preprocessing step (tbss_1_preproc), non-linear voxel-wise registration was used to transform each participant's FA image into MNI152 space, where they were averaged to create a mean FA image (tbss_2_reg and tbss_3_postreg). A common white matter tract skeleton was then created using the mean FA image. All participants FA data was then projected onto this skeleton which was thresholded at FA > 0.2 (tbss_4_prestats) to correct partial volume effects that may occur after warping across all participants. Radial diffusivity (RD) images were likewise processed with the same templates and transformations using tbss_non_FA.

DTI Masks of PV and Deep WM

The DTI ROI masks were generated from the JHU ICBM-81 WM ROI atlas (Mori et al., 2008). Several DTI ROIs were explored based on being major WM tracts with established connections between specific gray matter regions, located within either PV or deep WM regions and being well-aligned across participants in our DTI data. The PV ROI mask included the corpus callosum as it is the largest white matter structure in the brain connecting homologous structures across hemispheres (Fitsiori et al., 2011). Specific corpus callosum sub-sections were selected for being major partitions of the corpus callosum and well-aligned across participants (Splenium, Body, Tapetum). The deep ROI mask included the superior longitudinal fasciculus and external capsule which were chosen based on being major primary association fiber tracts in deep WM, and containing distant connections (connecting frontal and parietal regions and basal ganglia/claustrum with cortical regions, respectively; Mori et al., 2008). Furthermore, both tracts are believed to connect to cortical areas associated with several cognitive functions including language function, attention, and working memory/executive function (Mori et al., 2008; Wang et al., 2016; Nolze-Charron et al., 2020).

Mean FA and RD were extracted from each ROI tract, for each participant, using fslmeants. Mean values were computed across entire ROI WM tracts in order to provide anatomically meaningful diffusion estimates (i.e., estimates of tracts connecting specific gray matter regions). As a separate estimate, mean values were also computed across WM tracts after excluding values that overlapped with WMH voxels, resulting in ROIs restricted to only normal appearing white matter (NAWM). However, since the results were the same using each of these ROI methods, we present results using FA and RD values extracted from entire WM tracts to provide anatomically meaningful results. Extracted values from the entire ROIs were then used to create overall PV and deep FA and RD composite scores. These unweighted composite scores were created for each participant using the mean of the regional z-scored ROI tract values. This resulted in four composite scores for each participant: a PV FA composite score, a PV RD composite score, a deep FA composite score, and a deep RD composite score.

Statistical Analyses

Statistical analyses were performed using SPSS (IBM, Chicago, IL, USA, version 26), with results considered statistically significant at $p < 0.05$. Data was considered a statistical outlier and removed if it was >3 standard deviations from the mean. All images for all participants were visually inspected for quality

control. All predictors and dependent variables were tested for the assumption of normality using the Shapiro-Wilk test. Collinearity between predictors in all models was explored using the variance inflation factor (VIF), with a value of 5 implemented as a threshold value (Stine, 1995). CBF was z-scored across participants in the analyses to match the scale of the QSM and FA/DR composite scores. The coefficient of variation was calculated for unstandardized FA/DR, QSM, and CBF values in every ROI. This was done by dividing the standard deviation across participants by the mean signal across participants in every ROI. We also report the mean coefficient of variation across ROIs for FA/DR, QSM and CBF values. Finally, estimated total intracranial volume (eTIV) provided by FreeSurfer was z-scored across participants. This intracranial volume (ICV) measure was used as a covariate in subsequent analyses.

We first explored whether FA or DR better predicted PV and deep WMH volume (Section FA and RD as Predictors of WMH Volume). Separate linear regression models were run with FA and DR composite scores as the predictors and PV or deep WMH volume as the dependent variables. Age, sex, and ICV were included as covariates. The specific DTI metric, FA or RD, which had the larger effect size when predicting PV and deep WMH volume (partial r) was used in subsequent analyses.

Main effects of predictors on total WMH volume and predictor × WMH location interactions were initially explored using a general linear model repeated measures ANCOVA (Sections Imaging Modality Main Effects on WMH Volume and WMH Location Interactions and CBF Association With WMH Volume in Partial Models). CBF, QSM, and FA/DR, along with all possible interaction terms (CBF × QSM, QSM × FA/DR, and CBF × FA/DR) were the predictors of interest, with WMH volume as a 2-level dependent variable with PV and deep volume (not z-scored) as the levels. Age, sex, and ICV were included as covariates. For this analysis, white matter tracts from both PV and deep DTI ROIs were combined into a single FA/DR composite to reduce collinearity arising from including two DTI composites. We report the main effects of all predictors to examine effects on WMH volume more generally, and predictor interactions with WMH location to assess if any factors preferentially predict PV or deep WMH volume. Significant predictor by location interactions were followed-up with *post-hoc* analysis to identify relationships with WMH volume in each specific location (Section RD, CBF, and QSM Associations With Regional WMH Volumes). We were also interested in whether the accuracy of any of our predictors (CBF, QSM, or FA/DR) improves with increasing participant age. To test this possibility, we included age × predictor interaction terms in linear regression models predicting PV and deep WMH volume (Section Age Moderation Analysis).

Stepwise linear regression was used to further explore how much explained variance (R^2) each predictor added regarding WMH volume (Section Additive Effects of WMH Predictors Using R^2 Change). To accomplish this, we z-scored PV and deep WMH volume (the dependent variables used in the main ANCOVA model) across participants and then used the mean of the z-scores as our dependent variable (composite WMH volume). This was done to give equal weighting to WMH in both locations; using the more traditional total WMH volume would be largely driven by PV WMH volume which in general has much greater volume. The first step of the regression included only the covariates (age, sex, ICV). At each step, we added in the most significant predictor of WMH volume remaining as revealed by the initial ANCOVA. Interactions were excluded as they were not significant in the preceding analyses.

A retrospective power analysis was conducted to determine if our null between factor interaction findings were the result of insufficient power (Section Power Analysis). *Post-hoc* F-tests parameters were selected using G*power (version 3.1.9.2) with effect size, total sample size, number of tested predictors and total number of predictors specified. Cohen's f^2 was used as a guideline for interpreting effect size.

RESULTS

Participant and Data Characteristics

Participants summary demographic information is presented in **Table 1**. There were no outliers in any of the predictors (FA/DR composites, QSM composite, and CBF measurement) and one outlier in WMH data, which was excluded. Data from two other participants, one with a failed WMH segmentation and another with excessive motion in the QSM scan rendering it unusable, were also excluded. All the WMH distributions were skewed as is typical (PV; W statistic = 0.597; $p < 0.001$; Deep; W statistic = 0.318; $p < 0.001$) and were log transformed. The QSM composite and CBF measurement were normally distributed ($p = 0.725$; $p = 0.669$), while the FA/DR composites were mildly skewed but were not log transformed (W statistic = 0.924; $p < 0.001$), as this is not typically done in the DTI literature. Error residuals from all analyses were normally distributed indicating that the assumption of normality was met. Variance inflation factor for all predictors was <2 and tolerance was >0.5 in all analyses. The mean coefficient of variation was 0.0601 for FA (Superior Longitudinal Fasciculus ROI = 0.0585, External Capsule ROI = 0.0463, Body of Corpus Callosum ROI = 0.0556, Splenium of Corpus Callosum ROI = 0.0332, Tapetum of Corpus Callosum ROI = 0.107), and 0.0925 for DR (superior longitudinal fasciculus ROI = 0.0645, external capsule ROI = 0.0568, Body of Corpus Callosum ROI = 0.0955, Splenium of Corpus Callosum ROI = 0.0707, Tapetum of Corpus Callosum ROI = 0.175). The mean coefficient of variation was 0.362 for QSM (Caudate ROI = 0.395, Putamen ROI = 0.466, Cortical ROI = 0.225). The coefficient of variation was 0.174 for CBF (Gray Matter ROI = 0.174).

FA and RD as Predictors of WMH Volume

Participant's DTI PV and deep composite scores (for FA and RD) were computed by z-scoring individual participant's mean values in each tract in the mask and then calculating the mean of those z-scores across tracts (Section DTI Masks of PV and Deep WM). RD had a larger effect size than FA in a model predicting PV WMH volume (RD partial $r = 0.415$, $p < 0.001$; FA partial $r = -0.379$, $p = 0.001$) and deep WMH volume (RD partial $r = 0.323$, $p = 0.005$; FA partial $r = -0.141$, $p = 0.233$). Therefore,

TABLE 2 | Summary of main effects and interactions of predictors on WMH volume and location.

WMH Volume	Main Effects		Location Interaction	
Predictors	**F-value**	***p*-value**	**F-value**	***p*-value**
Age	0.658	0.420	0.302	0.584
Sex	1.161	0.285	2.250	0.138
ICV	3.032	0.086	0.103	0.750
CBF	3.530	0.065	0.029	0.866
QSM	5.107	0.027*	6.208	0.015*
RD	13.516	<0.001*	0.053	0.819
CBF × QSM	0.573	0.452	0.689	0.410
QSM ×RD	0.026	0.874	0.241	0.625
CBF × RD	0.018	0.894	0.127	0.723

The F- and p-values for the main effects of predictors on total WMH volume are on the left, with the interaction effects of WMH location on the right. QSM and RD had robust main effects, while CBF had a marginally significant main effect on total WMH volume. Only QSM interacted with WMH location.
**p < 0.05.*

RD was used as the DTI measure in PV and deep DTI ROIs in subsequent models.

Imaging Modality Main Effects on WMH Volume and WMH Location Interactions

The ANCOVA indicated a main effect of DTI-based RD ($F = 13.516$, partial Eta $= 0.412$, $p < 0.001$) and QSM-based iron concentration ($F = 5.107$, partial Eta $= 0.268$, $p = 0.027$) on total WMH volume (**Table 2**). The main effect of CBF on total WMH volume was marginally significant ($F = 3.530$, partial Eta $= -0.226$, $p = 0.065$). There was a QSM × WMH location interaction [explored in *post-hoc* analysis below (Section RD, CBF, and QSM Associations with Regional WMH Volumes), $F = 6.208$, partial Eta $= 0.293$, $p = 0.015$] such that QSM positively predicted deep but not PV WMH volume, but no CBF × WMH location ($F = 0.029$, $p = 0.866$) or RD × WMH location interactions ($F = 0.053$, $p = 0.819$). There were no significant interactions between predictors.

CBF Association With WMH Volume in Partial Models

Our ANCOVA with all 3 contributing factors revealed that CBF was only marginally significant in predicting total WMH volume. However, several previous studies report associations between CBF and total WMH volume. Therefore, we further explored if CBF was significantly associated with total WMH volume in partial models of the ANCOVA with standard covariates age, sex, and ICV included. The purpose of this analysis was to determine which predictor may account for some of the variance in the CBF-WMH relationship.

With CBF as the only predictor of interest, CBF negatively predicted total WMH volume ($F = 4.339$, $p = 0.041$). CBF still predicted total WMH volume when QSM (and CBF × QSM interaction) was entered into the model but RD was omitted ($F = 4.745$, $p = 0.033$), yet was only marginally significant when RD was entered into the model but QSM was omitted ($F = 3.777$, $p = 0.056$).

TABLE 3 | Total explained variance (Adjusted R^2) and explained variance attributed to the newest added predictor (Adjusted R^2 change) at each step of the linear regression predicting composite WMH volume.

Regression Step and Predictors	Adjusted R^2	Adjusted R^2 Change	*p*-value
Step 1	0.200	0.200	**<0.001***
Age	–	–	0.001*
Sex	–	–	0.417
ICV	–	–	0.025*
Step 2	0.336	0.136	**<0.001***
RD	–	–	<0.001*
Step 3	0.379	0.043	**<0.001***
QSM	–	–	0.018*
Step 4	0.406	0.027	**<0.001***
CBF	–	–	0.046*

Covariates alone predicted 20% of the variance. Including RD at step 2 increased the adjusted R^2 of the model to 0.336. After inclusion of QSM in step 3 and CBF in step 4, the total variance explained in total WMH volume exceeded 40%. The p-values in bold reflect the p-value of the model at the indicated step, whereas other p-values represent the indicated variable when they were first entered into the model.
**p < 0.05.*

TABLE 4 | Summary of main effects and interactions of predictors on WMH volume in periventricular and deep regions.

WMH Location	Periventricular			Deep		
Predictors	**Beta**	***F*-value**	***p*-value**	**Beta**	***F*-value**	***p*-value**
Age	0.016	3.453	0.065	0.008	0.341	0.529
Sex	−0.278	6.657	0.009*	−0.008	0.002	0.966
ICV	0.126	5.867	0.010*	0.118	1.848	0.170
CBF	−0.132	8.387	0.011*	−0.074	0.902	0.344
QSM	0.052	0.883	0.414	0.236	6.841	0.034*
RD	0.214	16.486	<0.001*	0.217	6.908	0.023*
CBF × QSM	−0.047	0.814	0.482	−0.054	0.312	0.562
QSM × RD	−0.028	0.125	0.755	0.062	0.339	0.593
CBF × RD	0.013	0.105	0.744	0.012	0.024	0.880

Displayed are unstandardized beta, F-and p-values for the main effects of all predictors, and interaction effects in both PV (left) and deep (right) WMH models. QSM was positively associated with deep but not PV WMH volume, while RD strongly predicted both. CBF negatively predicted PV WMH volume. There were no interactions between predictors in either model.
**p < 0.05.*

Additive Effects of WMH Predictors Using R^2 Change

In step 1, covariates alone accounted for 20% of the variance in composite WMH volume (Adjusted $R^2 = 0.200$; **Table 3**). Including RD in the model increased the variance explained to 33.6% (Adjusted R^2 change $= 0.136$). Further additions of QSM and CBF increased the variance explained to 37.9% at step 3 (Adjusted R^2 change $= 0.043$) and 40.6% (Adjusted R^2 change $= 0.027$) at step 4, respectively.

RD, CBF, and QSM Associations With Regional WMH Volumes

Separate linear regressions were next used as a *post-hoc* analysis for the initial ANCOVA to further explore the QSM × WMH volume location interaction, using CBF and RD as covariates. QSM positively predicted deep (bootstrapped Beta = 0.236, partial $r = 0.307$, $F = 6.841$; $p = 0.034$, SE = 0.109, 95% BCa CI = 0.032 to 0.388), but not PV WMH volume (bootstrapped Beta = 0.052, partial $r = 0.114$, $F = 0.883$; $p = 0.414$, SE = 0.063, 95% BCa CI = −0.055 to 0.121; **Table 4**).

Age Moderation Analysis

Linear regression models were used to explore the possibility of age × CBF, age × QSM, and age × DR interactions. Results indicated that the interaction terms were not statistically significant when predicting PV or deep WMH volume [age × CBF for PV ($p = 0.986$) and for deep ($p = 0.628$); age × QSM for PV ($p = 0.140$) and for deep ($p = 0.328$); and age × DR for PV ($p = 0.270$) and for deep ($p = 0.778$); **Supplementary Table 1**].

Power Analysis

If we assume that an interaction effect was present, this study had over 99% power to detect an interaction with a large effect ($f^2 = 0.35$), 92% power to detect an interaction with a medium effect ($f^2 = 0.15$), and 23% power to detect an interaction with a small effect ($f^2 = 0.15$). The actual f^2 for our most relevant interaction term (QSM × RD) was very small (0.005). This may suggest that the interactions in our models are not truly present; alternatively, the effect may be so small that it would require >1,500 participants to achieve 80% power.

DISCUSSION

We explored the main effects and interactions of DTI-based radial diffusivity (RD), QSM-based brain iron concentration and ASL-based cerebral blood flow (CBF) on WMH volume and location. Results indicated that RD was the strongest predictor of total WMH volume and was associated with WMH regardless of location. In contrast, iron concentration was more strongly associated with deep than periventricular (PV) WMH volume. Finally, CBF did not account for any unique variance in WMH volume or location after controlling for other predictors. Our findings demonstrate the importance of considering multiple predictors of WMHs simultaneously to identify the strongest individual predictors, after controlling for shared variance between predictors.

Additive Effects of Individual Predictors of WMH Volume

The covariates and predictors (WM microstructure, brain iron and CBF) explored in this study accounted for almost half of the total variance in composite WMH volume (**Table 3**). WM microstructure (assessed with RD) contributed the largest percentage of unique variance accounted for in composite WMH volume after accounting for covariates and other predictors, suggesting that WM microstructure is the most robust predictor of the three. While QSM and CBF were also significant predictors, each explained only modest percentages of WMH variance after accounting for covariates and other predictors indicating that a portion of their variance may be better explained by WM microstructure.

RD Predicts Both PV and Deep WMH Volume

DTI-based RD was strongly associated with WMH volume in both PV and deep locations. Our findings are in-keeping with results from previous cross-sectional studies suggesting that RD (Pelletier et al., 2016) and other DTI-based metrics (Maillard et al., 2011; Maniega et al., 2015; Promjunyakul et al., 2016) appear to predict global WMH volume in both PV and deep WM. However, we know of only one previous study using RD as a WMH predictor that controlled for other neuroimaging predictors (Promjunyakul et al., 2018). In that study, RD values predicted new PV and deep WMH growth ∼1.5 years later (Promjunyakul et al., 2018), and was a stronger WMH predictor than CBF.

The present results add to the literature, indicating that RD is associated with WMH volume in both PV and deep regions after controlling for CBF and brain iron concentration. Higher RD is associated with relatively lower myelination, axonal packing and axonal density (Madden et al., 2009). Thus, lower myelination and axonal packing/density appear to be associated with higher WMH volume, both independently of other neuroimaging metrics and across WM location.

Iron Concentration Is More Closely Associated With Deep Than PV WMH Volume

Non-heme brain iron concentration was quantified using QSM, which has been validated against postmortem tissue iron concentrations in both subcortical structures (Langkammer et al., 2012; Sun et al., 2015) and cortical structures (Fukunaga et al., 2010; Bulk et al., 2018). Our QSM ROI included both cortical and subcortical structures. We observed a significant main effect of cerebral iron concentration on total WMH volume after controlling for WM microstructural properties and cerebral blood flow. While non-heme iron is crucial for many cellular processes, it is also is a potent oxidizer that can generate reactive oxygen species (ROS), damaging neurons (Moos et al., 2007; Ward et al., 2014). Increased unbound iron is thought to contribute to demyelination resulting from free radical damage affecting oligodendrocytes and myelin sheaths (Todorich et al., 2009; Bartzokis, 2011). However, given that we controlled for myelin damage in our models (DTI-based RD was used as a covariate), the main effect of QSM on WMH we observed could reflect additional damage to neuronal cell bodies and/or axons (e.g., Wallerian degeneration).

One reason why iron was less predictive of total WMH volume than RD relates to the interaction we observed between brain iron and location on WMH volume. Specifically, brain iron concentration was more predictive of deep WMH volume than PV WMH volume. Several previous studies have had mixed findings, with some indicating that iron is associated with total

WMH volume (Yan et al., 2013; Valdés Hernández et al., 2016; Sun et al., 2017), although others have not (Gattringer et al., 2016). However, none of these studies accounted for CBF or FA/RD in their models or explored potential iron by WMH location interactions.

The interaction we observed between iron and location on WMH volume likely relates to deep WM ROIs containing more tracts with connections to iron-rich basal ganglia and other subcortical structures in our study. In particular, the deep ROI included the external capsule, a series of WM tracts situated between the putamen and claustrum. The external capsule includes extensive connections between the claustrum and subcortical structures such as the basal ganglia and thalamus (Smythies et al., 2013). In contrast, the PV WM ROI was primarily composed of the body and splenium of the corpus callosum, which connect homologous neocortical structures.

It is well-established that age-related cerebral iron accumulation is seen predominantly in subcortical structures of the basal ganglia (Zecca et al., 2004; Ward et al., 2014). Thus, it is possible that high concentrations of iron in basal ganglia structures may have contributed to Wallerian degeneration of deep tracts such as the external capsule. However, it should be noted that our analyses focused on major WM tracts. There are a number of smaller WM tracts in the PV region with connections to basal ganglia structures such as the lenticular fasciculus and nigrostriatal tracts which were not included in our study due to less optimal spatial alignment across participants.

CBF Does Not Predict WMH Volume After Controlling for Other Factors

Our results showed that CBF was negatively associated with total WMH volume when it was the only predictor of interest. This is consistent with results from a number of studies reporting a negative relationship between CBF and WMH volume (ten Dam et al., 2007; Brickman et al., 2009; Bahrani et al., 2017). However, our results indicated that CBF was only a marginally significant predictor of total WMH volume after controlling for other predictors ($p = 0.065$). In particular, we found that RD accounted for some of the variance in the CBF-WMH volume relationship (Section CBF Association With WMH Volume in Partial Models), and better predicted WMH volume than CBF in general (**Table 2**, section Additive Effects of WMH Predictors Using R^2 Change). One possible explanation for this is that CBF only predicts total WMH volume when reduced blood flow is pronounced enough to cause microstructural damage to myelin and WM tracts.

Age Did Not Moderate Relationships Between Predictors (CBF, QSM, DR) and WMH Volume

It is possible that CBF, QSM, or DR could better predict WMH volume at older age levels, as all these measures are known to correlate with age (Acosta-Cabronero et al., 2016; Beck et al., 2021; Juttukonda et al., 2021). We investigated this possibility by exploring whether age moderated the strength of relationship between any of our predictors and WMH volume. However, we did not find any evidence of age moderation in this study (**Supplementary Table 1**). As our study included mostly healthy older adults, future studies could examine the possibility that age may moderate the relationship between cSVD predictors and WMH volume at more advanced neurodegenerative states, such as those associated with mild cognitive impairment or dementia.

Study Strengths and Limitations

Strengths of our study include the consideration of multiple predictors (WM microstructure, brain iron concentration and CBF) of WMH volume, employing rigorous MRI analyses, a moderately large sample size and wide age range of older adults. Further, the integration of multiple WMH predictors in the same model controls for shared covariance between predictors, allowing identification of the best predictors through their unique variance on WMH volume. An additional strength of our study was consideration of interactions between predictors and spatial location (i.e., PV and deep WMHs).

This study also has limitations that highlight the need for additional follow-up studies. First, our cross-sectional study cannot determine how predictors would be associated with WMH growth. Future research with multiple time points is needed to identify baseline predictors of longitudinal WMH change. Second, as is true in most studies, ASL in our study had poorer spatial resolution than either DTI or QSM. The mean CBF signal used in our study consisted of a number of individual gray matter ROIs, including subcortical structures such as the caudate and putamen. Subcortical structures are surrounded by white matter where ASL signal is reduced compared to gray matter, and relatively large ASL voxels may have contributed to greater partial volume effects and averaging of lower CBF signal. For example, the putamen is bordered laterally by the external capsule, a long, thin WM tract. FreeSurfer segmentation, which we used, tends to overestimate the boundaries of the putamen by including the external capsule (Dewey et al., 2010; Perlaki et al., 2017). Although CBF did not predict total WMH volume when other predictors were controlled in our study, it is possible that CBF could contribute unique variance in total WMH volume using more advanced ASL techniques that are currently in development. Third, future studies should explore more than one clinical subset of participants. Our study focused on cognitively normal older adults and it is possible that our results may not generalize to individuals with more advanced WMH burden and cognitive impairment (Mild Cognitive Impairment and Alzheimer's Disease). Longitudinal follow-up is needed to identify if synergistic interactions begin to emerge at the onset of dementia.

This study employed a large-scale ROI approach to assess effects of more global CBF/QSM/DR predictors on overall measures of WMH volume (including total, PV and deep regions). In previous work in this area, both large-scale ROI approaches (ten Dam et al., 2007; Brickman et al., 2009; Leritz et al., 2014; Pelletier et al., 2016; Wiseman et al., 2018) and voxelwise or small ROI approaches (Maillard et al., 2011, 2014; Promjunyakul et al., 2016, 2018) have been employed. Each of these approaches have strengths and limitations. For example, local/small ROI approaches have the

potential to reveal fine-grained anatomical relationships but may have limitations associated with imperfect registration between imaging modalities. In contrast, large-scale ROI approaches such as the one used here may "blur" some fine-grained anatomical associations, but have the advantage of identifying network-level associations. Finally, as with several previous studies (ten Dam et al., 2007; Griffanti et al., 2018), this study focused on deep vs. PV WMH regions. Future work should explore the possibility that WMH predictors may have differential effects in additional ROIs, such as in lobar ROIs.

CONCLUSION

WM microstructure is strongly associated with both total and regional WMH volumes, even after controlling for other predictors. Brain iron concentration is also a significant predictor but adds only modest unique variance due to being selectively associated with deep but not PV WMH volume. Future studies should attempt to further clarify which predictors contribute additional, unique variance in WMH volume after controlling for WM microstructure and brain iron concentration.

DATA AVAILABILITY STATEMENT

The raw data supporting the conclusions of this article will be made available by the authors, without undue reservation.

ETHICS STATEMENT

The studies involving human participants were reviewed and approved by Institutional Review Board of the University of Kentucky. The patients/participants provided their written informed consent to participate in this study.

AUTHOR CONTRIBUTIONS

CB: conceptualization, data collection, data curation, methodology, formal analysis, writing (original draft), and writing (review and editing). VZ: data collection, data curation, methodology, formal analysis, visualization, and writing (review and editing). ES: data collection, data curation, methodology, and investigation. BG: conceptualization, data curation, methodology, formal analysis, writing (review and editing), supervision, project administration, and funding acquisition. All authors contributed to the article and approved the submitted version.

FUNDING

This work was supported by the National Institutes of Health (grant numbers NIA R01 AG055449, NIA P30 AG028383, and NIGMS S10 OD023573).

ACKNOWLEDGMENTS

The authors thank Beverly Meacham and Eric Forman for assistance with MRI scanning. We also thank Dr. David Powell for assistance in sequence preparation and troubleshooting of technical issues.

SUPPLEMENTARY MATERIAL

The Supplementary Material for this article can be found online at: https://www.frontiersin.org/articles/10.3389/fnagi.2021.617947/full#supplementary-material

REFERENCES

Acosta-Cabronero, J., Betts, M. J., Cardenas-Blanco, A., Yang, S., and Nestor, P. J. (2016). *In vivo* MRI mapping of brain iron deposition across the adult lifespan. *J. Neurosci.* 36, 364–374. doi: 10.1523/JNEUROSCI.1907-15.2016

Andersson, J. L. R., Skare, S., and Ashburner, J. (2003). How to correct susceptibility distortions in spin-echo echo-planar images: application to diffusion tensor imaging. *Neuroimage* 20, 870–888. doi: 10.1016/S1053-8119(03)00336-7

Andersson, J. L. R., and Sotiropoulos, S. N. (2016). An integrated approach to correction for off-resonance effects and subject movement in diffusion MR imaging. *Neuroimage* 125, 1063–1078. doi: 10.1016/j.neuroimage.2015.10.019

Aquino, D., Bizzi, A., Grisoli, M., Garavaglia, B., Bruzzone, M. G., Nardocci, N., et al. (2009). Age-related iron deposition in the basal ganglia: quantitative analysis in healthy subjects. *Neuroradiology* 252, 165–172. doi: 10.1148/radiol.2522081399

Bahrani, A. A., Powell, D. K., Yu, G., Johnson, E. S., Jicha, G. A., and Smith, C. D. (2017). White matter hyperintensity associations with cerebral blood flow in elderly subjects stratified by cerebrovascular risk. *J. Stroke Cerebrovasc. Dis.* 26, 779–786. doi: 10.1016/j.jstrokecerebrovasdis.2016.10.017

Bartzokis, G. (2011). Alzheimer's disease as homeostatic responses to age-related myelin breakdown. *Neurobiol. Aging* 32, 1341–1371. doi: 10.1016/j.neurobiolaging.2009.08.007

Beck, D., de Lange, A. M., Maximov, I. I., Richard, G., Andreassen, O. A., Nordvik, J. E., et al. (2021). White matter microstructure across the adult lifespan: a mixed longitudinal and cross-sectional study using advanced diffusion models and brain-age prediction. *Neuroimage* 224, 117441. doi: 10.1016/j.neuroimage.2020.117441

Besser, L., Kukull, W., Knopman, D. S., Chui, H., Galasko, D., Weintraub, S., et al. (2018). Version 3 of the National Alzheimer's Coordinating Center's uniform data set. *Alzheimer Dis. Assoc. Disord.* 32, 351–358. doi: 10.1097/WAD.0000000000000279

Boulouis, G., Charidimou, A., Pasi, M., Roongpiboonsopit, D., Xiong, L., Auriel, E., et al. (2017). Hemorrhage recurrence risk factors in cerebral amyloid angiopathy: comparative analysis of the overall small vessel disease severity score versus individual neuroimaging markers. *J. Neurol. Sci.* 380, 64–67. doi: 10.1016/j.jns.2017.07.015

Brickman, A. M., Zahra, A., Muraskin, J., Steffener, J., Holland, C. M., Habeck, C., et al. (2009). Reduction in cerebral blood flow in areas appearing as white matter hyperintensities on magnetic resonance imaging. *Psychiatry Res. Neuroimaging* 172, 117–120. doi: 10.1016/j.pscychresns.2008.11.006

Brown, C. A., Johnson, N. F., Anderson-Mooney, A. J., Jicha, G. A., Shaw, L. M., Trojanowski, J. Q., et al. (2016). Development, validation and application of a new fornix template for studies of aging and preclinical Alzheimer's disease. *Neuroimage Clin.* 13, 106–115. doi: 10.1016/j.nicl.2016.11.024

Brown, C. A., Schmitt, F. A., Smith, C. D., and Gold, B. T. (2019). Distinct patterns of default mode and executive control network circuitry contribute to present and future executive function in older adults. *Neuroimage* 195, 320–332. doi: 10.1016/j.neuroimage.2019.03.073

Bulk, M., Abdelmoula, W. M., Nabuurs, R. J. A., van der Graaf, L. M., Mulders, C. W. H., Mulder, A. A., et al. (2018). Postmortem MRI and histology demonstrate differential iron accumulation and cortical myelin organization in early- and late-onset Alzheimer's disease. *Neurobiol. Aging* 62, 231–242. doi: 10.1016/j.neurobiolaging.2017.10.017

Charidimou, A., Martinez-Ramirez, S., Reijmer, Y. D., Oliveira-Filho, J., Lauer, A., Roongpiboonsopit, D., et al. (2016). Total MRI small vessel disease burden in cerebral amyloid angiopathy: a concept validation imaging-pathological study. *JAMA Neurol.* 73, 994–1001. doi: 10.1001/jamaneurol.2016.0832

de Leeuw, F. E., De Groot, J. C., Achten, E., Oudkerk, M., Ramos, L. M. P., Heijboer, R., et al. (2001). Prevalence of cerebral white matter lesions in elderly people: a population based magnetic resonance imaging study: the Rotterdam Scan Study. *J. Neurol. Neurosurg. Psychiatry* 70, 9–14. doi: 10.1136/jnnp.70.1.9

Debette, S., and Markus, H. S. (2010). The clinical importance of white matter hyperintensities on brain magnetic resonance imaging: systematic review and meta-analysis. *BMJ* 341:c3666. doi: 10.1136/bmj.c3666

DeCarli, C., Maillard, P., and Fletcher, E. (2013). *Four Tissue Segmentation in ADNI II. Alzheimer's Disease Neuroimaging Initiative*. Available online at: https://files.alz.washington.edu/documentation/adni_proto.pdf (accessed July 26, 2019).

DeCarli, C., Murphy, D. G. M., Teichberg, D., Campbell, G., and Sobering, G. S. (1996). Local histogram correction of MRI spatially dependent image pixel intensity nonuniformity. *J. Magn. Reson. Imaging* 6, 519–528. doi: 10.1002/jmri.1880060316

Dewey, J., Hana, G., Russell, T., Price, J., McCaffrey, D., Harezlak, J., et al. (2010). Reliability and validity of MRI-based automated volumetry software relative to auto-assisted manual measurement of subcortical structures in HIV-infected patients from a multisite study. *Neuroimage* 51, 1334–1344. doi: 10.1016/j.neuroimage.2010.03.033

Fazekas, F., Kleinert, R., Offenbacher, H., Schmidt, R., Kleinert, G., Payer, F., et al. (1993). Pathologic correlates of incidental MRI white matter signal hyperintensities. *Neurology* 43, 1683–1683. doi: 10.1212/WNL.43.9.1683

Fischl, B., van der Kouwe, A., Destrieux, C., Halgren, E., Ségonne, F., Salat, D. H., et al. (2004). Automatically parcellating the human cerebral cortex. *Cereb. Cortex* 14, 11–22. doi: 10.1093/cercor/bhg087

Fitsiori, A., Nguyen, D., Karentzos, A., Delavelle, J., and Vargas, M. I. (2011). The corpus callosum: white matter or terra incognita. *Br. J. Radiol.* 84, 5–18. doi: 10.1259/bjr/21946513

Fukunaga, M., Li, T. Q., Van Gelderen, P., De Zwart, J. A., Shmueli, K., Yao, B., et al. (2010). Layer-specific variation of iron content in cerebral cortex as a source of MRI contrast. *Proc. Natl. Acad. Sci. U.S.A.* 107, 3834–3839. doi: 10.1073/pnas.0911177107

Gattringer, T., Khalil, M., Langkammer, C., Jehna, M., Pichler, A., Pinter, D., et al. (2016). No evidence for increased brain iron deposition in patients with ischemic white matter disease. *Neurobiol. Aging* 45, 61–63. doi: 10.1016/j.neurobiolaging.2016.05.008

Gouw, A. A., Seewann, A., van der Flier, W. M., Barkhof, F., Rozemuller, A. M., Scheltens, P., et al. (2011). Heterogeneity of small vessel disease: a systematic review of MRI and histopathology correlations. *J. Neurol. Neurosurg. Psychiatry* 82, 126–135. doi: 10.1136/jnnp.2009.204685

Grabner, G., Janke, A. L., Budge, M. M., Smith, D., Pruessner, J., and Collins, D. L. (2006). "Symmetric atlasing and model based segmentation: an application to the hippocampus in older adults," in *International Conference on Medical Image Computing and Computer-Assisted Intervention* (Copenhagen), 58–66.

Griffanti, L., Jenkinson, M., Suri, S., Zsoldos, E., Mahmood, A., Filippini, N., et al. (2018). Classification and characterization of periventricular and deep white matter hyperintensities on MRI: a study in older adults. *Neuroimage* 170, 174–181. doi: 10.1016/j.neuroimage.2017.03.024

Hachinski, V. C., Potter, P., and Merskey, H. (1987). Leuko-Araiosis. *Arch. Neurol.* 44, 21–23. doi: 10.1001/archneur.1987.00520130013009

Jenkinson, M., Beckmann, C. F., Behrens, T. E. J., Woolrich, M. W., and Smith, S. M. (2012). FSL. *Neuroimage* 62, 782–790. doi: 10.1016/j.neuroimage.2011.09.015

Juttukonda, M. R., Li, B., Almaktoum, R., Stephens, K. A., Yochim, K. M., Yacoub, E., et al. (2021). Characterizing cerebral hemodynamics across the adult lifespan with arterial spin labeling MRI data from the Human Connectome Project-Aging. *Neuroimage* 230:117807. doi: 10.1016/j.neuroimage.2021.117807

Kempton, M. J., Underwood, T. S. A., Brunton, S., Stylios, F., Schmechtig, A., Ettinger, U., et al. (2011). A comprehensive testing protocol for MRI neuroanatomical segmentation techniques: evaluation of a novel lateral ventricle segmentation method. *Neuroimage* 58, 1051–1059. doi: 10.1016/j.neuroimage.2011.06.080

Langkammer, C., Schweser, F., Krebs, N., Deistung, A., Goessler, W., Scheurer, E., et al. (2012). Quantitative susceptibility mapping (QSM) as a means to measure brain iron? A post mortem validation study. *Neuroimage* 62, 1593–1599. doi: 10.1016/j.neuroimage.2012.05.049

Leritz, E. C., Shepel, J., Williams, V. J., Lipsitz, L. A., Mcglinchey, R. E., Milberg, W. P., et al. (2014). Associations between T1 white matter lesion volume and regional white matter microstructure in aging. *Hum. Brain Mapp.* 35, 1085–1100. doi: 10.1002/hbm.22236

Liu, J., Liu, T., de Rochefort, L., Ledoux, J., Khalidov, I., Chen, W., et al. (2012). Morphology enabled dipole inversion for quantitative susceptibility mapping using structural consistency between the magnitude image and the susceptibility map. *Neuroimage* 59, 2560–2568. doi: 10.1016/j.neuroimage.2011.08.082

Liu, T., Khalidov, I., de Rochefort, L., Spincemaille, P., Liu, J., Tsiouris, A. J., et al. (2011). A novel background field removal method for MRI using projection onto dipole fields (PDF). *NMR Biomed.* 24, 1129–1136. doi: 10.1002/nbm.1670

Liu, T., Wisnieff, C., Lou, M., Chen, W., Spincemaille, P., and Wang, Y. (2013). Nonlinear formulation of the magnetic field to source relationship for robust quantitative susceptibility mapping. *Magn. Reson. Med.* 69, 467–476. doi: 10.1002/mrm.24272

Madden, D. J., Bennett, I. J., and Song, A. W. (2009). Cerebral white matter integrity and cognitive aging: contributions from diffusion tensor imaging. *Neuropsychol. Rev.* 19, 415–435. doi: 10.1007/s11065-009-9113-2

Maillard, P., Fletcher, E., Harvey, D., Carmichael, O., Reed, B., Mungas, D., et al. (2011). White matter hyperintensity penumbra. *Stroke* 42, 1917–1922. doi: 10.1161/STROKEAHA.110.609768

Maillard, P., Fletcher, E., Lockhart, S. N., Roach, A. E., Reed, B., Mungas, D., et al. (2014). White matter hyperintensities and their penumbra lie along a continuum of injury in the aging brain. *Stroke* 45, 1721–1726. doi: 10.1161/STROKEAHA.113.004084

Maniega, S. M., Valdés Hernández, M., Clayden, J. D., Royle, N. A., Murray, C., Morris, Z., et al. (2015). White matter hyperintensities and normal-appearing white matter integrity in the aging brain. *Neurobiol. Aging* 36, 909–918. doi: 10.1016/j.neurobiolaging.2014.07.048

Moos, T., Nielsen, T. R., Skjørringe, T., and Morgan, E. H. (2007). Iron trafficking inside the brain. *J. Neurochem.* 103, 1730–1740. doi: 10.1111/j.1471-4159.2007.04976.x

Mori, S., Oishi, K., Jiang, H., Jiang, L., Li, X., Akhter, K., et al. (2008). Stereotaxic white matter atlas based on diffusion tensor imaging in an ICBM template. *Neuroimage* 40, 570–582. doi: 10.1016/j.neuroimage.2007.12.035

Nasreddine, Z. S., Phillips, N. A., Bédirian, V., Charbonneau, S., Whitehead, V., Collin, I., et al. (2005). The Montreal Cognitive Assessment, MoCA: a brief screening tool for mild cognitive impairment. *J. Am. Geriatr. Soc.* 53, 695–699. doi: 10.1111/j.1532-5415.2005.53221.x

Nolze-Charron, G., Dufort-Rouleau, R., Houde, J. C., Dumont, M., Castellano, C. A., Cunnane, S., et al. (2020). Tractography of the external capsule and cognition: a diffusion MRI study of cholinergic fibers. *Exp. Gerontol.* 130, 1–7. doi: 10.1016/j.exger.2019.110792

Pantoni, L., and Garcia, J. H. (1995). The significance of cerebral white matter abnormalities 100 years after Binswanger's report. A review. *Stroke* 26, 1293–1301. doi: 10.1161/01.STR.26.7.1293

Pantoni, L., and Garcia, J. H. (1997). Pathogenesis of leukoaraiosis: a review. *Stroke* 28, 652–659. doi: 10.1161/01.STR.28.3.652

Pelletier, A., Periot, O., Dilharreguy, B., Hiba, B., Bordessoules, M., Chanraud, S., et al. (2016). Age-related modifications of diffusion tensor imaging parameters and white matter hyperintensities as inter-dependent processes. *Front. Aging Neurosci.* 7:255. doi: 10.3389/fnagi.2015.00255

Perlaki, G., Horvath, R., Nagy, S. A., Bogner, P., Doczi, T., Janszky, J., et al. (2017). Comparison of accuracy between FSL's FIRST and Freesurfer for caudate nucleus and putamen segmentation. *Sci. Rep.* 7, 1–9. doi: 10.1038/s41598-017-02584-5

Promjunyakul, N., Dodge, H. H., Lahna, D., Boespflug, E. L., Kaye, J. A., Rooney, W. D., et al. (2018). Baseline NAWM structural integrity and CBF predict periventricular WMH expansion over time. *Neurology* 90, e2107–e2118. doi: 10.1212/WNL.0000000000005684

Promjunyakul, N., Lahna, D. L., Kaye, J. A., Dodge, H. H., Erten-Lyons, D., Rooney, W. D., et al. (2016). Comparison of cerebral blood flow and structural penumbras in relation to white matter hyperintensities: a multi-modal magnetic resonance imaging study. *J. Cereb. Blood Flow Metab.* 36, 1528–1536. doi: 10.1177/0271678X16651268

Ryu, W. S., Woo, S. H., Schellingerhout, D., Chung, M. K., Kim, C. K., Jang, M. U., et al. (2014). Grading and interpretation of white matter hyperintensities using statistical maps. *Stroke* 45, 3567–3575. doi: 10.1161/STROKEAHA.114.006662

Sachdev, P. S., Wen, W., Christensen, H., and Jorm, A. F. (2005). White matter hyperintensities are related to physical disability and poor motor function. *J. Neurol. Neurosurg. Psychiatry* 76, 362–367. doi: 10.1136/jnnp.2004.042945

Smith, E. E., and Beaudin, A. E. (2018). New insights into cerebral small vessel disease and vascular cognitive impairment from MRI. *Curr. Opin. Neurol.* 31, 36–43. doi: 10.1097/WCO.0000000000000513

Smith, S. M. (2002). Fast robust automated brain extraction. *Hum. Brain Mapp.* 17, 143–155. doi: 10.1002/hbm.10062

Smith, S. M., Jenkinson, M., Johansen-Berg, H., Rueckert, D., Nichols, T. E., Mackay, C. E., et al. (2006). Tract-based spatial statistics: voxelwise analysis of multi-subject diffusion data. *Neuroimage* 31, 1487–1505. doi: 10.1016/j.neuroimage.2006.02.024

Smythies, J. R., Edelstein, L. R., and Ramachandran, V. S. (2013). *The Claustrum: Structural, Functional, and Clinical Neuroscience*. San Diego, CA: Academic Press.

Stine, R. A. (1995). Graphical interpretation of variance inflation factors. *Am. Stat.* 49, 53–56. doi: 10.1080/00031305.1995.10476113

Sun, H., Walsh, A. J., Lebel, R. M., Blevins, G., Catz, I., Lu, J. Q., et al. (2015). Validation of quantitative susceptibility mapping with Perls' iron staining for subcortical gray matter. *Neuroimage* 105, 486–492. doi: 10.1016/j.neuroimage.2014.11.010

Sun, Y., Ge, X., Han, X., Cao, W., Wang, Y., Ding, W., et al. (2017). Characterizing brain iron deposition in patients with subcortical vascular mild cognitive impairment using quantitative susceptibility mapping: a potential biomarker. *Front. Aging Neurosci.* 9:81. doi: 10.3389/fnagi.2017.00081

Taylor, W. D., Steffens, D. C., MacFall, J. R., McQuoid, D. R., Payne, M. E., Provenzale, J. M., et al. (2003). White matter hyperintensity progression and late-life depression outcomes. *Arch. Gen. Psychiatry* 60, 1090–1096. doi: 10.1001/archpsyc.60.11.1090

ten Dam, V. H., van den Heuvel, D. M. J., de Craen, A. J., Bollen, E. L., Murray, H. M., Westendorp, R. G., et al. (2007). Decline in total cerebral blood flow is linked with increase in periventricular but not deep white matter hyperintensities. *Radiology* 243, 198–203. doi: 10.1148/radiol.2431052111

Todorich, B., Pasquini, J. M., Garcia, C. I., Paez, P. M., and Connor, J. R. (2009). Oligodendrocytes and myelination: the role of iron. *Glia* 57, 467–478. doi: 10.1002/glia.20784

Valdés Hernández, M., Allerhand, M., Glatz, A., Clayson, L., Muñoz Maniega, S., Gow, A., et al. (2016). Do white matter hyperintensities mediate the association between brain iron deposition and cognitive abilities in older people? *Eur. J. Neurol.* 23, 1202–1209. doi: 10.1111/ene.13006

Valdés Hernández, M., Ritchie, S., Glatz, A., Allerhand, M., Muñoz Maniega, S., Gow, A. J., et al. (2015). Brain iron deposits and lifespan cognitive ability. *Age* 37:100. doi: 10.1007/s11357-015-9837-2

Wang, X., Pathak, S., Stefaneanu, L., Yeh, F. C., Li, S., and Fernandez-Miranda, J. C. (2016). Subcomponents and connectivity of the superior longitudinal fasciculus in the human brain. *Brain Struct. Funct.* 221, 2075–2092. doi: 10.1007/s00429-015-1028-5

Ward, R. J., Zucca, F. A., Duyn, J. H., Crichton, R. R., and Zecca, L. (2014). The role of iron in brain ageing and neurodegenerative disorders. *Lancet Neurol.* 13, 1045–1060. doi: 10.1016/S1474-4422(14)70117-6

Wardlaw, J. M., Smith, C., and Dichgans, M. (2013a). Mechanisms of sporadic cerebral small vessel disease: insights from neuroimaging. *Lancet Neurol.* 12, 483–497. doi: 10.1016/S1474-4422(13)70060-7

Wardlaw, J. M., Smith, E. E., Biessels, G. J., Cordonnier, C., Fazekas, F., Frayne, R., et al. (2013b). Neuroimaging standards for research into small vessel disease and its contribution to ageing and neurodegeneration. *Lancet Neurol.* 12, 822–838. doi: 10.1016/S1474-4422(13)70124-8

Wardlaw, J. M., Valdés Hernández, M. C., and Muñoz-Maniega, S. (2015). What are white matter hyperintensities made of? Relevance to vascular cognitive impairment. *J. Am. Heart Assoc.* 4:001140. doi: 10.1161/JAHA.114.001140

Wen, W., and Sachdev, P. (2004). The topography of white matter hyperintensities on brain MRI in healthy 60- to 64-year-old individuals. *Neuroimage* 22, 144–154. doi: 10.1016/j.neuroimage.2003.12.027

Wiseman, S. J., Booth, T., Ritchie, S. J., Cox, S. R., Muñoz Maniega, S., Valdés Hernández, M., et al. (2018). Cognitive abilities, brain white matter hyperintensity volume, and structural network connectivity in older age. *Hum. Brain Mapp.* 39, 622–632. doi: 10.1002/hbm.23857

Yan, S., Sun, J., Chen, Y., Selim, M., and Lou, M. (2013). Brain iron deposition in white matter hyperintensities: a 3-T MRI study. *Age* 35, 1927–1936. doi: 10.1007/s11357-012-9487-6

Zachariou, V., Bauer, C. E., Seago, E. R., Raslau, F. D., Powell, D. K., and Gold, B. T. (2020). Cortical iron disrupts functional connectivity networks supporting working memory performance in older adults. *Neuroimage* 223:117309. doi: 10.1016/j.neuroimage.2020.117309

Zecca, L., Youdim, M. B. H., Riederer, P., Connor, J. R., and Crichton, R. R. (2004). Iron, brain ageing and neurodegenerative disorders. *Nat. Rev. Neurosci.* 5, 863–873. doi: 10.1038/nrn1537

Disclaimer: The content is solely the responsibility of the authors and does not necessarily represent the official views of these granting agencies.

Conflict of Interest: The authors declare that the research was conducted in the absence of any commercial or financial relationships that could be construed as a potential conflict of interest.

frontiers in Aging Neuroscience

ORIGINAL RESEARCH
published: 15 July 2021
doi: 10.3389/fnagi.2021.681743

RNF213 p.R4810K (c.14429G > A) Variant Determines Anatomical Variations of the Circle of Willis in Cerebrovascular Disease

*Futoshi Eto[1,2†], Takeshi Yoshimoto[1†], Shuhei Okazaki[1,3], Kunihiro Nishimura[4], Shiori Ogura[1,2], Eriko Yamaguchi[1,2], Kazuki Fukuma[1], Satoshi Saito[1], Kazuo Washida[1], Masatoshi Koga[2], Kazunori Toyoda[2], Takaaki Morimoto[5,6], Hirofumi Maruyama[7], Akio Koizumi[6,8] and Masafumi Ihara[1]**

[1] Department of Neurology, National Cerebral and Cardiovascular Center, Suita, Japan, [2] Department of Cerebrovascular Medicine, National Cerebral and Cardiovascular Center, Suita, Japan, [3] Department of Neurology, Osaka University Graduate School of Medicine, Suita, Japan, [4] Department of Preventive Medicine and Epidemiologic Informatics, National Cerebral and Cardiovascular Center, Suita, Japan, [5] Department of Neurosurgery, Hyogo Prefectural Amagasaki General Medical Center, Amagasaki, Japan, [6] Department of Health and Environmental Sciences, Graduate School of Medicine, Kyoto University, Kyoto, Japan, [7] Department of Clinical Neuroscience and Therapeutics, Hiroshima University, Hiroshima, Japan, [8] Social Health Medicine Welfare Laboratory, Public Interest Incorporated Association Kyoto Hokenkai, Kyoto, Japan

Introduction: Dysregulation of the RING finger protein 213 *(RNF213)* gene impairs vascular formation in experimental animal models. In addition, vascular abnormalities in the circle of Willis are associated with cerebrovascular disease. Here, we evaluated the relationship between the East Asian founder variant *RNF213* p.R4810K and consequent anatomical variations in the circle of Willis in cerebrovascular disease.

Patients and Methods: The present study is an observational cross-sectional study. It included patients with acute anterior circulation non-cardioembolic stroke admitted to our institution within 7 days of symptom onset or last-known-well from 2011 to 2019, and those who participated in the National Cerebral and Cardiovascular Center Biobank. We compared anatomical variations of the vessels constituting the circle of Willis between *RNF213* p.R4810K (c.14429G > A) variant carriers and non-carriers using magnetic resonance angiography and assessed the association between the variants and the presence of the vessels constituting the circle of Willis. Patients with moyamoya disease were excluded.

Results: Four hundred eighty-one patients [146 women (30%); median age 70 years; median baseline National Institutes of Health Stroke Scale score 5] were analyzed. The *RNF213* p.R4810K variant carriers ($n = 25$) were more likely to have both posterior communicating arteries (PComAs) than the variant non-carriers ($n = 456$) (56% vs. 13%, $P < 0.01$). Furthermore, variant carriers were less likely to have an anterior communicating artery (AComA) than non-carriers (68% vs. 84%, $P = 0.04$). In a multivariate logistic regression analysis, the association of *RNF213* p.R4810K

OPEN ACCESS

Edited by:
Stefano Tarantini,
University of Oklahoma Health Sciences Center, United States

Reviewed by:
Raluca Pascalau,
Johns Hopkins University, United States
Adria Arboix,
Sacred Heart University Hospital, Spain

***Correspondence:**
Masafumi Ihara
ihara@ncvc.go.jp

[†] These authors have contributed equally to this work

Received: 17 March 2021
Accepted: 21 June 2021
Published: 15 July 2021

Citation:
Eto F, Yoshimoto T, Okazaki S, Nishimura K, Ogura S, Yamaguchi E, Fukuma K, Saito S, Washida K, Koga M, Toyoda K, Morimoto T, Maruyama H, Koizumi A and Ihara M (2021) RNF213 p.R4810K (c.14429G > A) Variant Determines Anatomical Variations of the Circle of Willis in Cerebrovascular Disease. Front. Aging Neurosci. 13:681743. doi: 10.3389/fnagi.2021.681743

variant carriers with the presence of both PComAs and the absence of AComA remained significant.

Conclusion: Our findings suggest that the *RNF213* p.R4810K variant is an important factor in determining anatomical variations in the circle of Willis.

Keywords: *RNF213* p.R4810K, the circle of Willis, cerebral circulation, magnetic resonance angiography, single nucleotide polymorphism

INTRODUCTION

RING finger protein 213 (*RNF213*) is a susceptibility gene for large artery atherosclerosis (LAA) (Okazaki et al., 2019) as well as moyamoya disease (MMD), which is a progressive steno-occlusive disease of the circle of Willis (Kamada et al., 2011; Liu et al., 2011). This gene encodes a large protein containing two AAA + ATPases and an E3 ligase domain (Liu et al., 2011; Morito et al., 2014), and plays an important role in regulating vascular endothelial function and angiogenesis (Koizumi et al., 2016). Several studies have revealed that MMD patients in East Asia commonly possess the *RNF213* p.R4810K (c.14429G > A) variant (Koizumi et al., 2016). Notably, in Japan, about 90% of MMD patients have this variant, compared with just 2–3% of the general population (Koizumi et al., 2013; Cao et al., 2016). Approximately 20–25% of Japanese patients with intracranial proximal arterial stenosis, but who do not meet the diagnostic criteria for MMD, also have this variant (Miyawaki et al., 2012).

Genetic variants have major effects on the development of cerebral vasculature, as demonstrated in both clinical and experimental studies. Different genetic backgrounds in mice significantly affect flow-mediated outward remodeling in the bilateral posterior communicating arteries (PComAs) after unilateral occlusion of the middle cerebral artery (MCA) (Faber et al., 2019). Moreover, knockdown of *RNF213* in zebrafish impairs the formation of the cerebral vasculature. A recent clinical study has also reported that the *RNF213* p.R4810K variant is associated with intracranial major artery stenosis or occlusion in anterior cerebral circulation (Matsuda et al., 2017).

We therefore sought to evaluate the relationship between the East Asian founder variant *RNF213* p.R4810K, associated with a single nucleotide polymorphism (SNP; rs112735431), and consequent anatomical variations in the circle of Willis in cerebrovascular disease.

MATERIALS AND METHODS

Study Design and Patients

This observational cross-sectional study was performed at the National Cerebral and Cardiovascular Center (NCVC), Osaka, Japan. The study was conducted in accordance with the Declaration of Helsinki and was approved by the local ethics committees at the NCVC Biobank and Kyoto University. The study was also approved by the Institutional Review Board of NCVC (approval numbers M29-003-9 and M30-145-5). All participants signed a comprehensive consent form at the NCVC.

All patients with ischemic stroke or transient ischemic attack (TIA) who were admitted to our institute within 7 days of symptom onset or last-known-well were prospectively registered to the NCVC Stroke Registry (Yoshimoto et al., 2021). Data for the period from January 2011 to July 2019 were retrospectively reviewed, and patients who met the following criteria were included: (1) admitted with acute anterior circulation non-cardioembolic stroke or TIA; (2) participated in the NCVC Biobank; and, (3) had magnetic resonance imaging (MRI) data available. Patients with MMD were excluded based on diagnostic criteria (Research Committee on the Pathology, and Treatment of Spontaneous Occlusion of the Circle of Willis, and Health Labour Sciences Research Grant for Research on Measures for Intractable Diseases, 2012).

Genotype Analysis

Peripheral blood samples were obtained from all patients. Genomic DNA was extracted from the buffy coat of blood samples using QIAsymphony SP equipment (Qiagen, Hilden, Germany). Genotyping was performed using TaqMan SNP Assays (Applied Biosystems, Foster City, CA, United States) as described previously (Liu et al., 2011). From the *RNF213* p.R4810K variant genotype analysis, individuals with the GA variant for p.R4810K or the homozygote AA genotype were defined as variant carriers, while individuals with the wild-type homozygote were defined as variant non-carriers.

Imaging Protocol

MRI was performed using a 3-tesla system (MAGNETOM Verio or Spectra, Siemens, Erlangen, Germany) at admission. Circle of Willis morphology was evaluated by magnetic resonance angiography (MRA) with maximum intensity protection, a method used to reconfigure and prevent overvaluation and overestimation.

The vessels constituting the circle of Willis were defined as follows: (i) the anterior communicating artery (AComA), (ii) the A1 segments of the anterior cerebral arteries (ACAs), (iii) the intracranial internal carotid arteries (ICAs) beyond the PComA bifurcation, (iv) the PComAs, (v) the P1 segments of the posterior cerebral arteries (PCAs), and (vi) the top of the basilar artery (BA) (**Figure 1**). Intracranial ICA was defined as the ICA from the PComA bifurcation to the top of the ICA.

Based on the MRA findings, the A1 segments of the ACAs, the intracranial ICAs, the PComAs, and the P1 segments of the PCAs were classified into the presence of both vessels (**Figure 2A**), a unilateral vessel (**Figure 2B**), or the absence of both vessels (**Figure 2C**). The AComA and the top of the BA

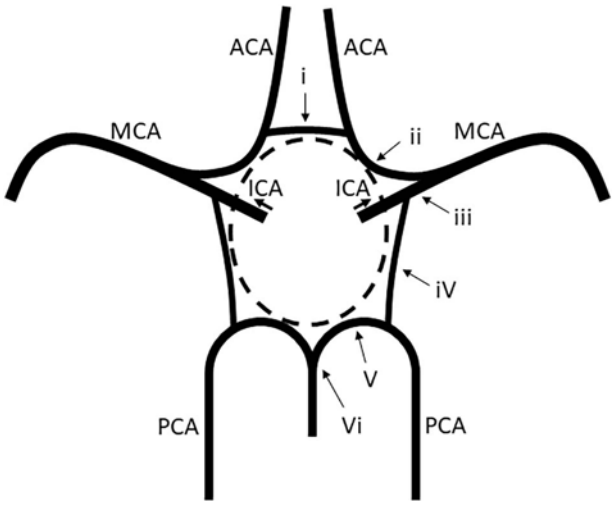

FIGURE 1 | Vessels constituting the circle of Willis. (i) The AComA, (ii) the A1 segment of the ACAs, (iii) the intracranial ICA beyond the PComA bifurcation, (iv) the PComAs, (v) the P1 segment of the PCAs, and (vi) the top of the BA. ACAs, anterior cerebral arteries; AComA, anterior communicating artery; BA, basilar artery; ICAs, internal carotid arteries; PCAs, posterior cerebral arteries; PComAs, posterior communicating arteries.

were classified by the presence and absence of the vessels. The absence of vessels included artery aplasia or hypoplasia (defined as an internal diameter under 1 mm Merkkola et al., 2006). To determine the anatomical variations, the MRA findings of the vessels constituting the circle of Willis and the focal narrowing of the M1 segment of the MCA were independently analyzed by two stroke neurologists (F.E. and T.Y.), who were blind to the clinical information. Joint assessments were carried out for consensus if required.

Clinical Data Collection

The baseline clinical characteristics were collected from the NCVC Stroke Registry: sex, age, prestroke modified Rankin Scale (mRS) score, medical history (hypertension, diabetes mellitus, dyslipidemia, ischemic heart disease, and chronic kidney disease), atrial fibrillation, current smoking, systolic blood pressure on admission, baseline National Institutes of Health Stroke Scale (NIHSS) score, Alberta Stroke Program Early Computed Tomographic Score (ASPECTS) on diffusion-weighted imaging (DWI) or computed tomography (CT), the presence of vessels constituting the circle of Willis (AComA, both A1 segments of the ACAs, both intracranial ICAs, and both PComAs), completeness of the circle of Willis, focal narrowing of the M1 segment of the MCA, stroke subtype, and clinical outcome (mRS score at discharge and in-hospital mortality). Hypertension was diagnosed at hospital discharge or from the use of antihypertensive medications before the index stroke/TIA. Diabetes mellitus was diagnosed at hospital discharge or from antidiabetic treatment before the index stroke/TIA. Dyslipidemia was diagnosed at hospital discharge or from lipid-lowering therapy before the index stroke/TIA. A complete circle of Willis was defined by the presence of all of the vessels that constitute the circle of Willis. Stroke subtype, including LAA, small vessel occlusion (SVO), and other/undetermined etiology, was determined by stroke neurologists according to the Trial of ORG 10172 in Acute Stroke Treatment criteria (Adams et al., 1993).

Statistical Analyses

Data are summarized as the median [interquartile range (IQR)] for continuous variables and the frequencies (percentages) for categorical variables. Patients were divided into two groups: *RNF213* p.R4810K variant carriers and non-carriers. The clinical characteristics, presence of vessels constituting the circle of Willis, and clinical outcomes were compared between groups using the Mann–Whitney *U*-test or Fisher's exact test, as appropriate. We assessed the correlations between anatomical variations of the circle of Willis (both PComAs and AComA) and the *RNF213* p.R4810K variant using the following models. For Model 1, a multivariate logistic regression model was created to investigate the association between anatomical variations of the circle of Willis (both PComAs and AComA) and the *RNF213* p.R4810K variant. Variables with $P < 0.10$ (women, age, focal narrowing of the M1 segment of MCA, and stroke subtype) were selected for the multivariate model. For Model

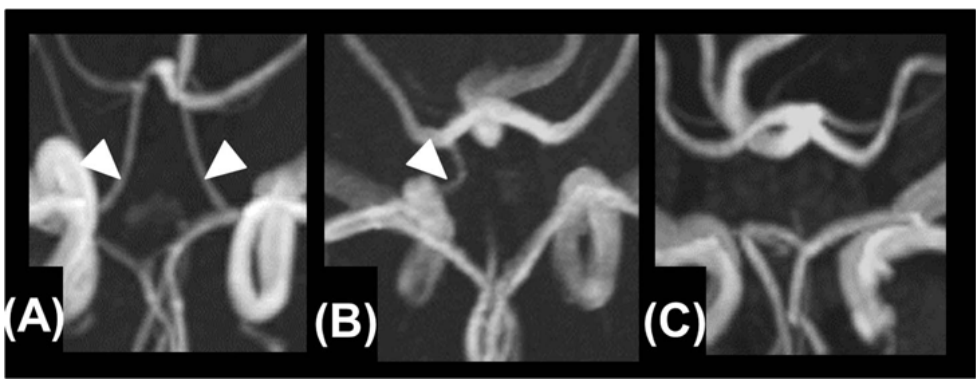

FIGURE 2 | Presence of both vessels **(A)**, unilateral presence of one vessel **(B)**, and bilateral absence of the vessels **(C)**.

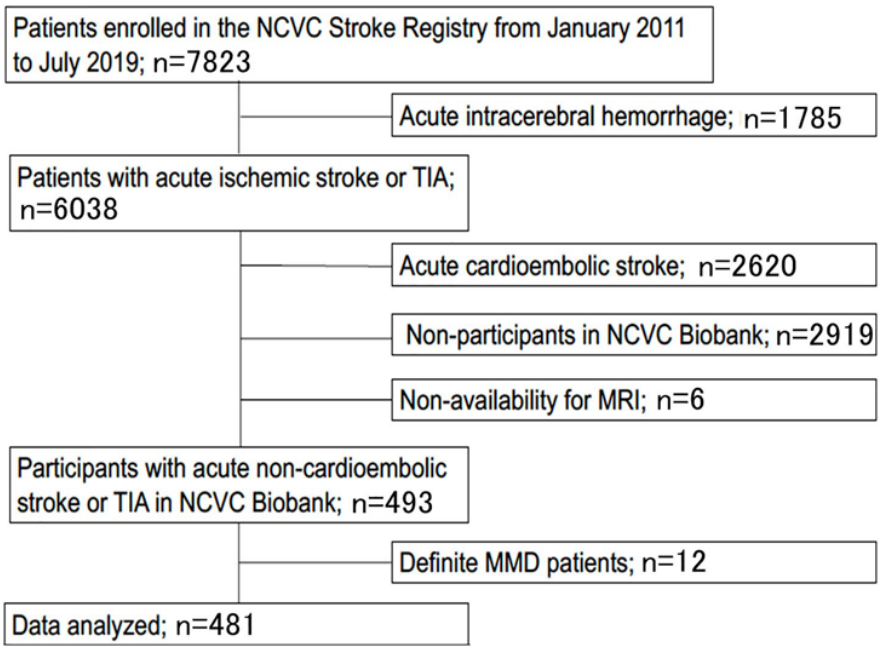

FIGURE 3 | Study flow chart. Patients were excluded based on acute intracerebral hemorrhage (n = 1,785), acute cardioembolic stroke (n = 2,620), non-participants at the NCVC Biobank (n = 2,919), non-availability of MRI (n = 6), and MMD cases (n = 12). MMD, moyamoya disease; MRI, magnetic resonance imaging; NCVC, National Cerebral, and Cardiovascular Center; TIA, transient ischemic attack.

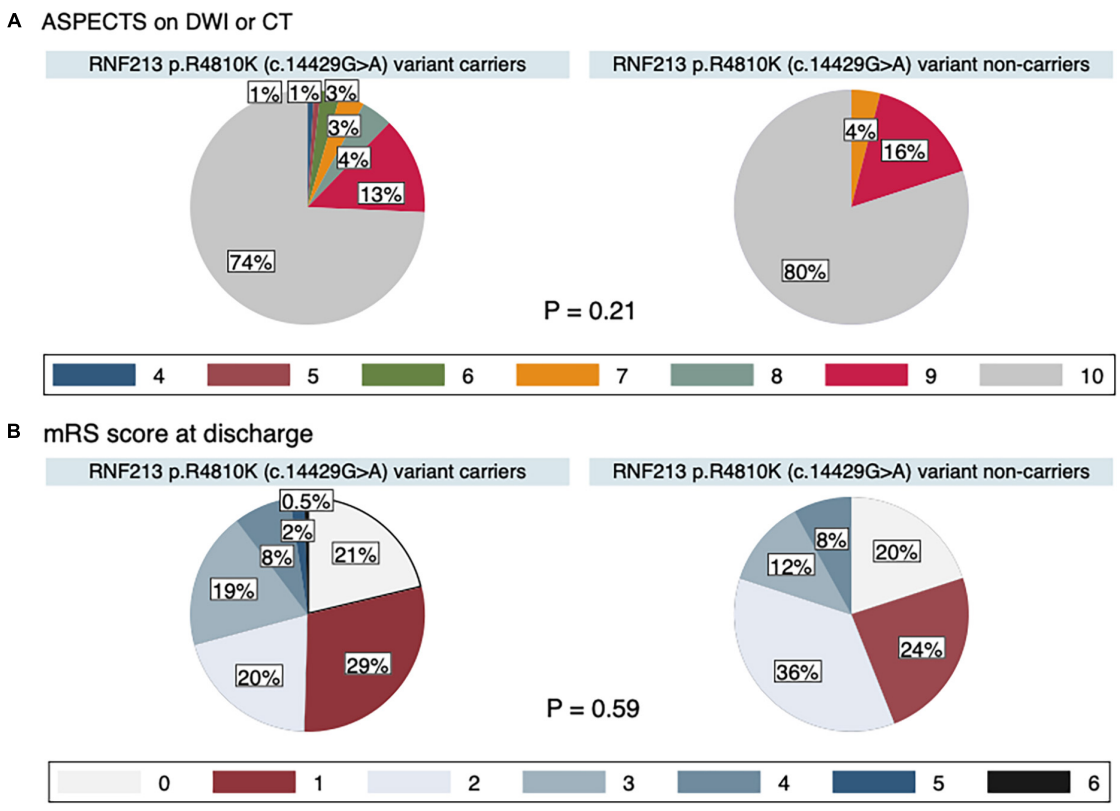

FIGURE 4 | Pie charts of ASPECTS on DWI or CT **(A)** and mRS score at discharge **(B)**.

2, associations between anatomical variations of the circle of Willis (both PComAs and AComA) and the *RNF213* p.R4810K variant were explored using a multivariate logistic regression model; the stepwise method was used for variable selection. To exclude statistically non-significant variables from the logistic regression model, bidirectional stepwise variable selection was used, with a *P*-value for entry of 0.05 and a *P*-value for removal of 0.10. Odds ratios (ORs) with 95% confidence intervals (CIs) were also calculated. We also analyzed the intraclass correlation coefficients for the evaluation of vessels constituting the circle of Willis.

The enrolled patients were then divided into three groups according to stroke subtype (LAA, SVO, and other/undetermined etiology). Baseline characteristics, including the presence of vessels constituting the circle of Willis, were compared. We evaluated the associations between the presence of vessels constituting the circle of Willis and the stroke subtype. All analyses were performed using JMP 14.0.0 statistical software (SAS Institute Inc., Cary, NC, United States).

RESULTS

The study flow chart is provided in **Figure 3**. From January 2011 to July 2019, 7823 patients were enrolled in the NCVC Stroke Registry. Of these, 481 patients [146 (30%) women, median (IQR) age of 70 (57–78) years] met our study criteria. Patients were excluded because of acute intracerebral hemorrhage ($n = 1785$), acute cardioembolic stroke ($n = 2620$), non-participants at the NCVC Biobank ($n = 2919$), non-availability of MRI ($n = 6$), and MMD cases ($n = 12$). Of the 481 patients [146 women (30%); median (IQR) age 70 (57–78) years, median NIHSS score 5 (2–5)] enrolled in the present study, 25 patients (5.2%) had the GA variant for p.R4810K and no patients had the homozygote AA genotype. The

TABLE 1 | Baseline characteristics between *RNF213* p.R4810K (c.14429G > A) variant carriers and non-carriers.

		***RNF213* p.R4810K (c.14429G > A) variant carriers**		
Variables	**All ($n = 481$)**	**Carriers ($n = 25$)**	**Non-carriers ($n = 456$)**	***P***
Women, *n* (%)	146 (30)	13 (52)	133 (29)	0.02
Age, median (IQR), years	70 (57–78)	62 (45–70)	70 (58–79)	<0.01
Prestroke mRS score, median (IQR)	0 (0–0)	0 (0–0)	0 (0–0)	0.57
Baseline systolic BP, median (IQR), mmHg	162 (144–177)	162 (140–175)	161 (150–177)	0.66
Medical history				
Hypertension, *n* (%)	384 (80)	20 (80)	364 (80)	1.00
Diabetes mellitus, *n* (%)	135 (28)	8 (32)	127 (28)	0.65
Dyslipidemia, *n* (%)	325 (68)	15 (60)	310 (68)	0.39
Ischemic heart disease, *n* (%)	21 (4)	2 (8)	25 (6)	0.64
Chronic kidney disease, *n* (%)	19 (4)	12 (48)	145 (32)	0.12
Atrial fibrillation, *n* (%)	9 (2)	0 (0)	9 (2)	1.00
Current smoking, *n* (%)	272 (57)	14 (56)	258 (57)	1.00
Baseline NIHSS score, median (IQR)	5 (2–5)	3 (2–6)	5 (2–5)	0.26
ASPECTS on DWI or CT, median (IQR) ($n = 465$)	10 (9–10)	10 (10–10)	10 (9–10)	0.43
Formation of vessels constituting the circle of Willis				
AComA, *n* (%)	401 (83)	17 (68)	384 (84)	0.04
Both A1 segments of ACAs, *n* (%)	424 (88)	19 (76)	403 (88)	0.11
Both intracranial ICAs, *n* (%)	467 (97)	23 (92)	444 (97)	0.16
Both PComAs, *n* (%)	75 (16)	14 (56)	61 (13)	<0.01
Both P1 segments of PCAs, *n* (%)	385 (80)	18 (72)	362 (79)	0.45
Top of BA, *n* (%)	478 (99)	24 (96)	455 (99)	0.10
Focal narrowing of the M1 segment of MCA, *n* (%)	66 (14)	11 (44)	55 (12)	<0.01
Complete circle of Willis, *n* (%)	49 (11)	5 (20)	43 (9)	0.09
Stroke subtype				<0.01
Large artery atherosclerosis, *n* (%)	139 (29)	14 (56)	125 (27)	
Small vessel occlusion, *n* (%)	135 (28)	5 (20)	130 (29)	
Other/undetermined etiology, *n* (%)	185 (38)	4 (16)	181 (40)	
Transient ischemic attack, *n* (%)	22 (5)	2 (8)	20 (4)	0.32
mRS score at discharge, median (IQR)	1 (1–3)	2 (1–2)	1 (1–3)	0.96
In-hospital mortality, *n* (%)	2 (0.4)	0	2 (0.4)	1.00

ACAs, anterior cerebral arteries; AComA, anterior communicating artery; ASPECTS, Alberta Stroke Program Early CT Score; BA, basilar artery; BP, blood pressure; CT, computed tomography; DWI, diffusion-weighted imaging; ICAs, internal carotid arteries; IQR, interquartile range; MCA, middle cerebral artery; mRS, modified Rankin Scale; NIHSS, National Institutes of Health Stroke Scale; PCAs, posterior cerebral arteries; PComAs, posterior communicating arteries.

most common comorbidities were hypertension (80%) and dyslipidemia (68%). Forty-nine patients (11%) had a complete circle of Willis. The median (IQR) mRS score at discharge was 1 (1–3) and the in-hospital mortality rate was 0.4%. The distributions of ASPECTS on DWI or CT and mRS scores at discharge in variant carriers and non-carriers are shown in **Figure 4**.

TABLE 2 | Baseline characteristics between patients with the presence and absence of both PComAs.

Variables	Both PComAs		*P*
	Presence (*n* = 75)	Absence (*n* = 406)	
Women, *n* (%)	31 (41)	115 (28)	0.03
Age, median (IQR), years	62 (46–73)	71 (60–79)	<0.01
Prestroke mRS score, median (IQR)	0 (0–0)	0 (0–0)	0.72
Baseline systolic BP, median (IQR), mmHg	162 (144–179)	158 (143–182)	0.75
Medical history			
Hypertension, *n* (%)	52 (69)	332 (82)	0.02
Diabetes mellitus, *n* (%)	20 (27)	115 (28)	0.89
Dyslipidemia, *n* (%)	46 (61)	279 (69)	0.23
Ischemic heart disease, *n* (%)	3 (4)	24 (6)	0.78
Chronic kidney disease, *n* (%)	12 (48)	145 (32)	0.12
Atrial fibrillation, *n* (%)	8 (2)	1 (1)	1.00
Current smoking, *n* (%)	19 (25)	138 (34)	0.18
Baseline NIHSS score, median (IQR)	5 (1–5)	5 (2–5)	0.33
ASPECTS on DWI or CT, median (IQR) (*n* = 465)	10 (9–10)	10 (10–10)	0.21
Formation of vessels constituting the circle of Willis			
AComA, *n* (%)	61 (81)	340 (84)	0.61
Both A1 segments of ACAs, *n* (%)	69 (92)	353 (87)	0.26
Both intracranial ICAs, *n* (%)	74 (99)	393 (97)	0.71
Both P1 segments of PCAs, *n* (%)	63 (84)	317 (78)	0.28
Top of BA, *n* (%)	75 (100)	404 (99)	1.00
Focal narrowing of the M1 segment of MCA, *n* (%)	15 (20)	51 (13)	0.10
Stroke subtype			<0.01
Large artery atherosclerosis, *n* (%)	16 (21)	123 (30)	
Small vessel occlusion, *n* (%)	18 (24)	117 (29)	
Other/undetermined etiology, *n* (%)	39 (52)	146 (36)	
Transient ischemic attack, *n* (%)	2 (3)	20 (5)	0.55
Outcome			
mRS score at discharge, median (IQR)	1 (0–3)	2 (1–3)	0.59
In-hospital mortality, *n* (%)	0	2 (0.5)	1.00
RNF213 p.R4810K (c.14429G > A) variant carriers, *n* (%)	14 (19)	11 (3)	<0.01

ACAs, anterior cerebral arteries; AComA, anterior communicating artery; ASPECTS, Alberta Stroke Program Early CT Score; BA, basilar artery; BP, blood pressure; CT, computed tomography; DWI, diffusion-weighted imaging; ICAs, internal carotid arteries; IQR, interquartile range; MCA, middle cerebral artery; mRS, modified Rankin Scale; NIHSS, National Institutes of Health Stroke Scale; PCAs, posterior cerebral arteries; PComAs, posterior communicating arteries.

TABLE 3 | Logistic regression analyses for the presence of both PComAs.

Variables	Unweighted univariable	Model 1	Model 2
	OR (95% CI)		
Women	1.78 (1.07–2.96)	1.50 (0.85–2.63)	–
Age (per 10-year increase)	0.67 (0.56–0.79)	0.73 (0.60–0.88)	0.71 (0.59–0.85)
Hypertension	0.50 (0.29–0.87)	0.76 (0.40–1.42)	–
Diabetes mellitus	0.92 (0.53–1.60)		–
Dyslipidemia	0.72 (0.43–1.20)	–	–
Ischemic heart disease	0.66 (0.19–2.26)	–	–
Chronic kidney disease	0.66 (0.38–1.15)	–	–
Atrial fibrillation	0.67 (0.08–5.46)	–	
Current smoking	0.59 (0.36–0.96)	–	–
Focal narrowing of the M1 segment of MCA	1.74 (0.91–3.29)	0.95 (0.43–2.12)	–
Large artery atherosclerosis	0.62 (0.35–1.13)	0.54 (0.26–1.10)	0.50 (0.25–0.99)
RNF213 p.R4810K (c.14429G > A) variant carriers	8.24 (3.58–18.98)	8.08 (3.17–20.59)	8.61 (3.48–21.31)

Model 1; adjusted for variables with p < 0.10 (women, age, focal narrowing of the M1 segment of MCA, and large artery atherosclerosis).
Model 2; forward–backward stepwise method.
CI, confidence interval; MCA, middle cerebral arteries; OR, odds ratio; PComAs, posterior communicating arteries.

Compared with *RNF213* p.R4810K (c.14429G > A) non-carriers ($n = 456$), carriers ($n = 25$) were more frequently women (52% vs. 29%, $P = 0.02$), younger (62 years vs. 70 years, $P < 0.01$), had focal narrowing of the M1 segment of the MCA (44% vs. 12%, $P < 0.01$), had a lower presence of AComA (68% vs. 84%, $P = 0.04$), and a higher presence of both PComAs (56% vs. 13%, $P < 0.01$). The baseline characteristics of *RNF213* p.R4810K variant carriers and non-carriers are shown in **Table 1**. Compared with patients with the unilateral presence or absence of PComAs ($n = 406$), patients with the presence of both PComAs ($n = 75$) were more frequently women (41% vs. 28%, $P = 0.03$), younger (median 62 years vs. 71 years, $P < 0.01$), less hypertensive (69% vs. 82%, $P = 0.02$), had more focal narrowing of the M1 segment of the MCA (26% vs. 12%, $P = 0.02$), and more frequently *RNF213* p.R4810K variant carriers (19% vs. 3%, $P < 0.01$). In the multivariate analysis using the stepwise model (Model 2), patients having both PComAs were more frequently younger (per 1-year increase; OR 0.71, 95% CI 0.59–0.85) and were significantly associated with the variant (OR 8.61, 95% CI 3.48–21.31). The patient baseline characteristics, stratified according to PComA patency state, are shown in **Table 2**. Two models were used to evaluate the associations between PComAs patency state and the factors shown in **Table 3**.

Compared with patients with AComA ($n = 401$), those without AComA ($n = 80$) were older (median 75 years vs. 69 years, $P = 0.03$), and more frequently the variant carriers (11% vs. 4%, $P = 0.04$). In the multivariate analysis using the stepwise model (Model 2), the absence of AComA were also significantly associated with the variant (OR 2.38, 95% CI 1.02–5.88), as shown in **Tables 4**, **5**. There were no associations between the other vessels constituting the circle of Willis and the *RNF213* p.R4810K variant.

The intraclass correlation coefficients for the evaluation of vessels constituting the circle of Willis were as follows: 0.97 (95% CI 0.97–0.98) for AComA, 0.98 (95% CI 0.98–0.99) for both A1 segments of the ACAs, 1.00 for both intracranial ICAs, 1.00 for the top of the BA, 0.97 (95% CI 0.97–0.98) for both PComAs, and 0.96 (95% CI 0.95–0.97) for both P1 segments of the PCAs.

There were no significant differences in the vessels constituting the circle of Willis for each stroke subtype, except that the presence of AComA was significantly higher in patients with SVO (LAA 89% vs. SVO 92% vs. other/undetermined etiology 79%, $P < 0.01$). Moreover, the frequency of *RNF213* p.R4810K variant carriers were significantly higher in patients with LAA (LAA 10% vs. SVO 4% vs. other/undetermined etiology 2%, $P < 0.01$). A comparison of the baseline characteristics by stroke subtype is shown in **Supplementary Table 1**, in the online-only Data Supplement.

TABLE 4 | Baseline characteristics between the presence and absence of AComA.

Variables	AComA		*P*
	Absence ($n = 80$)	Presence ($n = 401$)	
Women, *n* (%)	32 (40)	114 (28)	0.05
Age, median (IQR), years	75 (61–82)	69 (57–78)	0.03
Prestroke mRS score, median (IQR)	0 (0–0)	0 (0–0)	0.70
Baseline systolic BP, median (IQR), mmHg	158 (134–170)	162 (144–178)	0.05
Medical history			
Hypertension, *n* (%)	66 (83)	318 (79)	0.65
Diabetes mellitus, *n* (%)	16 (20)	119 (30)	0.10
Dyslipidemia, *n* (%)	54 (68)	271 (68)	1.00
Ischemic heart disease, *n* (%)	7 (9)	20 (5)	0.20
Chronic kidney disease, *n* (%)	37 (46)	120 (30)	<0.01
Atrial fibrillation, *n* (%)	4 (5.0%)	5 (1.2%)	0.05
Current smoking, *n* (%)	36 (45)	236 (59)	0.03
Baseline NIHSS score, median (IQR)	3 (2–5)	5 (2–5)	0.21
ASPECTS on DWI or CT, median (IQR) ($n = 465$)	10 (9–10)	10 (9–10)	0.81
Formation of vessels constituting the circle of Willis			
Both A1 segments of ACAs, *n* (%)	71 (89)	351 (88)	0.85
Both intracranial ICAs, *n* (%)	78 (98)	389 (97)	1.00
Both PComAs, *n* (%)	14 (18)	61 (15)	0.61
Both P1 segments of PCAs, *n* (%)	62 (78)	318 (79)	0.76
Top of BA, *n* (%)	80 (100)	399 (99)	1.00
Focal narrowing of the M1 segment of MCA, *n* (%)	6 (8)	60 (15)	0.11
Stroke subtype			<0.01
Large artery atherosclerosis, *n* (%)	16 (20)	123 (31)	
Small vessel occlusion, *n* (%)	11 (14)	124 (31)	
Other/undetermined etiology, *n* (%)	39 (49)	146 (36)	
Transient ischemic attack, *n* (%)	14 (17.5%)	8 (2.0%)	<0.01
Outcome			
mRS score at discharge, median (IQR)	1 (1–3)	2 (1–3)	0.50
In-hospital mortality, *n* (%)	0	2 (0.5)	1.00
RNF213 p.R4810K (c.14429G > A) variant carriers, *n* (%)	9 (11)	17 (4)	0.04

ACAs, anterior cerebral arteries; AComA, anterior communicating artery; ASPECTS, Alberta Stroke Program Early CT Score; BA, basilar artery; BP, blood pressure; CT, computed tomography; DWI, diffusion-weighted imaging; ICAs, internal carotid arteries; IQR, interquartile range; MCA, middle cerebral artery; mRS, modified Rankin Scale; NIHSS, National Institutes of Health Stroke Scale; PCAs, posterior cerebral arteries; PComAs, posterior communicating arteries.

TABLE 5 | Logistic regression analyses for the absence of AComA.

Variables	Unweighted univariable	Model 1	Model 2
	OR (95% CI)		
Women	1.67 (1.02–2.78)	1.18 (0.95–2.17)	–
Age (per 10-year increase)	1.15 (0.97–1.37)	1.10 (0.88–1.37)	–
Baseline systolic BP (per 10 mmHg increase)	0.91 (0.83–1.00)	0.89 (0.81–0.99)	0.91 (0.73–1.01)
Hypertension	2.00 (1.15–3.45)	–	
Diabetes mellitus	0.59 (0.33–1.06)	0.58 (0.31–1.10)	0.59 (0.32–1.09)
Dyslipidemia	1.00 (0.60–1.67)	–	–
Ischemic heart disease	1.82 (0.75–4.55)	–	–
Chronic kidney disease	2.00 (1.23–3.33)	1.49 (0.79–2.78)	1.96 (1.19–3.23)
Atrial fibrillation	4.17 (1.10–16.67)	–	
Current smoking	0.57 (0.35–0.93)	0.70 (0.39–1.25)	0.65 (0.40–1.08)
Focal narrowing of the M1 segment of MCA	0.46 (0.19–1.11)	–	
Large artery atherosclerosis	0.56 (0.31–1.02)	–	
RNF213 p.R4810K (c.14429G > A) variant carriers	2.56 (1.11–5.88)	2.50 (1.08–6.67)	2.38 (1.02–5.88)

Model 1; adjusted for variables with p < 0.10 (women, age, baseline systolic BP, diabetes mellitus, chronic kidney disease, and current smoking).
Model 2; forward–backward stepwise method.
AComA, anterior communicating artery; BP, blood pressure; CI, confidence interval; MCA, middle cerebral artery; OR, odds ratio.

DISCUSSION

The current study provides relevant new data about the associations between vessels constituting the circle of Willis and the *RNF213* p.R4810K variant carrier state. Our results indicate that the East Asian founder variant of *RNF213* affects the vascular formation of the circle of Willis. *RNF213* p.R4810K variant carriers had a higher frequency of the presence of both PComAs and the absence of AComA compared with non-carriers, even after adjusting for differences in baseline characteristics using a stepwise method. These findings reinforce the idea of anterior cerebral circulation failure even in *RNF213* p.R4810K variant carriers who do not satisfy the diagnostic criteria for MMD (Research Committee on the Pathology, and Treatment of Spontaneous Occlusion of the Circle of Willis, and Health Labour Sciences Research Grant for Research on Measures for Intractable Diseases, 2012). To our knowledge, no other SNPs have been reported to be associated with such substantial anatomical variations in the circle of Willis as in the current findings for the *RNF213* p.R4810K variant.

In terms of the variation of vessels constituting the circle of Willis, a previous study evaluated the intracranial arterial morphology of healthy subjects and reported that 21% (110/525) had an absence of AComA, 19% (100/525) had both PComAs, and 20.9% had a complete circle of Willis; however, the *RNF213* p.R4810K variant was not examined in this study (Kondori et al., 2017). In the variant carriers in the present study, the rate of absence of AComA was 32% (8/25), the rate of both PComAs was 56% (14/25), and a complete circle of Willis was present in 20% (5/25) of individuals. Thus, compared with the healthy subjects in the previous report (Kondori et al., 2017), our results showed higher rates of an absence of AComA and the presence of both PComAs in variant carriers. These results suggest that this variant affects anatomical variations in the circle of Willis. In the variant non-carriers, the rate of a complete circle of Willis was very low, at 9% (43/456), and the presence of both PComAs was only 13% (61/453); these findings likely reflect the fact that our study included only patients with a history of ischemic stroke/TIA.

In a previous study examining sex differences in stroke (Arboix et al., 2014), women generally had more stroke events at an older age and a higher number of stroke events than men because of a longer life expectancy. In the present study, although patients with the *RNF213* p.R4810K variant were more frequently women and younger, as previously reported (Kamimura et al., 2019; Okazaki et al., 2019), there were no differences in clinical outcomes, including mRS score at discharge and in-hospital mortality. To clarify the impact of this variant on clinical outcomes, long-term outcomes should be investigated in future research.

Advanced MMD is characterized by the discontinuity or disappearance of PComAs in Suzuki staging (Jin et al., 2011), probably as a result of arteriopathy extending proximally into these vessels. This seems to contradict our finding that variant carriers had increased patency of PComAs. However, this inconsistency may be explained by the different stages of *RNF213*-related vasculopathy between variant carriers with advanced MMD and those with sporadic ischemic stroke or TIA in our cohort (Okazaki et al., 2019; Hosoki et al., 2021), which excluded MMD. That is, patients with advanced MMD, who represent the extreme end of the disease spectrum of *RNF213*-related vasculopathy, have terminal ICA stenosis or occlusion. Anterior circulation insufficiency no longer activates compensatory mechanisms for collateral flow because of the arteriopathy of PComAs. In contrast, patients on the less severe end of the *RNF213*-related vasculopathy spectrum may still have activation of the mechanisms that compensate for insufficient anterior circulation through the PComAs, PCAs, and meningeal arteries (Song et al., 2019). Both the continuity and differences between MMD and non-moyamoya ischemic stroke in the same variant carriers should be further clarified to establish and stratify treatment strategies for *RNF213*-related vasculopathy.

Another explanation of PComA patency may be attributable to the embryonic development of cerebral circulation. In the embryonic stage, the neural crest gives rise to pericytes, thereby contributing to the formation of anterior cerebral circulation, which specifically includes primitive ICAs but not the vertebrobasilar arteries of mesodermal origin (Komiyama, 2017a). Therefore, failures in the differentiation and migration of neural crest cells may lead to the insufficiency of anterior cerebral circulation, including MMD, multisystemic smooth muscle dysfunction syndrome caused by *ACTA2* mutation, and PHACE syndrome, which are collectively named vascular neurocristopathy (cardio-cephalic neural crest syndrome) (Komiyama, 2017b). Thus, anatomical variations of the circle of Willis in variant carriers may not be acquired, but might be primarily determined in the embryonic stage. Additional studies in healthy carriers or other ischemic stroke and TIA cohorts are required to determine precisely when the *RNF213* p.R4810K variant leads to the observed arterial variations. This gene polymorphism may also be involved in the relationship between cerebrovascular pathology and Alzheimer's disease (AD) because vascular abnormalities affect the accumulation of amyloid protein and the progression of behavioral abnormalities in both AD patients and animal models (Farkas and Luiten, 2001). Another report (Roher et al., 2003) has demonstrated a relationship between circle of Willis atherosclerosis and AD, thus strengthening the importance of cerebrovascular architecture in AD.

There are several limitations in the present study. The first and major limitation was the lack of genetic and neuroimaging data from healthy volunteers, which was the result of ethical and procedural issues. Because only patients with previous ischemic stroke/TIA were enrolled in this study, it will be necessary to evaluate healthy subjects in a future validation cohort. Second, the anatomical variations of intracranial arteries were evaluated by MRA in the current study. Digital subtraction angiography is the gold standard technique and is superior to MRA in the evaluation of cerebrovascular architecture, although MRA has an advantage as a non-invasive imaging modality. Third, only 14% of patients enrolled in the study gave full consent for their data to be collected and stored at the NCVC Biobank;

such selection bias may have led to an overestimation of the prevalence of the *RNF213* p.R4810K variant. Fourth, although a previous whole-genome microarray analysis demonstrated associations between *RNF 213* polymorphisms and AD (Bai et al., 2014), cognitive status was not evaluated in the present study because the cerebrovascular disease affects cognitive function, and thus makes the diagnosis of AD difficult in an acute stroke setting. However, the results of the current study may stimulate future exploration of the association between AD and the *RNF 213* p.R4810K variant. Finally, we were unable to entirely rule out acquired changes in intracranial arteries caused by atherosclerosis. However, the association between the presence of both PComAs and the *RNF213* variant remained even after adjusting for baseline factors using the stepwise method.

CONCLUSION

RNF213 p.R4810K variant carriers had higher rates of the presence of both PComAs and an absence of AComA than non-carriers. In variant carriers, an insufficiency of anterior cerebral circulation arteries may be accompanied by compensatory collateral flow through the PComAs, thus affecting the anatomy of the circle of Willis.

DATA AVAILABILITY STATEMENT

The raw data supporting the conclusions of this article will be made available by the authors, without undue reservation.

ETHICS STATEMENT

The studies involving human participants were reviewed and approved by the National Cerebral and Cardiovascular Center Biobank and Kyoto University. The patients/participants provided their written informed consent to participate in this study.

AUTHOR CONTRIBUTION

FE wrote the first draft of the manuscript, evaluated MRA findings, performed the statistical analysis, and interpreted the data. TY revised the draft of the manuscript, evaluated the MRA findings, provided advice on the statistical analysis, and interpreted the data. KN provided advice on the statistical analysis. SOk, SOg, EY, KF, SS, KW, MK, KT, and HM critically revised the article for important intellectual content. TM and AK supported the genotyping from peripheral blood samples and critically revised the article for important intellectual content. MI designed the study, interpreted the data, and wrote the final draft of the manuscript. All authors contributed to the article and approved the submitted version.

FUNDING

This study was supported by the Japan Agency for Medical Research and Development (Grant No. 19ek0210120h0001) and the SENSHIN Medical Research Foundation.

ACKNOWLEDGMENTS

We thank Ahmad Khundakar for his intellectual input and article editing. We also thank Bronwen Gardner, from Edanz (https://jp.edanz.com/ac) for editing a draft of this manuscript. This research was performed using samples acquired from the National Center Biobank Network/NCVC Biobank resource. For further details see http://www.ncbiobank.org/ and http://www.ncvc.go.jp/biobank/.

SUPPLEMENTARY MATERIAL

The Supplementary Material for this article can be found online at: https://www.frontiersin.org/articles/10.3389/fnagi.2021.681743/full#supplementary-material

REFERENCES

Adams, H. P. Jr., Bendixen, B. H., Kappelle, L. J., Biller, J., Love, B. B., Gordon, D. L., et al. (1993). Classification of subtype of acute ischemic stroke. definitions for use in a multi-center clinical trial. TOAST. trial of Org 10172 in acute stroke treatment. *Stroke* 24, 35–41. doi: 10.1161/01.str.24.1.35

Arboix, A., Cartanya, A., Lowak, M., Garcia-Eroles, L., Parra, O., Oliveres, M., et al. (2014). Gender differences and woman-specific trends in acute stroke: results from a hospital-based registry (1986-2009). *Clin. Neurol. Neurosurg.* 127, 19–24. doi: 10.1016/j.clineuro.2014.09.024

Bai, Z., Stamova, B., Xu, H., Ander, B. P., Wang, J., Jickling, G. C., et al. (2014). Distinctive RNA expression profiles in blood associated with Alzheimer's disease after accounting for white matter hyperintensities. *Alzheimer Dis. Assoc. Disord.* 28, 226–233. doi: 10.1097/WAD.0000000000000022

Cao, Y., Kobayashi, H., Morimoto, T., Kabata, R., Harada, K. H., and Koizumi, A. (2016). Frequency of RNF213 p.R4810K, a susceptibility variant for moyamoya disease, and health characteristics of carriers in the Japanese population. *Environ. Health Prev. Med.* 21, 387–390. doi: 10.1007/s12199-016-0549-8

Faber, J. E., Zhang, H., Rzechorzek, W., Dai, K. Z., Summers, B. T., Blazek, C., et al. (2019). Genetic and environmental contributions to variation in the posterior communicating collaterals of the circle of Willis. *Transl. Stroke Res.* 10, 189–203. doi: 10.1007/s12975-018-0626-y

Farkas, E., and Luiten, P. G. M. (2001). Cerebral microvascular pathology in aging and Alzheimer's disease. *Prog. Neurobiol.* 64, 575–611. doi: 10.1016/s0301-0082(00)00068-x

Hosoki, S., Yoshimoto, T., and Ihara, M. (2021). A case of hemichorea in RNF213-related vasculopathy. *BMC Neurol.* 21:32. doi: 10.1186/s12883-021-02061-2067

Jin, Q., Noguchi, T., Irie, H., Kawashima, M., Nishihara, M., Takase, Y., et al. (2011). Assessment of moyamoya disease with 3.0-T magnetic resonance angiography and magnetic resonance imaging versus conventional angiography. *Neurol. Med. Chir. (Tokyo)* 51, 195–200. doi: 10.2176/nmc.51.195

Kamada, F., Aoki, Y., Narisawa, A., Abe, Y., Komatsuzaki, S., Kikuchi, A., et al. (2011). A genome-wide association study identifies RNF213 as the first Moyamoya disease gene. *J. Hum. Genet.* 56, 34–40. doi: 10.1038/jhg.2010.132

Kamimura, T., Okazaki, S., Morimoto, T., Kobayashi, H., Harada, K., Tomita, T., et al. (2019). Prevalence of RNF213 p.R4810K variant in early-onset stroke with

intracranial arterial stenosis. *Stroke* 50, 1561–1563. doi: 10.1161/strokeaha.118.024712

Koizumi, A., Kobayashi, H., Hitomi, T., Harada, K. H., Habu, T., Youssefian, S., et al. (2016). A new horizon of moyamoya disease and associated health risks explored through RNF213. *Environ. Health Prev. Med.* 21, 55–70. doi: 10.1007/s12199-015-0498-7

Koizumi, A., Kobayashi, H., Liu, W., Fujii, Y., Senevirathna, S. T. M. L. D., Nanayakkara, S., et al. (2013). P.R4810K, a polymorphism of RNF213, the susceptibility gene for moyamoya disease, is associated with blood pressure. *Environ. Health Prev. Med.* 18, 121–129. doi: 10.1007/s12199-012-0299-1

Komiyama, M. (2017a). Cardio-cephalic neural crest syndrome: a novel hypothesis of vascular neurocristopathy. *Interv. Neuroradiol.* 23, 572–576. doi: 10.1177/1591019917726093

Komiyama, M. (2017b). Moyamoya disease is a vascular form of neurocristopathy: disease of the embryologic cephalic neural crest. *Childs Nerv. Syst.* 33, 567–568. doi: 10.1007/s00381-017-3369-2

Kondori, B. J., Azemati, F., and Dadseresht, S. (2017). Magnetic resonance angiographic study of anatomic variations of the circle of Willis in a population in Tehran. *Arch. Iran. Med.* 20, 235–239.

Liu, W., Morito, D., Takashima, S., Mineharu, Y., Kobayashi, H., Hitomi, Y., et al. (2011). Identification of RNF213 as a susceptibility gene for moyamoya disease and its possible role in vascular development. *PLoS One* 6:e22542. doi: 10.1371/journal.pone.0022542

Matsuda, Y., Mineharu, Y., Kimura, M., Takagi, Y., Kobayashi, H., Hitomi, T., et al. (2017). RNF213 p.R4810K variant and intracranial arterial stenosis or occlusion in relatives of patients with Moyamoya disease. *J. Stroke Cerebrovasc. Dis.* 26, 1841–1847. doi: 10.1016/j.jstrokecerebrovasdis.2017.04.019

Merkkola, P., Tulla, H., Ronkainen, A., Soppi, V., Oksala, A., Koivisto, T., et al. (2006). Incomplete circle of Willis and right axillary artery perfusion. *Ann. Thorac. Surg.* 82, 74–80. doi: 10.1016/j.athoracsur.2006.02.034

Miyawaki, S., Imai, H., Takayanagi, S., Mukasa, A., Nakatomi, H., and Saito, N. (2012). Identification of a genetic variant common to moyamoya disease and intracranial major artery stenosis/occlusion. *Stroke* 43, 3371–3374. doi: 10.1161/STROKEAHA.112.663864

Morito, D., Nishikawa, K., Hoseki, J., Kitamura, A., Kotani, Y., Kiso, K., et al. (2014). Moyamoya disease-associated protein mysterin/RNF213 is a novel AAA+ ATPase, which dynamically changes its oligomeric state. *Sci. Rep.* 4:4442. doi: 10.1038/srep04442

Okazaki, S., Morimoto, T., Kamatani, Y., Kamimura, T., Kobayashi, H., Harada, K., et al. (2019). Moyamoya disease susceptibility variant RNF213 p.R4810K increases the risk of ischemic stroke attributable to large-artery atherosclerosis. *Circulation* 139, 295–298. doi: 10.1161/CIRCULATIONAHA.118.038439

Research Committee on the Pathology, and Treatment of Spontaneous Occlusion of the Circle of Willis, and Health Labour Sciences Research Grant for Research on Measures for Intractable Diseases (2012). Guidelines for the diagnosis and treatment of Moyamoya disease (spontaneous occlusion of the circle of Willis). *Neurol. Med. Chir. (Tokyo)* 52, 245–266. doi: 10.2176/nmc.52.245

Roher, A. E., Esh, C., Kokjohn, T. A., Kalback, W., Luehrs, D. C., Seward, J. D., et al. (2003). Circle of Willis Atherosclerosis is a risk factor for sporadic Alzheimer's disease. *Arterioscler. Thromb. Vasc. Biol.* 23, 2055–2062. doi: 10.1161/01.ATV.0000095973.42032.44

Song, P., Qin, J., Yu, Y., Shi, C., Qiao, P., Xie, A., et al. (2019). Comparative performance of magnetic resonance angiography and digital subtraction angiography in vessel involvement of pediatric moyamoya disease. *Iran. J. Radiol.* 16:e5559. doi: 10.5812/iranjradiol.55595

Yoshimoto, T., Inoue, M., Tanaka, K., Kanemaru, K., Koge, J., Shiozawa, M., et al. (2021). Identifying large ischemic core volume ranges in acute stroke that can benefit from mechanical thrombectomy. *J. NeuroInterv. Surg.* doi: 10.1136/neurintsurg-2020-016934 (in press).

Conflict of Interest: The authors declare that the research was conducted in the absence of any commercial or financial relationships that could be construed as a potential conflict of interest.

frontiers in Aging Neuroscience

ORIGINAL RESEARCH
published: 25 August 2021
doi: 10.3389/fnagi.2021.672548

Urinary 8-OxoGsn as a Potential Indicator of Mild Cognitive Impairment in Frail Patients With Cardiovascular Disease

Si-Min Yao[1,2], Pei-Pei Zheng[1,2], Wei He[1], Jian-Ping Cai[3], Hua Wang[1]* and Jie-Fu Yang[1]**

[1] Department of Cardiology, Beijing Hospital, National Center of Gerontology, Institute of Geriatric Medicine, Chinese Academy of Medical Sciences, Beijing, China, [2] Department of Cardiology, Peking University Fifth School of Clinical Medicine. No. 1, Beijing, China, [3] MOH Key Laboratory of Geriatrics, Beijing Hospital, National Center of Gerontology, Beijing, China

Oxidative RNA damage has been found to be associated with age-related diseases and 8-oxo-7,8-dihydroguanosine (8-oxoGsn) is a typical marker of oxidative modification of RNA. Urine tests are a feasible non-invasive diagnostic modality. The present study aimed to assess whether the measurement of urinary 8-oxoGsn could represent a potential early maker in mild cognitive impairment (MCI) of frail patients with cardiovascular disease (CVD). In this cross-sectional study performed in China from September 2018 to February 2019. Urinary 8-oxoGsn was measured in frail (Fried phenotype: 3–5) in patients with CVD and was adjusted by urinary creatinine (Cre) levels. Cognitive function was assessed by the Chinese version of the Mini-Mental State Examination (MMSE) and participants were classified into non-MCI (≥24) and MCI (<24) groups. Univariate and multivariate logistic regression models were used to determine the relationship between 8-oxoGsn/Cre and MCI. Receiver operating characteristic (ROC) curve analysis was used to assess the 8-oxoGsn/Cre ratio in relation to MCI in frail patients with CVD. A total of 106 elderly patients were enrolled in this study. The mean age of participants was 77.9 ± 6.8 years, the overall prevalence of MCI was 22.6% (24/106), and 57.5% (61/106) of participants were women. In the multivariate logistic regression analysis, urinary 8-oxoGsn/Cre was independently associated with MCI (odds ratio [OR] = 1.769, 95% confidence interval [CI] = 1.234–2.536, $P = 0.002$), after adjusting for age, sex, education level, marital status, and serum prealbumin levels. The area under the ROC curve was 0.786 (0.679–0.893) ($P < 0.001$), and the optimal cut-off value was 4.22 μmol/mol. The urinary 8-oxoGsn/Cre ratio showed a sensitivity of 87.5% and a specificity of 69.5%. The present study suggests the urinary 8-oxoGsn/Cre ratio may be a useful indicator for the early screening of MCI in frail patients with CVD.

Clinical Trial Registration: ChiCTR1800017204; date of registration: 07/18/2018. URL: http://www.chictr.org.cn/showproj.aspx?proj=28931.

Keywords: oxidative stress, 8-oxoGsn, mild cognitive impairment, frailty, cardiovascular disease

OPEN ACCESS

Edited by:
Stefano Tarantini, University of Oklahoma Health Sciences Center, United States

Reviewed by:
Anja Hviid Simonsen, Copenhagen University Hospital, Rigshospitalet, Denmark
Paola Garcia-delaTorre, Mexican Social Security Institute (IMSS), Mexico

****Correspondence:***
Jian-Ping Cai
caijp61@vip.sina.com
Hua Wang
wanghua2764@bjhmoh.cn
Jie-Fu Yang
yangjiefu2011@126.com

Received: *26 February 2021*
Accepted: *04 August 2021*
Published: *25 August 2021*

Citation:
Yao S-M, Zheng P-P, He W, Cai J-P, Wang H and Yang J-F (2021) Urinary 8-OxoGsn as a Potential Indicator of Mild Cognitive Impairment in Frail Patients With Cardiovascular Disease. Front. Aging Neurosci. 13:672548. doi: 10.3389/fnagi.2021.672548

INTRODUCTION

Mild cognitive impairment (MCI) is a transition between normal aging and dementia, and is an early indicator of dementing disorders in adults (Lovell and Markesbery, 2008). Subjects with MCI have a 10-fold increased risk of developing Alzheimer's disease (AD) at a rate of 15% annually (Geda et al., 2013). Distinguishing between MCI individuals from individuals with no evidence of MCI (no-MCI) is an important task and requires a complete understanding of risk factors and biomarkers for early detection of MCI.

In older adults, frailty represents a state of increased vulnerability to stressor events and increases the risk of early mortality, disability, falls, and hospitalization (Fried et al., 2001). Frailty is common in patients with cardiovascular disease (CVD). However, there is a bidirectional link between frailty and CVD (Uchikado et al., 2020), whereby frailty is associated with an earlier onset of CVD, and conversely, the presence of CVD is associated with a greater incidence of frailty (Fernandes et al., 2020). These two states influence each other and worsen the prognosis of these patients. Frail patients have been associated with a significantly increased risk of developing vascular dementia, over other types of dementia, compared to non-frail participants (Robertson et al., 2013). Early detection of MCI can help to prevent vascular dementia in frail patients.

The most commonly used markers of frailty and MCI are those related to inflammatory, nutritional, vascular, and metabolic factors (Ma and Chan, 2020). In addition, frailty and cognitive decline are associated with oxidative stress, a pro-inflammatory environment leading to endothelial dysfunction, which further promotes the occurrence of the above two states (Lin and Beal, 2006; Ma and Chan, 2020).

We and other groups have found that oxidative stress contributes significantly to the pathogenesis and progression of AD (Shan and Lin, 2006; Dai et al., 2018), as well as other forms of dementia (Nunomura et al., 2004). Oxidative RNA damage can impair protein translation, and the damaged RNA can be prematurely degraded, further impairing the synthesis of essential proteins (Butterfield and Halliwell, 2019). The oxidative stress marker 8-oxo-7,8-dihydroguanosine (8-oxoGsn) can reliably be quantified in urine using an ultra-performance liquid chromatography-mass spectrometry (UPLC-MS/MS) assay and is a valid marker of RNA damage (Weimann et al., 2002). Levels of 8-oxoGsn may be associated with the pathogenesis of bipolar disorder (Knorr et al., 2019), which is a mental disorder characterized by recurrent relapses of affective episodes, cognitive impairment, and disease progression (Schneider et al., 2012). In a study of 5 patients with MCI, increased oxidative modification of RNA was found in neurons and was associated with early neurofibrillary tangles in the hippocampus/parahippocampal gyrus (Lovell and Markesbery, 2008). However, these examinations are invasive, as both require sampling of the cerebrospinal fluid and the hippocampus. In the realm of biomarker discovery, the urine is a popular matrix due to its non-invasive collection in humans and its availability in large quantities (Cook et al., 2020), it provides a precious clinical sample for early non-invasive disease diagnosis. If patients with MCI could be detected early by examination of urine, the burden on patients will be reduced.

Our previous study showed that urinary 8-oxoGsn is independently associated with frailty in elderly patients with CVD (Liang et al., 2020). However, only a few studies have investigated RNA oxidation and MCI in frail patients with CVD. The aim of this study was to assess whether 8-oxoGsn could represent a potential indicator for the MCI among frail patients with CVD.

Abbreviations: MCI, Mild cognitive impairment; AD, Alzheimer's disease; CVD, Cardiovascular disease; 8-oxoGsn, 8-oxo-7,8-dihydroguanosine; MMSE, Mini-Mental State Examination; UPLC-MS/MS, Ultra-performance liquid chromatography-mass spectrometry; NO-MCI, Non-mild cognitive impairment; Cre, Creatinine; OR, Odds ratio; CI, Confidence interval; ROC, Receiver operating characteristic curve; AUC, Area under the ROC curve.

MATERIALS AND METHODS

Study Design and Participants

This study was a prospective cross-sectional study performed in China, which included inpatients aged ≥65 years old admitted to the Department of Cardiology from September 2018 to February 2019. Baseline assessments were carried out by experienced and trained investigators. Written informed consent was obtained from all participants. This study conformed to the Declaration of Helsinki and was approved by the Ethics Committee of Beijing Hospital (No.2018BJYYEC-121-02).

Inclusion criteria included: (1) definite diagnosis of CVD; (2) frail patients: Fried phenotype ≥3; and (3) sufficient urine samples for analysis. Exclusion criterion consisted of patients with a definite diagnosis of dementia.

Initially, 542 individuals with CVD participated in the baseline study. We excluded 348 robust individuals and 64 pre-frail participants. Of these, 24 participants without fresh urine samples were excluded, including 1 patient with AD. Finally, this study enrolled 106 participants for the determination of whether 8-oxoGsn is a useful marker for MCI in frail patients with CVD. In the supplementary materials, we also analyzed the data of 390 non-frail patients with qualified urine samples in order to establish a control group to verify the main conclusions.

Assessment of Frailty

The Fried phenotype was used to assess frailty (Fried et al., 2001) and is based on five criteria: unintentional weight loss, self-reported exhaustion, weakness, slow walking speed, and low physical activity. Participants meeting three or more criteria were categorized as frail based on: (1) unintentional weight loss: weight decreased by >5% in the previous year; (2) self-reported exhaustion: feeling tired all of the time (at least 3 or 4 days per a week); (3) weakness: maximum grip strength of the dominant hand at ≤20% of the population distribution, adjusted for sex and body mass index; (4) slow walking speed: using the average of timed walk test over a 4-meter course, defined as walking 4-m at <0.65m/s (height ≤ 173 cm for men or ≤159 cm for women) or <0.76 m/s (height > 173 cm for men or >159 cm for women);

and (5) low physical activity: <383 kcal per week for men or <270 kcal per week for women.

Cognitive Function Assessment

Cognitive function was assessed by the Chinese version of the Mini-Mental State Examination (MMSE) (An and Liu, 2016). The MMSE tests consists of 30 items within 6 dimensions: orientation, registration, attention, language, memory, and visual construction skills (Tsoi et al., 2015). The total MMSE score ranged from 0 to 30, with higher scores reflecting better cognitive function. We treated responses of "unable to understand and answer" as "wrong" (Lv et al., 2019). Participants were classified into non-MCI (NO-MCI, ≥24) and MCI (<24) groups using the cut-off score of 24.

Measurement of Urinary 8-OxoGsn, Creatinine and Prealbumin in All Patients

For this study, fresh midstream urine samples were obtained in the morning within 24 h after admission to hospital. All samples were coded at the moment of collection to ensure a blind study. Urine samples were stored at -80℃ until they were processed. The samples were thawed at 4℃, then after centrifugation at 7500 × *g* for 5 min to remove large particles, the supernatant was used for the analysis. Urinary 8-oxoGsn levels were determined by UPLC-MS/MS, as described elsewhere (Liang et al., 2020). Creatinine (Cre) concentrations were determined in urine samples using the MicroVue Creatinine EIA kit (Hitachi Koki; Tokyo, Japan). The results for 8-oxoGsn in urine were normalized for Cre. Prealbumin was measured with immunonephelometric assays on BN II system (Siemens Healthcare; Tarrytown, New York).

Statistical Analyses

The Kolmogorov-Smirnov test was used to verify whether continuous variables conformed to a normal distribution. Results were expressed as mean and standard deviation (normally distributed data) or median (interquartile range; non-normally distributed data). Categorical variables were expressed as numbers and percentages. The Student's *t*-test or Mann-Whitney test for continuous data and the Fisher's exact test or chi-square test for categorical data were used to identify statistical differences between the two groups. In our study, prealbumin was used to reflect nutritional status and high-sensitivity C-reactive protein was used to represent inflammatory state, which are commonly used markers of MCI. Univariate and multivariate logistic regression models were used to determine the relationship between the 8-oxoGsn/Cre ratio and MCI. Multivariate logistic regression was adjusted for age, sex, education level, marital status, and serum prealbumin levels (factors with a *P*-value < 0.10 in univariate analyses were entered into the multivariate model). Odds ratios (ORs) and 95% confidence intervals (CIs) were calculated in the results of the logistic regression models. Receiver operating characteristic (ROC) curve analysis was used considering the 8-oxoGsn/Cre ratio in relation to MCI in frail patients with CVD. The optimal cutoff point was calculated using the maximum value of the Youden Index (determined as sensitivity + [1-specificity]) (Schisterman et al., 2005). A *P*-value < 0.05 was considered statistically significant. All the data analyses were conducted using the IBM SPSS Statistics software program (version 24; IBM Corporation, Armonk, NY, United States). Graphs were created with GraphPad Prism version 7.0.0 for Windows (GraphPad Software San Diego, CA, United States).

RESULTS

The characteristics of the study population are presented in **Table 1**. Overall, a total of 106 elderly frail patients were enrolled in this study. The participants were classified into NO-MCI (n = 82) and MCI (n = 24) groups based on the MMSE scores. At baseline, the mean age of participants was 77.9 ± 6.8 years, 57.5% (61/106) of participants were women. Age (P < 0.001), sex (P = 0.003), education level (P < 0.001), and marital status (P = 0.007) showed statistically significant differences between groups. Among the five criteria of frailty, the MCI group had more patients exhibiting weakness (P = 0.029) compared to the NO-MCI group, no significant differences were observed regarding the proportion of individuals with unintentional weight loss (P = 0.183), self-reported exhaustion (P = 0.096), slow walking speed (P = 0.936), and low physical activity (P = 0.975). Furthermore, there were no differences in comorbidities or serum high sensitivity C-reactive protein levels among the two groups. Serum prealbumin was significantly higher in NO-MCI cases than in MCI cases (22.75 ± 5.11 vs. 19.04 ± 5.74 mg/dL; P = 0.003). Participants with MCI were more likely to have higher levels of urinary 8-oxoGsn/Cre [5.43 (4.39–6.38) vs. 3.60 (2.94–4.42) μmol/mol; P < 0.001] (**Figure 1**).

Three hundred and ninety non-frail patients with CVD were divided into two groups according to the MMSE. The characteristics of non-frail patients are shown in **Supplementary Table 1**. There was no difference in levels of urinary 8-oxoGsn/Cre between the two groups [NO-MCI: 3.20(2.48–4.14) μmol/mol vs. MCI: 3.69(3.10–4.54) μmol/mol, P = 0.186].

Univariate analysis demonstrated that age (P = 0.001), sex (P = 0.006), education level (P < 0.001), marital status (P = 0.009), serum prealbumin (P = 0.005), and urinary 8-oxoGsn/Cre (P = 0.005) were associated with MCI. To better explore the association between 8-oxoGsn/Cre and MCI, a multivariate logistic regression model was built. The urinary 8-oxoGsn/Cre ratio was independently associated with MCI (OR = 1.769, 95% CI = 1.234–2.536, P = 0.002), after adjusting for age, sex, education level, marital status, and serum prealbumin. Age (OR = 1.202, 95% CI = 1.045–1.383, P = 0.010) and education level (OR = 0.742, 95%CI = 0.621–0.886, P = 0.001) were independently associated with MCI in frail patients with CVD (**Table 2**). In non-frail patients, univariate logistic regression analysis demonstrated that urinary 8-oxoGsn/Cre was not associated with MCI in non-frail patients (OR = 1.152, 95%CI = 0.933–1.423, P = 0.189).

A ROC curve analysis was performed to estimate the diagnostic potential of urinary the 8-oxoGsn/Cre ratio for MCI. The area under the ROC curve (AUC) was 0.786 (0.679–0.893) (P < 0.001) (**Figure 2**). The optimal cut-off value of the

TABLE 1 | The baseline characteristics of study participants by cognitive function status.

	Overall (*n* = 106)	NO-MCI (*n* = 82)	MCI (*n* = 24)	*P*
Age, year	77.9 ± 6.8	76.7 ± 6.8	82.2 ± 5.2	<0.001
Sex, female (%)	61 (57.5)	41 (50.0)	20 (83.3)	0.003
Education level, year	10 (9–15)	12 (9–15)	6 (1–11)	<0.001
Married (%)	83 (78.3)	69 (84.1)	14 (58.3)	0.007
MMSE	28 (24–29)	28 (27–29)	20 (13–23)	<0.001
Unintentional weight loss (%)	34 (32.1)	29 (35.4)	5 (20.8)	0.183
Self-reported exhaustion (%)	94 (88.7)	75 (91.5)	19 (79.2)	0.096
Weakness (%)	85 (80.2)	62 (75.6)	23 (95.8)	0.029
Slow walking speed (%)	88 (83.0)	68 (82.9)	20 (83.3)	0.963
Low physical activity (%)	97 (91.5)	75 (91.5)	22 (91.7)	0.975
Prealbumin, mg/dL	21.90 ± 5.46	22.75 ± 5.11	19.04 ± 5.74	0.003
High sensitivity C-reactive protein, mg/L	1.28 (0.58–4.68)	1.14 (0.54–4.50)	1.70 (0.59–11.23)	0.269
Coronary artery disease (%)	59 (55.7)	45 (54.9)	14 (58.3)	0.767
Hypertension (%)	79 (74.5)	60 (73.2)	19 (79.2)	0.558
Heart failure (%)	22 (20.8)	16 (19.5)	6 (25.0)	0.564
Atrial fibrillation (%)	36 (34.0)	26 (31.7)	10 (41.7)	0.370
Diabetes (%)	45 (42.5)	38 (46.3)	17 (70.8)	0.137
Previous stroke (%)	25 (23.6)	16 (19.5)	9 (37.5)	0.069
Obesity (%)	23 (21.7)	19 (23.2)	4 (16.7)	0.501

NO-MCI, Non-mild cognitive impairment; MCI, mild cognitive impairment;
MMSE, Mini-Mental State Examination; Cre, creatinine.
Values are shown as mean ± standard deviation or median (interquartile range) or n (%).

urinary 8-oxoGsn/Cre ratio by the maximal Youden index was 4.22 μmol/mol. It showed a sensitivity of 87.5% and a specificity of 69.5%. Its positive predictive and negative predictive values were 74.2% and 84.8%, respectively, and its positive likelihood ratio and negative likelihood ratio were 2.87 and 0.18.

DISCUSSION

In this cross-sectional study, we reported the overall prevalence of MCI among frail patients with CVD was 22.6%, which was similar to previous findings (Petersen et al., 2010). We confirmed that urinary 8-oxoGsn/Cre ratios were significantly higher in MCI patients compared to patients with no evidence of MCI. We determined that urinary 8-oxoGsn/Cre could independently and effectively evaluate MCI in frail patients with CVD.

The oxidative modifications of RNA can be measured by urinary 8-oxoGsn levels (Larsen et al., 2019), which is the focus of the present study. The use of feasible and reliable biomarkers to identify patients with MCI is a challenge that needs to be addressed. Such indicators would provide a more accurate detection of dementia in early disease stages, when cognitive decline can still be potentially reverted. Individuals with MCI have shown alterations in the antioxidant system, which is designed to counteract the potentially hazardous reactions initiated by oxidative stress (Stephan et al., 2012). Nucleic acids are constantly oxidized within the cell and nuclear DNA is double stranded and is complexed with protective proteins. Pena-Bautista et al. showed that the DNA oxidation marker 8-hydroxy-2′-deoxyguanosine was able to distinguish between AD and healthy participants (Pena-Bautista et al., 2019). However, RNA is more vulnerable to oxidative stress than DNA because it is single-stranded and lacks protective histones (Liu et al., 2016). RNA damage is a valid marker that may provide useful information for early identification of MCI.

Accurate and early detection of oxidative modification markers indicative of chronic disease progression can provide useful diagnostic information. MCI reflects the transition between normal aging and dementia, and is the earliest clinical manifestation of AD. Perez et al. found that titanium dioxide nanoparticles induced strong oxidative stress in astrocytes, cells that play key roles in neuronal homeostasis and their dysfunction can lead to MCI (Perez-Arizti et al., 2020). Keller

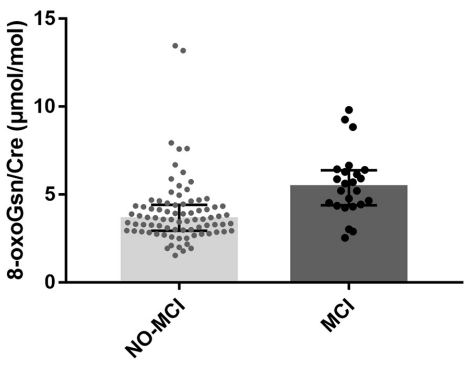

FIGURE 1 | Boxplot for 8-oxoGsn/Cre in the urine samples of NO-MCI and MCI individuals. Error bars represent median with interquartile distance. 8-oxoGsn, 8-oxo-7,8-dihydroguanosine; Cre, creatinine; NO-MCI, Non-mild cognitive impairment; MCI, mild cognitive impairment.

TABLE 2 | Univariate and multivariate logistic regression.

Variables	Univariate analysis				Multivariate analysis			
	OR	95% CI		*P*	OR	95% CI		*P*
		Lower	Upper			Lower	Upper	
Age, year	1.144	1.056	1.240	0.001	1.202	1.045	1.383	0.010
Female	5.000	1.570	15.910	0.006	0.290	0.059	1.424	0.127
Higher level of education, year	0.724	0.626	0.836	<0.001	0.742	0.621	0.886	0.001
Married	0.264	0.097	0.720	0.009	1.013	0.194	5.281	0.988
Unintentional weight loss	0.481	0.163	1.422	0.186	-	-	-	-
Self-reported exhaustion	1.027	0.199	5.302	0.975	-	-	-	-
Weakness	7.419	0.941	58.480	0.057	-	-	-	-
Slow walking speed	1.029	0.305	3.480	0.963	-	-	-	-
Low physical activity	0.355	0.101	1.242	0.105	-	-	-	-
8-oxoGsn/Cre, μmol/mol	1.415	1.112	1.800	0.005	1.769	1.234	2.536	0.002
Prealbumin, mg/dL	0.876	0.798	0.962	0.005	0.904	0.793	1.031	0.133
High sensitivity C-reactive protein, mg/L	1.018	0.979	1.059	0.362	-	-	-	-
Coronary artery disease	1.151	0.458	2.891	0.765	-	-	-	-
Hypertension	1.393	0.464	4.184	0.554	-	-	-	-
Heart failure	1.375	0.470	4.022	0.561	-	-	-	-
Atrial fibrillation	1.538	0.604	3.920	0.367	-	-	-	-
Diabetes	0.477	0.179	1.272	0.139	-	-	-	-
Previous stroke	2.475	0.919	6.665	0.073	-	-	-	-
Obesity	0.663	0.202	2.179	0.499	-	-	-	-

OR, odds ratio; CI, confidence interval; 8-oxoGsn, 8-oxo-7,8-dihydroguanosine; Cre, creatinine.

et al. showed significantly increased protein carbonyl formation and increased levels of lipid peroxidation in the temporal lobe of MCI subjects compared to healthy subjects (Keller et al., 2005). Ding et al. showed significantly elevated 8-hydroxyguanine immunoreactivity in the inferior parietal lobule of subjects early in disease progression (Ding et al., 2006).

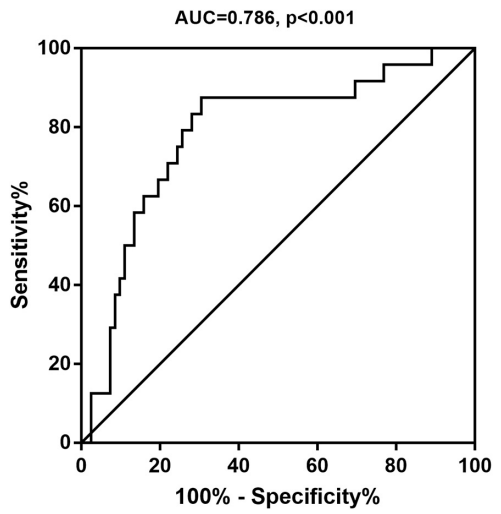

FIGURE 2 | Receiver operating characteristic curve for the 8-oxoGsn/Cre to predict MCI. 8-oxoGsn, 8-oxo-7,8-dihydroguanosine; Cre, creatinine; MCI, mild cognitive impairment; AUC, areas under the curve.

Our findings suggest that an increase in the urinary 8-oxoGsn/Cre ratio may be a useful indicator for the early screening of MCI in frail patients with CVD. Previous studies on oxidative stress and cognitive impairment have mainly focused on brain tissue and cerebrospinal fluid rather than on urine samples. Nunomura et al. suggested that RNA oxidation is a prominent feature of neuronal vulnerability in patients with AD (Nunomura et al., 1999) and dementia (Nunomura et al., 2002). Our previous study found that the presence of large amounts of 8-oxoGsn in the RNA could promote the secretion of pathogenic amyloid-β peptides *in vivo* (Dai et al., 2018), and this mechanism could contribute to the accumulation of amyloid-β plaques as is observed in the brains of AD patients. Lovell et al. described the presence of increased RNA oxidative modifications in neurons undergoing early neurofibrillary tangle formation in the hippocampus/parahippocampal gyrus of MCI and late-stage AD subjects (Lovell and Markesbery, 2008). Further, the levels of RNA oxidative damage observed in MCI were comparable to those observed in late-stage AD (Lovell and Markesbery, 2008).

The usual risk factors associated with conversion of individuals from cognitively normal status into dementia and AD are also possible risk factors for transitions into MCI (Kryscio et al., 2006). Our findings showing that age and education levels were independently associated with MCI are consistent with the current literature (O'Bryant et al., 2013; Wong et al., 2019). It is estimated that between 10 and 30% of all adults aged 65 and above experience MCI (Geda et al., 2013). In a longitudinal study at the University of Kentucky AD Center, it was shown that age affected the ORs of individuals transitioning

to MCI as well as that of onset of dementia or death (Kryscio et al., 2006). In an analysis of six international longitudinal studies, a higher education level was associated with a lower risk of transitioning from MCI in individuals with no prior evidence of MCI. Furthermore, those with a higher level of education and socioeconomic status experienced longer non-impaired life expectancies (Robitaille et al., 2018).

Cardiovascular risk factors and diseases are recognized as predictors of age-related cognitive decline and dementia (Sahathevan et al., 2012). MCI is an important under-researched complication of stroke and transient ischemic attack (Drozdowska et al., 2020). However, it is important to note that no clear correlation between cardiovascular risk factors or diseases and MCI was identified in our study. Nonetheless, these findings were not consistent with our hypothesis. One possible reason for this inconsistency may be that we excluded patients with dementia from our study, and only patients with mild cognitive decline were enrolled, and thus there was an insufficient number of cases with CVD to detect early changes in cognitive function. Second, previous studies have found that some forms of CVD and risk factors, such as heart failure (Yao et al., 2020), coronary artery disease (Ma et al., 2020), stroke (Chumha et al., 2020), atrial fibrillation (Guo et al., 2020), and obesity (Chan et al., 2020), are significantly associated with frailty, thus the relationship between CVDs or risk factors and MCI may be weakened in frail patients. Further research on CVDs and MCI in frail patients should be performed in the future.

The strengths of the current study include the analysis of oxidized nucleosides using UPLC-MS/MS, which is considered the reference standard method due to high specificity toward the RNA forms.

Our study has several limitations. First, the small sample size hampers the generalizability of our findings. Second, our cross-sectional study did not allow to draw any causative conclusions, nor could it identify risk factors associated with MCI. A long-term follow-up study in this population is currently being conducted by our group, which will verify whether these patients develop dementia in the future. Third, we studied the frail patients with CVD, which is a specific part of the population, and the results were not validated in the general population. Lastly, MMSE is a screening tool to identify MCI but it is not a diagnostic tool; thus, we failed to conduct a detailed subgroup analysis of patients with stratified by cognitive level. Nonetheless, the MMSE is the most widely used tool for evaluating MCI and is supported by a high degree of popularization and application.

In conclusion, the present study suggests the urinary 8-oxoGsn/Cre ratio may be a useful indicator for the early screening of MCI in frail patients with CVD. This indicator will enhance our understanding of the underlying pathological processes causative of MCI and the potential risk factors for early dementia progression. With the aging population, the number of frail patients with CVD may continue to increase. Early recognition of cognitive dysfunction and early intervention may help to improve the quality of life and prognosis of these patients.

DATA AVAILABILITY STATEMENT

The original contributions presented in the study are included in the article/**Supplementary Material**, further inquiries can be directed to the corresponding authors.

ETHICS STATEMENT

The study involving human participants was reviewed and approved by the Ethics Committee of Beijing Hospital, China (ID number: 2018BJYYEC-121-02), the version date of the protocol approved by ethics is September 18, 2018, and the version number is 1.0. The patients/participants provided their written informed consent to participate in this study.

AUTHOR CONTRIBUTIONS

HW, J-FY, and J-PC designed the research. S-MY and P-PZ contributed to the development of the conceptualization and methodology and wrote the manuscript. WH and S-MY analyzed data. All of the authors read the draft, made contributions, and approved the final manuscript.

FUNDING

This work was supported by the Beijing Municipal Science and Technology Commission (D181100000218003) and the Non-profit Central Research Institute Fund of Chinese Academy of Medical Sciences (No. 2019PT320013).

ACKNOWLEDGMENTS

We thank all study participants for their collaboration.

SUPPLEMENTARY MATERIAL

The Supplementary Material for this article can be found online at: https://www.frontiersin.org/articles/10.3389/fnagi.2021.672548/full#supplementary-material

REFERENCES

An, R., and Liu, G. G. (2016). Cognitive impairment and mortality among the oldest-old Chinese. *Int. J. Geriatr. Psychiatry* 31, 1345–1353. doi: 10.1002/gps.4442

Butterfield, D. A., and Halliwell, B. (2019). Oxidative stress, dysfunctional glucose metabolism and Alzheimer disease. *Nat. Rev. Neurosci.* 20, 148–160. doi: 10.1038/s41583-019-0132-6

Chan, G. C., Jack Kit-Chung, N. G., Chow, K. M., Kwong, V. W., Pang, W. F., et al. (2020). Interaction between central obesity and frailty on the clinical outcome

of peritoneal dialysis patients. *PLoS One* 15:e241242. doi: 10.1371/journal.pone.0241242

Chumha, N., Funsueb, S., Kittiwachana, S., Rattanapattanakul, P., and Lerttrakarnnon, P. (2020). An artificial neural network model for assessing Frailty-associated factors in the thai population. *Int. J. Environ. Res. Public Health* 17:6808. doi: 10.3390/ijerph17186808

Cook, T., Ma, Y., and Gamagedara, S. (2020). Evaluation of statistical techniques to normalize mass spectrometry-based urinary metabolomics data. *J. Pharm. Biomed. Anal.* 177:112854. doi: 10.1016/j.jpba.2019.112854

Dai, D. P., Gan, W., Hayakawa, H., Zhu, J. L., Zhang, X. Q., et al. (2018). Transcriptional mutagenesis mediated by 8-oxoG induces translational errors in mammalian cells. *Proc. Natl. Acad. Sci. U.S.A.* 115, 4218–4222. doi: 10.1073/pnas.1718363115

Ding, Q., Markesbery, W. R., Cecarini, V., and Keller, J. N. (2006). Decreased RNA, and increased RNA oxidation, in ribosomes from early Alzheimer's disease. *Neurochem. Res.* 31, 705–710. doi: 10.1007/s11064-006-9071-5

Drozdowska, B. A., Elliott, E., Taylor-Rowan, M., Shaw, R. C., Cuthbertson, G., et al. (2020). Cardiovascular risk factors indirectly affect acute post-stroke cognition through stroke severity and prior cognitive impairment: a moderated mediation analysis. *Alzheimers Res. Ther.* 12:85. doi: 10.1186/s13195-020-00653-y

Fernandes, J., Gomes, C., Guerra, R. O., Pirkle, C. M., Vafaei, A., et al. (2020). Frailty syndrome and risk of cardiovascular disease: analysis from the international mobility in aging study. *Arch. Gerontol. Geriatr.* 92:104279. doi: 10.1016/j.archger.2020.104279

Fried, L. P., Tangen, C. M., Walston, J., Newman, A. B., Hirsch, C., et al. (2001). Frailty in older adults: evidence for a phenotype. *J. Gerontol. Biol. Sci. Med. Sci.* 56, M146–M156. doi: 10.1093/gerona/56.3.m14

Geda, Y. E., Ragossnig, M., Roberts, L. A., Roberts, R. O., Pankratz, V. S., et al. (2013). Caloric intake, aging, and mild cognitive impairment: a population-based study. *J. Alzheimers Dis.* 34, 501–507. doi: 10.3233/JAD-121270

Guo, Q., Du, X., and Ma, C. S. (2020). Atrial fibrillation and frailty. *J. Geriatr. Cardiol.* 17, 105–109. doi: 10.11909/j.issn.1671-5411.2020.02.007

Keller, J. N., Schmitt, F. A., Scheff, S. W., Ding, Q., Chen, Q., et al. (2005). Evidence of increased oxidative damage in subjects with mild cognitive impairment. *Neurology* 64, 1152–1156. doi: 10.1212/01.WNL.0000156156.13641.BA

Knorr, U., Simonsen, A. H., Roos, P., Weimann, A., Henriksen, T., et al. (2019). Cerebrospinal fluid oxidative stress metabolites in patients with bipolar disorder and healthy controls: A longitudinal case-control study. *Transl. Psychiatry* 9:325. doi: 10.1038/s41398-019-0664-6

Kryscio, R. J., Schmitt, F. A., Salazar, J. C., Mendiondo, M. S., and Markesbery, W. R. (2006). Risk factors for transitions from normal to mild cognitive impairment and dementia. *Neurology* 66, 828–832. doi: 10.1212/01.wnl.0000203264.71880.45

Larsen, E. L., Weimann, A., and Poulsen, H. E. (2019). Interventions targeted at oxidatively generated modifications of nucleic acids focused on urine and plasma markers. *Free Radic. Biol. Med.* 145, 256–283. doi: 10.1016/j.freeradbiomed.2019.09.030

Liang, Y. D., Liu, Q., Du, M. H., Liu, Z., Yao, S. M., et al. (2020). Urinary 8-oxo-7,8-dihydroguanosine as a potential biomarker of frailty for elderly patients with cardiovascular disease. *Free Radic. Biol. Med.* 152, 248–254. doi: 10.1016/j.freeradbiomed.2020.03.011

Lin, M. T., and Beal, M. F. (2006). Mitochondrial dysfunction and oxidative stress in neurodegenerative diseases. *Nature* 443, 787–795. doi: 10.1038/nature05292

Liu, X., Gan, W., Zou, Y., Yang, B., Su, Z., et al. (2016). Elevated levels of urinary markers of oxidative DNA and RNA damage in type 2 diabetes with complications. *Oxid. Med. Cell Longev* 2016:4323198. doi: 10.1155/2016/4323198

Lovell, M. A., and Markesbery, W. R. (2008). Oxidatively modified RNA in mild cognitive impairment. *Neurobiol. Dis.* 29, 169–175. doi: 10.1016/j.nbd.2007.07.030

Lv, X., Li, W., Ma, Y., Chen, H., Zeng, Y., et al. (2019). Cognitive decline and mortality among community-dwelling Chinese older people. *BMC Med.* 17:63. doi: 10.1186/s12916-019-1295-8

Ma, L., and Chan, P. (2020). Understanding the physiological links between physical frailty and cognitive decline. *Aging Dis.* 11, 405–418. doi: 10.14336/AD.2019.0521

Ma, L., Chhetri, J. K., Liu, P., Ji, T., Zhang, L., et al. (2020). Epidemiological characteristics and related factors of frailty in older Chinese adults with hypertension: a population-based study. *J. Hypertens* 38, 2192–2197. doi: 10.1097/HJH.0000000000002650

Nunomura, A., Chiba, S., Kosaka, K., Takeda, A., Castellani, R. J., et al. (2002). Neuronal RNA oxidation is a prominent feature of dementia with Lewy bodies. *Neuroreport* 13, 2035–2039. doi: 10.1097/00001756-200211150-00009

Nunomura, A., Chiba, S., Lippa, C. F., Cras, P., Kalaria, R. N., et al. (2004). Neuronal RNA oxidation is a prominent feature of familial Alzheimer's disease. *Neurobiol. Dis.* 17, 108–113. doi: 10.1016/j.nbd.2004.06.003

Nunomura, A., Perry, G., Pappolla, M. A., Wade, R., Hirai, K., et al. (1999). RNA oxidation is a prominent feature of vulnerable neurons in Alzheimer's disease. *J. Neurosci.* 19, 1959–1964. doi: 10.1523/jneurosci.19-06-01959.1999

O'Bryant, S. E., Johnson, L., Reisch, J., Edwards, M., Hall, J., et al. (2013). Risk factors for mild cognitive impairment among Mexican Americans. *Alzheimers Dement* 9, 622–631. doi: 10.1016/j.jalz.2012.12.007

Pena-Bautista, C., Tirle, T., Lopez-Nogueroles, M., Vento, M., Baquero, M., et al. (2019). Oxidative damage of DNA as early marker of Alzheimer's disease. *Int. J. Mol. Sci.* 20, 6136. doi: 10.3390/ijms20246136

Perez-Arizti, J. A., Ventura-Gallegos, J. L., Galvan, J. R., Ramos-Godinez, M., Colin-Val, Z., et al. (2020). Titanium dioxide nanoparticles promote oxidative stress, autophagy and reduce NLRP3 in primary rat astrocytes. *Chem. Biol. Interact.* 317:108966. doi: 10.1016/j.cbi.2020.108966

Petersen, R. C., Roberts, R. O., Knopman, D. S., Geda, Y. E., Cha, R. H., et al. (2010). Prevalence of mild cognitive impairment is higher in men. The mayo clinic study of Aging. *Neurology* 75, 889–897. doi: 10.1212/WNL.0b013e3181f11d85

Robertson, D. A., Savva, G. M., and Kenny, R. A. (2013). Frailty and cognitive impairment–a review of the evidence and causal mechanisms. *Ageing Res. Rev.* 12, 840–851. doi: 10.1016/j.arr.2013.06.004

Robitaille, A., van den Hout, A., Machado, R., Bennett, D. A., Cukic, I., et al. (2018). Transitions across cognitive states and death among older adults in relation to education: a multistate survival model using data from six longitudinal studies. *Alzheimers Dement* 14, 462–472. doi: 10.1016/j.jalz.2017.10.003

Sahathevan, R., Brodtmann, A., and Donnan, G. A. (2012). Dementia, stroke, and vascular risk factors; a review. *Int. J. Stroke* 7, 61–73. doi: 10.1111/j.1747-4949.2011.00731.x

Schisterman, E. F., Perkins, N. J., Liu, A., and Bondell, H. (2005). Optimal cut-point and its corresponding Youden Index to discriminate individuals using pooled blood samples. *Epidemiology* 16, 73–81. doi: 10.1097/01.ede.0000147512.81966.ba

Schneider, M. R., DelBello, M. P., McNamara, R. K., Strakowski, S. M., and Adler, C. M. (2012). Neuroprogression in bipolar disorder. *Bipolar Disord.* 14, 356–374. doi: 10.1111/j.1399-5618.2012.01024.x

Shan, X., and Lin, C. L. (2006). Quantification of oxidized RNAs in Alzheimer's disease. *Neurobiol. Aging* 27, 657–662. doi: 10.1016/j.neurobiolaging.2005.03.022

Stephan, B. C., Hunter, S., Harris, D., Llewellyn, D. J., Siervo, M., et al. (2012). The neuropathological profile of mild cognitive impairment (MCI): a systematic review. *Mol. Psychiatry* 17, 1056–1076. doi: 10.1038/mp.2011.147

Tsoi, K. K., Chan, J. Y., Hirai, H. W., Wong, S. Y., and Kwok, T. C. (2015). Cognitive tests to detect dementia: a systematic review and meta-analysis. *JAMA Intern. Med.* 175, 1450–1458. doi: 10.1001/jamainternmed.2015.2152

Uchikado, Y., Ikeda, Y., and Ohishi, M. (2020). Current understanding of the role of frailty in cardiovascular disease. *Circ. J.* 84, 1903–1908. doi: 10.1253/circj.CJ-20-0594

Weimann, A., Belling, D., and Poulsen, H. E. (2002). Quantification of 8-oxo-guanine and guanine as the nucleobase, nucleoside and deoxynucleoside forms in human urine by high-performance liquid chromatography-electrospray tandem mass spectrometry. *Nucleic Acids Res.* 30:E7. doi: 10.1093/nar/30.2.e7

Wong, M., Tan, C. S., Venketasubramanian, N., Chen, C., Ikram, M. K., et al. (2019). Prevalence and risk factors for cognitive impairment and dementia in indians: a multiethnic perspective from a singaporean study. *J. Alzheimers Dis.* 71, 341–351. doi: 10.3233/JAD-190610

Yao, S. M., Zheng, P. P., Liang, Y. D., Wan, Y. H., Sun, N., et al. (2020). Predicting non-elective hospital readmission or death using a composite assessment of cognitive and physical frailty in elderly inpatients with cardiovascular disease. *BMC Geriatr.* 20:218. doi: 10.1186/s12877-020-01606-8

Conflict of Interest: The authors declare that the research was conducted in the absence of any commercial or financial relationships that could be construed as a potential conflict of interest.

Publisher's Note: All claims expressed in this article are solely those of the authors and do not necessarily represent those of their affiliated organizations, or those of the publisher, the editors and the reviewers. Any product that may be evaluated in this article, or claim that may be made by its manufacturer, is not guaranteed or endorsed by the publisher.

frontiers in Aging Neuroscience

ORIGINAL RESEARCH
published: 31 August 2021
doi: 10.3389/fnagi.2021.599724

The Association Between Perivascular Spaces and Cerebral Blood Flow, Brain Volume, and Cardiovascular Risk

Sirui Liu[1], Bo Hou[1], Hui You[1], Yiwei Zhang[1], Yicheng Zhu[2], Chao Ma[3], Zhentao Zuo[4,5] and Feng Feng[1]**

[1] Department of Radiology, Peking Union Medical College Hospital, Chinese Academy of Medical Sciences and Peking Union Medical College, Beijing, China, [2] Department of Neurology, Peking Union Medical College Hospital, Chinese Academy of Medical Sciences and Peking Union Medical College, Beijing, China, [3] Department of Human Anatomy, Histology and Embryology, School of Basic Medicine, Peking Union Medical College, Beijing, China, [4] State Key Laboratory of Brain and Cognitive Science, Institute of Biophysics, Chinese Academy of Sciences, Beijing, China, [5] Sino-Danish College, University of Chinese Academy of Sciences, Chinese Academy of Sciences, Beijing, China

Background: Basal ganglia perivascular spaces are associated with cognitive decline and cardiovascular risk factors. There is a lack of studies on the cardiovascular risk burden of basal ganglia perivascular spaces (BG-PVS) and their relationship with gray matter volume (GMV) and GM cerebral blood flow (CBF) in the aging brain. Here, we investigated these two issues in a large sample of cognitively intact older adults.

Methods: A total of 734 volunteers were recruited. MRI was performed with 3.0 T using a pseudo-continuous arterial spin labeling (pCASL) sequence and a sagittal isotropic T1-weighted sequence for CBF and GMV analysis. The images obtained from 406 participants were analyzed to investigate the relationship between the severity of BG-PVS and GMV/CBF. False discovery rate-corrected *P*-values (P_{FDR}) of <0.05 were considered significant. The images obtained from 254 participants were used to study the relationship between the severity of BG-PVS and cardiovascular risk burden. BG-PVS were rated using a 5-grade score. The severity of BG-PVS was classified as mild (grade <3) and severe (grade ≥ 3). Cardiovascular risk burden was assessed with the Framingham General Cardiovascular Risk Score (FGCRS).

Results: Severe basal ganglia perivascular spaces were associated with significantly smaller GMV and CBF in multiple cortical regions (P_{FDR} <0.05), and were associated with significantly larger volume in the bilateral caudate nucleus, pallidum, and putamen (P_{FDR} <0.05). The participants with severe BG-PVS were more likely to have a higher cardiovascular risk burden than the participants with mild BG-PVS (60.71% vs. 42.93%; $P = 0.02$).

Conclusion: In cognitively intact older adults, severe BG-PVS are associated with smaller cortical GMV and CBF, larger subcortical GMV, and higher cardiovascular risk burden.

Keywords: enlarged perivascular spaces, basal ganglia, magnetic resonance imaging, cerebral blood flow, gray matter volume, cardiovascular risk burden

OPEN ACCESS

Edited by:
Stefano Tarantini, University of Oklahoma Health Sciences Center, United States

Reviewed by:
Helmet Karim, University of Pittsburgh, United States
Henk J. M. M. Mutsaerts, VU University Amsterdam, Netherlands
Junliang Yuan, Capital Medical University, China

***Correspondence:**
Zhentao Zuo
ztzuo@bcslab.ibp.ac.cn
Feng Feng
cjr.fengfeng@vip.163.com

Received: *28 August 2020*
Accepted: *26 July 2021*
Published: *31 August 2021*

Citation:
Liu S, Hou B, You H, Zhang Y, Zhu Y, Ma C, Zuo Z and Feng F (2021) The Association Between Perivascular Spaces and Cerebral Blood Flow, Brain Volume, and Cardiovascular Risk. Front. Aging Neurosci. 13:599724. doi: 10.3389/fnagi.2021.599724

INTRODUCTION

Perivascular spaces, also known as Virchow–Robin spaces, are interstitial fluid-filled spaces surrounding the wall of small penetrating vessels (Arbel-Ornath et al., 2013; Yakushiji et al., 2014). Accumulating evidence has shown that the severity of basal ganglia perivascular spaces (PVS) (BG-PVS) is associated with vascular abnormalities and vascular cognitive decline (Kalaria, 2012; Banerjee et al., 2017; Duperron et al., 2018). BG-PVS can also be observed in elderly individuals (Zhu et al., 2010). However, the significance in an aging brain remains poorly understood. In addition, the relationship between the severity of BG-PVS and regional gray matter volume (GMV) and gray matter cerebral blood flow (CBF) remains unclear. A community-based study (Zhu et al., 2010) revealed that PVS are not associated with visually inspected brain atrophy and does not yield brain volume quantification. Therefore, the relationship between BG-PVS and the quantified volume of different brain regions remains to be explored further. CBF, which reflect hemodynamic alterations, is an imaging biomarker for the identification of vulnerable brain regions. Since BG-PVS are considered to be caused by vascular abnormalities (Kress et al., 2014; Kyrtsos and Baras, 2015; Ramirez et al., 2016), it was hypothesized that individuals with BG-PVS could have alterations in CBF and GMV. Previous studies have shown that BG-PVS are associated with various cardiovascular risk factors (such as age, sex, hypertension, and arteriolosclerosis) (Zhu et al., 2010; Aribisala et al., 2014). It is well established that cardiovascular risk factors are interrelated, making it difficult to isolate their individual effects on BG-PVS. The Framingham General Cardiovascular Risk Score (FGCRS), which combines multiple cardiovascular risk factors with demographic data, can be used to assess cardiovascular risk burden (D'Agostino et al., 2008). However, to the best knowledge of the authors, studies that link BG-PVS with cardiovascular risk burden are lacking. Hence, this study extended the research mentioned above and carried out cross-sectional estimation of cognitively intact older adults to determine whether GMV and CBF are associated with the severity of BG-PVS. This study also aimed to evaluate the relationship between BG-PVS and cardiovascular risk burden.

MATERIALS AND METHODS

Participants

This study was approved by the institutional review board of Peking Union Medical College Hospital (PUMCH), and a written informed consent was obtained from all the participants, who were recruited from two ongoing cohort studies (cohort A and cohort B). Cohort A is a community-based study that comprises elderly subjects from Beijing, China. Cohort B is a large-scale willed body donation program in the Chinese Academy of Medical Sciences and PUMCH (Zhang et al., 2018).

Figure 1 shows the flowchart of participant enrollment. This cross-sectional study included 734 participants (n = 301 for cohort A and n = 433 for cohort B). The exclusion criteria of participants were as follows: (1) under 55 years old; (2) a Mini-Mental State Exam (MMSE) score of <27 who might have apparent cortical hypoperfusion and atrophy (Schuff et al., 2009; Gao et al., 2013; Sun et al., 2016; Ten Kate et al., 2018); (3) an unavailable MMSE score; (4) left-handed participants; (5) a history of intracranial surgery before MRI; and (6) with brain tumor, stroke, and mental disorder. Thus, a total of 193 participants were excluded. The remaining 541 participants (n = 256 for cohort A and n = 285 for cohort B) were eligible for the subsequent analysis. Participants with inferior image quality (n = 18), unavailable pseudocontinuous arterial spin labeling (pcASL) data (n = 117), and/or incomplete clinical data (n = 287) were also excluded. Finally, the MRI images obtained from 406 participants were used to investigate the relationship between the severity of BG-PVS and GMV/CBF, while the MRI images obtained from 254 participants were used to investigate the relationship between the severity of BG-PVS and cardiovascular risk burden.

MRI Acquisition

The magnetic resonance imaging studies of cohort A were performed with a 3.0 T GE MRI scanner (GE Discovery MR750, GE Healtchare, Milwaukee, WI, United States). The MRI protocols used with cohort A comprised three serial sequences: an axial T2-PROPELLER sequence (TR/TE = 7,912/92 ms; slice thickness = 4 mm; and FOV = 256 × 256 mm^2), an axial pCASL sequence (TR/TE = 4,886/10.5 ms; FOV = 240 × 240 mm^2; slice thickness = 4 mm; post-labeling delay = 2,025 ms; labeling duration = 1,450 ms), and a sagittal 3D BRAVO sequence (TI/TR/TE = 400/6.9/2.6 ms; FOV = 256 mm^2 × 256 mm^2; slice thickness = 1. mm; matrix size = 256 × 256). The MRI studies of cohort B were performed with another 3.0 Tesla GE MRI scanner (GE SIGNA PET/MR, GE Healthcare Systems, Chicago IL, United States). The MRI protocols used for cohort B were as follows: an axial T2-PROPELLER sequence (TR/TE = 3,324/81 ms; slice thickness = 4 mm; and FOV = 256 × 256 mm^2), an axial pCASL sequence (TR/TE = 4,874/10.7 ms; FOV = 240 × 240 mm^2; slice thickness = 4 mm; post-labeling delay = 2,025 ms; labeling duration = 1,450 ms), and a sagittal T1-weighted 3D BRAVO sequence (TI/TR/TE = 450/7.4/3.2 ms; FOV = 256 mm^2 × 256 mm^2; slice thickness = 1.1 mm; matrix size = 256 × 256). The MR sequences and parameters used with cohort B were similar to those used with cohort A, which could greatly reduce the potential differences between the MRI scanners (Lundervold et al., 2000; Mutsaerts et al., 2015; Liu et al., 2020).

ASL Data Process

CBF maps of ASL were generated on GE AW 4.5 workstation by a software 3D ASL Functool kit (Lin et al., 2018). This software processes pcASL data in a standardized one-click mode. The same model used for CBF calculation was based on a previous study (Williams et al., 1992; Lin et al., 2020). Data were preprocessed using SPM12 (Wellcome Department of Cognitive Neurology, Institute of Neurology, London, United Kingdom) implemented on MATLAB (MathWorks,

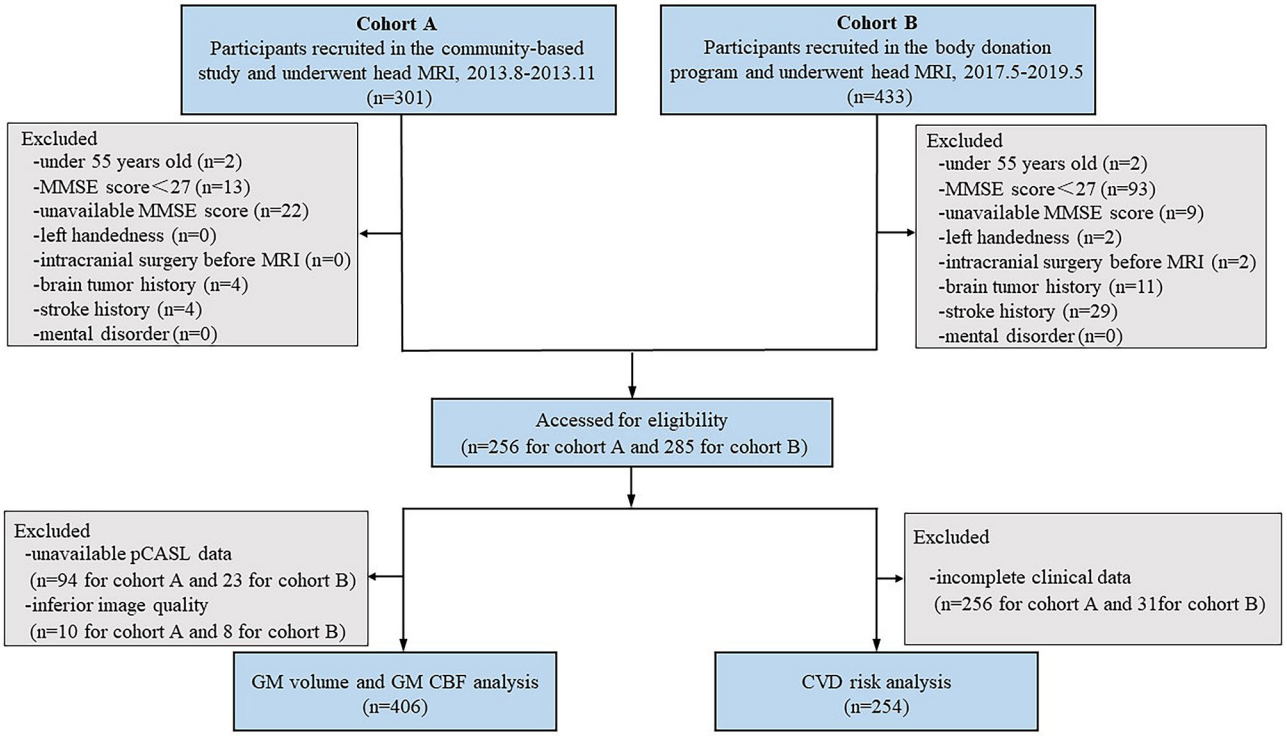

FIGURE 1 | Study flowchart shows the recruitment of study participants. MMSE, Mini-Mental State Exam; pCASL, pseudo-continuous arterial spin labeling.

Natick, MA, United States). First, the CBF maps were co-registered to 3D T1-weighted images. Second, the 3D T1-weighted images were segmented into the gray matter, white matter, and cerebrospinal fluid (CSF) based on tissue probability maps in each voxel and then normalized into a Montreal Neurological Institute (MNI) template. After that, the spatially normalized images were smoothed with an isotropic Gaussian kernel filter of 6 mm full width at half maximum (FWHM). The MNI-normalized smoothed gray matter was used to create a gray matter mask with a threshold value of 0.5. Finally, the Hammers atlas was used to extract the CBF of 68 brain regions.

Anatomic Morphometric Analysis

A morphometric analysis based on the 3D T1-weighted images was performed using CAT12 implemented on SPM12 (Wellcome Department of Cognitive Neurology, Institute of Neurology, London, United Kingdom) (Farokhian et al., 2017). The standard pipeline was first used to segment the 3D T1-weighted images into gray matter, white matter, and CSF. After that, the 3D T1-weighted images were normalized to the MNI template and smoothed with an isotropic Gaussian kernel filter of 8 mm FWHM. Then, the Hammers atlas was used to extract the GMV of 68 brain regions (Rodionov et al., 2009; Yaakub et al., 2020).

Rating of MRI-Visible BG-PVS

Basal ganglia perivascular spaces were identified according to the standards for reporting vascular changes on neuroimaging (Wardlaw et al., 2013). These were visually rated on axial T2-weighted images on a predefined slice (the first slice above the anterior commissure in the BG) (Banerjee et al., 2017) by a trained rater. Then, 82 (20%) individuals were randomly selected and visually assessed by another rater. Both raters were blinded to the clinical information. Only lesions that met the following conditions were regarded as BG-PVS: CSF-like signal lesions (hyperintense on T2 and hypointense on T1, and fluid-attenuated inversion recovery); lesions with a linear, round, or ovoid shape; lesions with a clear boundary; the maximum diameter of lesions <3 mm; lesions with no mass effect; and lesions in the areas supplied by perforating arteries (Zhu et al., 2010). Basal ganglia perivascular spaces were rated using a 5-grade score: grade 0 for no BG-PVS, grade 1 for <10 BG-PVS, grade 2 for 10 to 20 BG-PVS, grade 3 for 20 to 40 BG-PVS, and grade 4 for >40 BG-PVS (Doubal et al., 2010; Banerjee et al., 2017). Both hemispheres were counted, and the hemisphere with higher score was recorded. The number of individuals at each grade of BG-PVS varies greatly (Zhu et al., 2010; Yakushiji et al., 2014). Therefore, for statistical analysis, we categorized the severity of BG-PVS as mild (grade <3) or severe (grade ≥3). **Figure 2** presents the BG-PVS examples for each severity grade.

Assessment of Cardiovascular Risk Burden

We calculated FGCRS based on age, sex, high-density lipoprotein cholesterol, total cholesterol, systolic blood pressure (SBP), diabetes, and smoking history (D'Agostino et al., 2008). FGCRS is calculated by summing up the points from all of these risk factors.

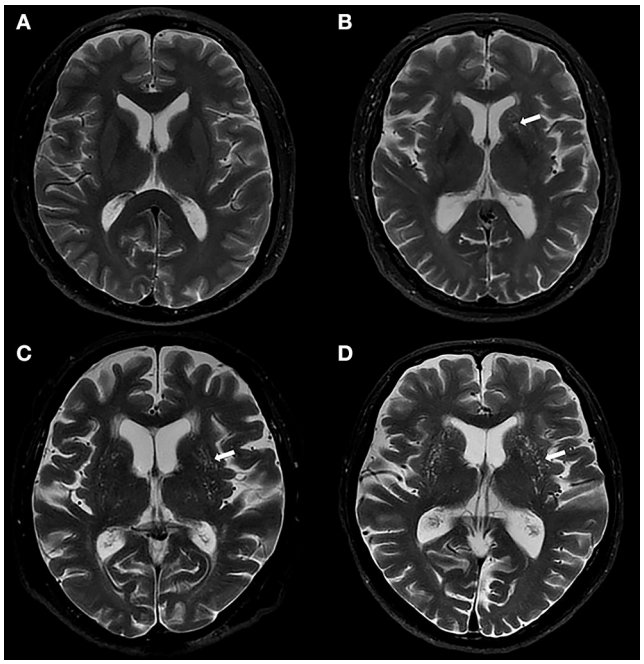

FIGURE 2 | Examples of MRI-visible BG-PVS. **(A,B)** Axial T2-weighted images show the mild grade of BG-PVS (arrow), **(C,D)** Axial T2-weighted images show the severe grade of BG-PVS (arrow).

According to FGCRS, the cardiovascular risk burden was divided into two categories for statistical analysis, lower (FGCRS <17) and higher (FGCRS ≥17) (Song et al., 2020).

Statistical Analysis

Statistical analysis was performed using SPSS (version 20, IBM Inc., Armonk, NY, United States). Categorical variables were tested by χ^2 test, and were described in both percentage and frequency. Continuous variables were tested by Student's *t*-test or Mann–Whitney U test, and were described with mean and SD estimates. The inter-rater consistency of the severity of BG-PVS was evaluated with kappa (κ) value.

Using age, sex, scanner, and total intracranial volume (TIV) as covariates, the difference in GMV between the mild and severe BG-PVS groups was analyzed using univariate linear models. Using age, sex, scanner, and regional GMV as covariates, the difference in CBF between the mild and severe BG-PVS groups was analyzed using univariate linear models. The Benjamini–Hochberg procedure was performed to control for false discovery rate (FDR). FDR-corrected *P*-values (P_{FDR}) of <0.05 were considered significant. Logistic regression analysis was performed to assess the difference in cardiovascular risk burden between the mild and severe BG-PVS groups.

RESULTS

Inter-rater Consistency

The inter-rater consistency was high for assessing the severity of BG-PVS (κ =0.883). The two raters reached a consensus on the classification of 81 images.

Basal Ganglia Perivascular Spaces, Gray Matter Volume, and Cerebral Blood Flow

A total of 406 participants (169 men and 237 women, mean age: 69.44 ± 7.89 years old) were included in the GMV and CBF analysis (see **Table 1** for the summary of details).

Among the 68 brain regions exacted from Hammers atlas, a total of 10 brain structures (e.g., ventricles and corpus callosum) that did not belong to the gray matter were excluded, and the remaining 58 brain regions were used for morphological and metabolic analysis.

The gray matter volume analysis revealed that the severe BG-PVS group had a significantly smaller GMV than the mild BG-PVS group, in the bilateral lateral occipital lobe, bilateral rectus gyrus, right orbitofrontal gyrus, right posterior temporal lobe, and right inferior middle temporal lobe (P_{FDR} <0.05, corrected for age, sex, scanner, and TIV, **Figure 3**) (see details in **Supplementary Material 1**). In addition, the severe BG-PVS group also showed a significantly larger volume in the bilateral caudate nucleus, pallidum, and putamen (P_{FDR} <0.05, corrected for age, sex, scanner, and TIV, **Figure 3**).

Figure 4 shows the statistical result of the CBF. Compared with the mild BG-PVS group, the severe BG-PVS group showed widespread hypoperfusion in the cortex and left thalamus (P_{FDR} <0.05, corrected for age, sex, scanner, and regional GMV, **Figure 4**) (see details in **Supplementary Material 1**).

BG-PVS and Cardiovascular Risk Burden

A total of 254 participants (107 men and 147 women, mean age: 71.27 ± 7.77 years old) were included in the analysis between the severity of BG-PVS and cardiovascular risk burden. **Table 2** presents the comparison of cardiovascular risk factors of all individuals stratified by the severity of BG-PVS. Severe BG-PVS were associated with male sex ($P = 0.023$) and age ($P < 0.001$). Those in the severe BG-PVS group were more likely to have hypertension ($P = 0.032$), higher SBP ($P = 0.001$), and higher total cholesterol ($P = 0.001$). The participants with severe BG-PVS were twice as likely to have a high cardiovascular risk burden than the participants with mild BG-PVS ($P = 0.02$; OR, 2.06; 95% CI, 1.12–3.77).

DISCUSSION

This study showed that BG-PVS were associated with cardiovascular risk burden and regional differences in CBF and GMV. This study advanced those of several groups (Kalaria, 2012; Banerjee et al., 2017; Duperron et al., 2018), which associated BG-PVS with vascular cognitive impairment with a larger population of cognitively intact individuals.

Previous MRI studies have shown no association between BG-PVS and whole-brain atrophy (Zhu et al., 2010, 2011; Yakushiji et al., 2014). However, a strong association between PVS and brain weight has been observed in a postmortem study (van Swieten et al., 1991). This study found that the severe BG-PVS group showed a significantly smaller volume in the occipital lobe, temporal lobe, orbitofrontal gyrus, and rectus gyrus. In the occipital lobe and posterior temporal lobe, these are regions

TABLE 1 | Demographic characteristics of the overall MRI sample classified according to the severity of BG-PVS.

	Mild BG-PVS group	Severe BG-PVS group	Statistical test	*P* value
Number	316 (77.83%)	90 (22.17%)		
Mean age at MRI (SD)	68.27 (7.45)	73.57 (8.03)	Student's t	<0.001***
Male (%)	120 (37.97)	49 (54.44)	$\chi 2$	0.005**
MMSE score	28.84 (1.06)	28.77 (1.02)	Mann-Whitney U	0.466

BG-PVS, basal ganglia perivascular spaces; MMSE, Mini-Mental State Exam; SD, standard deviation.
**P < 0.05; **P < 0.01; ***P < 0.001.*

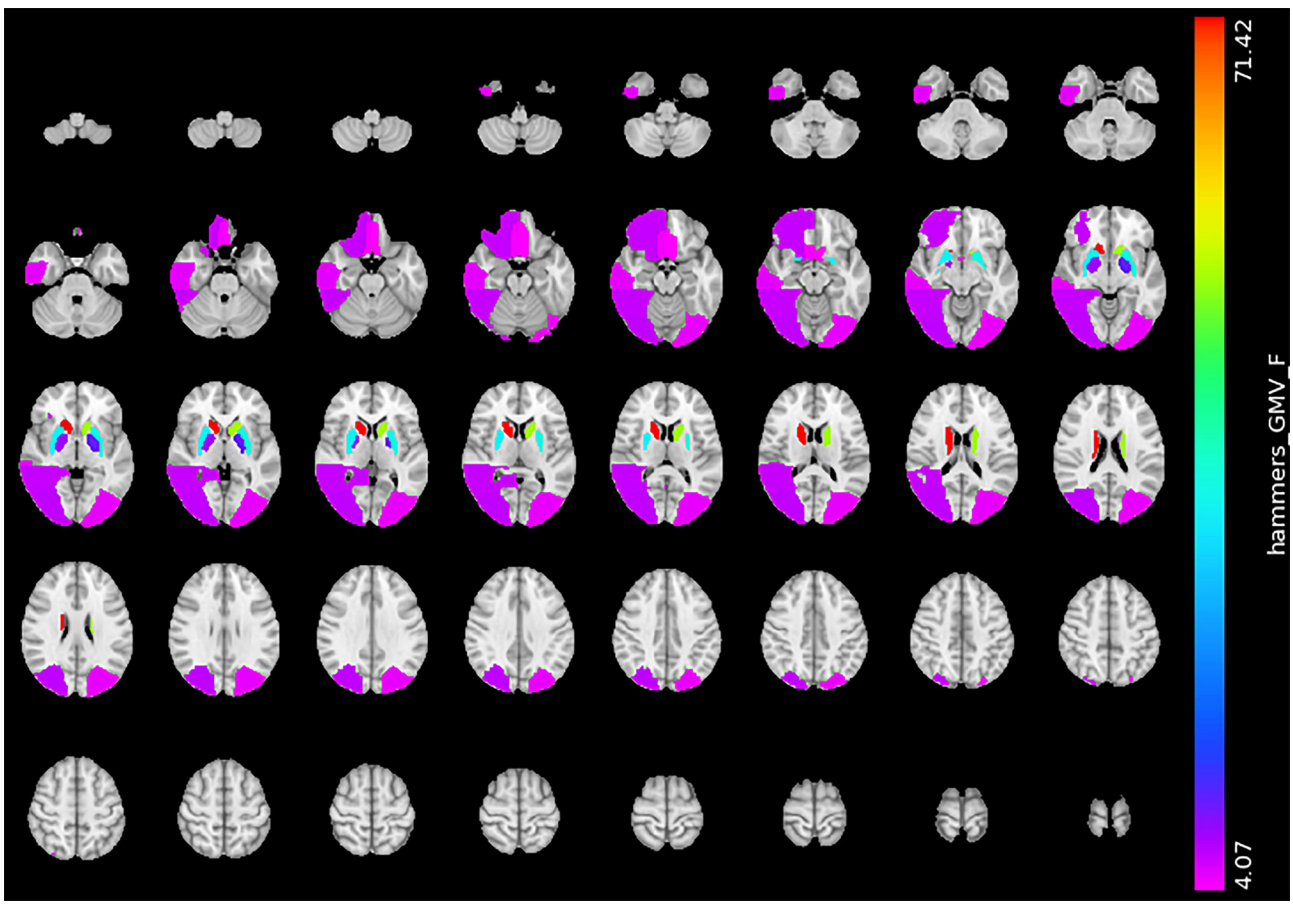

FIGURE 3 | Significant difference in GMV between the mild BG-PVS group and the severe BG-PVS group. The severe BG-PVS group shows a significantly smaller volume in multiple cortical areas and a larger volume in the bilateral caudate nucleus, pallidum, and putamen ($P_{FDR} < 0.05$, corrected for age, sex, scanner and TIV). The F-score bar is shown on the right. The left part of the figure represents the individual's right side. GMV, gray matter volume; BG-PVS, basal ganglia perivascular spaces; TIV, total intracranial volume.

that showed a smaller volume related to cognitive impairment and visuospatial processing deficits (Millington et al., 2017; Chen et al., 2019). Furthermore, the temporal lobe is also vulnerable to vascular abnormalities (De Jong et al., 1999; de Toledo Ferraz Alves et al., 2011). Next, the orbitofrontal gyrus and rectus gyrus are related to emotion and cognitive function (Suzuki et al., 2019; Xu et al., 2019). We also observed a significantly larger volume in the bilateral caudate nucleus, pallidum, and putamen in the severe BG-PVS group. Such volume differences in older adults have not been reported previously. The larger volume of the basal ganglia reflects functional changes in the cortico-basal ganglia-thalamocortical circuit and has been observed in patients with cognitive and behavioral impairment (Alexander and Crutcher, 1990; Frangou et al., 2004; Langen et al., 2007; Sandman et al., 2014).

After covarying CBF with regional GMV, we found a limited spatial overlap between the GMV and CBF pattern. Compared with the mild BG-PVS group, the severe BG-PVS group showed

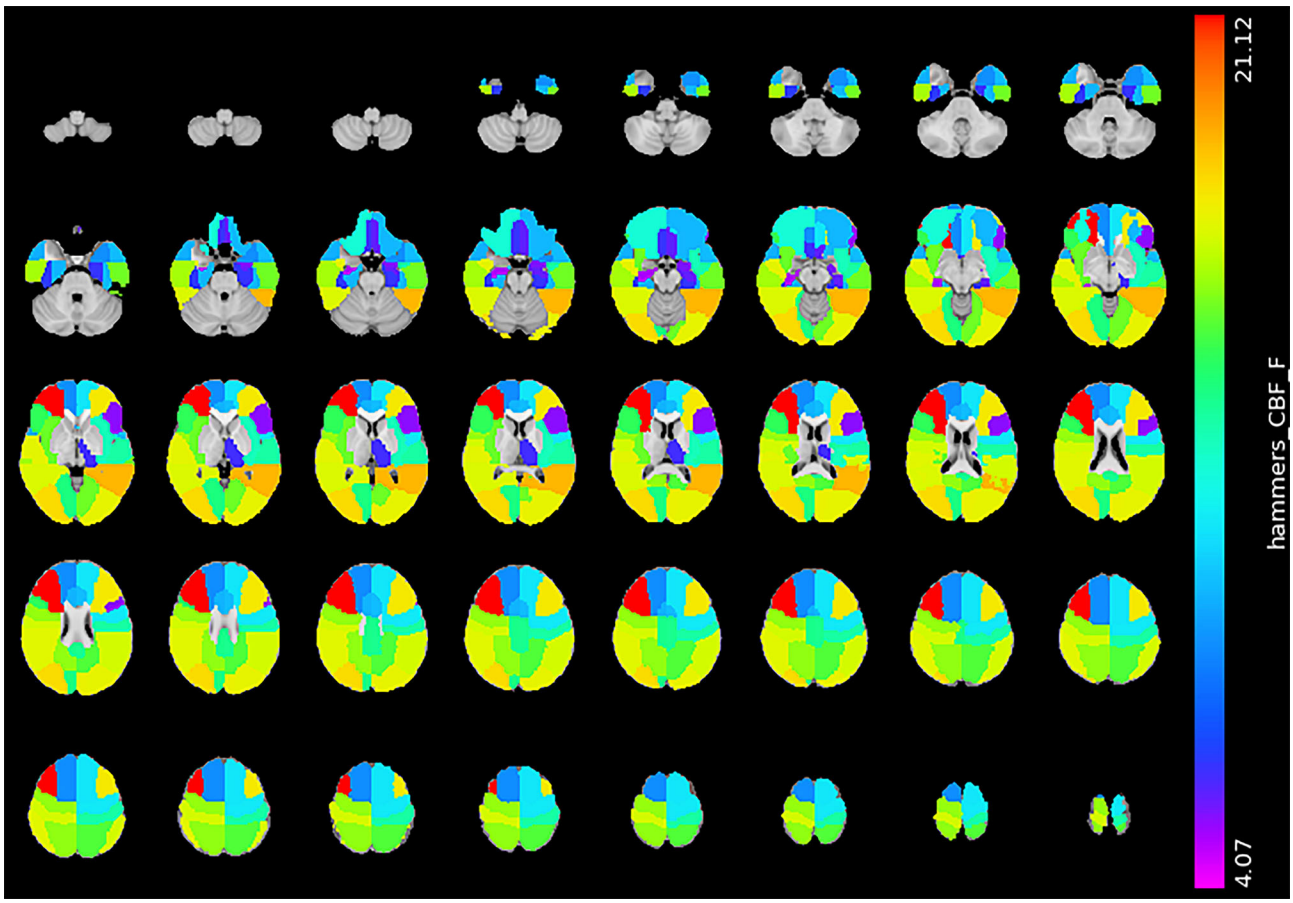

FIGURE 4 | Significant difference in CBF between the mild BG-PVS group and the severe BG-PVS group. The severe BG-PVS group shows a significantly lower CBF in the cortex and left thalamus ($P_{FDR} < 0.05$, corrected for age, sex, scanner and regional GMV). The F-score bar is shown on the right. The left part of the figure represents the right side of the individual. CBF, gray matter cerebral blood flow; BG-PVS, basal ganglia perivascular spaces; GMV, gray matter volume.

widespread hypoperfusion in the cortex, except for the right amygdala and right anterior middle temporal lobe. Therefore, it was hypothesized that BG-PVS were related to a whole-brain perfusion change rather than localized changes. The association between BG-PVS and CBF is in line with previous studies showing that CBF is negatively related to BG-PVS (Wang et al., 2020). However, the results contradicted with an MRI study of 132 memory clinic patients that observed no association between BG-PVS and total brain perfusion (Onkenhout et al., 2020). This discrepancy could be explained by differences in the study population. The normal cortex has a relatively high CBF to supply the metabolic activity of the cortex (Gregg et al., 2015). The presence of cerebral hypoperfusion can put older subjects at risk for neuronal injuries (Sowell et al., 2003; Gregg et al., 2015). Another study (Toth et al., 2017) found that even mild impairment of CBF can promote cognitive impairment in the elderly. These bodies of evidence led the authors of this study to consider severe BG-PVS, which were previously considered to be present in normal aging, as an abnormality.

The gray matter volume and cerebral blood flow analysis in this study showed that individuals with severe BG-PVS suffered chronic brain atrophy and hypoperfusion. Therefore, it is important to maintain brain health by controlling the severity of BG-PVS. The results revealed that BG-PVS are associated with numerous cardiovascular risk factors (such as age, sex, and hypertensive arteriopathy), consistent with previous studies (Zhu et al., 2010; Kress et al., 2014; Kyrtsos and Baras, 2015; Ramirez et al., 2016). This study also demonstrated the relationship between the severity of BG-PVS and cardiovascular risk burden, suggesting that BG-PVS can be used as an imaging marker to predict cardiovascular risk. Future studies can investigate whether CBF, GMV, and cardiovascular parameters are independently associated with BG-PVS, or whether there are any interaction effects between these different biomarkers.

This study focused on cognitively intact individuals and presented some new findings that might suggest directions for future research. There is a growing body of evidence that cerebral microvascular dysfunction and brain hypoperfusion play critical roles in the pathogenesis of dementia (Kalaria, 2012; Banerjee et al., 2017; Toth et al., 2017). However, the association between baseline BG-PVS and neurodegenerative disease still needs to be verified. In addition, the findings highlight the

TABLE 2 | Comparison of cardiovascular risk factors in subjects with mild or severe BG-PVS.

	Mild BG-PVS group	Severe BG-PVS group	Statistical test	*P* value
Number	198 (77.95%)	56 (22.05%)		
Mean age (SD)	69.55 (7.07)	77.32 (7.14)	Student's *t*	<0.001***
Male (%)	76 (38.38)	31 (55.36)	χ^2	0.023*
MMSE score	28.76 (1.07)	28.59 (0.93)	Mann-Whitney U	0.197
Higher cardiovascular risk burden (%)	85 (42.93)	34 (60.71)	Logistic regression	0.020*
Mean SBP mm Hg (SD)	132.53 (16.01)	140.91 (16.85)	Student's *t*	0.001**
TChol mg/dL (SD)	199.57 (39.79)	179.29 (43.98)	Student's *t*	0.001**
HDL-C mg/dL (SD)	51.87 (12.51)	55.05 (16.85)	Student's *t*	0.193
Smoker (%)	45 (22.73)	12 (21.43)	χ^2	0.837
Hypertension (%)	106 (53.53)	39 (69.64)	χ^2	0.032*
Diabetes (%)	41 (20.71)	11 (19.64)	χ^2	0.862

BG-PVS, basal ganglia perivascular spaces; MMSE, Mini-Mental State Exam; SD, standard deviation; SBP, systolic blood pressure; TChol, total cholesterol, HDL-C, high-density lipoprotein cholesterol.
**P < 0.05; **P < 0.01; ***P < 0.001.*

importance of controlling the cardiovascular risk burden in individuals with severe BG-PVS, which may have both public and clinical significance. This study is crucial for understanding the evolution of BG-PVS-related diseases and can improve future treatment decisions.

There are some limitations to this study. First, the visual scoring system was an observer-dependent task (Dubost et al., 2019). The automated quantification of BG-PVS was more effective and objective than visual scoring (Dubost et al., 2019). Furthermore, the automated quantification had great potential to evaluate the burden of BG-PVS as a continuous rather than categorical measure (Dubost et al., 2019). This would allow for an accurate diagnosis and better monitoring of BG-PVS progression. Second, the investigators used the number of classic BG-PVS to reflect the burden of BG-PVS. However, it was unclear whether single, large, and tumefactive BG-PVS would be more relevant in the clinic than multiple small BG-PVS (Ramirez et al., 2016). Third, FGCRS was based on the European population, which might influence its generalization to the Chinese population. Fourth, cardiovascular risk factors were categorically treated in this study. The relationship between BG-PVS and cardiovascular risk factors can be better elucidated by analyzing cardiovascular disease severity and duration of exposure.

CONCLUSION

This study indicated that for cognitively intact older adults, the presence of severe BG-PVS is associated with smaller cortical GMV and CBF, larger subcortical GMV, and a higher cardiovascular risk burden. This study suggested that early identification is crucial for understanding the evolution of BG-PVS-related diseases.

DATA AVAILABILITY STATEMENT

The datasets generated during the current study are available from the corresponding author on reasonable request.

ETHICS STATEMENT

The studies involving human participants were reviewed and approved by Institutional review board of Peking Union Medical College Hospital. The patients/participants provided their written informed consent to participate in this study.

AUTHOR CONTRIBUTIONS

SL, HY, ZZ, and FF: conception and design of the study. SL, BH, YCZ, and CM: acquisition of data. SL, YWZ, and ZZ: analysis and interpretation of data and SL, ZZ, and FF: drafting of the article. All authors contributed to the article and approved the submitted version.

FUNDING

This study was partially supported by the Ministry of Science and Technology of People's Republic of China (2016YFC1305901 and 2019YFA0707103), the Chinese Academy of Medical Sciences Innovation Fund for Medical Sciences (CIFMS #2017-I2M-3-008), the National Natural Science Foundation of China (Grant No: 82071899), and the Chinese Academy of Sciences (XDB32010300).

ACKNOWLEDGMENTS

The authors would like to thank the American Journal Experts for providing language help.

SUPPLEMENTARY MATERIAL

The Supplementary Material for this article can be found online at: https://www.frontiersin.org/articles/10.3389/fnagi.2021.599724/full#supplementary-material

REFERENCES

Alexander, G. E., and Crutcher, M. D. (1990). Functional architecture of basal ganglia circuits: neural substrates of parallel processing. *Trends Neurosci*. 13, 266–271. doi: 10.1016/0166-2236(90)90107-L

Arbel-Ornath, M., Hudry, E., Eikermann-Haerter, K., Hou, S., Gregory, J. L., Zhao, L., et al. (2013). Interstitial fluid drainage is impaired in ischemic stroke and Alzheimer's disease mouse models. *Acta Neuropathol*. 126, 353–364. doi: 10.1007/s00401-013-1145-2

Aribisala, B. S., Wiseman, S., Morris, Z., Valdes-Hernandez, M. C., Royle, N. A., Maniega, S. M., et al. (2014). Circulating inflammatory markers are associated with magnetic resonance imaging-visible perivascular spaces but not directly with white matter hyperintensities. *Stroke* 45, 605–607. doi: 10.1161/STROKEAHA.113.004059

Banerjee, G., Kim, H. J., Fox, Z., Jager, H. R., Wilson, D., Charidimou, A., et al. (2017). MRI-visible perivascular space location is associated with Alzheimer's disease independently of amyloid burden. *Brain* 140, 1107–1116. doi: 10.1093/brain/awx003

Chen, Y. S., Chen, H. L., Lu, C. H., Chen, M. H., Chou, K. H., Tsai, N. W., et al. (2019). Reduced lateral occipital gray matter volume is associated with physical frailty and cognitive impairment in Parkinson's disease. *Eur Radiol*. 29, 2659–2668. doi: 10.1007/s00330-018-5855-7

D'Agostino, R. B. Sr., Vasan, R. S., Pencina, M. J., Wolf, P. A., Cobain, M., Massaro, J. M., et al. (2008). General cardiovascular risk profile for use in primary care: the Framingham Heart Study. *Circulation* 117, 743–753. doi: 10.1161/CIRCULATIONAHA.107.699579

De Jong, G. I., Farkas, E., Stienstra, C. M., Plass, J. R., Keijser, J. N., de la Torre, J. C., et al. (1999). Cerebral hypoperfusion yields capillary damage in the hippocampal CA1 area that correlates with spatial memory impairment. *Neuroscience* 91, 203–210. doi: 10.1016/S0306-4522(98)00659-9

de Toledo Ferraz Alves, T. C., Scazufca, M., Squarzoni, P., de Souza Duran, F. L., Tamashiro-Duran, J. H., Vallada, H. P., et al. (2011). Subtle gray matter changes in temporo-parietal cortex associated with cardiovascular risk factors. *J Alzheimers Dis*. 27, 575–589. doi: 10.3233/JAD-2011-110827

Doubal, F. N., MacLullich, A. M., Ferguson, K. J., Dennis, M. S., and Wardlaw, J. M. (2010). Enlarged perivascular spaces on MRI are a feature of cerebral small vessel disease. *Stroke* 41, 450–454. doi: 10.1161/STROKEAHA.109.564914

Dubost, F., Yilmaz, P., Adams, H., Bortsova, G., Ikram, M. A., Niessen, W., et al. (2019). Enlarged perivascular spaces in brain MRI: Automated quantification in four regions. *Neuroimage* 185, 534–544. doi: 10.1016/j.neuroimage.2018.10.026

Duperron, M. G., Tzourio, C., Sargurupremraj, M., Mazoyer, B., Soumare, A., Schilling, S., et al. (2018). Burden of dilated perivascular spaces, an emerging marker of cerebral small vessel disease, is highly heritable. *Stroke* 49, 282–287. doi: 10.1161/STROKEAHA.117.019309

Farokhian, F., Beheshti, I., Sone, D., and Matsuda, H. (2017). Comparing CAT12 and VBM8 for detecting brain morphological abnormalities in temporal lobe epilepsy. *Front Neurol*. 8:428. doi: 10.3389/fneur.2017.00428

Frangou, S., Chitins, X., and Williams, S. C. (2004). Mapping IQ and gray matter density in healthy young people. *Neuroimage* 23, 800–805. doi: 10.1016/j.neuroimage.2004.05.027

Gao, Y. Z., Zhang, J. J., Liu, H., Wu, G. Y., Xiong, L., and Shu, M. (2013). Regional cerebral blood flow and cerebrovascular reactivity in Alzheimer's disease and vascular dementia assessed by arterial spinlabeling magnetic resonance imaging. *Curr. Neurovasc. Res*. 10, 49–53. doi: 10.2174/15672021380480601 6

Gregg, N. M., Kim, A. E., Gurol, M. E., Lopez, O. L., Aizenstein, H. J., Price, J. C., et al. (2015). Incidental cerebral microbleeds and cerebral blood flow in elderly individuals. *JAMA Neurol*. 72, 1021–1028. doi: 10.1001/jamaneurol.2015.1359

Kalaria, R. N. (2012). Cerebrovascular disease and mechanisms of cognitive impairment: evidence from clinicopathological studies in humans. *Stroke* 43, 2526–2534. doi: 10.1161/STROKEAHA.112.655803

Kress, B. T., Iliff, J. J., Xia, M., Wang, M., Wei, H. S., Zeppenfeld, D., et al. (2014). Impairment of paravascular clearance pathways in the aging brain. *Ann Neurol*. 76, 845–861. doi: 10.1002/ana.24271

Kyrtsos, C. R., and Baras, J. S. (2015). Modeling the role of the glymphatic pathway and cerebral blood vessel properties in Alzheimer's disease pathogenesis. *PLoS ONE* 10:e0e0139574. doi: 10.1371/journal.pone.0139574

Langen, M., Durston, S., Staal, W. G., Palmen, S. J., and van Engeland, H. (2007). Caudate nucleus is enlarged in high-functioning medication-naive subjects with autism. *Biol Psychiatry* 62, 262–266. doi: 10.1016/j.biopsych.2006.09.040

Lin, T., Lai, Z., Lv, Y., Qu, J., Zuo, Z., You, H., et al. (2018). Effective collateral circulation may indicate improved perfusion territory restoration after carotid endarterectomy. *Eur Radiol*. 28, 727–735. doi: 10.1007/s00330-017-5020-8

Lin, T., Qu, J., Zuo, Z., Fan, X., You, H., and Feng, F. (2020). Test-retest reliability and reproducibility of long-label pseudo-continuous arterial spin labeling. *Magn Reson Imaging*. 73, 111–117. doi: 10.1016/j.mri.2020.07.010

Liu, S., Hou, B., Zhang, Y., Lin, T., Fan, X., You, H., et al. (2020). Inter-scanner reproducibility of brain volumetry: influence of automated brain segmentation software. *BMC Neurosci*. 21:35. doi: 10.1186/s12868-020-00585-1

Lundervold, A., Taxt, T., Ersland, L., and Fenstad, A. M. (2000). Volume distribution of cerebrospinal fluid using multispectral MR imaging. *Med Image Anal*. 4, 123–136. doi: 10.1016/S1361-8415(00)00009-8

Millington, R. S., James-Galton, M., Maia Da Silva, M. N., Plant, G. T., and Bridge, H. (2017). Lateralized occipital degeneration in posterior cortical atrophy predicts visual field deficits. *Neuroimage Clin*. 14, 242–249. doi: 10.1016/j.nicl.2017.01.012

Mutsaerts, H. J., van Osch, M. J., Zelaya, F. O., Wang, D. J., Nordhøy, W., Wang, Y., et al. (2015). Multi-vendor reliability of arterial spin labeling perfusion MRI using a near-identical sequence: implications for multi-center studies. *Neuroimage*. 113, 143–152. doi: 10.1016/j.neuroimage.2015.03.043

Onkenhout, L., Appelmans, N., Kappelle, L. J., Koek, D., Exalto, L., de Bresser, J., et al. (2020). Cerebral perfusion and the burden of small vessel disease in patients referred to a memory clinic. *Cerebrovasc Dis*. 49, 481–486. doi: 10.1159/000510969

Ramirez, J., Berezuk, C., McNeely, A. A., Gao, F., McLaurin, J., and Black, S. E. (2016). Imaging the perivascular space as a potential biomarker of neurovascular and neurodegenerative diseases. *Cell Mol Neurobiol*. 36, 289–299. doi: 10.1007/s10571-016-0343-6

Rodionov, R., Chupin, M., Williams, E., Hammers, A., Kesavadas, C., and Lemieux, L. (2009). Evaluation of atlas-based segmentation of hippocampi in healthy humans. *Magn Reson Imaging* 27, 1104–1109. doi: 10.1016/j.mri.2009.01.008

Sandman, C. A., Head, K., Muftuler, L. T., Su, L., Buss, C., and Davis, E. P. (2014). Shape of the basal ganglia in preadolescent children is associated with cognitive performance. *Neuroimage* 99, 93–102. doi: 10.1016/j.neuroimage.2014.05.020

Schuff, N., Matsumoto, S., Kmiecik, J., Studholme, C., Du, A., Ezekiel, F., et al. (2009). Cerebral blood flow in ischemic vascular dementia and Alzheimer's disease, measured by arterial spin-labeling magnetic resonance imaging. *Alzheimers Dement*. 5, 454–462. doi: 10.1016/j.jalz.2009.04.1233

Song, R., Xu, H., Dintica, C. S., Pan, K. Y., Qi, X., Buchman, A. S., et al. (2020). Associations between cardiovascular risk, structural brain changes, and cognitive decline. *J Am Coll Cardiol*. 75, 2525–2534. doi: 10.1016/j.jacc.2020.03.053

Sowell, E. R., Peterson, B. S., Thompson, P. M., Welcome, S. E., Henkenius, A. L., and Toga, A. W. (2003). Mapping cortical change across the human life span. *Nat Neurosci*. 6, 309–315. doi: 10.1038/nn1008

Sun, Y., Cao, W., Ding, W., Wang, Y., Han, X., Zhou, Y., et al. (2016). Cerebral blood flow alterations as assessed by 3D ASL in cognitive impairment in patients with subcortical vascular cognitive impairment: a marker for disease severity. *Front Aging Neurosci*. 8:211. doi: 10.3389/fnagi.2016.00211

Suzuki, H., Venkataraman, A. V., Bai, W., Guitton, F., Guo, Y., Dehghan, A., et al. (2019). Associations of regional brain structural differences with aging, modifiable risk factors for dementia, and cognitive performance. *JAMA Netw Open*. 2:e1e1917257. doi: 10.1001/jamanetworkopen.2019.17257

Ten Kate, M., Dicks, E., Visser, P. J., van der Flier, W. M., Teunissen, C. E., Barkhof, F., et al. (2018). Atrophy subtypes in prodromal Alzheimer's disease are associated with cognitive decline. *Brain* 141, 3443–3456. doi: 10.1093/brain/awy264

Toth, P., Tarantini, S., Csiszar, A., and Ungvari, Z. (2017). Functional vascular contributions to cognitive impairment and dementia: mechanisms and consequences of cerebral autoregulatory dysfunction, endothelial impairment, and neurovascular uncoupling in aging. *Am J Physiol Heart Circ Physiol*. 312,H1–h20. doi: 10.1152/ajpheart.00581.2016

van Swieten, J. C., van den Hout, J. H., van Ketel, B. A., Hijdra, A., Wokke, J. H., and van Gijn, J. (1991). Periventricular lesions in the white matter on magnetic resonance imaging in the elderly. A morphometric correlation

with arteriolosclerosis and dilated perivascular spaces. *Brain* 114, 761–774. doi: 10.1093/brain/114.2.761

Wang, H., Nie, Z. Y., Liu, M., Li, R. R., Huang, L. H., Lu, Z., et al. (2020). Clinical characteristics of perivascular space and brain CT perfusion in stroke-free patients with intracranial and extracranial atherosclerosis of different extents. *Ann Transl Med*. 8:215. doi: 10.21037/atm.2020.01.35

Wardlaw, J. M., Smith, E. E., Biessels, G. J., Cordonnier, C., Fazekas, F., Frayne, R., et al. (2013). Neuroimaging standards for research into small vessel disease and its contribution to ageing and neurodegeneration. *Lancet Neurol*. 12, 822–838. doi: 10.1016/S1474-4422(13)70124-8

Williams, D. S., Detre, J. A., Leigh, J. S., and Koretsky, A. P. (1992). Magnetic resonance imaging of perfusion using spin inversion of arterial water. *Proc. Natl. Acad. Sci. USA*. 89, 212–216. doi: 10.1073/pnas.89.1.212

Xu, P., Chen, A., Li, Y., Xing, X., and Lu, H. (2019). Medial prefrontal cortex in neurological diseases. *Physiol Genomics* 51, 432–442. doi: 10.1152/physiolgenomics.00006.2019

Yaakub, S. N., Heckemann, R. A., Keller, S. S., McGinnity, C. J., Weber, B., and Hammers, A. (2020). On brain atlas choice and automatic segmentation methods: a comparison of MAPER and FreeSurfer using three atlas databases. *Sci. Rep*. 10:2837. doi: 10.1038/s41598-020-57951-6

Yakushiji, Y., Charidimou, A., Hara, M., Noguchi, T., Nishihara, M., Eriguchi, M., et al. (2014). Topography and associations of perivascular spaces in healthy adults: the Kashima scan study. *Neurology* 83, 2116–2123. doi: 10.1212/WNL.0000000000001054

Zhang, H., Chen, K., Wang, N., Zhang, D., Yang, Q., Zhang, Q., et al. (2018). Analysis of brain donors' demographic and medical characteristics to facilitate the construction of a human brain bank in China. *J Alzheimers Dis*. 66, 1245–1254. doi: 10.3233/JAD-180779

Zhu, Y. C., Dufouil, C., Mazoyer, B., Soumaré, A., Ricolfi, F., Tzourio, C., et al. (2011). Frequency and location of dilated Virchow-Robin spaces in elderly people: a population-based 3D MR imaging study. *AJNR Am J Neuroradiol*. 32, 709–713. doi: 10.3174/ajnr.A2366

Zhu, Y. C., Tzourio, C., Soumare, A., Mazoyer, B., Dufouil, C., and Chabriat, H. (2010). Severity of dilated Virchow-Robin spaces is associated with age, blood pressure, and MRI markers of small vessel disease: a population-based study. *Stroke* 41, 2483–2490. doi: 10.1161/STROKEAHA.110.591586

Conflict of Interest: The authors declare that the research was conducted in the absence of any commercial or financial relationships that could be construed as a potential conflict of interest.

Publisher's Note: All claims expressed in this article are solely those of the authors and do not necessarily represent those of their affiliated organizations, or those of the publisher, the editors and the reviewers. Any product that may be evaluated in this article, or claim that may be made by its manufacturer, is not guaranteed or endorsed by the publisher.

frontiers in Aging Neuroscience

ORIGINAL RESEARCH
published: 30 September 2021
doi: 10.3389/fnagi.2021.717391

The Effect of Mild Traumatic Brain Injury on Cerebral Microbleeds in Aging

*Luca Toth[1,2], Andras Czigler[1,2], Peter Horvath[1], Nikolett Szarka[2], Balint Kornyei[3], Arnold Toth[3], Attila Schwarcz[1], Zoltan Ungvari[4,5], Andras Buki[1] and Peter Toth[1,2,5,6]**

[1] Department of Neurosurgery, University of Pecs, Medical School, Pecs, Hungary, [2] Institute for Translational Medicine, University of Pecs, Medical School, Pecs, Hungary, [3] Department of Radiology, University of Pecs, Medical School, Pecs, Hungary, [4] Department of Biochemistry, Reynolds Oklahoma Center on Aging, University of Oklahoma Health Sciences Center, Oklahoma City, OK, United States, [5] Department of Public Health, Faculty of Medicine, Semmelweis University, Budapest, Hungary, [6] ELKH-PTE Clinical Neuroscience MR Research Group, Pecs, Hungary

A traumatic brain injury (TBI) induces the formation of cerebral microbleeds (CMBs), which are associated with cognitive impairments, psychiatric disorders, and gait dysfunctions in patients. Elderly people frequently suffer TBIs, especially mild brain trauma (mTBI). Interestingly, aging is also an independent risk factor for the development of CMBs. However, how TBI and aging may interact to promote the development of CMBs is not well established. In order to test the hypothesis that an mTBI exacerbates the development of CMBs in the elderly, we compared the number and cerebral distribution of CMBs and assessed them by analysing susceptibility weighted (SW) MRI in young (25 ± 10 years old, n = 18) and elder (72 ± 7 years old, n = 17) patients after an mTBI and in age-matched healthy subjects (young: 25 ± 6 years old, n = 20; aged: 68 ± 5 years old, n = 23). We found significantly more CMBs in elder patients after an mTBI compared with young patients; however, we did not observe a significant difference in the number of cerebral microhemorrhages between aged and aged patients with mTBI. The majority of CMBs were found supratentorially (lobar and basal ganglion). The lobar distribution of supratentorial CMBs showed that aging enhances the formation of parietal and occipital CMBs after mTBIs. This suggests that aging and mTBIs do not synergize in the induction of the development of CMBs, and that the different distribution of mTBI-induced CMBs in aged patients may lead to specific age-related clinical characteristics of mTBIs.

Keywords: microhemorrages, aging, cognitive decline, traumatic brain injury (TBI), microvascular injury

OPEN ACCESS

Edited by:
Stefano Tarantini, University of Oklahoma Health Sciences Center, United States

Reviewed by:
Istvan Jozsef Merchenthaler, University of Maryland, Baltimore, United States
Torgeir Hellstrøm, Oslo University Hospital, Norway
Fouad Antoine Zouein, American University of Beirut, Lebanon

***Correspondence:**
Peter Toth
toth.peter@pte.hu

Received: *30 May 2021*
Accepted: *27 August 2021*
Published: *30 September 2021*

Citation:
Toth L, Czigler A, Horvath P, Szarka N, Kornyei B, Toth A, Schwarcz A, Ungvari Z, Buki A and Toth P (2021) The Effect of Mild Traumatic Brain Injury on Cerebral Microbleeds in Aging. Front. Aging Neurosci. 13:717391. doi: 10.3389/fnagi.2021.717391

INTRODUCTION

A traumatic brain injury (TBI) has been shown to induce the formation of cerebral microbleeds (CMBs) (Huang et al., 2015; Toth et al., 2016, 2020; Ungvari et al., 2017; Irimia et al., 2018; Griffin et al., 2019). Cerebral microbleeds are hemosiderin deposits that are 5–10 mm in diameter as a result of bleeding from injured small cerebral arteries, arterioles, or capillaries. They are also

associated with the development of cognitive impairments, psychiatric disorders, and gait dysfunctions (Werring et al., 2010; de Laat et al., 2011; Wang et al., 2014, 2018; Huang et al., 2015; Toth et al., 2015, 2020; Akoudad et al., 2016; Ungvari et al., 2017, 2018; Irimia et al., 2018; Nyúl-Tóth et al., 2020). Due to orthostatic hypotension, dehydration, and impaired balance, the elderly population frequently suffers TBIs (Krishnamoorthy et al., 2015; Irimia et al., 2018; Rauen et al., 2020). The most common form of TBI affecting elderly people is mild brain trauma (mTBI) (Rachmany et al., 2013; Krishnamoorthy et al., 2015; Rauen et al., 2020). Similar to TBI, aging is also an independent risk factor for the development of CMBs (Toth et al., 2015, 2020; Ungvari et al., 2017; Irimia et al., 2018). The number of CMBs increases with age, and they are causally linked to age-related cognitive decline and gait disturbances. Interestingly, mechanisms leading to the formation of CMBs, such as cerebrovascular oxidative stress, the activation of matrix metalloproteinases, and the modification of the content of the cerebrovascular wall, are all induced by both aging and TBIs (Lewén et al., 2001; Werring et al., 2010; Rachmany et al., 2013; Abdul-Muneer et al., 2016; Ungvari et al., 2017, 2018; Griffin et al., 2019; Go et al., 2020). However, it is not well established and characterized how TBIs and aging interact to promote the development of CMBs, especially after an mTBI. In this brief study, we tested the hypothesis that an mTBI exacerbates the development of CMBs in the elderly compared with young patients, and aimed to characterize the location and distribution of CMBs in elderly patients after an mTBI.

MATERIALS AND METHODS

Study Population

The study was approved by the Regional Ethic Committee of the University of Pecs, Medical School, Hungary (7270-PTE 2018). We retrospectively analyzed the medical history and three Tesla susceptibility weighted (SWI) MRIs of 35 patients (15 males and 20 females) who had suffered mTBIs [Glasgow Coma Scale (GCS) 14–15] and were admitted to the Department of Neurosurgery, Medical School, University of Pecs, Hungary between April of 2014 and September of 2019. We also analyzed the SWI MRI images of 43 aged-matched control patients (17 males and 26 females) without a medical history of a TBI. For the TBI groups, the inclusion criteria were: young, age is between 18 and 40 years; aged, above 60 years old at the time of the injury; an mTBI in the history within 6 months of the MRI; an mTBI according to Mayo criteria: GCS 14–15, absence or a maximum of 30 min of loss of consciousness, and the absence of post-traumatic amnesia (PTA) (Malec et al., 2007). Exclusion criteria: any conditions associated with CMB formation in the medical history, such as epilepsy, a previous TBI, stroke, transient ischemic attack, cavernous malformations, cerebral amyloid angiopathy, chronic hypertensive encephalopathy, acute haemorrhagic leukoencephalitis, cerebral autosomal dominant arteriopathy with subcortical infarcts and leukoencephalopathy (CADASIL), Alzheimer's disease, cerebral vasculitis, cerebral metastases, haemorrhagic micrometastases, intracranial embolism, intravascular lymphoma, posterior reversible encephalopathy syndrome (PRES), progressive facial haemiatrophy, thrombotic microangiopathies, intracranial infection, and COL4A1 brain small-vessel disease (Greenberg et al., 2009; Yakushiji, 2015; Ungvari et al., 2017). For the control group, an additional exclusion criterion was a TBI in the medical records. Both in the TBI and control groups, two age groups were defined in a 2×2 study design: young (Y): $n = 20$, 10 females, 10 males, age: 25 ± 6 years; young + mTBI (Y + mTBI): $n = 17$, 11 females, 6 males, age: 25 ± 10 years; aged (A): $n = 23$, 16 females, 7 males, age: 68 ± 5 years; aged + mTBI (A + mTBI): $n = 17$, 9 females, 8 males, age: 72 ± 7 years.

Imaging Protocol

A brain MRI was performed using 3T (Magnetom Trio/Prismafit) Siemens MR scanners (Siemens, Munich, Germany). Susceptibility- and T1-weighted magnetization-prepared rapid acquisition with gradient echo (MPRAGE) and fluid-attenuated inversion recovery (FLAIR) images were obtained. The T1-weighted high-resolution images were then obtained using a three-dimensional (3D) MP-RAGE sequence [TI = 900–1,100 ms; TR = 1,900–2,530 ms; TE = 2.5–2.4 ms; slice thickness = 0.9–1 mm; field of view (FOV) = 256 mm × 256 mm; matrix size = 256 × 256], while 3D SWI images were acquired as follows: TR = 27–49 ms; TE = 20–40 ms; slice thickness = 1.2–3 mm; FOV = 137–201 mm × 230–240 mm; matrix size = 125–182 × 256–320, with no inter-slice gap. For image evaluation, the 3D Slicer 4.8.1[1] software was used.

Microbleed Analysis

Three independent neuroradiologists evaluated the images individually, blinded to medical history. In order to precisely identify CMBs, the exclusion of SWI lesions that mimic CMBs (intersection of veins, bottom of sulci, calcium deposits, artifacts caused by air-tissue interfaces, or macroscopic bleeding caused by, e.g., an intraventricular drain) was carried out (Greenberg et al., 2009; Yakushiji, 2015). The number and location of CMBs were obtained according to the clinically validated Microbleed Anatomic Rating Scale (MARS) (Gregoire et al., 2009). This scale distinguishes the number of definite and possible lesions and precisely localizes the CMBs according to anatomic regions as follows: (1) infratentorial: brainstem or cerebellum; (2) deep: basal ganglia, thalamus, internal or external capsule, corpus callosum, or either the periventricular or deep white matter; (3) lobar: cortex or subcortical white matter. In this study, we present only the definite lesions (**Figure 1**).

Statistical Analysis

A Kolmogorov–Smirnov test was performed to determine whether the sample data have the characteristics of a normal distribution. In order to compare the presence of microbleeds, the number of lesions, and specific distribution in different sample groups, Kruskal–Wallis with *post hoc* Dunn's multiple comparison tests and Mann–Whitney *U* tests were performed. To evaluate the effect of comorbidities on the number of CMBs, Fisher's exact tests were performed. Differences were considered

[1] http://www.slicer.org

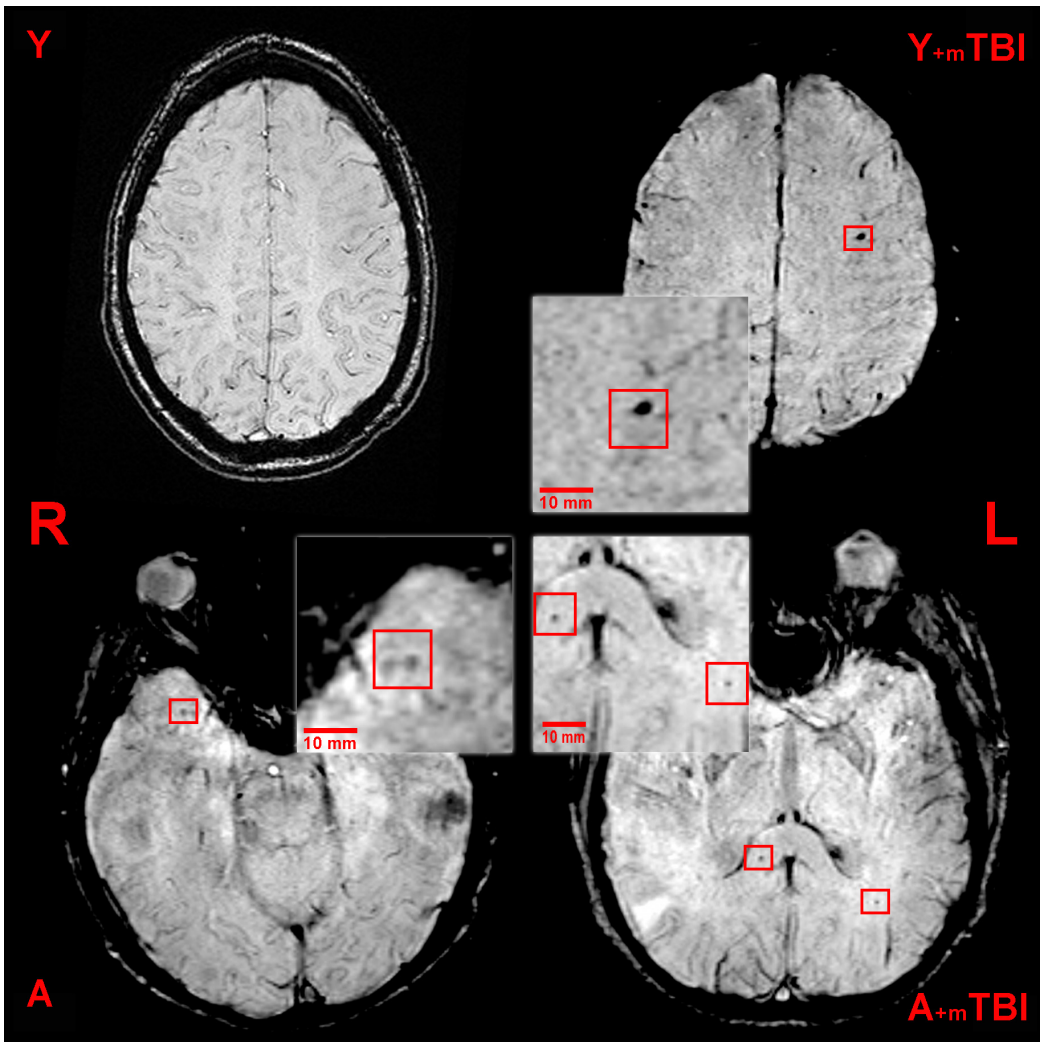

FIGURE 1 | Axial susceptibility weighted (SWI) MRI (three Tesla) of a young control patient (Y, 38-year-old, male), a young patient following mild traumatic brain injury (Y + mTBI, 36-year-old male, GCS: 15), an aged control patient (A, 67-year-old male), and an aged patient with a mild TBI (A + mTBI, 65-year-old male, GCS: 15). Cerebral microbleeds (CMBs) appear as ovoid, hypointense lesions and are indicated by the red squares (R, right; L, left).

significant at $p < 0.05$. Statistical analysis was performed using the Origin Pro 2018 software.

RESULTS

The Effect of Mild Traumatic Brain Injury on the Formation of Cerebral Microbleeds in Aging

The characteristics of the patients in each group are shown in **Table 1**. There were no differences in the assessed cerebrovascular risk factors between the groups.

We found that aging exacerbated the formation of CMBs significantly ($p < 0.05$) compared with young patients (**Figure 2A**), confirming the results of previous studies showing that aging is an independent risk factor for the development of CMBs (Greenberg et al., 2009; Toth et al., 2015; Irimia et al., 2018). Importantly, the number of CMBs in elderly patients was not further increased by mTBIs (**Figure 2A**). An mTBI did not enhance the number of CMBs in young patients either (**Figure 2A**). We found that aging also significantly exacerbated ($p < 0.05$) the incidence of patients with CMBs regardless of the number of bleedings (percent of patients with CMBs in the given group of patients) compared with the young patients (**Figure 2B**), who were not affected by mTBIs (**Figure 2B**).

Location Characteristics of Aging and Mild Traumatic Brain Injury-Induced Cerebral Microbleeds

We found the majority of CMBs in the supratentorial compartment (lobar and basal ganglion); however, a small

TABLE 1 | General description and main cardiovascular comorbidities of the study groups.

Group	Age (Mean ± SD)	Sex		Hypertension		Smoking		Urea		Creatinine		Totalcholesterol		Low density lipoprotein	
		Female	Male	Yes	No	Yes	No	Normal	Abnormal	Normal	Abnormal	Normal	Abnormal	Normal	Abnormal
Young control (Y)	25.09 ± 5.63	50%	50%	10.0%	90.0%	5.0%	95.0%	85.0%	15.0%	85.0%	15.0%	90.0%	10.0%	95.0%	5.0%
Young trauma (Y + mTBI)	24.65 ± 10.22	61.1%	35.3%	5.88%	94.12%	0%	100%	88.24%	11.76%	76.47%	26.53%	94.12%	5.88%	100.0%	0%
Aged control (A)	68.36 ± 4.88	69.6%	30.4%	60.87%	39.13%	4.35%	95.65%	91.3%	8.7%	91.3%	8.7%	56.52%	48.43%	78.26%	21.74%
Aged trauma (A + mTBI)	71.86 ± 7.31	52.9%	47.1%	88.24%	11.76%	17.65%	82.35%	82.35%	17.65%	52.94%	47.06%	82.35%	17.65%	100.0%	0%

number of microbleeds appear in the infratentorial location in aged patients after an mTBI. The difference did not reach statistical significance (**Figure 2C**). Analysing the distribution of supratentorial CMBs across cerebral lobes (frontal, temporal, parietal, and occipital), we found that aging enhances the number of parietal and occipital CMBs after an mTBI ($P < 0.05$ vs. Y + mTBI), and that an mTBI leads to the formation of more CMBs in the parietal lobes in aging ($P < 0.05$ vs. A; **Figure 2D**).

DISCUSSION

It has been shown previously that both TBIs and aging induce the development of CMBs (Huang et al., 2015; Toth et al., 2015; Ungvari et al., 2017; Irimia et al., 2018; Wang et al., 2018; Griffin et al., 2019). In both cases, CMBs are associated with long-term cognitive deficits and gait dysfunctions and determine the outcome of patients (Werring et al., 2010; de Laat et al., 2011; Huang et al., 2015; Toth et al., 2015, 2020; Yakushiji, 2015; Akoudad et al., 2016; Ungvari et al., 2017, 2018; Irimia et al., 2018; Nyúl-Tóth et al., 2020). Previous epidemiological studies have proposed that the TBI-related development of CMBs is exacerbated in aging (Irimia et al., 2018). However, the effect of an mTBI, which is the most frequent form of brain trauma, on the development of CMBs in aging, has not been established (Wang et al., 2014; Krishnamoorthy et al., 2015; Rauen et al., 2020). Here, we show (**Figure 2**) that significantly more microbleeds can be found in aging human brains than in the brains of young healthy individuals, confirming the results of previous studies (Greenberg et al., 2009; Werring et al., 2010; Toth et al., 2015; Akoudad et al., 2016; Wang et al., 2018). We also found significantly more CMBs in elderly patients after an mTBI compared with young patients with an mTBI; however, we did not observe a significant difference in the number of cerebral microhemorrhages between aged and aged patients with mTBIs. This suggests that aging and mTBIs do not synergize the induction of the development of CMBs.

The clinical consequences of CMBs, such as the development of cognitive decline, are most likely due to the cumulative effects of the lesions and the damage in specific anatomical locations (Werring et al., 2010; Ding et al., 2017; Ungvari et al., 2017). For example, damage to the fronto-subcortical circuits linking prefrontal areas to basal ganglia is associated with impairments in executive function, and the disarrangement of pathways from the mentioned areas projecting to the thalamus results in memory disturbances (Werring et al., 2010; Ding et al., 2017; Levit et al., 2020). Although morphological characteristics based on MRI examinations are not helpful in distinguishing CMBs of different etiologies, specific locations suggest the pathophysiological reasons of CMB formation (Greenberg et al., 2009; Wang et al., 2014; Yakushiji, 2015; Ding et al., 2017; Ungvari et al., 2017). For example, the typical brain areas for traumatic CMBs are the corona radiata and longitudinal fasciculus (Wang et al., 2014; Ungvari et al., 2017; Toth et al., 2020). Cerebral microbleeds in deep cerebral areas are thought to be due to cerebral angiopathy induced by hypertension, and lobar CMBs are likely due to amyloid angiopathy (Wang et al., 2014; Yakushiji, 2015; Ding et al., 2017; Ungvari et al., 2017). We found that aging alters the distribution of CMBs after an mTBI (**Figure 2**), namely, in elderly patients following an mTBI, the number of occipital and parietal bleedings was exacerbated compared with young patients. This may affect the functional consequences of these bleedings. Accordingly, the occipital and parietal lobes are responsible for integrating visual and cognitive information, and play an important role in voluntary coordination, posture and motor control, spatial cognition, and the rapid corrections of movements (Galletti et al., 2003; Niogi et al., 2008; Freedman and Ibos, 2018; MacKinnon, 2018). Specific tests should be part of the patient characterization after an mTBI to assess the region-specific consequences of CMBs in aging (and also in young patients), such as the trail making test, Beck's depression test, and Montreal Cognitive Assessment test. This possibility should be verified in the future.

Limitations and Perspectives

The major limitations of this study are its retrospective design and relatively small sample size. Future prospective studies should verify the findings of this study with a large number of healthy control volunteers. We used the Mayo criteria to define an mTBI. Since other guidelines suggest slightly different scoring systems, it would be important to compare the CMB formation

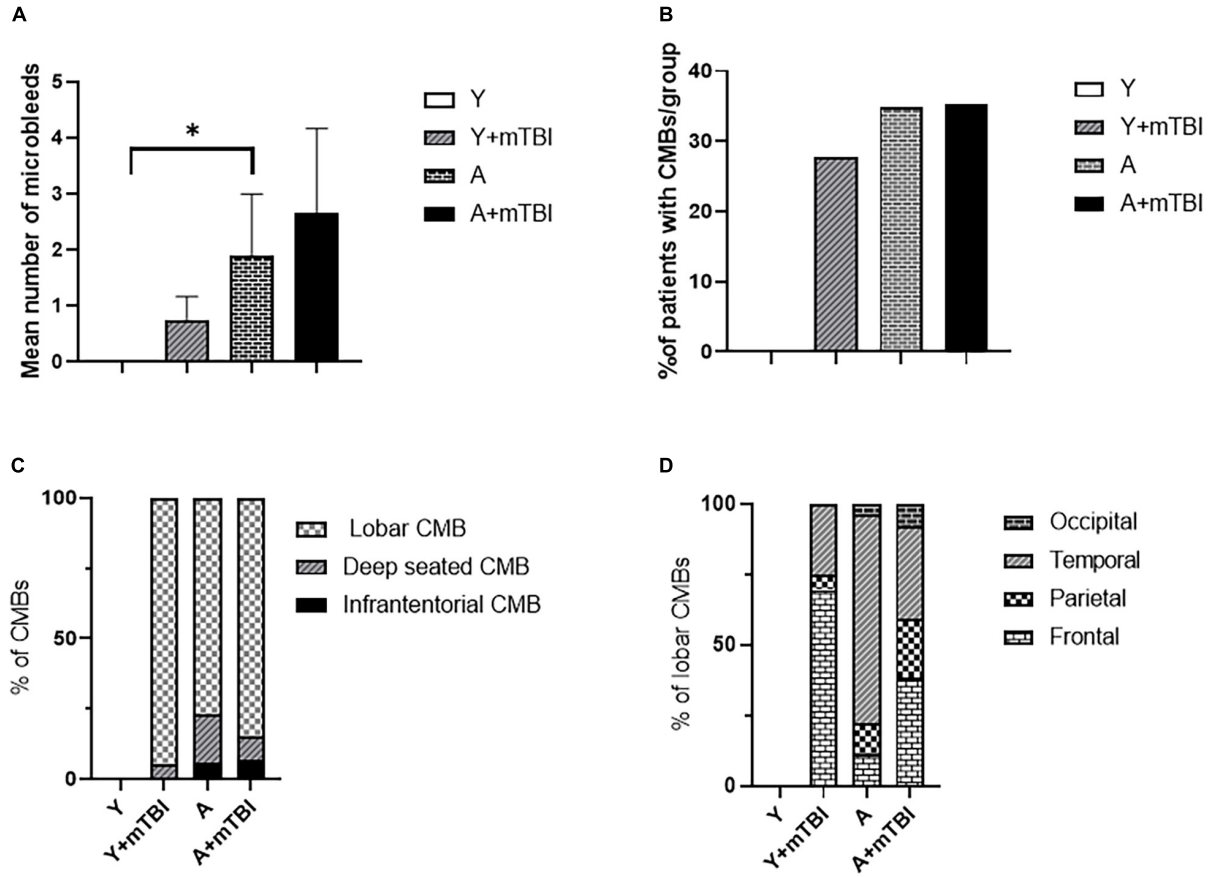

FIGURE 2 | Effect of mild traumatic brain injury on the development and characteristics of cerebral microbleeds in the elderly. **(A)** Mean number of CMBs in young control (Y) patients (n = 20, age: 25.09 ± 5.63 years), young patients after an mBTI (Y + mTBI) (n = 17, age: 24.65 ± 10.22 years), aged control patients (A) (n = 23, age: 68.36 ± 4.88 years), and aged patients with mTBIs (A + mTBI, n = 17, age: 71.86 ± 7.31 years). Data are mean ± SEM, *$P < 0.05$ vs. YC, ns: non-significant. **(B)** Number of patients with CMBs in the studied groups is expressed as the percent of the total number of patients in each group [young control (Y) patients (n = 20, age: 25.09 ± 5.63 years), young patients after mBTIs (Y + mTBI) (n = 17, age: 24.65 ± 10.22 years), aged control patients (A) (n = 23, age: 68.36 ± 4.88), and aged patients with mTBIs (A + mTBI) (n = 17, age: 71.86 ± 7.31 years)]. *$P < 0.05$ vs. YC. Panel **(C)** depicts the localization of CMBs in each group as number of lobar, deep-seated (basal ganglion), and infratentorial CMBs expressed as the percent (%) of the total number of CMBs. Note that the majority of CMBs can be found supratentorially (lobar and basal ganglion); however, a small number of microbleeds appear in the infratentorial location in aged patients after an mTBI. The difference did not reach statistical significance. **(D)** Lobar distribution of supratentorial CMBs in each studied group of patients (frontal, temporal, parietal, and occipital). Please note that aging enhances the number of parietal and occipital CMBs after an mTBI ($P < 0.05$ vs. Y + mTBI), and that an mTBI leads to the formation of more CMBs in the frontal, parietal, and occipital lobes in aging ($P < 0.05$ vs. A). (Y): n = 20, 10 females, 10 males, age: 25.09 ± 5.63 years; young + mTBI (Y + mTBI): n = 17, 11 females, 6 males, age: 24.65 ± 10.22 years; aged (A): n = 23, 16 females, 7 males, age: 68.36 ± 4.88 years; aged + mTBI (A + mTBI): n = 17, 9 females, 8 males, age: 71.86 ± 7.31 years.

in TBI groups as defined by various scoring systems. Aging and mTBIs may interact in altering regulatory mechanisms of cerebral blood flow (CBF) in a functional manner. Accordingly, the changes in neurovascular coupling, autoregulation of CBF, and cerebrovascular reactivity should be assessed and correlated with the cognitive and gait functions in different age groups after mTBIs. Finally, the possible mechanisms through which aging and TBIs may interact to alter cerebrovascular function and the formation of CMBs should be studied, with a special focus on mitochondrial oxidative stress, the activation of redox-sensitive matrix metalloproteinases, the modification of the cerebrovascular wall, the production of proinflammatory cytokines, and the disruption of the blood-brain barrier (Lewén et al., 2001; Greenberg et al., 2009; Werring et al., 2010; de Laat et al., 2011; Toth et al., 2015, 2020; Yakushiji, 2015; Ungvari et al., 2018; Levit et al., 2020).

DATA AVAILABILITY STATEMENT

The original contributions presented in the study are included in the article/supplementary material, further inquiries can be directed to the corresponding author.

ETHICS STATEMENT

The studies involving human participants were reviewed and approved by the study was approved by the Regional Ethic

Committee of the University of Pecs, Medical School, Hungary (7270-PTE 2018). Written informed consent for participation was not required for this study in accordance with the national legislation and the institutional requirements.

AUTHOR CONTRIBUTIONS

LT and PT designed the studies and protocols. AC, PH, BK, and NS performed the literature search and collected the patient data. LT, AC, BK, and AT performed the image analysis. LT, AC, and NS generated the figures. LT, AC, and PT wrote the manuscript. LT, AC, PH, BK, NS, AT, AS, ZU, AB, and PT edited and revised the manuscript. All authors contributed to the article and approved the submitted version.

FUNDING

This work was supported by grants from the National Research, Development and Innovation Office to PT (NKFI-FK123798) and AB (K-134555), the Hungarian Academy of Sciences Bolyai Research Scholarship to PT, ÚNKP-20-3-II-PTE-493 New National Excellence Program of the Ministry for Innovation and Technology to PT and LT, EFOP-3.6.2.-16-2017-00008, GINOP-2.3.2-15-2016-00048, GINOP-2.2.1-15-2017-00067 to PT and AB, Hungarian Brain Research Program 2.0 Grant No. 2017-1.2.1-NKP-2017-00002 to AB, the Higher Education Institutional Excellence Programme of the Ministry of Human Capacities to PT and AB, Thematic Excellence Program 2020-4.1.1-TKP2020 National Excellence Sub-program to LT, the National Institute of Health R01-AG055395, R01-NS100782, R01-AT006526 to ZU. This study was funded by the Hungarian Scientific Research Fund Grant No. OTKA/K-120356 to AS and AT.

REFERENCES

Abdul-Muneer, P. M., Pfister, B. J., Haorah, J., and Chandra, N. (2016). Role of matrix metalloproteinases in the pathogenesis of traumatic brain injury. *Mol. Neurobiol.* 53, 6106–6123. doi: 10.1007/s12035-015-9520-8

Akoudad, S., Wolters, F. J., Viswanathan, A., de Bruijn, R. F., van der Lugt, A., Hofman, A., et al. (2016). Association of cerebral microbleeds with cognitive decline and dementia. *JAMA Neurol.* 73, 934–943. doi: 10.1001/jamaneurol.2016.1017

de Laat, K. F., van den Berg, H. A., van Norden, A. G., Gons, R. A., Olde Rikkert, M. G., and de Leeuw, F. E. (2011). Microbleeds are independently related to gait disturbances in elderly individuals with cerebral small vessel disease. *Stroke* 42, 494–497. doi: 10.1161/strokeaha.110.596122

Ding, J., Sigurðsson, S., Jónsson, P. V., Eiriksdottir, G., Meirelles, O., Kjartansson, O., et al. (2017). Space and location of cerebral microbleeds, cognitive decline, and dementia in the community. *Neurology* 88, 2089–2097. doi: 10.1212/wnl.0000000000003983

Freedman, D. J., and Ibos, G. (2018). An integrative framework for sensory, motor, and cognitive functions of the posterior parietal cortex. *Neuron* 97, 1219–1234. doi: 10.1016/j.neuron.2018.01.044

Galletti, C., Kutz, D. F., Gamberini, M., Breveglieri, R., and Fattori, P. (2003). Role of the medial parieto-occipital cortex in the control of reaching and grasping movements. *Exp. Brain Res.* 153, 158–170. doi: 10.1007/s00221-003-1589-z

Go, V., Bowley, B. G. E., Pessina, M. A., Zhang, Z. G., Chopp, M., Finklestein, S. P., et al. (2020). Extracellular vesicles from mesenchymal stem cells reduce microglial-mediated neuroinflammation after cortical injury in aged Rhesus monkeys. *Geroscience* 42, 1–17. doi: 10.1007/s11357-019-00115-w

Greenberg, S. M., Vernooij, M. W., Cordonnier, C., Viswanathan, A., Al-Shahi Salman, R., Warach, S., et al. (2009). Cerebral microbleeds: a guide to detection and interpretation. *Lancet Neurol.* 8, 165–174. doi: 10.1016/s1474-4422(09)70013-4

Gregoire, S. M., Chaudhary, U. J., Brown, M. M., Yousry, T. A., Kallis, C., Jäger, H. R., et al. (2009). The Microbleed Anatomical Rating Scale (MARS): reliability of a tool to map brain microbleeds. *Neurology* 73, 1759–1766. doi: 10.1212/WNL.0b013e3181c34a7d

Griffin, A. D., Turtzo, L. C., Parikh, G. Y., Tolpygo, A., Lodato, Z., Moses, A. D., et al. (2019). Traumatic microbleeds suggest vascular injury and predict disability in traumatic brain injury. *Brain* 142, 3550–3564.

Huang, Y. L., Kuo, Y. S., Tseng, Y. C., Chen, D. Y., Chiu, W. T., and Chen, C. J. (2015). Susceptibility-weighted MRI in mild traumatic brain injury. *Neurology* 84, 580–585. doi: 10.1212/wnl.0000000000001237

Irimia, A., Van Horn, J. D., and Vespa, P. M. (2018). Cerebral microhemorrhages due to traumatic brain injury and their effects on the aging human brain. *Neurobiol. Aging* 66, 158–164. doi: 10.1016/j.neurobiolaging.2018.02.026

Krishnamoorthy, V., Distelhorst, J. T., Vavilala, M. S., and Thompson, H. (2015). Traumatic brain injury in the elderly: burden, risk factors, and prevention. *J. Trauma Nurs.* 22, 204–208. doi: 10.1097/jtn.0000000000000135

Levit, A., Hachinski, V., and Whitehead, S. N. (2020). Neurovascular unit dysregulation, white matter disease, and executive dysfunction: the shared triad of vascular cognitive impairment and Alzheimer disease. *Geroscience* 42, 445–465. doi: 10.1007/s11357-020-00164-6

Lewén, A., Fujimura, M., Sugawara, T., Matz, P., Copin, J. C., and Chan, P. H. (2001). Oxidative stress-dependent release of mitochondrial cytochrome c after traumatic brain injury. *J. Cereb. Blood Flow Metab.* 21, 914–920. doi: 10.1097/00004647-200108000-00003

MacKinnon, C. D. (2018). Sensorimotor anatomy of gait, balance, and falls. *Handb. Clin. Neurol.* 159, 3–26. doi: 10.1016/b978-0-444-63916-5.00001-x

Malec, J. F., Brown, A. W., Leibson, C. L., Flaada, J. T., Mandrekar, J. N., Diehl, N. N., et al. (2007). The mayo classification system for traumatic brain injury severity. *J. Neurotrauma* 24, 1417–1424. doi: 10.1089/neu.2006.0245

Niogi, S. N., Mukherjee, P., Ghajar, J., Johnson, C., Kolster, R. A., Sarkar, R., et al. (2008). Extent of microstructural white matter injury in postconcussive syndrome correlates with impaired cognitive reaction time: a 3T diffusion tensor imaging study of mild traumatic brain injury. *AJNR Am. J. Neuroradiol.* 29, 967–973. doi: 10.3174/ajnr.A0970

Nyúl-Tóth, Á, Tarantini, S., Kiss, T., Toth, P., Galvan, V., Tarantini, A., et al. (2020). Increases in hypertension-induced cerebral microhemorrhages exacerbate gait dysfunction in a mouse model of Alzheimer's disease. *Geroscience* 42, 1685–1698. doi: 10.1007/s11357-020-00256-3

Rachmany, L., Tweedie, D., Li, Y., Rubovitch, V., Holloway, H. W., Miller, J., et al. (2013). Exendin-4 induced glucagon-like peptide-1 receptor activation reverses behavioral impairments of mild traumatic brain injury in mice. *Age* 35, 1621–1636. doi: 10.1007/s11357-012-9464-0

Rauen, K., Späni, C. B., Tartaglia, M. C., Ferretti, M. T., Reichelt, L., Probst, P., et al. (2020). Quality of life after traumatic brain injury: a cross-sectional analysis uncovers age- and sex-related differences over the adult life span. *Geroscience* 43, 263–278. doi: 10.1007/s11357-020-00273-2

Toth, A., Kovacs, N., Tamas, V., Kornyei, B., Nagy, M., Horvath, A., et al. (2016). Microbleeds may expand acutely after traumatic brain injury. *Neurosci. Lett.* 617, 207–212. doi: 10.1016/j.neulet.2016.02.028

Toth, L., Czigler, A., Horvath, P., Kornyei, B., Szarka, N., Schwarcz, A., et al. (2020). Traumatic brain injury-induced cerebral microbleeds in the elderly. *Geroscience* 43, 125–136. doi: 10.1007/s11357-020-00280-3

Toth, P., Tarantini, S., Springo, Z., Tucsek, Z., Gautam, T., Giles, C. B., et al. (2015). Aging exacerbates hypertension-induced cerebral microhemorrhages in mice: role of resveratrol treatment in vasoprotection. *Aging Cell* 14, 400–408. doi: 10.1111/acel.12315

Ungvari, Z., Tarantini, S., Kirkpatrick, A. C., Csiszar, A., and Prodan, C. I. (2017). Cerebral microhemorrhages: mechanisms, consequences, and prevention. *Am. J. Physiol. Heart Circ. Physiol.* 312, H1128–H1143. doi: 10.1152/ajpheart.00780.2016

Ungvari, Z., Yabluchanskiy, A., Tarantini, S., Toth, P., Kirkpatrick, A. C., Csiszar, A., et al. (2018). Repeated Valsalva maneuvers promote symptomatic manifestations of cerebral microhemorrhages: implications for the pathogenesis of vascular cognitive impairment in older adults. *Geroscience* 40, 485–496. doi: 10.1007/s11357-018-0044-9

Wang, R., Liu, K., Ye, X., and Yan, S. (2018). Association between cerebral microbleeds and depression in the general elderly population: a meta-analysis. *Front. Psychiatry* 9:94. doi: 10.3389/fpsyt.2018.00094

Wang, X., Wei, X. E., Li, M. H., Li, W. B., Zhou, Y. J., Zhang, B., et al. (2014). Microbleeds on susceptibility-weighted MRI in depressive and non-depressive patients after mild traumatic brain injury. *Neurol. Sci.* 35, 1533–1539. doi: 10.1007/s10072-014-1788-3

Werring, D. J., Gregoire, S. M., and Cipolotti, L. (2010). Cerebral microbleeds and vascular cognitive impairment. *J. Neurol. Sci.* 299, 131–135. doi: 10.1016/j.jns.2010.08.034

Yakushiji, Y. (2015). Cerebral microbleeds: detection, associations and clinical implications. *Front. Neurol. Neurosci.* 37:78–92. doi: 10.1159/000437115

Conflict of Interest: The authors declare that the research was conducted in the absence of any commercial or financial relationships that could be construed as a potential conflict of interest.

Publisher's Note: All claims expressed in this article are solely those of the authors and do not necessarily represent those of their affiliated organizations, or those of the publisher, the editors and the reviewers. Any product that may be evaluated in this article, or claim that may be made by its manufacturer, is not guaranteed or endorsed by the publisher.

frontiers in Aging Neuroscience

ORIGINAL RESEARCH
published: 07 October 2021
doi: 10.3389/fnagi.2021.737359

White-Matter Hyperintensity Load and Differences in Resting-State Network Connectivity Based on Mild Cognitive Impairment Subtype

*Martina Vettore[1,2], Matteo De Marco[3], Claudia Pallucca[4,5], Matteo Bendini[6], Maurizio Gallucci[5] and Annalena Venneri[1,3]**

[1] Department of Neuroscience, University of Sheffield, Sheffield, United Kingdom, [2] Department of General Psychology, University of Padua, Padua, Italy, [3] Department of Life Sciences, Brunel University London, Uxbridge, United Kingdom, [4] Department of Clinical Neurosciences, University of Cambridge, Cambridge, United Kingdom, [5] Cognitive Impairment Center, Local Health Authority n.2 Marca Trevigiana, Treviso, Italy, [6] Unit of Neuroradiology, Treviso Regional Hospital, Treviso, Italy

"Mild cognitive impairment" (MCI) is a diagnosis characterised by deficits in episodic memory (aMCI) or in other non-memory domains (naMCI). Although the definition of subtypes is helpful in clinical classification, it provides little insight on the variability of neurofunctional mechanisms (i.e., resting-state brain networks) at the basis of symptoms. In particular, it is unknown whether the presence of a high load of white-matter hyperintensities (WMHs) has a comparable effect on these functional networks in aMCI and naMCI patients. This question was addressed in a cohort of 123 MCI patients who had completed an MRI protocol inclusive of T1-weighted, fluid-attenuated inversion recovery (FLAIR) and resting-state fMRI sequences. T1-weighted and FLAIR images were processed with the Lesion Segmentation Toolbox to quantify whole-brain WMH volumes. The CONN toolbox was used to preprocess all fMRI images and to run an independent component analysis for the identification of four large-scale haemodynamic networks of cognitive relevance (i.e., default-mode, salience, left frontoparietal, and right frontoparietal networks) and one control network (i.e., visual network). Patients were classified based on MCI subtype (i.e., aMCI vs. naMCI) and WMH burden (i.e., low vs. high). Maps of large-scale networks were then modelled as a function of the MCI subtype-by-WMH burden interaction. Beyond the main effects of MCI subtype and WMH burden, a significant interaction was found in the salience and left frontoparietal networks. Having a low WMH burden was significantly more associated with stronger salience-network connectivity in aMCI (than in naMCI) in the right insula, and with stronger left frontoparietal-network connectivity in the right frontoinsular cortex. Vice versa, having a low WMH burden was significantly more associated with left-frontoparietal network connectivity in naMCI (than in aMCI) in the left mediotemporal lobe. The association between WMH burden and strength of connectivity of resting-state functional networks differs between aMCI and naMCI patients. Although exploratory in nature, these findings indicate that clinical profiles reflect mechanistic interactions that may play a central role in the definition of diagnostic and prognostic statuses.

Keywords: dementia, Alzheimer's disease, haemodynamic, small vessel disease, independent component analysis

OPEN ACCESS

Edited by:
Prasad V. Katakam, Tulane University, United States

Reviewed by:
Peter Mukli, University of Oklahoma Health Sciences Center, United States
Zhiqun Wang, Aerospace Center Hospital, China

***Correspondence:**
Annalena Venneri
annalena.venneri@brunel.ac.uk

Received: *06 July 2021*
Accepted: *09 September 2021*
Published: *07 October 2021*

Citation:
Vettore M, De Marco M, Pallucca C, Bendini M, Gallucci M and Venneri A (2021) White-Matter Hyperintensity Load and Differences in Resting-State Network Connectivity Based on Mild Cognitive Impairment Subtype. Front. Aging Neurosci. 13:737359. doi: 10.3389/fnagi.2021.737359

INTRODUCTION

Mild cognitive impairment (MCI) is a diagnostic entity used to describe a disorder characterised by mild deficits in cognition that do not usually interfere with a patient's ability to lead an independent life. When first introduced, MCI described an intermediate stage between normal ageing and Alzheimer's disease (AD) dementia, and impairment in memory was required for the diagnosis to be made (Petersen et al., 1999). In time, the concept of MCI has been expanded to include cognitive impairments outside the memory domain and has become applicable to aetiologies other than AD (Winblad et al., 2004). Classification of MCI in different subtypes was introduced to recognise and distinguish among probable underlying aetiologies. A first classification is based on the impaired cognitive domain(s), with patients classified as "amnestic" MCI (aMCI) if their performance on tests of episodic memory is poor (usually 1–1.5 SD below the mean of age and education-matched peers), or, otherwise, as "non-amnestic" MCI (naMCI) for deficits in any other domains. This classification can be helpful to clinicians since aMCI is most commonly observed in patients who later progress to typical AD dementia, whereas naMCI is most likely associated with other, non-AD forms of dementia, such as dementia with Lewy bodies or frontotemporal dementia (Petersen, 2004; Yaffe et al., 2006; Albert et al., 2011; Ferman et al., 2013).

White-matter hyperintensities (WMHs), a neuroimaging feature associated with small-vessel disease, are a common finding in MCI patients, and do not seem to vary in severity across subtypes, at least on visual inspection (van de Pol et al., 2009; Boyle et al., 2016). WMHs are typically evidenced as areas of increased signal intensity in T2-weighted, proton-density and fluid-attenuated inversion recovery (FLAIR) MRI images. WMHs have been associated with a higher risk of developing MCI, vascular dementia and AD dementia, and overall appear to promote a faster decline in global cognitive performance (Debette and Markus, 2010; Boyle et al., 2016).

Experimental evidence suggests that small-vessel disease interacts with the diagnosis-defining pathological features of AD (i.e., amyloid plaques and neurofibrillary tangles). Both amyloid and TAU pathology, in fact, appear to affect the integrity of small vessels (Greenberg et al., 2020; Michalicova et al., 2020). In addition, a number of studies indicates that WMH burden may also contribute to neural pathophysiological changes, either in an additive or synergic way, by lowering the threshold for the clinical manifestation of dementia, or by being mechanistically linked to the core underlying pathophysiological processes (Breteler, 2000; Brickman et al., 2009; Gorelick et al., 2011; Kalaria and Ihara, 2013). On this note, a number of studies found a statistical association between WMH burden and amyloid β depositions (Brickman et al., 2015; Zhou et al., 2015; for a review, see Roseborough et al., 2017).

Recent studies have reported that WMH burden appears to disrupt the integrity of brain functional networks of healthy controls and MCI patients. Decreased functional connectivity within the default mode network (DMN) has been reported in association with WMH burden both in healthy adults (Reijmer et al., 2015; Liu et al., 2019) and in adults with cognitive impairment (Zhou et al., 2015; Liu et al., 2019). Positive associations between WMH burden and connectivity, on the other hand, have been found in the salience network (SN), suggesting a compensation mechanism (Cheng et al., 2017; De Marco et al., 2017b). The SN is involved in the detection and integration of endogenous and exogenous stimuli relevant for behaviour (Seeley et al., 2007; Menon, 2015) and a positive association would translate into the necessity of relying on more neural resources during the phase of stimulus selection and integration. There is also evidence linking WMH burden to executive dysfunction (Bombois et al., 2007; Debette and Markus, 2010), and Jacobs et al. (2012) studied the effect of WMH burden on functional networks involved in executive functions in MCI patients. WMHs affecting the territory underlying the frontoparietal and frontal–parietal-subcortical networks were indeed associated with decline in executive functions in MCI patients.

Most studies investigating associations of WMH burden with connectivity of resting state networks have considered MCI as a unique group, without any distinction of subtype. Since aMCI and naMCI present different clinical features and might have a different progression rate, they may originate from disruption of different underlying neural mechanisms and neuropathological processes. Distinct aetiologies may, therefore, interact differently with WMH burden to foster changes in functional connectivity, eventually determining the different clinical phenotypes.

In this study, we divided MCI patients into four groups based on WMH burden (high/low) and MCI subtype (aMCI/naMCI) to investigate how activity within major resting-state brain networks of cognitive relevance is modulated by the interaction of these two variables. We expected that WMH burden would be a statistically significant predictor of network connectivity, and that differences in network expression among subgroups would be reflective of patients' symptoms. In particular, we anticipated that effects in regions deputed to memory processing would be particularly relevant in aMCI patients, while effects in frontal and parietal regions would be relevant in naMCI patients, as this group typically shows a clinical profile characterised by executive or visuospatial impairment. Since this is, to our knowledge, the first study to investigate this interaction, we adopted an exploratory approach and analysed maps of connectivity voxel by voxel.

MATERIALS AND METHODS

Participants

This study included 123 patients with a clinical diagnosis of MCI enrolled as part of two initiatives: the Sheffield Ageing Database (United Kingdom) and the TREviso DEMentia (TREDEM) study (Italy) (Gallucci et al., 2012, 2018). Recruitment procedures were completed in the context of tertiary-care clinical facilities for memory disorders, where a diagnosis of MCI due to AD was formulated for each patient on the basis of published clinical criteria (Albert et al., 2011), and was confirmed by a consensus of clinicians, inclusive of a senior neurologist, a neuropsychologist and a neuroradiologist. Each patient underwent a brain MRI and

an extensive neuropsychological assessment. Exclusion criteria were defined as follows: clinical conditions of concern other than reduction in mental abilities, significant disabilities or psychiatric symptoms of concern, evidence of MRI abnormalities different from those expected in prodromal AD, pharmacological treatments with cholinergic drugs, psychotropic medications, drugs with toxic effects to internal organs or taken for research purposes, uncontrolled seizures (presence/diagnosis), sick sinus syndrome, peptic ulcer, neuropathy with conduction difficulties, abnormal levels of folates, vitamin B12 or thyroid stimulating hormone. Patients who did not undergo a full neuropsychological examination and that did not have structural and functional scans were also not considered for inclusion.

MRI Acquisition and Modelling

A harmonised protocol of anatomical and resting-state functional MRI images was devised as part of the study using 1.5 T systems (Philips Achieva and Siemens Avanto for patients recruited as part of the Sheffield Ageing Database and TREDEM initiatives, respectively). Anatomical images included three-dimensional T1-weighted and T2-weighted FLAIR sequences. Specifications for each sequence are detailed in **Table 1**.

Ten dummy volumes (20 s) were initially set up to allow the scanning environment to reach electromagnetic equilibrium prior to resting-state acquisitions. For these scans, patients were instructed to lay as still as possible with their eyes closed and in-scanner motion was minimised adapting the coil with foam padding to limit movement of the head.

The entire processing of MRI images was carried out with Matlab R2014a (Mathworks Inc., United Kingdom) and Statistical Parametric Mapping (SPM) 12 (Wellcome Centre for Human Neuroimaging, London, United Kingdom). T1-weighted scans were initially segmented to obtain native-space tissue-class maps of grey matter, white matter, and cerebrospinal fluid (Ashburner and Friston, 2005). The "get_totals" function[1] was then used to quantify each tissue-class map and thus obtain individual total intracranial volumes (TIVs).

T1-weighted and FLAIR scans were used to calculate WMH volumes *via* the Lesion Segmentation Tool toolbox (Schmidt et al., 2012; Birdsill et al., 2014). The Lesion Growth Algorithm (LGA) function was applied at a threshold of $\kappa = 0.3$ and the resulting individual WMH volume, expressed in ml, was divided by its respective TIV to obtain a fractional index of white matter lesion volume. A $\kappa = 0.3$ has been indicated as the best performing threshold by an earlier methodological study (Schmidt et al., 2012) and has been used in previous research as the optimal value to separate WMH from normal tissue (De Marco et al., 2017b; Bentham et al., 2019; Manca et al., 2021).

Resting state functional MRI scans were preprocessed and modelled using SPM and the CONN platform toolbox (Whitfield-Gabrieli and Nieto-Castanon, 2012). A first realignment was carried out using SPM to visualise and assess in-scanner motion plots for initial quality-check purposes. At this preliminary stage, scans with movement parameters in the range of ± 3 mm and $\pm 3°$ were considered acceptable. As a result, one scan was flagged up as problematic and was thus shortened to 135 consecutive volumes. All remaining scans included 240 volumes (equal to an 8-min acquisition) for all patients of the Sheffield Ageing Database, or 180 volumes (equal to a 6-min acquisition) for all patients recruited as part of the TREDEM initiative. Preprocessing was then restarted *via* CONN. Images were slice-timed, realigned, coregistered to their respective T1-weighted anatomical image, normalised to the Montreal Neurological Institute space template and smoothed with a 6-mm Gaussian kernel. A range of denoising methods was then applied to minimise the impact of artefactual sources of signal variability. This included band-pass filtering (0.01–0.1 Hz), scrubbing (volumes showing displacement larger than the 97th percentile were censored), regressing out of the first 10 principal components (aCompCor) calculated within the maps of white matter (5 components) and cerebrospinal fluid (5 components) and regressing out of 24 head motion parameters, including linear and rotational indices, their temporal derivatives and their squared values.

An independent component analysis (ICA) was run to obtain maps of network connectivity (Calhoun et al., 2001). This is a data-driven statistical analysis that assumes that independent sources of signal combine linearly and result in the observed data (Rosazza et al., 2012). The Fast-ICA reduction principle was used and 20 components were computed, in line with previously published research (Biswal et al., 2010). The spatial contour of the resulting components was inspected, four of which, spatially consistent with networks of interest, were selected. These networks (DMN, SN, and the left and right frontoparietal networks) play a major role in supporting cognitive functioning.

TABLE 1 | Technical specifications of the MRI sequences used in this study.

	Sheffield ageing database (n = 85)	TREDEM (n = 38)
T1-weighted		
Voxel size (mm^3)	1.1 × 1.1 × 0.6	1.0 × 1.0 × 1.0
Repetition time (ms)	7.42	9.50
Echo delay time (ms)	3.42	4.76
Matrix size	256 × 256	512 × 512
Number of slices	280	160
FLAIR		
Voxel size (mm^3)	0.75 × 0.75 × 4.93	0.45 × 0.45 × 6.50
Repetition time (ms)	8000	9000
Echo delay time (ms)	125	92
Matrix size	320 × 320	392 × 512
Number of slices	30	27
Resting-state fMRI		
Voxel size (mm^3)	2.87 × 2.87 × 6.00	3.81 × 3.81 × 5.00
Repetition time (ms)	2000	2000
Echo delay time (ms)	50	40
Matrix size	64 × 64	64 × 64
Field of view (mm)	230	244
Slices per volume	20	28

TREDEM, TREviso DEMentia study.

[1] http://www0.cs.ucl.ac.uk/staff/g.ridgway/vbm/get_totals.m

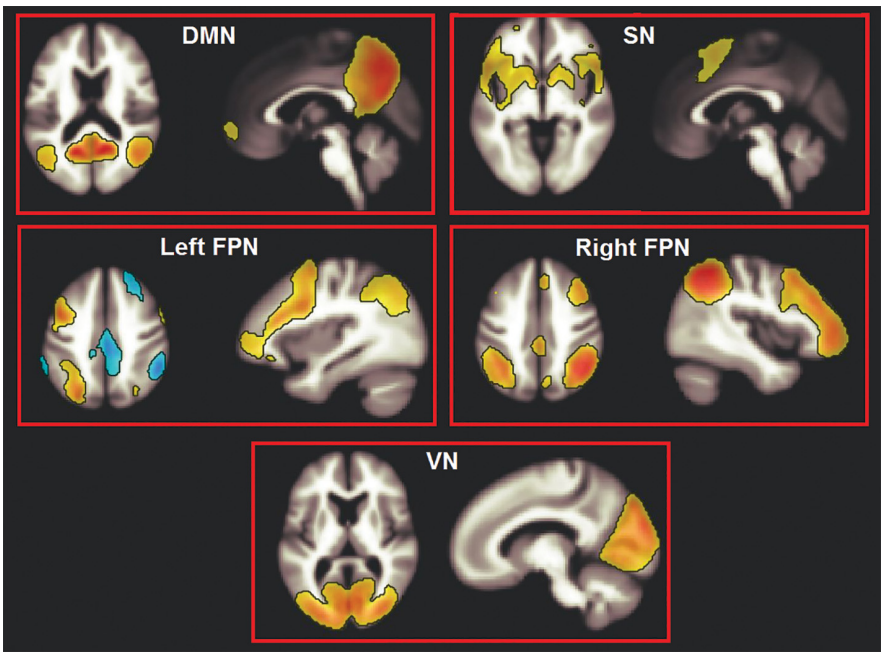

FIGURE 1 | The five large-scale haemodynamic networks investigated in this study. DMN, default mode network; SN, salience network; FPN, frontoparietal network; VN, visual network.

A fifth, non-cognitive network (the occipital visual network) was then selected as control component (**Figure 1**).

Data Modelling

Two statistical predictors of interest were defined to address the experimental hypothesis: WMH load and MCI subtype. A median split was carried out to separate normalised WMH volumes into "low WMH load" and "high WMH load". To define MCI subtypes, patients were classified as aMCI or naMCI based on their cognitive profile, i.e., patients were labelled as "aMCI" when impaired performance was recorded on at least one test of episodic memory, i.e., Rey-Osterrieth Complex Figure delayed recall, Prose Memory and Rey Auditory Verbal Learning Test (specific tests were used at each recruitment centre). Sub-sample numerosity distributed as follows: aMCI-low WMH load: $n = 43$; naMCI-low WMH load: $n = 19$; aMCI-high WMH load: $n = 42$; naMCI-high WMH load: $n = 19$.

The interaction between WMH load and MCI subtype was then modelled for each network of interest. Centre of recruitment, age, education level (in years), TIV, and global cognitive levels (i.e., Mini Mental State Examination score) were added as covariates. TIV also served to control for sex differences, since these two variables are strongly associated (Pintzka et al., 2015). Significance level was set at a cluster-forming threshold equal to $p < 0.001$ (uncorrected) and clusters surviving a cluster-level FWE-corrected threshold of $p < 0.05$ were reported as significant. Result coordinates were converted from Montreal Neurological Institute space into Talairach space and interpreted using the Talairach Daemon Client (Lancaster et al., 2000). To simplify the interpretation of the interaction contrasts, these were operationalised in terms of "low-WMH advantage" being larger among aMCI or naMCI. G*Power (version 3.1.9.7[2]) was used to estimate statistical power and ensure that our available sample size was sufficient to detect a significant statistical effect. With standard type I error and statistical power probabilities (5% and 80%, respectively), four groups and four covariates, a cohort size of $n = 123$ participants was sufficiently large to detect a medium effect size as significant ($f = 0.255$).

RESULTS

Demographic and neuropsychological characteristics of the groups are reported in **Table 2**. The distribution of individual WMH loads is shown in **Figure 2**. The median split separated the cohort into a homogeneous group of patients with low load and very low dispersion ($s^2 = 0.008$) and a group of patients with a load larger than 0.28% of their intracranial space and a significantly larger dispersion ($s^2 = 0.716$, Levene test's $p = 7.78^{-11}$). All significant main effects and interactions are listed in **Table 3** and illustrated in **Figures 3–5**. Patients with a high WMH load had more SN connectivity in right pericentral areas and in the right inferior frontal lobe (**Figure 3**). naMCI patients had more SN connectivity in the medial frontal gyrus, more DMN connectivity in the left dorsolateral prefrontal cortex and more left FPN connectivity in the precuneus (**Figure 4**).

A significant effect of the WMH-by-subtype interaction was found in the SN and left FPN (**Figure 5**). The low-WMH advantage was significantly stronger at the core of the SN (right

[2]https://stats.idre.ucla.edu/other/gpower/

TABLE 2 | Sample characterisation.

	aMCI		naMCI		*p* (ANOVA)
	Low WMH load	**High WMH load**	**Low WMH load**	**High WMH load**	
Demographic variables					
Age (years)	71.40 (6.40)	76.83 (5.85)	71.05 (5.82)	75.74 (5.30)	WMH ($p < 0.001$)
Education (years)	9.74 (3.80)	10.14 (4.43)	9.42 (4.15)	11.11 (3.93)	n.s.
Sex (f/m)	19/24	25/17	9/10	12/7	n.s.
Neurovolumetric variables					
TIV (ml)	1399.78 (152.94)	1454.49 (4.43)	1388.38 (171.74)	1488.98 (130.59)	WMH ($p = 0.008$)
WMH load fraction	0.0013 (0.0009)	0.0124 (0.0092)	0.0013 (0.0009)	0.0095 (0.0064)	WMH ($p < 0.001$)
Neurocognitive variables					
MMSE	27.48 (1.82)	26.52 (2.36)	27.11 (2.16)	27.89 (1.45)	Subtype-by-WMH ($p = 0.031$)
Digit cancellation test	46.23 (7.95)	44.76 (8.36)	47.78 (5.67)	50.63 (6.31)	Subtype ($p = 0.014$)
Letter fluency test	26.23 (9.53)	25.52 (11.85)	28.17 (12.72)	28.79 (10.62)	n.s.
Token test	32.17 (3.14)	31.57 (3.64)	31.58 (2.97)	32.21 (2.85)	n.s.
Immediate recall*	0.281 (0.157)	0.239 (0.105)	0.414 (0.106)	0.339 (0.100)	Subtype ($p < 0.001$); WMH ($p = 0.019$)
Delayed recall*	0.253 (0.186)	0.195 (0.157)	0.453 (0.130)	0.404 (0.137)	Subtype ($p < 0.001$)

*aMCI, amnestic mild cognitive impairment; MMSE, Mini-Mental State Examination; naMCI, non-amnestic mild cognitive impairment; TIV, total intracranial volume; WMHs, white-matter hyperintensities. *Variable expressed as a proportion of total score to harmonise scores obtained in different tests of memory between the two cohorts.*

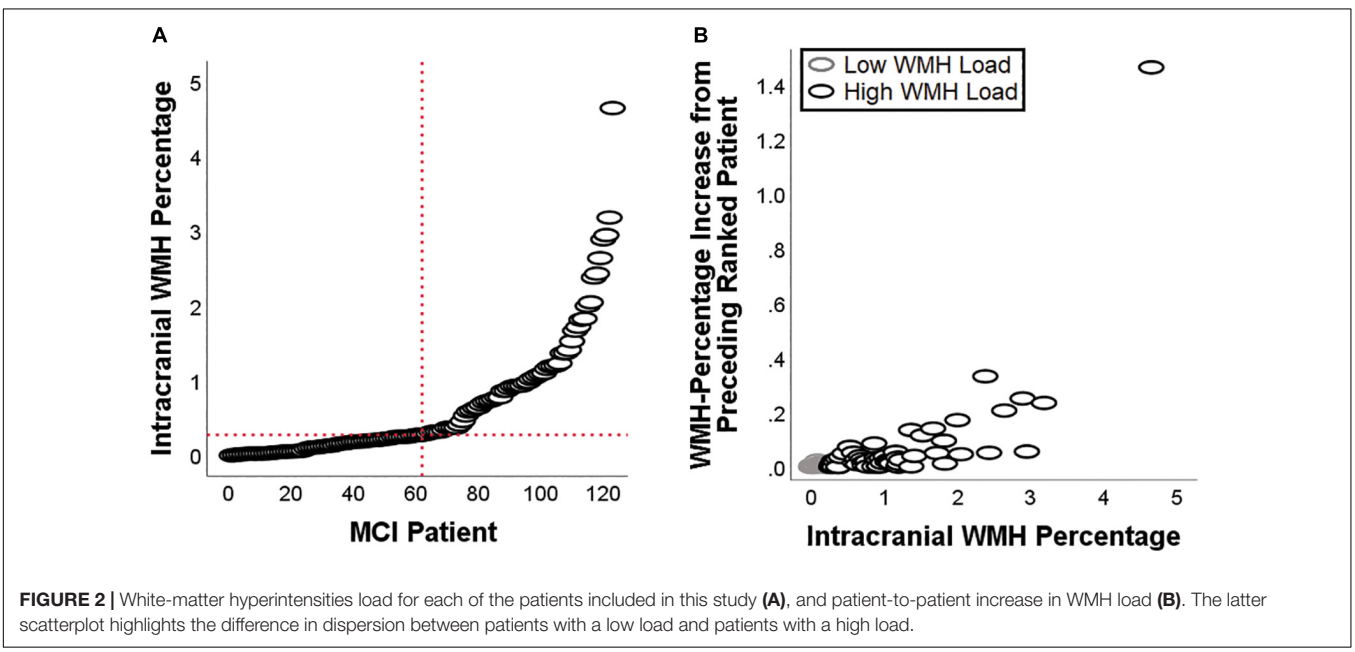

FIGURE 2 | White-matter hyperintensities load for each of the patients included in this study **(A)**, and patient-to-patient increase in WMH load **(B)**. The latter scatterplot highlights the difference in dispersion between patients with a low load and patients with a high load.

insula) among aMCI patients. Similarly, aMCI patients showed a more significant low-WMH advantage within the left FPN, in a right fronto-insular cluster extending to the right insula and right dorsolateral prefrontal territory. Conversely, naMCI patients showed a more significant low-WMH advantage within the left FPN in the left mediotemporal lobe.

DISCUSSION

Mild cognitive impairment is a clinical diagnosis that may be associated with a variety of neurodegenerative processes (Winblad et al., 2004). Although the prodromal phase of AD is more typically characterised by deficits in episodic memory, any MCI subtype may convert to dementia of the AD type (Fischer et al., 2007). It is, thus, clinically important to characterise the complexity of the mechanisms that are responsible for neurofunctional alterations in abnormal ageing. Since WMHs are common findings in older adults, in this study we investigated whether a low/high WMH load has a differential impact on resting-state circuitry in a way that depends on MCI subtype.

The effect of the WMH-by-subtype interaction was detectable in two large-scale pathways: the SN and left FPN. In the models analysing SN function, the "low-WMH load advantage" was significantly larger among aMCI patients in the right insula. This indicates that WMH burden plays a more central role in the expression of the SN when the profile is of the amnestic type. Integrity of the SN supports memory performance

TABLE 3 | Main effects and interactions emerged from the analyses.

Brain Region	Side	Cluster Size (voxels)	Cluster-Level *pFWE*	z Score	Talairach Coordinates		
					x	*y*	*z*
Main Effects							
High WMH Load > Low WMH Load – Salience Network							
Precentral Gyrus (BA4)	R	110	0.020	4.58	36	−26	64
Postcentral Gyrus (BA2)	R			3.41	30	−35	68
Inferior Frontal Gyrus (BA47)	R	102	0.029	4.04	38	26	−18
Non-Amnestic > Amnestic – Salience Network							
Medial Frontal Gyrus (BA11)	L	134	0.007	4.63	−10	63	−15
Non-Amnestic > Amnestic – Default-Mode Network							
Middle Frontal Gyrus (BA8)	L	99	0.026	4.33	−48	12	38
Inferior Frontal Gyrus (BA45)	L	151	0.002	3.89	−57	11	18
Inferior Frontal Gyrus (BA45)	L			3.79	−48	16	14
Inferior Frontal Gyrus (BA44)	L			3.74	−57	16	12
Non-Amnestic > Amnestic – Left Frontoparietal Network							
Precuneus (BA7)	L	94	0.028	4.20	−12	−50	54
Precuneus (BA7)	L			3.83	−6	−57	62
Precuneus (BA7)	L			3.18	−20	−46	56
Interaction Effects							
Low WMH Load Advantage Stronger in Amnestic – Salience Network							
Insula (BA13)	R	109	0.021	4.16	42	−16	1
Insula (BA13)	R			3.76	38	−25	3
Low WMH Load Advantage Stronger in Amnestic – Left Frontoparietal Network							
Insula (BA13)	R	131	0.008	4.57	30	17	−8
Middle Frontal Gyrus (BA9)	R			4.43	28	42	33
Superior Frontal Gyrus (BA9)	R			3.84	24	54	32
Superior Frontal Gyrus (BA10)	R			3.66	26	54	23
Low WMH Load Advantage Stronger in Non-Amnestic – Left Frontoparietal Network							
Parahippocampal Gyrus (BA35)	L	124	0.011	4.29	36	−26	64
Uncus	L			1.03	30	−35	68
Parahippocampal Gyrus (BA35)	L			3.65	38	26	−18

BA, Brodmann area; FWE, family-wise error; L, left; R, right; WMHs, white-matter hyperintensities.

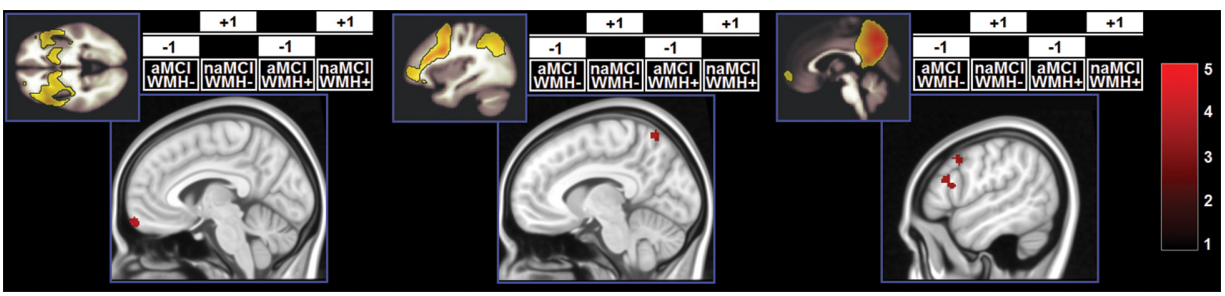

FIGURE 3 | Clusters in which a significant main effect of WMH load was found. *z*-Scores are indicated by the colour bar. aMCI, amnestic MCI; naMCI, non-amnestic MCI; WMH–, low WMH; WMH+, high WMH.

(Andreano et al., 2017), but studies characterising the SN profile in aMCI have led to conflicting findings, with some studies indicating reduction (He et al., 2014) and others reporting increases (Li et al., 2020) in SN expression. Although we found significant main effects of "subtype" and "WMH load", indicating that aMCI patients and patients with a low WMH load have reduced regional expression of the SN, these were superseded by a significant effect of the interaction. These findings indicate,

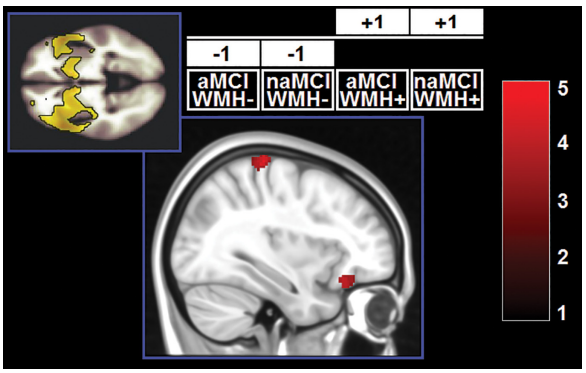

FIGURE 4 | Clusters in which a significant main effect of subtype was found. *z*-Scores are indicated by the colour bar. aMCI, amnestic MCI; naMCI, non-amnestic MCI; WMH–, low WMH; WMH+, high WMH.

therefore, that changes in functional connectivity of the SN may be driven by an interplay of mechanisms, and that WMH load may contribute to this interaction. This principle may play a central role at a clinical level, since neurofunctional alterations are at the basis of cognitive dysfunction. More specifically, from the analyses of the SN it was amnestic patients who were particularly susceptible to the detrimental effects of WMHs. Although episodic memory is supported by a wide-distributed large-scale network, its efficiency is dependent on the integrity of the hippocampus (Dickerson and Eichenbaum, 2010). On the other hand, the functions impaired in MCI patients with dysexecutive or visuospatial deficits are typically sustained by networks less homogeneously dependent on a single structure. We argue that this is the main reason why variability in WMHs has a smaller statistical impact among naMCI patients. Vice versa, aMCI patients whose white-matter tracts are relatively spared by WMH pathology can benefit more from higher level of SN neurofunctional integrity.

An interaction effect in the same direction also emerged from the analysis of the left FPN. Right frontoinsular regions are the core of SN processing and are responsible for transitional switching between DMN and FPN (Sridharan et al., 2008). Increased FPN expression in this region indicates tighter coupling between SN and FPN. Loss of inter-network functional connectivity between the right frontoinsular cortex accompanies cognitive decline in MCI patients (He et al., 2014). Along this interpretational line, we found that in patients with aMCI a low-WMH burden appears to be advantageous as it results in a tighter SN-FPN inter-network connectivity. Within the left FPN, however, an effect in the opposite direction was also found. Having a low-WMH load was associated with stronger network expression in the left mediotemporal lobe. This territory shows distinctive regional atrophy at the MCI stage of AD (Ferreira et al., 2011) and is, thus, particularly dysfunctional in those MCI patients who have underlying AD pathology. We argue that patients with naMCI benefit the most from a low-WMH burden because, as shown by their performance on episodic memory tests, their mediotemporal functioning is within normal levels, and, therefore, a "typical" effect of WMH load can be detected. Vice versa, WMH load would have little or no effect in patients with memory impairment due to dysfunctional mediotemporal areas.

No significant effect was found for the DMN. This expands the findings provided by previous exploratory studies carried out in small samples ($n < 50$) of patients with cognitive impairment (Zhou et al., 2015; Liu et al., 2019). The DMN is a neurofunctional system characterised by a degree of vulnerability to multiple processes, including ageing and AD pathology (Jagust, 2013). A recent meta-analysis, however, found considerable variability in the pattern of DMN alterations seen in patients with MCI (Eyler et al., 2019). Such heterogeneity suggests that there is no direct and clear-cut link between network dysfunction and a clinical diagnosis of MCI and that this link is likely to be influenced by various mechanisms and intervenient factors, such as neural compensation and reserve (Stern, 2009) that are at the basis of inter-individual differences in the functional circuitry that supports cognitive functioning. It has also been proposed that the pattern of regional atrophy typically seen in ageing may act as a promoter of functional plasticity, because task activation in older adults tends to increase in areas that are subjected to age-associated volumetric decrease (Greenwood, 2007). A recent study confirmed this negative association between regional structure and network expression in healthy adults, and also found inverse (positive) associations in patients with AD, indicating that those with reduced atrophy were also those with a stronger network expression (Sarli et al., 2021). Within this context, WMHs are a further contributor to the

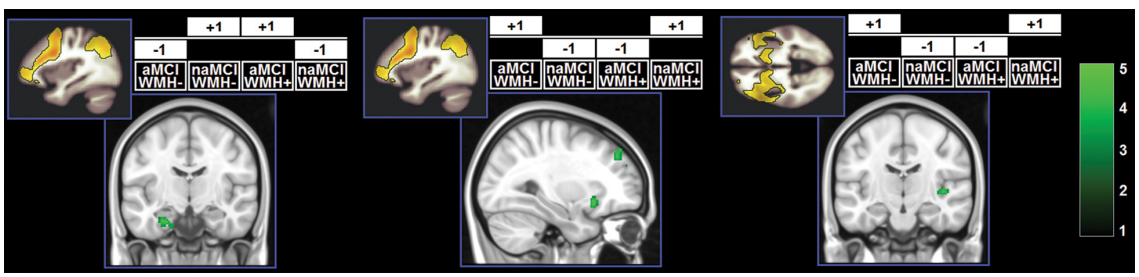

FIGURE 5 | Clusters in which a significant interaction was found. *z*-Scores are indicated by the colour bar. Specific contrasts are shown for each model associated with a significant findings. aMCI, amnestic MCI; naMCI, non-amnestic MCI; WMH–, low WMH; WMH+, high WMH.

reorganisation of the neurofunctional architecture, as reported by a number of investigations (Reijmer et al., 2015; Zhou et al., 2015; Cheng et al., 2017; De Marco et al., 2017b; Liu et al., 2019). The resulting picture is, thus, that of large-scale networks being under the effect of multiple concurrent (and, plausibly, interactive) processes. This study adds to this body of literature, providing evidence that significant interactions exist between WMH load and the expression of the neurofunctional architecture underlying distinct cognitive profiles. It is also worth noting that, while the four subgroups included in this study were, on average, between 71 and 76 years old, MCI is a condition that may be diagnosed at any point of middle-to-old adulthood. Since ageing is associated with increasing WMH load as well as physiological changes in network expression (and with a number of other neurological processes such as cortical atrophy and hypometabolism), it still needs to be confirmed whether the associations described in this study will hold valid at other stages of ageing. Also, since network alterations at the MCI stage may manifest either as a reduction or as an over-expression of neurofunctional pathways, plausibly the outcome of either compensatory and/or maladaptive processes (Gardini et al., 2015; De Marco et al., 2017a), it is important to be cautious when interpreting findings that are expressed as unidirectional (i.e., in the form of positive or negative associations) statistical effects.

There are two limitations to this study to take into consideration. First, we adopted a methodology that computes a global load of WMHs that does not allow a precise localisation within different brain regions (i.e., deep vs. periventricular white matter). Although this is a methodological aspect of potential improvement to investigate the impact of WMHs on neurofunctional pathways in the future, it is known that the frontal lobe seems to be particularly susceptible to this type of damage, regardless of where hyperintensities are located (Tullberg et al., 2004). This indicates that the calculation of a global WMH load measure is of interest, since the effect of this type of damage seems to converge toward a common target. The two groups of patients resulting from the median split showed different distributions, with patients with a low WMH load distributing homogeneously in proximity to 0 (ranging from 0 to 0.276% of intracranial space) and patients with a high-WMH load showing a significantly larger dispersion (ranging from 0.285 to 4.649% of intracranial space). In addition, a binary classification of patients (i.e., as having a "low"-vs.-"high" WMH load) is of clinical relevance, since this information is usually taken into account by clinicians to define the most adequate approach to treatment. In this respect, binarising the load of hyperintensities facilitates the operationalisation of the interaction term and helps draw clearer interpretations that are of immediate clinical value. Second, we did not separate our cohort of MCI patients into "single-domain" and "multiple-domain". This further subdivision would require larger cohorts and would also require a more extensive number of cognitive tests in order to characterise each domain in equal detail. Finally, although not a limitation, we acknowledge that additional or different correction factors might have been included in the models. Given that we corrected for those factors that account for the greatest influence on brain parameters, it is unlikely, however, that this might have led to substantial differences in the pattern of findings.

In conclusion, our study explored for the first time the interaction of WMH burden and MCI subtype. This topic will become increasingly more relevant as the contribution of vascular damage to cognitive deficits across different types of dementia outside the vascular type is being recognised. With the need of identifying individuals at risk for dementia earlier on, it is important to identify all the variables that can contribute to their cognitive phenotype and investigate how the interaction among these variables is reflected at the pathophysiological level.

DATA AVAILABILITY STATEMENT

The raw data supporting the conclusions of this article will be made available by the authors, without undue reservation.

ETHICS STATEMENT

Ethical review and approval was not required for the study on human participants in accordance with the local legislation and institutional requirements. The patients/participants provided their written informed consent to participate in this study.

AUTHOR CONTRIBUTIONS

MV carried out the literature search, ran the analyses, interpreted the findings, and wrote the manuscript. MD contributed to data collection, designed this study, ran the analyses, and interpreted the findings. CP and MB contributed to data collection and reviewed the manuscript. MG coordinated the data collection and reviewed the manuscript. AV coordinated the data collection, conceived this study, reviewed and finalised the manuscript. All authors contributed to the article and approved the submitted version.

FUNDING

Data collection and MRI scans acquisition were partially funded by grant No. 42/RF-2010-2321718 by the Italian Ministry of Health to AV.

REFERENCES

Albert, M. S., DeKosky, S. T., Dickson, D., Dubois, B., Feldman, H. H., Fox, N. C., et al. (2011). The diagnosis of mild cognitive impairment due to Alzheimer's disease: recommendations from the National Institute on Aging-Alzheimer's Association workgroups on diagnostic guidelines for Alzheimer's disease. *Alzheimers Dement.* 7, 270–279. doi: 10.1016/j.jalz.2011.03.008

Andreano, J. M., Touroutoglou, A., Dickerson, B. C., and Barrett, L. F. (2017). Resting connectivity between salience nodes predicts recognition memory. *Soc. Cogn. Affect. Neurosci.* 12, 948–955. doi: 10.1093/scan/nsx026

Ashburner, J., and Friston, K. J. (2005). Unified segmentation. *Neuroimage* 26, 839–851. doi: 10.1016/j.neuroimage.2005.02.018

Bentham, C., De Marco, M., and Venneri, A. (2019). The modulatory effect of cerebrovascular burden in response to cognitive stimulation in healthy ageing

and mild cognitive impairment. *Neural Plast.* 2019:2305318. doi: 10.1155/2019/2305318

Birdsill, A. C., Koscik, R. L., Jonaitis, E. M., Johnson, S. C., Okonkwo, O. C., Hermann, B. P., et al. (2014). Regional white matter hyperintensities: aging, Alzheimer's disease risk, and cognitive function. *Neurobiol. Aging* 35, 769–776. doi: 10.1016/j.neurobiolaging.2013.10.072

Biswal, B. B., Mennes, M., Zuo, X. N., Gohel, S., Kelly, C., Smith, S. M., et al. (2010). Toward discovery science of human brain function. *Proc. Natl. Acad. Sci. USA* 107, 4734–4739. doi: 10.1073/pnas.0911855107

Bombois, S., Debette, S., Delbeuck, X., Bruandet, A., Lepoittevin, S., Delmaire, C., et al. (2007). Prevalence of subcortical vascular lesions and association with executive function in mild cognitive impairment subtypes. *Stroke* 38, 2595–2597. doi: 10.1161/STROKEAHA.107.486407

Boyle, P. A., Yu, L., Fleischman, D. A., Leurgans, S., Yang, J., Wilson, R. S., et al. (2016). White matter hyperintensities, incident mild cognitive impairment, and cognitive decline in old age. *Ann. Clin. Transl. Neurol.* 3, 791–800. doi: 10.1002/acn3.343

Breteler, M. M. (2000). Vascular risk factors for Alzheimer's disease: an epidemiologic perspective. *Neurobiol. Aging* 21, 153–160. doi: 10.1016/S0197-4580(99)00110-4

Brickman, A. M., Guzman, V. A., Gonzalez-Castellon, M., Razlighi, Q., Gu, Y., Narkhede, A., et al. (2015). Cerebral autoregulation, beta amyloid, and white matter hyperintensities are interrelated. *Neurosci. Lett.* 592, 54–58. doi: 10.1016/j.neulet.2015.03.005

Brickman, A. M., Muraskin, J., and Zimmerman, M. E. (2009). Structural neuroimaging in Alzheimer's disease: do white matter hyperintensities matter? *Dialogues Clin. Neurosci.* 11, 181–190. doi: 10.31887/DCNS.2009.11.2/ambrickman

Calhoun, V. D., Adali, T., Pearlson, G. D., and Pekar, J. J. (2001). A method for making group inferences from functional MRI data using independent component analysis. *Hum. Brain Mapp.* 14, 140–151. doi: 10.1002/hbm.1048

Cheng, R., Qi, H., Liu, Y., Zhao, S., Li, C., Liu, C., et al. (2017). Abnormal amplitude of low-frequency fluctuations and functional connectivity of resting-state functional magnetic resonance imaging in patients with leukoaraiosis. *Brain Behav.* 7:e00714. doi: 10.1002/brb3.714

De Marco, M., Manca, R., Mitolo, M., and Venneri, A. (2017b). White matter hyperintensity load modulates brain morphometry and brain connectivity in healthy adults: A neuroplastic mechanism? *Neural Plast.* 2017:4050536. doi: 10.1155/2017/4050536

De Marco, M., Beltrachini, L., Biancardi, A., Frangi, A. F., and Venneri, A. (2017a). Machine-learning support to individual diagnosis of mild cognitive impairment using multimodal MRI and cognitive assessments. *Alzheimer Dis. Assoc. Disord.* 31, 278–286. doi: 10.1097/WAD.0000000000000208

Debette, S., and Markus, H. S. (2010). The clinical importance of white matter hyperintensities on brain magnetic resonance imaging: systematic review and meta-analysis. *BMJ* 341:c3666. doi: 10.1136/bmj.c3666

Dickerson, B. C., and Eichenbaum, H. (2010). The episodic memory system: neurocircuitry and disorders. *Neuropsychopharmacology* 35, 86–104. doi: 10.1038/npp.2009.126

Eyler, L. T., Elman, J. A., Hatton, S. N., Gough, S., Mischel, A. K., Hagler, D. J., et al. (2019). Resting state abnormalities of the default mode network in mild cognitive impairment: a systematic review and meta-analysis. *J. Alzheimers Dis.* 70, 107–120. doi: 10.3233/JAD-180847

Ferman, T. J., Smith, G. E., Kantarci, K., Boeve, B. F., Pankratz, V. S., Dickson, D. W., et al. (2013). Nonamnestic mild cognitive impairment progresses to dementia with Lewy bodies. *Neurology* 81, 2032–2038. doi: 10.1212/01.wnl.0000436942.55281.47

Ferreira, L. K., Diniz, B. S., Forlenza, O. V., Busatto, G. F., and Zanetti, M. V. (2011). Neurostructural predictors of Alzheimer's disease: a meta-analysis of VBM studies. *Neurobiol. Aging* 32, 1733–1741. doi: 10.1016/j.neurobiolaging.2009.11.008

Fischer, P., Jungwirth, S., Zehetmayer, S., Weissgram, S., Hoenigschnabl, S., Gelpi, E., et al. (2007). Conversion from subtypes of mild cognitive impairment to Alzheimer dementia. *Neurology* 68, 288–291. doi: 10.1212/01.wnl.0000252358.03285.9d

Gallucci, M., Di Battista, M. E., Battistella, G., Falcone, C., Bisiacchi, P. S., and Di Giorgi, E. (2018). Neuropsychological tools to predict conversion from amnestic mild cognitive impairment to dementia. The TREDEM Registry. *Neuropsychol. Dev. Cogn. B Aging Neuropsychol. Cogn.* 25, 550–560. doi: 10.1080/13825585.2017.1349869

Gallucci, M., Mariotti, E., Saraggi, D., Stecca, T., Oddo, M. G., Bergamelli, C., et al. (2012). The Treviso Dementia (TREDEM) study: a biomedical, neuroradiological, neuropsychological and social investigation of dementia in north-eastern Italy. *J. Frailty Aging* 1, 24–31.

Gardini, S., Venneri, A., Sambataro, F., Cuetos, F., Fasano, F., Marchi, M., et al. (2015). Increased functional connectivity in the default mode network in mild cognitive impairment: a maladaptive compensatory mechanism associated with poor semantic memory performance. *J. Alzheimers Dis.* 45, 457–470. doi: 10.3233/JAD-142547

Gorelick, P. B., Scuteri, A., Black, S. E., Decarli, C., Greenberg, S. M., Iadecola, C., et al. (2011). Vascular contributions to cognitive impairment and dementia: a statement for healthcare professionals from the american heart association/american stroke association. *Stroke* 42, 2672–2713. doi: 10.1161/STR.0b013e3182299496

Greenberg, S. M., Bacskai, B. J., Hernandez-Guillamon, M., Pruzin, J., Sperling, R., and van Veluw, S. J. (2020). Cerebral amyloid angiopathy and Alzheimer disease - one peptide, two pathways. *Nat. Rev. Neurol.* 16, 30–42. doi: 10.1038/s41582-019-0281-2

Greenwood, P. M. (2007). Functional plasticity in cognitive aging: review and hypothesis. *Neuropsychology* 21, 657–673. doi: 10.1037/0894-4105.21.6.657

He, X., Qin, W., Liu, Y., Zhang, X., Duan, Y., Song, J., et al. (2014). Abnormal salience network in normal aging and in amnestic mild cognitive impairment and Alzheimer's disease. *Hum. Brain Mapp.* 35, 3446–3464. doi: 10.1002/hbm.22414

Jacobs, H. I. L., Visser, P. J., Van Boxtel, M. P. J., Frisoni, G. B., Tsolaki, M., Papapostolou, P., et al. (2012). Association between white matter hyperintensities and executive decline in mild cognitive impairment is network dependent. *Neurobiol. Aging* 33, e1–e8. doi: 10.1016/j.neurobiolaging.2010.07.015

Jagust, W. (2013). Vulnerable neural systems and the borderland of brain aging and neurodegeneration. *Neuron* 77, 219–234. doi: 10.1016/j.neuron.2013.01.002

Kalaria, R. N., and Ihara, M. (2013). Dementia: vascular and neurodegenerative pathways-will they meet? *Nat. Rev. Neurol.* 9, 487–488. doi: 10.1038/nrneurol.2013.164

Lancaster, J. L., Woldorff, M. G., Parsons, L. M., Liotti, M., Freitas, C. S., Rainey, L., et al. (2000). Automated Talairach Atlas labels for functional brain mapping. *Hum. Brain Mapp.* 10, 120–131. doi: 10.1002/1097-0193(200007)10:3<120::AID-HBM30>3.0.CO;2-8

Li, X., Wang, F., Liu, X., Cao, D., Cai, K., Jiang, X., et al. (2020). Changes in brain function networks in patients with amnestic mild cognitive impairment: a resting-state fMRI study. *Front. Neurol.* 11:554032. doi: 10.3389/fneur.2020.554032

Liu, R., Wu, W., Ye, Q., Gu, Y., Zou, J., Chen, X., et al. (2019). Distinctive and pervasive alterations of functional brain networks in cerebral small vessel disease with and without cognitive impairment. *Dement. Geriatr. Cogn. Disord.* 47, 55–67. doi: 10.1159/000496455

Manca, R., Mitolo, M., Wilkinson, I. D., Paling, D., Sharrack, B., and Venneri, A. (2021). A network-based cognitive training induces cognitive improvements and neuroplastic changes in patients with relapsing-remitting multiple sclerosis: an exploratory case-control study. *Neural Regen. Res.* 16, 1111–1120. doi: 10.4103/1673-5374.300450

Menon, V. (2015). *Salience Network in Brain Mapping: An Encyclopedic Reference (Vol. 2)*. Amsterdam: Elsevier Inc. doi: 10.1016/B978-0-12-397025-1.00052-X

Michalicova, A., Majerova, P., and Kovac, A. (2020). Tau protein and its role in blood–brain barrier dysfunction. *Front. Mol. Neurosci.* 13:570045. doi: 10.3389/fnmol.2020.570045

Petersen, R. C. (2004). Mild cognitive impairment as a diagnostic entity. *J. Intern. Med.* 256, 183–194. doi: 10.1111/j.1365-2796.2004.01388.x

Petersen, R. C., Smith, G. E., Waring, S. C., Ivnik, R. J., Tangalos, E. G., and Kokmen, E. (1999). Mild cognitive impairment: clinical characterization and outcome. *Arch. Neurol.* 56, 303–308. doi: 10.1001/archneur.56.3.303

Pintzka, C. W. S., Hansen, T. I., Evensmoen, H. R., and Håberg, A. K. (2015). Marked effects of intracranial volume correction methods on sex differences

in neuroanatomical structures: a HUNT MRI study. *Front. Neurosci.* 9:238. 10.3389/fnins.2015.00238

Reijmer, Y. D., Schultz, A. P., Leemans, A., O'Sullivan, M. J., Gurol, M. E., Sperling, R., et al. (2015). Decoupling of structural and functional brain connectivity in older adults with white matter hyperintensities. *Neuroimage* 117, 222–229. doi: 10.1016/j.neuroimage.2015.05.054

Rosazza, C., Minati, L., Ghielmetti, F., Mandelli, M. L., and Bruzzone, M. G. (2012). Functional connectivity during resting-state functional MR imaging: study of the correspondence between independent component analysis and region-of-interest-based methods. *Am. J. Neuroradiol.* 33, 180–187. doi: 10.3174/ajnr.A2733

Roseborough, A., Ramirez, J., Black, S. E., and Edwards, J. D. (2017). Associations between amyloid ß and white matter hyperintensities: a systematic review. *Alzheimers Dement.* 13, 1154–1167. doi: 10.1016/j.jalz.2017.01.026

Sarli, G., De Marco, M., Hallikainen, M., Soininen, H., Bruno, G., and Venneri, A. (2021). Regional strength of large-scale functional brain networks is associated with regional volumes in older adults and in Alzheimer's disease. *Brain Connect.* 11, 201–212. doi: 10.1089/brain.2020.0899

Schmidt, P., Gaser, C., Arsic, M., Buck, D., Förschler, A., Berthele, A., et al. (2012). An automated tool for detection of FLAIR-hyperintense white-matter lesions in multiple sclerosis. *Neuroimage* 59, 3774–3783. doi: 10.1016/j.neuroimage.2011.11.032

Seeley, W. W., Menon, V., Schatzberg, A. F., Keller, J., Glover, G. H., Kenna, H., et al. (2007). Dissociable intrinsic connectivity networks for salience processing and executive control. *J. Neurosci.* 27, 2349–2356. doi: 10.1523/JNEUROSCI.5587-06.2007

Sridharan, D., Levitin, D. J., and Menon, V. (2008). A critical role for the right fronto-insular cortex in switching between central-executive and default-mode networks. *Proc. Natl. Acad. Sci. USA*. 105, 12569–12574. doi: 10.1073/pnas.0800005105

Stern, Y. (2009). Cognitive reserve. *Neuropsychologia* 47, 2015–2028. doi: 10.1016/j.neuropsychologia.2009.03.004

Tullberg, M., Fletcher, E., DeCarli, C., Mungas, D., Reed, B. R., Harvey, D. J., et al. (2004). White matter lesions impair frontal lobe function regardless of their location. *Neurology* 63, 246–253. doi: 10.1212/01.WNL.0000130530.55104.B5

van de Pol, L. A., Verhey, F., Frisoni, G. B., Tsolaki, M., Papapostolou, P., Nobili, F., et al. (2009). White matter hyperintensities and medial temporal lobe atrophy in clinical subtypes of mild cognitive impairment: the DESCRIPA study. *J. Neurol. Neurosurg. Psychiatry* 80, 1069–1074. doi: 10.1136/jnnp.2008.158881

Whitfield-Gabrieli, S., and Nieto-Castanon, A. (2012). Conn: A functional connectivity toolbox for correlated and anticorrelated brain networks. *Brain Connect.* 2, 125–141. doi: 10.1089/brain.2012.0073

Winblad, B., Palmer, K., Kivipelto, M., Jelic, V., Fratiglioni, L., Wahlund, L. O., et al. (2004). Mild cognitive impairment - beyond controversies, towards a consensus: report of the International Working Group on Mild Cognitive Impairment. *J. Intern. Med.* 256, 240–246. doi: 10.1111/j.1365-2796.2004.01380.x

Yaffe, K., Petersen, R. C., Lindquist, K., Kramer, J., and Miller, B. (2006). Subtype of mild cognitive impairment and progression to dementia and death. *Dement. Geriatr. Cogn. Disord.* 22, 312–319. doi: 10.1159/000095427

Zhou, Y., Yu, F., and Duong, T. Q., for the Alzheimer's Disease Neuroimaging Initiative. (2015). White matter lesion load is associated with resting state functional MRI activity and amyloid PET but not FDG in mild cognitive impairment and early Alzheimer's disease patients. *J. Magn. Reson. Imaging* 41, 102–109. doi: 10.1002/jmri.24550

Conflict of Interest: The authors declare that the research was conducted in the absence of any commercial or financial relationships that could be construed as a potential conflict of interest.

Publisher's Note: All claims expressed in this article are solely those of the authors and do not necessarily represent those of their affiliated organizations, or those of the publisher, the editors and the reviewers. Any product that may be evaluated in this article, or claim that may be made by its manufacturer, is not guaranteed or endorsed by the publisher.

frontiers in Aging Neuroscience

ORIGINAL RESEARCH
published: 08 October 2021
doi: 10.3389/fnagi.2021.738359

The Relationship Between ADAMTS13 Activity and Overall Cerebral Small Vessel Disease Burden: A Cross-Sectional Study Based on CSVD

Wenbo Sun[1], Yufan Luo[1], Shufan Zhang[1], Wenmei Lu[1], Luqiong Liu[2], Xiaoli Yang[1] and Danhong Wu[1]**

[1]*Department of Neurology, Shanghai Fifth People's Hospital, Fudan University, Shanghai, China,* [2]*Department of General Medicine, Shanghai Fifth People's Hospital, Fudan University, Shanghai, China*

Objectives: This study aimed to investigate the association between plasma von Willebrand factor (VWF) level, ADAMTS13 activity, and neuroimaging features of cerebral small vessel disease (CSVD), including the CSVD neuroimaging markers and the overall CSVD burden.

Methods: CSVD patients admitted to our hospital from 2016 to 2020 were recruited. Plasma VWF level and ADAMTS13 activity were measured. The overall effect of CSVD on the brain was described as a validated CSVD score. We evaluated the association between VWF levels, ADAMTS13 activity, and the increasing severity of CSVD score by the logistic regression model.

Results: We enrolled 296 patients into this study. The mean age of the sample was 69.0 years (SD 7.0). The mean VWF level was 1.31 IU/mL, and the ADAMTS13 activity was 88.01 (SD 10.57). In multivariate regression analysis, lower ADAMTS13 activity and higher VWF level was related to white matter hyperintensity (WMH) [$\beta = -7.31$; 95% confidence interval (CI) (−9.40, −4.93); $p<0.01$; $\beta = 0.17$; 95% confidence interval (0.11, 0.23); $p<0.01$], subcortical infarction (SI) [($\beta = -9.22$; 95% CI (−11.37, −7.06); $p<0.01$); $\beta = 0.21$; 95% confidence interval (0.15, 0.27); $p<0.01$] independently, but not cerebral microbleed (CMB) [($\beta = -2.3$; 95% CI (−4.95, 0.05); $p = 0.22$); $\beta = 0.02$; 95% confidence interval (−0.05, 0.08); $p = 0.63$]. Furthermore, ADAMTS13 activity was independently negatively correlated with the overall CSVD burden (odd ratio = 21.33; 95% CI (17.46, 54.60); $p < 0.01$) after adjustment for age, history of hypertension, and current smoking.

Conclusions: Reducing ADAMTS13 activity change is related to white matter hyperintensity, subcortical infarction, but not with cerebral microhemorrhage. In addition, ADAMTS13 may have played an essential role in the progression of CSVD.

Keywords: cerebral small vessel disease, ADAMTS13, von Willebrand factor, overall cerebral small vessel disease burden, white matter hyperintensity (WMH), subcortical infarction

OPEN ACCESS

Edited by:
Stefano Tarantini, University of Oklahoma Health Sciences Center, United States

Reviewed by:
Peter J. Toth, University of Pécs, Hungary
Federico Verde, Istituto Auxologico Italiano (IRCCS), Italy

****Correspondence:***
Danhong Wu
danhongwu@fudan.edu.cn
Xiaoli Yang
xiaoliyangsls@sina.com

Received: *08 July 2021*
Accepted: *23 August 2021*
Published: *08 October 2021*

Citation:
Sun W, Luo Y, Zhang S, Lu W, Liu L, Yang X and Wu D (2021) The Relationship Between ADAMTS13 Activity and Overall Cerebral Small Vessel Disease Burden: A Cross-Sectional Study Based on CSVD. Front. Aging Neurosci. 13:738359. doi: 10.3389/fnagi.2021.738359

INTRODUCTION

Cerebral small vessel disease (CSVD) is a syndrome with various structural or functional lesions involving perforating vessels that leads to parenchymal injury, which causes clinical, cognitive, neuroimaging, and neuropathological manifestation. Neuroimaging features are diverse so that the total CSVD score was created to capture the overall effect of CSVD on the brain, which incorporates white matter hyperintensity (WMH), cerebral microbleeds (CMB), lacunes, and enlarged perivascular spaces (EPVS; Huijts et al., 2013; Staals et al., 2014). The pathogenesis of the CSVD is not well known, but more evidence suggests that endothelial dysfunction is a crucial link leading to changes in cerebrovascular structure and function in patients with CSVD (Wardlaw et al., 2013; Jackman and Iadecola, 2015). Therefore, searching for endothelial biological markers will provide an essential theoretical basis for in-depth exploration of the pathogenesis of CSVD and the search for new therapeutic targets.

For CSVD, the related markers such as endothelial cell injury, inflammatory response, and coagulation/coagulation markers are well studied, and the connection between homocysteine, asymmetric dimethylarginine (ADMA), von Willebrand factor (VWF), and CSVD has been widely recognized (Wang et al., 2016; Janes et al., 2019; Nam et al., 2019). VWF is considered as a marker of endothelial dysfunction, which was synthesized in endothelial cells and released into the blood circulation *via* a constitutive pathway (released immediately after completion of molecular synthesis) or a stimulatory regulatory pathway that mediates initial platelet adhesion at sites of vascular injury (Ruggeri, 1999; Lenting et al., 2010). A disintegrin and metalloproteinase with a thrombospondin motif repeat 13 (ADAMTS13) regulate the activity of VWF by cutting ultra-long VWF multimers into smaller, less active molecules and exert its anti-inflammatory and antithrombotic properties (Gerritsen et al., 2001).

Several studies have reported that VWF levels are associated with the degree of WMH and the number of silent subcortical infarctions (Kario et al., 2001; Gottesman et al., 2009), but little is known about the association of VWF and ADAMTS13 activity with subtypes of CSVD and the overall CSVD burden. Therefore, we performed this study to investigate the independence or interactions correlation between multiple CSVD subtypes and the severity of CSVD.

MATERIALS AND METHODS

Study Population

"Investigation on the Status of Cerebrovascular Diseases and Establishing Cohort in Shang Hai Aging Population (ISCDECSHAP)" is a prospective, population-based, and cohort study of stroke incidence and risk factors in an ageing population from Shang Hai City. The ISCDECSHAP study aimed to establish a Chinese CSVD community cohort and was approved by the ethics committee of Hua Shan Hospital and the Fifth People's Hospital of Shanghai. Written informed consent was obtained from all the patients or their representatives before data collection (Yang et al., 2019). Based on protocol, all the subjects, at least 60 years old, performed cerebral magnetic resonance imaging (MRI), cerebral MRA, carotid artery ultrasound, cognitive function, and hematologic examination. Demographic and clinical data, including gender, age, hypertension, diabetes, smoking history, drinking history, and other health conditions were collected by neurologists through a standardized questionnaire. Three milliliters of fasting venous blood was drawn from the study subjects in the morning, all of which was completed within 1 week. According to the purpose of this study, our inclusion criteria: $\geq$60 years old CSVD patients; no neurological symptoms and signs; previous experience of non-specific neurological symptoms such as dizziness, vertigo, headache, and tinnitus can be included (the above symptoms should be completely relieved when evaluating the inclusion). Patients who met any one of the following criteria were excluded: history of stroke, cognitive dysfunction, heart disease, malignancies, hepatic or renal diseases, autoimmune diseases, or infection at enrollment. Contents are shown in **Figure 1**.

Brain MRI and Total CSVD Score

Brain MRI imaging sequences include T1-weighted images (T1WI), T2-weighted images (T2WI), fluid-attenuated inversion recovery (FLAIR), diffusion-weighted imaging (DWI), and susceptibility-weighted imaging (SWI). The field of view (FOV) is 240 mm $\times$ 240 mm, and the matrix = 320 $\times$ 256. Coronal and transaxial views of T1WI and T2WI, and transaxial views of T2-FLAIR, DWI, and SWI were collected. The imaging diagnosis of CSVD strictly follows the international CSVD guidelines (Wardlaw et al., 2013). Subcortical lesions (SI): round or oval lesions, 3–15 mm in diameter, with cerebrospinal fluid signal intensity on T1 and T2 sequences, isointensity on DWI, hypointensity on FLAIR, and ring hyperintensity in the periphery. Perivascular space enlargement (EPVS): round or oval, and usually $\leq$2 mm in diameter, most pronounced in the basal ganglia, with the cerebrospinal fluid signal on T1 and T2 sequences, isointensity on DWI, and hypointensity on FLAIR. White matter hyperintensity (WMH): abnormal signals of varying sizes in periventricular and deep white matter regions, which are hyperintense on T2, FLAIR, and isointense or hypointense on T1. Cerebral microbleed (CMB): it is round on SWI sequence, less than 10 mm in diameter, and hypointense. WMH was graded using a semi-quantitative Fazekas scale (Hainsworth et al., 2015), and high WMH was defined if the scale scored 2–3. According to Staals et al. (2014), the overall burden score of CSVD was rewarded with 1 point whenever one of the following occurred: $\geq$1 SI ($<$15 mm); $\geq$1 CMBs ($<$5 mm); moderate-severe basal ganglia PVS (semiquantitative scale 2–4 grades; Maclullich et al., 2004); deep WMH (Fazekas score 2/3) or periventricular WMH (Fazekas score 3). The total score of CSVD is 0–4 points, a higher score indicating that the CSVD is more severe. The MRI was independently evaluated by two neurologists, and inter-observer agreement values for the presence of CMB, WMH, EPVS, and lacune were 0.80, 0.83, 0.78, and 0.79,

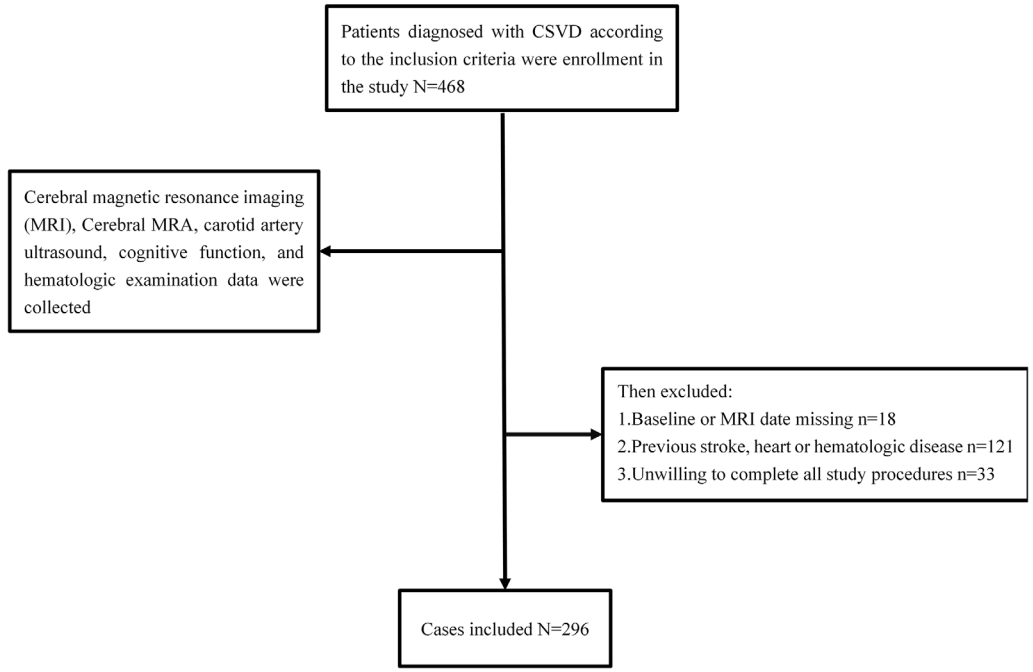

FIGURE 1 | Flowchart of patients included in this study.

respectively. Any disagreement regarding the presence of CSVD features was resolved by consensus with the third neuroimaging expert.

Measurement of ADAMTS13 Activity and VWF Level

Human VWF ELISA kit (Abcam) was used to quantitatively measure the VWF level directly in human fasting venous plasma samples obtained on admission. The samples were centrifuged (2,000 *g* for 5 min) immediately after collection, and plasma samples were stored in a −80 refrigerator. The assay was a sandwich ELISA and measurements were conducted according to the manufacturer's guidelines. ADAMTS13 enzyme activity was measured by the fluorescent substrate method, AnaSpecUSA provided FRETS-VWF73 (ADAMTS13 fluorescent substrate), and the percentage of enzyme activity indicated that the standard plasma activity was set at 100. The operation steps were performed according to the assay (Kokame et al., 2005). Standard plasma is a mixture of plasma from 20 healthy subjects and provided by the Physical Examination Center of Shanghai Fifth People's Hospital.

Statistical Analysis

SPSS 21.0 statistical software was applied for data analysis. For each demographic and clinical feature, normal distribution continuous variables were presented as mean ± standard deviation and compared by an independent sample *t*-test. Abnormal distribution continuous variables were presented as median (interquartile range) and compared by a nonparametric test. The categorical variables are expressed in frequency (percentage) and are expressed in χ^2 test or Fisher exact test. Associations between circulating biomarker (ADAMTS13 and VWF) levels and neuroimaging markers of CSVD and overall CSVD burden was performed by regression analysis. Multivariable linear regression was then conducted for each marker of CSVD in separate models adjusting for age, sex, hypertension, diabetes, smoking history, drinking history, and all brain variables. Kendall's tau-b correlation analysis was used to evaluate the correlation between the ADAMTS13 activity and the total CSVD score. For logistic regression models, age, sex, and variables showing a $p < 0.1$ on the respective univariate analyses were included in models. A *p*-value of 0.05 was considered significant.

RESULTS

Clinical Characteristics of Study Patients

A total of 296 patients with CSVD were included in this study, of which 125 were male. The mean age of the sample was s 69.0 years (SD 7.0), the median VWF level was 1.28 (1.01–1.50) IU/ml, and the ADAMTS13 activity was 88.04% (SD10.57). SI accounted for 42.3% ($n = 125$) of the total sample, CMB for 28.0% ($n = 83$), and high WMH (Fazekas score of 2–3) for 41.6% ($n = 123$). SI has higher total cholesterol than no SI ($p < 0.01$). We found that the high WMH and SI group had significantly increased VWF levels ($p < 0.01$) and decreased ADAMTS13 activity ($p < 0.01$) compared with the control group, but there was no significant difference in the changes of the above parameters in the CMB group (**Table 1**).

TABLE 1 | Sample characteristics by brain variable.

	Total Sample	No SI	SI	*P*	Low WMH	High WMH	*P*	No CMB	CMB	*P*
	n = 296	*n* = 171	*n* = 125		*n* = 162	*n* = 134		*n* = 213	*n* = 83	
Age, years	69 ± 7.0	66 ± 5.5	72 ± 7.7	<0.001	66 ± 6.3	72 ± 7.1	0.010	68 ± 7.2	70 ± 7.3	0.066
Male, *n* (%)	125 (42.2)	80 (46.8)	62 (49.6)	0.632	75 (46.3)	67 (50.0)	0.526	105 (49.3)	37 (44.6)	0.466
BMI, kg/m2	24.7 ± 4.0	24.5 ± 4.0	24.6 ± 3.1	0.762	24.7 ± 3.7	24.4 ± 3.5	0.243	24.6 ± 3.6	24.4 ± 3.7	0.592
Alcohol use, *n* (%)	72 (24.3)	27 (15.8)	45 (36)	<0.001	26 (16.0)	46 (34.3)	<0.001	42 (19.7)	30 (36.1)	<0.001
Current smoking, *n* (%)	99 (33.5)	29 (17.0)	70 (56.0)	<0.001	35 (21.6)	64 (47.8)	<0.001	72 (33.8)	27 (32.5)	0.835
Hypertension, *n* (%)	152 (51.4)	63 (36.8)	89 (71.2)	<0.001	54 (33.3)	98 (73.1)	<0.001	93 (43.7)	59 (71.1)	<0.001
Diabetes Mellitus, n (%)	80 (27.0)	30 (17.4)	52 (40.0)	<0.001	35 (21.6)	45 (36.2)	0.834	47 (22.1)	33 (39.8)	0.002
Total cholesterol, mmol/L	4.40 ± 1.20	4.07 ± 1.20	4.85 ± 1.04	0.007	4.39 ± 1.16	4.41 ± 1.23	0.222	4.37 ± 1.21	4.47 ± 1.14	0.545
HDL cholesterol, mmol/L	1.35 ± 0.59	1.38 ± 0.68	1.29 ± 0.44	0.212	1.29 ± 0.57	1.42 ± 0.62	0.062	1.38 ± 0.59	1.27 ± 0.60	0.153
LDL cholesterol, mmol/L	3.33 ± 0.79	3.30 ± 0.82	3.32 ± 0.77	0.748	3.37 ± 0.79	3.25 ± 0.79	0.180	3.26 ± 0.76	3.46 ± 0.85	0.048
VWF:Ag, IU/ml	1.31 ± 0.28	1.23 ± 0.31	1.41 ± 0.18	<0.001	1.25 ± 0.26	1.38 ± 0.27	<0.001	1.31 ± 0.28	1.29 ± 0.27	0.462
ADAMTS13 activity (%)	88.01 ± 10.57	91.44 ± 10.47	83.28 ± 8.61	0.006	90.29 ± 11.40	85.24 ± 8.60	0.001	88.37 ± 10.81	87.10 ± 9.74	0.545

Note: CMB, Cerebral Microbleed; IQR, Interquartile range; SI, Subcortical infarct; WMH, Median White Matter Hyperintensity; LDL cholesterol, low-density lipoprotein cholesterol; HDL cholesterol, high-density lipoprotein cholesterol.

Associations Between CSVD and the ADAMTS13 Activity

The association between different CSVD neuroimaging markers and ADAMTS13 activity was investigated. Adjusted for age, sex, alcohol, smoking, hypertension, and diabetes, lower ADAMTS13 activity and higher VWF level were related with high WMH [β= −6.26; 95% CI (−7.55, −2.82) $p<0.01$; β = 0.18; 95% CI (0.12, 0.25); $p<0.01$] and SI [β = −5.19; 95% CI (−7.55, −2.82) $p<0.01$; β = 0.13; 95% CI (0.07, 0.20); $p<0.01$]. Model II includes all brain variables, The presence of SI and WMH still remain associated with lower ADAMTS13 activity and higher VWF level (**Table 2**; **Supplementary Table 1**). In addition, we calculated the ADAMTS13:VWF ratio; the results showed that compared with ADAMTS13 alone, ADAMTS13:VWF ratio had a more pronounced association with SI [β = −23.24; 95% CI (−29.31, −17.16); $p<0.01$] and WMH [β = −17.35; 95% CI (−24.35, −10.35); $p < 0.01$] (**Table 3**). The final ADAMTS13:VWF model explained 32.3% (adjusted R squared) of the variance, which was higher than the 28.2% (adjusted R squared) of the ADAMTS13-only model in this study.

Associations Between Total CSVD Burden and the ADAMTS13 Activity

Patients were classified into four groups by ADAMTS13 activity and VWF level quartiles, respectively. In our study population, approximately half of the CSVD total score of patients was 1 (26.3%) or 2 (32.1%). A number of patients scored 3 (28.7%) and 4 (16.2%). Of the patients with a CSVD score of 4, the majority had ADAMTS13 activity (78.8%) among $ADAMTS13_{Q1<80.3\%}$. In addition, the correlation analysis shows that the ADAMTS13 activity was negatively related to the total CSVD score (Kendall's tau-b = −0.48, $p<0.01$; **Table 4**). In the adjusted statistical model (adjusted for age, sex, alcohol use, current smoking, hypertension, and diabetes mellitus), the increase in total CSVD score was negatively correlated with $ADAMTS13_{Q1<80.3\%}$ (OR = 21.33, 95% CI (17.46, 54.60) $p < 0.01$) and $ADAMTS13_{Q280.3–89.0\%}$ (OR = 2.89, 95% CI (1.75, 17.50) $p < 0.05$), respectively. Moreover, lower VWF levels ($VWF_{Q1<1.14\ IU/ml}$) can be regarded as a protective factor for CSVD (OR = 0.37, 95% CI (0.20, 0.66) $p < 0.01$; **Table 5**).

DISCUSSION

In our study, we investigated the association between plasma VWF level, ADAMTS13 activity, and neuroimaging features of CSVD, including the overall CSVD burden. After adjustment for established CSVD-related risk factors, we confirmed that ADAMTS13 activity was reversely correlated to WMH, SI, and overall CSVD burden independently.

The prevalence of CSVD in the elderly population over 60 years can reach 60%. Studies have shown that about 45% of dementia and 20% of stroke is caused by CSVD (Sudlow and Warlow, 1997; Gorelick et al., 2011). Furthermore, CSVD may double the risk of recurrent stroke (Debette and Markus, 2010). In recent years, large population-based studies report that low ADAMTS13 activity was correlated

TABLE 2 | Multivariate analysis of ADAMTS13 levels with brain variable.

	ADAMTS13 (Mode I)		ADAMTS13 (Mode II)	
	Coefficient	**95% confidence interval**	**Coefficient**	**95% confidence interval**
Subcortical infarct	−6.26*	[−9.08, −3.45]	−9.22*	[−11.37, −7.06]
Cerebral microbleeds	−0.51	[−3.17, 2.15]	−2.30	[−4.95, 0.05]
WMH	−5.19*	[−7.55, −2.82]	−7.31*	[−9.40, −4.93]

*Note: *p < 0.01. Mode I, adjusted for age, sex, alcohol use, current smoking, hypertension, diabetes mellitus; Mode II, Adjusted Mode I with all brain variables $R^2 = 0.28$.*

TABLE 3 | Multivariate analysis of ADAMTS13:VWF ratio with brain variable.

	ADAMTS13:VWF ratio (Mode I)		ADAMTS13:VWF ratio (Mode II)	
	Coefficient	**95% confidence interval**	**Coefficient**	**95% confidence interval**
Subcortical infarct	−14.89*	[−20.76, −9.01]	−23.24*	[−29.31, −17.16]
Cerebral microbleeds	4.25	[−1.22, 9.23]	−3.30	[−9.20, 2.38]
WMH	−12.22*	[−17.23, −7.26]	−17.35*	[−24.35, −10.35]

*Note: *p < 0.01. Mode I, adjusted for age, sex, alcohol use, current smoking, hypertension, diabetes mellitus; Mode II, adjusted model with all brain variables $R^2 = 0.32$.*

TABLE 4 | The characteristics of ADAMTS13 activity of the patients with total CSVD score.

		Total CSVD Score			
	***n* = 296**	**1 (*n* = 78)**	**2 (*n* = 95)**	**3 (*n* = 85)**	**4 (*n* = 38)**
ADAMTS13 activity, *n* (%)					
$Q1_{<80.3\%}$		2 (2.6)	10 (10.5)	29 (34.1)	30 (78.8)
$Q2_{80.3-89.0\%}$		18 (37.5)	24 (25.3)	27 (31.8)	4 (10.5)
$Q3_{89.0-97.1\%}$		25 (32.0)	28 (29.5)	20 (23.5)	4 (10.5)
$Q4_{>97.1\%}$		33 (42.3)	33 (34.7)	9 (10.6)	0

Note: Kendall's tau-b = 0.46, p < 0.01.

with a risk of ischemic stroke (Sonneveld et al., 2015) and dementia (Wolters et al., 2018) independent of other known demographic and cerebrovascular risk factors, but studies on the relationship between ADAMTS13 activity and CSVD are little. The association between VWF and neuroimaging markers of CSVD has been demonstrated, including silent lacunar cerebral infarcts, periventricular hyperintensity, and deep white matter hyperintensity (Kario et al., 2001; Gottesman et al., 2009; Nagai et al., 2012). However, it has not reflected changes between VWF with the overall CSVD burden. In our study, we demonstrated that higher VWF level and lower ADAMTS13 activity correlated with WMH and SI, but not with CMB after adjusting for traditional risk factors and brain variables. The complex mechanism involved is unknown, but there are several possible explanations as follows.

First, low ADAMTS13 activity may be associated with endothelial cell dysfunction. Endothelial dysfunction may lead to increased permeability of the blood-brain barrier (BBB), which not only interrupts the oxygen and nutrient supply to the brain but also leads to extravasation of blood components that damage the surrounding white matter regions (Zlokovic, 2008; Gorelick et al., 2011; Xu et al., 2015). Cao et al. (2019) observed that ADAMTS13-deficient mice promote BBB disruption and reduce microvascular and capillary perfusion, and cerebral blood flow by changing endothelial junctions. However, there is a tight link between WMH and BBB impairment that plays a crucial role in early white matter degeneration (Kerkhofs et al., 2021). For SI, its underlying mechanism may have partially overlapping pathophysiology with WMH, but somewhat different (Wardlaw et al., 2015; Lin et al., 2017). VWF, an indicator of endothelial dysfunction, is the first step in mediated adhesion of platelets to damaged endothelial cells in thrombus formation. When endothelial cells are dysfunctional, VWF will be released in the form of large-molecular-weight multimers, which aggravate vascular damage (Lip and Blann, 1997). ADAMTS13 alleviates thrombogenesis and inflammation by adjusting VWF size and regulates microvascular thrombosis by altering the interaction of VWF with platelets (Pillai et al., 2016; Gogia et al., 2017). A study has reported that increased levels of functional VWF accelerate the formation of more microthrombi in multiple SI elderly patients (Kario et al., 2001). In this study, we obtained similar results in VWF and found that low ADAMTS13 activity

TABLE 5 | Multiple ordinal regression analysis of total CSVD score with ADAMTS13.

	OR	**95% confidence interval**	***p*-value**
VWF:Ag (IU/ml)			
$Q1_{<1.14\ IU/ml}$	0.37	[0.20, 0.66]	<0.01
$Q2_{1.33-1.14\ IU/ml}$	0.68	[0.38, 1.23]	0.21
$Q3_{1.33-1.51\ IU/ml}$	0.50	[0.30, 0.79]	<0.05
$Q4_{>1.51\ IU/ml}$		Reference	
ADAMTS13 activity (%)			
$Q1_{<80.3\%}$	21.33	[17.46, 54.60]	<0.01
$Q2_{80.3-89.0\%}$	2.89	[1.75, 17.50]	<0.01
$Q3_{89.0-97.1\%}$	1.70	[0.91, 3.16]	0.09
$Q4_{>97.1\%}$		Reference	

Note: Adjusted for age, sex, alcohol use, current smoking, hypertension, diabetes mellitus.

was an independent risk factor for multiple SIs, and there was no association between ADAMTS13 activity and VWF levels, similar to previous studies (Andersson et al., 2012; Sonneveld et al., 2015; Denorme et al., 2017).The possible reason is that low local ADAMTS13 activity is not sufficient to cleave the supramaximal VWF multimers, eventually leading to the formation of microthrombiin microvascular injury. A second possible reason is that ADAMTS13 activity accelerates atherosclerosis. In animal models, lack of ADAMTS13 was found to promote the formation of plaques and vascular inflammation by generating signals for recruitment and extravasation of monocytes in the early stages of atherosclerosis, which are the pathological changes associated with CSVD (Gandhi et al., 2012; Jin et al., 2012). Ultimately, this may trigger or worsen the development of CSVD.

Furthermore, we confirmed that the severity of the overall CSVD burden was negatively correlated with ADAMTS13 activity. In another study, Nezu et al. (2015) observed that endothelial dysfunction was related to the severity of CSVD by using flow-mediated dilation (FMD) to measure endothelium-dependent vasodilation. However, ADAMTS13 was shown to be able to augment microvascular endothelial endothelium-dependent dilation (EDR) dependent on PI3K/Akt pathway *in vivo* (Zhou et al., 2019). Therefore, this implies ADAMTS13 may have played an essential role in the development of CSVD.

The innovation of this study is that we first reported the association between plasma VWF level, ADAMTS13 activity, and neuroimaging features of CSVD, including the overall CSVD burden in the community cohort. However, there are some limitations as follows. First, this study is a single-center cross-sectional study, with a relatively small number of study subjects and the included biological marker indicators are not comprehensive enough. Because we could not integrate multiple CSVD biomarkers into a panel, it will help us understand the pathogenesis of CSVD better. Second, the activity of ADAMTS13 was also demographically statistically different among different races and regions, and the subjects we included were all from Shanghai, China, so our results need to be validated in a more extensive prospective study.

In conclusion, reducing ADAMTS13 activity is related to white matter hyperintensity and subcortical infarction, but not with cerebral microhemorrhage. In addition, this implied that ADAMTS13 may have played an essential role in the development of CSVD. Exploring the differences of various biomarkers between various neuroimaging features of CSVD, and the association of these markers with clinical manifestations of CSVD will help to deeply elucidate the pathogenesis of CSVD and may provide a new theoretical basis and new targets for the early prevention and treatment of CSVD.

DATA AVAILABILITY STATEMENT

The raw data supporting the conclusions of this article will be made available by the authors, without undue reservation.

ETHICS STATEMENT

The studies involving human participants were reviewed and approved by Shanghai Fifth People's Hospital, Fudan University. The patients/participants provided their written informed consent to participate in this study.

AUTHOR CONTRIBUTIONS

WS: conceptualization, data collection, experiment, formal analysis, and writing original draft. SZ and YL: data collection. WL: validation, supervision, and experiment. XY and DW: review and editing, provide guidance. All authors contributed to the article and approved the submitted version.

FUNDING

This study was supported by grants from correlation between retinal vascular changes and cerebral small vessel disease of Shanghai Fifth People's Hospital (2018WYZD01), Shanghai Committee of Science and Technology (201409004900 and 20S31904400), Cooperation Programme of Fudan University—Minhang District Joint Health Center (2021FM22), Elite training of Shanghai Fifth People's Hospital (2020WYRCJY04), Beijing Bethune Charitable Foundation (AX083CS), and Minhang District High Level Specialist Backbone Physician Training Plan (2020MZYS09).

ACKNOWLEDGMENTS

We gratefully thank all the patients, general practitioners, and hospital colleagues who participated in our study.

SUPPLEMENTARY MATERIALS

The Supplementary Material for this article can be found online at: https://www.frontiersin.org/articles/10.3389/fnagi.2021.738359/full#supplementary-material.

REFERENCES

Andersson, H. M., Siegerink, B., Luken, B. M., Crawley, J. T., Algra, A., Lane, D. A., et al (2012). High VWF, low ADAMTS13 and oral contraceptives increase the risk of ischemic stroke and myocardial infarction in young women. *Blood* 119, 1555–1560. doi: 10.1182/blood-2011-09-380618

Cao, Y., Xu, H., Zhu, Y., Shi, M. J., Wei, L., Zhang, J., et al. (2019). ADAMTS13 maintains cerebrovascular integrity to ameliorate Alzheimer-like pathology. *PLoS Biol.* 17:e3000313. doi: 10.1371/journal.pbio.3000313

Debette, S., and Markus, H. S. (2010). The clinical importance of white matter hyperintensities on brain magnetic resonance imaging: systematic review and meta-analysis. *BMJ* 341:c3666. doi: 10.1136/bmj.c3666

Denorme, F., Kraft, P., Pareyn, I., Drechsler, C., Deckmyn, H., Vanhoorelbeke, K., et al. (2017). Reduced ADAMTS13 levels in patients with acute and chronic cerebrovascular disease. *PLoS One* 12:e0179258. doi: 10.1371/journal.pone.0179258

Gandhi, C., Khan, M. M., Lentz, S. R., and Chauhan, A. K. (2012). ADAMTS13 reduces vascular inflammation and the development of early

atherosclerosis in mice. *Blood* 119, 2385–2391. doi: 10.1182/blood-2011-09-376202

Gerritsen, H. E., Robles, R., Lämmle, B., and Furlan, M. (2001). Partial amino acid sequence of purified von Willebrand factor-cleaving protease. *Blood* 98, 1654–1661. doi: 10.1182/blood.v98.6.1654

Gogia, S., Kelkar, A., Zhang, C., Dayananda, K. M., and Neelamegham, S. (2017). Role of calcium in regulating the intra- and extracellular cleavage of von Willebrand factor by the protease ADAMTS13. *Blood Adv.* 1, 2063–2074. doi: 10.1182/bloodadvances.2017009027

Gorelick, P. B., Scuteri, A., Black, S. E., Decarli, C., Greenberg, S. M., Iadecola, C., et al. (2011). Vascular contributions to cognitive impairment and dementia:a statement for healthcare professionals from the american heart association/american stroke association. *Stroke* 42, 2672–2713. doi: 10.1161/STR.0b013e3182299496

Gottesman, R. F., Cummiskey, C., Chambless, L., Wu, K. K., Aleksic, N., Folsom, A. R., et al (2009). Hemostatic factors and subclinical brain infarction in a community-based sample:the ARIC study. *Cerebrovasc Dis.* 28, 589–594. doi: 10.1159/000247603

Hainsworth, A. H., Oommen, A. T., and Bridges, L. R. (2015). Endothelial cells and human cerebral small vessel disease. *Brain Pathol.* 25, 44–50. doi: 10.1111/bpa.12224

Huijts, M., Duits, A., van Oostenbrugge, R. J., Kroon, A. A., de Leeuw, P. W., and Staals, J. (2013). Accumulation of MRI markers of cerebral small vessel disease is associated with decreased cognitive function. A study in first-ever lacunar stroke and hypertensive patients. *Front Aging Neurosci* 5:72. doi: 10.3389/fnagi.2013.00072

Jackman, K., and Iadecola, C. (2015). Neurovascular regulation in the ischemic brain. *Antioxid. Redox Signal.* 22, 149–160. doi: 10.1089/ars.2013.5669

Janes, F., Cifù, A., Pessa, M. E., Domenis, R., Gigli, G. L., Sanvilli, N., et al (2019). ADMA as a possible marker of endothelial damage. a study in young asymptomatic patients with cerebral small vessel disease. *Sci. Rep.* 9:14207. doi: 10.1038/s41598-019-50778-w

Jin, S. Y., Tohyama, J., Bauer, R. C., Cao, N. N., Rader, D. J., and Zheng, X. L. (2012). Genetic ablation of Adamts13 gene dramatically accelerates the formation of early atherosclerosis in a murine model. *Arterioscler. Thromb. Vasc. Biol.* 32, 1817–1823. doi: 10.1161/ATVBAHA.112.247262

Kario, K., Matsuo, T., Kobayashi, H., Hoshide, S., and Shimada, K. (2001). Hyperinsulinemia and hemostatic abnormalities are associated with silent lacunar cerebral infarcts in elderly hypertensive subjects. *J. Am Coll. Cardiol.* 37, 871–877. doi: 10.1016/s0735-1097(00)01172-4

Kerkhofs, D., Wong, S. M., Zhang, E., Staals, J., Jansen, J. F. A., van Oostenbrugge, R. J., et al (2021). Baseline blood-brain barrier leakage and longitudinal microstructural tissue damage in the periphery of white matter hyperintensities. *Neurology* 96, e2192–e2200. doi: 10.1212/WNL.0000000000011783

Kokame, K., Nobe, Y., Kokubo, Y., Okayama, A., and Miyata, T. (2005). FRETS-VWF73, a first fluorogenic substrate for ADAMTS13 assay. *Br. J. Haematol.* 129, 93–100. doi: 10.1111/j.1365-2141.2005.05420.x

Lenting, P. J., Pegon, J. N., Groot, E., and de Groot, P. G. (2010). Regulation of von Willebrand factor-platelet interactions. *Thromb. Haemost.* 104, 449–455. doi: 10.1160/TH09-11-0777

Lin, J., Wang, D., Lan, L., and Fan, Y. (2017). Multiple factors involved in the pathogenesis of white matter lesions. *Biomed. Res. Int.* 2017:9372050. doi: 10.1155/2017/9372050

Lip, G. Y., and Blann, A. (1997). von Willebrand factor:a marker of endothelial dysfunction in vascular disorders. *Cardiovasc. Res.* 34, 255–265. doi: 10.1016/s0008-6363(97)00039-4

Maclullich, A. M., Wardlaw, J. M., Ferguson, K. J., Starr, J. M., Seckl, J. R., and Deary, I. J. (2004). Enlarged perivascular spaces are associated with cognitive function in healthy elderly men. *J. Neurol. Neurosurg. Psychiatry* 75, 1519–1523. doi: 10.1136/jnnp.2003.030858

Nagai, M., Hoshide, S., and Kario, K. (2012). Association of prothrombotic status with markers of cerebral small vessel disease in elderly hypertensive patients. *Am. J. Hypertens.* 25, 1088–1094. doi: 10.1038/ajh.2012.85

Nam, K. W., Kwon, H. M., Jeong, H. Y., Park, J. H., Kwon, H., and Jeong, S. M. (2019). Serum homocysteine level is related to cerebral small vessel disease in a healthy population. *Neurology* 92, e317–e325. doi: 10.1212/WNL.0000000000006816

Nezu, T., Hosomi, N., Aoki, S., Kubo, S., Araki, M., Mukai, T., et al. (2015). Endothelial dysfunction is associated with the severity of cerebral small vessel disease. *Hypertens. Res.* 38, 291–297. doi: 10.1038/hr.2015.4

Pillai, V. G., Bao, J., Zander, C. B., McDaniel, J. K., Chetty, P. S., Seeholzer, S. H., et al. (2016). Human neutrophil peptides inhibit cleavage of von Willebrand factor by ADAMTS13:a potential link of inflammation to TTP. *Blood* 128, 110–119. doi: 10.1182/blood-2015-12-688747

Ruggeri, Z. M. (1999). Structure and function of von Willebrand factor. *Thromb. Haemost* 82, 576–584.

Sonneveld, M. A., de Maat, M. P., Portegies, M. L., Kavousi, M., Hofman, A., Turecek, P. L., et al. (2015). Low ADAMTS13 activity is associated with an increased risk of ischemic stroke. *Blood* 126, 2739–2746. doi: 10.1182/blood-2015-05-643338

Staals, J., Makin, S. D., Doubal, F. N., Dennis, M. S., and Wardlaw, J. M. (2014). Stroke subtype, vascular risk factors and total MRI brain small-vessel disease burden. *Neurology* 83, 1228–1234. doi: 10.1212/WNL.0000000000000837

Sudlow, C. L., and Warlow, C. P. (1997). Comparable studies of the incidence of stroke and its pathological types. Results from an international collaboration. *Stroke* 28, 491–499. doi: 10.1161/01.str.28.3.491

Wang, X., Chappell, F. M., Valdes Hernandez, M., Lowe, G., Rumley, A., Shuler, K., et al. (2016). Endothelial function, inflammation, thrombosis and basal ganglia perivascular spaces in patients with stroke. *J. Stroke Cerebrovasc. Dis.* 25, 2925–2931. doi: 10.1016/j.jstrokecerebrovasdis.2016.08.007

Wardlaw, J. M., Smith, E. E., Biessels, G. J., Cordonnier, C., Fazekas, F., Frayne, R., et al. (2013). Neuroimaging standards for research into small vessel disease and its contribution to ageing and neurodegeneration. *Lancet. Neurol.* 12, 822–838. doi: 10.1016/S1474-4422(13)70124-8

Wardlaw, J. M., Valdés Hernández, M. C., and Muñoz-Maniega, S. (2015). What are white matter hyperintensities made of? Relevance to vascular cognitive impairment. *J. Am. Heart Assoc.* 4:001140. doi: 10.1161/JAHA.114.001140

Wolters, F. J., Boender, J., de Vries, P. S., Sonneveld, M. A., Koudstaal, P. J., de Maat, M. P., et al. (2018). Von Willebrand factor and ADAMTS13 activity in relation to risk of dementia:a population-based study. *Sci. Rep.* 8:5474. doi: 10.1038/s41598-018-23865-7

Xu, X., Chan, K. W., Knutsson, L., Artemov, D., Xu, J., Liu, G., et al. (2015). Dynamic glucose enhanced (DGE) MRI for combined imaging of blood-brain barrier break down and increased blood volume in brain cancer. *Magn. Reson. Med.* 74, 1556–1563. doi: 10.1002/mrm.25995

Yang, X., Zhang, S., Dong, Z., Zi, Y., Luo, Y., Jin, Z., et al. (2019). Insulin resistance is a risk factor for overall cerebral small vessel disease burden in old nondiabetic healthy adult population. *Front. Aging Neurosci.* 11:127. doi: 10.3389/fnagi.2019.00127

Zhou, S., Jiang, S., Guo, J., Xu, N., Wang, Q., Zhang, G., et al. (2019). ADAMTS13 protects mice against renal ischemia-reperfusion injury by reducing inflammation and improving endothelial function. *Am. J. Physiol. Renal Physiol.* 316, F134–F145. doi: 10.1152/ajprenal.00405.2018

Zlokovic, B. V. (2008). The blood-brain barrier in health and chronic neurodegenerative disorders. *Neuron* 57, 178–201. doi: 10.1016/j.neuron.2008.01.003

Conflict of Interest: The authors declare that the research was conducted in the absence of any commercial or financial relationships that could be construed as a potential conflict of interest.

Publisher's Note: All claims expressed in this article are solely those of the authors and do not necessarily represent those of their affiliated organizations, or those of the publisher, the editors and the reviewers. Any product that may be evaluated in this article, or claim that may be made by its manufacturer, is not guaranteed or endorsed by the publisher.

frontiers in Aging Neuroscience

ORIGINAL RESEARCH
published: 22 November 2021
doi: 10.3389/fnagi.2021.741881

Cerebral Hemodynamics and Carotid Atherosclerosis in Patients With Subcortical Ischemic Vascular Dementia

Xiao-Jiao Liu[1†], Ping Che[2†], Mengya Xing[2], Xiao-Bing Tian[2], Chunli Gao[2], Xiuyan Li[2] and Nan Zhang[1,2]*

[1] Department of Neurology, Tianjin Medical University General Hospital Airport Site, Tianjin, China, [2] Department of Neurology, Tianjin Neurological Institute, Tianjin Medical University General Hospital, Tianjin, China

A growing body of evidence indicates that atherosclerosis is correlated with cerebral small vessel disease and contributes to cognitive decline. This study aimed to explore the characteristics and contributions of intracranial hemodynamics and carotid atherosclerosis to cognitive dysfunction in subjects with subcortical ischemic vascular dementia (SIVD). Notably, 44 patients with SIVD, 30 patients with Alzheimer's disease (AD), and 30 healthy controls (HCs) were recruited from our longitudinal MRI study for AD and SIVD (ChiCTR1900027943). The cerebral mean flow velocity (MFV) and pulsatility index (PI) of both anterior and posterior circulations, artery plaque, and lumen diameter in carotid arteries were investigated using transcranial Doppler and carotid ultrasound, respectively. Their correlations with cognitive function were analyzed in patients with dementia. Decreased MFV and increased PI were found in patients with SIVD and AD. Patients with SIVD showed lower MFV and higher PI in the bilateral posterior cerebral arteries compared to patients with AD. Increases in lumen diameter, number of arteries with plaque, and total carotid plaque score were found in patients with SIVD. The Mini-Mental State Examination score was positively correlated with the MFV and negatively correlated with the PI of most major cerebral arteries, while it was negatively correlated with the lumen diameter of the common carotid artery, number of arteries with plaque, and total carotid plaque score in patients with dementia. There were also correlations between these parameters of some arteries and memory and executive function. Our results provide additional evidence suggesting that the pathological changes in macrovascular structure and function are correlated with cognitive impairment in dementia patients with SIVD and to a lesser extent AD.

Keywords: subcortical ischemic vascular dementia, Alzheimer's disease, transcranial Doppler, mean flow velocity, pulsatility index

OPEN ACCESS

Edited by:
Stefano Tarantini, University of Oklahoma Health Sciences Center, United States

Reviewed by:
Rita Moretti, University of Trieste, Italy
Chris Zarow, University of California, San Diego, United States

***Correspondence:**
Nan Zhang
nkzhangnan@yeah.net

[†] These authors have contributed equally to this work and share first authorship

Received: *15 July 2021*
Accepted: *21 October 2021*
Published: *22 November 2021*

Citation:
Liu X-J, Che P, Xing M, Tian X-B, Gao C, Li X and Zhang N (2021) Cerebral Hemodynamics and Carotid Atherosclerosis in Patients With Subcortical Ischemic Vascular Dementia. Front. Aging Neurosci. 13:741881. doi: 10.3389/fnagi.2021.741881

INTRODUCTION

Vascular dementia (VaD) is the second most commonly diagnosed type of dementia after Alzheimer's disease (AD) in people over the age of 70 years. According to the Vascular Impairment of Cognition Classification Consensus Study, VaD can be categorized into poststroke dementia, subcortical ischemic vascular dementia (SIVD), multi-infarct (cortical) dementia, and mixed dementia (Skrobot et al., 2018). SIVD is a clinically homogeneous subtype of VaD, typically characterized by cognitive impairment, mental and mood-behavioral disorders, gait instability, and incontinence. Approximately 36–67% of patients with VaD exhibit the pathological changes of cerebral small vascular disease, which is the main pathogenesis of SIVD (Roman et al., 2002).

Brain imaging features of patients with SIVD are characterized by white matter hyperintensities (WMH), lacunes, subcortical infarcts, enlarged perivascular spaces (PVS), microbleeds, and brain atrophy (Moretti and Caruso, 2020). Recent studies revealed correlations between hemodynamic and structural changes in large vessels and SIVD imaging features using transcranial Doppler (TCD) and carotid ultrasound. In a community-based study, elevated pulsatility index (PI) of the middle cerebral artery (MCA), increased plaque number, and enlarged diameter of carotid arteries are correlated with more lacunes and larger WMH volume (Mok et al., 2012). Cerebral perfusion and vascular resistance measured by TCD are significantly associated with WMH severity and executive function in non-demented elderly subjects (Vinciguerra et al., 2019). Moreover, PI of the MCA is significantly correlated with the scores on the Mini-Mental State Examination (MMSE), Trail Making Test-A (TMT-A), and TMT-B in patients with lacunar infarction (Altmann et al., 2016).

A large amount of clinical and postmortem evidence has revealed structural and functional changes in cerebral large vessels in patients with AD. Previous studies reported that patients with AD, in particular, apolipoprotein E (APOE) ε4 genotype carriers, have lower mean flow velocity (MFV) and higher PI of the MCA compared with age-matched non-demented individuals (Roher et al., 2011). A systematic review concluded that patients with mild cognitive impairment (MCI) show decreased cerebral blood flow velocity in the bilateral anterior cerebral artery (ACA) and MCA (especially among APOE ε4 carriers) compared with healthy subjects. This hemodynamic shift in patients with MCI also predicts their conversion to AD (Beishon et al., 2017). In addition, cerebral atherosclerotic stenosis is more common in patients with neuropathologically confirmed AD than non-demented individuals (Roher et al., 2004).

Major risk factors of arteriolosclerosis in small vessel diseases, such as aging, hypertension, diabetes, smoking, hyperhomocysteinemia, obesity, and dyslipidemia, also contribute to arteriosclerosis in large arteries. Moreover, cerebral hemodynamic changes indirectly accelerate cerebral edema, inter-arterial space dilation, and interstitial fluid retention. These changes are subsequently reflected on MRI, indicating the characteristics of SIVD. However, the pathological and functional changes in large vessels and their associations with cognitive function in patients with SIVD are still unknown. In this study, we investigated both anterior and posterior intracranial hemodynamics measured by TCD and carotid artery changes measured by carotid ultrasound in patients with SIVD. We compared the results to those in patients with AD, whose diagnosis was supported by fluorodeoxyglucose (FDG) and amyloid PET scans. Our results underscore the potential contributions of cerebral and carotid atherosclerosis to cognitive impairment in patients with SIVD and AD.

MATERIALS AND METHODS

Participants

A total of 104 participants, including 44 patients with SIVD, 30 patients with AD, and 30 age- and sex-matched healthy controls (HCs), were recruited from our longitudinal MRI study for AD and SIVD (ChiCTR1900027943). The diagnoses of AD and SIVD were supported by FDG and amyloid PET and multimodal MRI, respectively. All participants (aged from 50 to 85 years) underwent systematic evaluations, including medical history collection, physical and neurological examinations, neuropsychological assessment, laboratory tests, and brain MRI. The study was approved by the Ethics Committee of the Tianjin Medical University General Hospital (IRB2017-063-01). Written consent forms were signed by all participants and their legal guardians.

The diagnostic criteria for patients with dementia met the criteria for the major neurocognitive disorder (Sachdev et al., 2015) according to the fifth edition of the *Diagnostic and Statistical Manual of Mental Disorders*. They also had MMSE scores within the range of 10–26, and the Clinical Dementia Rating (CDR) scores within 0.5–2. Patients with SIVD met the diagnostic criteria for VaD according to the *Vascular Behavioral and Cognitive Disorders* (Sachdev et al., 2014). Patients with AD met the research diagnostic criteria for typical AD of International Working Group-2 (Dubois et al., 2014), presented with early and significant episodic memory impairment, and had positive results on ^{11}C-labeled Pittsburgh compound B PET. Patients with cognitive impairment caused by other neurological diseases, mental disorders, and medical conditions, such as frontotemporal lobar degeneration, dementia with Lewy bodies, Parkinson's disease, multiple sclerosis, hydrocephalus, severe depression, schizophrenia, thyroid dysfunction, vitamin B12 deficiency, and syphilis or human immunodeficiency virus infections, were excluded. All HCs demonstrated normal performances on neuropsychological assessments (MMSE score $>$ 26 and CDR score of 0) with no subjective cognitive decline.

The MRI criteria were also applied for each group. Patients with SIVD were characterized by the following: (1) multiple ($\geq$3) supratentorial subcortical lacunes (3–20 mm in diameter) with/without WMH of any degree; or (2) moderate-to-severe WMH in either periventricular region or deep white matter according to the Fazekas rating scale (score $\geq$ 2 with/without lacunes) (Fazekas et al., 1987); or (3) strategically located subcortical small infarcts in the deep gray matter; and (4) no

obvious hippocampal atrophy (Scheltens' medial temporal lobe atrophy scale < 2 for age ≤ 75 years old or < 3 for age > 75 years old) indicating the possibility of comorbid AD (Scheltens et al., 1992). Patients with AD were excluded by evidence of significant cerebrovascular diseases such as multiple cortical infarction or strategic infarction, >1 lacune in the basal ganglia, or severe WMH. There was no clinically significant atrophy in the medial temporal lobe or other brain areas or cerebrovascular diseases shown on MRI of HC.

All participants had no history of drug or alcohol abuse, no severe depression (Hamilton Depression Scale score < 18) (Hamilton, 1967), and no severe visual or auditory disability that could influence cognitive assessment performance. The doses of medication that might affect the cognitive function or cerebral hemodynamics were stable within 4 weeks before neuropsychological assessment and ultrasonography measurement.

Ultrasonography Measurement

The intracranial hemodynamics were measured by TCD (Delikai TC9-NB, Guangdong, China). During TCD assessment, all participants adopted a supine position in a quiet and warm indoor environment. The resting-state parameters of peak systolic blood flow velocity (PSV), end diastolic blood flow velocity (EDV), and MFV, which partly represent arterial stenosis and cerebral blood flow, were obtained through the bilateral temporal and occipital windows. PI, equivalent to pulse pressure, was used as an indicator to identify distal blood flow resistance and vessel wall elasticity and was calculated by the formula of (PSV−EDV)/MFV. We analyzed the MFV and PI of the bilateral intracranial carotid arteries (ICAs), ACAs, MCAs, posterior cerebral arteries (PCAs) and vertebral arteries (VAs), and basilar artery (BA), including the proximal BA (pBA) and distal BA (dBA).

Carotid artery plaque and lumen diameter were evaluated through high-resolution B-mode ultrasound (Hitachi HI VISION, Shenzhen, China) examination with a 7.5-MHz probe. The atherosclerotic plaque was measured at six carotid segments, namely, the left and right common carotid artery (CCA), carotid bifurcation, and extracranial internal carotid artery (EICA). The plaque was defined as focal structures that invaded the arterial lumen at least 0.5 mm or with thickness >1.5 mm measured from the media-adventitia interface to the intima-lumen interface (Touboul et al., 2007) and was evaluated at each carotid artery segment. Apart from the number of plaque and the number of arteries with plaque, the carotid plaque score (Ihle-Hansen et al., 2019) was also used to quantify plaque in this study. The largest plaque in each section was scored according to its diameter ($\geq$1.5, $\geq$2.5, and $\geq$3.5 mm were scored as 1, 2, and 3 points, respectively), and the total score of each segment was calculated and ranged from 0 to 18. Compared with the measurements of total plaque area and diameter, the plaque score was easier to evaluate and had better inter-operator reliability. The lumen diameters of the bilateral CCA, EICA, and VA during the diastole of each cardiac cycle were measured as the average of the distance between the leading edges of far- and near-wall lumen-intima interfaces (Brisset et al., 2013).

Neuropsychological Assessment

All participants underwent neuropsychological assessments. Global cognitive impairment was measured by the MMSE. Memory and executive function (i.e., the main cognitive functions impaired in patients with AD and SIVD, respectively) were also analyzed. The memory was calculated by the average *Z*-scores of the total learning, delayed recall, and recognition in the Rey Auditory Verbal Learning Test and the Brief Visuospatial Memory Test-Revised. The executive function was calculated by the average *Z*-scores of the TMT-B and the Stroop Color and Word Test. *Z*-scores were converted using the means and SDs of the HC group. All the cognitive data were collected within 1 week before or after the ultrasonographic measurements.

Statistical Analysis

All the data were analyzed by SPSS version 22.0 (IBM Corp. Armonk, NY, United States). The values are provided as a number or a percentage for categorical variables, mean $\pm$ SD for continuous variables, and 95% CIs for multiple logistic regression models. The differences in clinical characteristics and TCD and the carotid ultrasound parameters between patients with SIVD, patients with AD, and HCs were compared using the one-way ANOVAs for continuous variables or the Chi-square tests for categorical variables. The multiple logistic regression analysis was used for the correlation analysis of TCD and carotid ultrasound parameters with global cognition, memory, and executive function in patients with dementia (i.e., SIVD and AD). Age, sex, education, and vascular risk factors were adjusted during the regression analysis. $P < 0.05$ was considered statistically significant.

RESULTS

Demographic Characteristics

The demographic characteristics of all subjects are shown in **Table 1**. In total, 44 patients with SIVD (mean age of 71.6 years, median age of 72 years, 41.2% females), 30 patients with AD (mean age of 68.7 years, median age of 68 years, 70.3% females), and 30 HCs (mean age of 66.2 years, median age of 66 years, 63.3% females) were included in this study. All participants were right-handed. No statistically significant differences were found in age, educational level, and body mass index (BMI) among the three groups. However, the HC group was slightly younger than the SIVD and AD groups, but the differences were not statistically significant. Although all participants were between 50 and 85 years old, the age distribution was slightly different across three groups (SIVD vs. AD vs. HC: 50–59 years, 4.55 vs. 16.67 vs. 26.67%; 60–79 years, 84.09 vs. 73.33 vs. 70%; and 80–85 years, 11.36 vs. 10 vs. 3.33%). In addition, compared with the AD group, there was a lower proportion of females in the SIVD group. In terms of vascular risk factors, significantly higher incidences of stroke history (56.8 vs. 0 vs. 0%) and hypertension (72.7 vs. 26.7 vs. 46.7%) were found in patients with SIVD than in the AD and HC groups. A significantly higher proportion of diabetes mellitus (40.9 vs. 3.3%) was found in patients with SIVD compared to those with AD. A significantly

TABLE 1 | Group characteristics.

	SIVD (*n* = 44)	AD (*n* = 30)	HC (*n* = 30)	F/χ^2
Age, years	71.6 (7.90)	68.7 (8.81)	66.2 (6.29)	F = 4.81
Sex, female/male*	18/26	21/9	19/11	χ^2 = 7.10
Education, years	10.2 (2.57)	10.4 (4.48)	11.3 (3.37)	F = 0.33
BMI	24.3 (2.69)	24.2 (2.15)	24.5 (2.64)	F = 0.66
Hypercholesterolemia†, %	45.5	30.0	60.0	χ^2 = 5.45
Hypertension*‡, %	72.7	26.7	46.7	χ^2 = 15.63
Diabetes mellitus*, %	40.9	3.3	20.0	χ^2 = 14.17
Stroke, %	56.8	0	0	–
Coronary artery disease, %	22.7	6.7	6.7	χ^2 = 5.62
COPD, %	0	0	0	–
Statin use, %	36.4	13.3	20.0	χ^2 = 5.61
MMSE†‡	20.4 (3.22)	19.6 (2.44)	28.2 (1.20)	F = 129.24
Memory*†‡	−2.11 (0.87)	−2.90 (0.87)	0.08 (0.57)	F = 115.32
Executive function*†‡	−2.46 (0.98)	−2.10 (0.98)	0.02 (0.61)	F = 75.01

Values are provided as mean (SD) unless otherwise indicated. Memory and executive function were analyzed using composite Z-scores.
AD, Alzheimer's disease; BMI, body mass index; COPD, chronic obstructive pulmonary disease; HC, healthy control; MMSE, Mini-Mental State Examination; SIVD, subcortical ischemic vascular dementia.
**SIVD vs. AD, $P < 0.05$.*
‡*SIVD vs. HC, $P < 0.05$.*
†*AD vs. HC, $P < 0.05$.*

TABLE 2 | Mean flow velocities (MFVs) of insonated arteries by the group.

	SIVD (*n* = 44)	AD (*n* = 30)	HC (*n* = 30)	F
R ICA†‡	57.02 (13.09)	53.57 (8.99)	62.77 (10.44)	5.11
R ACA†‡	46.77 (9.93)	47.93 (7.43)	53.73 (9.93)	5.35
R MCA†‡	46.14 (5.20)	45.83 (4.72)	57.10 (10.92)	25.18
R PCA†‡	31.45 (6.66)	32.63 (5.49)	36.83 (7.80)	5.97
R VA†‡	28.30 (5.72)	30.43 (4.58)	44.10 (5.58)	83.93
pBA†‡	27.84 (5.94)	27.70 (5.13)	39.60 (6.93)	41.00
dBA†‡	23.32 (5.50)	25.60 (4.99)	35.83 (7.77)	45.87
L ICA‡	52.41 (13.06)	55.37 (11.25)	60.67 (12.19)	4.02
L ACA	48.11 (12.05)	50.87 (15.54)	53.13 (13.66)	1.25
L MCA	55.68 (12.65)	56.23 (7.04)	59.07 (8.65)	1.05
L PCA*†‡	29.09 (7.68)	36.73 (11.47)	42.90 (5.96)	23.89
L VA‡	25.61 (7.07)	28.47 (5.18)	29.53 (9.17)	2.90

Values (cm/s) are provided as mean (SD).
ACA, anterior cerebral artery; AD, Alzheimer's disease; dBA, distal basilar artery; HC, healthy control; ICA, intracranial internal carotid artery; L, left; MCA, middle cerebral artery; MFV, mean flow velocity; pBA, proximal basilar artery; PCA, posterior cerebral artery; R, right; SIVD, subcortical ischemic vascular dementia; VA, vertebral artery.
**SIVD vs. AD, $P < 0.05$.*
‡*SIVD vs. HC, $P < 0.05$.*
†*AD vs. HC, $P < 0.05$.*

lower incidence of hypercholesterolemia (30 vs. 60%) was found in patients with AD compared to HCs. No participants had comorbid chronic obstructive pulmonary disease (COPD). More patients with SIVD were using statins as compared to patients with AD and HCs (36.4 vs. 13.3 vs. 20.0%), but this difference was not significant. The SIVD and AD groups showed significantly lower MMSE score (20.4 ± 3.22 vs. 19.6 ± 2.44 vs. 28.2 ± 1.20) and lower *Z*-scores in memory assessments (−2.11 ± 0.87 vs. −2.90 ± 0.87 vs. 0.08 ± 0.57) and executive function tests (−2.46 ± 0.98 vs. −2.10 ± 0.98 vs. 0.02 ± 0.61) than the HC group. No significant difference in the MMSE score was found between the SIVD and AD groups. However, patients with SIVD had better performance in memory and worse performance in executive function than patients with AD.

Mean Flow Velocity Features

Significant differences in the MFV of the bilateral ICAs, PCAs, and VAs; right ACA and MCA; and pBA and dBA were found among the three groups (**Table 2**). Compared to the HC group, both patients with SIVD and AD showed lower MFVs of the bilateral PCAs; right ICA, ACA, MCA, and VA; and pBA and dBA. Patients with SIVD also showed lower MFVs of the left ICA and VA than HCs, as well as lower MFV of the left PCA than patients with AD.

Pulsatility Index Features

The PI of most measured arteries was significantly higher in patients with SIVD than in HCs, including the bilateral ACAs, MCAs, and PCAs; right ICA and VA; and pBA and dBA (**Table 3**). Patients with AD also demonstrated increased PI of the bilateral MCAs, left ACA, as well as pBA and dBA compared to HCs. Patients with SIVD had higher PI of the bilateral PCAs than patients with AD; meanwhile, patients with AD had higher PI of the pBA and dBA than patients with SIVD.

Lumen Diameter

Patients with SIVD showed significantly increased lumen diameters in the bilateral CCAs and left EICA compared to the AD and HC groups (**Table 4** and **Figure 1A**). No difference in lumen diameter of any measured artery was found between patients with AD and HCs.

Carotid Plaque Characteristics

Patients with SIVD showed significantly higher plaque number, number of arteries with plaque, and total carotid plaque score compared to HCs, as well as higher total carotid plaque score compared to patients with AD (**Table 5** and **Figure 1B**). An increasing trend in the index for the carotid plaque was found in patients with AD compared to HCs, but this was not statistically significant.

Association Between Mean Flow Velocity/Pulsatility Index and Cognitive Function in Patients With Dementia

Among all TCD parameters, the MMSE score was positively correlated with the MFV of the bilateral ICAs, MCAs, and PCAs; right ACA and VA; and pBA and dBA. It was negatively correlated with the PI of the bilateral MCAs; right ICA and VA; and pBA and dBA in all patients with either SIVD or AD. Sample plots for the MFV and PI in the right MCA

TABLE 3 | Pulsatility indices (PIs) of insonated arteries by the group.

	SIVD (*n* = 44)	AD (*n* = 30)	HC (*n* = 30)	F
R ICA‡	1.00 (0.15)	0.97 (0.18)	0.91 (0.84)	3.45
R ACA‡	1.02 (0.15)	0.97 (0.19)	0.92 (0.13)	3.51
R MCA†‡	1.19 (0.16)	1.18 (0.12)	0.88 (0.14)	11.67
R PCA*‡	1.03 (0.14)	0.94 (0.21)	0.91 (0.09)	6.40
R VA‡	1.02 (0.15)	0.98 (0.14)	0.93 (0.08)	4.84
pBA*†‡	0.98 (0.13)	1.11 (0.16)	0.85 (0.05)	31.75
dBA*†‡	0.94 (0.13)	1.06 (0.14)	0.82 (0.07)	28.43
L ICA	1.03 (0.14)	0.96 (0.20)	0.95 (0.10)	2.97
L ACA†‡	1.03 (0.13)	1.02 (0.20)	0.94 (0.10)	4.95
L MCA†‡	1.05 (0.14)	1.00 (0.12)	0.87 (0.16)	15.15
L PCA*‡	1.03 (0.14)	0.93 (0.21)	0.92 (0.10)	5.87
L VA	1.00 (0.14)	1.00 (0.14)	0.94 (0.10)	2.43

Values are provided as mean (SD).
ACA, anterior cerebral artery; AD, Alzheimer's disease; dBA, distal basilar artery; HC, healthy control; ICA, intracranial internal carotid artery; L, left; MCA, middle cerebral artery; pBA, proximal basilar artery; PCA, posterior cerebral artery; PI, pulsatility index; R, right; SIVD, subcortical ischemic vascular dementia; VA, vertebral artery.
**SIVD vs. AD, $P < 0.05$.*
‡SIVD vs. HC, $P < 0.05$.
†AD vs. HC, $P < 0.05$.

TABLE 4 | Lumen diameter of carotid arteries by the group.

	SIVD (*n* = 44)	AD (*n* = 30)	HC (*n* = 30)	F
R CCA*‡	0.79 (0.06)	0.72 (0.06)	0.73 (0.06)	14.54
R EICA	0.49 (0.03)	0.48 (0.02)	0.48 (0.02)	2.90
R VA	0.34 (0.05)	0.32 (0.02)	0.33 (0.03)	2.00
L CCA*‡	0.78 (0.06)	0.73 (0.07)	0.72 (0.06)	11.20
L EICA*‡	0.49 (0.03)	0.48 (0.03)	0.48 (0.02)	3.40
L VA	0.36 (0.05)	0.35 (0.04)	0.33 (0.04)	3.03

Values (cm) are provided as mean (SD).
AD, Alzheimer's disease; CCA, common carotid artery; EICA, extracranial internal carotid artery; HC, healthy control; L, left; R, right; SIVD, subcortical ischemic vascular dementia; VA, vertebral artery.
**SIVD vs. AD, $P < 0.05$.*
‡SIVD vs. HC, $P < 0.05$.
†AD vs. HC, $P < 0.05$.

as well as pBA and dBA from the linear regression analysis are shown in **Figure 2**. In terms of cognitive domains, the PI of the left MCA and PCA was negatively correlated with the memory composite score, and the MFV of the left ICA was positively correlated with the executive composite score. These correlations remained statistically significant after adjusting for age, sex, hypercholesterolemia, diabetes mellitus, coronary heart disease, hypertension, history of stroke, and BMI (**Supplementary Tables 1–3**).

Association Between Carotid Atherosclerosis and Cognitive Function in Patients With Dementia

Among all carotid ultrasound parameters, number of arteries with plaque, total carotid plaque score, and right CCA lumen diameter were negatively correlated with the MMSE score in all patients (**Supplementary Table 4**). Total carotid plaque score and right CCA lumen diameter were negatively correlated with either memory composite or executive composite scores (**Supplementary Table 5**). After adjusting for age, sex, hypercholesterolemia, diabetes mellitus, coronary heart disease, hypertension, history of stroke, and BMI, these correlations were still statistically significant.

DISCUSSION

In this study, TCD revealed significantly decreased MFV and increased PI in most major cerebral arteries in patients with SIVD compared with those in HCs. We also found increases in lumen diameter, number of arteries with plaque, and total carotid plaque score in patients with SIVD as compared to the HC group. Patients with AD also showed intracranial hemodynamic disruption without prominent carotid atherosclerosis. Furthermore, the changes in intracranial hemodynamics and carotid atherosclerosis were correlated with cognitive impairment in dementia patients with either SIVD or AD. These correlations were independent of age, sex, hypercholesterolemia, diabetes mellitus, coronary heart disease, hypertension, history of stroke, and BMI. These findings suggest that hemodynamic and structural changes in cerebral and carotid large blood vessels are involved in the pathogenesis of SIVD and to a lesser extent AD.

Although a study did not observe any robust difference in MFV or PI measured with TCD between patients with dementia and HCs (Malojcic et al., 2017), a meta-analysis concluded that the MFV of the MCA was decreased in patients with both VaD and AD (Sabayan et al., 2012). Consistently, we found decreased MFV and increased PI in arteries of both anterior and posterior circulations in patients with SIVD and AD. Moreover, we found lower MFV of the left PCA and higher PI of the bilateral PCAs in SIVD compared to AD. Our results were consistent with a previous study showing higher PI and lower MFV in patients with small vessel disease compared to those with AD (Sattel et al., 1996).

Our abovementioned findings of intracranial hemodynamics and carotid atherosclerosis in patients with SIVD and AD were potentially influenced by the differences in demographic and clinical features between groups. In this study, fewer subjects had vascular risk factors in the AD group compared to the HC group (hypercholesterolemia 30 vs. 60%, hypertension 26.7 vs. 46.7%, and diabetes mellitus 3.3 vs. 20.0%). Since we had strict MRI criteria (including variant cerebrovascular lesions) for both SIVD and AD, patients with significant vascular risk factors may have been excluded from the AD group. However, patients with AD still demonstrated worse intracranial hemodynamics than HCs, suggesting possible independence between cerebrovascular disruption in AD pathophysiology and vascular risk factors. Moreover, the prevalence of vascular risk factors is higher in men than in women. Accordingly, dementia patients with more cardiovascular risk factors or male sex are likely to be diagnosed with VaD or mixed dementia in clinical practice (Jiao et al., 2021). It is therefore reasonable that male patients accounted

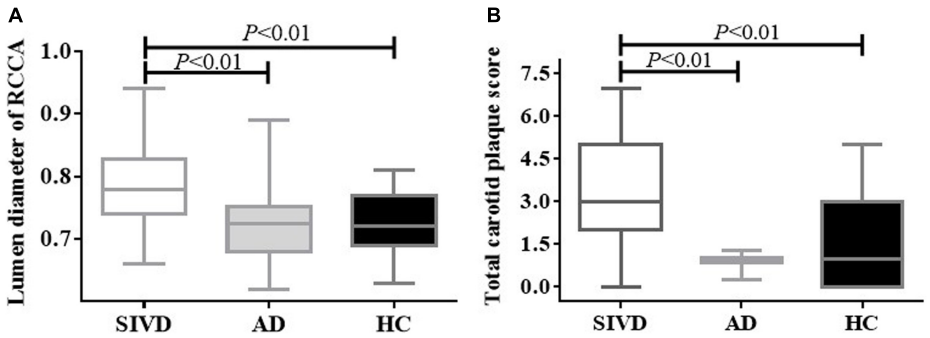

FIGURE 1 | Lumen diameter of the right CCA and total carotid plaque score by the group. Patients with SIVD showed significantly increased lumen diameter **(A)** and total carotid plaque score **(B)** compared with the AD and HC groups ($P < 0.01$). There was no difference between the AD and HC groups ($P > 0.05$). AD, Alzheimer's disease; CCA, common carotid artery; HC, healthy control; SIVD, subcortical ischemic vascular dementia.

TABLE 5 | Carotid plaque by the group.

	SIVD (*n* = 44)	AD (*n* = 30)	HC (*n* = 30)	F
Plaque numbers‡	2.36 (1.22)	1.77 (1.48)	1.40 (1.54)	4.49
Number of arteries with plaque‡	2.16 (1.12)	1.60 (1.30)	1.23 (1.30)	5.30
Total carotid plaque score*‡	3.23 (1.78)	2.00 (1.68)	1.60 (1.71)	9.02

Values are provided as mean (SD). Carotid arteries were divided into three segments on both sides (common carotid artery, bifurcation, and internal carotid artery), and plaques were quantified in each segment. The largest plaque in each segment was scored as 1, 2, or 3 according to its diameter (≥1.5, ≥2.5, and ≥3.5 mm, respectively). The total carotid plaque score was calculated as the sum of the scores for each segment, ranging from a minimum of 0 points to a maximum of 18 points.

AD, Alzheimer's disease; HC, healthy control; SIVD, subcortical ischemic vascular dementia.

**SIVD vs. AD, P < 0.05.*

‡SIVD vs. HC, P < 0.05.

†AD vs. HC, P < 0.05.

for 59% of the SIVD group, which was more than 30% in the AD group. Furthermore, the difference in sex proportion between the SIVD and AD groups was also caused by the epidemiological features of both diseases (Podcasy and Epperson, 2016); specifically, more women suffer from AD than men (Babapour and van der Flier, 2019). Although it was previously reported that women had higher MFVs of the ACA, MCA, and PCA than men in a healthy population (Krejza et al., 1999), this sex-related difference in TCD parameters has not been widely demonstrated in other studies, especially in older populations (Patel et al., 2016).

Decreased MFV is commonly caused by arterial stenosis and cerebral blood flow reduction. Elevated PI indicates an increase in distal vascular resistance, which could lead to a decrease in blood flow velocity and cerebral metabolism. Taken together, the hemodynamic changes detected by TCD in our study revealed a whole-brain model of increasing resistance to blood flow and subsequent hypoperfusion in patients with SIVD and AD. Cerebral hypoperfusion was found to be associated with a series of pathophysiological processes, including amyloid deposition, aberrant tau hyperphosphorylation, cholinergic dysregulation, and neurovascular unit disruption. Increasing evidence indicates a critical role of cerebral hypoperfusion in the pathogenesis and progression of VaD and neurodegenerative diseases, including AD (Fleisher et al., 2009; Iadecola, 2017; Caruso et al., 2019; Moretti and Caruso, 2020).

Previous studies suggested a correlation between carotid atherosclerosis and MRI features of SIVD (Poels et al., 2012; Moroni et al., 2016; Zhai et al., 2020). In a community-based study, patients with more carotid plaques showed an increased risk of concomitant microatheroma in perforator arterials, which potentially led to ischemic parenchymal lesions such as lacunes and WMH (Zhai et al., 2020). An enlarged CCA diameter measured by TCD was associated with WMH (Rundek et al., 2017) and lacunar infarction (Brisset et al., 2013) in stroke-free participants, and it was also associated with microbleeds and PVS (Zhai et al., 2020). These studies support our findings of the pathophysiological carotid artery changes in patients with SIVD, such as increased carotid plaques and enlarged lumen diameter, which might be the compensatory mechanisms to maintain cerebral perfusion against increased arterial wall stiffness and thickness, and were closely related to increased intima-media thickness and plaque burden (Bonithon-Kopp et al., 1996). Consistent with a prospective cardiovascular health study, showing that carotid atherosclerosis did not significantly correlate with the increased risk of AD (Newman et al., 2005), we did not find notable carotid atherosclerosis in patients with AD. However, this result was potentially caused by the lower burden of vascular risk factors in patients with AD in this study, as compared to the HC group.

Interestingly, the cognitive function measured by the MMSE was positively correlated with the MFV and was negatively correlated with the PI of most major cerebral arteries in dementia patients with SIVD or AD. A linear positive correlation between cognitive impairment and the MFV of the MCA in patients with severe unilateral internal carotid artery stenosis was previously reported (Marshall et al., 2020). Moreover, higher MFV was associated with higher MMSE score and larger hippocampal volume in a population-based study (Ruitenberg et al., 2005). The longitudinal studies reported that the increased PI of either ACA or PCA predicted conversion to dementia in individuals with subjective memory decline or MCI (Chung et al., 2017)

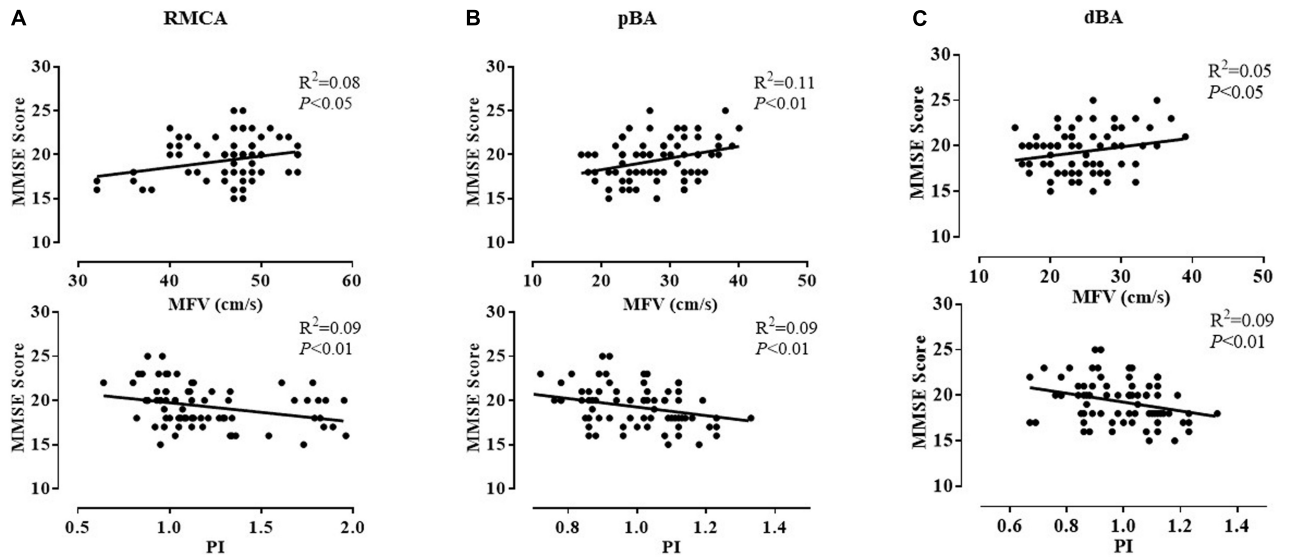

FIGURE 2 | Correlation between MMSE scores and the MFV and PI of three representative arteries in patients with dementia. After adjusting for age, sex, and vascular risk factors, the MMSE score was positively correlated with the MFV of the right MCA ($P < 0.05$) **(A)**, pBA ($P < 0.01$) **(B)**, and dBA ($P < 0.05$) **(C)** and negatively correlated with the PI of the right MCA ($P < 0.01$) **(A)**, pBA ($P < 0.01$) **(B)**, and dBA ($P < 0.01$) **(C)**. dBA, distal basilar artery; MCA, middle cerebral artery; MFV, mean flow velocity; MMSE, Mini-Mental State Examination; pBA, proximal basilar artery; PI, pulsatility index.

and the aggravation of cognitive decline in patients with mild-to-moderate AD (Lim et al., 2017). Apart from the global cognition, we also observed a negative correlation between memory and the PIs of the left MCA and PCA and a positive correlation between executive function and the MFV of the left ICA. These findings were supported by a previous study in which the PI of the MCA was correlated with information processing speed and executive function in patients with lacunar infarcts, even after the adjustment for vascular risk factors (Altmann et al., 2016).

Carotid atherosclerosis at early-to-mid stages characterized by intima-media thickening and plaques was associated with cognitive impairment in patients with dementia or MCI (Buratti et al., 2015; Gardener et al., 2017; Ihle-Hansen et al., 2019). Although the correlation between carotid artery lumen diameter and cognitive impairment has not been investigated in patients with cerebral vascular disease or AD, previous studies observed that the increased cerebral artery diameter that was measured by the time-of-flight MR angiogram was correlated with worse performance in memory and cognitive function in a population-based cohort of self-reported stroke-free individuals. In particular, participants with a larger left PCA diameter showed more declines in the scores of episodic memory, semantic memory, processing speed, and executive function in the 5-year follow-up (Gutierrez et al., 2018). Moreover, the cerebral arterial dilatation was related to AD pathology and was negatively correlated with the MMSE score in stroke-free participants (Gutierrez et al., 2019). Our findings provide new evidence of a correlation between carotid atherosclerosis (indicated by carotid plaque and lumen diameter) and cognitive function in dementia patients with either SIVD or AD, and this was independent of vascular risk factors.

We comprehensively investigated cerebral hemodynamics and carotid atherosclerosis using ultrasound technology and analyzed the correlations with cognitive impairment. However, this study was limited by the following factors. First, medical conditions associated with SIVD (e.g., metabolic syndrome and COPD) and statin use can potentially impact cerebral hemodynamics (Park et al., 2008; Giannopoulos et al., 2012; Hlavati et al., 2019). However, we did not analyze which factor most prominently contributed to hemodynamic changes. Second, since we only conducted the resting-state TCD measurement without end-tidal CO_2 or acetazolamide enhancement, it is necessary to investigate cerebrovascular reactivities in patients with SIVD in future studies. Finally, to confirm a causal relationship between cerebral hemodynamics and cognitive impairment, it will be important to perform repeated blood flow measurements and cognitive assessments in longitudinal studies.

CONCLUSION

In this study, we performed a non-invasive ultrasound and found prominent intracranial hemodynamic disruption and carotid atherosclerosis in patients with SIVD. The functional and pathological changes in cerebral and carotid large vessels were associated with cognitive impairment in dementia patients with SIVD or AD.

DATA AVAILABILITY STATEMENT

The original contributions presented in the study are included in the article/**Supplementary Material**, further inquiries can be directed to the corresponding author.

ETHICS STATEMENT

The studies involving human participants were reviewed and approved by the Ethics Committee of Tianjin Medical University General Hospital (IRB2017-063-01). The patients/participants provided their written informed consent to participate in this study.

AUTHOR CONTRIBUTIONS

X-JL and NZ drafted the manuscript. X-JL, PC, MX, and X-BT collected and organized the data. X-JL and PC performed the statistical analyses. CG and XL performed the ultrasound measurements. NZ designed the study. All authors contributed to the article and approved the submitted version.

FUNDING

This study was supported by the National Natural Science Foundation of China (Grant No. 81870831).

SUPPLEMENTARY MATERIAL

The Supplementary Material for this article can be found online at: https://www.frontiersin.org/articles/10.3389/fnagi.2021.741881/full#supplementary-material

REFERENCES

Altmann, M., Thommessen, B., Ronning, O. M., Benth, J. S., Reichenbach, A. S., and Fure, B. (2016). Middle cerebral artery pulsatility index is associated with cognitive impairment in lacunar stroke. *J. Neuroimaging* 26, 431–435. doi: 10.1111/jon.12335

Babapour, M. R., and van der Flier, W. M. (2019). Nature and implications of sex differences in AD pathology. *Nat. Rev. Neurol.* 15, 6–8. doi: 10.1038/s41582-018-0115-7

Beishon, L., Haunton, V. J., Panerai, R. B., and Robinson, T. G. (2017). Cerebral hemodynamics in mild cognitive impairment: a systematic review. *J. Alzheimers Dis.* 59, 369–385. doi: 10.3233/JAD-170181

Bonithon-Kopp, C., Touboul, P. J., Berr, C., Magne, C., and Ducimetiere, P. (1996). Factors of carotid arterial enlargement in a population aged 59 to 71 years: the EVA study. *Stroke* 27, 654–660. doi: 10.1161/01.str.27.4.654

Brisset, M., Boutouyrie, P., Pico, F., Zhu, Y., Zureik, M., Schilling, S., et al. (2013). Large-vessel correlates of cerebral small-vessel disease. *Neurology* 80, 662–669. doi: 10.1212/WNL.0b013e318281ccc2

Buratti, L., Balestrini, S., Altamura, C., Viticchi, G., Falsetti, L., Luzzi, S., et al. (2015). Markers for the risk of progression from mild cognitive impairment to Alzheimer's disease. *J. Alzheimers Dis.* 45, 883–890. doi: 10.3233/JAD-143135

Caruso, P., Signori, R., and Moretti, R. (2019). Small vessel disease to subcortical dementia: a dynamic model, which interfaces aging, cholinergic dysregulation and the neurovascular unit. *Vasc. Health Risk Manag.* 15, 259–281. doi: 10.2147/VHRM.S190470

Chung, C. P., Lee, H. Y., Lin, P. C., and Wang, P. N. (2017). Cerebral artery pulsatility is associated with cognitive impairment and predicts dementia in individuals with subjective memory decline or mild cognitive impairment. *J. Alzheimers Dis.* 60, 625–632. doi: 10.3233/JAD-170349

Dubois, B., Feldman, H. H., Jacova, C., Hampel, H., Molinuevo, J. L., Blennow, K., et al. (2014). Advancing research diagnostic criteria for Alzheimer's disease: the IWG-2 criteria. *Lancet Neurol.* 13, 614–629. doi: 10.1016/S1474-4422(14)70090-0

Fazekas, F., Chawluk, J. B., Alavi, A., Hurtig, H. I., and Zimmerman, R. A. (1987). MR signal abnormalities at 1.5 T in Alzheimer's dementia and normal aging. *AJR Am. J. Roentgenol.* 149, 351–356. doi: 10.2214/ajr.149.2.351

Fleisher, A. S., Podraza, K. M., Bangen, K. J., Taylor, C., Sherzai, A., Sidhar, K., et al. (2009). Cerebral perfusion and oxygenation differences in Alzheimer's disease risk. *Neurobiol. Aging.* 30, 1737–1748. doi: 10.1016/j.neurobiolaging.2008.01.012

Gardener, H., Caunca, M. R., Dong, C., Cheung, Y. K., Elkind, M., Sacco, R. L., et al. (2017). Ultrasound markers of carotid atherosclerosis and cognition: the Northern Manhattan study. *Stroke* 48, 1855–1861. doi: 10.1161/STROKEAHA.117.016921

Giannopoulos, S., Katsanos, A. H., Tsivgoulis, G., and Marshall, R. S. (2012). Statins and cerebral hemodynamics. *J. Cereb. Blood Flow Metab.* 32, 1973–1976. doi: 10.1038/jcbfm.2012.122

Gutierrez, J., Guzman, V., Khasiyev, F., Manly, J., Schupf, N., Andrews, H., et al. (2019). Brain arterial dilatation and the risk of Alzheimer's disease. *Alzheimers Dement.* 15, 666–674. doi: 10.1016/j.jalz.2018.12.018

Gutierrez, J., Kulick, E., Park, M. Y., Dong, C., Cheung, K., Ahmet, B., et al. (2018). Brain arterial diameters and cognitive performance: the Northern Manhattan study. *J. Int. Neuropsychol. Soc.* 24, 335–346. doi: 10.1017/S1355617717001175

Hamilton, M. (1967). Development of a rating scale for primary depressive illness. *Br. J. Soc. Clin. Psychol.* 6, 278–296.

Hlavati, M., Buljan, K., Tomic, S., Horvat, M., and Butkovic-Soldo, S. (2019). Impaired cerebrovascular reactivity in chronic obstructive pulmonary disease. *Acta Neurol. Belg.* 119, 567–575. doi: 10.1007/s13760-019-01170-y

Iadecola, C. (2017). The neurovascular unit coming of age: a journey through neurovascular coupling in health and disease. *Neuron* 96, 17–42. doi: 10.1016/j.neuron.2017.07.030

Ihle-Hansen, H., Vigen, T., Berge, T., Hagberg, G., Engedal, K., Ronning, O. M., et al. (2019). Carotid atherosclerosis and cognitive function in a general population aged 63-65 years: data from the Akershus Cardiac Examination (ACE) 1950 Study. *J. Alzheimers Dis.* 70, 1041–1049. doi: 10.3233/JAD-190327

Jiao, C., Wei, S., Liu, T., Bao, X., Chen, W., Liao, Z., et al. (2021). The prevalence of vascular dementia in China: a systematic review and meta-analysis from 2009-2019. *Iran. J. Public Health.* 50, 11–23. doi: 10.18502/ijph.v50i1.5068

Krejza, J., Mariak, Z., Walecki, J., Szydlik, P., Lewko, J., and Ustymowicz, A. (1999). Transcranial color Doppler sonography of basal cerebral arteries in 182 healthy subjects: Age and sex variability and normal reference values for blood flow parameters. *AJR Am. J. Roentgenol.* 172, 213–218. doi: 10.2214/ajr.172.1.9888770

Lim, J. S., Lee, J. Y., Kwon, H. M., and Lee, Y. S. (2017). The correlation between cerebral arterial pulsatility and cognitive dysfunction in Alzheimer's disease patients. *J. Neurol. Sci.* 373, 285–288. doi: 10.1016/j.jns.2017.01.001

Malojcic, B., Giannakopoulos, P., Sorond, F. A., Azevedo, E., Diomedi, M., Oblak, J. P., et al. (2017). Ultrasound and dynamic functional imaging in vascular cognitive impairment and Alzheimer's disease. *BMC Med.* 15:27. doi: 10.1186/s12916-017-0799-3

Marshall, R. S., Pavol, M. A., Cheung, Y. K., Asllani, I., and Lazar, R. M. (2020). Cognitive impairment correlates linearly with mean flow velocity by transcranial Doppler below a definable threshold. *Cerebrovasc. Dis. Extra.* 10, 21–27. doi: 10.1159/000506924

Mok, V., Ding, D., Fu, J., Xiong, Y., Chu, W. W., Wang, D., et al. (2012). Transcranial Doppler ultrasound for screening cerebral small vessel disease: a community study. *Stroke* 43, 2791–2793. doi: 10.1161/STROKEAHA.112.665711

Moretti, R., and Caruso, P. (2020). Small vessel disease-related dementia: an invalid neurovascular coupling? *Int. J. Mol. Sci.* 21:1095. doi: 10.3390/ijms21031095

Moroni, F., Ammirati, E., Magnoni, M., D'Ascenzo, F., Anselmino, M., Anzalone, N., et al. (2016). Carotid atherosclerosis, silent ischemic brain damage and brain atrophy: a systematic review and meta-analysis. *Int. J. Cardiol.* 223, 681–687. doi: 10.1016/j.ijcard.2016.08.234

Newman, A. B., Fitzpatrick, A. L., Lopez, O., Jackson, S., Lyketsos, C., Jagust, W., et al. (2005). Dementia and Alzheimer's disease incidence in relationship to cardiovascular disease in the Cardiovascular Health Study cohort. *J. Am. Geriatr. Soc.* 53, 1101–1107. doi: 10.1111/j.1532-5415.2005.53360.x

Park, J. S., Cho, M. H., Lee, K. Y., Kim, C. S., Kim, H. J., Nam, J. S., et al. (2008). Cerebral arterial pulsatility and insulin resistance in type 2 diabetic patients. *Diabetes Res. Clin. Pract.* 79, 237–242. doi: 10.1016/j.diabres.2007.08.029

Patel, N., Panerai, R. B., Haunton, V., Katsogridakis, E., Saeed, N. P., Salinet, A., et al. (2016). The Leicester cerebral haemodynamics database: normative values and the influence of age and sex. *Physiol. Meas.* 37, 1485–1498. doi: 10.1088/0967-3334/37/9/1485

Podcasy, J. L., and Epperson, C. N. (2016). Considering sex and gender in Alzheimer disease and other dementias. *Dialogues Clin. Neurosci.* 18, 437–446. doi: 10.31887/DCNS.2016.18.4/cepperson

Poels, M. M., Zaccai, K., Verwoert, G. C., Vernooij, M. W., Hofman, A., van der Lugt, A., et al. (2012). Arterial stiffness and cerebral small vessel disease: the Rotterdam Scan Study. *Stroke* 43, 2637–2642. doi: 10.1161/STROKEAHA.111.642264

Roher, A. E., Esh, C., Rahman, A., Kokjohn, T. A., and Beach, T. G. (2004). Atherosclerosis of cerebral arteries in Alzheimer disease. *Stroke* 35(11 Suppl. 1), 2623–2627.

Roher, A. E., Garami, Z., Tyas, S. L., Maarouf, C. L., Kokjohn, T. A., Belohlavek, M., et al. (2011). Transcranial Doppler ultrasound blood flow velocity and pulsatility index as systemic indicators for Alzheimer's disease. *Alzheimers Dement.* 7, 445–455. doi: 10.1016/j.jalz.2010.09.002

Roman, G. C., Erkinjuntti, T., Wallin, A., Pantoni, L., and Chui, H. C. (2002). Subcortical ischaemic vascular dementia. *Lancet Neurol.* 1, 426–436. doi: 10.1016/s1474-4422(02)00190-4

Ruitenberg, A., den Heijer, T., Bakker, S. L., van Swieten, J. C., Koudstaal, P. J., Hofman, A., et al. (2005). Cerebral hypoperfusion and clinical onset of dementia: the Rotterdam Study. *Ann. Neurol.* 57, 789–794. doi: 10.1002/ana.20493

Rundek, T., Della-Morte, D., Gardener, H., Dong, C., Markert, M. S., Gutierrez, J., et al. (2017). Relationship between carotid arterial properties and cerebral white matter hyperintensities. *Neurology* 88, 2036–2042. doi: 10.1212/WNL.0000000000003951

Sabayan, B., Jansen, S., Oleksik, A. M., van Osch, M. J., van Buchem, M. A., van Vliet, P., et al. (2012). Cerebrovascular hemodynamics in Alzheimer's disease and vascular dementia: a meta-analysis of transcranial Doppler studies. *Ageing Res. Rev.* 11, 271–277. doi: 10.1016/j.arr.2011.12.009

Sachdev, P. S., Mohan, A., Taylor, L., and Jeste, D. V. (2015). DSM-5 and mental disorders in older individuals: an overview. *Harv. Rev. Psychiatry.* 23, 320–328. doi: 10.1097/HRP.0000000000000090

Sachdev, P., Kalaria, R., O'Brien, J., Skoog, I., Alladi, S., Black, S. E., et al. (2014). Diagnostic criteria for vascular cognitive disorders: a VASCOG statement. *Alzheimer Dis. Assoc. Disord.* 28, 206–218. doi: 10.1097/WAD.0000000000000034

Sattel, H., Forstl, H., and Biedert, S. (1996). Senile dementia of Alzheimer type and multi-infarct dementia investigated by transcranial Doppler sonography. *Dementia* 7, 41–46. doi: 10.1159/000106851

Scheltens, P., Leys, D., Barkhof, F., Huglo, D., Weinstein, H. C., Vermersch, P., et al. (1992). Atrophy of medial temporal lobes on MRI in "probable" Alzheimer's disease and normal ageing: diagnostic value and neuropsychological correlates. *J. Neurol. Neurosurg. Psychiatry* 55, 967–972. doi: 10.1136/jnnp.55.10.967

Skrobot, O. A., Black, S. E., Chen, C., DeCarli, C., Erkinjuntti, T., Ford, G. A., et al. (2018). Progress toward standardized diagnosis of vascular cognitive impairment: guidelines from the Vascular Impairment of Cognition Classification Consensus Study. *Alzheimers Dement.* 14, 280–292. doi: 10.1016/j.jalz.2017.09.007

Touboul, P. J., Hennerici, M. G., Meairs, S., Adams, H., Amarenco, P., Bornstein, N., et al. (2007). Mannheim carotid intima-media thickness consensus (2004-2006). An update on behalf of the Advisory Board of the 3rd and 4th watching the risk symposium, 13th and 15th European Stroke Conferences, Mannheim, Germany, 2004, and Brussels, Belgium, 2006. *Cerebrovasc. Dis.* 23, 75–80. doi: 10.1159/000097034

Vinciguerra, L., Lanza, G., Puglisi, V., Pennisi, M., Cantone, M., Bramanti, A., et al. (2019). Transcranial Doppler ultrasound in vascular cognitive impairment-no dementia. *PLoS One* 14:e216162. doi: 10.1371/journal.pone.0216162

Zhai, F. F., Yang, M., Wei, Y., Wang, M., Gui, Y., Han, F., et al. (2020). Carotid atherosclerosis, dilation, and stiffness relate to cerebral small vessel disease. *Neurology* 94:e1811-19. doi: 10.1212/WNL.0000000000009319

Conflict of Interest: The authors declare that the research was conducted in the absence of any commercial or financial relationships that could be construed as a potential conflict of interest.

Publisher's Note: All claims expressed in this article are solely those of the authors and do not necessarily represent those of their affiliated organizations, or those of the publisher, the editors and the reviewers. Any product that may be evaluated in this article, or claim that may be made by its manufacturer, is not guaranteed or endorsed by the publisher.

frontiers in Aging Neuroscience

ORIGINAL RESEARCH
published: 03 February 2022
doi: 10.3389/fnagi.2022.759159

Increased RNA Transcription of Energy Source Transporters in Circulating White Blood Cells of Aged Mice

*Yukiko Takeuchi[1†], Orie Saino[1†], Yuka Okinaka[1], Yuko Ogawa[1], Rie Akamatsu[1], Akie Kikuchi-Taura[1], Yosky Kataoka[2,3], Mitsuyo Maeda[2,3], Sheraz Gul[4,5], Carsten Claussen[4,5], Johannes Boltze[1,6] and Akihiko Taguchi[1]**

[1] Department of Regenerative Medicine Research, Foundation for Biomedical Research and Innovation at Kobe, Hyogo, Japan, [2] Multi-Modal Microstructure Analysis Unit, RIKEN-JEOL Collaboration Center, RIKEN, Hyogo, Japan, [3] Laboratory for Cellular Function Imaging, RIKEN Center for Biosystems Dynamics Research, RIKEN, Hyogo, Japan, [4] Fraunhofer Institute for Translational Medicine and Pharmacology ITMP, Hamburg, Germany, [5] Fraunhofer Cluster of Excellence for Immune-Mediated Diseases (CIMD), Hamburg, Germany, [6] School of Life Sciences, University of Warwick, Coventry, United Kingdom

OPEN ACCESS

Edited by:
Stefano Tarantini,
University of Oklahoma Health Sciences Center, United States

Reviewed by:
Alejandro O. Sodero,
CONICET Institute for Biomedical Research (BIOMED), Argentina
Jose Felix Moruno-Manchon,
University of Texas Health Science Center at Houston, United States

***Correspondence:**
Akihiko Taguchi
taguchi@fbri.org

[†] These authors have contributed equally to this work and share first authorship

Specialty section:
This article was submitted to Neuroinflammation and Neuropathy, a section of the journal Frontiers in Aging Neuroscience

Received: 16 August 2021
Accepted: 12 January 2022
Published: 03 February 2022

Citation:
Takeuchi Y, Saino O, Okinaka Y, Ogawa Y, Akamatsu R, Kikuchi-Taura A, Kataoka Y, Maeda M, Gul S, Claussen C, Boltze J and Taguchi A (2022) Increased RNA Transcription of Energy Source Transporters in Circulating White Blood Cells of Aged Mice. Front. Aging Neurosci. 14:759159. doi: 10.3389/fnagi.2022.759159

Circulating white blood cells (WBC) contribute toward maintenance of cerebral metabolism and brain function. Recently, we showed that during aging, transcription of metabolism related genes, including energy source transports, in the brain significantly decreased at the hippocampus resulting in impaired neurological functions. In this article, we investigated the changes in RNA transcription of metabolism related genes (glucose transporter 1 [Glut1], Glut3, monocarboxylate transporter 4 [MCT4], hypoxia inducible factor 1-α [Hif1-α], prolyl hydroxylase 3 [PHD3] and pyruvate dehydrogenase kinase 1 [PDK1]) in circulating WBC and correlated these with brain function in mice. Contrary to our expectations, most of these metabolism related genes in circulating WBC significantly increased in aged mice, and correlation between their increased RNA transcription and impaired neurological functions was observed. Bone marrow mononuclear transplantation into aged mice decreased metabolism related genes in WBC with accelerated neurogenesis in the hippocampus. *In vitro* analysis revealed that cell-cell interaction between WBC and endothelial cells via gap junction is impaired with aging, and blockade of the interaction increased their transcription in WBC. Our findings indicate that gross analysis of RNA transcription of metabolism related genes in circulating WBC has the potential to provide significant information relating to impaired cell-cell interaction between WBC and endothelial cells of aged mice. Additionally, this can serve as a tool to evaluate the change of the cell-cell interaction caused by various treatments or diseases.

Keywords: aging, white blood cell, RNA transcription, energy source transporter, metabolism related gene, neurogenesis, hippocampus

Abbreviations: WBC, white blood cells; BM-MNC, bone marrow mononuclear cells; Hif1-α, hypoxia inducible factor 1-α; Glut1, glucose transporter 1; Glut3, glucose transporter 3; MCT4, monocarboxylate transporter 4; PHD3, prolyl hydroxylase 3; PDK1, pyruvate dehydrogenase kinase 1; qPCR, Quantitative PCR; Cx43, Connexin 43; Cx37, Connexin 37; BCECF, 2′,7′-bis-(2-carboxyethyl)-5-(6)-carboxyfluorescein; DCX, Doublecortin; HUVEC, Human umbilical vein endothelial cells; ANOVA, analysis of variance.

INTRODUCTION

Circulating white blood cells (WBC) have been shown to contribute to the maintenance of cerebral circulation, metabolism, development, neurogenesis and brain function (Taguchi et al., 2004a, 2008; Filiano et al., 2017; Smith et al., 2018; Pasciuto et al., 2020; Runtsch et al., 2020). Intravenous administration of immature blood cells, such as cord blood derived CD34-positive cells or bone marrow mononuclear cells (BM-MNC), have been shown to improve cerebral circulation and functions after ischemia (Taguchi et al., 2004b; Nakano-Doi et al., 2010). However, the direct link between circulating or intravenously injected cells, and cerebral circulation, metabolism, and function has to date been unclear.

Gap junction is an intercellular channel that allows direct diffusion of ions and small molecules, including metabolic substances, between adjacent cells. One gap junction channel is composed of two hemichannels termed connexons, each one being assembled of six proteins called Connexins (Okamoto et al., 2021). Connexins are a large family of proteins, and Connexin 43 (Cx43) is the most widespread Connexin in the cardiovascular system and is involved both in normal physiological and pathological conditions (Yuan et al., 2015). In the vascular system, connections between endothelial, pericyte and smooth muscle cells via gap junction, as well as between endothelial cells, allow for signaling to take place to endothelial cells as well as other related components (Nielsen et al., 2012). Recently, we showed that intravenously injected BM-MNC supplies an energy source, such as glucose, to endothelial cells via gap junction and activates injured endothelial cells by induction of hypoxia inducible factor 1-α (Hif1-α), which is one of the major activators of metabolism related genes (Kim et al., 2006), in a cerebral ischemia model (Kikuchi-Taura et al., 2020). Intravenous BM-MNC transplantation in aged mice was shown to increase transcription of glucose transporter 1 (Glut1) at hippocampus followed by improved memory functions through gap junction mediated cell-cell interaction between transplanted BM-MNC and endothelial cells (Takeuchi et al., 2020). Furthermore, we have shown that intravenously transplanted mesenchymal stem cells remove the energy source from endothelial cells via gap junction, and suppress their excessive activation in a cerebral ischemia model (Kikuchi-Taura et al., 2021). These findings indicate that circulating cells have a significant effect on the regulation of cerebral circulation, metabolism, and function via gap junction. These findings are consistent with our previous findings that patients with decreased number of circulating hematopoietic stem cells, which express Connexin (Pfenniger et al., 2013) and contain significant amount of glycolysis substrates due to anaerobic metabolism (Takubo et al., 2013), showed impaired cerebral circulation and function (Taguchi et al., 2004a, 2008).

Cerebral metabolism and function generally deteriorate during aging (Cunnane et al., 2020). It has been shown that metabolites pass through the gap junction (Okamoto et al., 2021) and expression of gap junctions are increased in early postnatal development of central nerve system and after brain injury (Belousov and Fontes, 2014). However, the significance of metabolite transfer via gap junction in the brain is not fully elucidated. Taken together, we hypothesize that impaired cerebral metabolism and function observed in aged animals would correlate to the impaired metabolism of circulating WBC. In this article, we had expected decreased expression of metabolism related genes in WBC with impaired brain function during aging, but found their expression increased with aging.

MATERIALS AND METHODS

All animal experiments were approved by the Animal Care and Use Committee of Foundation for Biomedical Research and Innovation at Kobe and comply with the Guide for the Care and Use of Animals published by the Japanese Ministry of Education, Culture, Sports, Science and Technology. Experiments and results are reported according to the ARRIVE guidelines.

Quantitative PCR (qPCR) Analysis of Circulating White Blood Cells, Hippocampus, and Human Umbilical Vein Endothelial Cells

Male CB-17 mice (C.B-17/Icr- + / + Jcl, Oriental Yeast, Tokyo, Japan) aged 5, 10, 52, and 104 weeks were used for this study (N = 5, each). Minimal variation of cerebrovascular structure is known in CB-17 mice (Taguchi et al., 2010) and CB-17 mice were used for the experiment of cerebrovascular disorders (Kasahara et al., 2013; Takeuchi et al., 2020). After deep anesthesia by pentobarbital, a blood sample was obtained by the puncture to left ventricle of heart. Total RNA was isolated using RNeasy Plus Universal Mini Kit (Qiagen, CA, United States) according to the manufacturer's instructions. cDNA was synthesized from 1μg total RNA using PrimeScript™ II 1st strand cDNA Synthesis Kit (TAKARA, Kyoto, Japan). Transcription of mRNA was analyzed using PowerUp™ SYBR™ Green Master Mix (Applied Biosystems, CA, United States) and the Agilent AriaMx real time PCR System. 18S ribosomal RNA was used for the reference gene. Relative quantification of RNA was analyzed by phaffle method. For the comparison of RNA transcription of Connexin 43 (Cx43) between young and aged mice, 5 and 80 weeks old Male CB-17 mice were used (N = 6, each). The list of target genes, primer sequences, and amplification protocols of qPCR are shown in **Table 1**.

Brain tissue was harvested from young (5W) and aged (more than 80 weeks) mice (N = 7, each). After harvesting the brain, coronal sections (4 mm thick) of the forebrain between 2 mm and 6 mm from frontal pole were cut followed by immersion in RNAlater (Thermo Fisher, Waltham, MA, United States) to prevent RNA degradation. Under stereoscopic microscope (Olympus, Tokyo, Japan), the part of the hippocampus, was dissected by medical tweezers, as we described previously (Takeuchi et al., 2020). Total RNA was isolated and cDNA was synthesized from 1 μg total RNA. The list of target genes, primer sequences, and amplification protocols are shown in **Table 1**.

Human umbilical vein endothelial cells (HUVEC, Kurabo, Osaka, Japan) were cultured with medium, serum and growth

TABLE 1 | Target genes, primer list and amplification protocol of qPCR.

Gene	NCBI accession no.		Sequences
18S	NR_003278.3	Forward	ACTCAACACGGGAAACCTCACC
		Reverse	CCAGACAAATCGCTCCACCA
Mouse Glut1	NM_011400.3	Forward	TGGCGGGAGACGCATAGTTA
		Reverse	CTCCCACAGCCAACATGAGG
Mouse Glut3	NM_011401.4	Forward	GAGGAACACTTGCTGCCGAG
		Reverse	CTGGAAAGAGCCGATCGTGG
Mouse MCT4	NM_001038653.1	Forward	GGCTGGCGGTAACAGAGTA
		Reverse	CGGCCTCGGACCTGAGTATT
Mouse Hif1-α	NM_001313919.1	Forward	AGCCAGCAAGTCCTTCTGAT
		Reverse	AGGCTGGGAAAAGTTAGGAGTG
Mouse PHD3	NM_028133.2	Forward	ATCCACATGAAGTCCAGCCC
		Reverse	ACACCACAGTCAGTCTTTAGCA
Mouse PDK1	NM_172665.5	Forward	TGCAAAGTTGGTATATCCAAAGCC
		Reverse	TGTGCCGGTTTCTGATCCTT
Mouse Cx37	NM_008120.3	Forward	CAGCTGCGCGCTATTTAAGG
		Reverse	CCATGTTTCCAGGGCCTCTC
Mouse Cx43	NM_010288.3	Forward	GAGTTCCACCACTTTGGCGT
		Reverse	GTGGAGTAGGCTTGGACCTT
Human Cx37	NM_002060.2	Forward	CACCATGCCCCACCTACAAT
		Reverse	TGGGGGTTTTTGGCCATTC
Human Cx43	NM_000165.4	Forward	AGGAGTTCAATCACTTGGCGT
		Reverse	CCCTCCAGCAGTTGAGTAGG

Segment	Plateau	Temperature (°C)	Duration time (seconds)	Cycle (times)
Hot Start	1	50	180	1
Hot Start 2	1	95	180	1
Amplification	1	95	5	40
Amplification	2	60	30	40
Melt	1	95	30	1
Melt	2	65	30	1
Melt	3	95	30	1

factors (HuMedia-EB2, Kurabo). Total RNA of HUVEC (1×10^5 cells) at passage 3 and 10 were was isolated and expression of Cx43 and Connexin 37 (Cx37) were evaluated by qPCR ($N = 4$). The list of target genes, primer sequences, and amplification protocols of qPCR are shown in **Table 1**.

Transfer of Low Molecular Weight Fluorescence Molecules in Cytoplasm of White Blood Cells to Endothelial Cells *in vitro*

Male CB-17 mice aged 5 and 80 weeks old were used for this study ($N = 5$, each). Blood sample was obtained by a puncture to the left ventricle of the heart and red blood cells were removed using lysing buffer (BD Biosciences, Woburn, MA, United States) (Muirhead et al., 1986). WBC were incubated with 5 μM of BCECF-AM (2′,7′-bis-(2-carboxyethyl)-5-(and-6)-carboxyfluorescein, acetoxymethyl ester, Dojindo, Kumamoto Japan) for 30 min at 37°C as we described previously (Kikuchi-Taura et al., 2020). BCECF-AM was converted to BCECF (2′,7′-bis-(2-carboxyethyl)-5-(6)-carboxyfluorescein) in the cytoplasm and BCECF loaded WBC were washed twice with PBS before use. HUVEC in passage 6 were used in the subsequent experimental work. BCECF loaded WBC (1×10^6 cells in 20 μl PBS) and HUVEC (1×10^5 cells in 100 μl PBS) were co-cultured at 37°C for 3 h. After co-incubation, the cell mixture was washed twice with PBS, and stained with PE-conjugated anti-human CD31 antibody (BD Biosciences, Woburn, MA, United States), FITC-conjugated anti-mouse CD45 antibody (BD Biosciences, Woburn, MA, United States) and 7-AAD (7-Amino-Actinomycin D) (BD Biosciences, Woburn, MA, United States). The level of BCECF in HUVEC (CD31-positive, CD45-negative and 7AAD-negative) was evaluated using a FACS Calibur fluorescence activated cell sorter (BD Biosciences, Woburn, MA, United States). Cell populations that communicate with HUVEC via gap junction were characterized using FACS as described previously (Kikuchi-Taura et al., 2021).

Effect of Gap-Junction Mediated Cell-Cell Interaction on Gene Expression of White Blood Cells by Co-culture With Endothelial Cells

HUVEC were treated with gap junction blocker (0.01 v/v 1-octanol. Wako, Osaka, Japan) or PBS for 10 min at 37°C. A blood sample was obtained by a puncture to the left ventricle of the

heart of male CB-17 mice (5 weeks old) and co-cultured at 37°C for 3 h with HUVEC that were treated or non-treated by gap junction blocker. The change of RNA transcription was evaluated by qPCR with mouse specific primers.

BM-MNC Transplantation to Aged Mice

Bone marrow was obtained from 5-week-old syngeneic male CB-17 mice and BM-MNC were prepared by Ficoll-Paque (GE-Healthcare, Little Chalfont, United Kingdom) density-gradient centrifugation as described elsewhere (Kikuchi-Taura et al., 2020). Aged (more than 80 weeks) mice received 1×10^5 BM-MNC in 100 μl PBS or PBS alone through the tail vein (5 times in total), and young (5 weeks) mice received PBS (N = 5, each). Each injection was performed without anesthesia and injection was finished in 10 s. Mouse behavior was evaluated using wire hang test and passive avoidance test before blood sample collection. The experimental design is shown in **Supplementary Figure 1A**. The Passive avoidance test is a fear-aggravated test used to evaluate learning and memory in rodent models. The apparatus (TMS-2; Melquest, Toyama, Japan) was divided into two compartments, an illuminated compartment (120 mm × 120 mm × 135 mm) and a dark compartment (120 mm × 120 mm × 135 mm), that were connected via a guillotine door. The dark compartment was equipped with a grid floor (6 mm in diameter spaced at 10 mm) through which a footshock (0.2 mA, 3 s) could be delivered. In the conditioning and acquisition phases, each mouse was placed in an illuminated compartment and habituated for 10 s before door opening. In the conditioning phase, a mild electric foot shock was administered 10 s after each mouse crossed the adjacent dark compartment and door closing. On the next day, each mouse was again placed in the illuminated compartment and habituated for 10 s, and the time to cross over to the dark compartment after door opening, up to a maximum of 180 s, was recorded as the test phase (Ogawa et al., 2020). The wire hang test evaluates muscular strength or motor function. In this test, each mouse was placed on the center of wire mesh plate (450 mm × 300 mm; mesh wire was 1.3 mm in diameter and spaced at 12 mm intervals, KK23-8331; Kohnan, Osaka, Japan) and allowed to accommodate to this environment for 5 s. The wire mesh plate was inverted and secured to the top of a cubic transparent open-topped glass box (250 mm × 250 mm × 250 mm). Latency to fall was recorded, up to a maximum of 180 s. This trial was repeated five times with an interval of 1 min and the average time to fall was calculated (Ogawa et al., 2020).

For immune historical analysis, aged mice (more than 80 weeks) received 1×10^5 BM-MNC in 100 μl PBS or PBS alone intravenously totally five times every 2 days from tail vein, and young (5 weeks) mice received PBS (N = 6,7,8, for aged + PBS, aged + BM-MNC and young + PBS, respectively). Twenty-four hours after the last injection, the brain was removed, fixed with 2% paraformaldehyde (PFA; Thermo Fisher, Waltham, MA, United States), and cut into coronal sections (20 μm) using a vibratome (Leica, Wetzlar, Germany). Sections were immunostained with primary antibodies against Nestin (Merck Millipore,1:200), Doublecortin (DCX; Merck Millipore, 1:350) and DAPI (Thermo Fisher, 1:1,000). Confocal images were obtained with fluorescence microscope (BZ-X810: Keyence, Osaka Japan). The number of Nestin positive fibers and DCX positive cells at the granular cell layer and sub granular zone of dentate gyrus, respectively, in the hippocampus of aged mice were counted by blinded investigator. The number of positive cells per 1 mm of each zone was evaluated.

Increased Expression of Gap-Junction in HUVEC by Co-culture With BM-MNC

HUVEC (1×10^5 cells in 100 μl PBS) and BM-MNC (1×10^6 cells in 20 μl PBS) were co-cultured at 37°C for 3 h, and the change in expression of Cx43 in HUVEC was evaluated with PE-conjugated anti-human CD31 antibody, FITC-conjugated anti-human Cx43 antibody (Santa Cruz Biotechnology, Santa Cruz, CA, United States) and 7-AAD (7-Amino-Actinomycin D) by FACS Calibur fluorescent cell sorter.

Statistics

Statistical comparisons among groups were performed using one-way ANOVA (analysis of variance) followed by *post hoc* analysis using Steel-Dwass test or Dunnett's test. Correlation between RNA transcription of metabolism related genes in circulating WBC and neurological functions was evaluated with linear regression analysis. Individual comparisons were performed using Student's t-test. All data are shown as mean ± SD.

RESULTS

Change in RNA Transcription of Metabolism-Related Genes in Circulating Whites Blood Cells With Aging

We previously observed that transcription of metabolism related genes, including energy source transport genes, in the brain are significantly decreased with aging with impaired neurological functions. We expected similar changes in WBC and investigated the sequential change in RNA transcription of these genes in circulating WBC. Contrary to our expectation, the energy source transport genes, including Glut1, Glut3, and monocarboxylate transporter 4 (MCT4), in WBC significantly increased with aging (**Figure 1A**). Hif1-α is one of the major transcriptional factors that regulates the expression of energy source transporters (Masoud and Li, 2015; Zorzano et al., 2005) and has been shown to decrease with aging in the brain (Takeuchi et al., 2020). The transcription of Hif1-α and its down-stream genes, prolyl hydroxylase 3 (PHD3) and pyruvate dehydrogenase kinase 1 (PDK1), in circulating WBC were investigated and it was found that transcription of PHD3 and PDK1 increased with aging (**Figure 1B**).

Cell-Cell Interaction Between WBC and Endothelial Cells via Gap Junction

We have shown low molecular weight molecules are transferred from BM-MNC to endothelial cells via gap junction mediated direct cell-cell interaction (Kikuchi-Taura et al., 2020; Takeuchi et al., 2020). To investigate gap junction mediated cell-cell

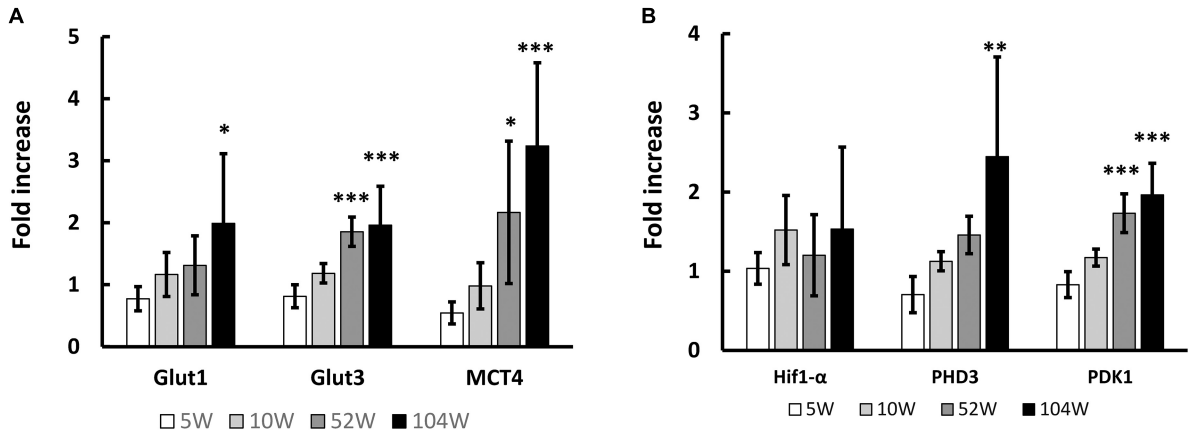

FIGURE 1 | Change in RNA transcription in circulating WBC with aging. **(A)** Significant increase of RNA transcription of energy source transport genes, including Glut1, Glut3 and MCT4, in WBC was observed with aging. **(B)** Similarly, RNA transcriptions of Hif1-α down-stream genes, PHD3 and PDK1, in WBC significantly increased with aging. $*p < 0.05$, $**p < 0.01$, $***p < 0.001$ by ANOVA followed by *post-hoc* analysis using Dunnett test (versus 5W). $N = 5$ in 10W, 104W and $N = 6$ in 5W, 52W **(A,B)**.

interaction between WBC and endothelial cells, low molecular weight fluorescence compound, namely BCECF, was loaded to WBC and co-cultured with HUVEC. Similar to BM-MNC, transfer of BCECF from WBC to HUVEC was observed and the level of BCECF transfer significantly decreased in WBC of aged mice, relative to that of young mice (**Figure 2A**). The change of RNA transcriptions with aging was evaluated and found the level of Cx43 in WBC was significantly decreased in aged mice, compared with young mice (**Figure 2B**). To confirm the significance of gap junction mediated cell-cell interaction on RNA transcription in WBC, WBC were co-cultured with HUVEC with or without blockade of gap junction. A significant increase of RNA transcription of Hif1-α and PDK1 was observed following blockade of gap junction (**Figure 2C**). These findings show the importance of gap junction mediated cell-cell interaction in the decrease of metabolism related gene expression in WBC, mainly monocytes and lymphocytes. The change in RNA transcription with passage number was evaluated in HUVEC and it was found that the level of Cx43 significantly decreased during passaging (**Figure 2D**). The change in RNA transcription with aging at hippocampus was evaluated and it was found that the level of Cx43 significantly decreased in aged mice, compared with young mice (**Figure 2E**). The change of RNA transcription of Cx37 was evaluated and found its expression decreased in HUVEC during passaging (**Figure 2F**) and in hippocampus with aging (**Figure 2G**).

Correlation in RNA Transcription of Metabolism Related Genes in Circulating White Blood Cells and Neurological Function in Aging Mice

Next, we evaluated the correlation between RNA transcription of metabolism related genes in circulating WBC and neurological function in mice, including aged mice that received BM-MNC transplantation. **Figures 3A-F** shows the correlation between increased RNA transcription of metabolism related genes and shortening of step through latency in passive avoidance test. A strong and significant correlation ($|r| > 0.7$ and $p < 0.05$) was observed for Glut1, MCT4, PHD3, and PDK1. **Supplementary Figure 2** shows the correlation between increased RNA transcription of metabolism related genes and shortening of latency to fall in wire hang test. A strong and significant correlation ($|r| > 0.7$ and $p < 0.05$) was observed for MCT4, PHD3, and PDK1. **Supplementary Figures 3, 4** show the correlation in aged mice, including those that received PBS or BM-MNC but not young mice, in the passive avoidance test (**Supplementary Figure 3**) and in the wire hang test (**Supplementary Figure 4**). A strong and significant correlation was observed for RNA transcription of MCT4 and PHD3. It should be noted that, a statistically significant reduction of the latency in passive avoidance test and wire hang test in aged mice with PBS, compared with young mice, was reported in our previous report. In contrast, BM-MNC injection to aged mice improved the scores of both tests and there had been no significant difference in the latencies between in aged mice with BM-MNC and young mice, though no statistically significant difference had been observed between in the scores of aged mice that received PBS or BM-MNC (Takeuchi et al., 2020).

Mice that received BM-MNC transplantation showed decreased RNA expression of Glut3, MCT4, PHD3, and PDK1 in circulating WBC (**Figures 4A,B**). To investigate the possible cause of decreased level of these genes by BM-MNC transplantation, endothelial cells were co-cultured with BM-MNC. We observed increased expression of Cx43 in HUVEC when co-cultured with BM-MNC (**Figure 4C**). These findings indicated that BM-MNC transplantation has a potential to improve cell-cell interaction between circulating WBC and endothelial cells through enhancing expression of Connexin on endothelial cells.

To further investigate the link between BM-MNC transplantation and increased memory function, the level

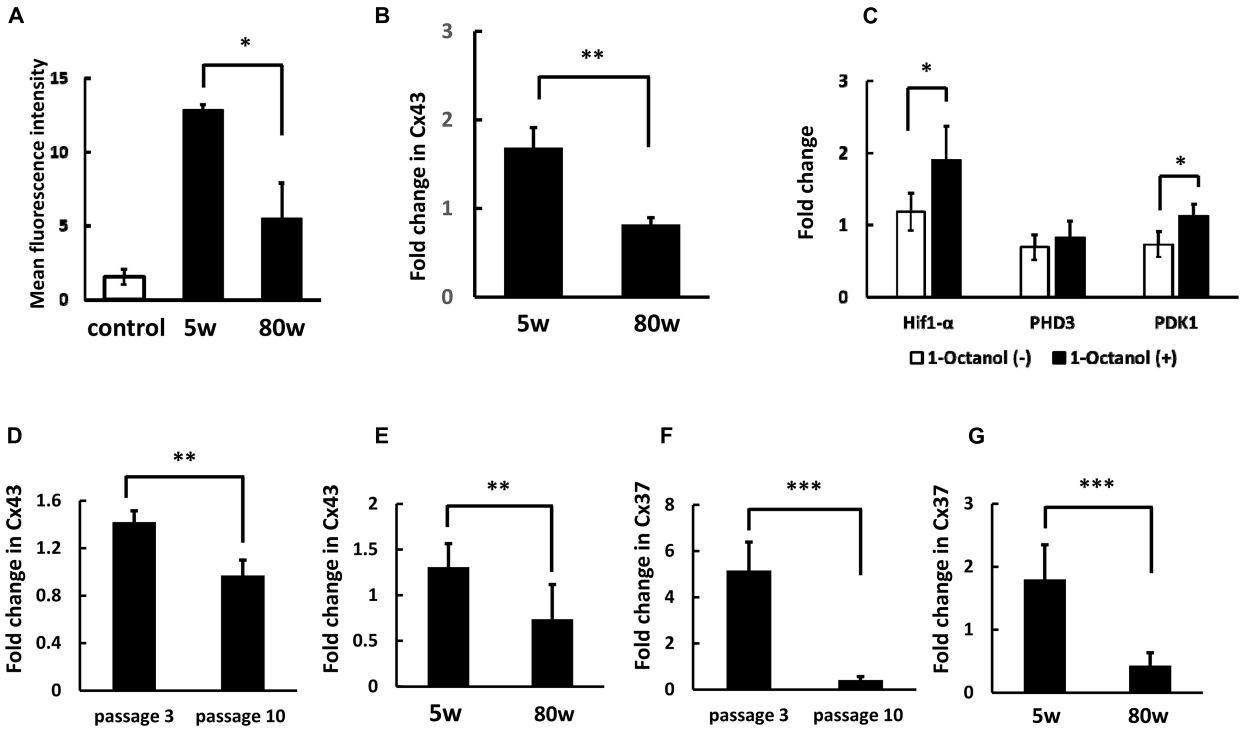

FIGURE 2 | Decreased cell-cell interaction between endothelial cells and WBC of aged mice. **(A)** Transfer of low molecular weight molecule (BCECF) from WBC to HUVEC significantly decreased at WBC of aged mice, compared with young mice. Control indicates background fluorescence level HUVEC without co-incubation of WBC. **(B)** The RNA transcription of Cx43 in WBC was significantly decreased with aging. **(C)** Blockade of cell-cell interaction between WBC and HUVEC via gap junction increased the expression of Hif1-α and PDK1 in WBC. **(D)** The RNA transcription of Cx43 in HUVEC was significantly decreased with passaging. **(E)** The RNA transcription of Cx43 at hippocampus was significantly decreased with aging. **(F)** The RNA transcription of Cx37 in HUVEC was significantly decreased with passaging. **(G)** The RNA transcription of Cx37 at hippocampus was significantly decreased with aging. $^{*}p < 0.05$ versus 5W ($N = 5$ in group **A**), $^{**}p < 0.01$ versus 5W ($N = 6$ in group **B**) by Student's *t*-test. $^{*}p < 0.05$ versus 1-Octanol (–) ($N = 4$ in group **C**). $^{**}p < 0.01$, $^{***}p < 0.001$ versus passage 3 ($N = 4$ in group **D, F**) by Student's *t*-test. ** $p < 0.01$, $^{***}p < 0.001$ versus 5W ($N = 7$ in group **E, G**) by Student's *t*-test.

of neurogenesis at hippocampus was evaluated using anti-Nestin and anti-DCX antibody, and it was found that the level of neurogenesis significantly increases with BM-MNC transplantation in aged mice (**Figures 5A-D**). These findings are consistent with our previous report that BM-MNC transplantation ameliorates memory disorder in aged mice (Takeuchi et al., 2020).

DISCUSSION

In this article, we have demonstrated that RNA transcription of metabolism related genes in circulating WBC, including Glut1, Glut3, MCT4, PHD3, and PDK1, are significantly increased during aging. Our results indicated that this is, at least in part, due to the decrease of cell-cell interactions to endothelial cells. Our findings indicate that the level of RNA transcription of metabolism related genes in circulating WBC can be potentially utilized as markers for decreased cell-cell interaction between circulating WBC and endothelial cells during aging.

Importantly, circulating WBC are known to contribute to the development and maintenance of brain function (Taguchi et al., 2004a, 2008; Filiano et al., 2017; Smith et al., 2018; Pasciuto et al., 2020; Runtsch et al., 2020). Recently, we demonstrated that direct cell-cell interaction between intravenously transplanted BM-MNC and endothelial cell via gap junction activates Hif1-α at endothelial cells followed by improvement of brain function (Kikuchi-Taura et al., 2020). In this article, we demonstrate that cell-cell interaction between circulating WBC and endothelial cell decreases with aging with impaired neurological function. As endothelial, pericyte, and smooth muscle cells are connected via gap junction in cerebral vasculature (Zhao et al., 2018), it would not be so surprising that metabolites and/or signals transfer between circulating cells and cerebral endothelial cells have a significant impact on cerebral circulation and function. Recently, we have demonstrated that intravenously transplanted mesenchymal stem cells remove energy source from endothelial cells via gap junction, and suppress excessed activation of endothelial cells in cerebral ischemia model (Kikuchi-Taura et al., 2021). Although further studies are required to fully elucidate the flow of metabolites and signals via gap junction with brain responses, our findings provide a novel paradigm linking cells in systemic circulation, endothelial cells and cerebral function (**Figure 6**).

Hif1-α is one of the major transcriptional factors that regulates the expression of energy source transporters (Zorzano et al., 2005;

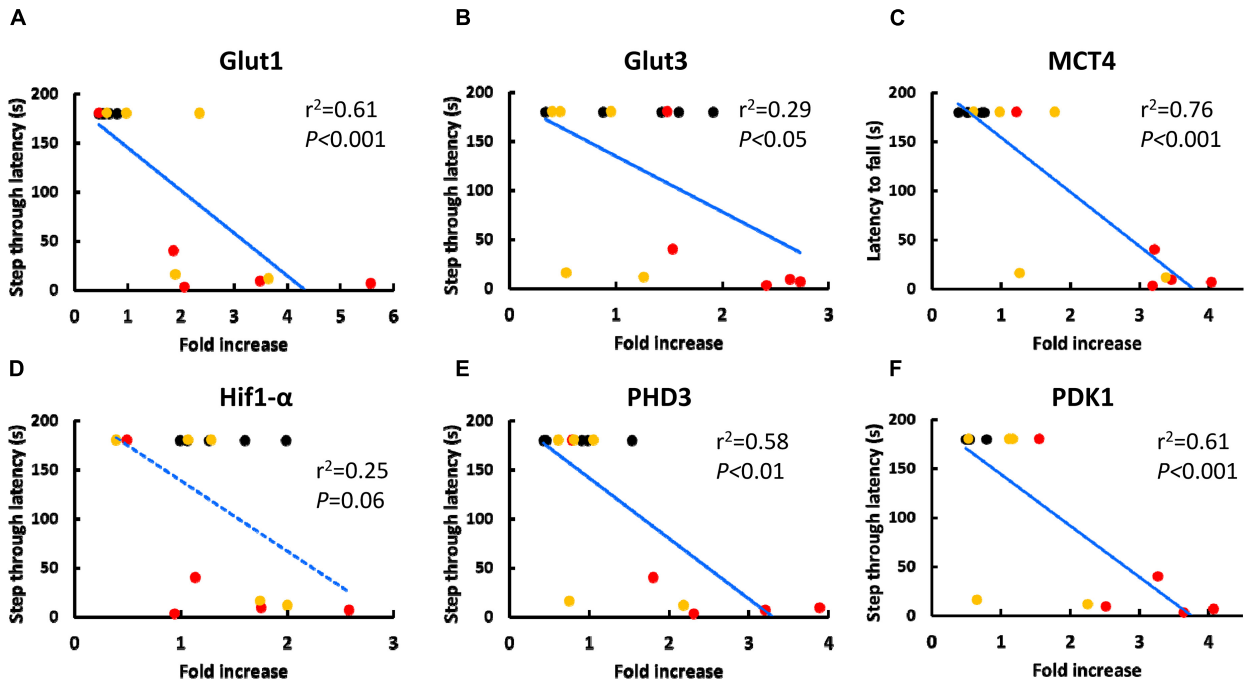

FIGURE 3 | Correlation between the score of passive avoidance test and RNA transcription of metabolism related genes in circulating WBC. **(A-F)** Correlation between increased in RNA transcription of Glut1 **(A)**, Glut3 **(B)**, MCT4 **(C)**, Hif1-α **(D)**, PHD3 **(E)** and PDK1 **(F)** and shorting of step through latency in passive avoidance test. Black, red or yellow dots indicate young mice, aged mice with PBS injection or aged mice with BM-MNC transplantation, respectively. Blue solid or dashed line indicate statistically highly ($p < 0.05$ and $|r| > 0.7$) or moderately ($p < 0.05$ and $|r| > 0.4$) correlating, respectively, by linear regression analysis ($N = 15$).

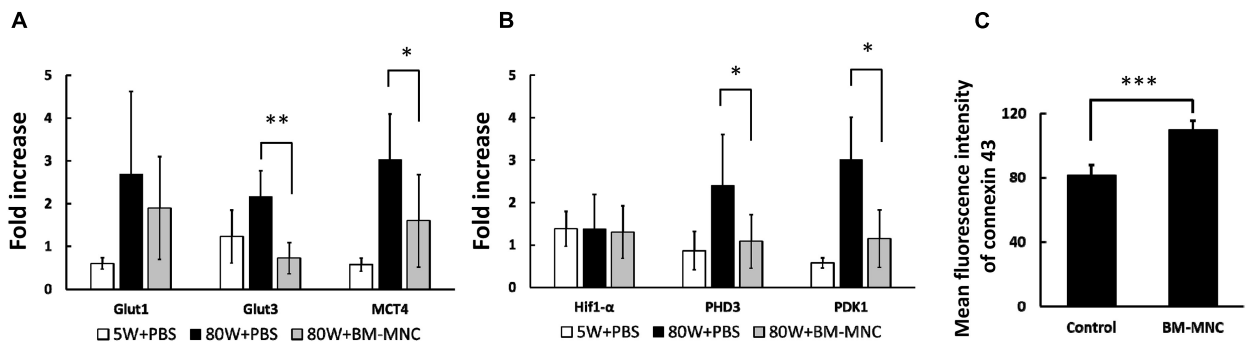

FIGURE 4 | BM-MNC transplantation decreased RNA expression of metabolism related genes in WBC. **(A,B)** BM-MNC transplantation to aged mice decreased the expression of Glut3, MCT4 **(A)**, PHD3 and PDK1 **(B)** in circulating WBC. **(C)** Co-culture with BM-MNC significantly increased the expression of Cx43 in endothelial cells. *$p < 0.05$ and **$p < 0.01$ vs. 80W + PBS by ANOVA followed by *post hoc* analysis using Dunnett's test (control, 80W + PBS; p values between aged mice were displayed in the figure). $N = 5$ in each group **(A,B)**. ***$p < 0.001$ by Student's t-test. $N = 6$ in each group **(C)**.

Masoud and Li, 2015) and PHD3 and PDK1 are known to be down-stream genes of Hif1-α(Ognibene et al., 2017; Takeuchi et al., 2020). As the activity of HIF1α protein can be regulated by its disassembly by HIF-prolyl hydroxylase in an oxidant dependent manner (Hill et al., 1992), our results shown in **Figures 1B**, **4B**, show there was a discrepancy between Hif1-α and PHD3 expression, which would be explained by the change of degradation rate rather than RNA transcription. Our previous results showed movement of small molecules, including glucose, from intravenously transplanted BM-MNC activates Hif1-α in recipient endothelial cells via gap junction mediated cell-cell interaction (Kikuchi-Taura et al., 2020). In this article, we show that movement of small molecules to endothelial cells via gap junction inactivates Hif1-α in donor WBC. These findings show that small molecule movement mediated Hif1-α regulation is the key mechanism for changes of metabolism related gene expression at circulating WBC and endothelial cells.

In this article, we have demonstrated that BM-MNC transplantation into aged mice enhanced neurogenesis in hippocampus and decreased metabolic related genes in WBC.

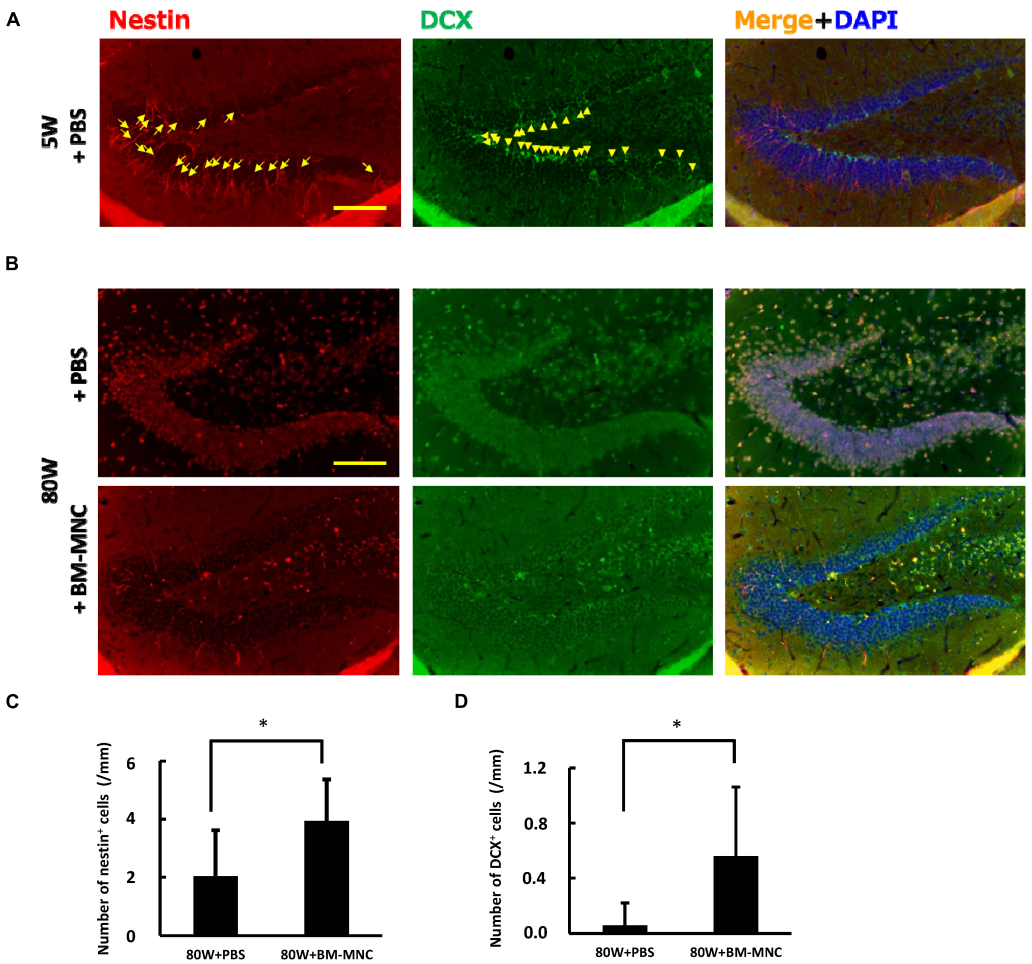

FIGURE 5 | BM-MNC transplantation activates age-related impaired neurogenesis at hippocampus. **(A)** A large number of Nestin-positive (arrow) and/or DCX-positive (allow head) neuronal progenitor cells were observed at dentate gyrus in young mice. **(B)** In contrast, only few Nestin-positive and/or DCX-positive neuronal progenitor cells were observed in aged mice that receive PBS or BM-MNC. **(C,D)** Quantitative analysis revealed that BM-MNC transplantation to aged mice increased the number of Nestin-positive **(C)** and DCX-positive neuronal progenitor cells **(D)**. *N* = 6 and 7 in PBS and BM-MNC transplanted group, respectively **(C,D)**. $*p < 0.05$ by Student's *t*-test. Scale bar: 100 μm **(A,B)**.

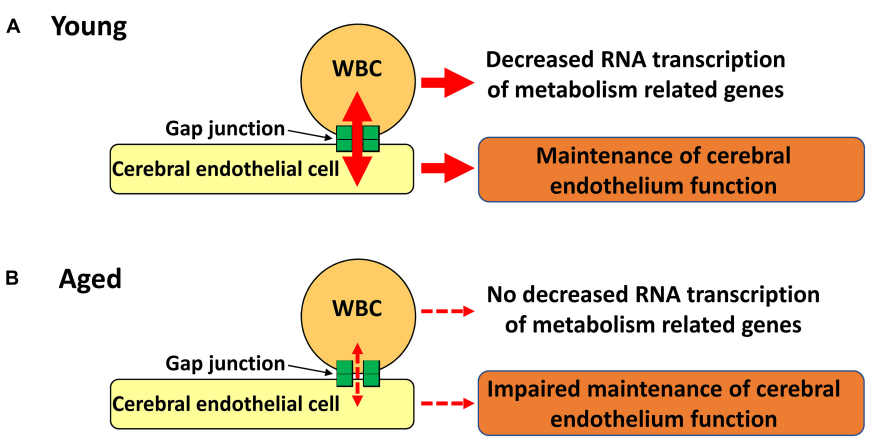

FIGURE 6 | Schematic illustration of our hypothesis. **(A)** Gap junction mediated cell-cell interaction between circulating WBC and endothelial cells decrease RNA transcription of metabolic related genes in WBC with maintenance of endothelial cell function. **(B)** Impaired gap junction mediated cell-cell interaction results in no decreased RNA transcription of metabolic related genes in WBC with impaired maintenance of endothelial cell function.

These findings are consistent with our previous report that BM-MNC transplantation to aged mice increases Glut1 and Na^+/K^+ ATPase expression in the hippocampus and ameliorates memory disorder (Takeuchi et al., 2020). New neurons in the hippocampus are known to have a pivotal role in improving memory (Moreno-Jimenez et al., 2019; Tobin et al., 2019) and our findings will have a significant impact that links cell therapy, improved neurogenesis, and improvement of memory. Once the mechanism of metabolite transfer via gap junction and activation of Hif1-α in brain is understood, this offers the potential to improve and develop novel therapies for dementia in the elderly whose main symptom is the disability of memory.

In vitro analysis revealed that BM-MNC enhanced the expression of Cx43 in endothelial cells. The turnover of Connexin molecules is only a few hours (Musil et al., 2000) that would require a significant amount of energy source. Although the reason of the fast turnover of Connexin and the regulator of Connexin transcription are unclear (Laird, 2006; Nielsen et al., 2012), it would not be surprising that gap junction mediated activation of Hif1-α increases energy source uptake and that upregulates the expression of Connexin. The enhanced expression of Cx43 in endothelial cells by BM-MNC transplantation would explain our result that aged mice that received BM-MNC transplantation showed decreased expression of metabolism related genes in circulating WBC. Our findings also show the potential that quantification of these metabolism related genes in WBC can serve as a tool to evaluate the change of the cell-cell interaction between WBC and endothelial cells caused by treatments that may affect the cell-cell interaction.

Limitations of our study include deciphering the mechanism of cell-cell interaction between WBC and endothelial cells which regulate Hif1-α gene expression in WBC and the differences in gene expression profiles between cell types, such as granulocytes, lymphocytes, and monocytes. Previous findings have shown that the lymphocytes and monocytes express Connexins, although no expression was observed in granulocytes under physiological conditions (Pfenniger et al., 2013). Although further mechanistic studies are required in order to determine the change of gene expression in each cell type, our findings demonstrate that the simple gross analysis of circulating WBC provides a marker for decreased cell-cell interaction between circulating WBC and endothelial cells with aging in mice. This parameter in mice does not require cell separation or cell specific group analysis and therefore is beneficial for screening individuals to assess the cell-cell interaction between circulating WBC and endothelial cells in mice. This information would also provide novel insights into pathology of various cardiovascular diseases. Another limitation is that we have used one strain of mice. To generalize the results obtained in this experiment, further studies using other strains and animal are required, especially for the assessment of human WBC with aging.

In conclusion, our novel findings show the potential that the simple gross analysis of RNA transcription of metabolism related genes in circulating WBC can provide a highly relevant insight into impaired cell-cell interaction between WBC and endothelial cells. This can also serve as a tool to evaluate the change of the cell-cell interaction caused by various treatments, diseases, and aging.

DATA AVAILABILITY STATEMENT

The original contributions presented in the study are included in the article/**Supplementary Material**, further inquiries can be directed to the corresponding author/s.

ETHICS STATEMENT

The animal study was reviewed and approved by Animal Care and Use Committee of Foundation for Biomedical Research and Innovation at Kobe.

AUTHOR CONTRIBUTIONS

YT, YOk, and AK-T performed the experiments and analyzed data. AT and OS prepared this manuscript the final figures and tables. YOg, RA, YK, MM, SG, CC, and JB supervised the project and revised the manuscript critically for important intellectual content. AT planned and designed the study. All authors gave their approval to the manuscripts.

FUNDING

This research was supported by the Japan Agency for Medical Research and Development (AMED) under Grant Number 20bm0404069.

SUPPLEMENTARY MATERIAL

The Supplementary Material for this article can be found online at: https://www.frontiersin.org/articles/10.3389/fnagi.2022.759159/full#supplementary-material

REFERENCES

Belousov, A. B., and Fontes, J. D. (2014). Neuronal gap junction coupling as the primary determinant of the extent of glutamate-mediated excitotoxicity. *J. Neural Transm.* 121, 837–846. doi: 10.1007/s00702-013-1109-7

Cunnane, S. C., Trushina, E., Morland, C., Prigione, A., Casadesus, G., Andrews, Z. B., et al. (2020). Brain energy rescue: an emerging therapeutic concept for neurodegenerative disorders of ageing. *Nat. Rev. Drug Discov.* 19, 609–633. doi: 10.1038/s41573-020-0072-x

Filiano, A. J., Gadani, S. P., and Kipnis, J. (2017). How and why do T cells and their derived cytokines affect the injured and healthy brain? *Nat. Rev. Neurosci.* 18, 375–384. doi: 10.1038/nrn.2017.39

Hill, S. L., Burnett, D., Lovering, A. L., and Stockley, R. A. (1992). Use of an enzyme-linked immunosorbent assay to assess penetration of amoxicillin into

lung secretions. *Antimicrob. Agents Chemother.* 36, 1545–1552. doi: 10.1128/AAC.36.7.1545

Kasahara, Y., Ihara, M., Nakagomi, T., Momota, Y., Stern, D. M., Matsuyama, T., et al. (2013). A highly reproducible model of cerebral ischemia/reperfusion with extended survival in CB-17 mice. *Neurosci. Res.* 76, 163–168. doi: 10.1016/j.neures.2013.04.001

Kikuchi-Taura, A., Okinaka, Y., Saino, O., Takeuchi, Y., Ogawa, Y., Kimura, T., et al. (2021). Gap junction-mediated cell-cell interaction between transplanted mesenchymal stem cells and vascular endothelium in stroke. *Stem Cells* 39, 904–912. doi: 10.1002/stem.3360

Kikuchi-Taura, A., Okinaka, Y., Takeuchi, Y., Ogawa, Y., Maeda, M., Kataoka, Y., et al. (2020). Bone Marrow Mononuclear Cells Activate Angiogenesis via Gap Junction-Mediated Cell-Cell Interaction. *Stroke* 51, 1279–1289. doi: 10.1161/STROKEAHA.119.028072

Kim, J. W., Tchernyshyov, I., Semenza, G. L., and Dang, C. V. (2006). HIF-1-mediated expression of pyruvate dehydrogenase kinase: a metabolic switch required for cellular adaptation to hypoxia. *Cell Metab.* 3, 177–185. doi: 10.1016/j.cmet.2006.02.002

Laird, D. W. (2006). Life cycle of connexins in health and disease. *Biochem. J.* 394, 527–543. doi: 10.1042/BJ20051922

Masoud, G. N., and Li, W. (2015). HIF-1alpha pathway: role, regulation and intervention for cancer therapy. *Acta Pharm. Sin. B.* 5, 378–389. doi: 10.1016/j.apsb.2015.05.007

Moreno-Jimenez, E. P., Flor-Garcia, M., Terreros-Roncal, J., Rabano, A., Cafini, F., Pallas-Bazarra, N., et al. (2019). Adult hippocampal neurogenesis is abundant in neurologically healthy subjects and drops sharply in patients with Alzheimer's disease. *Nat. Med.* 25, 554–560. doi: 10.1038/s41591-019-0375-9

Muirhead, K. A., Wallace, P. K., Schmitt, T. C., Frescatore, R. L., Franco, J. A., and Horan, P. K. (1986). Methodological considerations for implementation of lymphocyte subset analysis in a clinical reference laboratory. *Ann. N Y. Acad. Sci.* 468, 113–127. doi: 10.1111/j.1749-6632.1986.tb42034.x

Musil, L. S., Le, A. C., VanSlyke, J. K., and Roberts, L. M. (2000). Regulation of connexin degradation as a mechanism to increase gap junction assembly and function. *J. Biol. Chem.* 275, 25207–25215. doi: 10.1074/jbc.275.33.25207

Nakano-Doi, A., Nakagomi, T., Fujikawa, M., Nakagomi, N., Kubo, S., Lu, S., et al. (2010). Bone marrow mononuclear cells promote proliferation of endogenous neural stem cells through vascular niches after cerebral infarction. *Stem Cells* 28, 1292–1302. doi: 10.1002/stem.454

Nielsen, M. S., Axelsen, L. N., Sorgen, P. L., Verma, V., Delmar, M., and Holstein-Rathlou, N. H. (2012). Gap junctions. *Compr. Physiol.* 2, 1981–2035. doi: 10.1002/cphy.c110051

Ogawa, Y., Okinaka, Y., Takeuchi, Y., Saino, O., Kikuchi-Taura, A., and Taguchi, A. (2020). Intravenous Bone Marrow Mononuclear Cells Transplantation Improves the Effect of Training in Chronic Stroke Mice. *Front. Med.* 7:535902. doi: 10.3389/fmed.2020.535902

Ognibene, M., Cangelosi, D., Morini, M., Segalerba, D., Bosco, M. C., Sementa, A. R., et al. (2017). Immunohistochemical analysis of PDK1, PHD3 and HIF-1alpha expression defines the hypoxic status of neuroblastoma tumors. *PLoS One* 12:e0187206. doi: 10.1371/journal.pone.0187206

Okamoto, T., Park, E. J., Kawamoto, E., Usuda, H., Wada, K., Taguchi, A., et al. (2021). Endothelial connexin-integrin crosstalk in vascular inflammation. *Biochim. Biophys. Acta Mol. Basis. Dis.* 1867:166168. doi: 10.1016/j.bbadis.2021.166168

Pasciuto, E., Burton, O. T., Roca, C. P., Lagou, V., Rajan, W. D., Theys, T., et al. (2020). Microglia Require CD4 T Cells to Complete the Fetal-to-Adult Transition. *Cell* 182, 625-640.e24. doi: 10.1016/j.cell.2020.06.026

Pfenniger, A., Chanson, M., and Kwak, B. R. (2013). Connexins in atherosclerosis. *Biochim. Biophys. Acta* 1828, 157–166. doi: 10.1016/j.bbamem.2012.05.011

Runtsch, M. C., Ferrara, G., and Angiari, S. (2020). Metabolic determinants of leukocyte pathogenicity in neurological diseases. *J. Neurochem.* 158, 36–58. doi: 10.1111/jnc.15169

Smith, L. K., White, C. W. III, and Villeda, S. A. (2018). The systemic environment: at the interface of aging and adult neurogenesis. *Cell Tissue Res.* 371, 105–113. doi: 10.1007/s00441-017-2715-8

Taguchi, A., Kasahara, Y., Nakagomi, T., Stern, D. M., Fukunaga, M., Ishikawa, M., et al. (2010). A Reproducible and Simple Model of Permanent Cerebral Ischemia in CB-17 and SCID Mice. *J. Exp. Stroke Transl. Med.* 3, 28–33.

Taguchi, A., Matsuyama, T., Moriwaki, H., Hayashi, T., Hayashida, K., Nagatsuka, K., et al. (2004a). Circulating CD34-positive cells provide an index of cerebrovascular function. *Circulation* 109, 2972–2975. doi: 10.1161/01.CIR.0000133311.25587.DE

Taguchi, A., Soma, T., Tanaka, H., Kanda, T., Nishimura, H., Yoshikawa, H., et al. (2004b). Administration of CD34+ cells after stroke enhances neurogenesis via angiogenesis in a mouse model. *J. Clin. Invest.* 114, 330–338. doi: 10.1172/JCI20622

Taguchi, A., Matsuyama, T., Nakagomi, T., Shimizu, Y., Fukunaga, R., Tatsumi, Y., et al. (2008). Circulating CD34-positive cells provide a marker of vascular risk associated with cognitive impairment. *J. Cereb. Blood Flow Metab.* 28, 445–449. doi: 10.1038/sj.jcbfm.9600541

Takeuchi, Y., Okinaka, Y., Ogawa, Y., Kikuchi-Taura, A., Kataoka, Y., Gul, S., et al. (2020). Intravenous Bone Marrow Mononuclear Cells Transplantation in Aged Mice Increases Transcription of Glucose Transporter 1 and Na(+)/K(+)-ATPase at Hippocampus Followed by Restored Neurological Functions. *Front. Aging Neurosci.* 12:170. doi: 10.3389/fnagi.2020.00170

Takubo, K., Nagamatsu, G., Kobayashi, C. I., Nakamura-Ishizu, A., Kobayashi, H., Ikeda, E., et al. (2013). Regulation of glycolysis by Pdk functions as a metabolic checkpoint for cell cycle quiescence in hematopoietic stem cells. *Cell Stem Cell* 12, 49–61. doi: 10.1016/j.stem.2012.10.011

Tobin, M. K., Musaraca, K., Disouky, A., Shetti, A., Bheri, A., Honer, W. G., et al. (2019). Human Hippocampal Neurogenesis Persists in Aged Adults and Alzheimer's Disease Patients. *Cell Stem Cell* 24, 974–982.e973. doi: 10.1016/j.stem.2019.05.003

Yuan, D., Sun, G., Zhang, R., Luo, C., Ge, M., Luo, G., et al. (2015). Connexin 43 expressed in endothelial cells modulates monocyteendothelial adhesion by regulating cell adhesion proteins. *Mol. Med. Rep.* 12, 7146–7152. doi: 10.3892/mmr.2015.4273

Zhao, Y., Xin, Y., He, Z., and Hu, W. (2018). Function of Connexins in the Interaction between Glial and Vascular Cells in the Central Nervous System and Related Neurological Diseases. *Neural. Plast.* 2018:6323901. doi: 10.1155/2018/6323901

Zorzano, A., Palacin, M., and Guma, A. (2005). Mechanisms regulating GLUT4 glucose transporter expression and glucose transport in skeletal muscle. *Acta Physiol. Scand.* 183, 43–58. doi: 10.1111/j.1365-201X.2004.01380.x

Conflict of Interest: The authors declare that the research was conducted in the absence of any commercial or financial relationships that could be construed as a potential conflict of interest.

Publisher's Note: All claims expressed in this article are solely those of the authors and do not necessarily represent those of their affiliated organizations, or those of the publisher, the editors and the reviewers. Any product that may be evaluated in this article, or claim that may be made by its manufacturer, is not guaranteed or endorsed by the publisher.

frontiers in Aging Neuroscience

ORIGINAL RESEARCH
published: 09 March 2022
doi: 10.3389/fnagi.2022.788296

Increased Susceptibility to Cerebral Microhemorrhages Is Associated With Imaging Signs of Microvascular Degeneration in the Retina in an Insulin-Like Growth Factor 1 Deficient Mouse Model of Accelerated Aging

*Lauren R. Miller[1], Stefano Tarantini[2,3,4], Ádám Nyúl-Tóth[2,4,5], Morgan P. Johnston[1], Teryn Martin[1], Elizabeth C. Bullen[1], Marisa A. Bickel[1], William E. Sonntag[2], Andriy Yabluchanskiy[2], Anna Csiszar[2,4], Zoltan I. Ungvari[2,4], Michael H. Elliott[6,7] and Shannon M. Conley[1]**

[1] Department of Cell Biology, University of Oklahoma Health Sciences Center, Oklahoma City, OK, United States, [2] Vascular Cognitive Impairment and Neurodegeneration Program, Oklahoma Center for Geroscience and Healthy Brain Aging, Department of Biochemistry and Molecular Biology, University of Oklahoma Health Sciences Center, Oklahoma City, OK, United States, [3] Stephenson Cancer Center, University of Oklahoma, Oklahoma City, OK, United States, [4] International Training Program in Geroscience, Doctoral School of Basic and Translational Medicine/Department of Public Health, Semmelweis University, Budapest, Hungary, [5] International Training Program in Geroscience, Institute of Biophysics, Biological Research Centre, Eötvös Loránd Research Network, Szeged, Hungary, [6] Department of Ophthalmology, Dean McGee Eye Institute, University of Oklahoma Health Sciences Center, Oklahoma City, OK, United States, [7] Department of Physiology, University of Oklahoma Health Sciences Center, Oklahoma City, OK, United States

Age-related cerebrovascular defects contribute to vascular cognitive impairment and dementia (VCID) as well as other forms of dementia. There has been great interest in developing biomarkers and other tools for studying cerebrovascular disease using more easily accessible tissues outside the brain such as the retina. Decreased circulating insulin-like growth factor 1 (IGF-1) levels in aging are thought to contribute to the development of cerebrovascular impairment, a hypothesis that has been supported by the use of IGF-1 deficient animal models. Here we evaluate vascular and other retinal phenotypes in animals with circulating IGF-1 deficiency and ask whether the retina mimics common age-related vascular changes in the brain such as the development of microhemorrhages. Using a hypertension-induced model, we confirm that IGF-1 deficient mice exhibited worsened microhemorrhages than controls. The retinas of IGF-1 deficient animals do not exhibit microhemorrhages but do exhibit signs of vascular damage and retinal stress such as patterns of vascular constriction and Müller cell activation. These signs of retinal stress are not accompanied by retinal degeneration or impaired neuronal function. These data suggest that the role of IGF-1 in the retina is complex, and while IGF-1 deficiency leads to vascular defects in both the brain and the retina, not all brain pathologies are evident in the retina.

Keywords: insulin-like growth factor 1, retina, intracerebral hemorrhage, retinal vasculature, microhemorrhage, aging, cerebrovascular aging, vascular cognitive impairment

OPEN ACCESS

Edited by:
Daniel Ortuño-Sahagún, University of Guadalajara, Mexico

Reviewed by:
Krisztina Valter, Australian National University, Australia
Neetu Tyagi, University of Louisville, United States
Tamas Atlasz, University of Pécs, Hungary

****Correspondence:***
Shannon M. Conley
shannon-conley@ouhsc.edu

Specialty section:
This article was submitted to Neuroinflammation and Neuropathy, a section of the journal Frontiers in Aging Neuroscience

Received: *02 October 2021*
Accepted: *31 January 2022*
Published: *09 March 2022*

Citation:
Miller LR, Tarantini S, Nyúl-Tóth Á, Johnston MP, Martin T, Bullen EC, Bickel MA, Sonntag WE, Yabluchanskiy A, Csiszar A, Ungvari ZI, Elliott MH and Conley SM (2022) Increased Susceptibility to Cerebral Microhemorrhages Is Associated With Imaging Signs of Microvascular Degeneration in the Retina in an Insulin-Like Growth Factor 1 Deficient Mouse Model of Accelerated Aging. Front. Aging Neurosci. 14:788296. doi: 10.3389/fnagi.2022.788296

INTRODUCTION

Aging elicits multifaceted functional and structural impairment in the cerebral microcirculation, which has a critical role in the pathogenesis of vascular cognitive impairment and dementia (VCID) (Hajdu et al., 1990; Mayhan et al., 1990; Zlokovic, 2011; Jessen et al., 2015; Cooper et al., 2016; Daulatzai, 2016; Ighodaro et al., 2016). Within the spectrum of age-related microvascular pathologies [including microvascular rarefaction (Tarantini et al., 2016; Toth et al., 2017; Norling et al., 2020; Nyul-Toth et al., 2021), disruption of the blood–brain barrier (BBB) (Verheggen et al., 2020; Nyul-Toth et al., 2021), impaired regulation of cerebral blood flow (CBF) (Tarantini et al., 2017b, 2021), amyloid pathologies], recent studies highlighted the pathogenic role of cerebral microhemorrhages (CMHs) in the genesis of VCID (Poels et al., 2011, 2012; Ungvari et al., 2017). CMHs are small (<5 mm) bleeds that develop due to the rupture of cerebral arterioles and capillaries. Aging significantly increases microvascular fragility (in part due to microvascular degeneration), which exacerbates the genesis of CMHs, and CMH burden predicts cognitive decline in older adults (Kato et al., 2002; Vernooij et al., 2008; Ungvari et al., 2017).

Despite its pathophysiological importance, the human cerebral microcirculation is not readily accessible for imaging and functional assessment. The desire to identify novel, accessible biomarkers and tools for interrogating the cerebromicrovascular changes that contribute to VCID has led to much work utilizing the retinal vasculature as a proxy for the brain vasculature (Lipecz et al., 2019; McGrory et al., 2019; Czako et al., 2020). Cerebral and retinal vasculature share developmental and anatomical origins. The retina is considered part of the central nervous system, developing from the diencephalon, and exhibits similar anatomical features and physiological properties, including microvascular architecture, energy requirements, regulation of blood flow, and vascular barrier function (London et al., 2013; Tata et al., 2015; Lipecz et al., 2019). There is increasing evidence that age-related pathophysiological processes that affect the central nervous system and the cerebral microcirculation have a direct profound impact on the retina and retinal microcirculation as well (Stanton et al., 1995; Liew et al., 2008; Che Azemin et al., 2013; Csipo et al., 2019; Lipecz et al., 2019). Yet it is not clear whether the retina exhibits all of the tissue level pathologies that are associated with cerebrovascular aging. Importantly, the association between increases in microvascular fragility in the brain and the retina has not yet been investigated.

The mechanisms by which aging exacerbates functional and structural impairment in the cerebral microcirculation and promotes the genesis of CMHs include an age-related decline in circulating insulin-like growth factor 1 (IGF-1) (Sonntag et al., 2013; Toth et al., 2014, 2015a; Ashpole et al., 2017; Tarantini et al., 2017c, 2021; Fulop et al., 2018). IGF-1 is a vasoprotective growth factor largely produced by the liver, whose circulating levels significantly decrease with increasing age (Ungvari and Csiszar, 2012; Sonntag et al., 2013; Tarantini et al., 2017c). Animal models of circulating IGF-1 deficiency serve as models of accelerated aging, mimicking many age-related cerebrovascular pathologies. These include impaired myogenic autoregulation, impaired neurovascular coupling, microvascular rarefaction, decreased cerebral blood flow, and consequential impairment of higher brain functions (Bailey-Downs et al., 2012; Sonntag et al., 2013; Toth et al., 2014, 2015a; Fulop et al., 2018). Decreased circulating IGF-1 levels in rodent models are also associated with increased BBB permeability, pathological microvascular remodeling, increased microvascular fragility, and increased susceptibility to the hypertension-induced development of CMHs (Bake et al., 2014, 2016; Tarantini et al., 2017c). Yet, there are no studies extant investigating the role of circulating IGF-1 deficiency in microvascular pathologies in the retina.

The present study was designed to test the hypothesis that adult-onset circulating IGF-1 deficiency promotes the development of a pro-fragility microvascular phenotype both in the brain and the retina. To test our hypothesis, we used an established murine model of isolated endocrine IGF-1 deficiency: knockdown of IGF-1 specifically in the liver using Cre-lox technology ($Igf1^{f/f}$ + TBG-Cre-AAV8) (Tarantini et al., 2017c). To test microvascular fragility, we induced chronic hypertension in IGF-1 deficient mice and respective controls [by treatment with angiotensin II (Ang II) and L-NAME, a NO synthase inhibitor (Liu et al., 1998; Ho et al., 2008; Bailey-Downs et al., 2012; Toth et al., 2013, 2015a; Tarantini et al., 2017c)] and assessed occurrence of microhemorrhages in both the brain and retina. We also assessed the effects of circulating IGF-1 deficiency on the structural integrity of the retina and the retinal vessels.

MATERIALS AND METHODS

Experimental Animals

All animal work was reviewed and approved by the local Institutional Animal Care and Use Committee (IACUC; University of Oklahoma Health Sciences Center, Oklahoma City, OK, United States). Mice on the C57BL/6 background that were homozygous for an *Igf1* floxed allele ($Igf1^{f/f}$) were purchased from Jackson Laboratories (line 016831). These mice have exon 4 of the *Igf1* gene flanked by loxP sites, allowing for the excision of this entire exon via Cre recombinase. Transcripts of the altered Igf1 gene yield a protein that fails to bind the IGF-1 receptor. IGF-1 deficiency was induced in $Igf1^{f/f}$ mice by adeno-associated virus (AAV8)-mediated expression of Cre recombinase in the liver at 4 months of age, as previously reported (Bailey-Downs et al., 2012; Toth et al., 2014). The AAV8 vector was acquired from the University of Pennsylvania Viral Vector Core (Penn Vector Core, Philadelphia, PA, United States[1]). The thyroxine-binding globulin (TBG) promoter was used to restrict the expression of the AAV8 vector to hepatocytes. At 4 months of age, $Igf1^{f/f}$ mice were randomly assigned to two groups and were administered approximately 1.3×10^{10} viral particles of AAV8-TBG-Cre or AAV8-TBG-eGFP via retro-orbital injection, as described (Tarantini et al., 2017c). The majority of circulating IGF-1 is produced in the liver. Since IGF-1 is critical for the development of many organ systems during adolescence, including the cardiovascular system, this model was used to

[1]http://www.med.upenn.edu/gtp/vectorcore

specifically study the effects of adult-onset circulating IGF-1 deficiency (Toth et al., 2014). Animals were used for experiments at either approximately 1 year of age (12–14 months) or 2 years of age (24–27 months). Both male and female mice were used, however studies were not powered to evaluate the role of sex as a biological variable. Animals were housed in the Rodent Barrier Facility at OUHSC under specific pathogen-free barrier conditions, on a 12-h light/12-h dark cycle, with access to standard rodent chow (Purina Mills, Richmond, IN, United States) and water *ad libitum*. In-cage light levels during the light cycle were ∼30 lux.

Induction of Hypertension

To assess microvascular fragility, hypertension was induced in study animals at 12–14 months of age. AAV8-TBG-Cre and AAV8-TBG-eGFP mice were randomly assigned to either the "hypertensive" (HT) or "normotensive" (NT) groups. Hypertension was induced by a combination treatment with ω-nitro-$_L$-arginine-methyl ether [L-NAME (N5751, Millipore Sigma, St. Louis, MO, United States), 100 mg kg^{-1} day^{-1}, in drinking water] and administration of angiotensin II [Ang II; s.c. via osmotic mini-pumps (Alzet Model 2006, 0.15 μL h^{-1}, 42 days; Durect Co, Cupertino, CA, United States)]. Pumps were filled with either saline or a solution of angiotensin II (Sigma Chemical Co., St. Louis, MO, United States) that delivered 1 μg min^{-1} kg^{-1} of angiotensin II for up to 28 days. Mini-pumps were surgically placed in isoflurane anesthetized mice in the subcutaneous space on the back of the animal. This was accomplished by making a small incision in the intrascapular region, blunt dissection of the subcutaneous space, and closure of the incision with surgical sutures using aseptic techniques. Animals were given an s.c. injection of sustained release Buprenorphine (ZooPharm, Fort Collins, CO, United States) to manage post-operative pain. Animal blood pressure was measured via the tail-cuff method using the CODA Non-Invasive Blood Pressure System (Kent Scientific Co., Torrington, CT, United States) as described (Toth et al., 2015b). Mice were placed in a restrainer on an animal warmer for the duration of the measurement to encourage tail vein dilation for accurate blood pressure measurements.

Standardized Neurological Examination

Mice underwent daily neurological examination to predict the presence of clinically manifest hemorrhages. The scoring system evaluates spontaneous activity, symmetry in limb movement, forelimb outstretching, climbing ability, body proprioception, and response to vibrissae touch. Scores were summed on an 18-point scale as a measure of neurological function. A decline in this neurological score correlates with cerebral hemorrhage development (Toth et al., 2015b). Mice were euthanized at a neurological score of 15 or lower, or when they reached day 28 post-hypertension surgery, whichever came first. Mice were euthanized via transcardial perfusion with ice-cold 1× phosphate buffered saline (1× PBS, 137 mM NaCl, 2.7 mM KCl 10 mM Na_2HPO_4, 1.8 mM KH_2PO_4, pH 7.4, pH 7.2) for 10 min under ketamine/xylazine (84/14 mg kg^{-1}) anesthesia.

Fundoscopy and Fluorescein Angiography

To assess vascular damage in the retina, fundus imaging and fluorescein angiography were performed using the Micron III system (Phoenix Research Laboratories, Pleasanton, CA, United States) as described (Koirala et al., 2013; Chakraborty et al., 2020). Mice were anesthetized with ketamine/xylazine (84, 7 mg kg^{-1})) and eyes were dilated with 1% cyclopentolate eye drops (Family Medicine Pharmacy, University of Oklahoma Health Sciences Center, Oklahoma City, OK, United States). One drop of 2.5% Gonak (McKesson Medical Surgical, Richmond, VA, United States) was applied to each eye. Bright field images were collected, and then animals were injected intraperitoneally with 100 μL of 1% (w/v) fluorescein sodium (Sigma-Aldrich, St. Louis, MO, United States) for angiography. Angiogram images were captured using a GFP filter. All fundus images were captured using StreamPix software (Phoenix Research Labs, Bend, OR, United States). We observed repeated patterns of constriction in some retinal vessels, to semiquantitatively assess this phenotype, the number of affected vessels in each image was counted by an observer blinded to age and genotype.

Electroretinography

Electroretinography (ERG) measures the electrical responses of various cell types in the retina, including the photoreceptors, inner retinal cells (bipolar and amacrine cells), and the ganglion cells, which are sensitive to hypoxia and structural damage to the neural retina. To assess functional consequences of accelerated microvascular aging associated with IGF-1 deficiency, full-field ERG measurements were performed in the experimental mice as described by Chakraborty et al. (2020). Following dark adaptation, mice were anesthetized with ketamine/xylazine and eyes were dilated using 1% cyclopentolate eye drops. ERGs were recorded with the Diagnosys Espion E3 ERG system (Diagnosys LLC, Lowell, MA, United States). Scotopic ERGs were recorded with a strobe flash stimulus of 157 cd-s m^{-2} presented to the dark-adapted mouse followed by light-adaptation for 5 min at 29.03 cd m^{-2}. Photopic responses were recorded from 25 averaged flashes at 77 cd-s m^{-2} for white light. Flicker ERGs were recorded for 30 s in response to a 10 Hz flicker stimulus.

Neurovascular Coupling

Neurovascular coupling responses were tested in a subset of 2 year-old and young control mice (∼3–6 months of age) according to our previously reported protocol (Tarantini et al., 2017a, 2018; Yabluchanskiy et al., 2020). Mice were anesthetized with isoflurane (4% for induction and 1–2% for maintenance during the surgery and measurements). A femoral artery cannula was placed in each animal to monitor and maintain blood pressure in the physiological range during the procedure (between 90 and 110 mmHg). Mice were then endotracheally intubated and ventilated (MousVent G500; Kent Scientific Co., Torrington, CT, United States). Rectal temperature was maintained at 37°C using a thermostatic heating pad (Kent Scientific Co., Torrington, CT, United States). Mice were placed in a stereotaxic frame (Leica Microsystems, Buffalo Grove, IL,

United States) and a thinned-skull cranial window was prepared. To prepare the thinned-skull window, the scalp and periosteum were resected and the skull was thinned with a sterile scalpel blade. Nitrocellulose lacquer was then applied to the surface of the skull to allow for appropriate optics and light spreading. A laser speckle imager (Perimed, Järfälla, Sweden) was positioned 10 cm above the window. The change in CBF in response to whisker stimulation was measured by stimulating the whiskers on one side of the mouse for 30 s intervals and measuring the change in CBF of the contralateral whisker barrel cortex. The change in CBF is expressed as the percent increase from the baseline.

Enzyme-Linked Immunosorbent Assay

Blood was collected via puncture of the submandibular vein with a sterile lancet or 25G needle. The whole blood sample was allowed to coagulate for 20 min at room temperature and was then centrifuged at 2,500 × *g* for 20 min at 4°C. Serum was collected and stored at −80°C until use. IGF-1 concentration in the serum samples was measured by enzyme-linked immunosorbent assay (ELISA) (R&D Systems, Minneapolis, MN, United States) as previously reported (Toth et al., 2014). An IGF-1 control sample was included on each plate. Serum IGF-1 levels were reported in ng mL^{-1}.

Immunofluorescence

Whole eyes were collected from transcardially perfused mice and fixed in EM grade 4% paraformaldehyde (PFA) for 4 h at 4°C. Eyes were paraffin-embedded and sectioned at 6 μm thickness onto glass slides. After deparaffinization, slides underwent antigen retrieval in a solution of 10 mM citrate buffer (pH 6.0) for 20 min in a vegetable steamer and were then allowed to cool for 20 min at room temperature. Slides were then pre-treated with 1% sodium borohydride for 90 s, followed by three water washes and three 1× PBS washes. Blocking was performed in a blocking solution containing 5% BSA, 1% fish gelatin, 2% donkey serum, and 0.5% Triton in 1× PBS for 1 h at room temperature, followed by incubation in antibody overnight at 4°C in a humidity chamber (antibodies are listed in **Table 1**). The slides were then washed four times in 1× PBS for 10 min, incubated in secondary antibodies at a concentration of 1:500 for 1–2 h at room temperature, washed four additional times in 1× PBS, and then mounted with Prolong Diamond with 4',6-diamidino-2-phenylindole (DAPI) (Thermo Fisher Scientific, Waltham, MA, United States) and coverslipped. An Olympus BX62 microscope with a 20× air, 40× air, or 100× oil objective (Olympus Life Science, Waltham, MA, United States) was used for fluorescent imaging. To semiquantitatively assess the presence of GFAP labeling of gliosis, each image was scored by an observer blinded to age and genotype. Scores were assigned as follows: 0: no gliosis (GFAP labeling in endfeet only), 1: mild gliosis (very little sign of GFAP penetrating into other retinal layers), 2: moderate/intermittent gliosis, 3: elevated gliosis, 4: very high levels of gliosis.

Histological Analysis of Bleeds

Brains and eyes were collected from transcardially perfused mice (described above) and fixed in 4% paraformaldehyde for 48 or 4 h, respectively, at 4°C. Brains and eyes were stored in PBS at 4°C until they were embedded in paraffin. Serial coronal brain sections were cut at 8 μm thickness, yielding approximately 1,000 sections per brain. Every twelfth slide from each brain was stained with 3,3-diaminobenzidine (DAB) (Vector Laboratories/Maravai LifeSciences, San Diego, CA, United States) to reveal hemorrhages, and counterstained with Gill's No. 1 hematoxylin (Millipore Sigma, St. Louis, MO, United States) to show brain structure. DAB reacts with endogenous peroxidases in red blood cells generating a dark brown product that allows for easy and precise detection of extravasated blood in the brain parenchyma. All stained sections were imaged at 10× (for brains) or 20× (for retinas) using the VS120-L100-W Virtual Slide Microscope (Olympus Life Science, Waltham, MA, United States). Images were then analyzed by an observer blinded to genotype, group, and age. ImageJ 1.52p (NIH, Bethesda, MD, United States) software was used to

TABLE 1 | Antibodies.

Antigen	Species	Use	Source	References
4-HNE	Rbt-PC	IF	Alpha Diagnostics, cat# HNE11-S	Liou and Storz, 2015
Endomucin	Rat-MC	IF	Millipore Sigma, cat# MAB2624, clone V.5C7 RRID:AB_10807039	
GFAP	Ms-MC	IF	Millipore Sigma, cat# G3893-100UL	Wang et al., 2006
α-SMA	Ms-MC	IF	Millipore Sigma, cat# 113200 clone 1A4, RRID:AB_477010	Jackson-Weaver et al., 2020
Desmin	Ms-MC	IF	ThermoFisher, Cat# MS-376-S1 RRID:AB_61166	Boscolo Sesillo et al., 2019
Igf1R	Rbt-MC	IF	Abcam, cat# ab182408	Liu et al., 2018
Cone Arrestin (Arr4)	Rbt-PC	IF	Cheryl Craft, University of Southern California LUMIj-mCAR, RRID:AB_2314753	Brown et al., 2010; Chakraborty et al., 2010
Calbindin	Ckn-PC	IF	Synaptic Systems, Inc. Cat#214 006, RRID:AB_2619903	Rojek et al., 2019
SV2	Ms-MC	IF	Developmental Studies Hybridoma Bank,	Pang et al., 2018
Rhodopsin	Ms-MC	IF	Clone 1D4 generously shared by Muayyad Al-Ubaidi at the University of Houston. Can be purchased from Santa Cruz Biotechnology, cat# sc-57432, RRID:AB_785511	Kakakhel et al., 2020
VGLUT1	GP-PC	IF	Millipore Sigma, AB5905, AB_2301751	
M-opsin	Rbt-PC	IF	Novus Biologicals Cat# 110-74730 (opsin1),	

Rbt-PC, rabbit polyclonal; Rat-MC, rat monoclonal; Ms-MC, mouse monoclonal; Ckn-PC, chicken polyclonal; GP-PC, guinea pig polyclonal.

quantify and measure the size of hemorrhages. Images were color deconvolved and thresholded uniformly; then, the pixel intensity integrated density was measured on the selected bleed area using a protocol and ImageJ macro described in (Nyúl-Tóth et al., 2020). Identified hemorrhages were then mapped to specific brain regions by comparing images to the *Allen Mouse Brain Atlas*.[2] A similar workflow was followed for identifying microbleeds in eyes. Eyes were serially sectioned at 6 μm thickness, yielding approximately 200 sections per eye. Every sixth section was stained with hematoxylin and DAB. A brain section adjacent to one with a bleed was included in each batch of retinal staining to serve as a positive control for the DAB. However, no microbleeds were identified in the eye sections so bleeds could not be counted, measured, or mapped to regions of the eye.

Morphometry

Central retinal sections (through the optic nerve) were stained with hematoxylin and eosin (H&E), and then imaged at 20× on a VS120-L100-W Virtual Slide Microscope. Spidergrams were generated by measuring outer nuclear layer (ONL), outer plexiform layer (OPL), and inner nuclear layer (INL) thickness at defined distances from the optic nerve head. Values were captured from three sections per eye, by an observer blinded to age and genotype and at least three eyes per genotype/age/group were measured. Thickness measurements were made using Adobe Photoshop CS6.

Statistical Analysis

Statistical analyses were performed using Graphpad Prism version 9.2.0. Differences between groups were analyzed by two-tailed unpaired *t*-tests (to compare two groups), one-way ANOVA with Tukey's *post hoc* comparison (to compare more than two groups), or two-way ANOVA with Tukey's *post hoc* comparison (in cases where there were two different variables). Differences between survival curves were assessed by Log-rank (Mantel–Cox) test. When data were not normally distributed, the Mann–Whitney test was used.

RESULTS

Insulin-Like Growth Factor 1 Deficiency Exacerbates the Development of Hypertension-Induced Cerebral Microhemorrhages

To study the effects of IGF-1 deficiency on the development of vascular pathologies in the central nervous system, we used a mouse line in which exon 4 of the IGF-1 gene is floxed ($Igf1^{f/f}$). We knocked down circulating IGF-1 levels in young adult mice (4 months of age) by injection of an AAV carrying a liver-specific promoter driving Cre recombinase expression [TBG-Cre-AAV8, here referred to as IGF-1 KD ("knockdown")]. Control animals (also $Igf1^{f/f}$) received AAV8-TBG-eGFP at 4 months of age (here referred to as control). The liver is the primary source of paracrine IGF-1 (Ungvari and Csiszar, 2012; Blum et al., 2018), and knocking down IGF-1 production in hepatocytes causes a significant decrease in serum levels of IGF-1. Using ELISAs on serum harvested at 1 year of age, we confirmed that this AAV-mediated approach results in almost complete elimination of circulating IGF-1 levels in our knockdown animals (**Figure 1A**). We elicited CMHs at 1 year of age by inducing hypertension using a well-established paradigm (Toth et al., 2015b; Tarantini et al., 2017c) wherein Ang II is delivered via osmotic mini-pump and L-NAME is delivered in drinking water (**Figure 1B**). Normotensive control mice did not receive Ang II or L-NAME. To track the onset of neurological signs of CMHs, mice underwent daily neurological scoring which involved assessment of six different criteria on an 18-point scale. As expected, hypertensive IGF-1 KD mice experienced an earlier onset of neurological signs of CMHs (defined as a drop in neurological score from 18 to 17 or below) compared to control animals (**Figures 1C,D**). No normotensive animals (either IGF-1 KD or control) exhibited a change in neurological score. Tissues were collected when mice exhibited a neurological score of 15 or lower (or at 28 days after insertion of the mini-pumps). Consistent with their earlier onset of neurological signs of CMHs, hypertensive IGF-1 KD mice were removed from the study and euthanized at a significantly earlier time than control mice due to severe neurological decline (**Figure 1E**). CMHs were identified histologically by DAB staining (reddish brown color, **Figure 1G**) which reacts with endogenous peroxidases in red blood cells. We calculated the mean number of bleeds per brain section and found that hypertensive IGF-1 KD exhibited significantly more bleeds per section than hypertensive control animals (**Figures 1F,G**).

To further characterize CMHs, we measured the area of all identified bleeds. The cumulative size distribution of all detected bleeds is plotted in **Figure 2B**. IGF-1 deficient hypertensive mice had a greater number of bleeds of all sizes than hypertensive control mice but the overall size of bleeds in IGF-1 KD was significantly smaller than in controls (**Figures 2A,B**). Each identified bleed was mapped to its brain region using the online *Allen Mouse Brain Atlas* (last accessed 10/01/2021).[3] Each bleed was given a broad identifying region (shown in **Figure 2C**) as well as a specific brain region. In the hypertensive IGF-1 knockdown animals, the largest fraction of CMHs occurred in the cortex (42%), although CMHs were detected throughout the brain (examples shown in **Figures 2D–J**, black arrows indicate especially small or hard to see bleeds). In control animals the largest fraction of CMHs occurred in the brainstem and white matter (33 and 25%, respectively), though very few bleeds were detected in control brains overall. Some of the CMHs that occurred can be traced back to an adjacent arteriole or capillary in the brain (**Figures 2D–J**, red arrowheads indicate vessels). These findings demonstrate that hypertensive IGF-1 knockdown animals have an earlier onset and increased number of CMHs in the brain compared to hypertensive control animals, confirming that IGF-1 deficiency exacerbates microvascular fragility in the mouse brain, mimicking the aging phenotype.

[2]https://mouse.brain-map.org/static/atlas

[3]https://mouse.brain-map.org/

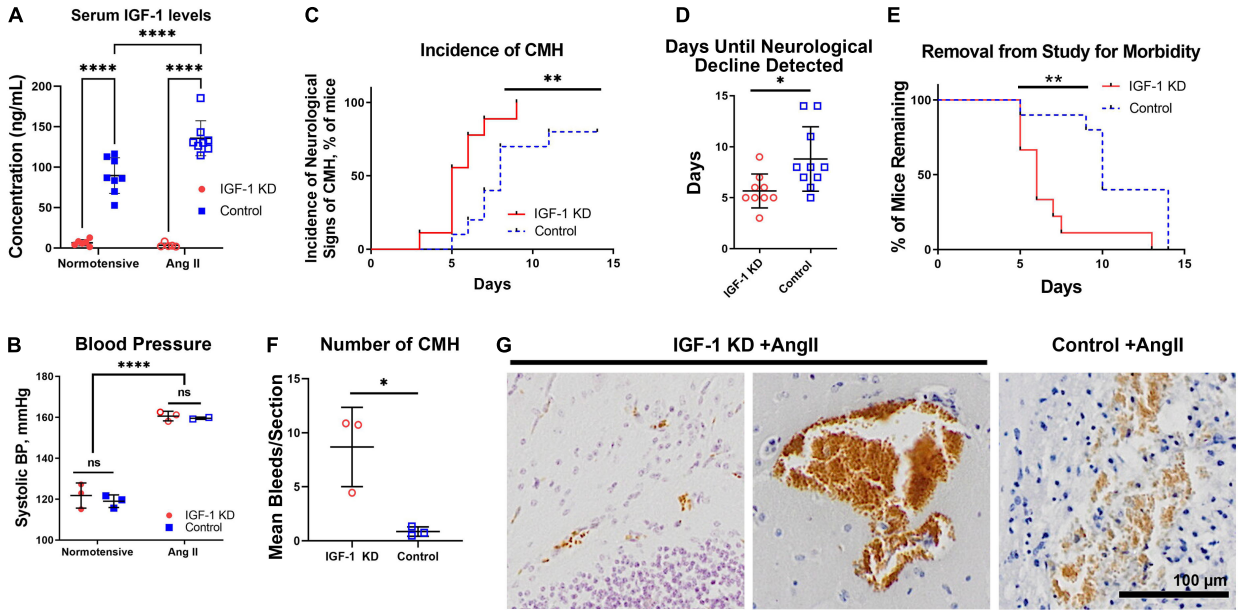

FIGURE 1 | Insulin-like growth factor 1 (IGF-1) deficiency exacerbates the development of hypertension-induced CMH at 1 year of age. **(A–G)** *Igf1*$^{f/f}$ mice were treated with TBG-Cre-AAV8 (IGF-1 KD) or TBG-GFP-AAV8 (control) at 4 months of age. At 1 year of age, hypertension was induced with Ang II and L-NAME. **(A)** At 1 year of age, serum ELISAs showed decreased circulating IGF-1 in IGF-1 KD mice (****$P < 0.0001$, by two-way ANOVA with Tukey's multiple comparisons correction). **(B)** Systolic blood pressures were significantly increased in mice receiving Ang II + L-NAME treatment versus untreated mice, regardless of genotype (****$P < 0.0001$, by two-way ANOVA with Tukey's multiple comparisons correction). **(C,D)** Hypertensive IGF-1 deficient (IGF-1 KD) mice exhibit neurological signs of CMH earlier than control hypertensive animals. Survival curves plot the day on which neurological score dropped below 18, day 0 is the day the Ang II delivery started [**$P \leq 0.01$, by Log-rank (Mantel–Cox) test **(C)** and *$P < 0.05$, by unpaired *t*-test, **(D)**]. **(E)** Hypertensive IGF-1 KD mice were removed from the study and sacrificed when neurological score dropped to 15 or lower [**$P \leq 0.01$, by Log-rank (Mantel–Cox) test]. **(F,G)** Bleeds were visualized by staining with DAB, reddish-brown. **(F)** Bleeds were counted in every twelfth section throughout of serially sectioned brains. The number of bleeds per section was averaged across all counted slides for a given mouse. Plotted is mean number of bleeds per section, each symbol reflects one mouse ($N = 3$ mice per group). Shown are mean ± SD (*$P < 0.05$, by unpaired *t*-test). **(G)** shows representative example bleeds. Scale bar, 100 µm, original magnification 10×.

Animals With Cerebral Bleeds Do Not Exhibit Signs of Retinal Bleeds

To assess whether mice in which CMHs developed in the brain also exhibited bleeds in the retina, we serially sectioned eyes collected from the same 1-year-old IGF-1 knockdown and control hypertensive and normotensive animals used for the experiments presented in **Figures 1**, **2**. Every 6th retinal section was stained with DAB to detect extravasated red blood cells (RBCs) and counterstained with hematoxylin. Our focus in these studies was identifying bleeds originating from the retinal vasculature. While the choroidal vasculature also supplies nutrients and oxygen to the retina, choroidal vessels are anatomically different from retinal and brain vessels (for example, choriocapillaris vessels are fenestrated and do not participate in the blood–retina barrier). In addition, the pigmented nature of the mouse choroid masks any DAB staining. The DAB stained retinal sections were scored by multiple blinded observers for the presence of any sign of bleed in the retina. However, no evidence of bleeds was detected in any retinal section examined in any region of the retina from any of the groups (example images are shown in **Figures 3A,B**). To confirm that this was not a staining artifact, brain sections adjacent to those in which cerebral bleeds had previously been detected were included in each retinal staining experiment as positive controls (**Figure 3C**). To verify that the retina carries receptors for IGF-1, we performed immunofluorescence labeling for IGF-1 receptor (red, **Figures 3D,E**). IGF-1 receptor is localized throughout the retina, and is particularly enriched in the retinal pigment epithelium (RPE) layer, in the two synaptic layers (inner and outer plexiform layers), and in blood vessels (white arrows). The labeling pattern for IGF-1 receptor is similar in IGF-1 KD and control retinas and in hypertensive and normotensive retinas (**Figure 3D**). IGF-1 receptor labeling in the brain with pronounced vascular labeling (white arrows) is shown in **Figure 3E**. These findings suggest that the retina is not as susceptible as the brain to the development of CMHs.

Circulating Insulin-Like Growth Factor 1 Deficiency Does Not Lead to Retinal Degeneration

As part of our general evaluation of the effects of circulating IGF-1 KD in the retina, we also undertook morphometric measurements to assess retinal degeneration (representative images shown in **Figures 4A,B**). One-year-old IGF-1 knockdown mice (regardless of whether they were hypertensive or normotensive) did not exhibit thinning of the ONL (photoreceptors, **Figure 4C**), INL (retinal interneurons, **Figure 4E**), or OPL (the layer where photoreceptor terminals

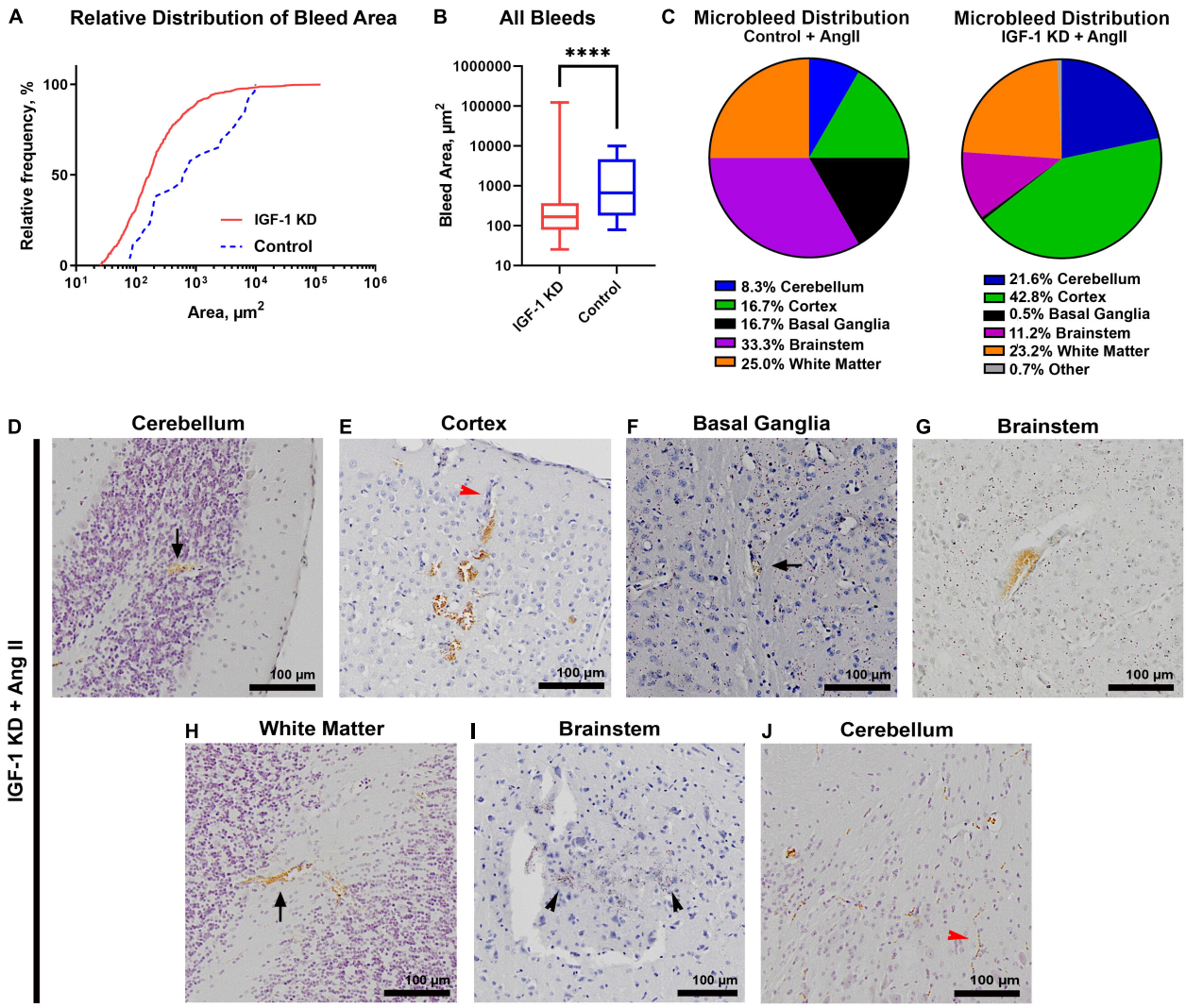

FIGURE 2 | Insulin-like growth factor 1 (IGF-1) deficiency increases the number of hypertension-induced cerebral microhemorrhages (CMHs) at 1 year of age. **(A)** The number of detected brain bleeds (from three control and three IGF-1 KD age-matched, 1-year-old brains) is plotted (relative frequency) as a function of bleed area. IGF-1 KD hypertensive mice have a greater relative frequency of smaller bleeds versus control hypertensive mice. **(B)** The mean bleed size was also smaller in IGF-1 KD mice versus controls (****$P < 0.0001$, Mann Whitney test for non-parametric data). Plotted is the median value, bars represent min/max. **(C)** The pie charts show the bleed locations in hypertensive IGF-1 KD ($N = 573$ bleeds) and control brains ($N = 12$ bleeds). Notably, IGF-1 KD mice had more bleeds in the cerebellum and cortex versus controls. Panels **(D–J)** show representative images of microbleeds in each of the brain regions represented in the pie charts from panel **(C)** (arrows show microbleeds). Black arrowheads denote darker brown 3,3-diaminobenzidine (DAB) staining showing older bleeds. Red arrowheads show bleeds emanating from blood vessels. Scale bars: 100 µm, original magnification 10×. IGF-1 KD: *Igf1*$^{f/f}$ + TBG-Cre-AAV8; control: *Igf1*$^{f/f}$ + TBG-GFP-AAV8.

form synapses with bipolar and horizontal cells, **Figure 4D**) compared to age-matched controls and young (3 month old) controls.

We next undertook a series of experiments designed to evaluate whether circulating IGF-1 deficiency had any general effects on the retina in aged mice (∼2 years of age). Similar to the case at 1 year of age, we observed no signs of retinal degeneration in IGF-1 KD or age-matched controls compared to young control mice (young control group replotted from **Figure 4** for ease of comparison) (**Figures 5A–D**). Incipient photoreceptor degeneration is often preceded by mislocalization of photoreceptor outer segment proteins such as rod and cone opsins, however, we observed no signs of this in 1 or 2-year-old IGF-1 KD animals (or age-matched controls, **Supplementary Figure 1**). Because retinal function does not correlate directly with retinal degeneration, and it has been well established that there is significant age-related loss of retinal function without significant structural degeneration (Li et al., 2001; Gresh et al., 2003; Samuel et al., 2011; Ferdous et al., 2021), we also conducted scotopic and photopic electroretinography on 2-year-old animals to assess rod and cone function. As expected, 2-year old mice (both IGF-1 knockdown and control) exhibited significant reductions in both dark adapted (rods, **Figure 5F**) and light-adapted (cones, **Figures 5G,H**) responses compared to young

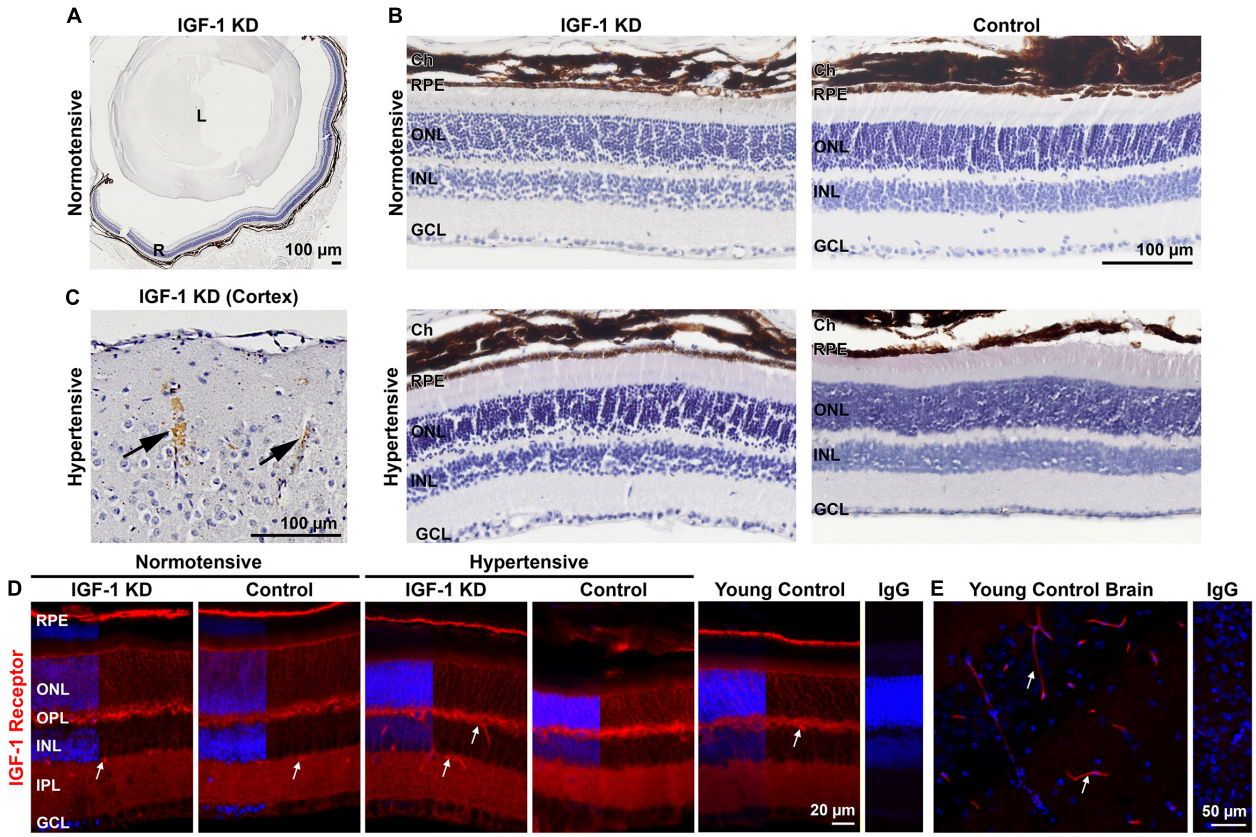

FIGURE 3 | Insulin-like growth factor 1 (IGF-1) deficient hypertensive mice do not show evidence of retinal microbleeds at 1 year of age. **(A,B)** Retinas from 1-year-old hypertensive IGF-1 knockdown (KD) and control animals were stained with hematoxylin and 3,3-diaminobenzidine (DAB). **(C)** Brain sections containing CMH were included as positive staining controls in each batch of retinal sections, 20 × (arrows denote microbleeds). **(D,E)** Retinal **(D)** and brain **(E)** sections were stained for IGF-1 receptor (red) and counterstained with DAPI (blue). *N* = 3 mice per group. Scale bars: 100 μm **(A–C)**, 20 μm **(D)**, 50 μm **(E)**, original magnification 10× **(A,C)**, 20× **(B,E)**, 40× **(D)**. R, retina; L, lens; Ch, choroid; RPE, retinal pigment epithelium; ONL, outer nuclear layer; INL, inner nuclear layer; GCL, ganglion cell layer; OPL, outer plexiform layer; IPL, inner plexiform layer. IGF-1 KD: $Igf1^{f/f}$ + TBG-Cre-AAV8; control: $Igf1^{f/f}$ + TBG-GFP-AAV8.

(3-month-old) controls. These findings are consistent with prior studies in C57BL/6 showing significant age-related loss in rod and cone function with little or no photoreceptor degeneration (Li et al., 2001; Gresh et al., 2003; Samuel et al., 2011; Ferdous et al., 2021). IGF-1 KD mice were partially protected from age-related decreases in rod and cone function compared to control mice (**Figures 5F–H**), exhibiting scotopic a- and b- wave amplitudes and photopic b-wave amplitudes that were slightly higher than those in age-matched controls.

These data were in contrast to findings in the brain, wherein circulating IGF-1 deficiency led to signs of neuronal dysfunction such as gait defects and cognitive decline as a result of impaired neurovascular coupling when assessed at 1 year of age (Toth et al., 2014; Tarantini et al., 2017c). Thus, we asked whether neurovascular coupling in the brain was also impaired in IGF-1 KD animals at 2 years of age. Measurements of CBF changes in the somatosensory cortex in response to whisker stimulation were performed on aged 2-year-old IGF-1 KD animals, age-matched controls, and young (3–6 month) controls. Both groups of 2-year-old mice exhibited significantly reduced neurovascular coupling compared to young mice (**Figure 5E**). IGF-1 KD mice had mean values slightly less than age-matched controls, however the difference did not achieve statistical significance. These data are consistent with the view that genetic IGF-1 deficiency at younger ages promotes accelerated cerebromicrovascular aging, which mimics the effects of age-related decline in circulating IGF-1 manifested at later ages in wild type mice.

Global IGF-1 knockout retinas exhibit loss of synapses in the OPL. To evaluate whether there are retinal synaptic defects in mice with adult-onset circulating IGF-1 deficiency, we labeled retinas from IGF-1 KD and control animals for VGLUT1 (photoreceptor and bipolar cell terminals) and SV2 (all presynaptic terminals, **Figure 6A**, magenta). Aged (2-year-old) IGF-1 KD and WT control animals exhibited a thinner layer of photoreceptor terminals in the OPL compared to young control mice, a phenotype that was more pronounced in the peripheral retina than in the central retina (**Figure 6A**). The OPL contains a mix of rod spherules and cone pedicles, but the terminals we observed in the 2-year-old animals exhibited morphological signs of cone pedicles. To verify this, we co-labeled retinal sections with the cone marker cone arrestin (CARR, yellow, **Figure 6B**) and SV2 (magenta, **Figure 6B**). In young control mice, cone terminals

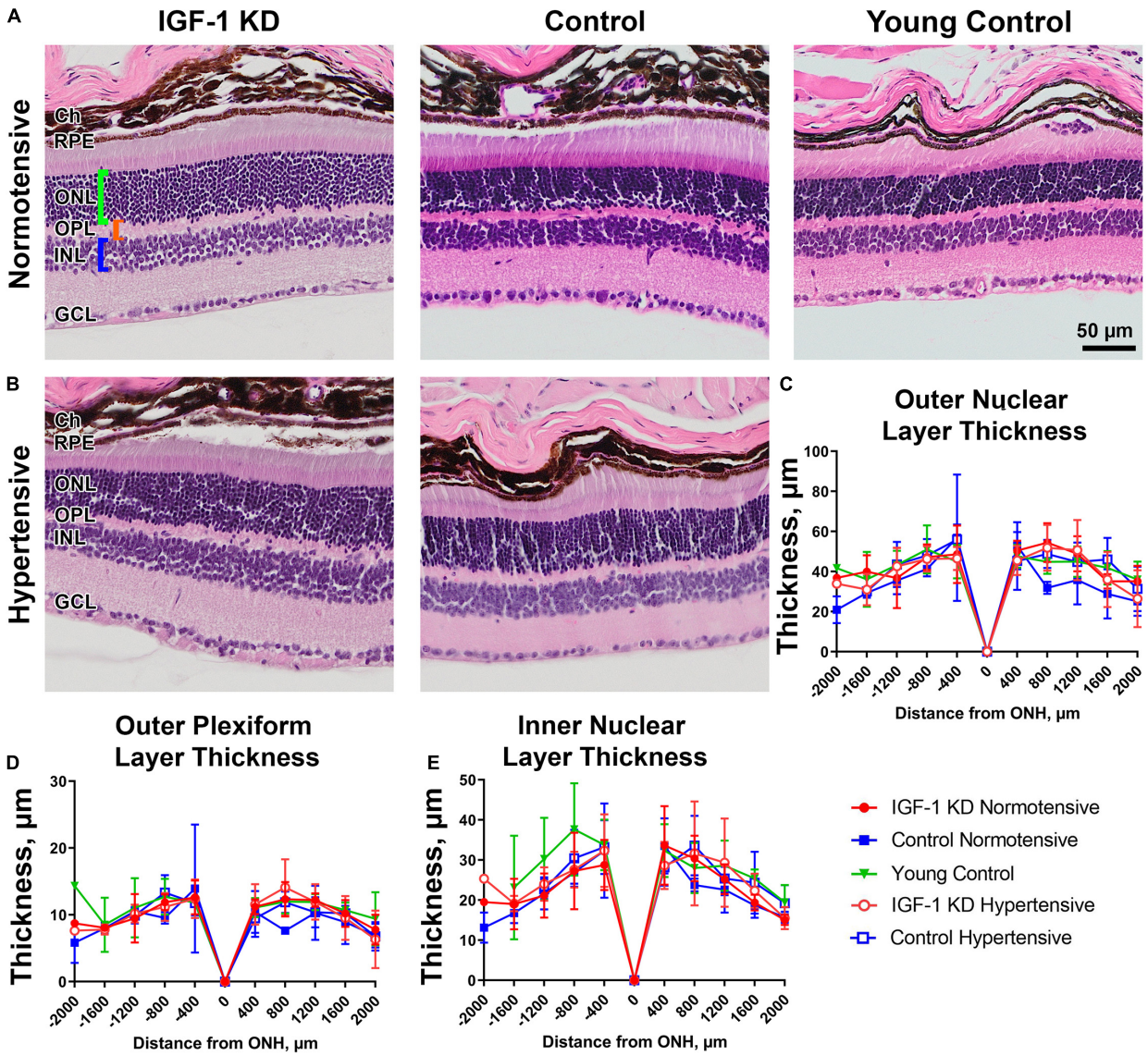

FIGURE 4 | Insulin-like growth factor 1 (IGF-1) deficient mice do not show signs of retinal degeneration at 1 year of age. Panels **(A,B)** shown are H&E stained retinal sections from 1-year-old normotensive/hypertensive IGF-1 KD, age-matched control, and young control mice. Green bracket highlights ONL, orange bracket highlights OPL, blue bracket highlights INL. **(C–E)** Spidergrams show the thickness of the ONL **(C)**, outer plexiform layer **(D)**, and inner nuclear layer **(E)** as measured from the optic nerve head (ONH). Plotted are means ± SD. *N* = 3–5 mice per group. Ch, choroid; RPE, retinal pigment epithelium; ONL, outer nuclear layer; OPL, outer plexiform layer; INL, inner nuclear layer; GCL, ganglion cell layer. Original magnification, 20×. Scale bar: 50 µm.

(white terminals are co-labeled with SV2/VGLUT1, and white arrows) and rod terminals (magenta label only, arrowheads highlight examples) are present, but the majority of terminals in aged retinas are co-labeled for CARR and SV2 indicating they originate from cones. To help evaluate whether second-order neurons were present at these synapses, we co-labeled retinal sections for SV2 (magenta, **Figure 6C**) and the horizontal cell marker calbindin (yellow, **Figure 6C**). Examination of high magnification images showed that horizontal cell process were properly present in 2 year old IGF-1 KD and control mice (**Figure 6C** bottom, arrows). We performed similar analyses on 1-year-old IGF-1 KD and control animals (**Supplementary Figure 2**) but found no abnormalities. Combined, these data suggest that circulating IGF-1 deficiency does not exacerbate age-related defects in retinal structure or function.

Circulating Insulin-Like Growth Factor 1 Deficiency Leads to Signs of Vascular Abnormalities and Gliosis in the Retina

To further analyze retinal phenotypes associated with circulating IGF-1 deficiency, we performed *in vivo* fluorescein angiography on both IGF-1 KD and control mice (all normotensive) at 1 and 2 years of age. On fluorescein angiograms, we

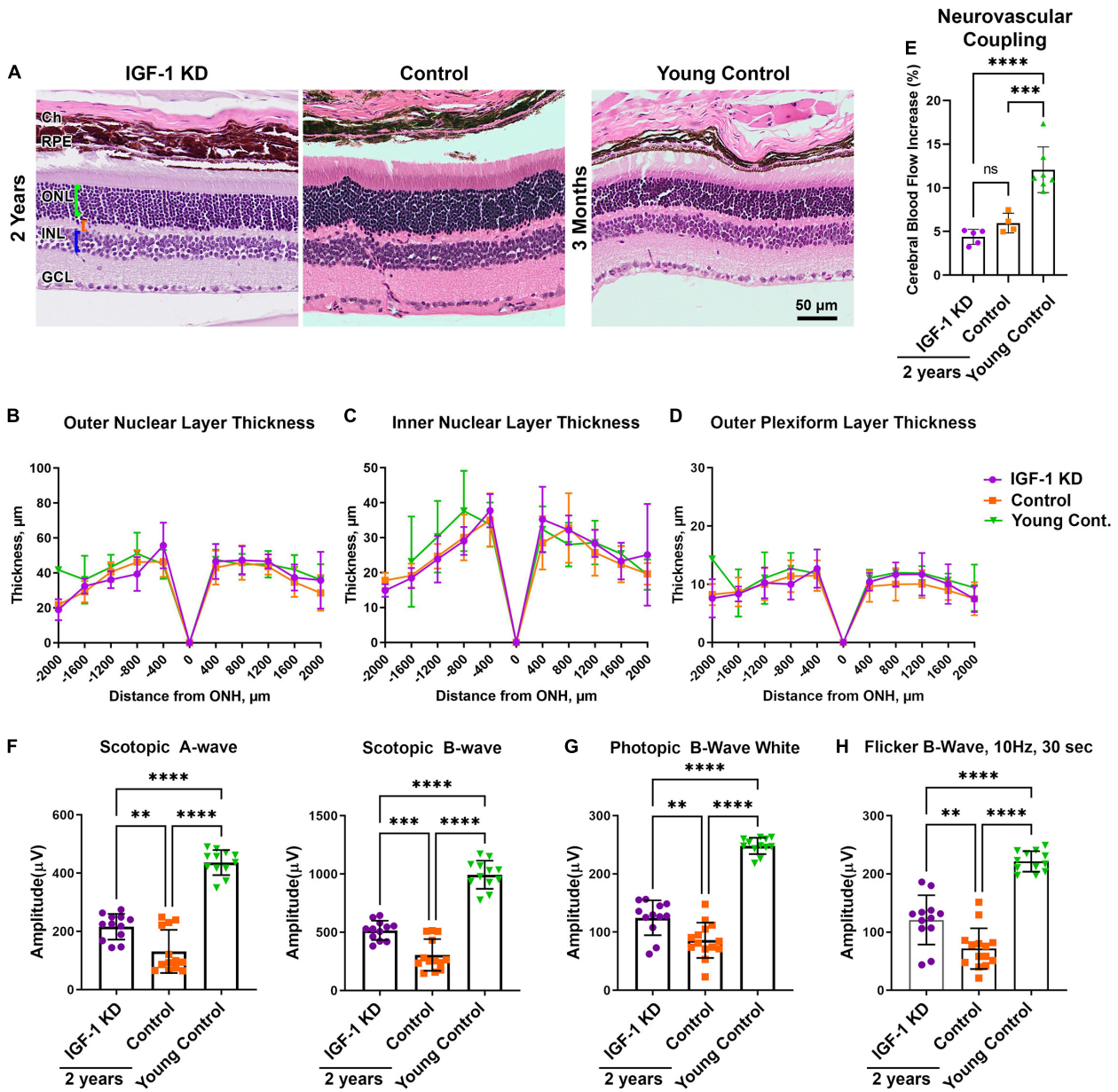

FIGURE 5 | Insulin-like growth factor 1 (IGF-1) deficiency slows age-related declines in retinal function at 2 years of age. **(A–D)** Retinas from 2-year-old IGF-1 KD, age-matched control, and young control animals were H&E stained and the thickness of retinal layers was measured. Green bracket highlights ONL, orange bracket highlights OPL, blue bracket highlights INL. **(B–D)** Spidergrams presenting the thickness of the outer nuclear layer **(B)**, inner nuclear layer **(C)**, and outer plexiform layer **(D)** are shown. Young control group is replotted from **Figure 4** as a control. There are no significant differences in thickness between the groups (N = 5–8 mice/group). **(E)** Change in blood flow in the somatosensory cortex in response to whisker stimulation was measured in 2-year-old mice as a measure of neurovascular coupling. **(F–H)** Two-year-old animals and controls underwent dark-adapted [**(F)** scotopic], light adapted [**(G)** photopic], or flicker [**(H)** photopic] electroretinography (ERG) to measure retinal function. N = 6–8 mice/group, each symbol represents an individual eye. Plotted are means ± SD $^{**}P < 0.01$, $^{***}P < 0.001$, $^{****}P < 0.0001$ by one-way ANOVA with Tukey's *post hoc* comparison. Ch, choroid; RPE, retinal pigment epithelium; ONL, outer nuclear layer; OPL, outer plexiform layer; INL, inner nuclear layer; GCL, ganglion cell layer. Scale bar: 50 µm. Original magnification, 20×. IGF-1 KD: $Igf1^{f/f}$ + TBG-Cre-AAV8; control: $Igf1^{f/f}$ + TBG-GFP-AAV8.

frequently observed patterns of repeated vascular constriction, referred to as "sausage on a string" phenotype (Jacobsen et al., 2002) in one or more retinal vessels in IGF-1 KD mice (**Figures 7A,B**, arrows). At 1 year of age, 5/6 IGF-1 KD, and only 2/5 age-matched controls exhibited this phenotype. This phenomenon persisted at 2 years of age: 7/12 IGF-1 KD mice had the severe constriction phenotype while only 1/5 age matched controls had the phenotype (**Figure 7B**). Young control animals did not exhibit this phenotype (**Figure 7C**).

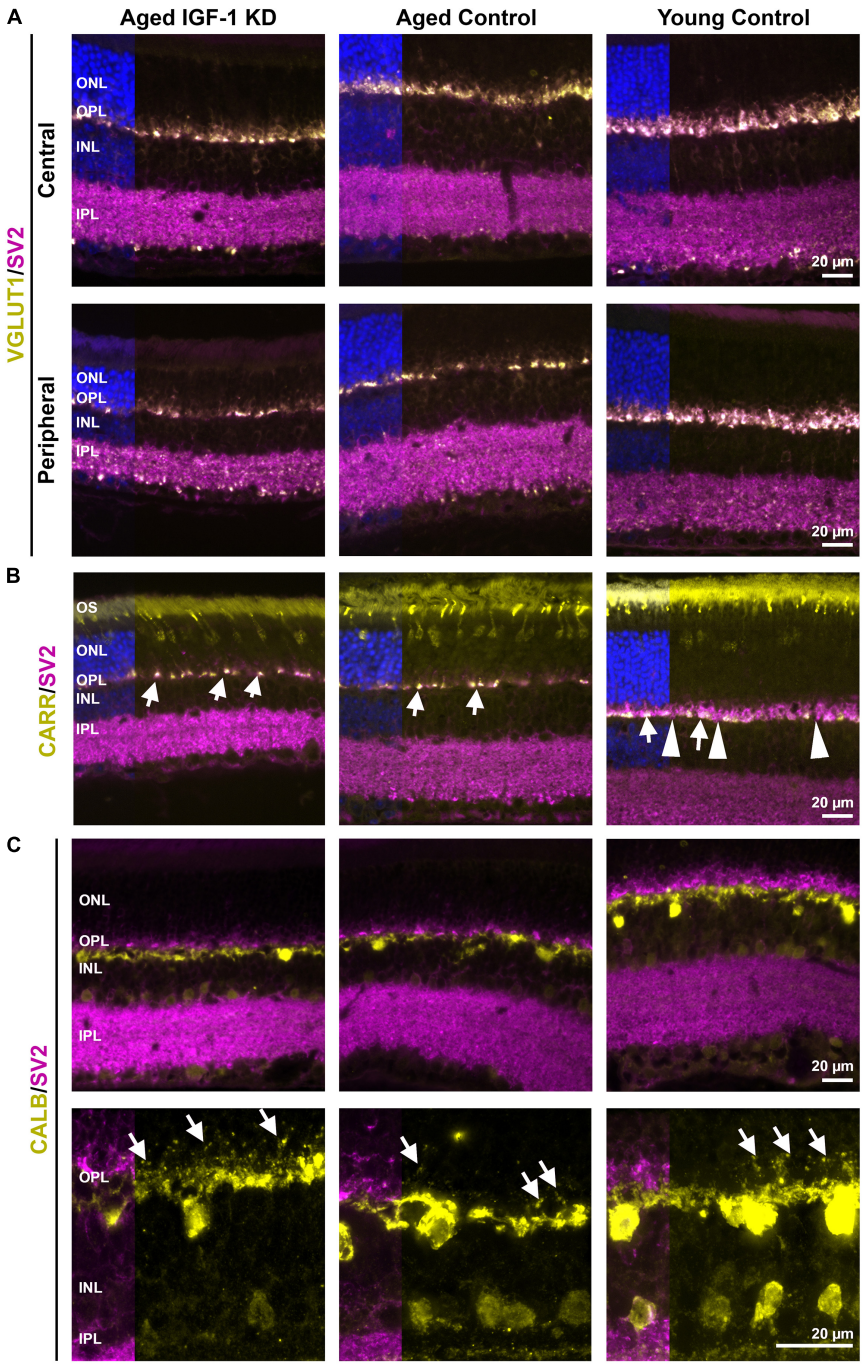

FIGURE 6 | Circulating insulin-like growth factor 1 (IGF-1) deficiency does not lead to gross synaptic abnormalities at 2 years of age. Retinal sections from the indicated groups were collected at 2 years of age (left and center) or at 3–6 months of age (right). Sections were labeled for VGLUT1 [yellow, **(A)**], cone arrestin [CARR, yellow, **(B)**], or calbindin [CALB, yellow, **(C)**] and SV2 [magenta, **(A–C)**]. Sections were counterstained with DAPI (blue). Panel **(A)** shown are representative images from both the central and peripheral retina. **(B)** Arrows highlight example cone pedicles co-labeled for CARR and SV2. Arrowheads highlight example rod spherules (SV2 positive, CARR negative). **(C)** Arrows highlight horizontal cell projections in the outer plexiform layer. Scale bars: 20 µm, original magnification 40× [**(A–C)**-top], and 100× [**(C)**-bottom]. *N* = 3–5 eyes per group. OPL, outer plexiform layer; INL, inner nuclear layer; IPL, inner plexiform layer; ONL, outer nuclear layer; OS, outer segment layer. IGF-1 KD: $Igf1^{f/f}$ + TBG-Cre-AAV8; control: $Igf1^{f/f}$ + TBG-GFP-AAV8.

We proceeded to evaluate other signs of stress in the retina. We used immunofluorescence to evaluate the expression of retinal glial fibrillary acidic protein (GFAP), an intermediate filament protein normally restricted to the endfeet of Müller glial cells (**Figures 8A–D**). Increased expression of GFAP leads to staining along the Müller cell body toward the outer layers of

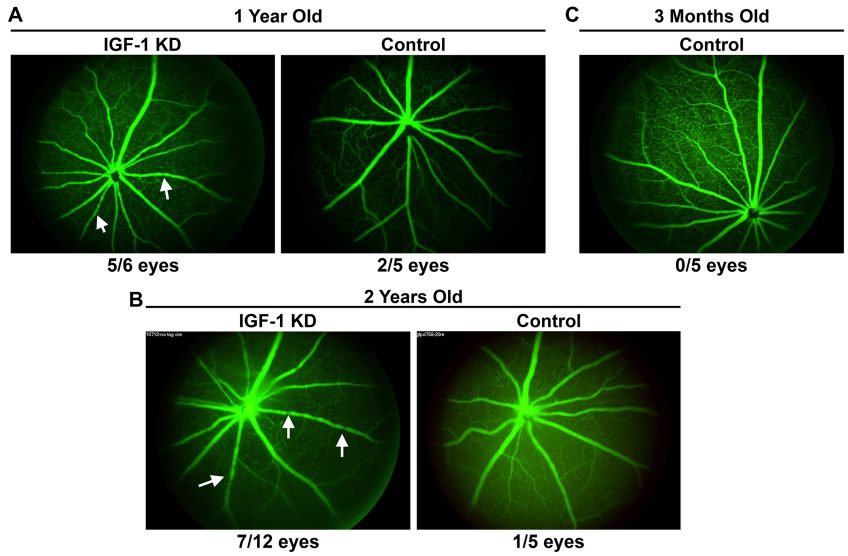

FIGURE 7 | Insulin-like growth factor 1 (IGF-1) deficient mice exhibit vascular abnormalities in the retina. **(A–C)** Fluorescein angiograms were performed in 1– and 2-year-old IGF-1 KD and control animals. Arrows highlight example vessels exhibiting a pattern of vascular constriction ("sausages-on-a-string" phenotype), numbers underneath denote the number of eyes/total eyes that exhibit at least one vessel with the pattern of constriction. IGF-1 KD: $Igf1^{f/f}$ + TBG-Cre-AAV8; control: $Igf1^{f/f}$ + TBG-GFP-AAV8.

the retina, and is a marker of gliosis and retinal stress. At 1 year of age, we observed some minor signs of glial cell activation in IGF-1 KD retinas (**Figure 8A**, arrowheads). This phenomenon was more pronounced at 2 years of age, wherein significantly increased GFAP labeling was frequently observed in IGF-1 KD retinas compared to age-matched control retinas (**Figure 8B**). We next scored GFAP-labeled retinas on a scale of 0–4 (0 = no gliosis, 4 = severe gliosis) (**Figure 8D**). At 1 year of age, gliosis was minor or not detected in all groups. At 2 years of age, there is a high degree of eye-to-eye variability, but even so, IGF-1 KD eyes had a higher median gliosis score than age-matched controls, and 3/9 IGF-1 KD eyes exhibited a high degree of gliosis (score 3 or higher) compared to 0/7 control eyes. To ask whether this gliosis was accompanied by increased oxidative stress, we labeled retinas with a marker of lipid peroxidative stress, 4-hydroxynonenal (4-HNE). However, 4-HNE expression was similar in IGF-1 KD and control mice at 1 and 2 years of age (**Figures 8E,G**), though staining was modestly increased in aged retinas compared to young controls (**Figure 8F**). These findings indicate that circulating IGF-1 deficiency leads to abnormalities in the retinal vasculature and retinal gliosis.

DISCUSSION

Here we confirm that the effects of adult-onset circulating IGF-1 deficiency phenocopy important aspects of cerebrovascular aging (Toth et al., 2015b; Tarantini et al., 2017c) and demonstrate that increased susceptibility to CMHs in IGF-1 deficient mice is associated with imaging signs of vascular defects in the retina. There has been significant research interest in using the eye to model or predict disease in the brain, and several neurodegenerative or cerebrovascular diseases have measurable ocular manifestations (Czako et al., 2020; Istvan et al., 2021). Previous human studies also provide *prima facie* evidence that retinal microvascular changes (microaneurysms and retinal hemorrhage) together with other imaging and histological signs [Müller cell gliosis, retinal nerve fiber layer (RNFL) thinning] predict a higher risk of subsequent stroke in humans (Wong et al., 2001a,b; London et al., 2013; Zhao et al., 2020).

Cerebral microhemorrhages are common in the aging human population and predict cognitive decline (Poels et al., 2012; Akoudad et al., 2016) as well as subsequent ischemic and hemorrhagic stroke (Poels et al., 2011). There is strong evidence that circulating IGF-1 deficiency is causally linked to the genesis of CMHs and larger intracerebral hemorrhages (Tarantini et al., 2017c). However, in spite of the shared anatomical origins and important functional and structural similarities between the retinal and cerebral microvasculature (Tata et al., 2015), we found that IGF-1 deficiency did not exacerbate hypertension-induced microbleeds in the retina.

Retinal hemorrhages can occur as part of a wide variety of retinal diseases and conditions, including diabetic retinopathy (Crabtree and Chang, 2021; Jena and Tripathy, 2021), age-related macular degeneration (Avery et al., 1996; Oh et al., 2009; Poels et al., 2012), head trauma in infants (D'Aloisio et al., 2020), and many others, but there is no systematic evidence for age-related retinal microhemorrhages paralleling those seen in the brain. It is not clear whether this is a physiological difference between the retina and the brain or a function of available tools and/or patient populations. How retinal hemorrhages are labeled in human studies may also contribute to a lack of clarity regarding the clinical presence of retinal hemorrhages in aging. A broad spectrum of retinal microvascular changes including retinal hemorrhages, microaneurysms, cotton wool spots, macular edema, other exudates and optic disc swelling

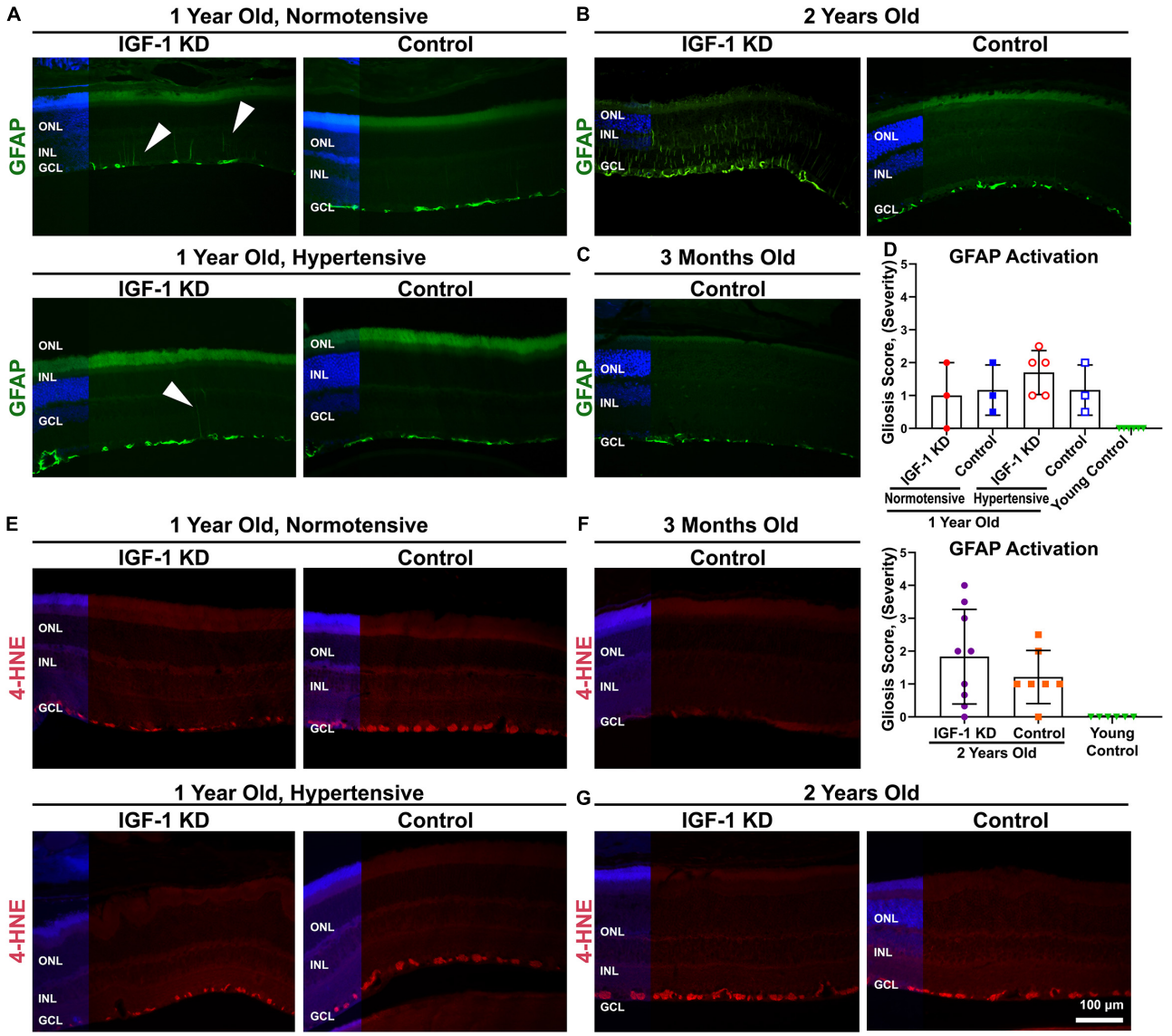

FIGURE 8 | Insulin-like growth factor 1 (IGF-1) deficient mice exhibit signs of reactive gliosis in the retina. **(A–D)** Retinal sections from 1– and 2-year-old IGF-1 KD were labeled for glial fibrillary acidic protein (GFAP) expression (green) and counterstained with DAPI (blue). Arrows highlight incipient Müller cell activation. **(D)** Müller cell activation (upregulation of GFAP, with penetration of labeling outside endfeet) was scored by a blinded observer on a 4-point scale (4 = severe gliosis, 0 = no gliosis). *N* = 3–9 eyes/group. **(E–G)** Oxidative stress was evaluated by labeling retinal sections with 4-HNE (red), a marker of lipid oxidative stress, and counterstained with DAPI (blue). *N* = 3–5 eyes/group. Scale bars: 100 μm. Original magnification, 20×. ONL, outer nuclear layer; INL, inner nuclear layer; GCL, ganglion cell layer. IGF-1 KD: $Igf1^{f/f}$ + TBG-Cre-AAV8; control: $Igf1^{f/f}$ + TBG-GFP-AAV8.

are often all grouped under the category of "retinopathy" (Wong et al., 2001b), and it can be challenging to refine individual microvascular manifestations. One of the few studies to specifically evaluate retinal microhemorrhages evaluated patients with cerebral amyloid angiopathy (CAA), a form of vascular dementia in which CMHs are common, found that CAA patients exhibited increased prevalence of retinal microhemorrhages compared to controls, and that there was a correlation between the presence of retinal microbleeds and cerebral bleeds (Alber et al., 2021). Further evaluation into the presence of retinal microhemorrhages in aging, and the extent to which these correlate with age-related CMH would be of great future interest.

There is an emerging body of literature suggesting that retinal microvascular rarefaction, typically measured by a decrease in retinal fractal dimension (a representation of microvascular network complexity) is associated with aging, cerebral microbleeds, cerebral small vessel disease, and the development of cognitive impairment (Hilal et al., 2014; Ong et al., 2014; Chua et al., 2020), although not all studies have confirmed these associations (O'Neill et al., 2021). We did not perform retinal microvascular imaging here, but we did

evaluate larger retinal vessels via fundus angiography. Aged IGF-1 deficient animals exhibited worsened patterns of vessel narrowing than control animals. This pattern is similar to the previously described "sausage-on-a-string" phenotype (so named because the constricted vessels resemble a chain of sausage links) and is thought to show regions of vascular instability (Jacobsen et al., 2002). Our "sausage-on-a-string" vessels also bear a resemblance to arteriovenous nicking and focal arteriolar narrowing, defects affecting larger retinal vessel in patients. There is clear evidence that cardiovascular risk factors such as hypertension are associated with changes in retinal microvessels (retinopathy) as well as these larger vessel changes [reviewed in Wong et al. (2001b)]. Combined, our findings suggest that while retinal microhemorrhages are not a part of the hypertensive response in mice with circulating IGF-1 deficiency, other vascular degenerative changes do occur in the retina, and are consistent with the presence of known cerebrovascular defects in IGF-1 knockdown models.

Insulin-like growth factor 1 in the retina in general has been widely evaluated, and as in the brain, the role of IGF-1 as either a protective pro-survival factor or a pro-inflammatory factor depends on the disease context. IGF-1 is an important pro-survival signal for photoreceptors and protects photoreceptors from apoptosis in the context of retinitis pigmentosa (RP) (Arroba et al., 2009; Arroba et al., 2018). IGF-1 is also known to be proangiogenic in eye pathologies associated with angiogenesis such as proliferative diabetic retinopathy (PDR) and wet age-related macular degeneration (AMD) (Arroba et al., 2018). In animal models, the findings have been similarly complicated. Similar to our findings from the circulating IGF-1 knockdown, global IGF-1 knockout animals exhibit signs of increased age-associated Müller cell gliosis in the retina but no overt retinal degeneration (Rodriguez-de la Rosa et al., 2012; Arroba et al., 2016). However, global IGF-1 knockout mice also exhibited significant decreases in rod and cone ERG function by 1 year of age. This is in contrast to our findings demonstrating that adult-onset circulating IGF-1 deficiency led not to declines in ERG function compared to control animals, but rather to a slight retardation of age-related loss of cone and rod function. One possible explanation for this counterintuitive effect is that cells resident to the retina may produce IGF-1 to compensate for any changes caused by circulating deficiency. IGF-1 is produced locally in the retina by multiple cell types including cones (Cao et al., 2001; Zygar et al., 2005; Lofqvist et al., 2009), and may therefore play a key role protecting the retina from circulating IGF-1 deficiency. Support for differential roles for circulating vs. locally-produced IGF-1 in the retina comes from studies utilizing transgenic mice that chronically overexpress IGF-1 in the retina (without increase in circulating IGF-1). Mice with chronic overexpression of intraocular IGF-1 exhibited significant impairments in the blood retinal barrier and loss of tight-junctional integrity, while mice with elevated circulating IGF-1 did not exhibit these phenotypes (Haurigot et al., 2009). However, these intraocular IGF-1 overexpressers also exhibited retinal degeneration, gliosis, and decreases in rod and cone function (Ruberte et al., 2004; Villacampa et al., 2013) similar to the global IGF-1 knockdowns, indicating that the role of IGF-1 in the retina is complex and levels are finely tuned. An additional layer of complexity arises from the fact that both the transgenic overexpression model and the global knockout model have modified IGF-1 levels from birth. Given the key role of IGF-1 in development, such early-onset models may not be the most relevant when studying age-related pathologies associated with IGF-1.

In conclusion, our work highlights the importance of IGF-1 in the maintenance of cerebrovascular and retinal stability and validates adult-onset circulating IGF-1 deficiency as an accelerated aging model. Critically, our findings also show that while the eye can serve as a model for the central nervous system, it does not always mimic every vascular pathology seen in the brain. The role of IGF-1 is complex in both the retina and the brain, but it clearly serves as a vasoprotective factor in both tissues, and further work to understand ways that retinal vascular changes can be used as biomarkers for cerebrovascular changes is urgently needed.

DATA AVAILABILITY STATEMENT

The original contributions presented in the study are included in the article/**Supplementary Material**, further inquiries can be directed to the corresponding author/s.

ETHICS STATEMENT

The animal study was reviewed and approved by Institutional Animal Care and Use Committee, University of Oklahoma Health Sciences Center.

AUTHOR CONTRIBUTIONS

LM, AC, ZU, and SC: conceptualization. LM, ST, WS, ME, AY, AC, and ZU: methodology. ÁN-T: software. LM, MJ, TM, EB, MB, and SC: validation. LM, ÁN-T, MJ, TM, MB, and SC: formal analysis. LM, ST, ÁN-T, MJ, TM, EB, MB, AY, and SC: investigation. WS, AC, ZU, and SC: resources. LM: writing—original draft. LM, ÁN-T, MJ, TM, EB, MB, WS, AY, AC, ZU, ME, and SC: writing—review and editing. SC and AC: supervision. LM, ST, ZU, AC, SC, and ME: funding acquisition. All authors contributed to the article and approved the submitted version.

FUNDING

This work was supported by grants from the National Institute on Aging (R01-AG047879, R01-AG038747, R01-AG055395, R01-AG070915, and K01AG073614), the National Institute of Neurological Disorders and Stroke (NINDS; R01-NS056218, and R01-NS100782), the NIA-supported Geroscience Training Program in Oklahoma (T32AG052363), the Oklahoma Nathan Shock Center (P30AG050911), the Cellular and Molecular GeroScience CoBRE (1P20GM125528), the National Eye Institute (R01-EY019494), the Oklahoma Center for the Advancement of Science and Technology, and by the NKFIH

(Nemzeti Szivlabor). Research reported in this publication was supported in part by the Molecular and Cellular Imaging core and Animal Model Development and Behavioral Analysis cores that are part of 1P20GM125528 Cellular and Molecular GeroScience CoBRE from the National Institute of General Medical Sciences, by the Dean McGee Eye Institute core, 5P30EY021725-10, and by the COBRE-initiated Histology, Microscopy, and Image Analysis (HMIA) Core at OUHSC, 5P30GM122744, and an unrestricted grant from Research to Prevent Blindness, Inc. The funding sources had no role in the study design; in the collection, analysis, and interpretation of data; in the writing of the report; and in the decision to submit the article for publication.

ACKNOWLEDGMENTS

We thank Neely Patel, Megan Runion, Cynthia Bulmer, Joshua Tatarian, and David Sherry for their technical assistance.

SUPPLEMENTARY MATERIAL

The Supplementary Material for this article can be found online at: https://www.frontiersin.org/articles/10.3389/fnagi.2022.788296/full#supplementary-material

REFERENCES

Akoudad, S., Wolters, F. J., Viswanathan, A., de Bruijn, R. F., van der Lugt, A., Hofman, A., et al. (2016). Association of cerebral microbleeds with cognitive decline and dementia. *JAMA Neurol.* 73, 934–943. doi: 10.1001/jamaneurol.2016.1017

Alber, J., Arthur, E., Goldfarb, D., Drake, J., Boxerman, J. L., Silver, B., et al. (2021). The relationship between cerebral and retinal microbleeds in cerebral amyloid angiopathy (CAA): a pilot study. *J. Neurol. Sci.* 423:117383. doi: 10.1016/j.jns.2021.117383

Arroba, A. I., Campos-Caro, A., Aguilar-Diosdado, M., and Valverde, ÁM. (2018). IGF-1, inflammation and retinal degeneration: a close network. *Front. Aging Neurosci.* 10:203. doi: 10.3389/fnagi.2018.00203

Arroba, A. I., Rodríguez-de la Rosa, L., Murillo-Cuesta, S., Vaquero-Villanueva, L., Hurlé, J. M., Varela-Nieto, I., et al. (2016). Autophagy resolves early retinal inflammation in Igf1-deficient mice. *Dis. Model. Mech.* 9, 965–974. doi: 10.1242/dmm.026344

Arroba, A. I., Wallace, D., Mackey, A., de la Rosa, E. J., and Cotter, T. G. (2009). IGF-I maintains calpastatin expression and attenuates apoptosis in several models of photoreceptor cell death. *Eur. J. Neurosci.* 30, 975–986. doi: 10.1111/j.1460-9568.2009.06902.x

Ashpole, N. M., Logan, S., Yabluchanskiy, A., Mitschelen, M. C., Yan, H., Farley, J. A., et al. (2017). IGF-1 has sexually dimorphic, pleiotropic, and time-dependent effects on healthspan, pathology, and lifespan. *Geroscience* 39, 129–145. doi: 10.1007/s11357-017-9971-0

Avery, R. L., Fekrat, S., Hawkins, B. S., and Bressler, N. M. (1996). Natural history of subfoveal subretinal hemorrhage in age-related macular degeneration. *Retina* 16, 183–189. doi: 10.1097/00006982-199616030-00001

Bailey-Downs, L. C., Mitschelen, M., Sosnowska, D., Toth, P., Pinto, J. T., Ballabh, P., et al. (2012). Liver-specific knockdown of IGF-1 decreases vascular oxidative stress resistance by impairing the Nrf2-dependent antioxidant response: a novel model of vascular aging. *J. Gerontol. A Biol. Sci. Med. Sci.* 67, 313–329. doi: 10.1093/gerona/glr164

Bake, S., Okoreeh, A. K., Alaniz, R. C., and Sohrabji, F. (2016). Insulin-like growth factor (IGF)-I modulates endothelial blood-brain barrier function in ischemic middle-aged female rats. *Endocrinology* 157, 61–69. doi: 10.1210/en.2015-1840

Bake, S., Selvamani, A., Cherry, J., and Sohrabji, F. (2014). Blood brain barrier and neuroinflammation are critical targets of IGF-1-mediated neuroprotection in stroke for middle-aged female rats. *PLoS One* 9:e91427. doi: 10.1371/journal.pone.0091427

Blum, W. F., Alherbish, A., Alsagheir, A., El Awwa, A., Kaplan, W., Koledova, E., et al. (2018). The growth hormone-insulin-like growth factor-I axis in the diagnosis and treatment of growth disorders. *Endocr. Connect.* 7, R212–R222. doi: 10.1530/EC-18-0099

Boscolo Sesillo, F., Fox, D., and Sacco, A. (2019). Muscle stem cells give rise to rhabdomyosarcomas in a severe mouse model of duchenne muscular dystrophy. *Cell Rep.* 26, 689.e6–701.e6. doi: 10.1016/j.celrep.2018.12.089

Brown, B. M., Ramirez, T., Rife, L., and Craft, C. M. (2010). Visual Arrestin 1 contributes to cone photoreceptor survival and light adaptation. *Invest. Ophthalmol. Vis. Sci.* 51, 2372–2380. doi: 10.1167/iovs.09-4895

Cao, W., Li, F., Steinberg, R. H., and Lavail, M. M. (2001). Development of normal and injury-induced gene expression of aFGF, bFGF, CNTF, BDNF, GFAP and IGF-I in the rat retina. *Exp. Eye Res.* 72, 591–604. doi: 10.1006/exer.2001.0990

Chakraborty, D., Conley, S. M., Stuck, M. W., and Naash, M. I. (2010). Differences in RDS trafficking, assembly and function in cones versus rods: insights from studies of C150S-RDS. *Hum. Mol. Genet.* 19, 4799–4812. doi: 10.1093/hmg/ddq410

Chakraborty, D., Strayve, D. G., Makia, M. S., Conley, S. M., Kakahel, M., Al-Ubaidi, M. R., et al. (2020). Novel molecular mechanisms for Prph2-associated pattern dystrophy. *FASEB J.* 34, 1211–1230. doi: 10.1096/fj.201901888R

Che Azemin, M. Z., Ab Hamid, F., Aminuddin, A., Wang, J. J., Kawasaki, R., and Kumar, D. K. (2013). Age-related rarefaction in retinal vasculature is not linear. *Exp. Eye Res.* 116, 355–358. doi: 10.1016/j.exer.2013.10.010

Chua, J., Hu, Q., Ke, M., Tan, B., Hong, J., Yao, X., et al. (2020). Retinal microvasculature dysfunction is associated with Alzheimer's disease and mild cognitive impairment. *Alzheimers Res. Ther.* 12:161. doi: 10.1186/s13195-020-00724-0

Cooper, L. L., Woodard, T., Sigurdsson, S., van Buchem, M. A., Torjesen, A. A., Inker, L. A., et al. (2016). Cerebrovascular damage mediates relations between aortic stiffness and memory. *Hypertension* 67, 176–182. doi: 10.1161/HYPERTENSIONAHA.115.06398

Crabtree, G. S., and Chang, J. S. (2021). Management of complications and vision loss from proliferative diabetic retinopathy. *Curr. Diab. Rep.* 21:33. doi: 10.1007/s11892-021-01396-2

Csipo, T., Mukli, P., Lipecz, A., Tarantini, S., Bahadli, D., Abdulhussein, O., et al. (2019). Assessment of age-related decline of neurovascular coupling responses by functional near-infrared spectroscopy (fNIRS) in humans. *Geroscience* 41, 495–509. doi: 10.1007/s11357-019-00122-x

Czako, C., Kovacs, T., Ungvari, Z., Csiszar, A., Yabluchanskiy, A., Conley, S., et al. (2020). Retinal biomarkers for Alzheimer's disease and vascular cognitive impairment and dementia (VCID): implication for early diagnosis and prognosis. *Geroscience* 42, 1499–1525. doi: 10.1007/s11357-020-00252-7

D'Aloisio, R., Nasillo, V., Gironi, M., and Mastropasqua, R. (2020). Bilateral macular hemorrhage in a patient with COVID-19. *Am. J. Ophthalmol. Case Rep.* 20:100958. doi: 10.1016/j.ajoc.2020.100958

Daulatzai, M. A. (2016). Cerebral hypoperfusion and glucose hypometabolism: key pathophysiological modulators promote neurodegeneration, cognitive impairment, and Alzheimer's disease. *J. Neurosci. Res.* 95, 943–972. doi: 10.1002/jnr.23777

Ferdous, S., Liao, K. L., Gefke, I. D., Summers, V. R., Wu, W., Donaldson, K. J., et al. (2021). Age-Related Retinal Changes in Wild-Type C57BL/6J Mice Between 2 and 32 Months. *Invest. Ophthalmol. Vis. Sci.* 62:9. doi: 10.1167/iovs.62.7.9

Fulop, G. A., Ramirez-Perez, F. I., Kiss, T., Tarantini, S., Valcarcel Ares, M. N., Toth, P., et al. (2018). IGF-1 deficiency promotes pathological remodeling of cerebral arteries: a potential mechanism contributing to the pathogenesis of intracerebral hemorrhages in aging. *J. Gerontol. A Biol. Sci. Med. Sci.* 74, 446–454. doi: 10.1093/gerona/gly144

Gresh, J., Goletz, P. W., Crouch, R. K., and Rohrer, B. (2003). Structure-function analysis of rods and cones in juvenile, adult, and aged C57bl/6 and Balb/c mice. *Vis. Neurosci.* 20, 211–220. doi: 10.1017/s0952523803202108

Hajdu, M. A., Heistad, D. D., Siems, J. E., and Baumbach, G. L. (1990). Effects of aging on mechanics and composition of cerebral arterioles in rats. *Circ. Res.* 66, 1747–1754. doi: 10.1161/01.res.66.6.1747

Haurigot, V., Villacampa, P., Ribera, A., Llombart, C., Bosch, A., Nacher, V., et al. (2009). Increased intraocular insulin-like growth factor-I triggers blood-retinal

barrier breakdown. *J. Biol. Chem.* 284, 22961–22969. doi: 10.1074/jbc.M109.014787

Hilal, S., Ong, Y. T., Cheung, C. Y., Tan, C. S., Venketasubramanian, N., Niessen, W. J., et al. (2014). Microvascular network alterations in retina of subjects with cerebral small vessel disease. *Neurosci. Lett.* 577, 95–100. doi: 10.1016/j.neulet.2014.06.024

Ho, K. J., Bass, C. E., Kroemer, A. H. K., Ma, C., Terwilliger, E., and Karp, S. J. (2008). Optimized adeno-associated virus 8 produces hepatocyte-specific Cre-mediated recombination without toxicity or affecting liver regeneration. *Am. J. Physiol. Gastrointest. Liver Physiol.* 295, G412–G419. doi: 10.1152/ajpgi.00590.2007

Ighodaro, E. T., Abner, E. L., Fardo, D. W., Lin, A. L., Katsumata, Y., Schmitt, F. A., et al. (2016). Risk factors and global cognitive status related to brain arteriolosclerosis in elderly individuals. *J. Cereb. Blood Flow Metab.* 37, 201–216. doi: 10.1177/0271678X15621574

Istvan, L., Czako, C., Elo, A., Mihaly, Z., Sotonyi, P., Varga, A., et al. (2021). Imaging retinal microvascular manifestations of carotid artery disease in older adults: from diagnosis of ocular complications to understanding microvascular contributions to cognitive impairment. *Geroscience* 43, 1703–1723. doi: 10.1007/s11357-021-00392-4

Jackson-Weaver, O., Ungvijanpunya, N., Yuan, Y., Qian, J., Gou, Y., Wu, J., et al. (2020). PRMT1-p53 pathway controls epicardial EMT and invasion. *Cell Rep.* 31:107739. doi: 10.1016/j.celrep.2020.107739

Jacobsen, J. C., Beierholm, U., Mikkelsen, R., Gustafsson, F., Alstrøm, P., and Holstein-Rathlou, N. H. (2002). "Sausage-string" appearance of arteries and arterioles can be caused by an instability of the blood vessel wall. *Am. J. Physiol. Regul. Integr. Comp. Physiol.* 283, R1118–R1130. doi: 10.1152/ajpregu.00006.2002

Jena, S., and Tripathy, K. (2021). *Vitreous Hemorrhage*. Treasure Island, FL: StatPearls Publishing Copyright.

Jessen, S. B., Mathiesen, C., Lind, B. L., and Lauritzen, M. (2015). Interneuron deficit associates attenuated network synchronization to mismatch of energy supply and demand in aging mouse brains. *Cereb. Cortex* 27, 646–659. doi: 10.1093/cercor/bhv261

Kakakhel, M., Tebbe, L., Makia, M. S., Conley, S. M., Sherry, D. M., Al-Ubaidi, M. R., et al. (2020). Syntaxin 3 is essential for photoreceptor outer segment protein trafficking and survival. *Proc. Natl. Acad. Sci. U.S.A.* 117, 20615–20624. doi: 10.1073/pnas.2010751117

Kato, H., Izumiyama, M., Izumiyama, K., Takahashi, A., and Itoyama, Y. (2002). Silent cerebral microbleeds on T2*-weighted MRI: correlation with stroke subtype, stroke recurrence, and leukoaraiosis. *Stroke* 33, 1536–1540. doi: 10.1161/01.str.0000018012.65108.86

Koirala, A., Makkia, R. S., Conley, S. M., Cooper, M. J., and Naash, M. I. S. (2013). /MAR-containing DNA nanoparticles promote persistent RPE gene expression and improvement in RPE65-associated LCA. *Hum. Mol. Genet.* 22, 1632–1642. doi: 10.1093/hmg/ddt013

Li, C., Cheng, M., Yang, H., Peachey, N. S., and Naash, M. I. (2001). Age-related changes in the mouse outer retina. *Optom. Vis. Sci.* 78, 425–430. doi: 10.1097/00006324-200106000-00015

Liew, G., Wang, J. J., Cheung, N., Zhang, Y. P., Hsu, W., Lee, M. L., et al. (2008). The retinal vasculature as a fractal: methodology, reliability, and relationship to blood pressure. *Ophthalmology* 115, 1951.e1–1956.e1. doi: 10.1016/j.ophtha.2008.05.029

Liou, G. Y., and Storz, P. (2015). Detecting reactive oxygen species by immunohistochemistry. *Methods Mol. Biol.* 1292, 97–104. doi: 10.1007/978-1-4939-2522-3_7

Lipecz, A., Csipo, T., Tarantini, S., Hand, R. A., Ngo, B. N., Conley, S., et al. (2019). Age-related impairment of neurovascular coupling responses: a dynamic vessel analysis (DVA)-based approach to measure decreased flicker light stimulus-induced retinal arteriolar dilation in healthy older adults. *Geroscience* 41, 341–349. doi: 10.1007/s11357-019-00078-y

Liu, J. L., Grinberg, A., Westphal, H., Sauer, B., Accili, D., Karas, M., et al. (1998). Insulin-like growth factor-I affects perinatal lethality and postnatal development in a gene dosage-dependent manner: manipulation using the Cre/loxP system in transgenic mice. *Mol. Endocrinol.* 12, 1452–1462. doi: 10.1210/mend.12.9.0162

Liu, Y., Liu, Y., Li, G., Chen, Z., and Gu, G. (2018). Ghrelin protects the myocardium with hypoxia/reoxygenation treatment through upregulating the expression of growth hormone, growth hormone secretagogue receptor and insulin-like growth factor-1, and promoting the phosphorylation of protein kinase B. *Int. J. Mol. Med.* 42, 3037–3046. doi: 10.3892/ijmm.2018.3886

Lofqvist, C., Willett, K. L., Aspegren, O., Smith, A. C., Aderman, C. M., Connor, K. M., et al. (2009). Quantification and localization of the IGF/insulin system expression in retinal blood vessels and neurons during oxygen-induced retinopathy in mice. *Invest. Ophthalmol. Vis. Sci.* 50, 1831–1837. doi: 10.1167/iovs.08-2903

London, A., Benhar, I., and Schwartz, M. (2013). The retina as a window to the brain-from eye research to CNS disorders. *Nat. Rev. Neurol.* 9, 44–53. doi: 10.1038/nrneurol.2012.227

Mayhan, W. G., Faraci, F. M., Baumbach, G. L., and Heistad, D. D. (1990). Effects of aging on responses of cerebral arterioles. *Am. J. Physiol.* 258(4 Pt 2), H1138–H1143. doi: 10.1152/ajpheart.1990.258.4.H1138

McGrory, S., Ballerini, L., Doubal, F. N., Staals, J., Allerhand, M., Valdes-Hernandez, M. D. C., et al. (2019). Retinal microvasculature and cerebral small vessel disease in the Lothian Birth Cohort 1936 and Mild Stroke Study. *Sci. Rep.* 9:6320. doi: 10.1038/s41598-019-42534-x

Norling, A. M., Gerstenecker, A. T., Buford, T. W., Khan, B., Oparil, S., and Lazar, R. M. (2020). The role of exercise in the reversal of IGF-1 deficiencies in microvascular rarefaction and hypertension. *Geroscience* 42, 141–158. doi: 10.1007/s11357-019-00139-2

Nyul-Toth, A., Tarantini, S., DelFavero, J., Yan, F., Balasubramanian, P., Yabluchanskiy, A., et al. (2021). Demonstration of age-related blood-brain barrier disruption and cerebromicrovascular rarefaction in mice by longitudinal intravital two-photon microscopy and optical coherence tomography. *Am. J. Physiol. Heart Circ. Physiol.* 320, H1370–H1392. doi: 10.1152/ajpheart.00709.2020

Nyúl-Tóth, Á, Tarantini, S., Kiss, T., Toth, P., Galvan, V., Tarantini, A., et al. (2020). Increases in hypertension-induced cerebral microhemorrhages exacerbate gait dysfunction in a mouse model of Alzheimer's disease. *Geroscience* 42, 1685–1698. doi: 10.1007/s11357-020-00256-3

Oh, I. K., Huh, K., and Oh, J. (2009). Risk factors for retinal hemorrhage after photodynamic therapy in age-related macular degeneration. *Ophthalmologica* 223, 78–84. doi: 10.1159/000173715

O'Neill, R. A., Maxwell, A. P., Paterson, E. N., Kee, F., Young, I., Hogg, R. E., et al. (2021). Retinal microvascular parameters are not significantly associated with mild cognitive impairment in the Northern Ireland Cohort for the Longitudinal Study of Ageing. *BMC Neurol.* 21:112. doi: 10.1186/s12883-021-02137-4

Ong, Y. T., Hilal, S., Cheung, C. Y., Xu, X., Chen, C., Venketasubramanian, N., et al. (2014). Retinal vascular fractals and cognitive impairment. *Dement. Geriatr. Cogn. Dis. Extra* 4, 305–313. doi: 10.1159/000363286

Pang, J. J., Yang, Z., Jacoby, R. A., and Wu, S. M. (2018). Cone synapses in mammalian retinal rod bipolar cells. *J. Comp. Neurol.* 526, 1896–1909. doi: 10.1002/cne.24456

Poels, M. M., Ikram, M. A., van der Lugt, A., Hofman, A., Krestin, G. P., Breteler, M. M., et al. (2011). Incidence of cerebral microbleeds in the general population: the Rotterdam Scan Study. *Stroke* 42, 656–661. doi: 10.1161/strokeaha.110.607184

Poels, M. M., Ikram, M. A., van der Lugt, A., Hofman, A., Niessen, W. J., Krestin, G. P., et al. (2012). Cerebral microbleeds are associated with worse cognitive function: the Rotterdam Scan Study. *Neurology* 78, 326–333. doi: 10.1212/WNL.0b013e3182452928

Rodriguez-de la Rosa, L., Fernandez-Sanchez, L., Germain, F., Murillo-Cuesta, S., Varela-Nieto, I., de la Villa, P., et al. (2012). Age-related functional and structural retinal modifications in the Igf1-/- null mouse. *Neurobiol. Dis.* 46, 476–485. doi: 10.1016/j.nbd.2012.02.013

Rojek, K. O., Krzemień, J., Doleżyczek, H., Boguszewski, P. M., Kaczmarek, L., Konopka, W., et al. (2019). Amot and Yap1 regulate neuronal dendritic tree complexity and locomotor coordination in mice. *PLoS Biol.* 17:e3000253. doi: 10.1371/journal.pbio.3000253

Ruberte, J., Ayuso, E., Navarro, M., Carretero, A., Nacher, V., Haurigot, V., et al. (2004). Increased ocular levels of IGF-1 in transgenic mice lead to diabetes-like eye disease. *J. Clin. Invest.* 113, 1149–1157. doi: 10.1172/JCI19478

Samuel, M. A., Zhang, Y., Meister, M., and Sanes, J. R. (2011). Age-related alterations in neurons of the mouse retina. *J. Neurosci.* 31, 16033–16044. doi: 10.1523/JNEUROSCI.3580-11.2011

Sonntag, W. E., Deak, F., Ashpole, N., Toth, P., Csiszar, A., Freeman, W., et al. (2013). Insulin-like growth factor-1 in CNS and cerebrovascular aging. *Front. Aging Neurosci.* 5:27. doi: 10.3389/fnagi.2013.00027

Stanton, A. V., Wasan, B., Cerutti, A., Ford, S., Marsh, R., Sever, P. P., et al. (1995). Vascular network changes in the retina with age and hypertension. *J. Hypertens.* 13(12 Pt 2), 1724–1728.

Tarantini, S., Tran, C. H. T., Gordon, G. R., Ungvari, Z., and Csiszar, A. (2017b). Impaired neurovascular coupling in aging and Alzheimer's disease: contribution of astrocyte dysfunction and endothelial impairment to cognitive decline. *Exp. Gerontol.* 94, 52–58. doi: 10.1016/j.exger.2016.11.004

Tarantini, S., Valcarcel-Ares, N. M., Yabluchanskiy, A., Springo, Z., Fulop, G. A., Ashpole, N., et al. (2017c). Insulin-like growth factor 1 deficiency exacerbates hypertension-induced cerebral microhemorrhages in mice, mimicking the aging phenotype. *Aging Cell* 16, 469–479. doi: 10.1111/acel.12583

Tarantini, S., Fulop, G. A., Kiss, T., Farkas, E., Zölei-Szénási, D., Galvan, V., et al. (2017a). Demonstration of impaired neurovascular coupling responses in TG2576 mouse model of Alzheimer's disease using functional laser speckle contrast imaging. *GeroScience* 39, 465–473. doi: 10.1007/s11357-017-9980-z

Tarantini, S., Nyul-Toth, A., Yabluchanskiy, A., Csipo, T., Mukli, P., Balasubramanian, P., et al. (2021). Endothelial deficiency of insulin-like growth factor-1 receptor (IGF1R) impairs neurovascular coupling responses in mice, mimicking aspects of the brain aging phenotype. *Geroscience* 43, 2387–2394. doi: 10.1007/s11357-021-00405-2

Tarantini, S., Tucsek, Z., Valcarcel-Ares, M. N., Toth, P., Gautam, T., Giles, C. B., et al. (2016). Circulating IGF-1 deficiency exacerbates hypertension-induced microvascular rarefaction in the mouse hippocampus and retrosplenial cortex: implications for cerebromicrovascular and brain aging. *Age* 38, 273–289. doi: 10.1007/s11357-016-9931-0

Tarantini, S., Valcarcel-Ares, N. M., Yabluchanskiy, A., Fulop, G. A., Hertelendy, P., Gautam, T., et al. (2018). Treatment with the mitochondrial-targeted antioxidant peptide SS-31 rescues neurovascular coupling responses and cerebrovascular endothelial function and improves cognition in aged mice. *Aging Cell* 17:e12731. doi: 10.1111/acel.12731

Tata, M., Ruhrberg, C., and Fantin, A. (2015). Vascularisation of the central nervous system. *Mech. Dev.* 138(Pt 1), 26–36. doi: 10.1016/j.mod.2015.07.001

Toth, P., Tarantini, S., Ashpole, N. M., Tucsek, Z., Milne, G. L., Valcarcel-Ares, N. M., et al. (2015a). IGF-1 deficiency impairs neurovascular coupling in mice: implications for cerebromicrovascular aging. *Aging Cell* 14, 1034–1044. doi: 10.1111/acel.12372

Toth, P., Tarantini, S., Springo, Z., Tucsek, Z., Gautam, T., Giles, C. B., et al. (2015b). Aging exacerbates hypertension-induced cerebral microhemorrhages in mice: role of resveratrol treatment in vasoprotection. *Aging Cell* 14, 400–408. doi: 10.1111/acel.12315

Toth, P., Tarantini, S., Csiszar, A., and Ungvari, Z. (2017). Functional vascular contributions to cognitive impairment and dementia: mechanisms and consequences of cerebral autoregulatory dysfunction, endothelial impairment, and neurovascular uncoupling in aging. *Am. J. Physiol. Heart Circ. Physiol.* 312, H1–H20. doi: 10.1152/ajpheart.00581.2016

Toth, P., Tucsek, Z., Sosnowska, D., Gautam, T., Mitschelen, M., Tarantini, S., et al. (2013). Age-related autoregulatory dysfunction and cerebromicrovascular injury in mice with angiotensin II-induced hypertension. *J. Cereb. Blood Flow Metab.* 33, 1732–1742. doi: 10.1038/jcbfm.2013.143

Toth, P., Tucsek, Z., Tarantini, S., Sosnowska, D., Gautam, T., Mitschelen, M., et al. (2014). IGF-1 deficiency impairs cerebral myogenic autoregulation in hypertensive mice. *J. Cereb. Blood Flow Metab.* 34, 1887–1897. doi: 10.1038/jcbfm.2014.156

Ungvari, Z., and Csiszar, A. (2012). The emerging role of IGF-1 deficiency in cardiovascular aging: recent advances. *J. Gerontol. A Biol. Sci. Med. Sci.* 67, 599–610. doi: 10.1093/gerona/gls072

Ungvari, Z., Tarantini, S., Kirkpatrick, A. C., Csiszar, A., and Prodan, C. I. (2017). Cerebral microhemorrhages: mechanisms, consequences, and prevention. *Am. J. Physiol. Heart Circ. Physiol.* 312, H1128–H1143. doi: 10.1152/ajpheart.00780.2016

Verheggen, I. C. M., de Jong, J. J. A., van Boxtel, M. P. J., Gronenschild, E., Palm, W. M., Postma, A. A., et al. (2020). Increase in blood-brain barrier leakage in healthy, older adults. *Geroscience* 42, 1183–1193. doi: 10.1007/s11357-020-00211-2

Vernooij, M. W., van der Lugt, A., Ikram, M. A., Wielopolski, P. A., Niessen, W. J., Hofman, A., et al. (2008). Prevalence and risk factors of cerebral microbleeds: the Rotterdam Scan Study. *Neurology* 70, 1208–1214. doi: 10.1212/01.wnl.0000307750.41970.d9

Villacampa, P., Ribera, A., Motas, S., Ramírez, L., García, M., de la Villa, P., et al. (2013). Insulin-like growth factor I (IGF-I)-induced chronic gliosis and retinal stress lead to neurodegeneration in a mouse model of retinopathy. *J. Biol. Chem.* 288, 17631–17642. doi: 10.1074/jbc.M113.468819

Wang, T. W., Stromberg, G. P., Whitney, J. T., Brower, N. W., Klymkowsky, M. W., and Parent, J. M. (2006). Sox3 expression identifies neural progenitors in persistent neonatal and adult mouse forebrain germinative zones. *J. Comp. Neurol.* 497, 88–100. doi: 10.1002/cne.20984

Wong, T. Y., Klein, R., Couper, D. J., Cooper, L. S., Shahar, E., Hubbard, L. D., et al. (2001a). Retinal microvascular abnormalities and incident stroke: the Atherosclerosis Risk in Communities Study. *Lancet* 358, 1134–1140. doi: 10.1016/s0140-6736(01)06253-5

Wong, T. Y., Klein, R., Klein, B. E., Tielsch, J. M., Hubbard, L., and Nieto, F. J. (2001b). Retinal microvascular abnormalities and their relationship with hypertension, cardiovascular disease, and mortality. *Surv. Ophthalmol.* 46, 59–80. doi: 10.1016/s0039-6257(01)00234-x

Yabluchanskiy, A., Tarantini, S., Balasubramanian, P., Kiss, T., Csipo, T., Fülöp, G. A., et al. (2020). Pharmacological or genetic depletion of senescent astrocytes prevents whole brain irradiation-induced impairment of neurovascular coupling responses protecting cognitive function in mice. *GeroScience* 42, 409–428. doi: 10.1007/s11357-020-00154-8

Zhao, Y., Yang, B., Xu, A. D., Ruan, Y. W., Xu, Y., Hu, H. L., et al. (2020). Retinal Microvascular Changes in Subtypes of Ischemic Stroke. *Front. Neurol.* 11:619554. doi: 10.3389/fneur.2020.619554

Zlokovic, B. V. (2011). Neurovascular pathways to neurodegeneration in Alzheimer's disease and other disorders. *Nat. Rev. Neurosci.* 12, 723–738. doi: 10.1038/nrn3114

Zygar, C. A., Colbert, S., Yang, D., and Fernald, R. D. (2005). IGF-1 produced by cone photoreceptors regulates rod progenitor proliferation in the teleost retina. *Brain Res. Dev. Brain Res.* 154, 91–100. doi: 10.1016/j.devbrainres.2004.10.009

Conflict of Interest: The authors declare that the research was conducted in the absence of any commercial or financial relationships that could be construed as a potential conflict of interest.

Publisher's Note: All claims expressed in this article are solely those of the authors and do not necessarily represent those of their affiliated organizations, or those of the publisher, the editors and the reviewers. Any product that may be evaluated in this article, or claim that may be made by its manufacturer, is not guaranteed or endorsed by the publisher.

frontiers | Frontiers in Public Health

ORIGINAL RESEARCH
published: 13 April 2022
doi: 10.3389/fpubh.2022.772592

A Transfer Learning Method for Detecting Alzheimer's Disease Based on Speech and Natural Language Processing

Ning Liu[1,2], *Kexue Luo*[3], *Zhenming Yuan*[4] *and Yan Chen*[5]*

[1] School of Public Health, Hangzhou Normal University, Hangzhou, China, [2] Department of Mathematics and Computer Science, Fujian Provincial Key Laboratory of Data-Intensive Computing, Quanzhou Normal University, Quanzhou, China, [3] Tongde Hospital of Zhejiang Province Geriatrics, Hangzhou, China, [4] School of Information Science and Technology, Hangzhou Normal University, Hangzhou, China, [5] International Unresponsive Wakefulness Syndrome and Consciousness Science Institute, Hangzhou Normal University, Hangzhou, China

OPEN ACCESS

Edited by:
Nicola Vanacore,
National Institute of Health (ISS), Italy

Reviewed by:
P. M. Durai Raj Vincent,
VIT University, India
Saturnino Luz,
University of Edinburgh,
United Kingdom
Yongzhao Du,
Huaqiao University, China

***Correspondence:**
Yan Chen
chen_yan@hznu.edu.cn

Specialty section:
This article was submitted to Aging and Public Health, a section of the journal Frontiers in Public Health

Received: 08 September 2021
Accepted: 24 February 2022
Published: 13 April 2022

Citation:
Liu N, Luo K, Yuan Z and Chen Y (2022) A Transfer Learning Method for Detecting Alzheimer's Disease Based on Speech and Natural Language Processing. Front. Public Health 10:772592. doi: 10.3389/fpubh.2022.772592

Alzheimer's disease (AD) is a neurodegenerative disease that is difficult to be detected using convenient and reliable methods. The language change in patients with AD is an important signal of their cognitive status, which potentially helps in early diagnosis. In this study, we developed a transfer learning model based on speech and natural language processing (NLP) technology for the early diagnosis of AD. The lack of large datasets limits the use of complex neural network models without feature engineering, while transfer learning can effectively solve this problem. The transfer learning model is firstly pre-trained on large text datasets to get the pre-trained language model, and then, based on such a model, an AD classification model is performed on small training sets. Concretely, a distilled bidirectional encoder representation (distilBert) embedding, combined with a logistic regression classifier, is used to distinguish AD from normal controls. The model experiment was evaluated on Alzheimer's dementia recognition through spontaneous speech datasets in 2020, including the balanced 78 healthy controls (HC) and 78 patients with AD. The accuracy of the proposed model is 0.88, which is almost equivalent to the champion score in the challenge and a considerable improvement over the baseline of 75% established by organizers of the challenge. As a result, the transfer learning method in this study improves AD prediction, which does not only reduces the need for feature engineering but also addresses the lack of sufficiently large datasets.

Keywords: transfer learning, Alzheimer's disease, natural language processing, BERT, machine learning

INTRODUCTION

Alzheimer's disease (AD) is a neurodegenerative and progressive disease that cannot be cured effectively (1). Mild cognitive impairment (MCI) is the early stage of AD. The study by the Lancet Public Health in 2020 found that the prevalence of dementia in people over 60 years old in China accounted for 6.04% of the population (approximately 1,507 ten thousand), and the number was 15.54% (3,877 ten thousand) for MCI cases (2). An epidemiological survey also found that a person's cost with AD in China was approximately $19,144.36 in 2015, while the total cost of the world's average level was $167,740 million, which was composed of $54,530 million (32.51%) direct medical cost, $26,200 million (15.62%) direct non-medical cost, and $87,010 billion (51.87%) indirect cost (3).

In the past 20 years, scholars have reported extensive studies on the relationship between the pathogenesis of AD and language fluency (4). They generally believed that mild word naming, retelling, hearing, understanding, and writing disorders already exist in the early stages of AD. One of the early signs of AD is an obvious decline in linguistic comprehension and expression form (5), and the linguistic manifestation of patients with AD usually includes the following:

1) Patients with AD talk less than ever before and are often silent, as they frequently forget the words they have just spoken, and have difficulty continuing with the topic that has just been discussed.
2) Sometimes, they are difficult to be understood with incoherent and repeated utterances.
3) They often call something the wrong name, for example, "watch" is regarded as "the clock on the wrist."

New studies have found that before the onset of AD, the β-amyloid has already gathered in the brain about 5 to 10 and even 20 years ago. If AD can be diagnosed at an early stage (6), a series of behavioral therapies can be prescribed to slow the progress of the disease. However, an AD diagnosis is challenging in clinical medicine because of the subtle differences between patients with AD and healthy individuals in terms of brain structure and behavior. At present, some medical diagnosis methods, such as pathological examination, MRI, PET, and reliable biomarkers (e.g., amyloid ligand imaging and cerebrospinal fluid testing), are usually used. However, these diagnosis methods cannot be widely popularized because of their high cost and invasive nature. Therefore, there is an urgent need to develop a convenient, inexpensive, and non-invasive AD diagnostic approach by AI technologies, such as speech processing and NLP. In contrast to earlier studies with manual expert-wise feature extraction in this field, this study used a reliable deep learning model to automatically find suspicious AD symptom features from speeches. Specifically, a pre-trained distilBert language model (7) was used as a feature extractor to obtain the features of the input sentence or document, and a simple logistic regression classifier, which has a good effect on binary classification, was used to classify AD from normal controls. Owing to its strong deep semantic feature extraction competency and an accurate binary classifier, this combination can effectively improve the classification effect. In addition, a grid search strategy (8) was used to tune the parameters to obtain the best parameters of the model. The results show that this method worked better on ADReSS datasets (9) in 2020, with an accuracy of 0.88, which was significantly higher than the baseline and almost equivalent to the best performance on the challenge (10).

The main contributions of this study are as follows:

1) A simple and effective model of AD diagnosis based on transcripts without complicated expertise is designed and implemented effectively.
2) A novel model architecture that combines deep learning with machine learning is proposed, and the best performance on the ADReSS dataset is obtained.
3) Our proposed approach has the advantages of reliability, low cost, and convenience and can provide a feasible solution for the screening of AD.

RELATED WORKS

Different technologies can be used to detect AD, such as molecular biomarkers combined with deep learning on gene expression datasets (11). However, we used transcripts combined with deep learning on speech datasets instead. Two approaches are mainly used in this field: machine learning with manual feature extraction based on expert knowledge and deep learning. Traditional machine learning algorithms have been widely studied with handcrafted features to predict AD. However, they have the disadvantage of lacking integrity, demanding good expertise, low accuracy, and poor portability. Moreover, these methods are generally applicable to a specific task scene. Once the scene changes, these manually designed features, and prior settings cannot be adapted to new scenes and need to be redesigned again; therefore, the portability of the model is not better overall. With the arrival of the deep learning paradigm, it has already become possible to extract high-level abstract features directly from transcripts that describe the distribution of datasets in low-dimensional manifolds internally. The advantage is that it can either extract input dataset patterns directly for both regression tasks or combine handcrafted features to the feature map of the input dataset without the certified professionals from the data source. Because language functions play an important role in the detection of cognitive deficits at different stages, the combination of NLP technology and deep learning provides an accurate and convenient solution for the detection of AD and MCI (12). In this study, a distilBERT model, which is a multi-layer perceptron with a self-attention mechanism, is used to extract deep semantic features; they are then passed through a strong binary classifier to recognize AD. The number of hidden layers is larger than that of traditional machine learning algorithms, thus, the model has a stronger semantic abstraction ability and classification performance, and the scalability is superior to traditional machine learning methods. Although the deep learning method does not need to extract features manually, it does not mean that we do not need to analyze manual features anymore, and the single deep learning model for diagnosing AD may perform better. Therefore, combining

it with some conspicuous markers and a stronger classifier may improve the classification results, which we will discuss in the discussion section.

Several studies have investigated language and speech features for AD diagnosis (13) and proposed many signal processing and machine learning algorithms to detect AD and MCI (14). However, in this field, there are still lacking benchmark datasets against which different methods can be systematically compared. The ADReSS Challenge (9), a subset of the DementiaBank dataset (15), uses a balanced dataset of AD and healthy controls to recognize the disease. Manual feature extraction methods have a better interpretation for classification tasks, although there are unremarkable results. As a basic study on the ADReSS dataset, Luz et al. (9) used 34 linguistic features, such as total utterances, a type-token ratio, percentages of parts of speech, duration, MLU, and a word ratio, combined with linear discriminant analysis, and obtained the best accuracy of 0.75 on the test dataset. Acoustic features, such as emobase (16), the extended Geneva minimalistic acoustic parameter set (eGeMAPS) (17), minimal features (18), Computational Paralinguistics ChallengE (ComParE), (19), and multi-resolution cochleagram (MRCG) (20), only obtained an accuracy of approximately 0.5 on the classifiers used frequently. Balagopalan et al. (21) used two approaches for the binary classification of AD and normal controls, i.e., acoustic and text-based feature extraction and the bidirectional encoder representation (BERT) model. Finally, the BERT model obtained the best accuracy of 0.8332, which was better than that of the manual feature extraction method. Syed et al. (22) and Yuan et al. (23) achieved accuracies of 85.45 and 89.6% using acoustic and linguistic features, respectively. Syed et al. (22) used acoustic features, such as bag-of-acoustic-words and INTERSPEECH 2010 Paralinguistic Challenge feature sets [a low-dimensional version of ComParE (19)], and obtained an accuracy of 76.85%. Luz et al. (24) used a combination of phonetic and linguistic features without human intervention and obtained an accuracy of 78.87%. Most of these earlier studies were based on features designed by experts and were unable to learn more informative and discriminative features, so a relatively poor performance was obtained.

The latest deep-learning methods, such as convolutional neural networks (CNN), recurrent neural networks (RNN), and BERT, can achieve good performances by automatically extracting high-level features. Mahajan et al. (25) used part-of-speech (POS) tags and word embeddings (GloVe) as inputs on a CNN-long short-term memory (LSTM) model (26) and obtained the best accuracy of 0.6875. Then, they replaced unidirectional LSTM with bidirectional LSTM layers (27) and obtained the best accuracy of 0.7292. Orimaye et al. (28) used a deep neural network to predict MCI in speech. Different from our datasets, they used part of the Pitt corpus of the DementiaBank dataset, comprising 19 controls and 19 MCI transcripts. Fritsch et al. (29) enhanced *n*-gram language models to create neural network models with LSTM cells, and an accuracy of 85.6% was obtained to classify HCs and AD on the Pitt dataset. Pan et al. (30) used a glove word embedding sequence as the input, combined with gated recurrent unit layers and a stacked bidirectional LSTM to diagnose AD on the Pitt dataset. These models differ from our model because we used deep learning and machine learning classifiers instead. Similar to our method, the study (31) demonstrated that the combination of $BERT_{Large}$ and logistic regression had the best performance in the classification problem. Different from our study, they used the Pitt DementiaBank dataset and data augmentation technology to enhance the classification performance and obtained a state-of-the-art (SOTA) accuracy of 88.08%.

Other tasks, except for the picture description task, can also be used to recognize AD. For example, Clarke et al. (32) used five different tasks to recognize AD, namely, conversation, procedural recall, picture description, narrative recall, and novel narrative retelling and obtained the best accuracy of 90% for AD vs. HC with linguistic features, combined with the support vector machine (SVM) model. In addition, many studies have used multimodal datasets to detect AD and MCI, and more accurate and differentiated information may be obtained from different models. Looze et al. (33) combined conversational features, neuropsychological testing, and structural MRI to explore temporal features, and a linear mixed model was used to diagnose AD, which differs from our corpus. They also found that slow turn-taking and slow speech are two useful factors for the early detection of cognitive decline. Martinc et al. (34) also used a multimodal approach to detect AD on the ADReSS dataset, using an active data representation approach (13), combining linguistic, acoustic, and temporal features and obtaining an accuracy of 93.75%. Jonell et al. (35) recorded participants' language, speech, motor signs, pupil dilation, thermal emission, facial gestures, gaze, and heart rate variability of 25 patients with AD and found that multi-modality improved clinical discrimination. Recently, the transfer learning model has been widely used to diagnose AD. For example, Laguarta et al. (36) presented an approach with multiple biomarkers, including sentiment, lung and respiratory tract, and vocal cords. They used the transfer learning model to learn the features from audio datasets and obtained an accuracy of 93% on the ADReSS datasets. Zhu et al. (37) used the transfer learning on the BERT model to detect AD with speech and text, achieving an accuracy of 89.58%. They also found that the text model was more discriminative than the speech model. Overall, strong representation learning ability and discriminative classifiers, multimodal information, and transfer learning are all effective factors in the accurate diagnosis of AD and MCI.

METHODS

Transfer Learning

One of the challenges in AD prediction research is the lack of training data, which is important for a better understanding of language models with semantic and syntactic structures when they are implemented. Transferring knowledge from one model to another is called transfer learning, which is learning information from pre-trained datasets and then converting it into weights to transfer to another neural network. Therefore, we need not to train a neural network from scratch. It eliminates the need for target-specific large datasets using a model that learns a probable distribution for classification. The general flow

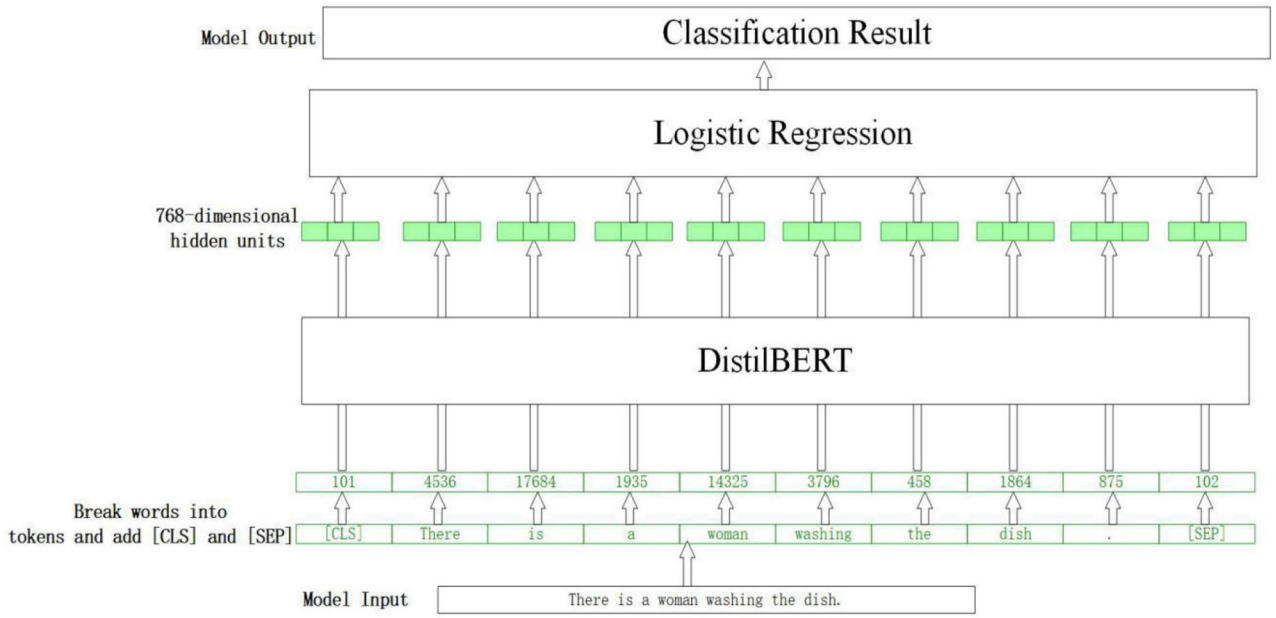

FIGURE 1 | The logical architecture of the model.

FIGURE 2 | A picture of a Boston Cookie-Theft description task.

of using a pre-trained model for classification consists of the following steps:

(1) Training a general language model on a large dataset.
(2) Fine-tuning a pre-trained language model on the target dataset.
(3) Using a target-specific pre-trained language model for classification.

In this paper, we argue that the attention mechanism allows the model to focus on some parts of the transcripts for decision-making, which is suitable for AD diagnosis because it can capture specific markers related to AD. We used a pre-trained BERT model for text embedding, which converts original sentences or transcripts to 768-dimensional vectors. In the next part, we will describe the architecture of our model.

Overall Classification Framework

The entire model architecture in this study mainly consists of two sections: the distilBert model (7) and the logistic regression classifier. The features transferred between the two models are 768-dimensional vectors, which are also embeddings for sentence classification.

Although BERT has become popular recently because of its excellent performance, the running speed with a hundred million parameters is a huge challenge for our computer system. Accordingly, we chose distilBert (7) developed by the team of Hugging Face, as an embedding feature extractor. It distills the BERT base from 12 layers to 6 layers and removes token-type embeddings and poolers. It can reach 60% of the faster speed and 40% smaller architecture but retains 97% language understanding capability of the BERT model (7). In this study, the distilBert model is used to extract deep semantic features, which are then passed to a logistic regression model to classify sentences. Specifically, the pretrained distilBert model is used as the feature extractor, the output layer of which is replaced by a logistic regression classifier for binary classification. The logical architecture of the model is shown in **Figure 1**. The embedding layer is a sentence or an entire transcript with a high-dimensional representation vector, and the classifier layer predicts the label of every embedded input. The main processes are as follows: Firstly, the words are divided into tokens using the distilBert tokenizer, and some special words are added to the text [i.e., (CLS) before the sentence and (SEP) at the end]. Then, the vocabulary table is searched from the pre-trained model to replace the tokens with

Algorithm 1 | The process of our algorithm description.

1: Input: Dataset $D = \{(x_i, y_i)\}_{i=1}^{N}$; x_i is the input sentence; y_i is the corresponding label.

2: The load pre-trained model tokenizes a sentence by splitting the sentence into words or subwords and then pads all lists to the same size.

3: Use the distilBert model to train the dataset to obtain the embedding vector.

4: Put the embedding vector into the logistic regression model to classify the dataset.

5: Model evaluation.

the corresponding numbers taken into the DistilBert model and a 768-dimensional output vector is obtained. Finally, this vector is inputted into a logistic regression classifier, and the final binary classification result is obtained. The algorithm description of the entire process is presented below.

DistilBert can capture long-distance dependencies by learning the global semantic message of input text thoroughly because it has some mechanisms, such as a multi-head self-attention and location code. It has excellent competence in feature extraction and semantic abstraction. The process is repeated six times and a 768-dimensional semantic feature vector is obtained, which is then input into a logistic regression model to get the final classification result. The transcripts in this study are a section of the description on a picture, the maximum length of which is no more than 500, so the length of word embedding is set as 500, considering speed and semantic completion.

Grid Search

Grid search is a simple and widely used hyperparametric search algorithm fit for small datasets and can obtain the optimal value by searching all the points in the range. In this study, the GridSearchCV function in the scikit-learn tool, including grid search and cross-validation, is used to search for the best parameters of the logistic regression model. The grid search adjusts the parameters in sequence within a specified parameter range and then trains the model by using the adjusted parameters with the best performance in the validation set. The last score is the average of the *k*-fold cross-verification scores in the test set. Considering speed and accuracy, the search scope of the GridSearchCV function ranges from 0.0001 to 100, and the step is set as 20.

EXPERIMENTS

ADReSS Datasets

The study is a picture description task from the Diagnostic Aphasia Examination (38), and participants are asked to describe a picture (**Figure 2**) as detailed as possible. The datasets (9), including full-wave audio and corresponding transcripts with 78 AD and 78 normal controls, are divided into 108 training sets and 48 test sets by challenge, which has a balanced distribution for classes, gender, and age. An example of a transcript from the dataset is shown below.

A boy and a girl are in a kitchen with their mothers. The little boy is getting a cookie for the little girl, but he is on a stool and is about to fall. The mother is washing dishes. She is obviously thinking of something else because the water pours out over the sink. She finished with some dishes. It seems to be summer because there are bushes. The window is open. There seems to be some kind of breeze because the curtains on the sill there blow. It must be fairly hot. The mother is in a sleeveless dress. The children are in short sleeve tops and have sandals. The little boy has tennis shoes. The mother obviously is unaware of what the children are doing. She will be aware of this shortly. How much more do you want to do?

The age distribution of the two groups at different intervals is presented in **Table 1**. The average values and standard deviations of age and mini-mental state examination (MMSE) scores are shown in **Table 2**.

Experiment Results

The experiment in this study was performed using the Windows 10 operating system. The computer was equipped with an Intel (R) Core I i5-6500 CPU @3.20 GHz, 3.19 GHz CPU, and 44. GB RAM. Library scikit learn was used to visit logistic regression, NumPy, and Pandas' libraries, and Python 3.6.13 was used as the programming language.

The experiment used the accuracy, precision, recall, and F1-score as indices to evaluate the performance of the model. **Table 3** lists the relationship between the predicted and true classes. TP is a sample predicted to be positive. TN is a negative sample that is predicted to be negative. FP is a negative sample that is predicted to be positive. FN is a positive sample that is predicted to be negative. The formula for the metric index is as follows:

$$Accuracy = \frac{TN + TP}{TN + FP + FN + TP} \tag{1}$$

$$Precision = \frac{TN}{TN + FP} \tag{2}$$

$$Recall = \frac{TP}{TP + FN} \tag{3}$$

$$F1 - Score = \frac{2TP}{2TP + FP + FN} \tag{4}$$

The parameters of the distilBert model are presented in **Table 4**. The champion of the ADReSS challenge obtained an accuracy of 0.896 by combining the Enhanced Language Representation with Informative Entities (ERNIE) model (39) and pause information in speech using acoustic align technology (10). We achieved 88% accuracy on the test set, which is almost equivalent to the SOTA result, and a 13% improvement over the baseline of 75%, established by the organizers of ADReSS (9). The champion used two models, acoustic and text, and combined the ERNIE model with discriminated markers to improve representation learning. We modified the

TABLE 1 | The basic composition of the participants in every group.

	AD (*N* = 78)		Non-AD (*N* = 78)	
Age interval	**Male**	**Female**	**Male**	**Female**
50,55	2	0	2	0
55,60	7	6	7	6
60,65	4	9	4	9
65,70	9	14	9	14
70,75	9	11	9	11
75,80	4	3	4	3
Total	35	43	35	43

TABLE 2 | The average and SD of age and MMSE.

	Non-AD (*N* = 78)		AD (*N* = 78)	
Measure	**AVG**	**SD**	**AVG**	**SD**
Age	66.56	6.60	66.79	6.83
MMSE	29.01	1.16	17.79	5.48

TABLE 3 | Relationship between predicted class and true class.

	True class	
Predicted class	**Positive**	**Negative**
Positive	True positive(TP)	False positive (FP)
Negative	False negative(FN)	True negative (TN)

TABLE 4 | Parameters of the distilBert model.

Parameters	**Value**
Epoch	1
DistilBatch_size	156
Pad_size	500
Pre-trained model	distilBert-base-uncased
Hidden_size	768

model architecture of the distilBert model to achieve a strong classification performance using only text.

We used the popular models of BERT and ERNIE (39) for comparison. To check the influence of different classifiers with the DistilBert model, the CNN, random forest, SVM, and AdaBoost classifiers were also used for comparison with our logistic regression (LR) classifier. **Table 5** shows that the LR classifier obtains the best performance. The LR is one of the simplest classifiers with a good performance in binary classification and has become a prior selection classifier in clinical diagnosis. For example, a study (31) demonstrated the superiority of the combination of BERT and LR models in the classification problem.

TABLE 5 | The performance of different models.

Model	**Accuracy**	**Precision**	**Recall**	**F1-score**
Linear discriminant analysis (9)	0.625	0.60	0.75	0.67
DistilBert	0.48	0.51	0.48	0.48
ERNIE (39)	0.42	0.46	0.42	0.30
DistilBert +CNN	0.58	0.34	0.58	0.43
DistilBert+RF	0.79	0.79	0.79	0.79
DistilBert+SVM	0.625	0.629	0.625	0.622
DistilBert+Ada	0.73	0.73	0.73	0.73
ERNIE+Pause (10)*	**0.896**	**0.952**	0.833	**0.889**
DistilBert+ LR	0.88	0.88	**0.88**	0.87

**ERNIE+Pause (10) is the model of a champion, distilBert +LR is our method, RF and Ada are the abbreviations of random forest and adaboost classifier, respectively. The best performance in a column of measure.*

DISCUSSION

Pre-trained models are considered important and effective nowadays because they attempt to learn the features and structure of the language from large datasets and regulate the model effectively to perform best on new datasets by only updating a few parameters. Accordingly, our model was highly trained with the best initial parameters. The best performance indicates that our model has learned useful features for classification, which not only reduces the need for expert-defined linguistic features but also makes it possible for accurate, complex, and comprehensive features to be extracted from the dataset. The advantage of sentence embedding is that it considers the entire transcript and does not have any out-of-context word embedding layer, which converts every word into a vector representation, considering its context. The ADReSS challenge also includes MMSE evaluation, a detailed interactive exam to evaluate cognitive skills, including memory, language, delayed recall, and visuospatial. However, whether our model is suitable for the evaluation of MMSE scores needs to be further verified. In addition, the transcripts were annotated in CHAT format (40), which is convenient for manual feature extraction. We performed the experiment with and without annotation and found that the performance did not differ. Using automatic speech recognition (ASR)-generated transcripts directly without the need for further annotation, our method has more advantages than the manual feature extraction method.

Many studies have demonstrated that manual features, combined with the deep learning model, can improve the performance of the model, and manual features also provide a better interpretation, which is important for clinical diagnosis. For example, Looze CD et al. (33) found that the temporal characteristics of speech may reflect underlying cognitive deficits. Nasreen et al. (32) used linguistic features, such as pauses, overlaps, and dysfluencies, to detect AD on the ADReSS dataset. They obtained 90% accuracy and demonstrated the importance of dysfluency and pauses in detecting AD. The champion of the ADReSS challenge (10) combined deep learning with pauses and obtained SOTA accuracy of 89.6%, proving that pauses are important for AD diagnosis. Sadeghian et al. (41) extracted

acoustic features, including pauses more than 5 s in duration, and obtained the best accuracy of 95.8%. Features, such as pauses, are important features that deep learning cannot learn effectively (i.e., cannot give enough weight for pauses), so the combination of both can improve the performance of AD detection. In clinical medicine, patients with AD often pause and cannot continue treatment. This is not only a memory decline problem but may also be related to some language function obstacles caused by brain damage. A successful computer model can guide doctors to focus more on the early clinical symptoms of patients with AD, such as pauses and dysfluency. The largest limitation of our study is the difficulty to interpret the performance of a model with so many parameters (42). That is, our model cannot understand the reason for a wrong verdict, but we can identify the words that the network has paid more attention to in the case of a correct prediction. This function is particularly useful because such an interpretation can reveal the important linguistic attributes of patients with AD, which can help in speech therapy and communication with patients with AD.

The practice of pre-trained and fine-tuning paradigms has achieved excellent performance in many downstream tasks. In recent years, research in academia and industry has indicated that the pre-trained model is developing in a larger and deeper direction. However, there are still some problems that need to be solved in large models, such as the dataset quality, huge training energy consumption, carbon emission problems, and a lack of common sense and reasoning ability. These problems should be addressed in future studies.

FUTURE WORKS

In the future, we will focus on the following two directions for AD diagnosis.

Implicit sentiment analysis is an expression that does not contain any polarity markers but can still convey a clear human awareness sentiment polarity in the context; it exists widely in the recognition of aspect-based sentiments (43). For example, the comment "The waiter poured water on my clothes and walked away" contains no opinion words but can be interpreted as clearly negative toward "the waiter"; some sentences, such as "the service of the hotel is great," "the food of the restaurant is delicious," contain obvious sentimental words that neural network can give enough weights for the words of "great," "delicious," but the non-sentiment-related aspects of such words are often ignored by the model. The transcripts used for the AD diagnosis of spontaneous speech contain no polarity markers; however, most previous studies in this field generally pay little attention to implicit sentiment expressions. The study (44) used supervised contrastive learning to capture implicit sentiment using an advanced method. That is, the expressions with the same sentiment polarity were pulled together, and those with different sentiment orientations were pushed apart. In the future, we will focus on implicit sentiment analysis for AD diagnosis using a contrastive learning method.

One of the most popular language models is the multilingual one. With a proper multilingual model, the problem of lacking large datasets can be addressed by transferring the knowledge of AD prediction from another language in which a large dataset is available, which is similar to the approaches proposed by Fraser et al. (45). Only in this manner can the need for a target task be addressed for expert-defined linguistic features. In the future, we will commit to improving multilingual AD recognition using cross-lingual transfer learning, including the multilingual BERT and transformer models.

DATA AVAILABILITY STATEMENT

The datasets presented in this study can be found in online repositories. The names of the repository/repositories and accession number(s) can be found in the article/supplementary material.

ETHICS STATEMENT

Written informed consent was obtained from the individual(s) for the publication of any potentially identifiable images or data included in this article.

AUTHOR CONTRIBUTIONS

ZY designed the research. KL analyzed the data and interpreted the analysis. NL and YC wrote the main manuscript text and revised it carefully. All authors reviewed and approved the final manuscript.

FUNDING

This research was funded by Natural Science Foundation of Zhejiang Province (Grant Number LQ22H090002), the initial fee for introducing doctoral research of Natural Science Foundation of Zhejiang Provincial (Grant Number LGF20F020009) and the 4th Graduate Student innovation and Entrepreneurship Competition of Hangzhou Normal University.

REFERENCES

1. Sousa RM, Ferri CP, Acosta D, Albanese E, Guerra M, Huang YQ, et al. Contribution of chronic diseases to disability in elderly people in countries with low and middle incomes: a 10/66 Dementia Research Group population-based survey. *Lancet.* (2009) 374:1821–30. doi: 10.1016/S0140-6736(09)61829-8
2. Jia LF, Du Y, Chu L, Zhang Z, Qiu Q. Prevalence, risk factors, and management of dementia and mild cognitive impairment in adults aged 60 years or older in China: a cross-sectional study. *Lancet Public Health.* (2020) 5:e661–71. doi: 10.1016/S2468-2667(20)30185-7
3. Jia JP, Wei C, Chen S, Li F, Gauthier S. The cost of Alzheimer's disease in China and re-estimation of costs worldwide. *Alzheimer's Dementia.* (2018) 14:483–91. doi: 10.1016/j.jalz.2017.12.006

4. Appell J, Kertesz A, Fisman M. A study of language functioning in Alzheimer patients. *Brain Lang.* (1982) 17:73–91. doi: 10.1016/0093-934X(82)90006-2
5. Wang J, Wang YH. A neuropsychological study of linguistic disorder in Alzheimer's disease. *Chin Mental Health J.* (1999) 5: 263–5.
6. Sperling RA, Aisen PS, Beckett LA, Bennett DA, Craft S, Fagan AM, et al. Toward defining the preclinical stages of Alzheimer's disease: recommendations from the National Institute on Aging-Alzheimer's Association workgroups on diagnostic guidelines for Alzheimer's disease. *Alzheimers Dement.* (2011) 7:280–92. doi: 10.1016/j.jalz.2011.03.003
7. Sanh V, Debut L, Chaumond J, Wolf T. DistilBERT, a distilled version of BERT: Smaller, faster, cheaper and lighter. *arXiv preprint arXiv:1910.01108.* (2019) Available online at: https://github.com/saurabhkulkarni77/DistillBERT.
8. Rtayli N, Enneya N. Enhanced credit card fraud detection based on SVM-recursive feature elimination and hyper-parameters optimization. *J Inf Secur Appl.* (2020) 55:102596. doi: 10.1016/j.jisa.2020.102596
9. Luz S, Haider F, Fuente SDL,Fromm D, Macwhinney B. Alzheimer's dementia recognition through spontaneous speech: the address challenge. *arXiv preprint arXiv:2004.06833.* (2020) p. 2571. doi: 10.21437/Interspeech.2020-2571
10. Yuan J, Cai X, Bian Y, Ye Z, Church K. Pauses for detection of Alzheimer's disease. *Front Comput Sci.* (2021) 2:57. doi: 10.3389/fcomp.2020.624488
11. Mahendran N, Vincent PMDR, Srinivasan K, Chang CY. Improving the classification of alzheimer's disease using hybrid gene selection pipeline and deep learning. *Front Genet.* (2021) 12:784814. doi: 10.3389/fgene.2021.784814
12. Pulido MLB. Hern'andez JBA, Ballester MAF, Gonz'alez C, Mekyska J, Sm'ekal Z, Alzheimer'sdisease and automatic speech analysis: a review. *Expert Syst Appl.* (2020) 150:113213. doi: 10.1016/j.eswa.2020.113213
13. Saturnino L, Fasih H, Sofia DLFG, Davida F, Brian MW. Editorial: Alzheimer's dementia recognition through spontaneous speech. *Front Comput Sci.* (2021) 3:1–5. doi: 10.3389/fcomp.2021.780169
14. Petti U, Baker S, Korhonen A, A. systematic literature review of automatic Alzheimer's disease detection from speech and language. *J Am Med Inform Assoc.* (2020) 27:1784–97. doi: 10.1093/jamia/ocaa174
15. Becker JT, Boiler F, Lopez OL, Saxton J, Mcgonigle KL. The natural history of Alzheimer's disease: description of study cohort and accuracy of diagnosis. *Arch Neurol.* (1994) 51:585–94. doi: 10.1001/archneur.1994.00540180063015
16. Eyben F, Wöllmer M, Schuller B. Opensmile: the munich versatile and fast open-source audio feature extractor. In: *Proceedings of the 18th ACM international conference on Multimedia.* (2010) p. 1459–62. doi: 10.1145/1873951.1874246
17. Eyben F, Scherer KR, Schuller BW, Sundberg J, Andr'e E, Busso C, et al. The Geneva minimalistic acoustic parameter set GeMAPS for voice research and affective computing. *IEEE Trans Affect Comput.* (2015) 7:190–202. doi: 10.1109/TAFFC.2015.2457417
18. Luz S. Longitudinal monitoring and detection of Alzheimer's type dementia fromspontaneous speech data. In: *2017 IEEE 30th International Symposium on Computer-Based Medical Systems (CBMS).* (2017) p. 45–46. doi: 10.1109/CBMS.2017.41
19. Eyben F,Weninger F, Groß F, Schuller B. Recent developments in openSMILE, the Munich open-source multimedia feature extractor. In: *Proceedings of the 21st ACM international conference on Multimedia.* (2013). p. 835–8. doi: 10.1145/2502081.2502224
20. Chen J, Wang Y, Wang D. A feature study for classification-based speech separation at low signal-to-noise ratios. In: *IEEE/ACM Transactions on Audio Speech & Language Processing.* (2014) vol. 22. p. 1993–2002. doi: 10.1109/TASLP.2014.2359159
21. Balagopalan A, Eyre B, Robin J,Rudzicz F, Novikova J. Comparing pre-trained and feature-based models for prediction of Alzheimer's disease based on speech. *Front Aging Neurosci.* (2021) 13:635945. doi: 10.3389/fnagi.2021.635945
22. Syed MSS, Syed ZS, Lech M, Pirogova E. Automated screening for Alzheimer's dementia through spontaneous speech. In: *INTERSPEECH 2020.* (2020) p. 2222–6. doi: 10.21437/Interspeech.2020-3158
23. Yuan J, Bian Y, Cai X, Huang J,Ye Z, Church K, Disfluencies and fine-tuning pre-trained language models for detection of Alzheimer's disease. In: *INTERSPEECH 2020.* (2020) p. 2162–6. doi: 10.21437/Interspeech.2020-2516
24. Luz S, Haider F, Fuente S, Fromm D, Macwhinney B. Detecting cognitive decline using speech only: the ADReSS O Challenge. *arXiv preprint arXiv:2104.09356.* (2021) doi: 10.1101/2021.03.24.212504263
25. Mahajan P, Baths V. Acoustic and language based deep learning approaches for Alzheimer's dementia detection from spontaneous speech. *Front Aging Neurosci.* (2021) 13:20. doi: 10.3389/fnagi.2021.623607
26. Karlekar S, Niu T, Bansal M. Detecting linguistic characteristics of Alzheimer's dementia by interpreting neural models. *arXiv preprint arXiv:1804.06440.* (2018). doi: 10.18653/v1/N18-2110
27. Di Palo F, Parde N. Enriching neural models with targeted features for dementia detection. *arXiv preprint arXiv1906.05483.* (2019). doi: 10.18653/v1/P19-2042
28. Orimaye SO, Wong JSM, Fernandez JSG. Deep-deep neural network language models for predicting mild cognitive impairment. In: *25th IJCAI Advances in Bioinformatics and Artificial Intelligence: Bridging the Gap*. (2016) p. 14–20. Available online at: http://ceur-ws.org/Vol-1718/paper2.pdf.
29. Fritsch J, Wankerl S, Noth E. Automatic diagnosis of alzheimer's disease using neural network language models. In: *ICASSP 2019-2019 IEEE International Conference on Acoustics, Speech and Signal Processing (ICASSP)*. (2019) p. 5841–5. Available online at: https://publications. idiap.ch/downloads/papers/2019/Fritsch_ICASSP_2019.pdf. doi: 10.1109/ICASSP.2019.8682690
30. Pan Y, Mirheidari B, Reuber M, et al. Automatic hierarchical attention neural network for detecting AD[C]//Proceedings of Interspeech 2019. In: *International Speech Communication Association (ISCA).* (2019) p. 4105–9. doi: 10.21437/Interspeech.2019-1799
31. Roshanzamir A, Aghajan H, Baghshah M S. Transformer-based deep neural network language models for Alzheimer's disease risk assessment from targeted speech. *BMC Med Inform Decis Mak.* (2021) 21:1–14. doi: 10.1186/s12911-021-01456-3
32. Clarke N, Barrick TR, Garrard P. A Comparison of Connected Speech Tasks for Detecting Early Alzheimer's Disease and Mild Cognitive Impairment Using Natural Language Processing and Machine Learning. *Front Comput Sci.* (2021) 3:1–17. doi: 10.3389/fcomp.2021.634360
33. Looze CD, Dehsarvi A, Crosby L, Vourdanou A, Coen RF, Lawlor BA, et al. Cognitive and structural correlates of conversational speech timing in mild cognitive impairment and mild-to-moderate Alzheimer's disease: relevance for early detection approaches. *Front Aging Neurosci.* (2021) 13:1–17. doi: 10.3389/fnagi.2021.637404
34. Matej M, Fasih H, Senja P, Saturnino L. Temporal integration of text transcripts and acoustic features for Alzheimer's diagnosis based on spontaneous speech. *Front Aging Neurosci.* (2021) 13:1–15. doi: 10.3389/fnagi.2021.642647
35. Jonell P, Moëll B, Håkansson K, Henter GE, Kucherenko T, Mikheeva O, et al. Multimodal capture of patient behaviour for improved detection of early dementia: clinical feasibility and preliminary results. *Front Comput Sci.* (2021) 3:1–22. doi: 10.3389/fcomp.2021.642633
36. Soler JL, Subirana B. Longitudinal speech biomarkers for automated Alzheimer's detection. *Front Comput Sci.* (2021) 3:624694. doi: 10.3389/fcomp.2021.624694
37. Zhu YX, Liang XH, Batsis JA, Roth RM. Exploring deep transfer learning techniques for Alzheimer's dementia detection. *Front Comput Sci.* (2021) 3:1–15. doi: 10.3389/fcomp.2021.624683
38. Goodglass H, Kaplan E, Barresi B. *Boston Diagnostic Aphasia Examination (3rd ed.) (BDAE-3).* Publisher: Pro-Ed, 8700 Shoal Creek Blvd, Austin, TX 787576897 (2001).
39. Zhang Z, Han X, Liu Z, Jiang X, Sun M, Liu Q. ERNIE: enhanced language representation with informative entities. In: *The Association for Computational Linguistics in 2019.* (2019) p. 1–11. doi: 10.18653/v1/P19-1139
40. Macwhinney B. *The CHILDES Project: Tools for Analyzing Talk.* Volume I: Transcription Format and Programs. New York, NY; Hove, ES: Psychology Press. (2014).
41. Sadeghian R, Schaffer JD, Zahorian SA. Towards an automatic speech-based diagnostic test for Alzheimer's disease. *Front Comput Sci.* (2021) 3:13. doi: 10.3389/fcomp.2021.624594

42. Jawahar G, Sagot B, Seddah D. What does BERT learn about the structure of language? In: *Proceedings of the 57th Annual Meeting of the Association for Computational Linguistics.* (2019) p. 3651–7. doi: 10.18653/v1/P19-1356
43. Russo I, TCaselli T, Strapparava C. SemEval-2015 task 9: CLIPEval implicit polarity of events. In: *Proceedings of the 9th International Workshop on Semantic Evaluation (SemEval 2015).* (2015) p. 443–450. doi: 10.18653/v1/S15-2077
44. Li Z, Zou Y, Zhang C, Zhang Q, Wei Z. Learning implicit sentiment in aspect-based sentiment analysis with supervised contrastive pre-training. In: *Proceedings of the 2021 Conference on Empirical Methods in Natural Language Processing.* (2021) p. 246–256. doi: 10.18653/v1/2021.emnlp-main.22
45. Johnson M, Schuster M, Le QV, Krikun M, Dean J. Google's multilingual neural machine translation system: Enabling zero-shot translation.. *Trans Assoc Comput Linguist.* (2017) 5:339–51. doi: 10.1162/tacl_a_00065

Conflict of Interest: The authors declare that the research was conducted in the absence of any commercial or financial relationships that could be construed as a potential conflict of interest.

frontiers | Frontiers in Aging Neuroscience

ORIGINAL RESEARCH
published: 18 May 2022
doi: 10.3389/fnagi.2022.892343

The Effects of Aerobic Exercise Training on Cerebrovascular and Cognitive Function in Sedentary, Obese, Older Adults

Edward S. Bliss[1], Rachel H. X. Wong[2,3], Peter R. C. Howe[2,3,4] and Dean E. Mills[1,2]*

[1] Respiratory and Exercise Physiology Research Group, School of Health and Medical Sciences, University of Southern Queensland, Ipswich, QLD, Australia, [2] Centre for Health Research, Institute for Resilient Regions, University of Southern Queensland, Ipswich, QLD, Australia, [3] Clinical Nutrition Research Centre, School of Biomedical Sciences and Pharmacy, University of Newcastle, Callaghan, NSW, Australia, [4] Allied Health and Human Performance, University of South Australia, Adelaide, SA, Australia

Cerebrovascular function and cognition decline with age and are further exacerbated by obesity and physical inactivity. This decline may be offset by aerobic exercise training (AT). We investigated the effects of 16 weeks AT on cerebrovascular and cognitive function in sedentary, obese, older adults. Twenty-eight participants were randomly allocated to AT or a control group. Before and after the intervention, transcranial Doppler ultrasonography was used to measure the cerebrovascular responsiveness (CVR) to physiological (hypercapnia, 5% carbon dioxide) and cognitive stimuli. AT increased the CVR to hypercapnia (98.5 ± 38.4% vs. 58.0 ± 42.0%, $P = 0.021$), CVR to cognitive stimuli (25.9 ± 6.1% vs. 16.4 ± 5.4%, $P < 0.001$) and total composite cognitive score (111 ± 14 vs. 104 ± 14, $P = 0.004$) compared with the control group. A very strong relationship was observed between the number of exercise sessions completed and CVR to cognitive stimuli ($r = 0.878$, $P < 0.001$), but not for CVR to hypercapnia ($r = 0.246$, $P = 0.397$) or total composite cognitive score ($r = 0.213$, $P = 0.465$). Cerebrovascular function and cognition improved following 16 weeks of AT and a dose-response relationship exists between the amount of exercise sessions performed and CVR to cognitive stimuli.

Keywords: aerobic exercise training, cerebrovascular function, cognition, aging, obesity

OPEN ACCESS

Edited by:
Stefano Tarantini, University of Oklahoma Health Sciences Center, United States

Reviewed by:
Peter Mukli, University of Oklahoma Health Sciences Center, United States
Ferdinando Franzoni, University of Pisa, Italy

****Correspondence:***
Edward S. Bliss
Edward.Bliss@usq.edu.au

Specialty section:
This article was submitted to Neurocognitive Aging and Behavior, a section of the journal Frontiers in Aging Neuroscience

Received: *08 March 2022*
Accepted: *11 April 2022*
Published: *18 May 2022*

Citation:
Bliss ES, Wong RHX, Howe PRC and Mills DE (2022) The Effects of Aerobic Exercise Training on Cerebrovascular and Cognitive Function in Sedentary, Obese, Older Adults. Front. Aging Neurosci. 14:892343. doi: 10.3389/fnagi.2022.892343

INTRODUCTION

Aging is associated with the development of cognitive decline which may be preceded by reduced cerebrovascular function and unfavorable neuroanatomical changes (Bangen et al., 2014; Toth et al., 2017). There is also increased chronic low-grade systemic inflammation and reactive oxygen species production with aging, which promotes endothelial dysfunction and reduced cerebrovascular function and cognition (Pikula et al., 2009; Toth et al., 2017; Chang et al., 2018; Rossman et al., 2018; Bliss et al., 2021). Both cerebrovascular function and cognition are exacerbated in sedentary and obese individuals because physical inactivity and obesity promote oxidative stress, which increases the chronic low-grade inflammation, resulting in uncoupling of endothelial nitric oxide synthase which further promotes oxidative stress and inflammation leading to endothelial dysfunction (Pikula et al., 2009; Toth et al., 2017; Chang et al., 2018; Rossman et al., 2018; Bliss et al., 2021).

Hence, sedentary behavior and obesity further impair cerebrovascular function, due to a reduction in capillary density and increased arterial stiffness (i.e., reduced blood flow and vasoreactivity due to decreased endothelial function) (Woods et al., 2011; Toda, 2012; Bangen et al., 2014; Toth et al., 2017). These changes diminish the metabolic capacity of the brain, as the brain is no longer supplied as efficiently as it once was with essential nutrients and oxygen and its metabolic waste is no longer removed as efficiently as in earlier adulthood. If cerebrovascular function is further reduced, the development of cerebral pathologies, cerebral dysfunction and, eventually, a neurodegenerative disease, such as dementia, can ensue as severely reduced cerebrovascular function is associated neurodegenerative changes, including tauopathies and β-amyloid deposition (Kearney-Schwartz et al., 2009; Smith and Greenberg, 2009; Bliss et al., 2021).

The population of older adults who are sedentary and obese is growing and this can lead to the development of comorbidities, including dementia (Beydoun et al., 2008; Taylor, 2014; Brown et al., 2017). The prevalence of dementia is expected to treble over the next 30 years to 150 million people globally (AIHW, 2012; Nichols et al., 2019). Thus, it is important to find and implement cost-effective and evidence-based strategies that promote improvements in cerebrovascular function and cognition which can slow or prevent the normal age-related decline and dementia. One such intervention is aerobic exercise training (AT), which has been shown to maintain cerebral perfusion and cognitive capacity in healthy aging and potentially reduce the risk of individuals developing dementia (Rogers et al., 1990; Ainslie et al., 2008; Bailey et al., 2013).

Previous research has demonstrated that moderate intensity AT interventions between 12 and 24 weeks improve cognition in middle-aged to older adults who were sedentary (Lautenschlager et al., 2008; Erickson et al., 2011; Anderson-Hanley et al., 2012; Chapman et al., 2013; Guadagni et al., 2020), suffer from mild cognitive impairment (Baker et al., 2010), or had a diagnosis of a dementia (Hoffmann et al., 2016; Sobol et al., 2016). This in contrast to the findings of a recent systematic review, which indicated that AT may not improve cognition in older adults who were both health and cognitively healthy (Young et al., 2015). Thus suggesting more research is needed in the area and that healthy older adults may be less sensitive to exercise than those who are not. Improvements in cerebral perfusion have also been reported in sedentary older adults who participated in 12 weeks of moderate intensity AT (Chapman et al., 2013; Maass et al., 2014) and in older adults with coronary artery disease following 24 weeks of AT (Anazodo et al., 2016). Cerebral pulsatility index (CPI), which determines arterial resistance and compliance of a vessel's ability to stretch and recoil following left ventricular ejection, provides an estimation of arterial stiffness. CPI increases as compliance decreases and resistance increases, thus reflecting structural changes in the arterial walls (i.e., less elasticity) and reduced ability to adequately perfuse the area in which the vessel is supplying (Afkhami et al., 2021). CPI has been reported to decrease in patients with amnestic mild cognitive impairment who participated in 12 months AT (Tomoto et al., 2021) and following 6 months of moderate intensity AT, the cerebrovascular responsiveness (CVR) to hypercapnia increased in older, sedentary adults (Vicente-Campos et al., 2012; Kleinloog et al., 2019; Guadagni et al., 2020) and stroke patients (Ivey et al., 2011).

There are several important limitations to these studies. Firstly, the effects of AT on both cerebrovascular function and cognition are not as well defined particularly in older obese and sedentary adults who are at greater risk of developing impaired cognitive function (Beydoun et al., 2008; Pikula et al., 2009; Woods et al., 2011; Toda, 2012; Bangen et al., 2014; Toth et al., 2017; Chang et al., 2018; Rossman et al., 2018; Bliss et al., 2021). Secondly, studies have not typically measured cerebrovascular and cognitive function together. Since these functions are interrelated and contribute to overall brain health, both should be measured together to determine the effect these combined parameters exert (Bliss et al., 2021). Thirdly, no study has performed measurements of CVR to cognitive stimuli (i.e., neurovascular coupling, NVC). This is of importance because CVR to both physiological and cognitive stimuli are imperative to maintaining cerebral function because both reflect the ability of the microvasculature to maintain cerebral autoregulation and NVC (Duchemin et al., 2012; Toth et al., 2017; Miller et al., 2018). The measurement of both parameters in conjunction with cognition is essential to holistically determine the effects of AT on overall brain health. Finally, few of the studies cited have deviated from the recommended physical activity guideline of 150–300 min of moderate intensity exercise. Many older adults are not meeting these guidelines and are not participating in exercise (AIHW, 2018a; Piercy et al., 2018; Guadagni et al., 2020). The evaluation of the dose response relationship between AT and cerebrovascular and cognition function is important, as we currently do not know how much AT is required to elicit improvements in cerebrovascular and cognitive function in older adults. It may be that some exercise is better than none at delaying or preventing further cerebrovascular and cognitive decline. This may also encourage sedentary adults to exercise with a future goal of reaching the recommended physical activity guidelines.

Accordingly, the aim of the study was to evaluate the effects of 16 weeks AT performed for 2–4 days per week on cerebrovascular and cognitive function in sedentary, obese, older adults. We hypothesized that compared with control participants: (1) AT would improve both cognition and cerebrovascular function determined by the CVR to physiological and cognitive stimuli; (2) the greater the dose of AT, the greater the improvements in cerebrovascular and cognitive function.

MATERIALS AND METHODS

Participants

Participants were recruited from the Ipswich Region, Australia between April 2019 and March 2021 *via* an approved media campaign that incorporated physical advertisement *via* media releases (flyers and newspaper articles), social media and a radio interview. Inclusion criteria were: age between 50 and 80 years; were physically inactive based on classed as physically inactive based on the physical activity guidelines of 150 min of

TABLE 1 | Composition of the exercise sessions, including session content, intensity and rating of perceived exertion.

Week/s	Day/s	Session	Intensity	Rating of perceived exertion (0–10)
1–2	Monday/Friday	30 Min walking	Moderate	5
	Tuesday/Thursday	15 Min walking 15 min circuit	Moderate Moderate-to-vigorous	5 6–7
3–5	Monday	35 min walking	Moderate	5–6
	Tuesday/Thursday	15 Min walking, cycling, arm ergometry, rowing 15 min circuit	Moderate Vigorous	5–6 7–8
	Friday	15 Min walking 3 × 6 min circuits	Moderate	5–6
6–8	Monday/Friday	15 Min walking, cycling, arm ergometry, rowing 3 × 5 min circuits	Moderate Moderate	6 6
	Tuesday/Thursday	15 Min walking, cycling, arm ergometry, rowing 15 min circuit	Moderate Vigorous	6 7–8
9–12	Monday/Friday	15 Min walking, cycling, arm ergometry, rowing 3 × 5 min circuits	Moderate Moderate	6 6
	Tuesday/Thursday	15 Min walking, cycling, arm ergometry, rowing 15 min circuit	Moderate Vigorous	6 7–8
13–14	Monday/Friday	5 Min walking, cycling, arm ergometry, rowing 7 × 4 min circuits	Moderate Moderate-to-vigorous	6 7
	Tuesday/Thursday	10 Min walking, cycling, arm ergometry, rowing 20 min circuit	Moderate Vigorous	6 8
15–16	Monday/Friday	5 Min walking, cycling, arm ergometry, rowing 7 × 4 min circuits	Moderate Moderate-to-vigorous	6 7
	Tuesday/Thursday	5 Min walking, cycling, arm ergometry, rowing 2 × 15 min circuits	Moderate Vigorous	6 8

moderate-vigorous intensity aerobic exercise per week (AIHW, 2018b); and had a body mass index (BMI) of $>$ 25 kg/m^2. The exclusion criteria were: aged under 50 years or over 80 years; participation in regular physical activity and meeting the physical activity guidelines of 150 min of moderate-vigorous intensity aerobic exercise per week (AIHW, 2018b); body mass index (BMI) of $<$ 25 kg/m^2; current smoker; blood pressure $\geq$ 160/100 mmHg; prescribed insulin, hormone-replacement therapy, or oral anticoagulants; had significant history of cardiovascular, cerebrovascular, kidney, liver disease or cancer; and had a diagnosis of cognitive impairment and/or a neurodegenerative disease. Participants were only included in the study if they were on a stable medication treatment plan that did not contradict the exclusion criteria. The Yale Physical Activity Survey (Dipietro et al., 1993), the Exercise and Sports Science Australia Adult Pre-exercise Screening System (Norton and Norton, 2011), and a customized health and wellbeing screen were used to determine whether participants met the inclusion and/or exclusion criteria, as well as their physical activity status and exercise behaviors. All study procedures were approved by the University of Southern Queensland Research Ethics Committee (H19REA007), which adheres to the Declaration of Helsinki. The study was registered with the Australian and New Zealand Clinical Trial Registry (ACTRN12619000988156). Participants provided written, informed consent.

Experimental Design

The study adopted a randomized control design. The intervention lasted 16 weeks. Before and approximately 1 week following the completion of the intervention, participants visited the laboratory on two occasions, at a similar time of day, separated by a minimum of 24 h and a maximum of 7 days. Participants fasted and abstained from coffee, tea and other stimulants for 2 h before visit 1 and 8–12 h before visit 2. They were also requested to refrain from moderate-vigorous intensity exercise for 24 h before each visit and to take their daily supplements and medication after each visit was completed. During visit 1, participants undertook anthropometric, cardiovascular, exercise performance, strength, cerebrovascular and cognitive measurements. During visit 2, participants undertook body composition measurements, blood collection and the Profile of Moods State questionnaire. The Profile of Mood States questionnaire calculated mood disturbance by adding the scores of the negative mood state scales (i.e., anger-hostility, confusion-bewilderment, depression-dejection, fatigue inertia, tension-anxiety) and subtracting the positive mood state scale (i.e., vigor-activity) (Heuchert and McNair, 2012). Lower values in the negative mood states and total mood disturbance indicated better mood, while higher values in the positive mood state portion of the questionnaire are associated with positive mood. Between visits 1 and 2, participants were asked to complete a nutritional questionnaire (Automated Self-Administered 24 h Dietary Assessment Tool; National Institute of Health, Bethesda, MA, United States) to estimate energy intake over a typical 24 h period (Pannucci et al., 2018).

Exercise Intervention

Participants were then randomly allocated to one of two arms of the study using Altman's minimization method (prioritizing BMI and sex) to ensure that the groups were balanced (Altman and Bland, 2005). The two arms of the study included a control group, which did not participate in any exercise training, and an exercise group. Participants allocated to the exercise group were asked to participate in AT for between 2–4 days per week (i.e., they could participate in either two, three, or four sessions per week). These sessions were conducted as group classes supervised by a clinical exercise physiologist. **Table 1** provides an overview of the exercise session content. All sessions lasted for approximately 40–45 min and incorporated both a 5 min warm-up and cool-down. The body of the sessions was performed at a rating of perceived exertion for leg discomfort of 5–8 on the Borg (CR-10) scale, which indicated that the exercise was being performed at a moderate (5–6) or high intensity (7–8) (Borg, 1998). Additionally, the participants were asked to perform these exercise sessions at a higher intensity at approximately every 4 weeks if possible (**Table 1**). The circuit comprised functional exercises including wall press-ups, marching, step-ups, sit-to-stands, squats and basic resistance exercises. Compliance was measured by a roll call at the start of every exercise session to determine participation. Participants were contacted by either by phone, email, or in person each week for the first 2 weeks

of the study, then fortnightly until 8 weeks at which time they were contacted every 4 weeks to ensure protocol familiarity, personal reassurance and motivation and as a check of their general wellbeing. This practice can assist in ensuring participant compliance (Lautenschlager et al., 2008). An attendance rate of 40% of all of the available exercise sessions at the end of the 16 weeks was considered compliant (Rejeski et al., 1997; Claxton et al., 2001; Lautenschlager et al., 2008).

Basal Cerebral Hemodynamics

Transcranial Doppler ultrasonography (TCD; DopplerBox X; Compumedics DWL, Singen, Germany) was used to measure basal cerebrovascular hemodynamics, including minimum, maximum and mean values for both CBF_V and cerebral pulsatility, as well as CVR in response to hypercapnia and cognitive stimuli following at least 10 min of quiet rest in a seated position (Edmonds et al., 2011; Barbour et al., 2017; Evans et al., 2017). Participants were seated and fitted with a headpiece which housed two 2-MHz TCD ultrasound probes that were fixed and aligned bilaterally to the left and right cranial temporal bone windows to insonate the middle cerebral arteries (MCA) at a depth of approximately 40–65 mm through the transtemporal window using standardized techniques as previously described (Edmonds et al., 2011; Willie et al., 2011). Once a suitable blood flow signal was obtained, participants were asked to sit quietly while basal measurements were recorded for 30 s. If the MCA could not be insonated, the participant was excluded from the study.

Cerebrovascular Responsiveness to Hypercapnia

Participants were subsequently challenged with a hypercapnic stimulus for 3 min and monitored for another 1 min following removal. This process was performed in duplicate following a 5 min rest period (whilst participants breathed in room air) to ensure mean velocity returned to baseline values (Barbour et al., 2017; Evans et al., 2017). Participants breathed through a two-way non-rebreathing valve (model 2730, Hans Rudolph, Kansas City, MO, United States) whilst wearing a nose-clip. The inspiratory port of the two-way valve was connected to 1 m of wide bore tubing distal to a 100 L Douglas bag which contained carbogen gas (5% carbon dioxide and 95% oxygen; Carbogen 5; BOC, Toowoomba, Australia). Flow was measured from the expiratory port of the two-way valve using a pneumotachograph (MLT 300L; AD Instruments, Bella Vista, Australia) which was calibrated with a 3 L syringe prior to the commencement of each test. Volume was obtained by numerical integration of the flow signal. End-tidal partial pressures of carbon dioxide ($P_{ET}CO_2$) were sampled from the expiratory port of the two-way valve connected to a gas analyzer (ADI ML206; AD Instruments, Bella Vista, Australia) that was calibrated across the physiological range with known gas concentrations (BOC, Toowoomba, Australia). Flow and $P_{ET}CO_2$ measurements were sampled at 200 Hz using a 4-channel Powerlab analog-to-digital converter (AD Instruments, Bella Vista, Australia) interfaced with a computer and displayed in real time during testing. Data were stored for subsequent offline analysis using LabChart software (version 7.2, AD Instruments, Bella Vista, Australia).

Cognitive Function and Cerebrovascular Responsiveness to Cognitive Stimuli

Cognitive tests included the Trail Making Task Parts A and B which assessed central executive function, Spatial Span Test (visuospatial short-term working memory) and a National Institute of Health (NIH) Toolbox, which is a battery of cognitive examinations (Strauss et al., 2006; Evans et al., 2017). The NIH Toolbox is comprised of the Dimensional Change Card Sort Test (cognitive flexibility and attention), Picture Vocabulary Test (language and crystallized cognition), List Sorting Working Memory Test (working memory), Oral Reading Recognition Test (language and crystallized cognition), Flanker Inhibitory Control and Attention Test (attention and inhibitory control), Picture Sequence Memory Test (episodic memory), Pattern Comparison Processing Speed Test (processing speed) (Slotkin et al., 2012; Heaton et al., 2014). An age adjusted total composite cognitive function score was also derived from the above (Heaton et al., 2014). All NIH Toolbox test scores were automatically computed within the program to control for examiner bias. The outputs for all tests were normalized based on the demographics entered into the program (age, education level, familial education history, sex, ethnicity, and occupation). A full description of how these tests are administered, how these scores are calculated and the validation of these tests and scores have been previously described in detail (Slotkin et al., 2012; Heaton et al., 2014; Weintraub et al., 2014). All tests excluding the Trail Making Task were delivered using an iPad (6th generation, Apple Inc., Cupertino, CA, United States). The CVR to cognitive stimuli was assessed during each cognitive task and 30 s of baseline data was recorded before the start of each cognitive task.

Data Capture and Processing for Cerebrovascular Responsiveness

Beat-to-beat measurements of CBF_V were recorded from the MCA onto software (QL Reader; Compumedics DWL, Singen, Germany) sampling at 100 Hz and were stored for subsequent offline analysis. If a bilateral signal was not obtained, then analysis took place with only the side that was able to be obtained. These data were then normalized and analyzed using Curve Expert Professional software (Hyams Development, Chattanooga, TE, United States) to determine peak CBF_V, resting CBF_V and resting cerebral pulsatility index (CPI). CVR and CPI were calculated based on Equations (1) and (2) from previous work (Bakker et al., 2004; Wong R. H. X. et al., 2016; Harris et al., 2018).

$$\text{CPI} = \frac{\text{peak systolic CBFv} - \text{end diastolic CBFv}}{\text{mean CBFv during a cardiac cycle}} \quad (1)$$

$$\text{CVR (\%)} = \frac{(\text{peak CBFv} - \text{resting CBFv})}{\text{resting CBFv}} \times 100 \div \text{resting CPI} \quad (2)$$

Anthropometrics and Body Composition

Participants were instructed to wear light clothing prior to testing and subsequently asked to remove their shoes for measurements. Body mass was measured to the nearest 100 g using an electronic scale (Tanita Ultimate Scale, 2000; Tokyo, Japan) and waist and hip circumferences was recorded to the nearest 1 cm using a standard tape measure as previously described (Welborn et al., 2003). Height was recorded to the nearest 1 cm using a wall-mounted telescopic stadiometer (Seca220; Vogel and Halke, Hamburg, Germany). Height, body mass and waist and hip circumference measurements were measured in duplicate and the mean of the two measurements were analyzed. BMI and a waist to hip ratio were calculated as previously described (Keys et al., 1972; Welborn et al., 2003). Dual-energy X-ray absorptiometry was used to obtain the following measures of whole body composition: lean mass, body fat percentage, bone mineral content and density (Luna Corp. Prodigy Advance Model GE; Madison, WI, United States).

Cardiovascular Function

Systolic and diastolic blood pressure, mean arterial pressure, heart rate and arterial elasticity were measured non-invasively using a HDI/Pulsewave^{TM} CR-2000 Research Cardiovascular Profiling System (Hypertension Diagnostics, Eagan, MN, United States) (Prisant et al., 2002). Participants rested in a seated position for 10 min prior to measurements. Four consecutive readings were recorded approximately 5 min apart by an automated oscillometer, using an appropriately size blood pressure cuff over the left brachial artery, to assess blood pressure and a tonometer, placed over the right radial artery, to assess heart rate and estimate arterial elasticity, cardiac output and cardiac index by pulse wave analysis (Prisant et al., 2002; Barbour et al., 2017). The first reading was discarded and the mean of the three subsequent readings was used for analysis.

Biochemical Analyses

Approximately 20 ml of venous blood was sampled using a suitable method (i.e., either evacuated tube system or winged-infusion set for difficult collections) from the veins of the antecubital fossa into a thrombin-based clot activator serum separator tubes (BD, Macquarie Park, NSW, Australia). Following collection, blood was left to stand for 30 min at 18–25°C prior to centrifugation at 1,300 g and 18°C for 10 min, as outlined by the tube manufacturer and the testing laboratory (BD, 2019; QML, 2019). Following centrifugation, blood was separated as serum and analyzed for the general chemistry profile and high-sensitivity C-reactive protein (hs-CRP) on a Siemens ADVIA® Labcell® (Siemens Healthcare, Bayswater, VIC, Australia), which utilizes spectrophotometric (enzymes, metabolites, proteins, lipids), turbidimetric (hs-CRP) and potentiometric (electrolytes) techniques (Healthineers, 2019).

Exercise Performance and Handgrip Strength

Exercise performance was assessed using a 6 min walk test (6MWT) according to published guidelines (ATS, 2002). Handgrip strength was determined using hand dynamometry as previously described (Hillman et al., 2005). Participants were permitted three attempts with both their dominant and non-dominant hands. The first reading for each hand was discarded and was used as a familiarization and the second and third readings for each hand were averaged for each hand and were used for analysis. Both the 6MWT and handgrip strength were used to provide an estimate of endurance exercise capacity and whole-body strength (ATS, 2002; Hillman et al., 2005).

Statistical Analysis

Statistical analyses were performed using SPSS for Windows (IBM, Chicago, United States). An initial power calculation was performed on the basis of previous research that has investigated the differences in CVR between participants who had undergone an intervention study (Wong R. et al., 2016; Wong R. H. X. et al., 2016; Barbour et al., 2017; Evans et al., 2017). It indicated that 32 participants would give 80% power to detect a significant ($p < 0.05$) 5% increase in the CVR to hypercapnia following exercise training. This was based on a 10% standard deviation observed in previous studies and a medium sized effect (Wong R. et al., 2016; Wong R. H. X. et al., 2016; Barbour et al., 2017; Evans et al., 2017). Recruitment was limited to 28 participants due to the impacts of COVID-19 and the restrictions placed on gathering, research and travel by the Queensland Government. Normality of data was assessed using a Shapiro-Wilk test. Comparisons between groups for anthropometric, body composition, cardiovascular, cognitive, exercise performance, strength and biochemical measures were determined using an independent *t*-test or a Mann-Whitney *U*-test for parametric and non-parametric data, respectively. A two-way analysis of variance (ANOVA) was used to determine the effects of "treatment" (exercise vs. control) and "intervention" (week 0 vs. week 16). A three-way ANOVA was used to determine the effects of "treatment," "intervention" and "time" (baseline vs. peak) for the CVR to hypercapnia and cognitive stimuli measures. Significant interaction effects were followed by planned pairwise comparisons between groups using the Bonferroni method. Pearson product-moment correlation coefficients were calculated to assess the relationship between the number of exercise sessions completed and the relative percentage change from week 0 to week 16 for the CVR to hypercapnia, total composite CVR to cognitive stimuli and total composite cognitive score in the exercise group (Schober et al., 2018). The relative percentage change for each of these variables were determined by the following formula:

$$\text{relative percentage increase} = \frac{(\text{week 16 value} - \text{week 0 value})}{\text{week 0 value}} \times 100 \quad (3)$$

Statistical significance was set at $P < 0.05$. Effect sizes were determined using Cohen's *d* using the following thresholds: ≤ 0.19 = trivial, ≥ 0.2 ≤ 0.49 = small, ≥ 0.5 ≤ 0.79 = medium, and ≥ 0.8 = large (Cohen, 1988). Results are presented as means ± SD.

RESULTS

Participant Characteristics

Figure 1 shows the CONSORT participant flow diagram. Twenty-seven participants were included in the final data and statistical analysis. Thirteen participants were in the control arm of the study. Fourteen participants completed the exercise intervention and compliance was good with 40 ± 3 (63 ± 5%) exercise sessions completed.

Baseline characteristics are shown in **Table 2**. No differences were observed between the groups except for the number of flights of stairs climbed daily which was higher in the control compared to the exercise group with a medium effect size (d = 0.68). Baseline general biochemistry profiles and hs-CRP are shown in **Table 3**. There were no differences between the groups. The participants were obese, had low-grade inflammation and met the International Diabetes Federation criteria of the metabolic syndrome (Alberti et al., 2005).

Body Composition, Grip Strength, Exercise Performance, Cardiovascular Function

Body composition, grip strength, exercise performance and cardiovascular function measurements are shown in **Table 4**. The 6MWT distance at week 0 was higher in the exercise compared to the control group with a medium effect size (main effect of treatment, d = 0.74). Total lean mass (d = 0.18), 6MWT distance, and large arterial compliance (d = 0.08) increased in both groups (main effect of intervention), while total body fat percentage (d = 0.69), systolic blood pressure (d = 0.19), mean arterial pressure (d = 0.04) and total vascular impedance (d = 0.01) decreased in both groups (main effect of intervention). There were no significant treatment x intervention interaction effects in any of the parameters, although the 6MWT distance (d = 1.33) and total bone mineral content (d = 0.31) were approaching significance.

Cerebrovascular Responsiveness to Hypercapnia

The CVR to hypercapnia and the cerebrovascular and respiratory parameters are shown in **Figure 2** and **Table 5**. All variables measured increased during hypercapnia (main effect of time; $P < 0.001$), except for CPI which decreased (main effect of time; $P < 0.001$) and breathing frequency, which did not change. The CVR to hypercapnia increased to a greater extent in the exercise than the control group (+ 40%; treatment x intervention interaction; $P = 0.021$, $d > 0.82$). Although Week 0 CBF_V was lower in the exercise group than the control group, the increase in CBF_V during hypercapnia (treatment × intervention × time interaction) was greater following the intervention (+ 36%) in the exercise group (d = 0.81). CPI decreased (main effect of intervention, $P = 0.001$, d = 0.24) in both the exercise and control groups following the intervention but there were no interaction effects. Maximum tidal volume and minute ventilation (treatment x intervention interaction) increased to a greater extent in the exercise compared to the control group following the intervention ($d > 0.82$ and d = 0.28).

Cognitive Function and Cerebrovascular Responsiveness to Cognitive Stimuli

Cognitive function and the CVR to cognitive stimuli are shown in **Figure 2** and **Table 6**. There were no differences between the groups in any of the cognitive parameters at week 0. Following the intervention, the exercise group had higher overall cognitive function than the untrained group, which was demonstrated by a higher total cognitive composite score with a small effect size (3 vs. 10% improvement; treatment × intervention interaction; $P = 0.004$, d = 0.49). The exercise group also had increased working memory capacity compared to the control group with a large effect size following the intervention, demonstrated by the List Sorting Working Memory Test ($d > 0.82$).

At week 0, there were no differences between the groups in any CVR measures except for the CVR to Part B of the Trail Making Task which was higher in the control than the exercise group with a small effect size (main effect of treatment, d = 0.23). Following the intervention, the exercise group had a higher total composite CVR to all cognitive stimuli (10% higher; treatment x intervention interaction; $P < 0.001$, $d > 0.82$) than the control group with a large effect size, as well as a higher CVR to all of the individual cognitive stimuli with a large effect size ($d > 0.82$), excluding the Picture Vocabulary Test and the Flanker Inhibitory Control and Attention Test (treatment × intervention interaction).

Correlations Between Exercise Sessions Completed and Cerebrovascular Function and Cognition

Figure 3 shows the correlations between the number of exercise sessions completed and the percentage increase from week 0 to week 16 for the CVR to hypercapnia, total composite CVR to cognitive stimuli and total composite cognitive score in the exercise group. There were no significant differences in the frequency of sessions in which participants chose to participate in on a weekly basis over the 16-week period (2.5 ± 0.3 sessions). There was a very strong positive correlation between the number of exercise sessions completed and the total composite CVR to cognitive stimuli. There were no significant correlations between the number of exercise sessions completed and either the CVR to hypercapnia or the total composite cognitive score.

DISCUSSION

Main Findings

The aim of the study was to evaluate the effects of 16 weeks AT on cerebrovascular and cognitive function in sedentary, obese, older adults. We hypothesized that compared with control participants: (1) AT would improve both cognition and cerebrovascular function determined by the CVR to physiological and cognitive stimuli; and (2) the greater the dose of AT, the greater the improvements in cerebrovascular and cognitive function. The

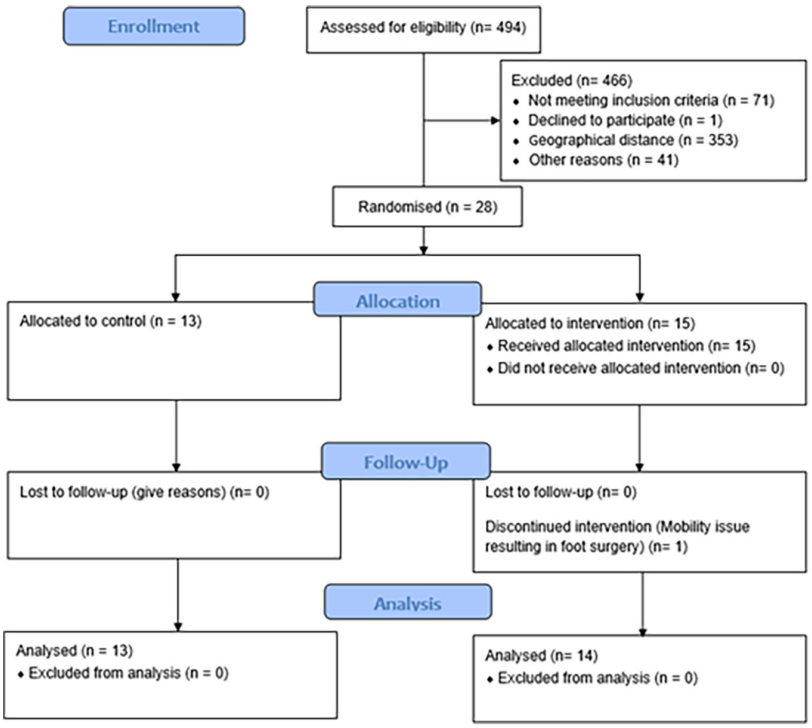

FIGURE 1 | CONSORT participant flow diagram.

TABLE 2 | Baseline demographics, anthropometrics, nutritional intake and physical activity levels for the control and exercise groups.

Variable	Control (*n* = 13)	Exercise (*n* = 14)	*P*-value
Demographics			
Age (years)	66 ± 9	67 ± 7	0.553
Sex (male/female)	2/11	4/10	0.618
Education (years)	16 ± 4	14 ± 3	0.440
Anthropometrics			
Body mass (kg)	93.5 ± 23	88.7 ± 11	0.928
Height (m)	1.64 ± 0.08	1.68 ± 0.09	0.208
Body mass index (kg/m^2)	34.6 ± 6.55	31.4 ± 1.99	0.339
Hip circumference (cm)	126 ± 15	117 ± 5	0.118
Waist circumference (cm)	114 ± 15	107 ± 8	0.217
Hip-to-waist ratio	0.91 ± 0.07	0.91 ± 0.08	0.730
Nutritional intake			
Total energy intake (kcal)	2,375 ± 769	2,688 ± 1,035	0.393
Physical activity levels			
Energy expenditure (kcal/min)	70 ± 34	94 ± 73	0.560
Vigorous activity index	5 ± 5	1 ± 2	0.131
Leisurely walking index	5 ± 5	8 ± 10	0.527
Moving index	7 ± 3	8 ± 4	0.705
Standing index	5 ± 1	6 ± 4	0494
Sitting index	4 ± 2	4 ± 2	0.560
Flights of stairs climbed per day	2 ± 3	1 ± 2	**0.036**
Seasonal adjustment score	1 ± 0	1 ± 0	0.274

Values are means ± SD.
Bold values represent significant differences.

main findings were that AT increased the CVR to hypercapnia, CVR to cognitive stimuli and total composite cognitive score compared with the control group. A very strong relationship was observed between the number of exercise sessions completed and CVR to cognitive stimuli, but not for CVR to hypercapnia or total composite cognitive score. These results demonstrate that in sedentary, obese, older adults 16 weeks of AT can improve both improve both cognition and cerebrovascular function and there

TABLE 3 | Baseline biochemical analyses for the control and exercise groups.

Variable	Control (*n* = 11)	Exercise (*n* = 14)	*P*-value
Glucose (mmol/L)	5.7 ± 1.4	5.6 ± 1.0	0.683
Urea (mmol/L)	6.1 ± 1.5	5.9 ± 1.1	0.610
Creatinine (mmol/L)	74 ± 21	67 ± 10	0.959
Estimated glomerular filtration rate (ml/min)	80 ± 14	84 ± 10	0.384
Total bilirubin (μmol/L)	9 ± 4	9 ± 3	0.574
Alkaline phosphatase (U/L)	92 ± 26	75 ± 27	0.123
Gamma-glutamyl transferase (U/L)	35 ± 25	29 ± 16	0.760
Alanine aminotransferase (U/L)	37 ± 20	30 ± 10	0.443
Aspartate aminotransferase (U/L)	35 ± 15	27 ± 5	0.384
Lactate dehydrogenase (U/L)	234 ± 69	202 ± 30	0.474
Total protein (g/L)	70 ± 3	69 ± 4	0.555
Albumin (g/L)	40 ± 3	42 ± 2	0.164
Globulins (g/L)	30 ± 5	27 ± 3	0.101
Total cholesterol (mmol/L)	5.3 ± 1.0	5.6 ± 1.0	0.330
Triglycerides (mmol/L)	1.4 ± 0.8	1.4 ± 0.6	0.931
High-density lipoprotein (mmol/L)	1.47 ± 0.22	1.45 ± 0.35	0.827
Low-density lipoprotein (mmol/L)	2.71 ± 0.87	3.18 ± 0.83	0.186
Total cholesterol-to-high-density lipoprotein ratio	3.7 ± 0.9	4.1 ± 0.8	0.292
High-sensitivity C-reactive protein (mg/L)	4.8 ± 2.8	3.0 ± 2.6	0.066

Values are means ± SD.

TABLE 4 | Body composition, grip strength, exercise performance and cardiovascular function at week 0 and week 16 for the control and exercise groups.

Variable	Control (*n* = 13)		Exercise (*n* = 14)		*P*-value		
	Week 0	Week 16	Week 0	Week 16	Treatment	Intervention	Treatment × intervention
Body composition							
Total lean mass (kg)	45.6 ± 8.6	46.8 ± 9.6	48.2 ± 10.4	48.7 ± 10.3	0.551	**0.029**	0.299
Total body fat (%)	48.4 ± 6.7	47.1 ± 7.4	43.5 ± 5.6	42.7 ± 5.5	0.064	**<0.001**	0.353
Total bone mineral density (g/cm^2)	1.24 ± 0.13	1.24 ± 0.13	1.22 ± 0.14	1.22 ± 0.14	0.673	0.762	0.827
Total bone mineral content (g/cm)	2,478 ± 458	2,439 ± 476	2,598 ± 557	2,602 ± 565	0.484	0.113	0.052
Grip strength							
Dominant hand (kg)	27.0 ± 7.8	27 ± 7.6	28.7 ± 9.7	31.3 ± 10.3	0.332	0.364	0.324
Non-dominant hand (kg)	26.1 ± 6.3	25.8 ± 7.0	26.8 ± 8.7	30.1 ± 9.6	0.336	0.242	0.147
Exercise performance							
6-Min walk test distance (m)	461 ± 73	469 ± 92	511 ± 61	576 ± 66	**0.004**	**0.015**	0.058
Cardiovascular function							
Heart rate (beats/min)	76 ± 12	75 ± 10	72 ± 6	71 ± 10	0.213	0.719	0.810
Systolic blood pressure (mmHg)	144 ± 15	133 ± 14	139 ± 9	130 ± 10	0.347	**<0.001**	0.473
Diastolic blood pressure (mmHg)	78 ± 8	73 ± 10	76 ± 6	72 ± 5	0.401	0.055	0.714
Mean arterial pressure (mmHg)	104 ± 9	95 ± 10	99 ± 11	95 ± 8	0.336	**0.012**	0.183
Large arterial compliance (ml/mmHg × 10)	9.3 ± 3.4	11.5 ± 3.9	9.7 ± 3.4	11.8 ± 4.1	0.735	**0.007**	0.885
Small arterial compliance (ml/mmHg × 10)	3.9 ± 1.8	4.5 ± 2.0	4.5 ± 2.0	4.8 ± 3.3	0.501	0.291	0.532
Systemic vascular resistance (dyne/sec/cm^{-5})	1,663 ± 316	1,534 ± 263	1,630 ± 261	1,543 ± 229	0.836	0.125	0.708
Total vascular impedance (dyne/sec/cm^{-5})	202 ± 59	161 ± 48	178 ± 39	161 ± 44	0.431	**0.010**	0.218

Values are means ± SD.
Bold values represent significant differences.

is a dose response relationship between the number of exercise sessions completed and CVR to cognitive stimuli.

Cerebrovascular Responsiveness to Hypercapnia

We observed an increase in the CVR to hypercapnia following AT in the exercise compared with the control group. This finding is similar to others who have also reported an increased CVR to hypercapnia in older, sedentary adults (Vicente-Campos et al., 2012; Guadagni et al., 2020) and stroke patients (Ivey et al., 2011) following 6 months of moderate intensity AT. We also observed that the increase in CBF_V during hypercapnia was greater following the intervention in the exercise compared to the control group. Increased cerebral perfusion, whether measured

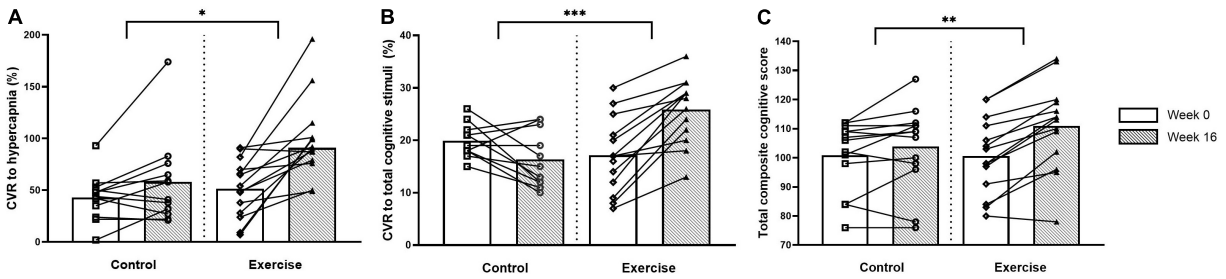

FIGURE 2 | Cerebrovascular responsiveness (CVR) to hypercapnia **(A)**, CVR to total composite of cognitive stimuli **(B)** and total composite cognitive score **(C)** at weeks 0 and 16 for the control and exercise groups. Significant difference between groups * ($P < 0.05$), ** ($P < 0.005$), *** ($P < 0.001$).

directly or indirectly, following at least 12 weeks of AT is consistent with other studies that reported increases in either CBF or CBF_V in older adults who were previously sedentary (Vicente-Campos et al., 2012; Chapman et al., 2013; Maass et al., 2014) and those with coronary artery disease who undertook 6 months of AT (Anazodo et al., 2016). We found that CPI decreased in both the exercise and control groups following the intervention, but there were no differences between the groups. A previous study reported no change in basal CPI in middle-aged to older sedentary adults who undertook a 12 week moderate intensity AT (Akazawa et al., 2018). However, it was reported that these adults did have a decreased CPI following 30 min of acute exercise. The limitation of this study was that it was not a randomized control trial and only compared CPI changes between weeks 0 and 12. The decreased CPI reported following an acute bout of exercise may largely reflect post-exercise recovery, making it difficult to ascertain if an AT intervention can cause a sustained improvement of CPI in older adults (Akazawa et al., 2018). The participants in that study differed from ours in that they were not obese and did not have cardiometabolic disease, thus suggesting that changes in CPI in those who are sedentary, obese and older may take longer than 12–16 weeks to elicit following an AT intervention. Further studies in this area are warranted to determine if AT can reduce arterial stiffness. In any case, our results collectively indicate that 16 weeks of AT can improve cerebrovascular function. The mechanisms for this improvement may be due to an increased ability of the microvasculature to respond to local chemical changes, modify regional blood flow in response to these changes and maintain cerebral autoregulation *via* improved endothelial function and its ability to synthesize nitric oxide (NO) in response to shear stress (Serrador et al., 2000; Willie et al., 2011; Duchemin et al., 2012; Toth et al., 2017). This may translate to improvements in the cerebrovasculature enabling it to respond to increased neuronal metabolism during times of increased cognitive demand.

Cognitive Function and Cerebrovascular Responsiveness to Cognitive Stimuli

We observed that AT increased the total cognitive composite score and working memory capacity compared with the control group. We used the total composite score because this is a collective measurement that is more aligned with the demands of daily living. It is also an appropriate measure to use because TCD does not focus on a specific brain region mediating a particular cognitive function. Rarely is only a single individual cognitive domain or subtype used in isolation and the domains are interdependent (Harvey, 2019). However, we also observed an increase in individual cognitive domains, including working memory. This is consistent with previous studies that have reported an increase in individual cognitive domains following 12–24 weeks of AT in older adults who were sedentary (Lautenschlager et al., 2008; Erickson et al., 2011; Anderson-Hanley et al., 2012; Chapman et al., 2013; Guadagni et al., 2020), suffered from mild cognitive impairment (Baker et al., 2010), or had a diagnosis of a dementia (Hoffmann et al., 2016; Sobol et al., 2016). How AT improves cognitive function is not clear, with potential mechanisms being summarized in detail elsewhere (see Bliss et al., 2021). Briefly, those who have reported improvements in cognition have indicated that this may be associated with improved vascular function, cerebral perfusion and/or increased systemic brain-derived neurotrophic factor, which promotes synaptogenesis, neurogenesis and angiogenesis centrally (Lautenschlager et al., 2008; Erickson et al., 2011; Anderson-Hanley et al., 2012; Chapman et al., 2013; Guadagni et al., 2020; Bliss et al., 2021). Acute exercise increases cardiac output, which induces arterial shear stress, promoting endothelial NO synthase expression, which subsequently results in increased NO production (Toda, 2012; Rossman et al., 2018). β-2 adrenoceptor activated endothelial vasodilatation, as occurs in skeletal muscle beds during aerobic exercise, may also induce increased NO production centrally. In any case, NO not only promotes vasodilatation and reduces arterial stiffness, but reduces oxidative stress and inflammation, as well as improving endothelial function and vascular health (Toda, 2012; Rossman et al., 2018). Centrally, this results in improved cerebral perfusion where it also promotes the delivery of systemic molecules, such as BDNF, to the brain, where its effects can be exerted and further promote cognition (Vaynman et al., 2004; Devika and Jaffar Ali, 2013; Sleiman et al., 2016). Therefore, our findings and those from previous studies suggest that improvements in cognition following AT may be due to improved vascular health, which promotes improved cerebral perfusion and CVR during times of increased neuronal metabolism (i.e., improved NVC) (Guadagni et al., 2020). This is supported by the increased cerebrovascular function we also observed.

We observed that following the intervention, the exercise group had a higher total composite CVR to cognitive stimuli

TABLE 5 | Cerebrovascular and respiratory parameters at baseline and peak hypercapnia at week 0 and week 16 for the control and exercise groups.

Variable	Control (n = 13)				Exercise (n = 14)				Treatment	Intervention	Treatment × intervention	Treatment × intervention × time
	Week 0		Week 16		Week 0		Week 16					
	Baseline	Peak	Baseline	Peak	Baseline	Peak	Baseline	Peak				
Cerebrovascular variables												
CBF_V (cm/s)	37.4 ± 9.3	52.3 ± 15.4	41.6 ± 13.5	61.2 ± 18.2	31.0 ± 8.9	47.0 ± 14.0	33.5 ± 5.3	61.2 ± 8.7	0.147	**< 0.001**	0.116	**0.045**
CPI	1.22 ± 0.44	1.05 ± 0.50	1.00 ± 0.25	0.83 ± 0.19	1.20 ± 0.32	0.93 ± 0.18	0.95 ± 0.16	0.80 ± 0.13	0.971	**0.001**	0.319	0.350
Respiratory variables												
$P_{ET}CO_2$ (mmHg)	32.5 ± 5.1	37.1 ± 5.0	33.8 ± 5.2	38.6 ± 5.4	29.6 ± 3.2	35.9 ± 4.3	30.9 ± 4.1	37.2 ± 3.5	0.982	0.332	0.997	0.884
Tidal volume (L)	0.79 ± 0.29	1.13 ± 0.46	0.62 ± 0.27	0.93 ± 0.37	0.80 ± 0.28	0.98 ± 0.39	1.00 ± 0.25	1.34 ± 0.49	0.099	0.280	**0.002**	0.166
Breathing frequency (breaths/min)	16 ± 8	18 ± 8	16 ± 7	18 ± 10	15 ± 5	16 ± 7	13 ± 4	15 ± 6	0.406	0.434	0.200	0.812
Minute ventilation (L/min)	12.0 ± 4.1	16.8 ± 9.1	9.3 ± 4.1	14.8 ± 8.3	11.3 ± 4.9	14.6 ± 5.2	12.0 ± 4.9	17.0 ± 7.5	0.619	0.885	**0.035**	0.663
$CBF_V/P_{ET}CO_2$ (cm/s/mmHg)	1.24 ± 0.20	1.53 ± 0.31	1.24 ± 0.35	1.59 ± 0.42	1.10 ± 0.20	1.41 ± 0.31	1.10 ± 0.26	1.65 ± 0.23	0.232	0.263	0.853	0.384

CBF_V, cerebral blood flow velocity; CPI, cerebral pulsatility index; $P_{ET}CO_2$, partial pressure of end tidal carbon dioxide.
Values are means ± SD.
Bold values represent significant differences.

than the control group, as well as a higher CVR to each of the individual cognitive stimuli, excluding the Picture Vocabulary Test and the Flanker Inhibitory Control and Attention Test. To our knowledge, we are the first to evaluate the effects of AT in sedentary, obese, older adults who are at risk of cognitive decline. Our findings support those of others who have measured the effects of an AT intervention on NVC and another study which measured differences in NVC between aerobic exercise trained and sedentary older adults. Ozturk et al. (2021) demonstrated that CVR to a working memory task improved following 6 months of AT in young adults with spinal-cord injuries and Fabiani et al. (2014) reported that older adults with greater aerobic fitness had higher NVC capacity. Both studies suggest that improvements in NVC are due to improvements in cardiovascular function, specifically endothelial function. Ozturk et al. (2021) suggested that those suffering from spinal cord injuries have reduced cognitive and endothelial function, which is partly demonstrated by increased arterial stiffness. In other words, a reduction in endothelial function may result from increased arterial stiffness, which reduces the capacity of the cerebrovasculature to supply oxygen and nutrient rich blood to the brain, thus resulting in reduced cognitive function. The authors also suggested that AT reduced arterial stiffness and improved endothelial function in this cohort, thus improving cognition. The characteristics of our participants with metabolic syndrome and those with spinal cord injury are very different. However, one central theme shared among those with spinal cord injuries and those with the metabolic syndrome is that they have reduced endothelial function and increased chronic low-grade systemic inflammation and, therefore, poor cardiometabolic status (Lteif et al., 2005; Mohammadi et al., 2015). Hence, it is clear that improved endothelial function is pivotal in improving cerebrovascular function and cognition. Further, the total composite CVR to cognitive stimuli decreased in the control group. Since this measurement describes NVC and is reflective of the relationship between the brain and its vasculature, this finding also indicates that reduced endothelial function promotes further decline in cerebrovascular and cognitive function and that improving endothelial health is pivotal to improving overall brain health (Duchemin et al., 2012; Toth et al., 2017).

Correlations Between Exercise Sessions Completed and Cerebrovascular Function and Cognition

The exercise group completed 40 AT sessions on average over the 16 weeks. This equates to approximately 2.5 sessions per week or approximately 100 min of mixed intensity AT per week. This is less than that of the current physical activity guidelines described by both the Australian Department of Health and the American College of Sports Medicine (DOH, 2014; Piercy et al., 2018). Only one other study has deviated from these guidelines and it was reported that 90 min of moderate intensity exercise per week for 12 weeks improved cerebral perfusion and cognition in older, apparently healthy adults (Maass et al., 2014). We observed a very strong positive correlation between the number of exercise sessions completed and the total composite

TABLE 6 | Cognitive function and cerebrovascular responsiveness to cognitive stimuli at week 0 and week16 for the control and exercise groups.

Variable	Control (n = 13)		Exercise (n = 14)		P-value		
	Week 0	Week 16	Week 0	Week 16	Treatment	Intervention	Treatment × intervention
Cognitive function							
Dimensional change card sort*	7.46 ± 1.33	7.78 ± 0.15	7.32 ± 2.00	7.58 ± 1.25	0.708	0.313	0.939
Pattern comparison processing speed*	43 ± 11	44 ± 11	47 ± 10	53 ± 13	0.164	**0.006**	0.078
Picture vocabulary test*	6.16 ± 1.86	6.06 ± 2.10	5.14 ± 2.37	5.99 ± 2.24	0.492	0.215	0.118
Flanker inhibitory control and attention*	7.80 ± 0.49	7.79 ± 0.40	8.09 ± 0.47	8.16 ± 0.43	0.062	0.443	0.365
Picture sequence memory*	–0.67 ± 0.84	–0.36 ± 0.98	–0.90 ± 0.58	–0.62 ± 0.18	0.379	**0.005**	0.886
List sorting working memory*	16 ± 2	16 ± 3	15 ± 3	19 ± 3	0.352	**< 0.001**	**<0.001**
Oral reading recognition*	4.61 ± 2.41	5.10 ± 2.59	4.16 ± 2.32	5.71 ± 2.57	0.921	**0.002**	0.080
Trail making task (Part A)							
Time (s)	36.3 ± 13.1	36.5 ± 14.1	37.0 ± 14.1	28.6 ± 12.4	0.410	0.173	0.152
Errors made	0.7 ± 0.9	0.9 ± 1.3	0.6 ± 0.9	0.1 ± 0.4	0.107	0.602	0.164
Trail making task (Part B)							
Time (s)	83.4 ± 48.9	66.6 ± 23.9	77.9 ± 29.2	67.2 ± 47.3	0.723	0.216	0.621
Errors made	2.4 ± 1.9	2.5 ± 4.6	1.5 ± 2.2	0.6 ± 0.7	0.052	0.550	0.687
Part B–Part A time difference	47.1 ± 38.8	30.0 ± 16.5	40.9 ± 20.3	38.5 ± 36.8	0.951	0.315	0.262
Spatial span test							
Time (s)	100.9 ± 20.5	104.3 ± 38.4	97.4 ± 35.9	105.3 ± 22.6	0.769	0.504	0.752
Total spans completed	5.6 ± 0.9	5.2 ± 1.6	4.8 ± 1.3	5.4 ± 0.7	0.215	0.697	0.129
Total composite cognitive score	101 ± 12	104 ± 14	101 ± 13	111 ± 14	0.508	**< 0.001**	**0.004**
Cerebrovascular responsiveness (%)							
Dimensional change card sort test	16.9 ± 8.9	12.1 ± 5.0	13.3 ± 7.0	20.8 ± 6.1	0.329	0.289	**0.001**
Pattern comparison processing speed test	20.0 ± 6.5	18.7 ± 10.2	18.0 ± 6.8	24.5 ± 7.1	0.517	0.179	**0.048**
Picture vocabulary test	23.1 ± 7.0	21.9 ± 11.9	20.0 ± 9.4	27.2 ± 7.9	0.797	0.192	0.083
Flanker inhibitory control and attention test	13.1 ± 8.5	14.0 ± 6.7	12.3 ± 6.1	19.2 ± 5.6	0.342	**0.026**	0.080
Picture sequence memory test	21.9 ± 7.3	17.5 ± 6.0	20.6 ± 9.2	27.2 ± 11.6	0.238	0.529	**0.010**
List sorting working memory test	21.0 ± 5.9	16.8 ± 5.7	17.8 ± 7.2	28.1 ± 8.0	0.112	**< 0.001**	**0.040**
Oral reading recognition test	19.9 ± 4.2	10.4 ± 6.5	14.0 ± 8.0	26.9 ± 10.0	0.067	0.572	**< 0.001**
Trail making task (Part A)	24.0 ± 9.2	16.6 ± 5.2	20.0 ± 9.7	25.8 ± 8.4	0.405	0.441	**< 0.001**
Trail making task (Part B)	17.4 ± 6.5	16.9 ± 5.4	19.5 ± 10.4	30.6 ± 5.5	**0.016**	0.153	**0.002**
Spatial span test	22.3 ± 4.3	16.3 ± 6.1	16.4 ± 9.3	25.8 ± 7.3	0.511	0.226	**< 0.001**
Total composite CVR to cognitive stimuli	19.9 ± 3.3	16.4 ± 5.4	19.5 ± 10.4	25.9 ± 6.1	0.114	**0.026**	**< 0.001**

**Normalized, computed and standardized automatically by NIH Toolbox, based on validated measures (Slotkin et al., 2012).*
Values are means ± SD.
Bold values represent significant differences.

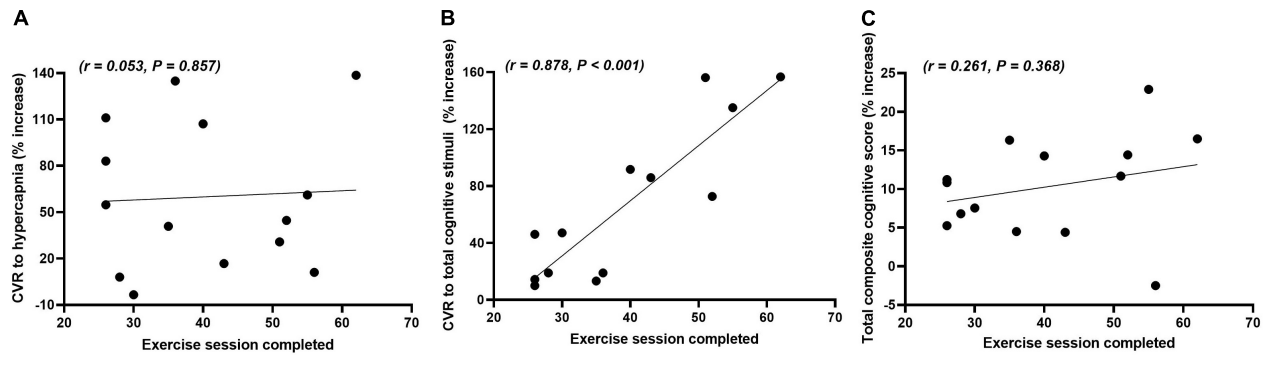

FIGURE 3 | Correlations between the number of exercise sessions completed and the relative percentage change (% increase) in the cerebrovascular responsiveness (CVR) to hypercapnia **(A)**, total composite CVR to cognitive stimuli **(B)** and total composite cognitive score **(C)** from weeks 0 to 16 in the exercise group.

CVR to cognitive stimuli. This finding indicates that a dose-response relationship between these variables may exist and that NVC, a vital regulatory function in cerebrovascular function and neuronal metabolism, can be improved with less than 100 min of AT per week for 16 weeks. There were no significant correlations between the number of exercise sessions completed and the CVR to hypercapnia and total composite cognitive scores. This finding may suggest one of three things: Firstly, some exercise is better than none in improving cognition and CVR to hypercapnia, which reflects the autoregulatory function of the cerebrovasculature. Secondly, a dose-response relationship between these variables exists, but it was too low a dose to be determined in this study. Thirdly, NVC is more sensitive to exercise training than both CVR to hypercapnia and total cognitive capacity. In any case, further studies examining this relationship between the amount of exercise and improvements in overall brain health are warranted because it may be more attainable to promote and prescribe shorter bouts of exercise to improve exercise compliance and engagement in the community, particularly in older adults.

Methodological Considerations

While we aimed to recruit an even number of men and women, it was not possible due to several confounding factors, such as geographical distance from the study location and potential participants not meeting the inclusion criteria. We acknowledge that the sex differences between the participants of this study may have cofounded our data, even though there were no significant differences between the groups in distribution of men and women. Additionally, **Figure 1** reflects the relatively low engagement of the target region (i.e., Ipswich) in health or at least health-related studies. This may have also contributed to the low uptake of the study by men. We noted that there were no significant treatment × intervention interaction effects in any of the data that was collected to define participant characteristics at baseline. This may have been influenced by the fact that the exercise group appeared marginally healthier than the control group at baseline, thus masking potential covariates that may lead to improvements in both cerebrovascular function and cognition. Additionally, the majority of exercise prescription was AT with a small component of resistance training. The resistance exercises were utilized and prescribed in a manner which predominantly focused on the recruitment of the aerobic energy system (i.e., aerobic-resistance training). In any case, we cannot exclude that resistance training may have influenced the results of this study. It must be acknowledged that another potential limitation to this study was that those in the control group may have participated in exercise sessions outside of the study or chose to make lifestyle changes, such as altering their nutritional intake. All included participants agreed at the start of the trial to continue with their current lifestyle and nutritional choices. In an attempt to encourage this, we informed all participants in the control group at Week 0 that once the study concluded that they would be provided with the entire exercise regime, including instructions on how to perform the exercises. We also made regular contact with the control group in an attempt to ensure compliance. Future studies may benefit from having a sham exercise group as a control or another arm added to the study, in which participants do not participate in exercise, rather they interact socially. The latter may be particularly important to control for given that there is evidence that socialization and re-socialization following isolation can improve cognitive performance and brain activity in animals (Rivera et al., 2020) and older adults (Gallucci et al., 2009). We did not use the gold-standard maximal oxygen uptake test to quantify aerobic exercise capacity in this study. Instead, a 6MWT was used, because it is a safe, inexpensive, tolerable and reliable measure of functional exercise capacity commonly utilized in older populations that may also increase compliance for future testing in this population (ATS, 2002; Maniscalco et al., 2006; Ross et al., 2010).

CONCLUSION

In conclusion, 16 weeks of AT increased the CVR to hypercapnia, CVR to cognitive stimuli and total composite cognitive score in sedentary, obese, older adults compared with the control group. A very strong relationship was observed between the number of exercise sessions completed and CVR to cognitive stimuli, but not for CVR to hypercapnia or total composite cognitive score. These results indicate that cognition and the responsiveness of the cerebrovasculature to physiological stimuli can be improved by as little as 100 min of exercise per week in previously sedentary, older, obese adults with metabolic syndrome. These individuals are at an increased risk of developing cognitive impairment and, potentially, a neurodegenerative disease such as dementia. Future studies should ascertain the minimum dose of AT needed to improve total cognitive capacity and CVR to hypercapnia in a cohort of older adults.

DATA AVAILABILITY STATEMENT

The original contributions presented in the study are included in the article/supplementary material, further inquiries can be directed to the corresponding author/s.

ETHICS STATEMENT

The studies involving human participants were reviewed and approved by the University of Southern Queensland Human Research Ethics Committee. The patients/participants provided their written informed consent to participate in this study.

AUTHOR CONTRIBUTIONS

EB, RW, PH, and DM conceptualized, designed the study protocol and experiments, and contributed to revisions of intellectual content. EB and DM designed the training protocol for the study. EB collected the data and analyzed the data. EB and DM performed statistical analysis, with all authors contributing to data interpretation. All authors approved the final manuscript.

FUNDING

This study was supported in part by a University of Southern Queensland Strategic Funding Grant. EB was also supported by the Australia Postgraduate Award.

ACKNOWLEDGMENTS

We would like to acknowledge the University of Southern Queensland for assistance in funding the production of this manuscript. We would also like to thank QML Pathology for their timely reporting of some of the biochemical analyses performed at their laboratory. We would also like to thank all study participants for their time and effort to ensure this project was completed. Finally, we would like to thank the University of Southern Queensland Sports and Exercise Clinic, including staff and students, who greatly assisted in ensuring this project was completed. Without your assistance, this study could not be performed. We would also like to thank Prof. Laine Cameron for her guidance and advice in exercise prescription for participants with specific ailments.

REFERENCES

Afkhami, R., Walker, F. R., Ramadan, S., Wong, R., and Johnson, S. J. (2021). Indexing cerebrovascular health using near-infrared spectroscopy. *Sci. Rep.* 11:14812. doi: 10.1038/s41598-021-94348-5

AIHW (2012). *Dementia in Australia*. Canberra: Australian Institute of Health and Welfare.

AIHW (2018a). *Australia's Health 2018*. Canberra: Australian Institute of Health and Welfare.

AIHW (2018b). *Physical Activity Across the Life Stages*. Canberra: Australian Institute of Health and Welfare.

Ainslie, P. N., Cotter, J. D., George, K. P., Lucas, S., Murrell, C., Shave, R., et al. (2008). Elevation in cerebral blood flow velocity with aerobic fitness throughout healthy human ageing. *J. Physiol.* 586, 4005–4010. doi: 10.1113/jphysiol.2008.158279

Akazawa, N., Tanahashi, K., Kosaki, K., Ra, S.-G., Matsubara, T., Choi, Y., et al. (2018). Aerobic exercise training enhances cerebrovascular pulsatility response to acute aerobic exercise in older adults. *Physiol. Rep.* 6:e13681. doi: 10.14814/phy2.13681

Alberti, K. G., Zimmet, P., and Shaw, J. (2005). The metabolic syndrome: a new worldwide definition. *Lancet* 366, 1059–1062. doi: 10.1016/s0140-6736(05)67402-8

Altman, D. G., and Bland, J. M. (2005). Treatment allocation by minimisation. *Br. Med. J.* 330, 843–843. doi: 10.1136/bmj.330.7495.843

Anazodo, U. C., Shoemaker, J. K., Suskin, N., Ssali, T., Wang, D. J. J., and Lawrence, K. S. (2016). Impaired cerebrovascular function in coronary artery disease patients and recovery following cardiac rehabilitation. *Front. Aging Neurosci.* 7:224. doi: 10.3389/fnagi.2015.00224

Anderson-Hanley, C., Arciero, P. J., Brickman, A. M., Nimon, J. P., Okuma, N., Westen, S. C., et al. (2012). Exergaming and older adult cognition: a cluster randomized clinical trial. *Am. J. Prev. Med.* 42, 109–119. doi: 10.1016/j.amepre.2011.10.016

ATS (2002). ATS statement: guidelines for the six-minute walk test. ATS Committee on Proficiency Standards for Clinical Pulmonary Function Laboratories. *Am. J. Respir. Crit. Care Med.* 166, 111–117. doi: 10.1164/ajrccm.166.1.at1102

Bailey, D. M., Marley, C. J., Brugniaux, J. V., Hodson, D., New, K. J., Ogoh, S., et al. (2013). Elevated aerobic fitness sustained throughout the adult lifespan is associated with improved cerebral hemodynamics. *Stroke* 44, 3235–3238. doi: 10.1161/STROKEAHA.113.002589

Baker, L. D., Frank, L. L., and Foster-Schubert, K. (2010). Effects of aerobic exercise on mild cognitive impairment: a controlled trial. *Arch. Neurol.* 67, 71–79. doi: 10.1001/archneurol.2009.307

Bakker, S. L., de Leeuw, F. E., den Heijer, T., Koudstaal, P. J., Hofman, A., and Breteler, M. M. (2004). Cerebral haemodynamics in the elderly: the Rotterdam study. *Neuroepidemiology* 23, 178–184. doi: 10.1159/000078503

Bangen, K. J., Nation, D. A., Clark, L. R., Harmell, A. L., Wierenga, C. E., Dev, S. I., et al. (2014). Interactive effects of vascular risk burden and advanced age on cerebral blood flow. *Front. Aging Neurosci.* 6:159. doi: 10.3389/fnagi.2014.00159

Barbour, J. A., Howe, P. R. C., Buckley, J. D., Bryan, J., and Coates, A. M. (2017). Cerebrovascular and cognitive benefits of high-oleic peanut consumption in healthy overweight middle-aged adults. *Nutri. Neurosci.* 20, 555–562. doi: 10.1080/1028415X.2016.1204744

BD (2019). *Specimen Collection Resource Library [Internet]*. [Online]. Franklin Lakes, NJ: Dickinson and Company.

Beydoun, M. A., Beydoun, H. A., and Wang, Y. (2008). Obesity and central obesity as risk factors for incident dementia and its subtypes: a systematic review and meta-analysis. *Obes. Rev.* 9, 204–218. doi: 10.1111/j.1467-789X.2008.00473.x

Bliss, E. S., Wong, R. H., Howe, P. R., and Mills, D. E. (2021). Benefits of exercise training on cerebrovascular and cognitive function in ageing. *J. Cereb. Blood Flow Metab.* 41, 447–470. doi: 10.1177/0271678x20957807

Borg, G. (1998). *Borg's Perceived Exertion and Pain Scales*. Canada: Human kinetics.

Brown, L., Hansnata, E., and La, H. A. (2017). *Economic Cost of Dementia in Australia*. Canberra: Alzheimer's Australia.

Chang, F., Flavahan, S., and Flavahan, N. A. (2018). Superoxide inhibition restores endothelium-dependent dilatation in aging arteries by enhancing impaired adherens junctions. *Am. J. Physiol. Heart Circ. Physiol.* 314, H805–H811. doi: 10.1152/ajpheart.00681.2017

Chapman, S., Aslan, S., Spence, J., DeFina, L., Keebler, M., Didehbani, N., et al. (2013). Shorter term aerobic exercise improves brain, cognition, and cardiovascular fitness in aging. *Front. Aging Neurosci.* 5:75. doi: 10.3389/fnagi.2013.00075

Claxton, A. J., Cramer, J., and Pierce, C. (2001). A systematic review of the associations between dose regimens and medication compliance. *Clin. Ther.* 23, 1296–1310. doi: 10.1016/S0149-2918(01)80109-0

Cohen, J. (1988). *Statistical Power Analysis for the Behavioral Sciences*. Hillsdale, NJ: Lawrence Erlbaum Associates, Inc.

Devika, N. T., and Jaffar Ali, B. M. (2013). Analysing calcium dependent and independent regulation of eNOS in endothelium triggered by extracellular signalling events. *Mol. BioSyst.* 9, 2653–2664. doi: 10.1039/C3MB70258H

Dipietro, L., Caspersen, C. J., Ostfeld, A. M., and Nadel, E. R. (1993). A survey for assessing physical activity among older adults. *Med. Sci. Sports Exerc.* 25, 628–642.

DOH (2014). *Australia's Physical Activity and Sedentary Behaviour Guidelines*. Canberra: Australian Government Deparment of Health.

Duchemin, S., Boily, M., Sadekova, N., and Girouard, H. (2012). The complex contribution of NOS interneurons in the physiology of cerebrovascular regulation. *Front. Neural. Circ.* 6:51. doi: 10.3389/fncir.2012.00051

Edmonds, H. L. Jr., Isley, M. R., Sloan, T. B., Alexandrov, A. V., and Razumovsky, A. Y. (2011). American Society of Neurophysiologic Monitoring and American Society of Neuroimaging joint guidelines for Transcranial Doppler ultrasonic monitoring. *J. Neuroimaging* 21, 177–183. doi: 10.1111/j.1552-6569.2010.00471.x

Erickson, K. I., Voss, M. W., Prakash, R. S., Basak, C., Szabo, A., Chaddock, L., et al. (2011). Exercise training increases size of hippocampus and improves memory. *Proc. Natl. Acad. Sci. U S A.* 108, 3017–3022. doi: 10.1073/pnas.1015950108

Evans, H., Howe, P., and Wong, R. (2017). Effects of resveratrol on cognitive performance, mood and cerebrovascular function in post-menopausal women; A 14-week randomised placebo-controlled intervention trial. *Nutrients* 9:27. doi: 10.3390/nu9010027

Fabiani, M., Gordon, B. A., Maclin, E. L., Pearson, M. A., Brumback-Peltz, C. R., Low, K. A., et al. (2014). Neurovascular coupling in normal aging: a combined optical, ERP and fMRI study. *Neuroimage* 85, 592–607. doi: 10.1016/j.neuroimage.2013.04.113

Gallucci, M., Antuono, P., Ongaro, F., Forloni, P., Albani, D., Amici, G., et al. (2009). Physical activity, socialization and reading in the elderly over the age

of seventy: what is the relation with cognitive decline? Evidence from "The Treviso Longeva (TRELONG) study. *Arch. Gerontol. Geriat.* 48, 284–286. doi: 10.1016/j.archger.2008.02.006

Guadagni, V., Drogos, L. L., Tyndall, A. V., Davenport, M. H., Anderson, T. J., Eskes, G. A., et al. (2020). Aerobic exercise improves cognition and cerebrovascular regulation in older adults. *Neurology* 94, e2245–e2257. doi: 10.1212/wnl.0000000000009478

Harris, S., Reyhan, T., Ramli, Y., Prihartono, J., and Kurniawan, M. (2018). Middle cerebral artery pulsatility index as predictor of cognitive impairment in hypertensive patients. *Front. Neurol.* 9:538. doi: 10.3389/fneur.2018.00538

Harvey, P. D. (2019). Domains of cognition and their assessment. *Dialogues Clin. Neurosci.* 21, 227–237. doi: 10.31887/DCNS.2019.21.3/pharvey

Healthineers (2019). *ADVIA Chemistry XPT System* [Online]. Germany: Siemens Healthcare.

Heaton, R. K., Akshoomoff, N., Tulsky, D., Mungas, D., Weintraub, S., Dikmen, S., et al. (2014). Reliability and validity of composite scores from the NIH Toolbox Cognition Battery in adults. *J. Int. Neuropsychol. Soc.* 20, 588–598. doi: 10.1017/s1355617714000241

Heuchert, J. P., and McNair, D. M. (2012). *Profile of Mood States 2nd Edition^{TM}: POMS 2*. North Tonawanda, NY: Multi-Health Systems Inc.

Hillman, T. E., Nunes, Q. M., Hornby, S. T., Stanga, Z., Neal, K. R., Rowlands, B. J., et al. (2005). A practical posture for hand grip dynamometry in the clinical setting. *Clin. Nutr.* 24, 224–228. doi: 10.1016/j.clnu.2004.09.013

Hoffmann, K., Sobol, N. A., Frederiksen, K. S., Beyer, N., Vogel, A., Vestergaard, K., et al. (2016). Moderate-to-high intensity physical exercise in patients with Alzheimer's disease: a randomized controlled trial. *J. Alzheimer's Dis.* 50, 443–453. doi: 10.3233/jad-150817

Ivey, F. M., Ryan, A. S., Hafer-Macko, C. E., and Macko, R. F. (2011). Improved cerebral vasomotor reactivity after exercise training in hemiparetic stroke survivors. *Stroke* 42, 1994–2000. doi: 10.1161/STROKEAHA.110.607879

Kearney-Schwartz, A., Rossignol, P., Bracard, S., Felblinger, J., Fay, R., Boivin, J.-M., et al. (2009). Vascular structure and function is correlated to cognitive performance and white matter hyperintensities in older hypertensive patients with subjective memory complaints. *Stroke* 40, 1229–1236. doi: 10.1161/STROKEAHA.108.532853

Keys, A., Fidanza, F., Karvonen, M. J., Kimura, N., and Taylor, H. L. (1972). Indices of relative weight and obesity. *J. Chronic Dis.* 25, 329–343. doi: 10.1016/0021-9681(72)90027-6

Kleinloog, J. P. D., Mensink, R. P., Ivanov, D., Adam, J. J., Uludağ, K., and Joris, P. J. (2019). Aerobic exercise training improves cerebral blood flow and executive function: a randomized, controlled cross-over trial in sedentary older men. *Front. Aging Neurosci.* 11:333. doi: 10.3389/fnagi.2019.00333

Lautenschlager, N. T., Cox, K. L., and Flicker, L. (2008). Effect of physical activity on cognitive function in older adults at risk for alzheimer disease: a randomized trial. *J. Am. Med. Assoc.* 300, 1027–1037. doi: 10.1001/jama.300.9.1027

Lteif, A. A., Han, K., and Mather, K. J. (2005). Obesity, insulin resistance, and the metabolic syndrome. *Circulation* 112, 32–38. doi: 10.1161/CIRCULATIONAHA.104.520130

Maass, A., Düzel, S., Goerke, M., Becke, A., Sobieray, U., Neumann, K., et al. (2014). Vascular hippocampal plasticity after aerobic exercise in older adults. *Mol. Psychiatry* 20:585. doi: 10.1038/mp.2014.114

Maniscalco, M., Zedda, A., Giardiello, C., Faraone, S., Cerbone, M. R., Cristiano, S., et al. (2006). Effect of bariatric surgery on the six-minute walk test in severe uncomplicated obesity. *Obes. Surg.* 16, 836–841. doi: 10.1381/096089206777822331

Miller, K. B., Howery, A. J., Harvey, R. E., Eldridge, M. W., and Barnes, J. N. (2018). Cerebrovascular reactivity and central arterial stiffness in habitually exercising healthy adults. *Front. Physiol.* 9:1096. doi: 10.3389/fphys.2018.01096

Mohammadi, V., Khalili, M., Eghtesadi, S., Dehghani, S., Jazayeri, S., Aghababaee, S., et al. (2015). The effect of alpha-lipoic acid (ALA) supplementation on cardiovascular risk factors in men with chronic spinal cord injury: a clinical trial. *Spinal Cord* 53, 621–624. doi: 10.1038/sc.2015.35

Nichols, E., Szoeke, C. E. I., Vollset, S. E., Abbasi, N., Abd-Allah, F., Abdela, J., et al. (2019). Global, regional, and national burden of Alzheimer's disease and other dementias, 1990–2016: a systematic analysis for the Global Burden of Disease Study 2016. *Lancet Neurol.* 18, 88–106. doi: 10.1016/S1474-4422(18)30403-4

Norton, K., and Norton, L. (2011). *Pre-Exercise Screening: Guide to the Australian Adult Pre-Exercise Screening System*. Australia: Exercise and Sport Science Australia.

Ozturk, E. D., Lapointe, M. S., Kim, D.-I., Hamner, J. W., and Tan, C. O. (2021). Effect of 6-month exercise training on neurovascular function in spinal cord injury. *Med. Sci. Sports Exerc.* 53, 38–46. doi: 10.1249/mss.0000000000002452

Pannucci, T. E., Thompson, F. E., Bailey, R. L., Dodd, K. W., Potischman, N., Kirkpatrick, S. I., et al. (2018). Comparing Reported Dietary Supplement Intakes between Two 24-Hour Recall Methods: the Automated Self-Administered 24-Hour Dietary Assessment Tool and the Interview-Administered Automated Multiple Pass Method. *J. Acad. Nutr. Diet* 118, 1080–1086. doi: 10.1016/j.jand.2018.02.013

Piercy, K. L., Troiano, R. P., Ballard, R. M., Carlson, S. A., Fulton, J. E., Galuska, D. A., et al. (2018). The physical activity guidelines for Americans. *J. Am. Med. Assoc.* 320, 2020–2028. doi: 10.1001/jama.2018.14854

Pikula, A., Böger, R. H., Beiser, A. S., Maas, R., DeCarli, C., Schwedhelm, E., et al. (2009). Association of plasma ADMA levels with MRI markers of vascular brain injury: framingham offspring study. *Stroke* 40, 2959–2964. doi: 10.1161/STROKEAHA.109.557116

Prisant, L. M., Pasi, M., Jupin, D., and Prisant, M. E. (2002). Assessment of repeatability and correlates of arterial compliance. *Blood Press. Monitor.* 7, 231–235. doi: 10.1097/00126097-200208000-00005

QML (2019). *QML Pathology Test Reference Manual [Internet]*. [Online]. Brisbane: QML Pathology.

Rejeski, W. J., Brawley, L. R., Ettinger, W., Morgan, T., and Thompson, C. (1997). Compliance to exercise therapy in older participants with knee osteoarthritis: implications for treating disability. *Med. Sci. Sports Exerc.* 29, 977–985. doi: 10.1097/00005768-199708000-00001

Rivera, D. S., Lindsay, C. B., Oliva, C. A., Codocedo, J. F., Bozinovic, F., and Inestrosa, N. C. (2020). Effects of long-lasting social isolation and re-socialization on cognitive performance and brain activity: a longitudinal study in Octodon degus. *Sci. Rep.* 10, 1–21. doi: 10.1038/s41598-020-75026-4

Rogers, R. L., Meyer, J. S., and Mortel, K. F. (1990). After reaching retirement age physical activity sustains cerebral perfusion and cognition. *J. Am. Geriat. Soc.* 38, 123–128. doi: 10.1111/j.1532-5415.1990.tb03472.x

Ross, R. M., Murthy, J. N., Wollak, I. D., and Jackson, A. S. (2010). The six minute walk test accurately estimates mean peak oxygen uptake. *BMC Pulm. Med.* 10:31. doi: 10.1186/1471-2466-10-31

Rossman, M. J., LaRocca, T. J., Martens, C. R., and Seals, D. R. (2018). Healthy lifestyle-based approaches for successful vascular aging. *J. Appl. Physiol.* 125, 1888–1900. doi: 10.1152/japplphysiol.00521.2018

Schober, P., Boer, C., and Schwarte, L. A. (2018). Correlation coefficients: appropriate use and interpretation. *Anesth. Analg.* 126, 1763–1768. doi: 10.1213/ane.0000000000002864

Serrador, J. M., Picot, P. A., Rutt, B. K., Shoemaker, J. K., and Bondar, R. L. (2000). MRI measures of middle cerebral artery diameter in conscious humans during simulated orthostasis. *Stroke* 31, 1672–1678. doi: 10.1161/01.str.31.7.1672

Sleiman, S. F., Henry, J., Al-Haddad, R., El Hayek, L., Abou Haidar, E., Stringer, T., et al. (2016). Exercise promotes the expression of brain derived neurotrophic factor (BDNF) through the action of the ketone body β-hydroxybutyrate. *eLife* 5:e15092. doi: 10.7554/eLife.15092

Slotkin, J., Nowinski, C., Hays, R., Beaumont, J., Griffith, J., Magasi, S., et al. (2012). *NIH Toolbox Scoring and Interpretation Guide*. Washington, DC: National Institutes of Health, 6–7.

Smith, E. E., and Greenberg, S. M. (2009). B-amyloid, blood vessels, and brain function. *Stroke* 40, 2601–2606. doi: 10.1161/STROKEAHA.108.536839

Sobol, N. A., Hoffmann, K., Vogel, A., Lolk, A., Gottrup, H., Høgh, P., et al. (2016). Associations between physical function, dual-task performance and cognition in patients with mild Alzheimer's disease. *Aging Ment. Health* 20, 1139–1146. doi: 10.1080/13607863.2015.1063108

Strauss, E., Sherman, E., and Spreen, O. (2006). *A Compendium of Neuropsychological Tests*. New York, NY: Oxford University Press.

Taylor, D. (2014). Physical activity is medicine for older adults. *Postgrad. Med. J.* 90, 26–32. doi: 10.1136/postgradmedj-2012-131366

Toda, N. (2012). Age-related changes in endothelial function and blood flow regulation. *Pharmacol. Ther.* 133, 159–176. doi: 10.1016/j.pharmthera.2011.10.004

Tomoto, T., Liu, J., Tseng, B. Y., Pasha, E. P., Cardim, D., Tarumi, T., et al. (2021). One-year aerobic exercise reduced carotid arterial stiffness and increased cerebral blood flow in amnestic mild cognitive impairment. *J. Alzheimers. Dis.* 80, 841–853. doi: 10.3233/jad-201456

Toth, P., Tarantini, S., Csiszar, A., and Ungvari, Z. (2017). Functional vascular contributions to cognitive impairment and dementia: mechanisms and consequences of cerebral autoregulatory dysfunction, endothelial impairment, and neurovascular uncoupling in aging. *Am. J. Physiol. Heart Circ. Physiol.* 312, H1–H20. doi: 10.1152/ajpheart.00581.2016

Vaynman, S., Ying, Z., and Gomez-Pinilla, F. (2004). Hippocampal BDNF mediates the efficacy of exercise on synaptic plasticity and cognition. *Eur. J. Neurosci.* 20, 2580–2590. doi: 10.1111/j.1460-9568.2004.03720.x

Vicente-Campos, D., Mora, J., Castro-Piñero, J., González-Montesinos, J. L., Conde-Caveda, J., and Chicharro, J. L. (2012). Impact of a physical activity program on cerebral vasoreactivity in sedentary elderly people. *J. Sports Med. Phys. Fit.* 52, 537–544.

Weintraub, S., Dikmen, S. S., Heaton, R. K., Tulsky, D. S., Zelazo, P. D., Slotkin, J., et al. (2014). The cognition battery of the NIH toolbox for assessment of neurological and behavioral function: validation in an adult sample. *J Int. Neuropsychol. Soc.* 20, 567–578. doi: 10.1017/s1355617714000320

Welborn, T. A., Dhaliwal, S. S., and Bennett, S. A. (2003). Waist-hip ratio is the dominant risk factor predicting cardiovascular death in Australia. *Med. J. Aust.* 179, 580–585. doi: 10.5694/j.1326-5377.2003.tb05704.x

Willie, C. K., Colino, F. L., Bailey, D. M., Tzeng, Y. C., Binsted, G., Jones, L. W., et al. (2011). Utility of transcranial Doppler ultrasound for the integrative assessment of cerebrovascular function. *J. Neurosci. Methods* 196, 221–237. doi: 10.1016/j.jneumeth.2011.01.011

Wong, R., Raederstorff, D., and Howe, P. (2016). Acute resveratrol consumption improves neurovascular coupling capacity in adults with type 2 diabetes mellitus. *Nutrients* 8:425. doi: 10.3390/nu8070425

Wong, R. H. X., Nealon, R. S., Scholey, A., and Howe, P. R. C. (2016). Low dose resveratrol improves cerebrovascular function in type 2 diabetes mellitus. *Nutr. Metab. Cardiovasc. Dis.* 26, 393–399. doi: 10.1016/j.numecd.2016.03.003

Woods, J. A., Wilund, K. R., Martin, S. A., and Kistler, B. M. (2011). Exercise, inflammation and aging. *Aging Dis.* 3, 130–140.

Young, J., Angevaren, M., Rusted, J., and Tabet, N. (2015). Aerobic exercise to improve cognitive function in older people without known cognitive impairment. *Cochrane Datab. Syst. Rev.* 4:5381. doi: 10.1002/14651858.CD005381.pub4

Conflict of Interest: The authors declare that the research was conducted in the absence of any commercial or financial relationships that could be construed as a potential conflict of interest.

Publisher's Note: All claims expressed in this article are solely those of the authors and do not necessarily represent those of their affiliated organizations, or those of the publisher, the editors and the reviewers. Any product that may be evaluated in this article, or claim that may be made by its manufacturer, is not guaranteed or endorsed by the publisher.

Advantages of publishing in Frontiers

OPEN ACCESS
Articles are free to read for greatest visibility and readership

FAST PUBLICATION
Around 90 days from submission to decision

HIGH QUALITY PEER-REVIEW
Rigorous, collaborative, and constructive peer-review

TRANSPARENT PEER-REVIEW
Editors and reviewers acknowledged by name on published articles

Frontiers
Avenue du Tribunal-Fédéral 34
1005 Lausanne | Switzerland

Visit us: www.frontiersin.org
Contact us: frontiersin.org/about/contact

REPRODUCIBILITY OF RESEARCH
Support open data and methods to enhance research reproducibility

DIGITAL PUBLISHING
Articles designed for optimal readership across devices

FOLLOW US
@frontiersin

IMPACT METRICS
Advanced article metrics track visibility across digital media

EXTENSIVE PROMOTION
Marketing and promotion of impactful research

LOOP RESEARCH NETWORK
Our network increases your article's readership